UNIVERSIDAD NACIONAL DEL LITORAL

DOCTORADO EN INGENIERÍA

Caracterización y control de sistemas biomédicos: diabetes mellitus tipo 1 e infección por SARS-CoV-2

Pablo Abuin

FICH
FACULTAD DE INGENIERÍA Y CIENCIAS HÍDRICAS

INTEC
INSTITUTO DE DESARROLLO TECNOLÓGICO PARA LA INDUSTRIA QUÍMICA

CIMEC
CENTRO DE INVESTIGACIÓN DE MÉTODOS COMPUTACIONALES

sinc(*i*)
INSTITUTO DE INVESTIGACIÓN EN SEÑALES, SISTEMAS E INTELIGENCIA COMPUTACIONAL

Tesis de Doctorado **2023**

UNIVERSIDAD NACIONAL DEL LITORAL
Facultad de Ingeniería y Ciencias Hídricas
Instituto de Desarrollo Tecnológico para la Industria Química
Centro de Investigacón de Métodos Computacionales
Instituto de Investigaciones en Señales, Sistemas e Inteligencia Computacional

CARACTERIZACIÓN Y CONTROL DE SISTEMAS BIOMÉDICOS: DIABETES MELLITUS TIPO 1 E INFECCIÓN POR SARS-COV-2

Pablo Abuin

Tesis remitida al Comité Académico del Doctorado
como parte de los requisitos para la obtención
del grado de
DOCTOR EN INGENIERÍA
Mención Inteligencia Computacional Señales y Sistemas
de la
UNIVERSIDAD NACIONAL DEL LITORAL
2023

Comisión de Posgrado, Facultad de Ingeniería y Ciencias Hídricas, Ciudad Universitaria, Paraje: El Pozo, S3000, Santa Fe, Argentina.

UNIVERSIDAD NACIONAL DEL LITORAL
Facultad de Ingeniería y Ciencias Hídricas
Instituto de Desarrollo Tecnológico para la Industria Química
Centro de Investigacón de Métodos Computacionales
Instituto de Investigaciones en Señales, Sistemas e Inteligencia Computacional

CARACTERIZACIÓN Y CONTROL DE SISTEMAS BIOMÉDICOS: DIABETES MELLITUS TIPO 1 E INFECCIÓN POR SARS-COV-2

Pablo Abuin

Lugar de trabajo:
INTEC
Instituto de Desarrollo Tecnológico para la Industria Química
Facultad de Ingeniería y Ciencias Hídricas
Universidad Nacional del Litoral

Director:
Dr. Alejandro Hernán González (INTEC-CONICET-UNL)

Co-director:
Dr. Antonio Ferramosca (Departamento de Ingeniería en Gestión, Información y Producción, Universidad de Bergamo, Italia)

Jurado evaluador:
Dra. Marta Basualdo (CIFASIS – CONICET)
Dr. Fabricio Garelli (UNLP-CONICET)
Dr. Patricio Colmegna (Universidad de Virginia, Estados Unidos de América)

2023

DECLARACIÓN LEGAL DEL AUTOR

Esta Tesis ha sido remitida como parte de los requisitos para la obtención del grado académico de Doctor en Ingeniería ante la Universidad Nacional del Litoral y ha sido depositada en la Biblioteca de la Facultad de Ingeniería y Ciencias Hídricas para permanecer a disposición de sus lectores bajo las condiciones por el reglamento de la mencionada Biblioteca.

Se permiten citaciones breves de esta Tesis sin la necesidad de un permiso especial, en la suposición de que la fuente sea correctamente citada. El portador legal del derecho de propiedad intelectual de la obra concederá por escrito solicitudes de permiso para la citación extendida o para la reproducción parcial o total de este manuscrito.

TESIS POR COMPILACIÓN

La presente tesis se encuentra organizada bajo el formato de Tesis por Compilación, aprobado en la resolución No 255/17 (Expte. No 888317-17) por el Comité Académico de la Carrera Doctorado en Ingeniería, Facultad de Ingeniería y Ciencias Hídricas, Universidad Nacional del Litoral (UNL). De dicha resolución: "En el caso de optar por la Tesis por Compilación, ésta consistirá en una descripción técnica de al menos 30 páginas, redactada en español e incluyendo todas las investigaciones abordadas en la tesis. Se deberán incluir las secciones habituales indicadas a continuación en la Sección Contenidos de la Tesis. Los artículos científicos publicados por el autor, en el idioma original de las publicaciones, deberán incluirse en un Anexo con el formato unificado al estilo general de la Tesis indicado en la Sección Formato. El Anexo deberá estar encabezado por una sección donde el tesista detalle para cada una de las publicaciones cuál ha sido su contribución. Esta sección deberá estar avalada por su director de Tesis. El documento central de la Tesis debe incluir referencias explícitas a todas las publicaciones anexadas y presentar una conclusión que muestre la coherencia de dichos trabajos con el hilo conceptual y metodológico de la tesis. Los artículos presentados en los anexos podrán ser artículos publicados, aceptados para publicación (en prensa) o en revisión."

AGRADECIMIENTOS

A Alejandro que fue mi guía durante de este proceso y, que mediante su pasión y optimismo, me orientó en la puesta en práctica del método científico.
A Antonio, que aun estando lejos, implusó la integración de las ideas labradas como condición inicial para futuras colaboraciones.
A mis compañeros del laboratorio, Agustina, Alejandro, Ignacio, Juan y Mara, por su paciencia y predisposición para abordar nuevos proyectos, y posibilitarme participar en sus temas de investigación.
A mi familia y amigos, por acompañarme y brindarme su apoyo durante este proceso.
A Marianela, por cuidarme con todo su amor a lo largo de estos años.

UNIVERSIDAD NACIONAL DEL LITORAL
Facultad de Ingeniería y Ciencias Hídricas

Santa Fe, 31 de Julio de 2023.

Como miembros del Jurado Evaluador de la Tesis de Doctorado en Ingeniería titulada ***"Caracterización y Control de Sistemas Biomédicos: Diabetes Mellitus Tipo 1 e Infección por SARS-CoV-2"***, desarrollada por el Bioing. Pablo ABUIN, en el marco de la Mención "Inteligencia Computacional, Señales y Sistemas", certificamos que hemos evaluado la Tesis y recomendamos que sea aceptada como parte de los requisitos para la obtención del título de Doctor en Ingeniería.

La aprobación final de esta disertación estará condicionada a la presentación de dos copias encuadernadas de la versión final de la Tesis ante el Comité Académico del Doctorado en Ingeniería.

Dra. Marta Basualdo	Dr. Fabricio Garelli	Dr. Patricio Colmegna

Santa Fe, 31 de Julio de 2023.

Certifico haber leído la Tesis, preparada bajo mi dirección en el marco de la Mención "Inteligencia Computacional, Señales y Sistemas" y recomiendo que sea aceptada como parte de los requisitos para la obtención del título de Doctor en Ingeniería.

Dr. Antonio Ferramosca Codirector de Tesis	Dr. Alejandro González Director de Tesis

FACULTAD DE INGENIERÍA Y CIENCIAS HÍDRICAS * SANTA FE *
Dr. JOSE LUIS MACOR
SECRETARIO DE POSGRADO
Ingeniería y Cs. Hídricas

Universidad Nacional del Litoral
Facultad de Ingeniería y Ciencias Hídricas

Secretaría de Posgrado

Ciudad Universitaria
C.C. 217
Ruta Nacional Nº 168 – Km. 472,4
(3000) Santa Fe
Tel: (54) (0342) 4575 229
Fax: (54) (0342) 4575 224
E-mail: posgrado@fich.unl.edu.ar

Índice general

Índice de figuras

Resumen

Con el advenimiento de nuevas estrategias terapéuticas existe hoy en día una marcada tendencia hacia el uso de modelos matemáticos como soporte a la optimización de dosis, las predicciones de la evolución de la patología en el corto y mediano plazo, el análisis y comprensión de las mismas para distintos escenarios, entre otros aspectos. Frente a esta realidad, resulta crucial realizar una caracterización de los modelos que las representan, analizando aspectos como su identificabilidad, observabilidad y controlabilidad a los fines del diseño de estrategias de identificación, estimación y control pertinentes. Siguiendo este paradigma, en la presente tesis se propone, por un lado, (i) el diseño de estrategias de control con garantías de convergencia asintótica a objetivos terapéuticos (específicos) para la diabetes tipo 1 y, por otro, (ii) la caracterización de modelos para infecciones agudas, incluyendo el efecto del tratamiento con antivirales.

Capítulo 1

Introducción

1.1. Antecedentes y motivación

Con el avance de la práctica médica hay una tendencia hacia el uso de modelos matemáticos para caracterizar ciertas patologías (tipo y estabilidad de equilibrios) [Ciupe and Heffernan, 2017, Nangue, 2019], comprender la evolución de las mismas para distintos escenarios y/o perturbaciones [Goodwin et al., 2018,Goodwin and Seron, 2019], estimar parámetros (ej. sensibilidad a la insulina [Schiavon et al., 2014,Pillonetto et al., 2006], tasa de infección de las células susceptibles [Baccam et al., 2006], producción de interferón [Dobrovolny et al., 2013], etc.), diseñar estrategias de control a los fines de conducir las variables controladas a ciertos objetivos terapéuticos [Pérez et al., 2022], entre otras. Frente a esta realidad, la teoría de sistemas dinámicos juega un papel clave, brindando las bases para el estudio del sistema en base a un modelo matemático del mismo [Haddad and Chellaboina, 2008]. En el marco de esta teoría, el sistema puede ser particularizado de acuerdo a una serie de herramientas matemáticas, posibilitando así una caracterización del mismo, determinado aspectos como su identificabilidad [Raue et al., 2009], observabilidad [Anderson and Moore, 2012] y controlabiliad [Sontag, 2013].

En lo que respecta a la etapa de control, previo al diseño de un controlador, se debe especificar el objetivo de control, es decir, hacia donde se desea guiar el sistema y de qué forma [Rawlings et al., 2017, Blanke et al., 2006, Goodwin et al., 2006]. Normalmente, en aplicaciones biomédicas, se detalla un objetivo terapéutico (o rango/ventana de referencia) [Sikaris, 2014, Committee and Committee:, 2022, Vegvari et al., 2016], y el objetivo de control consistente entonces en guiar el sistema hacia dicho objetivo, y mantenerlo allí . Sin embargo, en vistas de mantener el sistema en el objetivo, aparece el concepto de conjunto invariante [Blanchini and Miani, 2008] como un conjunto admisible, es decir, un conjunto de estados para los cuales existe una ley de control tal que la evolución del estado quede contenida en el mismo para todo tiempo futuro. De esta forma, vemos que al controlador podría resultarle infactible guiar el sistema hacia un objetivo terapéutico que no contenga un invariante de control del sistema dinámico a lazo cerrado [Liu et al., 2019, Sanchez et al., 2023]. Más concretamente, debemos corroborar si el objetivo terapéutico contiene un conjunto invariante de control (asintóticamente estable) del sistema dinámico a los fines de garantizar: a) la convergencia hacia la ventana, b) la permanencia en la misma [Sopasakis et al., 2015, Rivadeneira et al., 2018, D'Jorge et al., 2020]. De esta forma, vemos que esta etapa conlleva una análisis y caracterización del modelo previa a cualquier estrategia de control. Siguiendo esta metodología de trabajo, como objetivo común a las distintas aplicaciones, a lo largo de esta tesis estudiaremos la existencia de distintos tipos de conjuntos invariantes contenidos en las regiones terapéuticas, entre los que se destacan: equilibrios generalizados para sistemas pulsátiles, trayectorias basales para sistemas periódicos y conjuntos de equilibrio para modelos de infecciones agudas limitado por células. Además, dado que este tipo de sistemas normalmente se encuentra sujeto a restricciones fisiológicas y de seguridad, y puesto que presentan dinámicas complejas (ej. no-lineales, familia de modelos, variante en el tiempo, impulsionales), intentar hacerlo con controladores clásicos resultaría dificultoso [Rawlings et al., 2017,Rakovic and Levine, 2018]. Frente a esta situación, otra contribución de esta tesis será la propuesta de controladores optimizantes sujetos a restricciones, o más comúnmente, controles predictivos basados en modelos (MPC, por sus siglas en inglés).

Motivados por las ideas presentadas, en la presente tesis exploraremos: i) el control de glucemia en pacientes diabéticos tipo 1 mediante el cómputo óptimo del suministro de insulina, como así también, ii) la caracterización de un modelo de infecciones agudas, con la consideración del efecto de antivirales.

1.1.1. Control basado en modelos de la glucemia en pacientes diabéticos tipo 1

La diabetes tipo 1 (DT1) es una enfermedad crónica caracterizada por una destrucción de las células beta del páncreas, lo que conlleva a una deficiencia absoluta en la producción endógena de insulina, con la consecuente elevación de la concentración de glucosa en sangre (BG, del inglés, *blood glucose*) (BG en ayunas: $>$ 126 mg/dL, BG postprandial -2hs-:200 mg/dL) [American Diabetes Association, 2019]. Representa del 5 al 15 % de aproximadamente 422 millones de pacientes con diabetes en todo el mundo, y su incidencia está en aumento a un ritmo del 3,9 % anual [Katsarou et al., 2017]. Debido a la condición crónica de hiperglucemia, los pacientes diabéticos son propensos a desarrollar complicaciones de largo plazo, como nefropatía, neuropatía, cardiopatía coronaria y enfermedad periférica arterial, así como complicaciones de corto plazo, como cetoacidosis diabética (complicación aguda metabólica grave de la DT1 debida a la descomposición de lípidos en cetonas como fuente alternativa de glucosa).

A los fines de restablecer los niveles de normoglicemia (BG en ayunas: 80-140 mg/dL, pico BG postprandial (2hs): $<$ 180 mg/dL), evitando episodios de hipoglucemia en el trayecto (BG: $<$ 70 mg/dL, hipoglucemia severa incrementa el riesgo de complicaciones graves, como desmayo, coma o incluso la muerte), se propuso el tratamiento funcional con insulina (FIT, del inglés, *functional insulin treatment*) como un modo terapéutico de administrar inyecciones de insulina de forma exógena, imitando los patrones de secreción fisiológicos del páncreas. En este sentido, se suministra una dosis basal para mantener la glucemia constante durante períodos de ayuno, y bolos para compensación de hiperglucemia postprandial y/o por incremento de glucemia por encima de valores referencia, bolos prandiales y bolos correctores, respectivamente. Aunque estas dosis pueden ser calculadas mediante herramientas de soporte al FIT (ej. factor de corrección (CF, del inglés, *correction factor*), relación insulina-carbohidrato (CR , del inglés, *carb ratio*), duración de la acción de la insulina (DIA, del inglés, *duration of insulin action*)) [Walsh and Roberts, 2017] acorde a mediciones de glucemia y conteo de carbohidratos, los pacientes DT1 deben estimar y administrar las dosis de insulina por sí mismos, lo que inherentemente conlleva riesgos, como episodios de hipoglucemia e hiperglucemia (debido a una supra/subestima de la ingesta de comidas, variaciones no previstas de la sensibilidad a la insulina, entre otras causas).

Frente a esta realidad, el suministro de insulina de forma automática basada en mediciones de glucemia (AP, del inglés *artificial pancreas*) fue propuesto como un medio de implementar el FIT a lazo cerrado. Básicamente, el AP es un dispositivo médico integrado por un monitor continuo de glucosa (CGM, del inglés, *continuous glucose monitor*), una bomba de insulina (CSII, del inglés, *continuous subcutaneous insulin infusion*) y un algoritmo de control, que en base a lecturas del CGM, ajusta la infusión de insulina a los fines de mantener la concentración de glucosa en sangre en niveles normales. Múltiples algoritmos de control han sido propuestos, entre los que se destacan, el control proporcional-integral-derivativo (PID) [Steil, 2013], el control por lógica difusa (FL) [Mauseth et al., 2013], el control predictivo basado en modelo (MPC) [Incremona et al., 2018, Gondhalekar et al., 2018], entre otros; los cuales han sido validados tanto en ensayos 'in-sílico' (UVA/Padova [Man et al., 2014] , Cambridge [Hovorka et al., 2002], Medtronic Virtual Patient [Kanderian et al., 2009]) como en pruebas 'in-vivo' [Castle et al., 2018, Sánchez-Peña et al., 2018, Cameron et al., 2017]. De todas estas formulaciones , el MPC se ha mostrado como el más promisorio, debido a su capacidad para computar acciones de control óptimas (insulina para configuración single-hormonal, e insulina y glucagón para configuración bi-hormonal) basado en la solución de un problema de optimización que tiene en cuenta un modelo de predicción de la dinámica glucosa-insulina y restricciones de entrada y salida (o de estado). Si bien varias configuraciones de MPC han sido propuestas, entre las que se destacan: MPC no restricto [Incremona et al., 2018], MPC multi-modelo [Wilinska et al., 2016, Cameron et al., 2012], MPC por zonas [Gondhalekar et al., 2018], MPC para regulación mejorado (eMPC) [Lee et al., 2016], MPC adaptativo [Hajizadeh et al., 2019b, Shi et al., 2019], MPC bi-hormonal [Boiroux et al., 2018a] y MPC estocástico [Goodwin et al., 2016, Seron et al., 2016], la mayoría de ellas carece de ingredientes estabilizantes (esto es, costo y restricciones terminales). Algunas excepciones pueden encontrarse en [Messori et al., 2018, Soru et al., 2012, González et al., 2020, Penet, 2013]. A los fines de evitar incrementar el costo computacional asociado a la consideración de condiciones terminales (consideración de conjunto terminal mediante restricciones adicionales), suelen emplearse horizontes de predicción suficientemente largos de modo que el estado terminal alcance una condición de equilibrio. En este sentido, dado que las comidas representan las mayores perturbaciones, y teniendo presente que el período postprandial después de un bolo bien configurado dura aproximadamente 4 horas, suelen emplearse horizontes de predicción del orden de 6-10 horas. Además, la mayoría de ellos están formulados para minimizar la desviación entre la glucemia predicha y un punto de operación fijo (ej. MPC integral [Incremona et al., 2018], MPC mejorado

de punto de ajuste [Lee et al., 2016]) o un intervalo establecido (ej. MPC por zonas [Gondhalekar et al., 2018, Gondhalekar et al., 2016]). Por lo tanto, dado que las condiciones terminales dependerán del objetivo seleccionado, si es modificado (ej. zona de normoglucemia variante a lo largo del día [Gondhalekar et al., 2016], punto de referencia dependiente del nivel de glucemia [Boiroux et al., 2018b], entre otros), el problema de optimización podría volverse infactible, con la consecuente pérdida de factibilidad recursiva del controlador. Frente a este inconveniente, en la presente tesis se extenderá el uso de la formulación de MPC para tracking [Limón et al., 2008] al problema del control glucémico de forma automática en pacientes DT1. Esta formulación, mediante el empleo de variables artificiales (set-points artificiales), incrementa el dominio de atracción del controlador (en contraposición al MPC estándar para regulación), brindando garantías de estabilidad y factibilidad recursiva, bajo la suposición de estados completamente observables y perturbaciones no-persistentes.

Por otro lado, dado que el control glucémico con insulina puede modelarse como un sistema híbrido (sistema a lazo cerrado híbrido) [Huang et al., 2012, González et al., 2020], particularmente, como un sistema con entradas impulsivas (bolos) que se suministran frente a eventos de comidas y/o para la corrección de la glucemia, se priorizarán formulaciones de MPC que consideren acciones de control tipo impulsionales, o de modo más general, acciones de control pulsátiles. Esto último viene a colación, dado que los algoritmos formulados serán ideados en vistas de su implementación mediante bombas de infusión, la cual administra la dosis mediante una acumulación de microbolos [Ziegler et al., 2021, Jørgensen et al., 2019]- es decir, micro-infusiones de tiempo discreto distribuidas a lo largo del período de muestreo - que son comparables con inyecciones pulsátiles. Más aún, es importante destacar, que el uso de infusiones pulsátiles presenta beneficios terapéuticos (de hecho, el páncreas segrega la insulina de forma pulsátil, cada 5-10 min aprox.) [Tokarz et al., 2018]. Ensayos 'in-vivo', han mostrado un mejor control de la producción hepática de glucosa, mediante la administración intravenosa de insulina en forma pulsátil [Satin et al., 2015]. Además, algunos trabajos han mostrado tanto experimentalmente [Juhl et al., 2012, Walsh and Roberts, 2017] como teóricamente [Goodwin et al., 2015b, Goodwin et al., 2018], que se logra un mejor control postprandial con pulsos de corta duración (bolos), especialmente en el caso de comidas con alto índice glucémico.

Otro aspecto a considerar, será el uso de modelos relevante a control de largo término (predicción postprandial y de estado basal) [Magdelaine et al., 2015, Ruan et al., 2016] a los fines de posibilitar que el controlador pueda calcular, de forma unificada, el suministro para condiciones basales y postprandiales. De esta forma, el conjunto controlable/estabilizable del sistema (restringido positivamente) se incrementa drásticamente, dado que cuando un evento de hipoglucemia es predicho (no solo medido, sino anticipado por el modelo), el controlador es capaz de suspender rápidamente la administración basal de insulina. También se priorizarán el uso de modelos cuyos parámetros se vinculen explícitamente con herramientas FIT, a los fines de mejorar la identificabilidad [Garcia-Tirado et al., 2018] de los mismos, como así también, posibilitar el diseño de restricciones para la insulina administrada [Bondia et al., 2018].

1.1.2. Caracterización de modelos para infecciones agudas, considerando la efectividad de antivirales. Caso de estudio: infección por SARS-CoV-2

A los fines de estudiar la proliferación de un patógeno en un organismo, resulta de utilidad considerar modelos dinámicos de la progresión de los mismos conforme evoluciona la enfermedad. Dependiendo del tipo de patógeno (virus, bacteria, parásito, hongo) el modelo debe incluir características fundamentales de la dinámica de la infección en el huésped, entre las que se destacan, el tipo de células blanco (ej. células epiteliales en tracto respiratorio para el virus de la influenza; linfocitos tipo CD4+, macrófagos y células dendríticas para el virus VIH), la duración de la infección respecto a la dinámica vital del paciente (infecciones crónicas - persistentes y de larga duración - *vs* infecciones agudas - comienzo súbito y de corta duración) y el ciclo de vida del patógeno (mecanismos por los cuales el patógeno se propaga en el huésped) [Nowak and May, 2000, Bocharov et al., 2018, Wodarz, 2007]. En lo que respecta a la dinámica vital respecto a la duración de la patología, suelen emplearse modelos crónicos y agudos, siendo los segundos una simplificación de los primeros (despreciando la producción y muerte de células susceptibles por causas naturales). En tal punto, partiendo de un modelo para infecciones crónicas (duración media: > 3 meses), [Baccam et al., 2006] realizaron una extensión del mismo al virus de influenza A H1N1 (duración media: 7 días post-infección), considerando: (i) modelo limitado por células (sin/con fase de latencia), es decir, se asume que la propagación de la infección se encuentra limitada por la disponibilidad de células susceptibles, sin la consideración explícita de la respuesta inmunológica, y se brinda la opción de un estado de latencia para las células infectadas (estado intermedio sin producción de virus libre), y (ii) modelo con

respuesta inmunológica innata, es decir, la propagación de la infección se encuentra limitada, además de la disponibilidad de células susceptibles, por la producción de interferón tipo 1 (característica de la respuesta inmunológica innata por infección viral) [Murphy and Weaver, 2016]. Posteriormente, otros trabajos incorporaron la respuesta inmunológica adaptativa [Eftimie et al., 2016, Wodarz, 2007] a los fines de valorar la respuesta humoral y celular en el control de infecciones agudas [Dobrovolny et al., 2013, Boianelli et al., 2015, Cao and McCaw, 2017]. Si bien el modelo limitado por células (sin/con respuesta inmunológica) fue ampliamente empleado para el estudio del virus de la influenza A en el huésped, otros trabajos extendieron su uso para distintos agentes infecciosos, como el virus del Dengue [Nikin-Beers and Ciupe, 2018], del Zika [Best and Perelson, 2018], del Ébola [Nguyen et al., 2015], y más recientemente, para la infección por SARS-CoV-2 [Ke et al., 2021, Hernandez-Vargas and Velasco-Hernandez, 2020, Gonçalves et al., 2021, Kim et al., 2021].

A diferencia de los modelos para infecciones crónicas, caracterizadas por puntos de equilibrios aislados (equilibrios sanos y equilibrios infectados) [Ciupe and Heffernan, 2017], los modelos para infecciones agudas están caracterizados por un continuo de puntos de equilibrio (conjunto de equilibrio sano) [Abuin et al., 2020a, Pérez et al., 2022, Dobrovolny et al., 2011]. Esto se debe a que para el caso de infecciones agudas, el único equilibrio factible es aquel libre de infección, puesto que para este tipo de infecciones, el agente infeccioso se elimina al final de la infección, independientemente del número de reproducción del huésped [Baccam et al., 2006, Cao and McCaw, 2017]. La existencia de un conjunto de equilibrio sano implica que el análisis de estabilidad se pueda realizar considerando conjuntos de equilibrio como generalizaciones de puntos de equilibrio, lo que da un marco para la aplicación de métodos de análisis basados en conjuntos [Rawlings et al., 2017, Blanchini and Miani, 2008]. En ese sentido, se procederá a estudiar la estabilidad de conjuntos de equilibrio. Como se comenta más adelante en la presente tesis (Sección 4.3), este tipo de modelos presenta la particularidad de tener conjuntos de equilibrio atractivos, cuyos puntos no necesariamente lo son. De hecho, se demuestra que el conjunto de equilibrio para infecciones agudas se encuentra formado por un subconjunto inestable y un subconjunto estable, delimitados por un valor crítico de células susceptibles, por encima del cual la carga viral en el huésped no puede disminuir (valor análogo a la inmunidad de rebaño en los modelos epidemiológicos) [Allen et al., 2008]. Si bien los puntos de equilibrio del segundo son estables (en el sentido de Lyapunov o $\epsilon - \delta$) [Haddad and Chellaboina, 2008], no son atractivos (es decir, dada una condición inicial arbitrariamente cercana, no se garantiza la convergencia al punto de equilibrio). Sin embargo, se demuestra que el conjunto estable es a la vez el mínimo conjunto atractivo (el máximo viene dado por el conjunto de equilibrio), y por ende, el único conjunto asintóticamente estable del sistema (es decir, el máximo estable y mínimo atractivo).

Por otra parte, el control de una infección se puede modelar considerando la respuesta inmune, donde la infección es autocontrolada de acuerdo a una combinación de reacciones inespecíficas y específicas, o puede incluirse el efecto inducido por tratamientos farmacológicos. La inclusión de modelos farmacocinéticos (PK, del inglés, *pharmacokinetic*) y farmacodinámicos (PD, del inglés, *pharmacodynamic*) permite la incorporación de efectos terapéuticos (efectividad) sobre la propagación del patógeno, lo que se reduce a modificaciones paramétricas del modelo (ej. tasa de infección de células susceptibles, tasa de replicación de virus libre, etc.) dada por a la frecuencia y cantidad de la dosis suministrada [Zou et al., 2020, Ciupe and Heffernan, 2017]. Naturalmente, este efecto está limitado por el potencial inhibitorio del fármaco (expresado en términos de la concentración del fármaco que inhibe el 50 % de partículas de antígeno [EC50]) y su efecto citotóxico (expresado en términos de la concentración del fármaco que provoca la muerte del 50 % de las células susceptibles [CI50]). En este sentido, acorde a la concentración de la droga en el tejido blanco y su concentración inhibitoria (EC50), puede estimarse la efectividad del mismo. Si bien para modelos de infecciones crónicas se caracterizó una efectividad media, denominada efectividad crítica (η^c) [Dahari et al., 2007], tal que para (i) efectividades menores a η^c, el número de reproducción en el huésped (R_0) es mayor a 1, y por ende el equilibrio sano es inestable (con la consecuente propagación de la infección), (ii) mientras que para efectividades mayores o iguales a η^c, $R_0 \leq 1$, y el equilibrio sano es asintóticamente estable (con la consecuente eliminación del patógeno en el huésped y efecto terapéutico favorable), para modelos de infecciones agudas la existencia de tal efectividad no fue abordada. Frente a esta limitante, uno de los objetivos de la presente tesis, será estudiar la existencia de una efectividad crítica para infecciones agudas, y el comportamiento dinámico del modelo para efectividades supra y subcríticas. En este punto, dado que las drogas se suministran, normalmente, por vía oral o por inyecciones intravenosas, se observan saltos instantáneos en la concentración de la droga en el plasma sanguíneo y/o tejido blanco, lo que se puede modelar como un sistema impulsivo de control [Rivadeneira et al., 2018, Hernandez-Mejia et al., 2019]. Basados en este esquema de modelado, se procederá además a evaluar la dinámica del sistema (en sus regí-

menes transitorio y estacionario) considerando esquemas de suministro por intervalo simple/múltiple (dosis fijas, aplicadas durante ciertos períodos de tiempo), consistentes con efectividades supra y subcríticas, y con objetivos adicionales a la mera minimización de la carga viral (ej. maximización de las células susceptibles al final de infección, sujeto a evitar repunte de la carga viral al discontinuar tratamiento).

1.2. Objetivos

1.2.1. Objetivo General

El objetivo general de la presente tesis consiste en la caracterización dinámica y el control de sistemas biomédicos empleando técnicas de control avanzado, centrando el estudio en la diabetes tipo 1 y en infecciones agudas (particularmente la infección por SARS-CoV-2).

1.2.2. Objetivos Particulares

- Análisis de modelos de la dinámica glucosa-insulina en pacientes diabéticos tipo 1.
- Diseño de formulaciones de MPC estabilizantes bajo suministros pulsátiles que permitan el control glucémico con garantías de estabilidad, manteniendo la factibilidad recursiva para cambios de referencia y/o prominentes perturbaciones.
- Desarrollo de formulaciones que consideren restricciones para la insulina a bordo variantes en el tiempo (con mayor controlabilidad) y posibiliten el uso de restricciones suaves.
- Extensión de las formulaciones estabilizantes de MPC al caso con variabilidad paramétrica (específicamente sensibilidad a la insulina).
- Caracterización de modelos de infecciones agudas limitados por células.
- Caracterización de modelos considerando efectividad crítica de los antivirales.
- Propuesta de estrategias preliminares de control basadas en los resultados de los dos ítems anteriores.

1.3. Organización del documento

En el Capítulo 1 se provee una introducción a la teoría de control de sistemas biomédicos, brindado una descripción de los casos de aplicación, conformados por la diabetes tipo 1 e infecciones agudas (tomando como caso particular la infección por SARS-CoV-2). En el Capítulo 2, se describe una estrategia de control pulsátil aplicada al control glucémico en DT1 junto con la propuesta de observadores de perturbación y el uso de un modelo de largo término. Además, se aporta una formulación para la restricción de la insulina a bordo basada en eventos de comidas (la cual posibilita incrementar la controlabilidad del sistema, respecto al perfil exponencial) y se extiende el controlador considerando restricciones suavizadas. Por otro lado, en el Capítulo 3 se presenta una estrategia de control basado en el seguimiento de trayectorias basales periódicas como objetivos admisibles para condiciones con variabilidad circadiana de la sensibilidad a la insulina. Finalmente, en el Capítulo 4 se describe la caracterización del conjunto de equilibrio para un modelo de infecciones agudas. Además, se estudia el efecto del tratamiento con antivirales, caracterizando la efectividad crítica para este tipo de modelos (control de duración infinita) y una estrategia de control óptimo (single, duración finita). Para esta última, y basados en el análisis dinámico del modelo, se formula un objetivo de control consistente en evitar el rebote de la carga viral mientras se maximizan las células susceptibles al final de la infección. Finalmente, en el Capítulo 5 se presentan las conclusiones respecto a los objetivos particulares formulados y se bosquejan potenciales líneas de trabajo futuras.

Capítulo 2

Control glucémico mediante controlador pulsátil por zonas

2.1. Antecedentes

2.1.1. Control pulsátil

En lo que respecta al suministro de insulina de forma exógena mediante AP, diversas propuestas han sido formuladas, entre las que se destacan: a) control basal por algoritmo de control [Colmegna et al., 2018, Hughes et al., 2011], b) control basal por algoritmo de control y bolos por paciente [Gondhalekar et al., 2016, Shi et al., 2019], c) control basal por algoritmo de control y bolos por algoritmos dedicados (ej. detectores y estimadores de comida) [Sala-Mira et al., 2019, Harvey et al., 2014, Samadi et al., 2018], d) control basal y bolos por algoritmo de control (cómputo del suministro basal y prandial/correctora acorde a objetivos de control) [Incremona et al., 2018, Abuin et al., 2020b]. Dado que para d) ambas dosis se calculan en función de la estimación del estado, la controlabilidad del sistema se incrementa notablemente, pudiendo por ejemplo reducir el suministro basal e incrementar el bolus para satisfacer objetivos de control específicos (ej. alcanzar la zona de normoglucemia en tiempo menores a 4 horas, sujeto a picos de hiperglucemia por debajo de 180 mg/dL). Más aún, dado que los bolos pueden modelarse como infusiones de corta duración (en relación con el período de muestreo), resulta de utilidad considerar acciones de control tipo impulsionales (o de modo más general, pulsátiles). Esto último conlleva a tener un sistema de control pulsátil, que como se verá mas adelante, implica que la evolución del sistema en tiempo continuo presente intervalos de evolución libre (o no forzada) lo cual repercutirá en que el sistema no pueda ser guiado a un equilibro convencional. Frente a esta situación, se hará uso de equilibrios generalizados respecto a conjuntos terapéuticos, como objetivos de control admisibles para este tipo de sistemas. Es importante destacar, tal como se manifiesta en la Sección 1, Apéndice A, que el usos de pulsos podría tener beneficios terapéuticos adiciones.

2.1.2. Control para seguimiento de zonas

Como se comentó en la Capítulo 1, los objetivos de terapéuticos para sistemas biomédicos normalmente distan de ser puntuales, optándose por zonas de operación. Tal es el caso del control glucémico, donde normalmente interesa guiar la variable controlada a una zona de normoglucemia, no penalizando los niveles glucémicos pertenecientes a la misma. Más aún, producto de intentar controlar el sistema con pulsos de corta duración, resulta inviable guiar la glucemia a un valor de equilibrio particular, por lo que se espera que las evoluciones libres queden contenidas en el objetivo. Considerando este escenario, en el presente capítulo emplearemos un controlador para el seguimiento de zonas [Ferramosca et al., 2010], el cual al emplear set-points artificiales como objetivos de control, posibilita un incremento del dominio de atracción (DOA, del inglés, *domain of attraction*) del controlador respecto al caso estándar de regulación. Esto último resulta de utilidad, para el mantenimiento de la factibilidad recursiva de la estrategia, frente a (i) cambios no-previstos de la referencia (zona de normoglucemia dependiente del nivel/tasa de cambio de la glucemia), y (ii) eventuales perturbaciones (o modos de falla) que pongan al sistema en lazo cerrado fuera de su dominio de atracción (ej. comidas no anunciadas, cambios de la relación insulina/glucemia, desconexión de la guía

de suministro, etc.). Además, extenderemos la formulación considerando restricciones suaves, puesto que como se comenta a continuación, suelen emplearse restricciones de seguridad para la insulina a bordo y cuya activación resulta una estrategia de mitigación de riesgos asociados a la sobreactuación del controlador (ej. producto de perturbaciones externas e incertidumbre de modelado).

2.1.3. Restricción para la insulina a bordo

En los sistemas de AP , a los fines de limitar la máxima infusión admisible, suelen emplearse restricciones para la insulina a bordo (IOB, del inglés, *insulin on board*), es decir, el nivel de insulina remanente en sangre y tejidos subcutáneos. En el contexto de controladores MPC, esta restricción de seguridad suele implementarse, directamente, mediante restricciones asociadas a los estados de insulina plasmática y/o IOB [Hajizadeh et al., 2019a, Abuin et al., 2020b] o, indirectamente, mediante restricciones vinculadas a la tasa de suministro de insulina $u(t)$ [U/min] [Messori et al., 2015, Ellingsen et al., 2009]. Respecto a las primeras, es importante mencionar, que para formulaciones no restrictas [Fushimi et al., 2018, Bondia et al., 2018], se ha considerado un circuito de limitación externo, denominado SAFE (por sus siglas en inglés, *safety auxiliary feedback element*), a los fines de mantener la IOB dentro de limites predefinidos. Siguiendo esta línea de trabajo, pero explotando el hecho de que aquí se emplea un modelo con estados intrínsicamente vinculados a la IOB, en el presente capítulo se abordarán dos modos alternativos de restricción: (i) una restricción para la IOB constante por tramos (dependiente de franja horaria), y (ii) una restricción dependiente del evento de comida de soporte postprandial finito (limitando la máxima dosis acumula acorde al tiempo de accionamiento de la restricción). Además, para esta última estrategia, se propone un modo adaptativo que permite incrementar la amplitud de la restricción (y con esto, la amplitud de los pulsos suministrados) conforme la velocidad y la aceleración de la glucemia sobrepasan umbrales específicos.

En este capítulo se abarcarán los objetivos particulares 1, 2 y 3.

2.2. Modelo de la dinámica glucosa-insulina en DT1

Los modelos glucosa-insulina pueden ser fisiológicos o basado en datos [Oviedo et al., 2017, Aiello et al., 2020]. Los primeros se basan normalmente en representaciones compartimentales [Man et al., 2007, Hovorka et al., 2002, Bergman et al., 1979], mientras que los segundos se caracterizan por enfoques basados en series temporales [Hajizadeh et al., 2017, van Heusden et al., 2011]. Si bien, ambos tipos de enfoques han sido ampliamente empleados para modelos relevante a control (es decir, modelos empelados para el diseño de controladores), los modelos fisiológicos resultan beneficiosos debido a su descriptibilidad inherente e interpretabilidad de parámetros . Como se introdujo anteriormente (Capítulo 1), en esta tesis se empleará un modelo mínimo fisiológico de largo término basado en la propuesta de [Ruan et al., 2017], el cual deriva de una linealización del modelo de Bergman [Bergman et al., 1979](consumo de glucosa dependiente de insulina; independiente del nivel de glucosa en sangre) y bajo asunción de estado en condición quasi-estacionaria (insulina remota en equilibrio con respecto a insulina en compartimento plasmático).

2.2.1. Descripción de subsistemas

El modelo de la dinámica glucosa-insulina con la consideración del efecto de las comidas puede ser analizado mediante dos subsistemas, dados por el **subsistema glucosa-insulina** 2.1 y el **subsistema de comidas** 2.2, donde el primero describe el efecto de la insulina en el metabolismo de la glucosa, y el segundo representa la absorción de carbohidratos (CHO):

$$\dot{x}(t) = A_x x(t) + B_u u(t) + B_z z(t) + E, \;\; x(0) = x_0, \tag{2.1}$$

$$\dot{z}(t) = A_z z(t) + B_r r(t), \;\; z(0) = z_0, \tag{2.2}$$

donde $x(t) = [x_1(t) \;\; x_2(t) \;\; x_3(t)]'$ es el vector de estados, x_1 es la concentración de glucosa en sangre [mg/dL], x_2 es la tasa de suministro de insulina en plasma [U/min] y x_3 es la tasa de suministro de insulina en tejido subcutáneo [U/min]. Por otro lado, $z(t) = [z_1(t) \;\; z_2(t)]'$ es el vector de perturbaciones asociadas a las comidas, donde z_1 y z_2 son las tasas de absorción gastro-intestinales de CHO [g/min]. Además, $u(t)$ es la tasa de suministro de insulina [U/min] y $r(t)$ la tasa de ingesta de carbohidratos ($CHO/\Delta T_{CHO}$)[g/min].

En este modelo, las matrices de transición y de entrada están dadas por:

$$A_x=\begin{bmatrix}-\theta_1 & -\theta_2 & 0\\ 0 & -\frac{1}{\theta_4} & \frac{1}{\theta_4}\\ 0 & 0 & -\frac{1}{\theta_4}\end{bmatrix}, B_u=\begin{bmatrix}0\\0\\\frac{1}{\theta_4}\end{bmatrix}, E=\begin{bmatrix}\theta_0\\0\\0\end{bmatrix}, B_z=\begin{bmatrix}\theta_3 & 0\\0 & 0\\0 & 0\end{bmatrix}, A_z=\begin{bmatrix}-\frac{1}{\theta_5} & \frac{1}{\theta_5}\\0 & -\frac{1}{\theta_5}\end{bmatrix}, B_r=\begin{bmatrix}0\\\frac{1}{\theta_5}\end{bmatrix},$$

donde θ_2 es la sensibilidad a la insulina [mg/(dL·U)], θ_3 es el factor de carbohidratos [mg/(dL·g)] y θ_1 es la efectividad de la glucosa [min^{-1}] o auto-regulación de la glucemia (ej. estimulación de la captura de glucosa por tejidos periféricos y supresión hepática de la liberación de glucosa). θ_0 representa la producción endógena de glucosa (EGP) en niveles basales EGP_b ($\theta_0 = \theta_1 x_{1b} + \theta_2 u_b$, siendo x_{1b} y u_b los niveles basales de glucemia e insulina, respectivamente) [mg/(dL · min)]. Además, θ_4 y θ_5 son constantes de tiempo asociadas a la absorción insulina y comidas, respectivamente [min]. Es importante destacar que el efecto del subsistema de comidas en el subsistema de insulina, viene dado por $R_a(t) = \theta_3 z_1(t)$, siendo R_a la tasa de aparición de glucosa en plasma [mg/(dL· min)]. Las salidas del subsistema 2.1 vienen dadas por:

$$\begin{aligned} G(t) &= C_1 x(t),\\ IOB(t) &= C_2 x(t),\end{aligned}$$

donde $C_1 = [1\ 0\ 0]$ y $C_2 = [0\ \theta_4\ \theta_4]$, siendo $IOB(t)$ la insulina a bordo [U] (insulina remanente en sangre y tejidos subcutáneos procedente de infusiones previas) [Magdelaine et al., 2020]. Se destaca que una de las bondades del modelo propuesto es que incluye un modelo de farmacocinética, lo que posibilita obtener una estimación de la IOB prescindiendo de curvas de decaimiento poblacionales [Ellingsen et al., 2009].

Observación 1. *Bajo la asunción que $\theta_1 \approx 0$ [Magdelaine et al., 2015, Bock et al., 2015], herramientas de soporte al FIT pueden obtenerse del análisis dinámico de los subsistemas 2.1 y 2.2. En ese caso, el factor de corrección (o factor de sensibilidad a la insulina) $CF = \theta_2$ [mg/(dL U)], el factor de incremento $RF = \theta_3$ [mg/(dL g)] y la relación carbohidrato-insulina (cantidad de carbohidratos cubiertos por una unidad de insulina) $CR = \theta_2/\theta_3$ [g/U]. Es importante mencionar que dado que el efecto autorregulatorio de la glucosa se desprecia (tener en cuenta que contrarresta el efecto de la insulina en la reducción de BG), las herramientas obtenidas resultan conservadoras en relación a los valores óptimos alcanzables [Goodwin et al., 2015a, Toffanin et al., 2017b, Schiavon et al., 2018].*

Observación 2. *Si bien en [Abuin et al., 2020b] el modelo fue presentado considerando ambos subsistemas de forma integrada, dado que el subsistema de comidas representa una perturbación exógena, para simplificar el análisis y unificar notación, a lo largo de esta tesis se los presenta de forma separada y acoplados mediante la matriz de entrada B_z.*

2.2.2. Especificación de restricciones

Debido a limitaciones físicas y por motivos de seguridad, el subsistema glucosa-insulina 2.1 se asume restringido en estados y entradas, tal que $x \in \mathcal{X}$ y $u \in \mathcal{U}$, con $\mathcal{U} = \{u \in \mathbb{R}_{\geq 0} \mid u \leq U_{max}\}$ siendo $U_{max} \approx 15$ [U/min] (*i.e.*: máxima dosis admisible suministrada por bomba de insulina) [min, 2015]. Además, $\mathcal{X}$ se asume variante con el tiempo a lo largo del día, debido a i) suministros adicionales de insulina durante períodos postprandiales y ii) variaciones temporales de parámetros (ej.: variaciones circadianas de la sensibilidad a la insulina [Visentin et al., 2015,Hinshaw et al., 2013], mayor riesgo de eventos de hipoglucemia durante períodos nocturnos producto del decremento de la respuesta simpatoadrenal a disminuciones de glucemia [El-Khatib et al., 2017]):

$$\mathcal{X}(t) \doteq \{x \in \mathbb{R}^3_{\geq 0} \mid G_{hypo} \leq x_1(t) \leq G_{hyper},\ \theta_4(x_2(t)+x_3(t)) \leq \overline{IOB}(t)\}, \tag{2.3}$$

donde $\overline{IOB}(t) = IOB_b + \tilde{IOB}(t)$, con $IOB_b := \theta_4(x_{2b}+x_{3b})$ la máxima IOB admisible correspondiente a condiciones basales e $\tilde{IOB}(t)$ la máxima IOB admisible correspondiente a períodos postprandiales. Como se verá a continuación, esta última puede adoptar un valor constante o variante en el tiempo durante el intervalo postprandial, en concordancia con distintos tipos de cotas para el suministro de la insulina. Por otro lado, el estado de glucemia x_1 se encuentra acotado por limites fisiológicos dados por $G_{hypo} = 60$ [mg/dL] y $G_{hyper} = 250$ [mg/dL]. Es importante destacar que los estados del subsistema de comida 2.2 se asumen irrestrictos, puesto que no son controlables y, por ende, no es factible incluir restricciones en su evolución (dependientes de la ingesta de comida).

Restricción constante (franja horaria) para la insulina a bordo

En este caso, se asume un perfil constante por tramos para la restricción, tal que en períodos nocturnos $IOB(t)$ se limita a la dosis basal (IOB_b), mientas que en períodos diurnos $IOB(t)$ se limita a la dosis bajo condiciones basales y prandiales. De esta forma, durante períodos nocturnos $[22, 6)$ [horas], y puesto que el riesgo a eventos de hipoglucemia está aumentado producto de la pérdida de respuesta simpatoadrenal, se logra mitigarlo limitando la máxima infusión admisible a la correspondiente a períodos de ayuno o basales (enfoque similares pueden verse en [Toffanin et al., 2013, Gondhalekar et al., 2018, Bertachi et al., 2020]). Por otro lado, durante períodos diurnos $[6, 22)$ [horas], la $IOB(t)$ se limita considerando dosis correspondientes a bolos prandiales (convencionales: CHO_{ub}/CR, y super-bolos: $CHO_{ub}/CR + \tau U_b$) , con CHO_{ub} un umbral superior en el anuncio de CHO y τ un tiempo admisible de interrupción del suministro basal (para más detalle, referirse a la Sección 2.4, Apéndice A). Si bien, no fueron contemplados bolos correctores, las dosis correspondientes a los mismos podrían añadirse, incorporando al umbral de $\overline{IOB}(t)$ la función $dist(G(t), \mathcal{Y}^{Tar})/CR$, siendo $dist(\cdot)$ una función distancia y $\mathcal{Y}^{Tar}$ la zona de normoglucemia.

Restricción basada en eventos para la insulina a bordo

Si bien, la restricción anteriormente presentada, limitaba la amplitud de la dosis, tenía como desventajas que i) la dosis acumulada durante el período postprandial no estaba acotada a un intervalo específico -solo dependiente del tiempo de activación de la restricción (ej. período diurno) -y ii) el disparo de la misma no tenía correlación con eventos de comida (por lo que dosis adicionales, debido a lecturas erróneas/modos de falla [Kölle et al., 2019, Meneghetti et al., 2018], eran admisibles durante el período diurno). Por ende, en esta sección, se propone una restricción cuyo disparo es dependiente del evento de comida (avisado/detectado) y la dosis (acumulada) durante el período postprandial puede configurarse acorde a la especificación del paciente. Respecto a esto último, si bien es corriente emplear perfiles exponenciales, dado que estos podrían limitar la controlabilidad del sistema, siguiendo la propuesta de [Fushimi et al., 2018], se propone un perfil constante para la IOB (durante una ventana temporal, ΔT_{IOB}) proseguido luego, por un perfil exponencial. De esta forma, se propicia un: i) incremento de la controlabilidad del sistema (principalmente en condiciones de hiperglucemia) y ii) una limitación de la dosis acumulada admisible durante el intervalo de accionamiento de la restricción (ΔT_{IOB}). Se presenta además, una versión adaptativa, tal que cuando condiciones relacionadas con eventos hiperglucemiantes son detectadas (ej. derivada de primer y segundo orden de BG mayores a umbral), la amplitud de la restricción es aumentada, posibilitando la administración de bolos de mayor amplitud. Es importante destacar, que tanto para configurar la amplitud del bolo durante el disparo de la restricción, como así también, la máxima dosis acumulada durante el intervalo ΔT_{IOB} se emplea un modelo poblacional de conteo de carbohidratos (Sección 3.2, Apéndice B).

2.2.3. Análisis de condiciones basales: estabilidad del conjunto de equilibrio

Para el sistema 2.1, el conjunto de equilibrio de estados factibles [1] viene dado por

$$\mathcal{X}_s \doteq \{x_s |\ x_s \in \mathcal{X}(t), x_{s,1} = (\theta_0 - \theta_2 x_{s,2})/\theta_1,\ x_{s,2} = x_{s,3} = u_s\}$$

con $u_s \in \mathcal{U}_s$ siendo $\mathcal{U}_s = \{u_s | u_s \in \mathcal{U}, 0 \leq u_s \leq U_{b,max}\}$ el conjunto de las entradas basales admisibles, con $U_{b,max} := (\theta_0 - \theta_1 G_{b,min})/\theta_2$. Debido al efecto autorregulatorio de la glucemia ($\theta_1 \neq 0$) los estados de equilibrio de control (x_s, u_s) son asintóticamente estables (AE). Nótese que las raíces λ del polinomio característico $det(\lambda I - A) = 0$ se corresponden con los elementos de la diagonal principal de A, $\lambda = diag(A)$, por ser A una matriz triangular superior. De esta forma, al aplicar un suministro basal u_b, el sistema convergerá asintóticamente al punto de equilibrio x_b que se le corresponde. Esto resulta una diferencia principal respecto al modelo propuesto por [Magdelaine et al., 2015], donde se asume que $\theta_1 = 0$, y por ende, los puntos de equilibrio resultantes son marginalmente estables, es decir, solo existirá un único suministro basal para todos los pares de equilibrio. De la Figura 2.1 (a) puede observarse el conjunto de equilibrio correspondiente a 2.1 y el pertinente al modelo máximo [Man et al., 2014, Dalla Man et al., 2007] (simulador UVAPadova), lo que muestra la aproximación local obtenida por el modelo propuesto. Tal análisis puede efectuarse también para condiciones transitorias, donde tanto para el modelo de Ruan [Ruan et al., 2017] como para el modelo UVAPadova [Man et al., 2014], al perturbar el sistema con un bolo de

[1] Se entiende por equilibrio factible a los pares (x_s, u_s) con $x_s \in \mathcal{X}$ y $u_s \in \mathcal{U}$, tales que $0 = f(t, x_s, u_s)$ para todo $t \geq 0$.

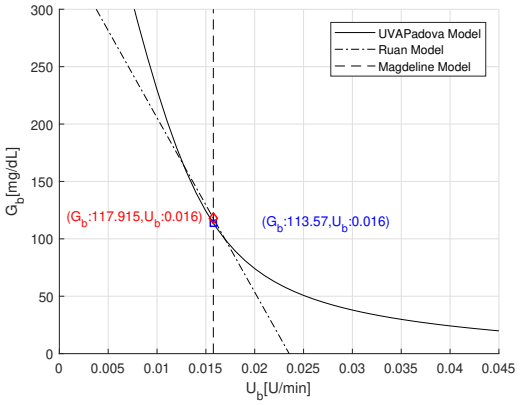

Figura 2.1: Conjunto de equilibrio de entrada-salida para distintos modelos.

corrección , debido a la naturaleza AE de su conjunto de equilibrio, se logra la convergencia asintótica del sistema al par (G_b, u_b).

2.2.4. Estimación de parámetros

A pesar de que el modelo, dado por los subsistemas 2.1 y 2.2 es estructuralmente identificable, debido a (i) la diferencia paciente-modelo y (ii) la indisponibilidad de mediciones de estados internos (ej.: EGP, Ra, IOB), existen problemas de identificabilidad práctica. Por ende resulta necesario regularizar el objetivo de la identificación a los fines de explorar soluciones que se correspondan con el espacio de soluciones plausibles del problema en cuestión (buscando incrementar la generalización de las predicciones) [Cobelli and Carson, 2019, Pillonetto et al., 2022]. En este sentido, para mejorar el condicionamiento del problema, se procedió a incluir una regularización del funcional acorde a parámetros de FIT conocidos. A continuación, se detalla la rutina de estimación paramétrica basada en mínimos cuadrados regularizados (RLS, del inglés, *regularized least square*) propuesta. El costo a minimizar está dado por:

$$V_N(\theta) \quad = \quad \frac{\|y(k) - \hat{y}(k)\|^2}{\|y(k) - \overline{y}(k)\|^2} + \theta^0 \alpha \theta^{0'} \tag{2.4}$$

donde $y(k)$ es la glucemia medida, $\overline{y}(k)$ es su valor promedio, $\hat{y}(k)$ es la predicción del modelo, y $\theta^0 = [(\theta_2 - CR^0\theta_3) \;\; (\theta_4 - \theta_4^0) \;\; (\theta_5 - \theta_5^0)]$, siendo CR^0, θ_4^0 y θ_5^0 valores 'a-priori' de la relación carbohidrato-insulina, tiempo de máxima concentración de insulina y tiempo de máxima concentración de glucosa en tracto gastro-intestinal.

Observación 3. *Si bien, el ajuste del hiperparámetro α fue realizado de forma empírica, adoptando $\alpha = diag(1, 1, 1/(\theta_5^0)^2)$ para todos los pacientes; tal sintonía puede optimizarse empleando criterios como minimización del error de validación cruzada, maximización de función de verosimilitud (método de bayes empírico), método SURE, entre otros [Chen et al., 2012, Pillonetto et al., 2022].*

2.3. Análisis del modelo en tiempo discreto: entradas pulsátiles

Puesto que tanto, los estimadores de estado como los controladores se implementan de forma computacional, resulta necesario contar con una discretización de los subsistemas (2.1 y 2.2) (mediante un muestreo apropiado). Dependiendo del ancho de pulso a emplear, ΔT, esta puede adoptar los siguientes tipos: i) retenedor de orden cero (zoh, del inglés, *zero-order-hold*), si el ancho pulso es coincidente con el período de muestreo ($\Delta T = T_s$), ii) pulsátil, si ancho pulso es menor que el período de muestreo ($\Delta T \in [0, T_s)$), o iii) impulsional, para el caso que ($\Delta T \to 0$). Dado que ii) brinda una representación general, con i) y iii) como casos límites de la duración del pulso, en la siguiente sección se empleará esta discretización para los susbsistemas 2.1 y 2.2.

2.3.1. Sistemas pulsátiles: sistema en tiempo discreto subyacente

Considerando los subsistemas 2.1 y 2.2 sujetos a entradas pulsátiles, $u(\cdot)$ y $r(\cdot)$, y muestreando la evolución en tiempo continuo $\varphi_x(t; x(kT_s), z(kT_s), u(\cdot))$ y $\varphi_z(t; z(kT_s), r(\cdot))$ de los mismos, resultan los siguientes subsistemas discretos:

$$\begin{aligned} x(k+1) &= F_x(x(k), u(k), z(k)), && (2.5)\\ z(k+1) &= F_z(z(k), r(k)), && (2.6)\\ G(k) &= C_1 x(k), \quad IOB(k) = C_2 x(k), \end{aligned}$$

con $F_x(x(\cdot), u(\cdot), z(\cdot)) = A_x^d x(\cdot) + B_u^d(\cdot)u(\cdot) + B_z^d(\cdot)z(\cdot) + E^d$ y $F_z(z(\cdot), r(\cdot)) = A_z^d z(\cdot) + B_r^d r(\cdot)$. Si asumimos que i) $r(t) = r(kT_s)$ con $t \in [kT_s, (k+1)T_s)$ (zoh), ii) $z(t) = z(kT_s)$ con $t \in [kT_s, (k+1)T_s)$ (zoh), y iii) $\theta_1 \neq 0$ ($\exists A_x^{-1}$), las matrices de estado y salida de dichos subsistemas resultan:

$$\begin{aligned} A_x^d &:= e^{A_x T_s},\\ B_u^d &:= e^{A_x(T_s-\Delta T)} \int_0^{\Delta T} e^{A_x(\Delta T-\zeta)} d\zeta B_u = e^{A_x(T_s-\Delta T)} A_x^{-1}(e^{A_x \Delta T} - I_3) B_u,\\ B_z^d &:= \int_0^{T_s} e^{A_x(T_s-\zeta)} d\zeta B_z = A_x^{-1}(e^{A_x T_s} - I_3) B_z,\\ E^d &:= \int_0^{T_s} e^{A_x(T_s-\zeta)} d\zeta E = A_x^{-1}(e^{A_x T_s} - I_3) E,\\ A_z^d &:= e^{A_z T_s},\\ B_r^d &:= \int_0^{T_s} e^{A_z(T_s-\zeta)} d\zeta B_r = A_z^{-1}(e^{A_z T_s} - I_2) B_r. \end{aligned}$$

Por otro lado, el conjunto de restricciones de estado en tiempo discreto, viene dado por $\mathcal{X}(k) := \mathcal{X}(kT_s)$ con $k \in \mathbb{I}_{[0,\infty)}$.

2.3.2. Conjunto de equilibrio generalizado

Del subsistema glucosa-insulina 2.1, se observa que debido al termino afín (E), el modelo presenta equilibrios fuera del origen. Por ende, al intentar controlarlo mediante acciones de control pulsátiles, el sistema en tiempo continuo no podrá alcanzar un punto de equilibrio en el sentido convencional ($\dot{x} = 0$ para todo $t \geq 0$). Siguiendo la caraterización presentada en [Rivadeneira et al., 2018], se propone entonces empelar un conjunto de equilibrio generalizado como objetivo de control, el cual es un conjunto de equilibrio del subsistema en tiempo discreto 2.5, tal que se asegura que la evolución no forzada (o respuesta libre del subsistema en tiempo continuo) queda contenida en un determinado conjunto objetivo (respecto al cual se lo define). Formalmente:

Definición 1 (Conjunto de equilibrio generalizado)**.** *Un conjunto $\mathcal{X}_s^{Tar} \subseteq \mathcal{X}^{Tar}$ es un conjunto de equilibrio generalizado para el subsistema 2.1 (sujeto a entradas pulsátiles), con respecto al conjunto $\mathcal{X}^{Tar}$, si para todo $x_s \in \mathcal{X}_s^{Tar}$ existe una entrada $u_s \in \mathcal{U}$ tal que (i) $x(kT_s) = x(k)$, $k \in \mathbb{N}_{\geq 0}$ permanece en x_s, cuando u_s es aplicada ($u(kT) = u_s$), y (ii) $x(t) \in \mathcal{X}^{Tar}$ para $t \in (kT, (k+1)T]$, $k \in \mathbb{N}$.*

Dada una zona de normoglicemia $\mathcal{Y}^{Tar} := \{G \in \mathbb{R}_{\geq 0} |\ \underline{G} \leq G \leq \overline{G}\}$, con $\underline{G} = 90$ y $\overline{G} = 120$ [mg/dL], y el conjunto de restricciones de estado 2.3, puede expresarse el conjunto objetivo $\mathcal{X}^{Tar}$, como un conjunto de estados $x \in \mathbb{R}^3$ tal que $C\mathcal{X}^{Tar} = \mathcal{Y}^{Tar}$. En la Figura 2.2 se muestra el conjunto de equilibrio generalizado $\mathcal{X}_s^{Tar}$ para el subsistema glucosa-insulina 2.1 con acciones de control pulsátiles considerando distintos tiempo entre pulsos (T_s). Se destaca la reducción del equilibrio generalizado conforme el tiempo entre pulsos es mayor; producto del incremento de las evoluciones libres del sistema. Por otro lado, al emplear insulina de acción lenta (Figura 2.3), puesto que las evoluciones libres están más acotadas (para igual tiempo entre pulsos) se logra extender el conjunto $\mathcal{X}_s^{Tar}$. De hecho, para $T_s = 240$ [min], vemos que $\mathcal{X}_s^{Tar}$ continua abarcando prácticamente la totalidad del conjunto objetivo $\mathcal{X}^{Tar}$, lo que da indicios de la potencialidad de este tipo de insulina para el control basal (o de equilibrio) con modos pulsátiles (o impulsionales) restringidos en tiempo de aplicación.

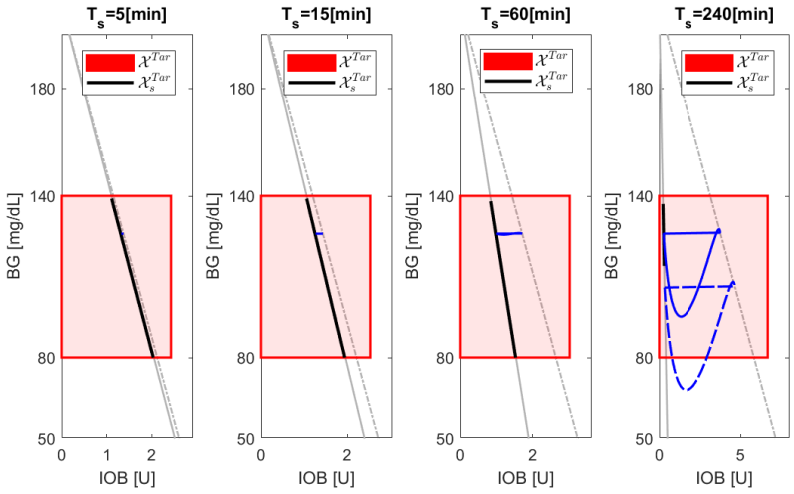

Figura 2.2: Conjunto $\mathcal{X}_s^{Tar}$ para insulina de acción rápida (subsistema de insulina 2.1)

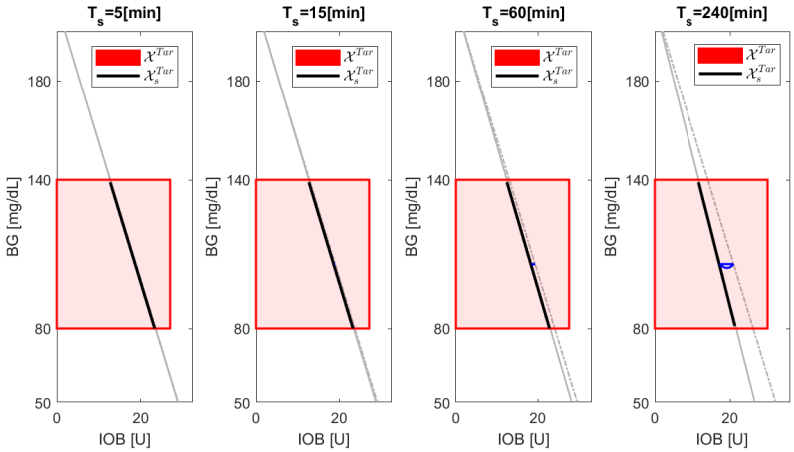

Figura 2.3: Conjunto $\mathcal{X}_s^{Tar}$ para insulina de acción lenta (subsistema de insulina, [Schiavon et al., 2019]).

2.4. Observadores de perturbación

Habiendo introducido la discretización pulsátil del sistema dinámico, en esta sección, procederemos a la descripción de observadores de perturbación de estado aumentado. Es decir, estimadores de estado cuyas matrices de transición se encuentran aumentadas incluyendo dinámicas adicionales para perturbaciones externas (no modeladas). En tal punto, presentaremos 2 propuestas de observadores, donde la idea principal estriba en considerar perturbaciones aditivas para i) estado de salida y ii) estado de entrada. Además, incluiremos la consideración de restricciones de positividad para los estados estimados, siguiendo un procedimiento de proyección de los estados estimados al conjunto admisible $\mathcal{X}_{aug}(t) := \{(x, z)|x \in \mathcal{X}(t), z \in \mathbb{R}^2_{\geq 0}\}$ [Simon, 2010]. Los observadores presentados serán implementados mediante un filtro de Kalman.

2.4.1. Observador de perturbación de salida

En este caso, la asunción principal es que las componentes no-modeladas del estado de salida $x_1(k)$ se corresponden con una perturbación aleatoria $d_1(k)$ de orden $p = 2$, lo que posibilita eliminar el error de estimación cuando las componentes no-modeladas se corresponden con un impulso, un escalón o una

rampa. De esta forma, el modelo ampliado a ser empleado por el estimador de estados, resulta:

$$\begin{bmatrix} x^*(k) \\ d_1(k) \\ d_2(k) \end{bmatrix} = \underbrace{\begin{bmatrix} A^d & B & 0 \\ 0 & 1 & T_s \\ 0 & 0 & 1 \end{bmatrix}}_{A_{aug}} \underbrace{\begin{bmatrix} x^*(k-1) \\ d_1(k-1) \\ d_2(k-1) \end{bmatrix}}_{x_{aug}} + \underbrace{\begin{bmatrix} B^d \\ 0 \\ 0 \end{bmatrix}}_{B_{aug}} \underbrace{\begin{bmatrix} u(k-1) \\ r(k-1) \\ 1 \end{bmatrix}}_{u_{aug}} + G\, w(k-1)$$

$$y(k) = [C\ 0\ 0]\, x_{aug} + v(k) \tag{2.7}$$

con $x^*(k) = [x(k), z_1(k)]'$, $A^d = [A_x^d, B_z^d; 0_{n_x x n_x}, A_z^d]$, $B^d = [B_u^d\ \ B_r^d\ \ E^d]$, $C = [1\ 0\ 0\ 0\ 0]$ y $B = B^o = [1\ 0\ 0\ 0\ 0]'$. Vemos que B determina la forma en que la componente no-modelada $d_1(k)$ afecta al sistema $F = [F_x, F_z]'$. Si bien, en este caso, se asume que solo afecta al estado de salida, en la Sección 2.4.2 se detalla la formulación bajo el supuesto que afecta a más de un estado del sistema. Es importante aclarar, que dado que la matriz de entrada está dada por $G := [0\ \ k_i\ \ k_i\ \ 0\ \ 0\ \ 0\ \ k_d]'$, se asume que el ruido de proceso $w(k) \sim N(0, \sigma^2)$ modifica a $d_1(k)$ mediante k_d. Por otro lado, $v(k)$ es el ruido de medición que se asume $v(k) \sim N(0, R_{KF})$, siendo $R_{KF} = \sigma^2_{CGM}$ (varianza del ruido del CGM).

Observación 4. *Dada una perturbación de orden p, expresada mediante el siguiente polinomio $d(t) = a_{p-1}t^{p-1} + a_{p-2}t^{p-2} + ... + a_0$, de acuerdo a [Gourishankar et al., 1977] la misma puede expresarse mediante el siguiente sistema, $\dot{d} = Ed$ con $E = [0_{px1}\ \ M_{px1}]$, siendo $M_{px1} = [I_{p-1}; 0]$. Más aún, el sistema en tiempo discreto resultante, viene dado por $d(k) = e^{ET_s} d(k-1)$. Por ende, si asumimos que la perturbación sigue una dinámica de segundo orden $d(t) = at + b$, el sistema exógeno en tiempo discreto resultante es $d(k) = E^d d(k-1)$, con $E^d = [1\ \ T_s; 0\ \ 1]$.*

Empleando el modelo aumentado 2.7, bajo las asunciones de ruido detalladas, puede obtenerse una estimación de $\hat{x}_{aug} = [\hat{x},\ \hat{d}_1,\ \hat{d}_2]'$ mediante un filtro de Kalman. Puesto que 2.7 es de estado completamente observable, es decir, $rango(A_{aug}, C_{aug}) = n_x + n_z + n_d$, siendo $rango(A)$ el rango de una matriz A, puede demostrarse [Anderson and Moore, 2012] que $\hat{x}_{aug}(k) \to x_{aug}(k)$ conforme $k \to \infty$.

2.4.2. Observador de perturbación de entrada

A diferencia del caso anterior, en este apartado se asume que la perturbación d_1 representa i) solo incerteza en el anuncio de comidas, o ii) incerteza en el anuncio de comidas y componentes no-modeladas en el estado de salida. Si bien, esto último es equivalente a considerar 2 modos de perturbación, $d^o(t)$ y $d^i(t)$, siendo $d^o(t)$ la perturbación relacionada con el estado de salida y $d^i(t)$ la perturbación vinculada al anuncio de comida, a los fines de simplificar el análisis (preservando la observabilidad del modelo) se asumirá que $d^o(t) \propto d^i(t)$. Bajo estas condiciones, la matriz de entrada (o de perturbación) viene dada por $B = B^i = \theta_5 \cdot RF \cdot B^0 + \mu B_r^d$.

2.4.3. Restricciones de positividad

Un aspecto importante en los observadores presentados es la consideración explícita de restricciones de positividad para los estados estimados $\hat{x}_{aug}(k)$. A los fines de proyectar $\hat{x}_{aug}(k)$ (irrestricto) en $\mathcal{X}_{aug}(k)$ se resuelve el siguiente problema de optimización

$$\begin{aligned} \tilde{x}_{aug}(k) = \arg\min_{x} \quad & (x - \hat{x}_{aug}(k))^T W (x - \hat{x}_{aug}(k))^T \\ s.t. \quad & x \in \mathcal{X}_{aug}(k) \end{aligned}$$

siendo $\tilde{x}_{aug}(k)$ estimación restricta (o proyectada) y W una matriz positiva definida.

2.5. Formulación MPC pulsátil por zonas

En esta sección se presenta una formulación MPC para el sistema pulsátil presentado anteriormente, extendiendo el controlador impulsivo presentado en [González et al., 2020] al caso pulsátil. La glucosa (y estados) son estimados mediante los observadores de perturbación especificados en la Sección 2.4. En la Figura 2.4 se detalla la estructura de la estrategia de control, integrada por el controlador pulsátil por zonas (pZMPC) y observadores de perturbación. Respecto al primero, se anticipa que debido a la consideración

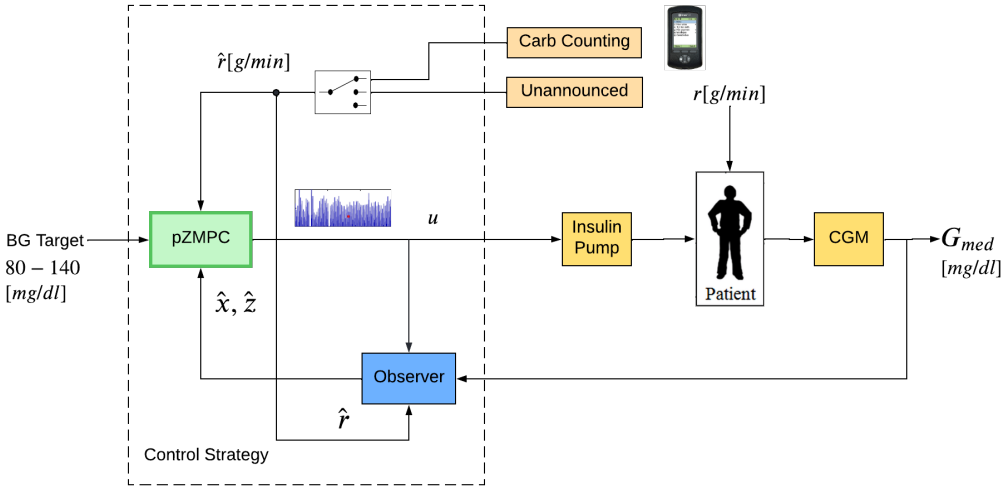

Figura 2.4: Páncreas artificial. Controlador pulsátil MPC por zonas (pZMPC): configuración con/sin anuncio de comidas.

de equilibrios generalizados como objetivos de control, se impone como condición terminal que el estado alcance el equilibrio generalizado al final del horizonte. Sin embargo, siguiendo la propuesta presentada en [Sanchez et al., 2023] se podrían emplear restricciones de pertenencia a conjuntos invariantes (de control, según una ley local), que contienen los equilibrios anteriores, y amplían significativamente el dominio de atracción resultante. Si bien se probó dicha estrategia, no se incluye aquí, para hacer más sencilla la presentación de los conceptos generales.

2.5.1. Problema de control

Dada una zona de normoglucemia $\mathcal{Y}^{Tar}$ y un conjunto objetivo asociado $\mathcal{X}^{Tar}$, $C\mathcal{X}^{Tar} = \mathcal{Y}^{Tar}$, el problema de control consiste en guiar al sistema de glucosa-insulina (afectado por perturbación de comidas) (2.1 y 2.2) mediante acciones de control pulsátiles, al conjunto de equilibrio generalizado $X_s^{Tar} \subseteq \mathcal{X}^{Tar}$, cumpliendo restricciones de estado $\mathcal{X}(t)$ y entrada $\mathcal{U}$ para todo $t \geq 0$.

Para resolver este problema de control con restricciones se emplea un MPC por zonas [Ferramosca et al., 2010] utilizando como conjunto objetivo $\mathcal{Y}_s^{Tar} = C\mathcal{X}^{Tar}$ y como modelo de predicción la discretización pulsátil 2.5 del sistema de glucosa-insulina (afectado por perturbación de comidas 2.6). Nótese que si bien, se utiliza como conjunto objetivo $\mathcal{Y}_s^{Tar}$, el cual se corresponde con un conjunto de salida, dado que la formulación del MPC a emplear (Sección 2.5.2) guía los estados del sistema a un conjunto de equilibrio $\mathcal{X}_s$; la convergencia a $\mathcal{X}_s^{Tar}$ queda garantizada conforme el estado de salida $y(k) \to \mathcal{Y}_s^{Tar}$.

2.5.2. Función de costo

La función de costo del problema de optimización que el MPC resuelve en-línea resulta:

$$V_N(\hat{x}, \hat{r}, \mathcal{Y}_s^{Tar}; \mathbf{u}, u_a, y_a) \doteq V_{dyn}(\hat{x}, \hat{r}; \mathbf{u}, u_a, y_a) + V_s(\mathcal{Y}_s^{Tar}; u_a, y_a),$$

donde $V_{dyn}(\hat{x}, \hat{r}; \mathbf{u}, u_a, y_a)$ (costo de etapa) es un término dedicado a dirigir el sistema hacia las variables artificiales de equilibrio $(u_a, y_a) \in \mathcal{U}_s \times \mathcal{Y}_s$ y $V_s(\mathcal{Y}_s^{Tar}; u_a, y_a)$ (costo de offset) es un término que penaliza la distancia entre el set-point artificial y_a y el conjunto objetivo de equilibrio $\mathcal{Y}_s^{Tar}$. En este costo, $\hat{x}$, $\hat{r}$ y $\mathcal{Y}_s^{Tar}$ son parámetros de optimización, mientras que $\mathbf{u} = \{u(0), u(1), \cdots, u(N-1)\}$, u_a y y_a, son las variables de optimización, siendo N el horizonte de control.

Observación 5. *A diferencia de las estrategias de control para regulación [Rawlings et al., 2017], dado que en este tipo de controladores se emplean variables artificiales de equilibrio como objetivos de control [Limón et al., 2008], la excursión de la trayectoria predicha se penaliza respecto a estas últimas. Por ende, la función de costo suele estar integrada por 3 componentes principales: un costo de etapa (o transitorio) que penaliza la excursión transitoria del sistema respecto a un set-point artificial, un costo terminal*

que pondera la distancia del estado terminal y el set-point artificial (nulo en caso de emplear restricción terminal de igualdad), y un costo de offset que penaliza la distancia entre el set-point artificial y un punto de equilibrio perteneciente a la zona. Si bien esta formulación guía los estados del sistema a un estado de equilibrio dentro de la zona [Ferramosca et al., 2010], también pueden emplearse otro tipo de conjuntos invariante de control dentro de la misma. Por ejemplo, en el Capítulo 3 se emplearán trayectorias periódicas como conjuntos objetivo contenidos dentro de la misma.

2.5.3. Problema de optimización

A los fines de calcular la secuencia de entradas óptimas, en cada instante de muestreo k, el MPC resuelve el siguiente problema de optimización

$P_{MPC}(\hat{x}, \hat{r}, \mathcal{Y}_s^{Tar})$:

$$
\begin{aligned}
\underset{\mathbf{u}, u_a, y_a}{\text{mín}} \quad & V_N(\hat{x}, \hat{\mathbf{r}}, \mathcal{Y}_s^{Tar}; \mathbf{u}, u_a, y_a) \\
s.a. \quad & \\
& x(0) = \hat{x}, \;\; z(0) = \hat{z} \\
& x(j+1) = F_x(x(j), u(j), z(j)), \qquad j \in \mathbb{I}_{[0,N-1]} \\
& z(j+1) = F_z(z(j), r(j)), \qquad j \in \mathbb{I}_{[0,N-1]} \\
& u(j) \in \mathcal{U}, \;\; x(j) \in \mathcal{X}(k+j), \qquad j \in \mathbb{I}_{[0,N-1]} \\
& x(N) = x_a, \;\; y_a = x_{1,a} \\
& x_a = F_x(x_a, u_a, 0) \\
& x_a \in \mathcal{X}_s, u_a \in \mathcal{U}_s(\mathcal{X}_s).
\end{aligned}
$$

Dado que solo los estados correspondientes a $F_x(x(\cdot), u(\cdot), z(\cdot))$ son controlables, se impone una restricción de estado $x \in \mathcal{X}(k)$, donde $\mathcal{X}(k)$ es una discretización del conjunto $\mathcal{X}(t)$ introducido en 2.3. Además, puesto que no se consideran comidas futuras, r solo se utiliza para el primer paso de predicción. Nótese que se supone que las comidas se ingieren durante un período de muestreo T_s, aunque esta formulación admite la distribución del anuncio en un intervalo arbitrario (D_t), de forma tal que $D_t = nT_s$ con $n \in \mathbb{I}_{1:N-1}$. Por otro lado $x(N) = x_a$ es una restricción terminal que fuerza a que el estado al final del horizonte de control, $x(N)$, alcance el equilibrio artificial $x_a \in \mathbb{R}^3$. Finalmente, la restricción $x_a = F_x(x_a, u_a, 0)$, con $x_a \in \mathcal{X}_s$ y $u_a \in \mathcal{U}_s(\mathcal{X}_s)$, impone que el par de variables artificiales (u_a, x_a) sean un equilibrio factible del sistema en tiempo discreto 2.5.

Una vez que se resuelve el problema $P_{MPC}(\hat{x}, \hat{r}, \mathcal{Y}_s^{Tar})$, la solución (óptima) se denota como $(\mathbf{u}^0, u_a^0, x_a^0)$, mientras que la función de costo óptima está dada por $V_N^0\ (\hat{x}, \hat{r}, \mathcal{Y}_s^{Tar}) \doteq V_N(\hat{x}, \hat{r}, \mathcal{Y}_s^{Tar}; \mathbf{u}^0, u_a^0, x_a^0)$. La ley de control de la estrategia de horizonte deslizante (RHC, del inglés, *receding horizon control*) resulta $\kappa_{MPC}(\hat{x}, \hat{r}, \mathcal{Y}_s^{Tar}) = u^0(0; x)$, con $u^0(0; x)$ es el primer elemento de la secuencia solución $\mathbf{u}^0(x)$.

2.5.4. Costo asimétrico de offset , V_s

El problema del control glucémico en DT1 con insulina exógena es naturalmente asimétrico debido a (i) decremento en la producción de hormonas antagonistas a la insulina (ej. glucógeno) [Bisgaard Bengtsen and Møller, 2021], por lo que una sobredosis de insulina puede causar una reducción de la concentración de glucosa en sangre que no puede ser compensada de forma endógena, (ii) debido al decremento de permeabilidad a la glucosa de la barrera hematoencefálica, un evento de hipoglucemia es más severo que uno de hiperglucemia (más rápido y perjudicial) [Katsarou et al., 2017], (iii) la insulina no puede ser removida, entre otras. Frente a esta situación, resulta necesario incluir componentes asimétricos [Gondhalekar et al., 2018, Deshpande et al., 2023, Boiroux et al., 2018b], a los fines de penalizar, mayoritariamente, excursiones hipoglucemiantes respecto a zonas de normoglucemia. Siguiendo tal lineamiento, se propuso un costo de offset asimétrico, dado por $V_s(\mathcal{Y}_s^{Tar}; u_a, y_a) \doteq \hat{p}\delta_{hyper,s}^2 + \check{p}\delta_{hypo,s}^2$, donde $\hat{p}$ y $\check{p}$ son los pesos correspondientes a excursiones hiper e hipoglucemiantes, respectivamente, y $\delta_{hipo,s}$ y $\delta_{hiper,s}$ variables de optimización (no negativas) tales que $\underline{G} - \delta_{hipo,s} \leq y_a \leq \overline{G} + \delta_{hiper,s}$. De esta forma, seleccionando $\check{p} \gg \hat{p}$, la convergencia a la zona resulta más prominente conforme y_a se aproxima por debajo ($y_a \nearrow G$).

Observación 6. *Si bien, la idea de emplear un costo de offset asimétrico fue introducida en (Sección 5.1, Apéndice A), en el Apéndice B fue extendida basada en información de la tasa de cambio de la glucemia, mientras que en [Abuin et al., 2022a] se propuso un ajuste basado en información del residuo (considerando incertidumbre en la estimación de la sensibilidad a la insulina).*

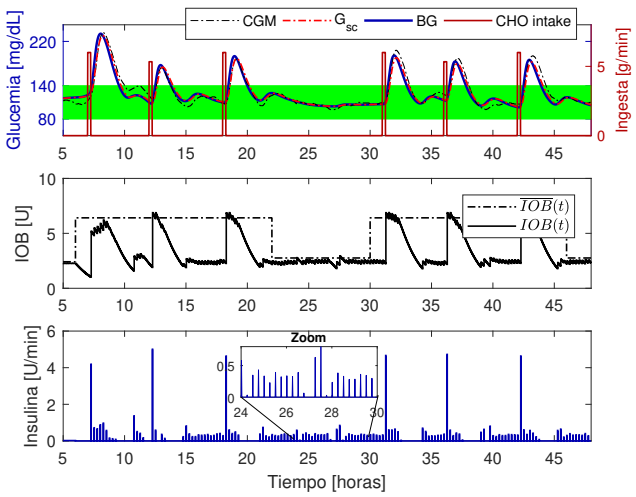

Figura 2.5: pZMPC con anuncio perfecto (PA). Horizonte de predicción: 6 [horas] ($N = 30$ y $T_s = 15$ [min] - $\Delta T = 1$ [min]).

De la Figura 2.5 puede observarse el control glucémico empleando pulsos ($\Delta T = 1$ [min], $T_s = 15$ [min]). Se destaca la aplicación de un bolo de comida como resultado del aviso de la misma y solución del problema de optimización P_N. Por otro lado, durante períodos nocturnos, se percibe que mediante la ley de control propuesta se guía la glucemia a la zona (convergencia asintótica al equilibrio generalizado). Se destaca además, producto del empleo de un costo asimétrico de offset, la promoción de la convergencia de la glucemia hacia la zona por arriba (es decir, desde la región de hiperglucemia).

2.5.5. Formulación con restricciones suavizadas

Un extensión (estabilizante) del controlador presentado, puede verse en el Anexo B, donde la idea principal consiste en incorporar variables de holgura para relajar la restricciones de estado $\mathcal{X}(k)$ en caso de activación de la misma (recuperando la factibilidad de la estrategia). De esta forma, se logra incrementar el dominio de atracción respecto al caso original. Puesto que el uso de variables de holgura podría incrementar la función de costo V_N, a los fines de garantizar que la misma continúe siendo una función de Lyapunov para el sistema en lazo cerrado (y con ello, se preserve la convergencia asintótica a $\mathcal{Y}_s^{Tar}$), se incluye una variable de holgura de equilibrio ϵ_s.

2.5.6. Propiedades de las controladores presentados

Normalmente, las estrategias de control predictivo suelen evaluarse en términos de su i) factibilidad recursiva, ii) estabilidad y iii) desempeño (o performance). En lo que respecta a i), debido al empleo de equilibrios generalizados como conjunto objetivo, y teniendo en cuenta que los mismos son invariantes de control para sistemas controlados mediantes pulsos, la factibilidad recursiva del controlador queda garantizada. Por otro lado, en lo que respecta a ii), siguiendo [Rivadeneira et al., 2018] puede demostrarse que el equilibrio generalizado para el sistema con la ley de control presentada es asintóticamente estable (AE). De hecho en [D'Jorge et al., 2022] se demuestra que la evolución en tiempo continuo queda contenida en el conjunto de órbitas para el sistema en tiempo discreto. Finalmente, en lo que respecta a iii), producto de personalizar la estrategia de control (uso de modelos calibrados por paciente, asimetría en costo de offset, restricciones para la IOB variantes en el tiempo y basadas en herramientas FIT) se mejora notablemente el control glucémico respecto a estrategias con modelos poblacionales y/o asimetrías fijas. Para más detalle, referirse a la Sección 5, Apéndice A y a la Sección 6.4, Apéndice B.

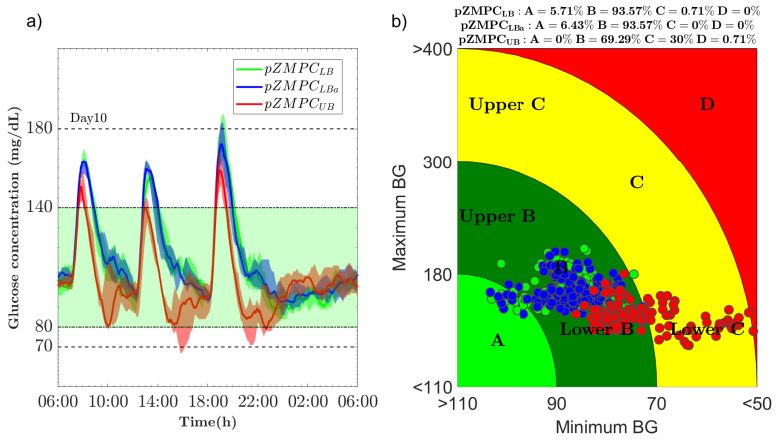

Figura 2.6: (a) Control glucémico mediante $pZMPC_{LB}$, $pZMPC_{LBa}$ y $pZMPC_{UB}$ para 10 pacientes virtuales (día 10). (b) Diagrama CVGA para los 10 pacientes considerando escenario de 14 días. Caso: anuncio de comidas con $(+50\,\%)$ error.

2.6. Resultados

En esta sección se incluyen resultados relevantes al control glucémico considerando, a) el control con anuncio de comidas (con distintos grados de error) y empleando la restricción para IOB basada en eventos de comida (2.2.2) y b) el control si anuncio de comidas y empleando restricción para IOB constante (franja horaria) 2.2.2 . Para el caso b), se incoporan resultados utilizando un costo de offset asimétrico dependiente de la velocidad de cambio de la glucemia.

2.6.1. Configuración híbrida: con anuncio de comidas

En la Figura 2.6 se contrasta el desempeño del controlador empleando la restricción dependiente del evento de comida presentada en la Sección 2.2.2 y considerando un aviso por exceso $(+50\,\%)$ del conteo de carbohidratos. Puede observarse, que tanto en la configuración $pZMPC_{LB}$ como en la $pZMPC_{LBa}$, gracias a que la amplitud del bolo máximo está limitado por $U_0 = CHO_{lb}/CR$, se evitan excursiones en zonas de hipoglucemia. Por otro lado, para el caso $pZMPC_{UB}$, debido a no considerar un límite de seguridad admisible, siendo $U_0 = CHO_{ub}/CR$, el incremento del tiempo en zonas de hipoglucemia es significativo. Por otro lado, en la Figura 2.7 se compara el desempeño del controlador considerando un aviso por defecto $(-50\,\%)$. Puede advertirse, que gracias a la configuración adaptativa del $pZMPC_{LBa}$, se logra un desempeño similar al $pZMPC_{UB}$. Sin embargo, para el controlador $pZMPC_{LB}$ se registra un incremento del número de eventos de hipoglucemia, producto de una infusión extendida en el tiempo (consecuente con una sobreactuación del controlador). Esta da cuenta, que: i) el perfil de $\overline{IOB}$ a emplear no es indistinto, y ii) $\overline{IOB}$ brinda protecciones parciales frente a sobreinfusiones, requiriéndose de estrategias accesorias (ej. costos asimétricos, formulaciones robustas -modelo de predicción conservadores-, entre otras).

Limitaciones: si bien, la configuración de la restricción usando un modelo de comidas posibilita limitar la amplitud del bolo al caso conservador, luego el controlador podría seguir aplicando insulina a una tasa dada por $\hat{u}(t)$, lo que conllevaría a riesgos por acumulación de esta hormona en el tejido subcutáneo/plasma, con el posterior descenso de la glucemia. Motivados por esta esta situación, a los fines de acotar el intervalo ΔT_{IOB}, resultaría oportuno dotar a la restricción de una etapa de detección y diagnóstico del riesgo de sobreactuación del controlador (R_{CO}), siendo $\overline{IOB}(t; R_{CO})$ [Meneghetti et al., 2018,Manzoni et al., 2023, Blanke et al., 2006].

2.6.2. Configuración automática: sin anuncio de comidas

Para esta configuración, se eliminó el anuncio de comidas y a los fines de tener una estimación de la tasa de aparición de glucosa en sangre ($\hat{R}_a$), se empleó el observador de perturbación de entrada (Sección 2.4.2) considerando distintas configuraciones de la matriz de perturbación (B). Además, se configuró el

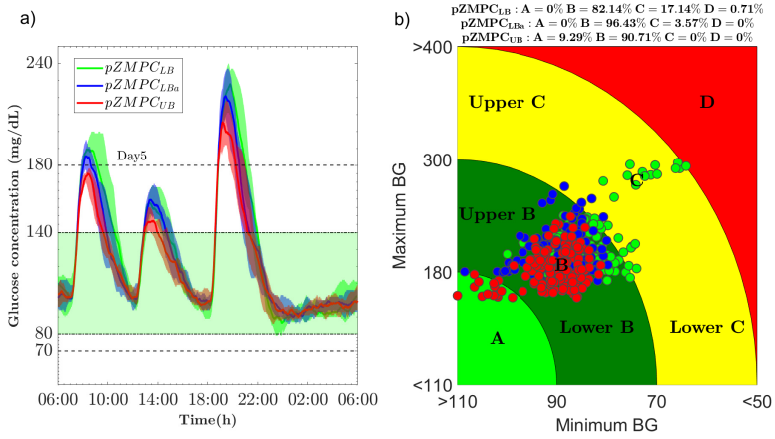

Figura 2.7: (a) Control glucémico mediante $pZMPC_{LB}$, $pZMPC_{LBa}$ y $pZMPC_{UB}$ para 10 pacientes virtuales (día 10). (b) Diagrama CVGA para los 10 pacientes considerando escenario de 14 días. Caso: anuncio de comidas con $(-50\,\%)$ error.

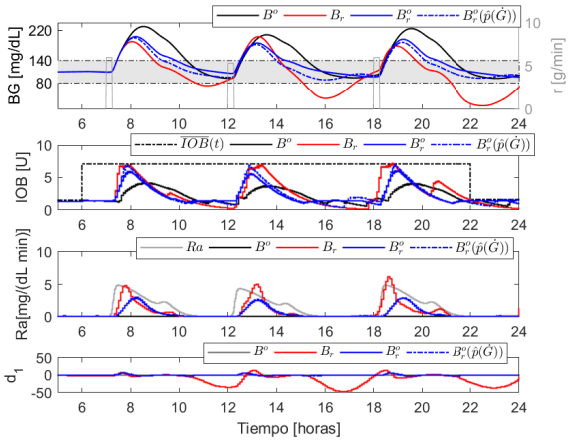

Figura 2.8: Control sin anuncio de comidas para distintas configuraciones del observador de perturbación de entrada: $B = B^o$ ($\mu = 0$), $B = B_r$ ($\mu = 1$), $B = B_r^o$ ($\mu = 0{,}3$) y $B = B_r^o(\hat{p}(\dot{G}))$ ($\mu = 0{,}3$). Sensibilidad a la insulina (aumento 30 %): $S_I = 1{,}3S_{In}$. Paciente: adulto 005 (para más detalle, referirse a la Sección 2.5., Apéndice A).

controlador pZMPC con el costo de offset asimétrico presentado en la Sección 2.5.4), con $\hat{p} = 1$ y $\check{p} = 10^9$. Para el caso $B = B_r^o(\hat{p}(\dot{G}))$, se implementó un costo de offset dependiente de la velocidad de cambio de la glucemia, con $\hat{p}(\dot{G}) = 10^2\hat{p}$ si $\dot{G} \geq 2$ [mg/(dL · min] y $\hat{p}(\dot{G}) = \hat{p}$ (otro caso).

De la Figura 2.8 se observa que al incrementar el nivel de asimetría en el funcional, se logra una mejora en la compensación de la sobreactuación del controlador (en caso de emplear un observador de perturbación de entrada). Por ende, al recurrir a este tipo de observador, resultaría recomendable: i) configurar el factor μ a los fines de moderar la relación de la perturbación que se expresa como comida no-anunciada, y ii) incluir un costo de offset asimétrico dependiente de la glucemia a los fines de moderar la agresividad del controlador (esto último puede mejorarse a partir de una estimación de la tasa de cambio de BG).

Capítulo 3

Seguimiento de trayectorias basales

3.1. Antecedentes

3.1.1. Variaciones circadianas de la sensibilidad a la insulina

Múltiples fuentes de variabilidad (intra e interdía) pueden considerarse para el problema de control glucémico en DT1, entre las que se destacan, variabilidad por ejercicio físico [Dalla Man et al., 2009, Riddell et al., 2017, Riddell et al., 2020], alteraciones de la producción hepática de glucosa [Visentin et al., 2018], estrés [Mansell et al., 2017], variaciones circadianas por efectos neuroendócrinos [Stenvers et al., 2019, Van Cauter et al., 1997, Mansell et al., 2017], aumento/decremento del peso [Kudva et al., 2014], entre otras. Entre estas, las variaciones circadianas de la sensibilidad a la insulina se corresponden con un tipo de alteración caracterizadas por un perfil pseudo-periódico (debido a la variabilidad entre días) [Hinshaw et al., 2013, Visentin et al., 2015]. A diferencia de los pacientes sanos (donde es alta a la mañana y más baja a lo largo del día, producto de la compensación endógena de hormonas hiperglucemiantes) [Saad et al., 2012], para los pacientes DT1 la misma tiene patrones irregulares . Esto conlleva un desafío adicional para los sistemas de AP, requiriendo de módulos estimadores [Schiavon et al., 2018, Reiterer and Freckmann, 2019], no pudiendo asumir un patrón regular para todos los pacientes.

3.1.2. Control periódico para seguimiento de trayectorias

Teniendo en cuenta la periodicidad del sistema (para este tipo de variabilidad) diversas estrategias de control han sido formuladas, entre las que se destacan: MPC para el seguimiento de trayectorias [Gondhalekar et al., 2016], MPC basado en procesos gaussianos [Ortmann et al., 2017], MPC adaptativos [Boiroux et al., 2018a] y MPC iterativos [Toffanin et al., 2017b, Shi et al., 2019], entre otros. Por ejemplo, bajo la asunción de periodicidad en la administración de insulina, [Toffanin et al., 2017a] desarrollaron una estrategia iterativa (R2R, del inglés, *run-to-run*) para el cómputo del suministro basal con garantía de convergencia al suministro óptimo (en términos de maximización del tiempo en zona). Más aún, producto de la periodicidad del sistema, suelen emplearse trayectorias periódicas como objetivos de control [Gondhalekar et al., 2016], normalmente basadas en la expertise del médico y/o en registros diarios de infusión de insulina [Del Favero et al., 2019, Hajizadeh et al., 2019b]. Sin embargo, debido a la consideración de restricciones y dinámicas del modelo, las mismas podrían no ser admisibles, por lo que el sistema en lazo cerrado no lograría converger a estas últimas [Limon et al., 2015, Köhler et al., 2020]. Motivadas por este marco contextual, en el presente capítulo, se proponen formulaciones de MPC para el seguimiento de trayectorias basales, entendiéndose como tal, a aquellas trayectorias admisibles que minimizan la distancia a una referencia dada. A los fines de mejorar el desempeño de las estrategias, se proponen modelos periódicos ajustados en sintonía con variaciones circadianas del paciente.

En este capítulo se abarcarán los objetivos particulares 1 y 4.

3.2. Modelo variante en el tiempo de la dinámica glucosa-insulina en DT1

Para el caso de variaciones intradía de la sensibilidad a la insulina, resulta el siguiente modelo variante en el tiempo, dado por:

$$\dot{x}(t) = A_x(t)x(t)+B_u u(t)+B_z z(t) + E(t), \;\; x(0) = x_0, \tag{3.1}$$
$$\dot{z}(t) = A_z z(t)+B_r r(t), \;\; z(0) = z_0, \tag{3.2}$$

Al igual que lo presentado en el Capítulo 2, las matrices de transición y de entrada vienen dadas por:

$$A_x(t)=\begin{bmatrix} -\theta_1 & -\theta_2(t) & 0 \\ 0 & -\frac{1}{\theta_4} & \frac{1}{\theta_4} \\ 0 & 0 & -\frac{1}{\theta_4} \end{bmatrix}, B_u=\begin{bmatrix} 0 \\ 0 \\ \frac{1}{\theta_4} \end{bmatrix}, E=\begin{bmatrix} \theta_0(t) \\ 0 \\ 0 \end{bmatrix}, B_z=\begin{bmatrix} \theta_3 & 0 \\ 0 & 0 \\ 0 & 0 \end{bmatrix}, A_z=\begin{bmatrix} -\frac{1}{\theta_5} & \frac{1}{\theta_5} \\ 0 & -\frac{1}{\theta_5} \end{bmatrix}, B_r=\begin{bmatrix} 0 \\ \frac{1}{\theta_5} \end{bmatrix},$$

donde $\theta_2(t)$ es la sensibilidad a la insulina, la cual se asume variante en el tiempo y cuya expresión está dada por $\theta_2(t) := \bar{\theta}_2 + \tilde{\theta}_2(t)$, siendo $\bar{\theta}_2$ una componente nominal y $\tilde{\theta}_2(t)$ una componente periódica ($\tilde{\theta}_2(t) = \tilde{\theta}_2(t+T)$). Respecto a esta última, dado que su variabilidad se debe solo a efectos circadianos, se asume un período T igual a 24 [horas]. Además, $\theta_2(t) > 0$ para todo $t \geq 0$. Por otro lado, de [Ruan et al., 2017] se observa que la producción endógena en condiciones basales viene dada por $\theta_0(t) = \theta_1 G_b + \theta^2_{\sigma(t)} x_{b,2}(t)$ [mg/(dL · min)], con $x_{b,2}(t)$ correspondiente a un suministro basal que mantiene la glucemia en un valor constante, G_b (ej. perfiles diurnos de $u_b(t)$ [Rilstone et al., 2021]). Dado que $x_{b,2}(t)$ puede asumirse inversamente proporcional a $\theta_2(t)$, a los fines de simplificar el análisis, en el siguiente apartado se supondrá que $\theta_0(t) \equiv \theta_0$ (constante).

Observación 7. *(Sensibilidad a la insulina, S_I) La sensibilidad a la insulina S_I es un parámetro que mide la capacidad de la insulina para fomentar la utilización de glucosa (tejidos insulino-dependientes) e inhibir la producción endógena de esta última (vías hepáticas). Puede ser estimada en condiciones de estado estacionario [Bergman et al., 1979] como así también en condiciones transitorias [Pillonetto et al., 2006]. De la linealización del modelo mínimo de Bergman según las hipótesis detalladas en la Sección 2.2, puede demostrarse que $\theta_2 = S_I G_b$, siendo S_I la sensibilidad a la insulina en condiciones de estado estacionario ($S_I = p_3/p_2$) y (G_b, u_b) un par de equilibrio basal.*

3.2.1. Especificación de restricciones

Teniendo en cuenta la variabilidad cíclica de parámetros, el conjunto de restricciones de estado $\mathcal{X}(t)$ se lo define como un conjunto periódico, $\mathcal{X}(t) = \mathcal{X}(t+T)$, tal que para todo $t \geq 0$,

$$\mathcal{X}(t) \doteq \{x \in \mathbb{R}^3_{\geq 0} \mid G_{hypo} \leq x_1(t) \leq G_{hyper},\; \theta_4(x_2(t) + x_3(t)) \leq \overline{IOB}(t)\},$$

donde $\overline{IOB}(t) := \theta_4(x_{b,2}(\cdot) + x_{b,3}(\cdot)) + C\hat{H}O/CR(t)$, siendo $(x_{b,2}, x_{b,3})$ elementos de la trayectoria basal de seguridad (ej. $x_b(t)$ tal que $x_{b,1}(t) = G_{b,min}$, con $G_{b,min} = 60$ [mg/dL] un límite de seguridad para la glucemia). Además, $C\hat{H}O$ se corresponde con el conteo de carbohidratos, y $CR(t)$ con la relación carbohidrato-insulina [g/U] (ej. $CR(t) := \theta_2(t)/\theta_3$). Respecto a esto último, es importante aclarar que la especificación de $CR(\cdot)$ es versátil a la estrategia de estimación de la misma, entre las que se destacan: i) R2R [Toffanin et al., 2017b], ii) ILC [Shi et al., 2019] y iii) OP [Schiavon et al., 2018, Reiterer and Freckmann, 2019]). Al igual que la formulación presentada en el Capítulo 2, $G_{hypo} = 60$ y $G_{hyper} = 300$ [mg/dL] (acorde a límites fisiológicos).

3.2.2. Análisis de condiciones basales: trayectorias basales

Al igual que el estudio realizado en el Capítulo 2, en condiciones de ayuno ($r(t) \equiv 0$ y $z(t) \equiv 0$), el subsistema glucosa-insulina describe la evolución dinámica del sistema de DT1. Bajo estas condiciones, vemos que la evolución dinámica del sistema puede ser analizada dependiendo del perfil de $\theta_2(\cdot)$.

- *Perfil nominal* ($\theta_2(t) \equiv \bar{\theta}_2$). En este caso, el conjunto de equilibrio de estados factibles está dado por

$$\mathcal{X}_s \doteq \{x_s \mid x_s \in \mathcal{X}(t), x_{s,1} = (\theta_0 - \theta_2 x_{s,2})/\theta_1,\; x_{s,2} = x_{s,3} = u_s\}$$

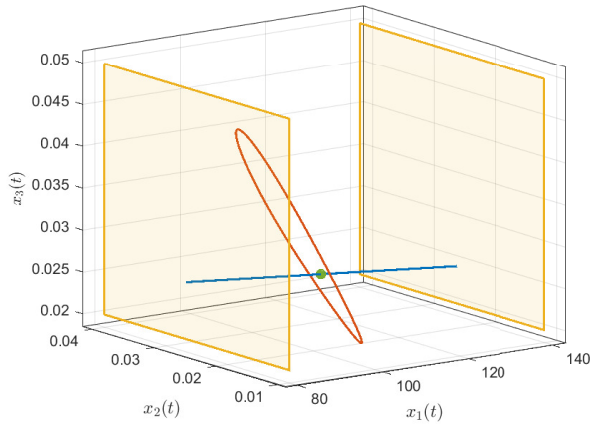

Figura 3.1: Conjunto de equilibrio $\mathcal{X}_s$ (línea azul), equilibrio basal x_b (punto verde) y trayectoria basal correspondiente a $\bar{G}_b = 110$ (trayectoria periódica roja), para el subsistema 3.1. Restricciones para $G = x_1$ (planos amarillos).

con $u_s \in \mathcal{U}_s$, siendo $\mathcal{U}_s = \{u_s | u_s \in \mathcal{U}, 0 \leq u_s \leq U_{b,max}\}$ un conjunto de entradas admisibles asociadas al conjunto de equilibrio $\mathcal{X}_s$ y $U_{b,max} := (\theta_0 - \theta_1 G_{b,min})/\theta_2$. De la Figura 3.1, vemos que entre $(x_s, u_s) \in \mathcal{X}_s \times \mathcal{U}_s$, el par (x_b, u_b) (punto verde) que se corresponde con un valor específico de $x_{s,1} := \bar{G}_b$, el cual está dado por $x_b = [\bar{G}_b, u_b, u_b]'$ y $u_b = \frac{\theta_0 - \theta_1 \bar{G}_b}{\theta_2}$.

- *Perfil periódico* ($\theta_2(t) = \bar{\theta}_2 + \tilde{\theta}_2(t)$, con $\tilde{\theta}_2(t) = \tilde{\theta}_2(t+T)$). Si se consideramos la variabilidad circadiana de $\theta_2(t)$, vemos que para el sistema bajo condiciones basales, no existe una entrada de equilibrio, u_s, tal que $x(t) \in \mathcal{X}_s$ para todo $t \geq 0$, es decir, $\nexists u_s$ tal que $0 = -\theta_1 x_{s,1} + \theta_2(t) u_s + \theta_0$ para todo $t \geq 0$. Sin embargo, teniendo en cuenta la periodicidad de $\theta_2(t)$, es posible definir el conjunto de trayectorias T-periódicas factibles $x(\cdot) : \mathbb{R}_{[0,\infty)} \to \mathbb{R}^n$ como

$$\mathcal{X}_T(t) \doteq \{x \mid x(t) \in \mathcal{X}(t), \dot{x}(t) = A_x(t)x(t) + B_u u(t) + E, x(0) = x(T)\}$$

con $u(t) \in \mathcal{U}_T(t)$ siendo $\mathcal{U}_T(t) \doteq \{u \mid u(t) \in \mathcal{U}, u(0) = u(T)\}$ un conjunto de entradas periódicas admisibles asociadas al conjunto $\mathcal{X}_T(t)$. De la Figura 3.1, se deduce que entre $(x(t), u(t)) \in \mathcal{X}_T(t) \times \mathcal{U}_T(t)$, la trayectoria $x_b(t)$ (línea roja) tal que $x_1(t) = \bar{G}_b$ viene dada por

$$\begin{bmatrix} x_{b,1} \\ x_{b,2} \\ x_{b,3} \end{bmatrix} = \begin{bmatrix} \bar{G}_b \\ \frac{\theta_0 - \bar{G}_b \theta_1}{\theta_2(t)} \\ \frac{\theta_0 - \bar{G}_b \theta_1}{\theta_2(t)} - \frac{(\theta_0 - \bar{G}_b \theta_1)\theta_4 \dot{\theta}_2(t)}{\theta_2^2(t)} \end{bmatrix}.$$

Sin embargo, la trayectoria presentada es una de las admisibles $x(t) \in \mathcal{X}_T(t)$. En un modo más específico, a los fines de seleccionar una trayectoria del conjunto $\mathcal{X}_T(t)$, introduciremos el concepto de trayectoria basal como aquella cuyo estado de salida $C_1 x_b(t)$ minimiza la distancia respecto a una referencia dada, $G_b^{ref}(t)$, para todo $t \geq 0$.

Definición 2 (Trayectoria basal de estado y entrada)**.** *Considérese el subsistema 3.1 con restricciones de estado $\mathcal{X}$ y entrada $\mathcal{U}$, y una referencia periódica de glucemia $G_b^{ref}(\cdot) : \mathbb{R}_{[0,\infty)} \to \mathbb{R}_{[G_{hypo}, G_{hyper}]}$ con período T (ej. $G_b^{ref}(t) = G_b^{ref}(t+T)$, para $t \geq 0$). Una trayectoria basal de estado y entrada está dada por la trayectoria periódica de estado $x_b(\cdot) : \mathbb{R}_{[0,\infty)} \to \mathcal{X}$ y la correspondiente trayectoria de entrada $u_b(\cdot) : \mathbb{R}_{[0,\infty)} \to \mathcal{U}$ que minimiza la distancia $\|C_1 x_b(t) - G_b^{ref}(t)\|$.*

En la Figura 3.1 se muestra la trayectoria basal de estado para una referencia $G_b^{ref}(\cdot)$ constante y considerando el subsistema glucosa-insulina con $\theta_2(t)$ periódica.

Observación 8. *Del análisis del modelo en condiciones basales, puede observarse que el conjunto de equilibrio $\mathcal{X}_s$ no es admisible para el caso de variaciones temporales de $\theta_2(t)$. Sin embargo, si $\theta_2(t)$ y*

$\theta_0(t)$ se asumieran variantes en el tiempo; $\mathcal{X}_s := \{x_s \mid x_{s,1} = (\theta_0(t) - \theta_2(t)u_s)/\theta_1, x_{s,2} = x_{s,3} = u_s\}$ sería un conjunto admisible bajo el supuesto que $\dot{\theta}_0(t) = \dot{\theta}_2(t)u_s$ para todo $t \geq 0$ (lo cual, sin embargo, puede ser restrictivo).

3.2.3. Identificación de ritmos circadianos de la sensibilidad a la insulina

A los fines de contar con una estimación de $\theta_2(t)$ debido a variaciones circadianas, se propuso un enfoque basado en mínimos cuadrados regularizados (RLS), con el funcional de costo regularizado por una función (i) periódica y (ii) constante por tramos $\theta_{2T}(t)$. Además, se incorporaron restricciones fisiológicas para la estimación de $\theta_2(t)$, tal que $\theta_2(t) \in \Theta$, con $\Theta = \mathbb{R}_{[0,8\alpha\bar{\theta}_2,1,2\bar{\theta}_2]}$ ($\alpha = 0{,}4$) y $\bar{\theta}_2$ el valor nominal de la sensibilidad a la insulina. Se asumió una variabilidad interdiaria del $\pm 20\,\%$ ([Visentin et al., 2015]). De esta forma, bajo la asunción de una base periódica diaria ($T = 1440$ min), la sensibilidad a la insulina debido a ritmos circadianos puede ser estimada de la solución del siguiente problema de optimización:

$$\begin{aligned}
\theta_2^* = \arg\min_{\theta_2,\theta_{2T}} \quad & \textstyle\sum_{j=1}^{N_{CI}} \|G_m(j) - G(j)\|_2^2 + \lambda_1\|\theta_2(j) - \theta_{2T}(j)\|_2^2 + \lambda_2\|\Delta\theta_{2T}(j)\|_1 \\
s.t. \quad & G(j) = C_1[\tfrac{(q-1)I}{T_s} - A_x(j)]^{-1}(B_u u(j) + B_z z(j) + E), \\
& z(j) = [\tfrac{(q-1)I}{T_s} - A_z]^{-1} B_r r(j), \\
& \theta_{2T}(j) = \theta_{2T}(j+T), \\
& \theta_2(j) \in \Theta,
\end{aligned}$$

donde θ_2^* denota la estimación óptima de la sensibilidad insulina durante un intervalo temporal N_{CI} ($N_{CI} = N_{days} \cdot (288/\text{día})$ para $T_s = 5$ [min]). $G_m(j)$ se corresponde con la glucemia medida y $G(j)$ con la glucemia estimada para el instante $j-$ésimo. Por otro lado, $A_x(j)$ indica que la matriz de transición de estado varía a lo largo del horizonte debido a $\theta_2(j)$. A los fines de mantener la estructura del modelo lineal en sus parámetros, los subsistemas 3.1 y 3.2 fueron muestreados mediante una discretización de Euler. Es importante aclarar, que en el problema de optimización presentado, $\theta_{2T}(j)$ representa una variable auxiliar respecto a la cual se regulariza la excursión de $\theta_2(j)$. Para el caso enunciado, se asume que $\theta_{2T}(j)$ es (i) periódica y (ii) constante por tramos, tal que (i) se satisface mediante restricción de periodicidad y (ii) mediante penalización *sparse* (norma 1) del incremento temporal $\Delta\theta_{2T}(j) = \theta_{2T}(j) - \theta_{2T}(j-1)$. Enfoques similares pueden encontrarse en [Ohlsson et al., 2010, Ohlsson and Ljung, 2013, Carlson et al., 2018].

En la Figura 3.2 se compara la estimación de $\theta_2(t)$ acorde a distintas penalizaciones en el funcional de costo. Si $\lambda_1 = 0$ y $\lambda_2 = 0$ (Figura 3.2 (a)(c)), el perfil estimado queda sobreajustado, y por ende, todos los efectos no-modelados (ej. utilización de glucosa en tejidos insulino-dependientes variante con la concentración de glucosa, efectos no-lineales en el vaciado gástrico, secreción de glucagón, entre otras) son expuestos como variaciones de la sensibilidad a la insulina. Por otro lado, si la componente de regularización es considerada, $\lambda_1 = 1 \cdot 10$ y $\lambda_2 = 1 \cdot 10^3$ (Figura 3.2 (b)(d)), la tendencia del perfil periódico de $S_I(t)$ es capturada, incluso cuando variabilidades interdiarias [Visentin et al., 2015] son consideradas.

Observación 9. *De la Figura 3.2, se observa que cuando se incorpora la etapa de regularización, se evita el sobreajuste del modelo a los datos de entrenamiento, por lo que se espera una capacidad de generalización mayor. Si bien, el desempeño fue comparado considerando pesos fijos, a los fines de optimizar la relación bias/varianza en pos de minimizar el error de estimación [Pillonetto et al., 2022], resultaría oportuno implementar una estrategia de calibración de los hiperparámetros (λ_1 y λ_2).*

3.2.4. Representación en tiempo-discreto

A los fines de emplear los modelos en tiempo-continuo 3.1 y 3.2 en controladores de tiempo-discreto, se seleccionó el esquema pulsátil presentado en el Capítulo 2, el cual, para un tiempo de muestreo dado T_s (T múltiplo de T_s) y una duración de pulso $\Delta T \in [0, T_s)$, consiste en el siguiente sistema de tiempo discreto:

$$\begin{aligned}
x(k+1) &= F_x(k, x(k), u(k), z(k)), \\
z(k+1) &= F_z(z(k), r(k)), \\
G(k) &= C_1 x(k), \quad IOB(k) = C_2 x(k),
\end{aligned} \tag{3.3}$$

con $F_x(k, x(\cdot), u(\cdot), z(\cdot)) := A_x(k)^d x(\cdot) + B_u(k)^d(\cdot)u(\cdot) + B_z(k)^d(\cdot)z(\cdot) + E(k)^d$ y $F_z(z(\cdot), r(\cdot)) := A_z^d z(\cdot) + B_r^d r(\cdot)$. Las matrices de transición y de entrada son equivalentes a las presentadas anteriormente

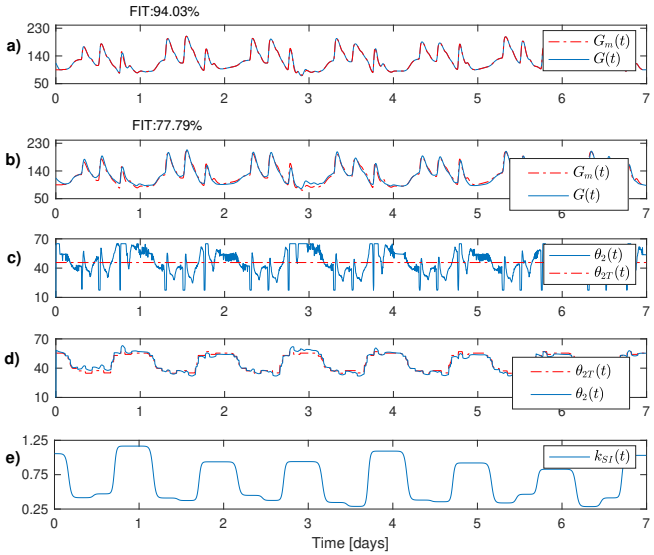

Figura 3.2: Identificación del patrón periódico de sensibilidad a la insulina, $\theta_2(t)$, empleando el algoritmo de estimación de parámetros con distintas configuraciones (Adulto #2, Simulador UVA/Padova, T1DMS2013). Caso 1 (sobreajustado): $\lambda_1 = 0$ y $\lambda_2 = 0$ (a,c). Caso 2: $\lambda_1 = 1 \cdot 10$ y $\lambda_2 = 1 \cdot 10^3$ (b,d). Variabilidad interdiaria k_{SI}.

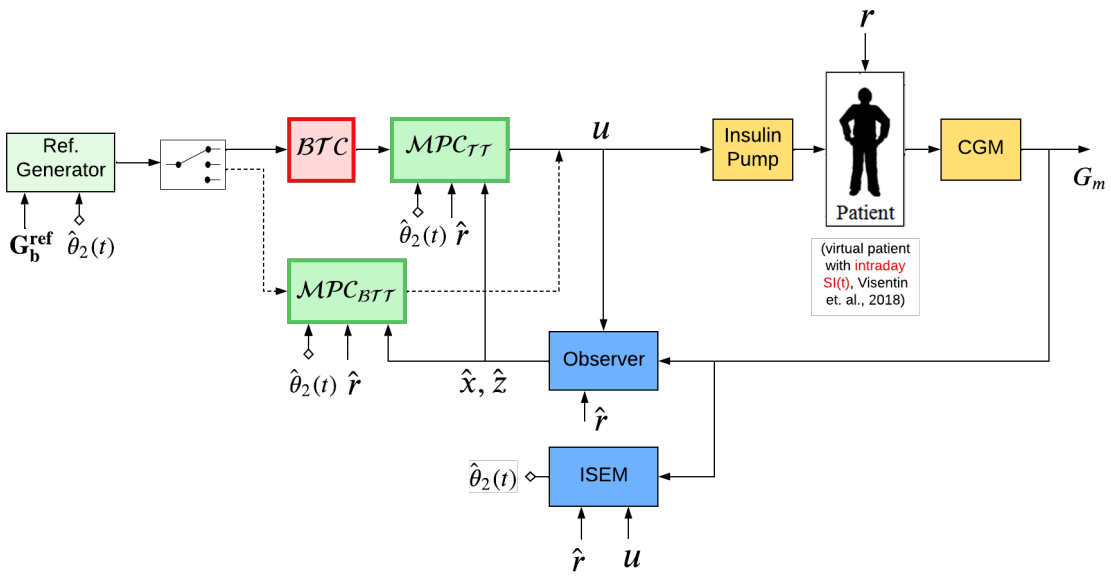

Figura 3.3: Páncreas artificial. Esquema combinado de $\mathcal{BTC} - \mathcal{MPC}_{\mathcal{TT}}$ y $\mathcal{MPC}_{\mathcal{BTT}}$.

(véase Sección 2.3), con la salvedad que se asume que el parámetro variante en el tiempo es constante por tramos, es decir, $\theta_2(t) := \theta_2(kT_s)$, $t \in [kT_s, (k+1)T_s)$. Por otro lado, $\mathcal{X}(k) := \mathcal{X}(kT_s)$ es una versión muestreada del conjunto de restricciones de estado variante en el tiempo, $\mathcal{X}(t)$.

3.3. Formulaciones para seguimiento de trayectorias basales

En esta sección, se define el problema de control relevante al seguimiento de trayectorias basales y se presentan 2 estrategias principales para la resolución del mismo.

3.3.1. Problema de control

Considerando el sistema 3.3 sujeto a restricciones de estado $\mathcal{X}(k)$ y entrada $\mathcal{U}$, y una referencia basal para la glucemia $\mathbf{G}_b^{ref} : \mathbb{I}_{[0,\infty)} \rightarrow \mathbb{R}_{[G_{hypo},G_{hyper}]}$ (la cual es una versión muestreada $G_b^{ref}(\cdot)$). Luego, dados $\hat{x}$, $\hat{z}$, y $\hat{r}$ para un tiempo k, el problema de control consiste en guiar el sistema 3.3 a la trayectoria basal de estado y entrada, $\mathbf{x}_b(\cdot) : \mathbb{I}_{[0,\infty)} \rightarrow \mathcal{X}$ y $\mathbf{u}_b(\cdot) : \mathbb{I}_{[0,\infty)} \rightarrow \mathcal{U}$ respectivamente, la cual, como se presentó en la sección anterior, es aquella que minimiza la distancia $\|C_1 x_b(k) - G_b^{ref}(k)\|$ para todo tiempo $k \geq 0$.

A continuación, a los fines de resolver el problema de control enunciado, se detallarán 2 estrategias basadas en MPC para seguimiento de trayectorias.

3.3.2. Seguimiento trayectoria basal, 2 etapas: $\mathcal{BTT} - \mathcal{MPC}_{\mathcal{TT}}$

Dada una referencia $G_b^{ref}(\cdot)$, sobre el intervalo [0,T], en una primera etapa se computa la trayectoria basal $(\bar{\mathbf{u}}_b, \bar{\mathbf{x}}_b)$ mediante la solución del siguiente problema de optimización (problema de planeamiento) $\mathcal{BTC}(\mathbf{G}_b^{ref})$

$$
\begin{array}{ll}
\underset{\bar{\mathbf{u}}_b, \bar{\mathbf{x}}_b}{\text{mín}} & V_{traj}(\mathbf{G}_b^{ref}; \bar{\mathbf{u}}_b, \bar{\mathbf{x}}_b) \\
s.t. & \bar{u}_b(j) \in \mathcal{U}, \;\; \bar{x}_b(j) \in \mathcal{X}(k+j), \qquad\qquad j \in \mathbb{I}_{[0,T]} \\
& \bar{x}_b(j+1) = F_x(k+j, \bar{x}_b(j), \bar{u}_b(j), 0), \\
& \bar{x}_b(0) = F_x(k+T-1, \bar{x}_b(T-1), \bar{u}_b(T-1), 0).
\end{array}
$$

De esta forma, se obtienen una trayectoria seguible [1] para el sistema a lazo cerrado, la cual es un conjunto invariante de control para el sistema restricto 3.3. Nótese además, que la misma es óptima, en el aspecto que es aquella que minimiza la distancia respecto a una referencia dada. Debido a la convexidad del problema de optimización anterior, la unicidad de la misma queda garantizada. En el contexto de estrategias de control predictivo para el seguimiento de trayectorias [Limon et al., 2015, Köhler et al., 2020] suele denominársela *trayectoria óptima alcanzable*.

En una segunda etapa, con la trayectoria basal calculada $(\bar{\mathbf{u}}_b^o, \bar{\mathbf{x}}_b^o)$, se procede a emplearla como objetivo alcanzable para un controlador de seguimiento de trayectorias, $\mathcal{MPC}_{\mathcal{TT}}(\hat{x}, \hat{z}, \mathbf{r}, \mathbf{u}_b, \mathbf{x}_b, k)$. De esta forma, para un tiempo k, dados $\hat{x}, \hat{z}, \mathbf{r}, \mathbf{u}_b, \mathbf{x}_b$ se resuelve el siguiente problema de optimización (problema de seguimiento),

$$
\begin{array}{ll}
\underset{\mathbf{u}}{\text{mín}} & V_{track}(\hat{x}, \hat{z}, \mathbf{r}, \mathbf{u}_b, \mathbf{x}_b, k; \mathbf{u}) \\
s.t. & x(0) = \hat{x}, \;\; z(0) = \hat{z} \\
& x(j+1) = F_x(k+j, x(j), u(j), z(j)), \quad j \in \mathbb{I}_{[0,N]} \\
& z(j+1) = F_z(z(j), r(j)), \qquad\qquad\quad j \in \mathbb{I}_{[0,N]} \\
& u(j) \in \mathcal{U}, \;\; x(j) \in \mathcal{X}(k+j), \qquad\quad j \in \mathbb{I}_{[0,N-1]} \\
& x(N) = x_b(N).
\end{array}
$$

Es importante aclarar, que en este caso, se emplea la trayectoria basal como parámetro de optimización en la etapa de seguimiento de trayectoria $\mathcal{MPC}_{\mathcal{TT}}$, lo cual constituye una diferencia principal respecto a la configuración de una etapa, donde esta última resulta una variable de optimización. A los fines de garantizar la convergencia asintótica a la trayectoria $(\bar{\mathbf{u}}_b, \bar{\mathbf{x}}_b)$, vemos que esta formulación emplea una restricción terminal de igualdad $x(N) = x_b(N)$. Si bien, esto último, junto a propiedades del costo $V_{track}(\cdot)$ [Limon et al., 2015] garantiza que la trayectoria basal sea asintóticamente estable para el sistema en lazo cerrado, impone que la trayectoria predicha por el controlador la alcance en N pasos. Por ende, en esta formulación, el horizonte de control es crítico a los fines de contar con un DOA compatible con perturbaciones características del problema bajo análisis (ej. comidas con elevado índice glucémico).

3.3.3. Seguimiento trayectoria basal, 1 etapa: $\mathcal{MPC}_{\mathcal{BTT}}$

A diferencia de $\mathcal{BTT} - \mathcal{MPC}_{\mathcal{TT}}$, en este apartado, se presenta una formulación para seguimiento de trayectorias donde se emplea una trayectoria artificial como conjunto objetivo del controlador. Se incorpora

[1] Una trayectoria se denomina seguible si satisface restricciones de estado y de modelo para todo tiempo.

además un costo de planeamiento, $V_{traj}(\cdot)$, a los fines de penalizar la distancia entre la trayectoria artificial de salida, $C_1 x_a(k)$, y la referencia G_b^{ref}.

$$\begin{aligned}
\min_{\mathbf{u},\mathbf{u}_a,\mathbf{x}_a} \quad & V_N(\hat{x},\hat{z},\mathbf{r},\mathbf{G}_b^{ref},k;\mathbf{u},\mathbf{u}_a,\mathbf{x}_a) \\
s.t. \quad & x(0)=\hat{x},\ \ z(0)=\hat{z} \\
& x(j+1)=F_x(k+j,x(j),u(j),z(j)), \quad j\in\mathbb{I}_{[0,N]} \\
& z(j+1)=F_z(z(j),r(j)), \quad j\in\mathbb{I}_{[0,N]} \\
& u(j)\in\mathcal{U},\ \ x(j)\in\mathcal{X}(k+j), \quad j\in\mathbb{I}_{[0,N-1]} \\
& x(N)=x_a(N), \\
& x_a(j+1)=F_x(k+j,x_a(j),u_a(j),0),\ j\in\mathbb{I}_{[0,T-1]} \\
& u_a(j)\in\mathcal{U}, \quad x_a(j)\in\mathcal{X}(k+j), \quad j\in\mathbb{I}_{[0,T-1]} \\
& x_a(0)=F_x(k+T-1,x_a(T-1),u_a(T-1),0).
\end{aligned}$$

La misma consiste en el empleo de trayectorias artificiales $(\mathbf{u}_a,\mathbf{x}_a)$ como variables de optimización, las cuales son objetivos parciales utilizados por el controlador. De esta forma, mediante el uso de un costo de seguimiento, $V_{track}(\cdot)$, el cual penaliza la distancia entre las trayectorias predichas y la trayectoria artificial (o trayectoria basal en-línea), y gracias a la utilización de ingredientes terminales estabilizantes, se logra la convergencia asintótica del sistema en lazo cerrado a esta última. Es importante aclarar, que debido al uso de trayectorias artificiales como conjunto objetivo, se incrementa el DOA respecto a $\mathcal{BTT}-\mathcal{MPC}_{\mathcal{TT}}$. Para más detalle, en la Sección 3.4 se contrastan los DOAs de ambas formulaciones mediante un índice asociado a la pérdida de factibilidad (IE, del inglés, *infeasibility episodes index*). Finalmente, tal como enunció en el Capítulo 2, ante un cambio de la trayectoria de referencia $G_b^{ref}(\cdot)$ (ej. por niveles de BG compatibles con hipoglucemia, perturbaciones por ejercicio físco, entre otras) esta formulación conserva la factibilidad recursiva del problema de seguimiento.

3.3.4. Seguimiento trayectoria basal, 1 etapa: Basal tube tracking

En este último caso, se presenta un controlador para seguimiento de trayectorias basales contenidas en zonas terapéuticas (variantes en el tiempo). A diferencia del controlador por zonas $pZMPC$ presentado en la Capítulo 2, en este caso, la zona consiste en un conjunto de trayectorias periódicas. A los fines de implementar esta estrategia, teniendo en cuenta las ventajas relacionadas al uso de trayectorias artificiales, se reemplaza el costo de planeamiento, $V_{traj}(\cdot)$, por

$$V_{traj}(\mathbf{G}_b^{ref},k;\mathbf{u}_a,\mathbf{x}_a,\mathbf{G}*) := \sum_{j=0}^{T-1} S\|C_1 x_a(j)-G^*(j)\|_2^2,$$

con $G^*(j)$ una variable de optimización adicional, restringida por $G^*(j)\in[G_b^{ref}(k+j)-G_{b,min}^z, G_b^{ref}(k+j)+G_{b,max}^z]$, siendo $G_{b,min}^z$ y $G_{b,max}^z$ los limites superiores e inferiores de la zona, respectivamente.

3.3.5. Propiedades de la estrategias

Bajo la estrategia de control a lazo cerrado ideal, la trayectoria basal $(\mathbf{u}_b,\mathbf{x}_b)$ es asintóticamente estable (AE). Respecto a la factibilidad recursiva, debido a que se emplean trayectorias basales como objetivos de control, y teniendo en cuenta la naturaleza periódica del sistema, puede garantizarse la existencia de una secuencia de control factible para todo tiempo. Por ende, para todo estado inicial perteneciente al dominio de atracción del controlador, la factibilidad del problema de optimización queda garantizada. Sin embargo, para 1 etapa, puesto que la trayectoria basal "artificial" $(\mathbf{u}_a,\mathbf{x}_a)$ es una variable de decisión, se obtiene un DOA mayor (para el mismo horizonte de control). Respecto a la estabilidad, dado que la trayectoria basal es un objetivo asintóticamente estable para el sistema en lazo cerrado (tanto, para leyes de control: $\kappa_N(\hat{x},\hat{z},\hat{\mathbf{r}},\mathbf{u_b},\mathbf{x_b},k)$ y $\kappa_N(\hat{x},\hat{z},\hat{\mathbf{r}},\mathbf{G}_b^{ref},k)$) [Limon et al., 2015], la convergencia asintótica a la misma queda garantizada. Es importante destacar, que debido a que el modelo resulta una aproximación local del sistema, existe un error de modelado, lo que en términos prácticos demandaría caracterizar la estabilidad práctica de la formulación [Limon et al., 2009, Bujarbaruah et al., 2020]. Finalmente, en relación al desempeño, debido al uso de un modelo lineal variante en el tiempo (LTV, por sus siglas en inglés) la performance de la estrategia es significativamente superior respecto caso de un modelo lineal invariante en el tiempo (LTI, por sus siglas en inglés). Además, la configuración de la trayectoria basal considerando variaciones

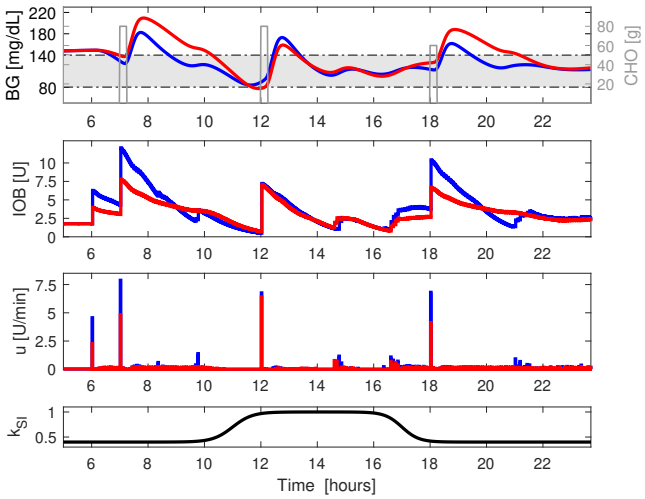

Figura 3.4: Control glucémico empleando $\mathcal{MPC}_{\mathcal{TT}}$, modelo nominal LTI (rojo) y modelo LTV (azul). Patrón de variabilidad de la sensibilidad a la insulina: $k_{SI}(t)$.

de $S_I(t)$ (ej. trayectoria de referencia $G_b^{ref}(\cdot)$ dependiente del patrón de $\theta_2(t)$, Sección 6.2., Apéndice C) posibilita incrementar la robustez de la formulación, principalmente para escenarios con incerteza paramétrica relacionada a la sensibilidad a la insulina.

3.4. Resultados de simulación

A continuación se muestran resultados relevantes al seguimiento de trayectorias basales, ensayando los controladores en un paciente DT1 'in-silico' (simulador virtual UVAPadova) [Man et al., 2014]. Para mayores precisiones remitirse a la Sección 6, Apéndice C.

3.4.1. Evaluación de $\mathcal{MPC}_{\mathcal{TT}}$ y $\mathcal{MPC}_{\mathcal{BTT}}$: configuración LTI vs LTV

En este caso, se comparan las formulaciones, con y sin etapa de planeamiento, $\mathcal{MPC}_{\mathcal{TT}}$ y $\mathcal{MPC}_{\mathcal{BTT}}$ respectivamente, cuando se emplea un modelo de predicción nominal (LTI) y uno variante en el tiempo (LTV). Para ambas configuraciones, se utiliza un horizonte de control $N = 30$ (2.5 [horas]) a los fines de evidenciar, las ventajas potenciales de emplear trayectorias basales (artificiales) como objetivo de control en lugar de una trayectoria fija. En ambos casos, se asume una referencia constante, dada por $G_b^{ref} = 110$ [mg/dL].

De la Figura 3.4, se destaca que la configuración variante en el tiempo optimiza el suministro de insulina de acuerdo a las variaciones temporales de S_I (representadas por $k_{SI}(t)$). Se observa además, que la administriación de insulina es reducida de forma anticipativa durante transiciones de S_I de niveles S_I^l (baja) a S_I^h (alta) (ej. reducción de IOB entre 10:00 to 12:00 h). Para el caso $\mathcal{MPC}_{\mathcal{TT}}$, como su dominio de atracción es menor, se reporta un aumento del número de eventos de pérdida de factibildiad recursiva (Tabla 3.1).

Tabla 3.1: Episodios de pérdida de factibilidad recursiva (IE) para un escenario de 7 días

	$\mathcal{MPC}_{\mathcal{TT}}$		$\mathcal{MPC}_{\mathcal{BTT}}$	
	LTI	LTV	LTI	LTV
#IE	15	52	1	0

Capítulo 4

Caracterización dinámica de modelo *in-host* para infecciones agudas

4.1. Antecedentes

4.1.1. Modelo limitado por células

Como se comentó en el Capítulo 1, en esta segunda parte se caracterizará un modelo para la descripción de infecciones virales. Estas pueden ser crónicas o agudas dependiendo de la virulencia del agente infeccioso. A los fines de describir la evolución de las mismas, suelen emplearse modelos basados en sistemas de ecuaciones diferenciales ordinarias (ODE, del inglés, *ordinary differential equation*), cuyos estados representan la concentración de células susceptibles, células infectadas, virus libre, células y mediadores de respuesta inmunológica, entre otras. Suelen incorporase además diversas dinámicas a lo largo del ciclo de vida la infección, entre las que se destacan: a) dinámica vital (producción y muerte de células susceptibles por causas naturales), b) estadios con fase de latencia para las células infectadas, c) producción de mediadores de respuesta inmunológica con dinámicas no-lineales y con retardo, entre otras. Además, para infecciones con evolución progresiva en distintos tejidos blancos, se han considerado modelos con evolución espacial y temporal. Particularmente, en esta capítulo, bajo la asunción de dinámica vital despreciable, realizaremos la caracterización dinámica de un modelo para infecciones virales agudas. Cabe aclarar, tal como se enunció en el Capítulo 1, que debido a que no se considera explícitamente la respuesta inmunológica, se corresponde a un modelo "limitado por células".

4.1.2. Tratamiento con antivirales

A los fines de valorar el efecto de los antivirales en las células blanco, suelen emplearse modelos de la farmacodinámica (PD) y farmacocinética (PK) de los mismos, tal que la primera representa el efecto (o acción terapéutica) del antiviral en las células blanco, mientras que la segunda representa la dinámica de absorción del mismo en el organismo. Normalmente, la PD suele modelarse mediante funciones sigmoideas (Michaelis-Menten, términos logísticos) las cuales, basadas en dinámicas de saturación de receptores de membrana [Canini and Perelson, 2014, Ciupe and Heffernan, 2017], relacionan la concentración del agente terapéutico en el compartimento circundante (normalmente, el plasma) y el efecto del mismo en la propagación de la infección. Por otro lado, la PK suele representarse mediante modelos compartimentales, cuyo partición es dependiente de las vías de suministro (oral, intravenosa, parenteral, entre otras). Además, dado que la administración del antiviral suele realizarse en forma de pastillas, suelen emplearse modelos con dinámicas impulsiones. Siguiendo esta línea de trabajo, en el presente capítulo examinaremos el modelo para infecciones agudas, considerando distintas efectividades de antivirales, y formalizaremos la existencia de una efectividad crítica, la cual resulta un punto de inflexión en la propagación de la infección.

En esta capítulo se abarcarán los objetivos particulares 5, 6 y 7.

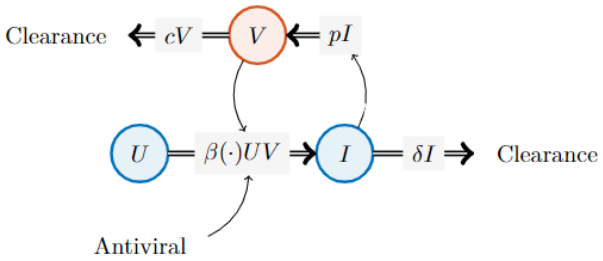

Figura 4.1: Esquema del modelo UIV

4.2. Modelo *in-host* limitado por células

Sea el siguiente modelo limitado por células, donde U es la concentración de células susceptibles [células/mm^3], I es la concentración de células infectadas [cell/mm^3] y V es la concentración de virus libre [copias/mL],

$$\dot{U}(t) = -\beta U(t)V(t), \qquad U(0) = U_0, \tag{4.1}$$
$$\dot{I}(t) = \beta U(t)V(t) - \delta I(t), \qquad I(0) = I_0, \tag{4.2}$$
$$\dot{V}(t) = pI(t) - cV(t), \qquad V(0) = V_0 \tag{4.3}$$

siendo β [mL.day^{-1}/copias] la tasa de infección de las células susceptibles U por parte del virus libre V, δ [día^{-1}] la tasa de muerte de las células infectadas, p [(copias.mm^3/célula.mL).day^{-1}] la tasa reproducción del virus libre (en células infectadas), y c [dia^{-1}] la tasa de eliminación (o 'clearance') del virus V mediante el sistema inmunológico. En este modelo, se asume que la dinámica vital (es decir, la producción y muerte de células susceptibles por causas naturales) es despreciable respecto a la duración de la infección. Como se verá a lo largo de este capítulo, esta asunción repercute en el conjunto de equilibrio del modelo, pasando de ser equilibrios aislados (sanos/enfermos) a un continuo de puntos de equilibrio sano (puesto que concluida la infección, el remanente de células infectadas y virus libre es nulo). Un diagrama esquemático del modelo propuesto se observa en la Figura 4.1

Observación 10. *Es importante destacar, que si bien en el modelo se asume que U, I y V se encuentran homogéneamente distribuidas (compartimento), dado que no necesariamente se satisfice un balance de masa para cada estado (por ejemplo, la producción de virus libre no implica un decremento de la concentración de células infectadas), resulta que el mismo no se corresponde con un esquema de modelado compartimental. En contraposición resulta análogo a un modelo de poblaciones [Murray, 2002], donde se observa (i) una relación predador-presa de la interacción entre U y V, (ii) relación de mutualismo de la interacción entre I y V. Sin embargo, es bueno aclarar, que si redefinimos la tasa de infección $\beta(V) := \beta V(\cdot)$, con $V(\cdot)$ la carga de virus libre que satisface la siguiente dinámica $\dot{V}(t) = pI(t) - cV(t)$, y circunscribimos los compartimentos a U e I, el sistema podría ser caracterizado bajo un esquema estrictamente compartimental (con una tasa de transferencia dependiente de la concentración de virus libre).*

Efecto de antivirales

Un aspecto importante relacionado al análisis del modelo anterior resulta de determinar el tipo de mecanismos de control que pueden moderar la progresión de la infección en el huésped. Entre ellos se distinguen dos grandes grupos: i) agentes terapéuticos (antivirales, corticoides) [Canini and Perelson, 2014] y ii) mecanismos mediadores de respuesta inmunológica innata (interferón tipo I) y adaptativa (linfocitos T citotóxicos, anticuerpos) [Ciupe and Heffernan, 2017]. Si bien, ambos efectos pueden actuar de forma sinérgica, en el presente capítulo solo consideraremos acciones de control mediadas por agentes terapéuticos, más precisamente, antivirales. Respecto a estos últimos, dependiendo de la fase en el ciclo de vida del virus, pueden modelarse como:

- Agentes mediadores de la infección de células susceptibles: $\beta(1-\eta)$ (ej. bloqueadores de receptores de membrana).

- Agentes mediadores de la replicación y maduración en células infectadas: $p(1-\eta)$ (ej. bloqueadores de ARN polimerasa).

siendo η la efectividad del antiviral. Es importante destacar, que $\eta(t)$ puede relacionarse con la concentración del antiviral en el tejido blanco, $D(t)$, mediante modelos de saturación de receptores. Por ejemplo, mediante dinámicas de Michaelis-Menten (Sección 2.4., Apéndice F).

4.2.1. Numero básico de reproducción

Definición 3. *Dada una población de células susceptibles $U(t)$, se define el numero básico de reproducción $\mathcal{R}(t)$ como la cantidad de células infectadas que se producen a lo largo de la vida-media de una célula infectada. Para el modelo 4.1 viene dado por:*

$$\mathcal{R}(t) := U(t)\frac{\beta p}{c\delta}. \tag{4.4}$$

Para el caso de condiciones iniciales, $t = 0$, y asumiendo que una pequeña cantidad de virus libre V_0 es introducida en un población de células susceptibles, U_0, resulta

$$\mathcal{R}_0 := U_0\frac{\beta p}{c\delta}. \tag{4.5}$$

Antes de proceder a un análisis dinámico del sistema, resulta de utilidad definir el valor crítico de las células susceptibles $\mathcal{U}_c$, el cual como se verá más adelante, es un umbral fundamental para distinguir la estabilidad del conjunto de equilibrio $\mathcal{X}_s$.

Definición 4. *Se define el valor crítico de U, $\mathcal{U}_c$, como*

$$\mathcal{U}_c := \frac{c\delta}{p\beta}, \tag{4.6}$$

el cual, para valores fijos de los parámetros β, p, δ y c, es constante y solo dependiente de parámetros del modelo. Nótese además que de 4.5, el nivel crítico $\mathcal{U}_c = \frac{U_0}{\mathcal{R}_0}$.

Observación 11. *Es importante destacar que la expresión matemática presentada para $\mathcal{R}_0$, puede derivarse de aplicar el método de matrices generacionales [van den Driessche, 2017] al modelo original. Sin embargo, en lo que respecta a la estabilidad de los puntos de equilibrio, puesto que dicho método demanda que los mismos sean hiperbólicos (a los fines de conservar la aproximación local de la linealización), la condición $\mathcal{R}_0 \leq 1$ no es suficiente para caracterizar la estabilidad asintótica de los mismos. Por otro lado, de lo visto en la Sección 4.2.2 y dado que $\mathcal{R}_0 = \mathcal{U}_0/\mathcal{U}_c$, se anticipa que aquellos puntos de equilibrio $\overline{x} = (\mathcal{U}_0, 0, 0)$, cuyo $\mathcal{U}_0 > \mathcal{U}_c$ (o $\mathcal{R}_0 > 1$) resultan inestables.*

Observación 12. *Respecto a la propagación del virus, en el Apéndice D, se demuestra que si el virus está en fase de propagación ($\dot{V}(t^*) > 0$) con $t^* \in [\check{t}_V, \hat{t}_V)$, siendo $\check{t}_V$ y $\hat{t}_V$ los tiempos donde $V(t)$ alcanza un mínimo y máximo respectivamente, entonces dado que $\mathcal{R}(t)$ es monótonamente decreciente y $\mathcal{R}(\check{t}_V) > 1$, resulta que $\mathcal{R}(0) > 1 + \alpha(0)$, para una dada función positiva $\alpha(\cdot)$. Esto último denota una condición suficiente para el crecimiento de la carga viral.*

4.2.2. Conjunto de equilibrio

Del análisis del modelo para condiciones de estado estacionario ($\dot{U}(t)$, $\dot{I}(t)$ y $\dot{V}(t)$ igual a cero para todo $t \geq 0$), resulta el siguiente conjunto de equilibrio:

$$\mathcal{X}_s := \{(U, I, V) \in \mathbb{R}^3 : U \in [0, \infty),\ I = 0,\ V = 0\}. \tag{4.7}$$

Realizando un estudio de la estabilidad del conjunto $\mathcal{X}_s$ (método indirecto de Lyapunov), se observa que para aquellos puntos de equilibrio $x_s := (U_s, 0, 0)$, con $U_s > \mathcal{U}_c$, al menos 1 autovalor de $J(x_s) := \frac{\partial f}{\partial x}$ presenta parte real positiva ($\lambda_1 = 0, \lambda_2 < 0, \lambda_3 > 0$). Por ende, el subconjunto de puntos de equilibrio, con $U_s > \mathcal{U}_c$, resulta inestable (Figura 4.2). Por otro lado, para $U_s \leq \mathcal{U}_c$, si bien, $J(x_s)$ no presenta autovalores con parte real positiva ($\lambda_1 = 0, \lambda_2 < 0, \lambda_3 \leq 0$), dado que tiene un autovalor con parte real cero, no

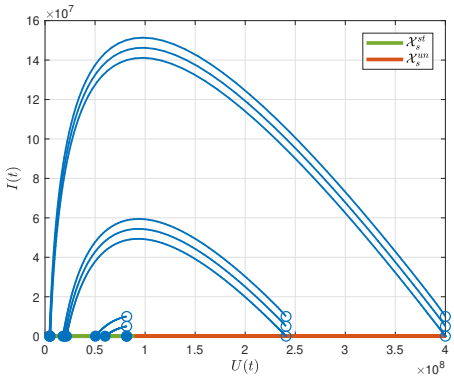

Figura 4.2: Conjunto de equilibrio: $\mathcal{X}_s = \mathcal{X}_s^{st} \cup \mathcal{X}_s^{un}$ $(U^* = 1/R)$

pueden obtenerse resultados concluyentes respecto a su estabilidad. Sin embargo, del análisis realizado, una primera observación es que el conjunto de equilibrio $\mathcal{X}_s$ puede ser desagregado en 2 subconjuntos, siendo

$$\mathcal{X}_s^{un} \quad := \quad \{(U, I, V) \in \mathcal{X} : U \in (\mathcal{U}_c, +\infty),\ I = 0,\ V = 0\}, \tag{4.8}$$

inestable, y

$$\mathcal{X}_s^{st} \quad := \quad \{(U, I, V) \in \mathcal{X} : U \in [0, \mathcal{U}_c],\ I = 0,\ V = 0\} \tag{4.9}$$

(presumiblemente) estable. Se anticipa igualmente, que aplicando el método directo de Lyapunov a puntos de equilibrio de $\mathcal{X}_s^{st}$, se puede concluir que el mismo es estable. De hecho, como resultado de un análisis de atractividad del conjunto $\mathcal{X}_s^{st}$, se puede concluir además, que resulta asintóticamente estable. Por ese motivo, a lo largo del capítulo lo denotaremos como $\mathcal{X}_s^{st}$.

4.2.3. Efectividad crítica

En el contexto de modelos *in-host*, se entiende por efectividad crítica, al nivel de efectividad del antiviral tal que por encima de esta se produce el decremento de la propagación de la infección. Normalmente, suele interpretársela como un punto de bifurcación del modelo, $\mathcal{R}(t_{tr}) = 1$ [Dobrovolny et al., 2011, Dahari et al., 2007, Canini and Perelson, 2014], tal que para efectividades superiores a la crítica, los puntos de equilibrio sanos resultan asintóticamente estables, mientras que los enfermos inestables. A los fines de caracterizar este umbral, definamos el numero básico de reproducción $\mathcal{R}$ al inicio del tratamiento t_{tr},

$$\mathcal{R}(t_{tr}) = \frac{U(t_{tr})p(1-\eta_p)\beta(1-\eta_\beta)}{c\delta}, \tag{4.10}$$

con $\check{t}_V < t_{tr} < \hat{t}_V$. Entonces los valores críticos de η_p y η_β son aquellos para los cuales $\mathcal{R}(t_{tr}) = 1$, es decir,

$$\eta_p^c(t_{tr}) \quad := \quad 1 - \frac{c\delta}{U(t_{tr})\beta p} \tag{4.11}$$

$$\eta_\beta^c(t_{tr}) \quad := \quad 1 - \frac{c\delta}{U(t_{tr})\beta p} = \eta_p^c(t_{tr}). \tag{4.12}$$

De las ecuaciones 4.11 y 4.12 se puede inferir que $\eta_p^c(t_{tr})$ y $\eta_\beta^c(t_{tr})$ son funciones decrecientes con la reducción de $U(t_{tr})$. Puesto que $U(t_{tr})$ es monotónicamente decreciente con el tiempo de inicio de tratamiento, t_{tr}, de la Figura 4.3, se observa que $\eta_p^c(t_{tr})$ decrece conforme $t_{tr} \to t_c$. Respecto a esto último, del análisis del modelo, vemos que $\eta_p^c(t_{tr}) \approx 1 - c\delta/(U_0\beta p)$ para $t_{tr} \to t_0$ y $\eta_p^c(t_{tr}) \approx 1 - c\delta/(\mathcal{U}_c\beta p) = 0$ para $t_{tr} \to \hat{t}_V$ $(t_c \approx \hat{t}_V)$.

Observación 13. *Si bien, la efectividad crítica fue definida como un umbral, tal que para efectividades superiores a la crítica, $\mathcal{R}(t_{tr}) < 1$, vemos que esta condición tiene implicancias tanto en i) la propagación*

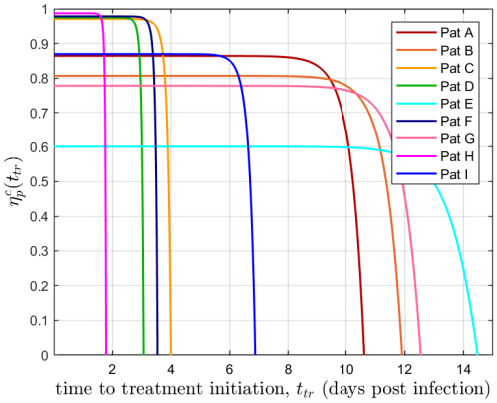

Figura 4.3: $\eta_p^c(t_{tr})$ vs t_{tr} correspondiente a 9 pacientes COVID-19

del virus, como así también, en ii) la estabilidad del conjunto de equilibrio. Respecto a i), adoptando el modelo aproximado (véase Sección 7.2., Apéndice E), resulta $\dot{V}(t_{tr}) = (\mathcal{R}(t_{tr})-1)\delta V(t_{tr})$. *Por ende, para efectividades* $\eta_p(t_{tr}) > \eta_p^c(t_{tr})$ *(o* $\eta_\beta(t_{tr}) > \eta_\beta^c(t_{tr})$*),* $\dot{V}(t_{tr}) < 0$ *por lo que se produce el decremento de la propagación de la infección. Respecto a ii), sea* $\mathcal{X}_s(t_{tr}) := [0, U(t_{tr})]$ *el conjunto de equilibrio admisible al momento del tratamiento, vemos que para efectividades superiores a la crítica,* $U(t_{tr}) < \mathcal{U}_c(t_{tr}) := p(1 - \eta_p^c(t_{tr}))\beta/(c\delta)$*, por lo que (siguiendo resultado Sección 4.3)* $\mathcal{X}_s(t_{tr})$ *resulta asintóticamente estable. Es decir, para este modelo, puede interpretarse la efectividad crítica como un punto de bifurcación transcrítica para el modelo UIV.*

4.2.4. Positividad de la soluciones

Si bien, en los trabajos (Apéndices D, E y F), se asumió que dadas condiciones iniciales $x_0 = (U(t_0), I(t_0), V(t_0)) \in \mathcal{X} := \mathbb{R}^3_{\geq 0}$, la solución del sistema $x(t) := (U(t), I(t), V(t)) \in \mathcal{X}$ pertenece al conjunto $\mathcal{X}$ para todo $t \geq t_0$, es importante aclarar que, siguiendo a [Nangue, 2019] puede demostrarse (desigualdad diferencial) la positividad de la solución para todo tiempo. De esta forma, vemos que $\mathcal{X} := \mathbb{R}^3_{\geq 0}$ es un conjunto invariante (positivo) para el modelo UIV.

4.3. Estabilidad asintótica del conjunto de equilibrio

A continuación procederemos a caracterizar la estabilidad y atractividad del conjunto de equilibrio $\mathcal{X}_s$, extendiendo el concepto de estabilidad $\epsilon - \delta$ de puntos de equilibrio a conjuntos de equilibrio. Nótese que debido a la compacidad del conjunto, bastará con demostrar la estabilidad de sus puntos para generalizar la estabilidad de este último. Respecto a la atractividad, puesto que todo conjunto que contenga un subconjunto atractivo, es también atractivo, a los fines de caracterizarla procederemos a determinar atractividad del mínimo conjunto atractivo (subconjunto) contendido en el mismo. Como se verá a lo largo de esta sección, puesto que este subconjunto es estable, se anticipa que será el único conjunto asintóticamente estable del modelo bajo análisis.

4.3.1. Estabilidad $\epsilon - \delta$

Puesto que el método de indirecto de Lyapunov no puede emplearse para determinar la estabilidad local del conjunto $\mathcal{X}_s^{st}$ (autovalor igual a cero) se propone realizar el análisis empleando el método directo de Lyapunov. En este punto, es importante destacar que si bien el objetivo es estudiar la estabilidad local $\epsilon - \delta$ del conjunto $\mathcal{X}_s$ (Definición 5), debido a la compacidad (cerrado y acotado) de este último, bastará con estudiar la estabilidad local de sus puntos.

Definición 5 (Estabilidad local $\epsilon - \delta$ de $\mathcal{X}_s$)**.** *Considérese el sistema 4.1 restringido por* $\mathcal{X}$*. Un conjunto de equilibrio cerrado,* $\mathcal{X}_s \subset \mathcal{X}$*, es* $\epsilon - \delta$ *localmente estable si para todo* $\epsilon > 0$ *existe* $\delta > 0$ *tal que si* $\|x\|_{\mathcal{X}_s} < \delta$ *entonces* $\|\phi(t; x)\|_{\mathcal{X}_s} < \epsilon$*, para todo* $t \geq 0$*.*

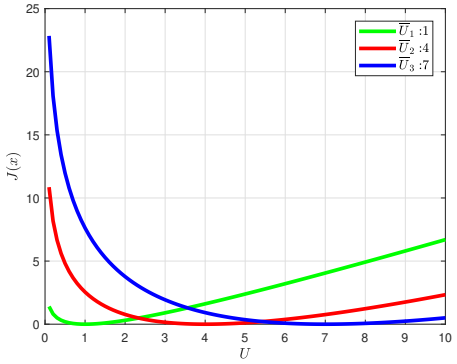

Figura 4.4: Función de Lyapunov, $J(x)$

Sea $\overline{x} = (\bar{U}, 0, 0)$ un punto de equilibrio perteneciente al conjunto $\mathcal{X}_s$ (con $\bar{U} \in (0, U_0]$). Para evaluar la estabilidad del mismo, proponemos una función candidata de Lyapunov, dada por

$$J(x) := U - \overline{U} - \overline{U}\ln(\frac{U}{\overline{U}}) + I + \frac{\delta}{p}V.$$

la cual es continuamente diferenciable en un dominio $\mathcal{X}$, y satisface i) $J(x) = 0$ para $x = \bar{x}$ y ii) $J(x) > 0$ para todo $x \in \mathcal{X} - \bar{x}$ (véase. Figura 4.4). Evaluando la derivada de $J(\cdot)$ a lo largo de una trayectoria $x(\cdot)$ solución del sistema 4.1, resulta

$$\dot{J}(x(t)) = \frac{\partial J}{\partial x}\dot{x}(t) = V(t)\beta\left(\bar{U} - \frac{\delta c}{p\beta}\right) = V(t)\beta\left(\bar{U} - \mathcal{U}_c\right).$$

De la expresión de $\dot{J}(x(t))$, se destaca que su dependencia con la trayectoria $x(t) = (U(t), I(t), I(t))$ viene dada por $V(t)$. Por ende, independientemente del valor del parámetro $\bar{U}$, $\dot{J}(x(t)) = 0$ para $V(t) \equiv 0$. Entonces para cualquier condición inicial $x(0) \in \mathcal{X}_s$ ($V(0) = I(0) = 0$), resulta que $V(t) = 0$ para todo $t \geq 0$. Por ende, $\dot{J}(x(t)) \equiv 0$ para cualquier $x(0) \in \mathcal{X}_s$, es decir, no solo resulta nula para $x(0) = \bar{x}$, sino para todo $x(0) \in \mathcal{X}_s$. Esto implica que no es cierto que $\dot{J}(x(t)) < 0$ para cada $x \neq \bar{x}$, por lo que puede adelantarse que los puntos de equilibrio del conjunto $\mathcal{X}_s$ (o más particularmente, $\mathcal{X}_s^{st}$) no pueden ser asintóticamente estables.

Por otro lado, para $x(0) \notin \mathcal{X}_s$, vemos que $\dot{J}(x(t))$ es negativa, cero o positiva, dependiendo de si $\bar{U}$ es menor, igual o mayor que $\mathcal{U}_c = \frac{\delta c}{\beta p}$, respectivamente. Nótese que esto se satisface para todo $x(0) \in \mathcal{X}$ y para todo $t \geq 0$. Particularmente, para cualquier punto de equilibrio $\bar{x} \in \mathcal{X}_s^{st}$, vemos que $\dot{J}(x(t)) \leq 0$ (siendo $\dot{J}(x(t)) = 0$ para el caso $\bar{x} = (\bar{U}, 0, 0) = (\mathcal{U}_c, 0, 0)$). Por ende, se puede concluir que cada $\bar{x} \in \mathcal{X}_s^{st}$ es localmente $\epsilon - \delta$ estable. Por otro lado, puesto que $\dot{J}(x(t)) > 0$ para todo $\bar{x} \in \mathcal{X}_s^{un}$, el conjunto $\mathcal{X}_s^{un}$ es inestable (tal como se demostró en la Sección 4.2.2).

Observación 14. *Notese que si $\bar{U} = 0$, es decir, $\bar{x} = (0, 0, 0)$, el funcional anteriormente definido no resulta una función candidata de Lyapunov. Por ende, para estudiar la estabilidad $\epsilon - \delta$ se puede emplear la siguiente función $J(x) = U - I + \delta/pV$. Procediendo de forma análoga, se demuestra que el $\bar{x} = (0, 0, 0)$ es un punto de equilibrio estable para el modelo 4.1.*

Finalmente, puesto que cada estado en $\mathcal{X}_s^{st}$ es localmente $\epsilon - \delta$ estable, y dado que $\mathcal{X}_s^{st}$ es compacto, el conjunto de equilibrio $\mathcal{X}_s^{st}$ resulta locamente estable. Para mas detalle, remitirse a la Sección 2.3.4., Apéndice F.

4.3.2. Atractividad

A continuación, procederemos a caracterizar la atractividad del conjunto de equilibrio, $\mathcal{X}_s$. A diferencia de la prueba de estabilidad, donde la estabilidad de un conjunto compacto puede ser determinada en base a la estabilidad de sus puntos, para el caso de la atractividad, esta no es una condición suficiente. Es decir, dado

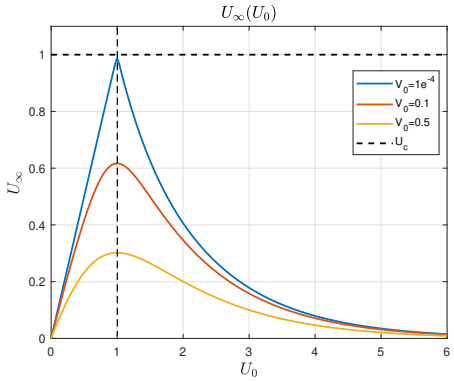

Figura 4.5: Función $U_\infty(U,V)$ para diferentes valores de ϵ, para $U \in [0, U_{\text{máx}}]$, $V = \epsilon$ e $I = 0$. Se destaca que el supremo de U_∞ (dado por $\mathcal{U}_c$) es alcanzado para $U = \mathcal{U}_c$ e $I \to 0$.

un conjunto atractivo (en el sentido de la Definición 6), no necesariamente todo conjunto cerrado contenido en el mismo (por ejemplo, un punto de equilibrio) debe ser atractivo. De hecho, del análisis realizado en la Sección 4.3.1, vemos que los puntos del equilibrio del conjunto $\mathcal{X}_s^{st}$ no son atractivos, aunque como se verá a continuación, $\mathcal{X}_s^{st}$ como conjunto satisface esta propiedad.

Definición 6 (Atractividad local $\mathcal{X}_s$)**.** *Sea el sistema 4.1 restringido por $\mathcal{X}$ y un conjunto $\mathcal{Y} \subseteq \mathcal{X}$. Un conjunto de equilibrio cerrado $\mathcal{X}_s \subset \mathcal{X}$ es atractivo en $\mathcal{Y}$ si $\lim_{t\to\infty} \|\phi(t;x)\|_{\mathcal{X}_s} = 0$ para todo $x \in \mathcal{Y}$. Si $\mathcal{Y}$ es una ε-vecindad de $\mathcal{X}_s$ para algún $\eta > 0$, decimos que $\mathcal{X}_s$ es localmente atractivo.*

Dado un conjunto atractivo, a los fines acotar el conjunto de condiciones iniciales que convergen asintóticamente al mismo, suele especificarse su dominio de atracción (DOA). Es decir, dado conjunto atractivo para el sistema 4.1, se define su DOA al conjunto de estados iniciales x tales que $\|\phi(t;x)\|_{\mathcal{X}_s} \to 0$ conforme $t \to \infty$. Si bien, para el caso presentado puede determinarse de forma analítica el DOA, para la mayoría de las aplicaciones, solo puede obtenerse una estima del mismo (por ejemplo, mediante el uso de curvas de nivel de una función de Lyapunov) [Haddad and Chellaboina, 2008]. Frente a esta situación, suele emplearse el término de región de atracción para denotar cualquier conjunto contenido en el DOA.

Analizando el modelo 4.1 para condición a tiempo infinito resulta

$$U_\infty(\sigma, U(t_0), I(t_0), V(t_0)) = -\frac{W(-\sigma U(t_0) e^{-\sigma(U(t_0)+I(t_0)+\frac{\delta}{p}V(t_0))})}{\sigma}$$

donde $W(\cdot)$ es la rama principal de una función de Lambert y $(U(t_0), I(t_0), V(t_0))$ una condición inicial arbitraria ($t_0 \geq 0$). Sea $\Omega(\epsilon)$ un dominio de $\mathcal{X}$, tal que para cada $\epsilon \geq 0$, viene dado por:

$$\Omega(\varepsilon) = \{(U, I, V) \in \mathcal{X} : I \geq \varepsilon, V \geq \varepsilon\}.$$

Entonces, acorde al (Lemma 2.7., Apéndice F) puede demostrarse, que para cada $\epsilon \geq 0$, la función $U_\infty(\sigma, U, I, V) := -W(-f(U,I,V))/\sigma$, con $f(U,I,V) = \sigma U e^{-\sigma(U+I+\delta/pV)}$ alcanza un máximo en $\Omega(\varepsilon)$ dado por $U_\infty(\mathcal{U}_c, \epsilon, \epsilon)$. En particular, el valor máximo de U_∞ sobre $\Omega(0)$ viene dado por $U_\infty(U^*, 0, 0) = \mathcal{U}_c$, con $\mathcal{U}_c = 1/\sigma$. De esta forma, dada una condición inicial arbitraria, $x(t_0) = (U(t_0), I(t_0), V(t_0))$, vemos que $U_\infty(\sigma, U(t_0), I(t_0), V(t_0)) \in [0, \mathcal{U}_c]$. Basados en este resultado, se puede probar que $\mathcal{X}_s^{st}$ es un conjunto atractivo en $\mathcal{X}$, es decir, que $\lim_{t\to\infty} \|\phi(t;x)\|_{\mathcal{X}_s^{st}} = 0$ para todo $x \in \mathcal{X}$ y valores de σ (véase Sección 2.3.3., Apéndice F). Por otro lado, considerando una condición inicial $(U^*, I(t_0), 0)$, con $I(t_0) \geq 0$, y teniendo en cuenta que $W(\cdot)$ es una función biyectiva, puede demostrarse que para todo $x_s \in \mathcal{X}_s^{st}$ existe un condición inicial $I(t_0) \geq 0$ tal que $(U^*, I(t_0), 0)$ converge a x_s. Por ende, dado que cada punto interior de $\mathcal{X}_s^{st}$ es necesario para su atractividad, el mínimo conjunto atractivo del conjunto de equilibrio, $\mathcal{X}_s$, viene dado por $\mathcal{X}_s^{st}$.

4.3.3. Estabilidad asintótica de $\mathcal{X}_s^{st}$

Finalmente, puesto que $\mathcal{X}_s^{st}$ es (i) el único conjunto $\epsilon - \delta$ estable de $\mathcal{X}_s$ y (ii) además el mínimo conjunto atractivo, resulta que es el *máximo conjunto asintóticamente estable* del modelo 4.1 con un dominio de atracción (DOA) dado por $\mathcal{X} \backslash \mathcal{X}_s^{un}$. Por otro lado, $\mathcal{X}_s^{un}$ es inestable.

4.4. Tratamiento con antivirales

Con el modelo caracterizado, en esta sección, procederemos a analizar el efecto de los antivirales. Como se anticipó en la introducción, los mismos modifican la dinámica del modelo, dependiendo su interacción en el ciclo de vida del virus. En esta sección, estudiaremos el comportamiento transitorio del modelo para infecciones agudas considerando efectividades sub y supracríticas. Además, presentaremos una estrategia de control -basada en el análisis de estabilidad del conjunto de equilibrio $\mathcal{X}_s$- tal que se posibilita, para un esquema de administración de antiviral en tiempo finito, el cumplimiento de objetivos de control relacionados con (i) la prevención de rebrotes de la carga viral al discontinuar el tratamiento y (ii) minimizar el pico de la carga viral.

4.4.1. Efectividad del tratamiento con antivirales

Caracterización de la efectividad

Con la efectividad crítica definida (ver Sección 4.2.3) se procedió a estudiar el comportamiento dinámico del modelo para efectividades supra y subcríticas. Respecto a las primeras, se notó que conforme la efectividad del antiviral se incrementa, la velocidad de descenso de la carga viral es mayor. Esto último contribuye a i) un menor tiempo de infección y ii) a un aumento de las células sanas al final de la infección. Por ende, este tipo de efectividades es compatible con una reducción de los síntomas y del tiempo que el paciente propaga la infección en la población (implicancias epidemiológicas). Por otro lado, para efectividades subcríticas, se denotó la existencia de una tiempo ($t^e < t_V$) tal que para tratamientos iniciados durante intervalos menores a t^e se produce un incremento monotónico del tiempo que el paciente está activo conforme la efectividad tiende por arriba a la crítica. Esto último puede explicarse, dado que para este tipo de efectividades, la dinámica de la propagación del virus experimenta un enaltecimiento, que si bien no es suficiente para producir su decrecimiento, disminuye la tasa de propagación a una relación del orden de magnitud que la tasa de *clearance* del mismo.

Caracterización de la efectividad considerando efectos combinados

En esta instancia se caracterizó una efectividad crítica considerando efectos combinados, es decir, antivirales con más de un blanco en el ciclo de vida de la carga viral. Particularmente, se estudió el efecto en la reproducción (ARNpolimerasa) y en el contagio (receptores de membrana) para distintas efectividades. Se observaron comportamientos dinámicos similares respecto al caso anterior conforme la efectividad combinada tiende a la crítica.

4.4.2. Control óptimo por intervalo simple

A pesar de que la caracterización presentada anteriormente fundó las bases para el estudio de la alteración de la dinámica de una infección mediante un tratamiento (acción de control), tenía como principal limitante que se restringía a tratamientos de duración infinita. Por ende, ante una interrupción del tratamiento, existía un riesgo que se produzca un rebrote de la carga viral (principalmente, en el caso que las células susceptibles al final del tratamiento estuvieran por encima del nivel crítico -equilibrio inestable-). Frente a esta situación, en la siguiente sección, se calcula una acción de control para tratamientos de duración finita, tal que se asegura que una vez discontinuada, el rebrote de la carga viral es evitado.

Tratamiento con antivirales: esquema impulsional

Considerando el modelo 4.1 a lazo cerrado bajo un esquema de administración impulsional de antivirales (ejemplo, toma de pastillas/infusiones intravenosas) [Rivadeneira et al., 2018, Hernandez-Mejia et al.,

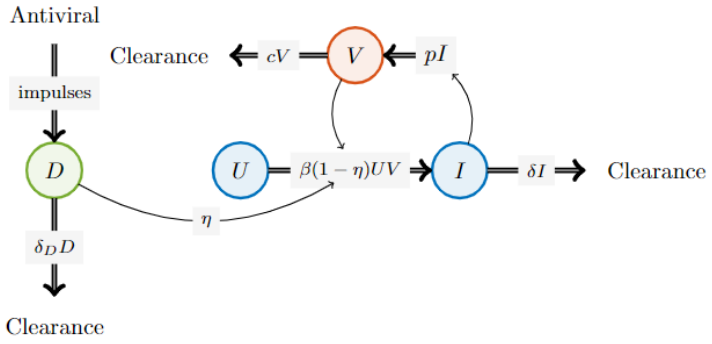

Figura 4.6: Esquema del modelo UIV con tratamiento antiviral

2019], resulta el siguiente sistema de control impulsivo:

$$\dot{U}(t) = -\beta(1-\eta(t))U(t)V(t), \quad t \neq t_k, \tag{4.13a}$$

$$\dot{I}(t) = \beta(1-\eta(t))U(t)V(t) - \delta I(t), \quad t \neq t_k, \tag{4.13b}$$

$$\dot{V}(t) = pI(t) - cV(t), \quad t \neq t_k, \tag{4.13c}$$

$$\dot{D}(t) = -\delta_D D(t), \quad t \neq t_k, \tag{4.13d}$$

$$D(t_k) = D(t_k^-) + u_{k-1}, \quad k \in \mathbb{I} \tag{4.13e}$$

donde $D(t)$ representa la concentración de la droga en el compartimento circundante al órgano blanco, δ_D su tasa de eliminación (o clearance), y u_k la dosis del antiviral en el tiempo $t_k := kT$, con $T > 0$ un intervalo de suministro fijo y $k \in \mathbb{I}$. Notese que t_k^- denota el tiempo justo antes de t_k, es decir, $D(t_k^-) = \lim_{\delta \to 0^+} D(t_k - \delta)$.

Dada la concentración $D(t)$, el efecto de la misma $\eta(t)$ en el ciclo de propagación del virus, se modela por:

$$\eta(t) \quad = \quad \frac{D(t)}{D(t) + EC_{50}} \tag{4.14}$$

siendo EC_{50} la concentración de la droga correspondiente a una efectividad del $50\,\%$ de su máxima efectividad. Se asume que $\eta(t) \in [0, \eta_{\text{máx}})$, con $\eta_{\text{máx}} < 1$. Un diagrama esquemático del modelo propuesto se detalla en la Figura 4.6.

Objetivo de control

Los **objetivos de control** para infecciones agudas pueden ser definidos de distintos tipos. Dado que el pico de la carga viral se encuentra íntimamente ligado con la severidad de la infección y la inefectividad del huésped para neutralizar la infección, es común considerar objetivos tendientes a minimizar el pico. Sin embargo, bajo este tipo de paradigmas, el nivel de células susceptibles al final de la infección podría quedar por encima $\mathcal{U}_c$, por lo que al discontinuar el tratamiento existiría un rebrote de la infección. Frente a este marco contextual, y basados en la caracterización dinámica del modelo, definimos el siguiente objetivo de control:

Definición 7 (Objetivo de control)**.** *Sea el sistema a lazo cerrado 4.13, el objetivo de control consiste en (1) maximizar el valor de las células susceptibles al final de la infección, U_∞, y (2) minimizar el pico de la carga vial, $\hat{V}$. Estos objetivos serán denotados como Objetivo 1 y Objetivo 2, respectivamente.*

Como se enunció en la sección anterior, los antivirales afectan la tasa de infección β mediante el factor tiempo-variante $(1 - \eta(t))$. De esta forma, el número de reproducción (relativo) σ resulta también variante con el tiempo, y viene expresado por

$$\sigma(t) := \frac{\beta(1-\eta(t))p}{c\delta}. \tag{4.15}$$

En este punto, es importantes aclarar, que a lo largo de esta sección denotaremos con, $\sigma(0)$, al número de reproducción (relativo) al inicio de la infección (es decir, correspondiente al caso sin acción terapéutica $u_0 = 0$ y $\eta = 0$). Sea u_k una acción de control de intervalo simple,

$$u_k = u(t_k) = \begin{cases} 0 & \text{for } t_k \in [0, t_i), \\ u_i & \text{for } t_k \in [t_i, t_f], \\ 0 & \text{for } t_k \in (t_f, \infty). \end{cases} \tag{4.16}$$

con $t_i < \hat{t}(\sigma(0))$, siendo $\hat{t}(\sigma(0))$ el tiempo de pico del virus libre $V(\tau)$ (bajo condiciones sin administración de antiviral), $u_i \in [0, u_{\text{máx}}]$ ($u_{\text{máx}}$ máxima dosis admisible) y t_f tiempo (finito) de interrupción del suministro. Se destaca que para tiempos mayores a t_f, $u(t_k) = 0$, por lo que $\eta(t) \to 0$, y consecuentemente $\sigma(t) \to \sigma(0)$.

Por ende, dados los objetivo de control (Definición 7), la meta principal será computar el perfil de tratamiento u_k tal que el mismos puedan ser satisfechos.

Estrategia de control: Objetivo 1

En lo que respecta a este objetivo, en una primera instancia (véase Sección 2.5.1., Apéndice F), se propone una dosis de antiviral $u^g = u^g(t_i)$ (GAD, del inglés, *goldilocks antiviral dose*), tal que si es aplicada para un tiempo $t_i < \hat{t}(\sigma(0))$, el nivel de células susceptibles al final de la infección, $U_\infty(\sigma_n^g, U(t_i), I(t_i), V(t_i)) = \mathcal{U}_c$, con σ_n^g determinado por u^g. Por ende, bajo este esquema de suministro, se logra maximizar el nivel de células susceptibles al final de la infección, sujeto a evitar el rebrote de la infección al interrumpir el tratamiento en el tiempo t_f. Esto último se debe, a que mediante u^g, se guía al sistema en lazo cerrado 4.13 al conjunto de equilibrio estable $\mathcal{X}_s^{st}$ (sin antiviral). Sin embargo, puesto que mediante u^g se logra la convergencia asintótica al conjunto de equilibrio, vemos que t_f resultaría infinito. En vistas de esta situación, y bajo la asunción de un tiempo (finito) de tratamiento, resulta más oportuna la propuesta de un esquema de suministro, u_i (con t_f finito), tal que el estado del sistema $(U(t_f), I(t_f), V(t_f))$ se encuentre arbitrariamente cerca de $(\mathcal{U}_c, 0, 0)$. Puesto que bajo este escenario, el sistema 4.13 alcanzaría una condición de quasi-estado estacionario (QSS, del inglés, *quasi-stationary state*) [1] al final del tratamiento, se denomina a tal esquema terapéutico *esquema de tratamiento quasi-óptimo de intervalo simple*. Para más detalle, en (Sección 5.1., Apéndice F) se contrastan esquemas terapéuticos respecto a este último, tal que a) $(U(t_f), I(t_f), V(t_f))$ en condición QSS y $U(t_f) < \mathcal{U}_c$, b) $(U(t_f), I(t_f), V(t_f))$ en condición QSS y $U(t_f) > \mathcal{U}_c$, y c) $(U(t_f), I(t_f), V(t_f))$ no alcanza condición QSS (interrupción temprana del tratamiento, t_f reducido).

Estrategia de control: Objetivo 2

En lo que respecta al Objetivo 2, puesto que el área bajo la curva de la carga viral $AUC_V := \int_{t_i}^{t_f} V(t)dt \approx \frac{1}{c}[\frac{p}{\delta}(U(t_i) - U(t_f))]$, vemos que para un mismo nivel $U(t_f)$, dependiendo del esquema de suministro durante el intervalo $[t_i, t_f]$, podrían obtenerse múltiples comportamientos transitorios. Esto da cuenta que el Objetivo 1 puede ser independiente del Objetivo 2 (principalmente al emplear acciones de control de intervalo múltiple, Sección 5.2., Apéndice F). Por otro lado, es importante aclarar, que para el caso de una acción de control de intervalo simple, el pico de la carga viral $V(\hat{t_v})$ se encuentra biunívocamente relacionado con $U(t_f)$ (Apéndice E), por lo que cumplimiento del Objetivo 1, $U(t_f) = \mathcal{U}_c$, restringe el cumplimiento del Objetivo 2 a un $V(\hat{t_v})$ en concordancia con $U(t_f) = \mathcal{U}_c$.

4.5. Resultados de simulación

A los fines de tener un mayor grado de comprensión de los conceptos presentados a lo largo del capítulo, a continuación se presentan ensayos de simulación considerando el modelo UIV con parámetros identificados de pacientes COVID-19 (para mayores precisiones referirse a los Apéndices D, E y F).

[1] Dado un sistema dinámico con escalas temporales rápidas y lentas, se dice que el mismo se encuentra en una condición de quasi-estado estacionario (QSS), cuando puede asumirse que la dinámica rápida está en condición de estado estacionaria respecto a la lenta (aunque esta última se encuentre en fase transitoria) [Kokotović et al., 1999]

4.5.1. Comportamiento dinámico: pacientes SARS-CoV-2

De la Figura 4.7, se observa que el estado $U(t)$ converge al conjunto $\mathcal{X}_s^{st}$, aunque resultados variados son obtenidos para los distintos pacientes. De hecho, puede advertirse que el nivel de células susceptibles al final de la infección U_∞ se encuentra reducido para pacientes con elevado número de reproducción $\mathcal{R}_0$ (independientemente que en todos los casos, se asume el mismo nivel de células susceptibles al inicio de la infección U_0). Esto puede ser explicado por el hecho que $W(\mathcal{R}_0 e^{-\mathcal{R}_0})$ es una función monotónicamente decreciente con $\mathcal{R}_0 > 1$, y en consecuencia, $0 < U_\infty(\mathcal{R}_{01}) < U_\infty(\mathcal{R}_{02})$ para $\mathcal{R}_{01} > \mathcal{R}_{02} > 1$ (Sección 5., Apéndice D).

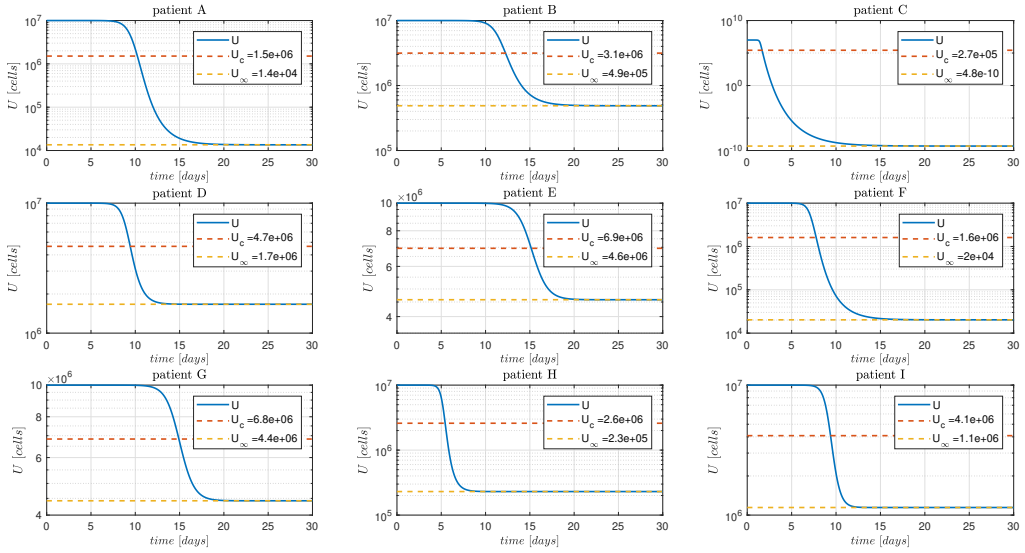

Figura 4.7: Evolución dinámica de células susceptibles para modelo UIV identificado con datos de 9 pacientes COVID-19 [Wölfel et al., 2020].

4.5.2. Tratamiento con efectividades sub y supracríticas

En este caso, la Figura 4.8 muestra la evolución de la carga viral (simulada) correspondiente a 9 pacientes COVID-19, cuando el tratamiento es iniciado al momento de detección (PCR positivo) ($t_{tr} = t_{DL}$, siendo t_{DL} el tiempo en que la carga viral $V(t_{DL}) = 100$ copias/mL). Puesto que $\hat{t}_V < t_{tr} < t^e < \hat{t}_V$ ($0{,}3\hat{t}_V \approx 0{,}40t^e$), el sistema se encuentra bajo las hipótesis del Teorema 3.1. (véase Sección 3., Apéndice E). De esta forma, se visualiza que para efectividades superiores a la crítica ($\eta_p > \eta_p^c(t_{tr})$) se produce un decremento de la carga viral al momento del inicio del tratamiento. Además, conforme $\eta_p \to \eta_p^c(t_{tr})$ el tiempo de duración de la infección experimenta un incremento (producto de enaltecimiento de la propagación del virus). Por otro lado, para efectividades ($\eta_p < \eta_p^c(t_{tr})$) vemos que si bien, el tiempo de pico se reduce, la amplitud de la carga viral aumenta, por lo que es esperable una mayor severidad de la infección (para más detalle, remitirse a la Sección 5., Apéndice E).

4.5.3. Control óptimo por intervalo simple

Finalmente, de la Figura 4.9, se observa el esquema de tratamiento considerando una acción de control quasi-óptima. Se destaca que el nivel de células suscpetibles al final de la infección alcanza una condición QSS ($U(t_f) \approx \mathcal{U}_c = 1/\sigma(0)$). Por ende, al discontinuar el tratamiento ($t_f = 30$ h), se evita el rebrote de la carga viral (véase Sección 6.3, Apéndice F).

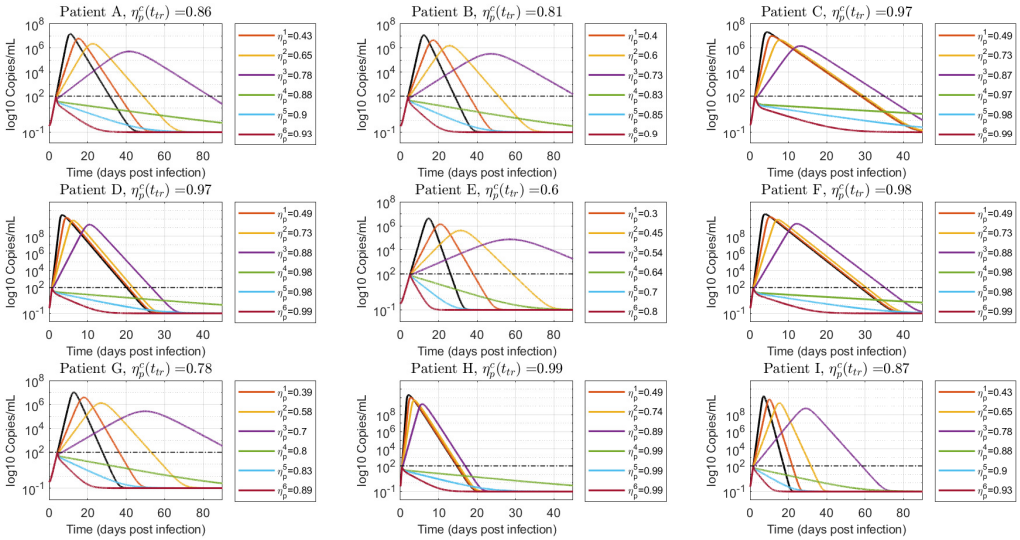

Figura 4.8: Evolución de la carga viral cuando el tratamiento es iniciado en ($t_{tr} = t_{DL}$) para distintas efectividades η_p (en línea negra se denota el caso no tratado).

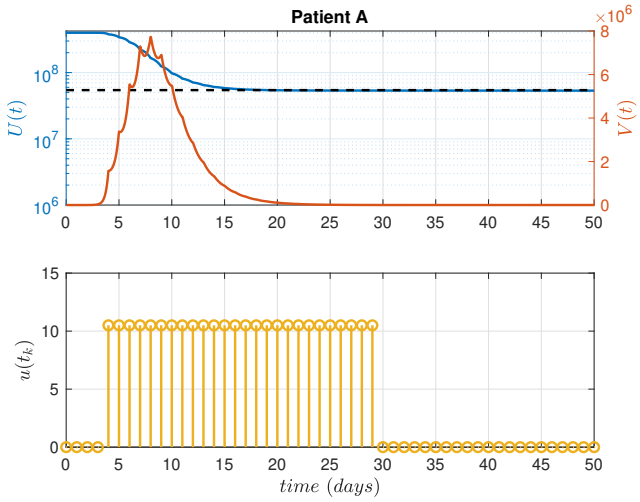

Figura 4.9: Evolución de carga viral para el paciente A, con $u_i = u^g = 10{,}5$ mg de antiviral (esquema de tramiento quasi-óptimo por intervalo simple).

Capítulo 5

Conclusiones

La propuesta de estrategias de control y estimación en sistemas biomédicos conlleva un análisis dinámico del modelo a emplear a los fines de determinar la controlabilidad, identificabilidad y observabilidad del mismo. A lo largo de esta tesis, tales aspectos fueron estudiados, tomando como ejemplos particulares el caso del suministro de insulina en diabéticos tipo 1 y la caracterización de un modelo dinámico para la descripción de infecciones virales. Respecto a los objetivos particulares, se pueden discutir los siguientes resultados:

- En lo que respecta al objetivo particular 1, se pudo vislumbrar la importancia del análisis de modelos dinámicos de la relación glucosa-insulina previo a intentar controlarlos. Por otro lado, los mismos pudieron ser identificados y relacionados estructuralmente con modelos máximos usualmente empleados en la bibliografía para la representación de pacientes diabéticos tipo 1.

- En lo que respecta al objetivo particular 2, se logró efectuar el control mediante un controlador pulsátil por zonas, observándose la factibilidad de emplear equilibrios generalizados como objetivos de control. Se formularon observadores de perturbación para la compensación de diferencias paciente-modelo, denotándose que los mismos posibilitan una estima de los estados relacionados a perturbaciones exógenas no modeladas.

- En lo que respecta al objetivo particular 3, se formuló una restricción para la insulina a bordo tiempo-variante, la cual dada un evento de comida combina un perfil exponencial con un perfil constante, lo cual incrementa la controlabilidad del sistema. Para este tipo de restricción se propuso un versión adaptativa. Puesto que tanto el empleo del costo asimétrico y la restricción pueden interpretarse como estrategias de mitigación de riesgos, como trabajos futuros, sería oportuno extender la propuesta de otro tipo de estrategias de mitigación de riesgos. De hecho, sería conveniente extender el diseño considerando controladores tolerante a fallas.

- Respecto al objetivo particular 4, mediante el uso de trayectorias basales como objetivos de control, se logró extender la formulaciones al caso de variaciones circadianas en la sensibilidad a la insulina. Esto posibilitó: a) mejorar la performance en entornos con variabilidad periódica respecto a formulaciones con modelos LTI -adecuando los suministros de insulina acorde a la franja horaria-, b) brindar garantías de convergencia asintótica a trayectorias basales alcanzables (seguridad) e c) incrementar el dominio de atracción del sistema a lazo cerrado (lo que posibilita preservar la factibilidad del problema frente a modos de falla que puedan poner el sistema fuera de su dominio de atracción, ej. comidas no anunciadas, desconexión guía suministro). Respecto a esto último, actualmente se están formulando invariantes de tracking para sistemas periódicos, lo que posibilitaría relajar el requerimiento del alcanzar una trayectoria basal terminal (ej. de utilidad en entornos perturbados).

- En lo que confiere al objetivo particular 5, se caracterizó el conjunto de equilibrio para un modelo de infecciones agudas, demostrándose la estabilidad asintótica de un subconjunto de éste. Como trabajos futuros sería oportuno caracterizar tales modelos considerando efectos inmunológicos de forma explícita.

- En lo que respecta al objetivo particular 6, extendimos el concepto de efectividad crítica al caso dinámico, demostrándose la existencia de una efectividad crítica para modelos de infecciones agudas.

Además se formalizó la existencia de un tiempo temprano tal que se cumple el crecimiento monotónico de la duración de la infección.

- Respecto al objetivo particular 7, se formuló un perfil de suministro de la insulina por intervalo simple que maximiza la concentración de células susceptibles al final de la infección (evitando rebrote de esta al discontinuar el tratamiento). Dado que este esquema de infusión limita la minimización del pico de la carga viral, como trabajos futuros resultaría pertinente explorar acciones de control por intervalo múltiple.

Capítulo 6

Contribuciones

6.1. Paper A

En este trabajo se presenta una formulación de MPC pulsátil con garantía de estabilidad para el control glucémico de pacientes diabéticos, tanto en configuraciones (i) *híbridas* (anuncio de comida de modo feedforward), como (ii) *full closed-loop* (lazo cerrado puro, sin anuncio de comidas). Como modelo de predicción, se emplea un modelo de largo término el cual surge de suposiciones de linealidad y análisis de estado quasi-estacionario (QSS) para el modelo de Bergman extendido (ej. modelo de Bergman con subsistemas de comidas e insulina subcutánea). Además, como rutina de identificación, debido a limitantes de identificabilidad práctica del modelo, se realiza una regularización de la función objetivo basada en información 'a-priori' de los parámetros a estimar (los cuales se pueden vincular explícitamente con herramientas de soporte al FIT -conocidas para el paciente en cuestión). Por otro lado, debido a diferencias planta-modelo, se formuló un observador de perturbación con restricciones de positividad, tanto para compensación de offset de salida como para compensación del error/no aviso en la ingesta de carbohidratos. Finalmente, empelando un MPC estable por zonas bajo suministro pulsátil, se procedió a valorar el desempeño de la estrategia frente a distintas condiciones en el aviso de comida (sin error/con error/no aviso) y contemplando variaciones paramétricas de la sensibilidad a la insulina. Esta línea de investigación fue presentada en [Godoy et al., 2018a, Godoy et al., 2018b, Abuin et al., 2019], dando lugar a las siguientes publicaciones [Rivadeneira et al., 2019, Abuin et al., 2020b].

6.2. Paper B

En este trabajo [Abuin et al., 2023], se presenta una versión mejorada de la propuesta previa. Se incluyen dos novedades principales, (i) una restricción de insulina a bordo (IOB) variante en el tiempo, que promueve la administración de insulina distinta de cero después de una infusión de bolo estándar (aumentando la controlabilidad del sistema durante períodos posprandiales) y (ii) una versión con restricciones suaves del controlador con garantías de estabilidad. Se propone además, un método para configurar la restricción basado en información de conteo de carbohidratos, y se proporciona un algoritmo de ajuste de la amplitud de la restricción acorde a información de la tasa de cambio de la glucemia.

6.3. Paper C

Dado que para el sistema analizado, bajo variaciones temporales en la sensibilidad a la insulina, no existiría una infusión basal admisible tal que el sistema permanezca en un equilibrio para todo tiempo, se propone una extensión del conjunto invariante objetivo mediante una secuencia de conjuntos invariantes. Motivados por la periodicidad de la variación circadiana de la sensibilidad a la insulina, se optó por emplear trayectorias basales periódicas como conjunto objetivo. En base a esta hipótesis de trabajo, resultó natural extender el problema de control a una estrategia de control predictivo para seguimiento de trayectorias. En este punto, se optó por emplear dos versiones de MPC para seguimiento de trayectoria, donde en ambos casos se computa una trayectoria objetivo periódica (factible), aunque en solo una se la emplea como variable de decisión durante la ejecución del controlado, incrementando de esta forma el dominio de atracción.

Se destaca que esta formulación también puede operar con modelos invariantes en el tiempo (LTI), conservando las garantías, y de hecho para este caso, respecto a MPCs para tracking se logra un incremento del dominio de atracción significativo. Como otra contribución de la línea de trabajo, se propuso una estrategia de estimación de parámetros offline (semi-paramétrica) para modelo variante en tiempo (LTV) basada en un condicionamiento del parámetro que determina la sensibilidad a la insulina, con una regularización del costo acorde a información 'a-priori' (ej. pseudo-periodicidad, restricción de constante a tramos, valores factibles/uso de información a priori relacionada a herramientas FIT). Es importante aclarar que debido a la característica estable de estos sistemas, y teniendo en cuenta que la perturbación (comidas) es asintóticamente convergente al cero, se pueden relajar las restricciones terminales, aumentando de este modo el dominio de atracción del lazo cerrado (sin perder garantía de estabilidad y factibilidad recursiva). Un primer abordaje al problema de variaciones circadianas, siguiendo la estrategia de referencias variante en el tiempo, fue presentado en [Abuin et al., 2020c]. Por otro lado, una versión actualizada de la línea de trabajo, fue presentada en el congreso de IFAC2022 [Abuin et al., 2022b], y actualmente, está en preparación un trabajo [Abuin et al., 2022c] para ser enviado a una revista especializada.

6.4. Paper D

En este trabajo se abordó la caracterización dinámica, tanto en estado estacionario como en condiciones transitorias, de un modelo compartimental "in-host" para infecciones agudas limitado por células. Puesto que del análisis de estado estacionario se vislumbró la existencia de un conjunto de equilibrio sano, en lugar de equilibrios aislados (sanos y enfermos), se optó por realizar el análisis de estabilidad en base a conjuntos. Se detectaron dos subconjuntos de equilibrio (estable e inestable) dependiendo de si el nivel inicial de células susceptibles se encontraba por encima o por debajo de un umbral crítico, el cual es un valor fijo, solo dependiente de los parámetros del modelo. Para el subconjunto estable, debido a la imposibilidad de caracterizarlo mediante método indirecto de Lyapunov (existe un autovalor nulo), se optó por proponer una función de Lyapunov (utilizada en modelos epidemiológicos), demostrando la estabilidad de cada punto de equilibrio del conjunto. En este ítem, es importante aclarar, que debido a la compacidad del conjunto, se pudo inferir la estabilidad (épsilon-delta) del conjunto en base a la mera estabilidad (épsilon-delta) de puntos de equilibrio pertenecientes al mismo. Por otro lado, mediante el uso de funciones de Lambert, fue posible demostrar la atractividad del conjunto de equilibrio, y más aún, la existencia de un mínimo conjunto atractivo, que de hecho, es coincidente con el subconjunto de equilibrio estable. De esta forma, se pudo concluir que el subconjunto de equilibrio estable es a la vez el único conjunto asintóticamente estable del modelo en cuestión (estabilidad), lo que permite interpretar que una vez iniciada a la infección (independientemente del número de reproducción), el nivel de células susceptibles concluida la infección convergerá asintóticamente a este subconjunto de forma global. Además, se incluyó un análisis de la evolución de la carga viral, demostrando que aún para ciertas combinaciones de los parámetros el virus podría no propagarse, y se obtuvieron condiciones para que esto ocurra. Los trabajos [Abuin et al., 2020a] y [Pérez et al., 2022] se corresponden con resultados de esta línea de investigación.

6.5. Paper E

En esta línea de trabajo, aprovechando la caracterización dinámica del modelo para infecciones agudas, se procedió a evaluar la existencia de una efectividad crítica, $\eta^c(t_{tr})$, dependiente del tiempo de tratamiento (t_{tr}). Empleando un modelo aproximado (previo análisis QSS, bajo el supuesto que la tasa de clearance del virus libre (c) es significativamente mayor que la tasa de muerte de células infectadas (δ)) se demostró que para efectividades supracríticas, $\eta(t_{tr}) > \eta^c(t_{tr})$, la carga viral es estrictamente decreciente, alcanzado su valor máximo en t_{tr}. Más aún, se evidenció un aumento monotónico de la tasa de decrecimiento del virus libre conforme $\eta(t_{tr})$ tiende a la máxima efectividad admisible. Por otro lado, para efectividades subcríticas, $\eta(t_{tr}) < \eta^c(t_{tr})$, y bajo supuesto de $t_{tr} \leq t^e < \hat{t}_V$ (siendo t^e una cota para el tiempo de inicio de tratamiento y $\hat{t}_V$ el tiempo de pico del virus libre sin tratamiento) se reportó un aumento del tiempo de pico con tratamiento, $\hat{t}_{V,t_{tr}} > \hat{t}_V$, conforme $\eta(tr)$ tiende a $\eta^c(t_{tr})$ por defecto. En este punto, es importante aclarar, que si bien (i) el tiempo detección de carga viral es más prolongado respecto al caso no tratado -lo que tendría implicancias epidemiológicas, requiriendo un mayor tiempo de aislamiento del paciente tratado-; (ii) el pico de la carga viral y la fracción de células infectadas al final de la infección (indicador de

severidad) son menores, lo que da indicios de un compromiso entre objetivos contrapuestos (i) y (ii) para efectividades subcríticas. El artículo [Abuin et al., 2021] corresponde a esta línea de trabajo.

6.6. Paper F

En este trabajo, se formalizó la caracterización del conjunto de equilibrio para el modelo de infecciones agudas limitadas por células. Además, del análisis del modelo, se formularon objetivos de control orientados a 1) maximizar el nivel de células susceptibles al final de la infección, U_∞, y 2) minimizar el pico de la carga viral $\hat{V}$. Posteriormente, y bajo la consideración de dinámicas impulsionales, se idearon acciones de control por intervalo simple orientadas al cumplimiento de tales objetivos, sujeto a evitar el rebrote de la infección al discontinuar el tratamiento. Respecto al objetivo 1, se estudió la existencia de una (única) dosis de antiviral (denominada *goldilock antiviral dose*) tal que se evita el repunte de la carga viral, discontinuado el tratamiento, y se maximiza la disponibilidad de células susceptibles al final de la infección. Respecto al Objetivo 2, previo análisis del área bajo la curva de la carga viral, pudo concluirse que para esquemas de infusión por intervalo múltiple, resulta independiente del Objetivo 1.

Apéndice A

Artificial pancreas under stable pulsatile MPC: improving the closed-loop performance

Artificial pancreas under stable pulsatile MPC: improving the closed-loop performance.

P. Abuin[a], P. S. Rivadeneira[b], A. Ferramosca[c], A. H. González[a]

[a]*Institute of Technological Development for the Chemical Industry (INTEC), CONICET-Universidad Nacional del Litoral, Güemes 3450, (3000), Santa Fe, Argentina*
[b]*Universidad Nacional de Colombia, Facultad de Minas, Cra. 80#65-224, Medellín, Colombia.*
[c]*CONICET, UTN - Facultad Regional de Reconquista, 27 de Abril 1000 (3560), Reconquista, Argentina.*

Abstract

This work presents a pulsatile Zone Model Predictive Control (pZMPC) for the control of blood glucose concentration (BGC) in patients with Type 1 Diabetes Mellitus (T1DM). The main novelties of the algorithm - in contrast to other existing strategies - are: (i) it controls the patient glycemia by injecting short duration insulin boluses for both, the basal and bolus infusions, in an unified manner, (ii) it performs the predictions and estimations (critical to anticipate both, hypo and hyperglycemia) based on a physiological individualized long-term model, (iii) it employs disturbance observers to compensate plant-model mismatches, (iv) it ensures, under standard assumptions, closed-loop stability, and (v) it can be used - under minor modifications -as an optimal basal-bolus calculator to emulate conventional therapies. Because of the latter characteristic, a significantly better performance is achieved, not only in terms of classical indexes (time in the normoglycemia zone, avoidance of hypoglycemia in the short term, avoidance of hyperglycemia in the long term) but also in terms of its applicability (use of the pump or injections). Such a performance is tested in a cohort of in-silico patients from the FDA-accepted UVA/Padova simulation platform, considering the most challenging scenarios.

Keywords: Pulsatile Control, Hybrid Control, Model Predictive Control, Artificial Pancreas, Insulin Functional Therapy, Stability.

1. Introduction

Type 1 Diabetes Mellitus (T1DM) is a chronic disease, affecting approximately 42 million people around the world (10-15% of all diabetes cases) [1]. It is characterized by a destruction of pancreatic β cells due to an auto-immune response (T1DMa, 70-90% cases) or idiopathic causes (T1DMb) [2] leading to a complete deficiency of endogenous insulin production, thus resulting in higher blood glucose (BG) levels (fasting BG: $> 126\ mg/dL$, postprandial BG (2hs): $\geq 200\ mg/dL$) [3].

In order to restore euglycemia levels (fasting BG: $80 - 130\ mg/dL$, peak postprandial BG (2hs): $< 180\ mg/dL$)[4] the functional insulin treatment (FIT) was proposed as therapeutic way to administer exogenous insulin injections, imitating healthy secretion patterns. This way, a basal insulin is delivered to keep glycemia flat during fasting periods, while a bolus insulin is delivered to counteract postprandial hyperglycemia or bring high glucose levels back to target. Although these doses can be estimated with FIT support tools (i.e., correction factor (CF), insulin to carbs ratio (CR), duration of insulin action (DIA)) [5] according to BG readings and carb counting values, T1DM patients still need to estimate and administrate insulin by itself, which inherently entails risks, as hypoglycemic and hyperglycemic episodes (due to over/under estimation of meal intake, unpredicted physiological variabilities, among others) [6].

Facing this situation, the automatic insulin delivery based on glycemia measurement (artificial pancreas, AP) was proposed as a way to implement FIT in a closed-loop manner [7]. Basically, it is a medical equipment composed of a continuous glucose monitoring (CGM) sensor, an insulin

*Corresponding author: pabloabu.g@gmail.com

pump (CSII) and a control algorithm which, based on CGM readings, adjusts the insulin delivery in order to maintain blood glucose concentration in normoglycemia levels. Relying on user interaction requirements (i.e., meal announcements, meal boluses, hypoglycemia treatments, patient-specified correction boluses), APs are classified as hybrid closed-loop (HCL) systems or fully automated closed-loop (FCL) systems [8], being the former dependent on manual user inputs to compensate meals or exercise, while the latter gives corrections insulin doses autonomously.

Multiple control algorithms have been proposed for current AP systems, including Proportional-Integral-Derivative (PID) [9], Fuzzy-Logic [10] and Model Predictive Control (MPC) [11]. Of these strategies, MPCs has shown to be the most promissory one, because of its ability to anticipate undesired glucose excursion and to compute the insulin dosage fulfilling variable constraints (positivity and maximum constraints). Furthermore, MPC can include, without further complexities, meal digestion dynamics, insulin absorption delays, glucose-insulin dynamics and physical exercise effect by considering the corresponding mathematical prediction model [12]. Many version of MPCs has been implemented in AP systems. They can be classified as [13]: unconstrained MPC [14], multiple-model adaptive MPC [15], zone MPC [16], set-point-based enhanced MPC (eMPC) [17], adaptive MPC [18, 19], bi-hormonal MPC [20] and policy-based stochastic MPC [21, 22]. These strategies were tested under in-silico simulators (UVA/Padova [23], Cambridge [24], Medtronic Virtual Patient [25]) and also, under in-vivo clinical trials.

Most of the MPCs assume a continuous and constant infusion delivery $u(t)[U/min]$ over the time interval between samples (referred as zero-order hold, ZOH, assumption) in spite of the fact that pulsatile injections have shown to be preferable in many senses. On one hand, pumps administer insulin by means of micro boluses [26, 27]; that is, discrete time micro-infusions distributed along the sampling time interval, which are comparable to pulsatile injections. On the other hand, the use of pulses has several physiological benefits (in fact, the healthy pancreas segregates insulin in such a way, every $5-10\ min$, [28, 29]). Studies have shown both, experimentally [6, 5, 30] and theoretically [31, 32], that a better postprandial control is achieved by shot boluses, especially in the case of meals with high glycemic index (HGI). Moreover, a pulsatile insulin delivery suppresses more effectively the hepatic glucose release, as stated in [29, 33].

According to the latter discussion, the objective of this article is to control the glycemia only by insulin pulses, employing a physiological individualized long-term minimal model of glucose-insulin evolution [34], and a pulsatile Zone Model Predictive Controller (pZMPC) based on the use of artificial optimization variables. This approach shows a number of benefits (in contrast to standard zone MPCs) and guarantees, under full state information and non-persistent disturbance assumptions, recursive feasibility and stability of the closed-loop [35, 36]. Furthermore, given that the model describes T1DM glycemia evolution under fasting and prandial conditions, the controller administers both, the basal and postprandial infusions simultaneously (opposite to what is done in all the cited AP controllers). This way, the controllable/stabilizable set of the (positively constrained) system is drastically enlarged, given that when hypoglycemia is predicted (not just seen, but anticipated by the model), the controller is able to quickly suspend the basal insulin infusion. Moreover, this infusion mode permits a super-bolus scheme of administration [5]; that is, an increment in the meals correction bolus while the basal insulin rate is temporarily suspended. This infusion scheme, indeed, shows a better postprandial glycemic control than the conventional ones, mainly due to an increase in the rate of insulin absorption speed [30].

Regarding the meals, even though MPC-based AP is naturally robust to bad announced meals, studies have revealed that its performance is significantly degraded when the size of meals increases [37]. To deal with this condition, two augmented double-integrator observers are proposed to have an offset-free behavior under both, partially-announced and unannounced meals scenarios, as well as to cope with moderate plant-model uncertainties. This way, the proposed controller avoids the need of additional meal detection/estimation algorithms [38]. The general control loop proposed in this work is depicted in Figure 1, where it can be seen that no additional blocks, such as safety algorithms, boluses corrections, basal corrections, etc., are utilized.

The outline of the paper is as follows. After the introduction of Section 1, Section 2 presents the details of glucose-insulin long-term model, including compartment description and parameter estimation strategy. Later, in Section 3, the relative discretization schemes are formulated in order to get a pulsatile representation of glucose-insulin model, useful for pulse control. In Section 4, the state observer using an augmented double integrator model is formulated; while in

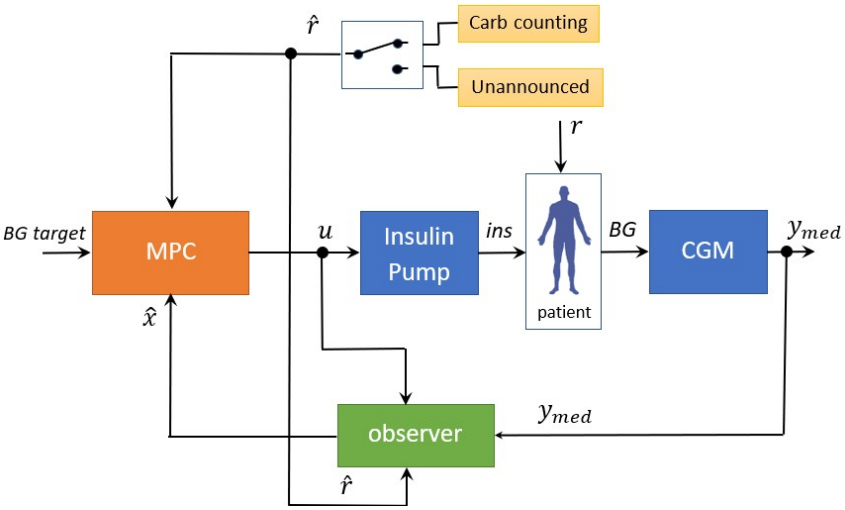

Figure 1: Control Scheme. The control objective is to maintain the blood glucose (BG) in a safety range (BG target) by manipulating the pulsatile insulin (u) injected to the patient by means of a pump. The blood glucose is measured by a CGM while the meal intake (r) can be (or not) announced by means of meal signal $\hat{r}$ (carb counting associated with meal r or $\hat{r} \equiv 0$ in case of unannounced meal scenario). An observer is used to estimate the current model states $\hat{x}$, based on the CGM signal y_{med}, the insulin infusion rate u and the meal signal $\hat{r}$.

Section 5 the pulsatile zone MPC is described including the use of artificial variables and terminal cost to ensure asymptotic stability. Later, in Section 6, an optimal basal-bolus calculator based on an event-triggered formulation is presented. Then, in Section 7 in-silico trials are presented considering announced and unannounced meals scenarios, and a comparison with conventional FIT strategy is done to evaluate the potential advantages of an optimal bolus administration scheme. Finally, in Section 8 some concluding remarks are given.

2. Blood glucose-insulin model

Blood glucose-insulin models can be physiological or data-driven [39, 40]. The former are usually based on a compartmental representation [41, 24, 42], while the latter ones normally rely on time-series approaches [43, 44]. Although both kinds of approaches have been used for control-oriented models [45, 44, 43], physiological-based models are preferable due to their inherent descriptive ability and parameter interpretability. In this work a physiological long-term minimal model based on Ruan proposal [34] is selected as the control-oriented model to be used for both, the state estimator and the pZMPC.

2.1. Glucose Dynamics

The glycemia evolution is described by a single compartment:

$$\frac{dG(t)}{dt} = \theta_0 - \theta_1 G(t) - \theta_2 Q_i(t) + \theta_3 Q_g(t) \tag{1}$$

where $G(t)$ is the blood glucose concentration $[mg/dL]$, $Q_i(t)$ is the insulin delivery rate in plasma $[U/min]$ and $Q_g(t)$ represents the rate of carbohydrate absorption from the gut $[g/min]$. Furthermore, θ_2 is the insulin sensitivity $[mg/(dL \cdot U)]$ and θ_3 is the carbohydrate factor $[mg/(dL \cdot g)]$, being the rate of glucose appearance in plasma $Ra(t) = \theta_3 Q_g(t) [mg/(dL \cdot min)]$. In contrast to Bergman model [42, 46], equation (1) considers the insulin action on glucose consumption independent of the glycemia level (as proposed in [47, 34]). Moreover, θ_0 is the endogenous glucose production (EGP) at basal levels EGP_b ($\theta_0 = \theta_1 G_b + \theta_2 U_b$, being G_b and U_b the glucose and insulin basal rates, respectively) $[mg/(dL \cdot min)]$ while θ_1 is the glucose effectiveness $[/min]$ or glucose self-regulation effect to promote its own metabolism (i.e. stimulating glucose uptake by peripheral tissues and suppressing hepatic glucose release) [48].

Remark 1. *Note that the FIT tools can be easily derived from equation 1. The correction factor (or insulin sensitivity factor) $CF = \theta_2[mg/(dL \cdot U)]$, the raise factor (or carbohydrate factor) $RF = \theta_3[mg/(dL \cdot g)]$, the carbohydrate-to-insulin ratio (or the number of carbohydrates covered by 1 unit of insulin) $CR = CF/RF = \theta_2/\theta_3[g/U]$ and the insulin basal rate $U_b = (\theta_0 - \theta_1 G_b)/\theta_2[U/min]$.*

2.2. Insulin Absorption Subsystem

The insulin absorption subsystem represents the insulin pharmacokinetics with the subcutaneous and blood compartments [47, 34, 49]:

$$\begin{aligned} \frac{dQ_i(t)}{dt} &= -\frac{1}{\theta_4}Q_i(t) + \frac{1}{\theta_4}Q_{i_{sub}}(t), \\ \frac{dQ_{i_{sub}}(t)}{dt} &= -\frac{1}{\theta_4}Q_{i_{sub}}(t) + \frac{1}{\theta_4}u(t) \end{aligned} \tag{2}$$

where $Q_{i_{sub}}(t)$ stands for the insulin delivery rate in the subcutaneous compartment $[U/min]$, θ_4 is the time constant (or time-to-maximum effective insulin concentration)$[min]$ and $u(t)$ is the insulin infusion rate (bolus and basal) $[U/min]$. Moreover, the insulin on board (IOB) $[U]$ (the amount of insulin remaining in the body from previous insulin boluses), can be expressed as $IOB(t) = \int_0^t (u(\tau) - Q_i(\tau))\, d\tau$ where $Q_i(\tau)$ is the plasma insulin infusion rate consumed by insulin-dependent tissues and $[0, t]$ the interval where insulin boluses were administrated . Since $u(\tau) - Q_i(\tau) = \theta_4(\dot{Q}_i + \dot{Q}_{i_{sub}})$ (from (2)) and assuming initial conditions equal to zero ($u(0) = 0, Q_i(0) = 0$), the IOB becomes $IOB(t) = \theta_4(Q_i(t) + Q_{i_{sub}}(t))$, which is the expression used hereafter for IOB estimation.

2.3. Meals Absorption Subsystem

The meal absorption subsystem describes the meal-glucose absorption from the stomach to the gut by a two compartmental model [15, 47]:

$$\begin{aligned} \frac{dQ_g(t)}{dt} &= -\frac{1}{\theta_5}Q_g(t) + \frac{1}{\theta_5}Q_{sto}(t), \\ \frac{dQ_{sto}(t)}{dt} &= -\frac{1}{\theta_5}Q_{sto}(t) + \frac{1}{\theta_5}r(t) \end{aligned} \tag{3}$$

where Q_{sto} stands for the glucose delivery rate from the stomach $[g/min]$, θ_5 is the time constant (or time-of-maximum appearance rate of glucose in gut $Q_g(t))[min]$ and $r(t)$ is the rate of oral ingested carbohydrates $[g/min]$.

2.4. Affine state space model

According to control purposes, the following affine continuous-time state space model is considered:

$$\begin{aligned} \dot{x}(t) &= Ax(t) + B_u u(t) + B_r r(t) + E, \;\; x(0) = x_0, \\ y(t) &= Cx(t), \end{aligned} \tag{4}$$

where $x(t) = [x_1(t) \;\; x_2(t) \;\; x_3(t) \;\; x_4(t) \;\; x_5(t)]'$, with $x_1 = G$, $x_2 = Q_i$, $x_3 = Q_{i_{sub}}$, $x_4 = Q_g$ and $x_5 = Q_{sto}$. The output $y(t)$ is given by the state component x_1, i.e., the glycemia to be controlled. As before, $u(t)$ is the insulin infusion $[U/min]$ and $r(t)$ is the rate of carbohydrate (CHO) intake $[g/min]$. E is a constant matrix (affine term) accounting for the basal steady-state endogenous glucose production (θ_0). The model matrices are given by:

$$A = \begin{pmatrix} -\theta_1 & -\theta_2 & 0 & \theta_3 & 0 \\ 0 & -\frac{1}{\theta_4} & \frac{1}{\theta_4} & 0 & 0 \\ 0 & 0 & -\frac{1}{\theta_4} & 0 & 0 \\ 0 & 0 & 0 & -\frac{1}{\theta_5} & \frac{1}{\theta_5} \\ 0 & 0 & 0 & 0 & -\frac{1}{\theta_5} \end{pmatrix}, \; B_u = \begin{pmatrix} 0 \\ 0 \\ \frac{1}{\theta_4} \\ 0 \\ 0 \end{pmatrix}, \; B_r = \begin{pmatrix} 0 \\ 0 \\ 0 \\ 0 \\ \frac{1}{\theta_5} \end{pmatrix}, \; E = \begin{pmatrix} \theta_0 \\ 0 \\ 0 \\ 0 \\ 0 \end{pmatrix}, \; C = \begin{pmatrix} 1 \\ 0 \\ 0 \\ 0 \\ 0 \end{pmatrix}'. \tag{5}$$

Constraints for both, states and inputs are considered, in such a way that $u \in \mathcal{U}$, $x \in \mathcal{X}$, where $\mathcal{U}$ is given by $\mathcal{U} = \{u \in \mathbb{R}_{\geq 0} \mid u \leq U_{max}\}$, with $U_{max} \approx 15\ [U/min]$. Given the cyclic variability of parameters (according to circadian cycle) and the risk of hypoglycemia during the night, $\mathcal{X}$ is assumed to take two different values along the day:

$$\mathcal{X} = \mathcal{X}(t) \doteq \{x \in \mathbb{R}^5_{\geq 0} \mid G_{hypo} \leq x_1(t) \leq G_{hyper},\ \theta_4(x_2(t)+x_3(t)) \leq \overline{IOB}(t)\}, \tag{6}$$

where

$$\overline{IOB}(t) \quad \doteq \quad \begin{cases} IOB_s + (CHO_{u_b}/CR + \tau \cdot U_b), & t \in [6,\ 22)\ h \\ IOB_s, & t \in [22,\ 6)\ h \end{cases},$$

$IOB_s = \theta_4 \cdot (x_{2s} + x_{3s}) = \theta_4 \cdot 2U_b$, τ is the temporal allowable interval of basal suspension during post-prandial period (i.e.: under superbolus mode of infusion) $[min]$ and CHO_{ub} is the meal size upper bound in $[g]$ [50]. The bounds for x_1 are given by $G_{hypo} = 60$ and $G_{hyper} = 300\ mg/dL$. Note that $\mathcal{X}(t)$ is unbounded for x_4, x_5, which is consistent with the fact that these two state component (associated to the meal ingestion) are uncontrollable.

As part of the system/problem description, a target set $\mathcal{Y}^{Tar}$ representing the normoglycemia is defined as $\mathcal{Y}^{Tar} \doteq \{y \in \mathbb{R} : G_{min} \leq y \leq G_{max}\}$, where G_{min} and G_{max} are between $70 - 80\ mg/dL$ and $140 - 180\ mg/dL$, respectively. [1]

2.5. Parameter Estimation

Although model (4) is *a-priori* uniquely identifiable, the lack of internal fluxes measurements (i.e. EGP, Ra, IOB) jeopardizes the model plausibility; that is, the physiological feasibility of estimated parameters [51]. Consequently, an identification technique based on regularized least-squares (RLS) by carbohydrate-to-insulin ratio (CR^0), time-to-maximum effective insulin concentration (θ_4^0) and time-to-maximum appearance rate of glucose in gut (or plasma) (θ_5^0) is considered. The proposed objective function is:

$$V_N(\theta) \quad = \quad \frac{\|y(k) - \hat{y}(k)\|^2}{\|y(k) - \overline{y}(k)\|^2} + \theta^0 \alpha \theta^{0\prime} \tag{7}$$

where $y(k)$ is the measured blood glucose from in-silico patient of UVA/Padova simulator, $\overline{y}(k)$ is its average, $\hat{y}(k)$ is the model predicted output and $\theta^0 = [(\theta_2 - CR^0\theta_3)\ \ (\theta_4 - \theta_4^0)\ \ (\theta_5 - \theta_5^0)]$ a regularization term, with $\alpha = diag(1, 1, 1/(\theta_5^0)^2)$. The minimization of (7) is performed using Matlab *fmincon* routine, with individualized initial parameters given by: $\theta_0(0) = \theta_1(0)G_b + \theta_2(0)U_b$, $\theta_1(0) = \theta_1^0$, $\theta_2(0) = CF$, $\theta_3(0) = RF$, $\theta_4(0) = \theta_4^0$ and $\theta_5(0) = \theta_5^0$, with $\theta_1^0 = 0.004$[min] [34] and $G_b = y(1)$. Note that it is assumed that glycemia is at equilibrium at the beginning of identification.

The parameter CR^0 is established according to CR value of each patient while θ_5^0 is set in $40[min]$ [15] for all patients (Table 1). Moreover, since an accurate estimation of θ_4 is crucial to avoid insulin stacking problems [49], θ_4^0 is determined by minimizing the sum of squared residuals (least-squares, LS) between the estimated IOB and the real value of the simulator (see Remark 2).

The proposed model achieved an acceptable goodness of fit (GoF) [2] : median $[25th, 75th]$ of $48.53\,[43.30, 52.90]$ for 10 individualized in-silico patients (Table 2). Messori et. al. [45], using a linearized model of UVA/Padova Model (13 states), reached a GoF of $55.68\,[41.22, 66.54]$ for 100 in-silico adults.

Remark 2. *Following the same ideas of Section 2.2, the IOB of the UVA/Padova simulator can be computed as* $IOB(t) = \int_0^t (u(\tau) - \frac{BW}{6000} R_{ai}(\tau))\, d\tau = \frac{BW}{6000}(I_{SC1}(t) + I_{SC2}(t))$, *where BW is the body weight* $[kg]$, R_{ai} *is the rate of appearance of insulin in plasma* $[pmol/(min \cdot kg)]$ *and,* $I_{SC1}(t)$ *and* $I_{SC2}(t)$ *are the insulin in the first and second subcutaneous compartment* $[pmol/kg]$, *respectively (see [23]).*

[1] Note the difference between a constraint set $\mathcal{X}$ and a target set $\mathcal{Y}^{Tar}$, in the sense that the system may be outside the latter during the transient regime, while it must be inside the former at any time. $\mathcal{X}$ is associated to the domain of validity of the model.

[2] The goodness of fit (GoF) is calculated according to $GoF = 100\ (1 - \frac{\|y(k) - \hat{y}(k)\|}{\|y(k) - \overline{y}(k)\|})$.

Table 1: *A-priori* parameters for individualization of 10 in-silico adults.

Patient	**001**	**002**	**003**	**004**	**005**	**006**	**007**	**008**	**009**	**010**
$\theta_4^0\ [min]$	56.0	40.0	52.5	59.5	45.5	52.5	47.5	50.0	47.5	50.0
$\theta_5^0\ [min]$	40.0	40.0	40.0	40.0	40.0	40.0	40.0	40.0	40.0	40.0
$CR\ [g/U]$	19.161	22.484	14.552	19.703	13.469	8.995	18.145	8.793	19.763	13.773
$CF\ [mg/(dL \cdot U)]$	43.854	42.101	35.151	53.204	48.019	25.890	42.604	37.062	53.445	39.503

Table 2: Estimated parameters of 10 individualized in-silico adults.

Patient	**001**	**002**	**003**	**004**	**005**	**006**	**007**	**008**	**009**	**010**
$\theta_0\ [mg/(dL \cdot min)]$	1.327	2.011	0.757	1.252	1.036	2.181	1.901	1.057	2.073	1.074
$\theta_1\ [/min]$	0.0034	0.0063	0.0010	0.0027	0.00218	0.0081	0.0018	0.0028	0.0058	0.0032
$\theta_2\ [mg/(dL \cdot U)]$	44.223	54.185	25.271	58.349	49.843	37.488	79.44	38.425	88.105	34.591
$\theta_3\ [mg/(dL \cdot g)]$	2.308	2.410	1.737	2.961	3.871	4.173	4.379	4.370	4.459	2.51
$\theta_4\ [min]$	56.001	40.004	52.202	59.502	46.782	52.503	47.505	50.007	50.505	50.503
$\theta_5\ [min]$	21.840	14.624	21.516	25.429	28.638	23.511	22.023	26.854	24.461	23.317

3. Discrete-time modeling for pulsatile input signals

As discussed before, a better control of BG is achieved by short duration insulin actions [5, 31, 32]. In this context, pulsatile models - in contrast to zero-order hold assumptions - are necessary to properly describe the patient dynamics.

If the boluses duration is significantly short in comparison with the time period, the impulsive approach (i.e., pulses of infinitesimal duration) is valid [35]. However, in the AP problem, it is not so clear if the (probably fast) insulin injection is quick enough to have a good representation by the impulsive approach. In any case, having a general pulsatile representation (i.e., pulses of arbitrary duration) that accounts for both, the zero-order hold input and impulsive input as particular extreme cases is desired.

Let us consider system (4), a fixed time period (sampling time) $T > 0$ and a pulsatile input signal of the form

$$u(t) \quad = \quad \begin{cases} u(kT), & t \in [kT, kT + \Delta T) \\ 0, & t \in [kT + \Delta T, (k+1)T) \end{cases} \quad , \tag{8}$$

for $k \in \mathbb{N}_{\geq 0}$, where $\Delta \in (0, 1]$ is the (arbitrary small) time duration of the pulses. Furthermore consider that the disturbance $r(t)$ is given by $r(t) = r(kT)$, $t \in [kT, (k+1)T)$, $k \in \mathbb{N}_{\geq 0}$, which is the typical zero-order hold assumption.

Now, by sampling the continuous-time solution of system (4) at times $t = kT$, the following discrete-time system is obtained (see Appendix 10.1 for details):

$$x((k+1)T) \quad = \quad A^d x(kT) \ + \ B_u^d u(kT) \ + \ B_r^d r(kT) + E^d, \tag{9}$$

where, assuming that $\theta_1 \neq 0$ (in such a way that A is invertible), $A^d \doteq e^{AT}$, $B_u^d \doteq e^{A(T-\Delta T)} A^{-1}(e^{A\Delta T} - I_5)B_u$, $B_r^d \doteq A^{-1}(e^{AT} - I_5)B_r$, $E^d \doteq A^{-1}(e^{AT} - I_5)E$. Matrices A^d, B_r^d and E^d are the discrete-time counterpart of A, B_r and E, respectively, for the fixed time period T, when r and E are piece-wise constant with a period T. On the other side, B_u^d, which depends on ΔT, accounts for the effect of the input u, which is null from ΔT to T.

Remark 3. *Discrete-time system* (9) *accounts for the two extreme cases in which u is a piece-wise constant signal with period T (i.e., the zero-order hold assumption) and in which u is an impulsive input* $u(t) = u(kT)\delta(t - kT)$, $t \in [kT, (k+1)T)$, $k \in \mathbb{N}_{\geq 0}$, *where* $\delta(t)$ *is a Dirac delta. In the first case it is* $\Delta T = T$ *and, so,* $B_u^d = A^{-1}(e^{AT} - I_5)B_u$. *In the second case it is* $\Delta T \to 0$ *and, so,* $B_u^d = e^{AT}B_u$ *(see [35] for details).*

The main dynamical characteristic of pulsatile systems (i.e., system (4), controlled by inputs (8), with $\Delta \in (0, 1]$) is that there is a free-response (no control) lapse of time, at each period T. This way, a periodic or pseudo-periodic behavior for the states is observed, even when the sampled system reaches an equilibrium. Next, a characterization of such a concept is made, to proceed, in Section 5, with a rigorous MPC formulation for pulsatile systems.

3.1. Equilibrium characterization under pulsatile inputs

Given that the control objective is to steer the continuous-time system output (glucose) to a desired set, $\mathcal{Y}^{Tar}$, and maintain it there by only applying pulsatile controls, the concept of equilibria for pulsatile systems needs to be defined first. Opposite to the zero-order hold sampling case, the equilibria of the discrete-time system (9) is not a formal equilibrium of the continuous-time system (4). In fact, no formal equilibrium of system (4) can be reached when it is controlled by pulses and, so, a more general equilibiurm definition needs to be used.

Consider a bounded and compact set $\mathcal{X}^{Tar} \subseteq \mathcal{X}(t)$, for all $t \geq 0$, such that $C\mathcal{X}^{Tar} = \mathcal{Y}^{Tar}$.

Definition 1 (Generalized equilibrium set [35])**.** *A set $\mathcal{X}_s^{Tar} \subseteq \mathcal{X}^{Tar}$ is a generalized equilibrium set for* (4)*, with respect to $\mathcal{X}^{Tar}$, if for every $x_s \in \mathcal{X}_s^{Tar}$ it there exists an input $u_s \in \mathcal{U}$ such that (i) states $x(kT)$, $k \in \mathbb{N}_{\geq 0}$, remain at x_s, when u_s is applied (i.e., $u(kT) = u_s$), and (ii) $x(t) \in \mathcal{X}^{Tar}$, for $t \in (kT, (k+1)T]$, $k \in \mathbb{N}$.*

Given a set $\mathcal{X}^{Tar}$, two conditions are necessary (under the fasting condition $r(t) \equiv 0$), for a pair (u_s, x_s) to be a generalized equilibrium. The pair (u_s, x_s) must be an equilibrium of the pulsatile discrete-time system (9): $x_s = A^d x_s + B_u^d u_s + E^d$, and the free state evolution starting at x_s, when u_s is applied to the system by pulses, $\varphi(t; x_s, u_s, 0)$, must remains in $\mathcal{X}^{Tar}$ (see Appendix 10.1 for details): $\varphi(t; x_s, u_s, 0) \in \mathcal{X}^{Tar}$, for $t \in [0, T]$.

The later condition is relevant given that the continuous-time evolution of physiological state variables needs to be controlled at any time (not just at the sampling time), when a stationary condition is reached. Particularly, it ensures that $y(t) \in \mathcal{Y}^{Tar}$, for all t upon convergence.

Given the sets $\mathcal{Y}^{Tar}$ and $\mathcal{X}(t)$ (defined in section 2.4), it is easy to find an associated state set [3] $\mathcal{X}^{Tar} \subseteq \mathcal{X}(t)$, $t \geq 0$, such that $C\mathcal{X}^{Tar} = \mathcal{Y}^{Tar}$. However, to find a nonempty generalized equilibrium set with respect to it, say $\mathcal{X}_s^{Tar}$, is not trivial. By following similar steps to the ones in [35], Property 3, it is possible to establish mild conditions on system (4) and time period $T > 0$ under which $\mathcal{X}_s^{Tar}$ can be determined. Sets $\mathcal{X}_s^{Tar}$ and $\mathcal{Y}_s^{Tar} = C\mathcal{X}_s^{Tar}$ will be used in Section 5, to formulate a novel pulsatile MPC for AP.

4. State estimation under pulsatile models

Two state observers are proposed in this work to account for plant-model mismatches, considering meals as the more significant disturbance. First, an output disturbance observer (ODO) is formulated under the main assumption that the plant-model mismatch is due to model uncertainty, without considering any external disturbance effect (i.e., unmodeled meal dynamics). Then, an input disturbance observer (IDO) is proposed assuming a plant-model mismatch related to unannounced meals and unmodeled glucose dynamics.

4.1. Output Disturbance Observer (ODO)

In this case, the main assumption is that the measurable state $y(k) = x_1(k)$ is perturbed by a double integrated white noise process $w(k) \sim N(0, \sigma^2)$, which allows for an offset-free estimation when the plant-model mismatch is an impulse, a step or a ramp. Therefore, this disturbance model is proposed in order to cancel unmodeled glycemia effects during fasting (i.e.: constant mismatch) as well as during postprandial (i.e.: ramp mismatch) periods. The augmented model used for the state estimator is given by:

$$\begin{bmatrix} x(k) \\ d_1(k) \\ d_2(k) \end{bmatrix} = \underbrace{\begin{bmatrix} A^d & B^o & 0 \\ 0 & 1 & T \\ 0 & 0 & 1 \end{bmatrix}}_{A_{aug}} \underbrace{\begin{bmatrix} x(k-1) \\ d_1(k-1) \\ d_2(k-1) \end{bmatrix}}_{x_{aug}} + \underbrace{\begin{bmatrix} B^d \\ 0 \\ 0 \end{bmatrix}}_{B_{aug}} \underbrace{\begin{bmatrix} u(k-1) \\ r(k-1) \\ 1 \end{bmatrix}}_{u_{aug}} + G\, w(k-1)$$

$$y(k) = [C \;\; 0 \;\; 0]\, x_{aug} + v(k) \tag{10}$$

[3] For instance, $\mathcal{X}^{Tar} = \{x \in \mathbb{R}^5_{\geq 0} \mid \mathcal{Y}_s^{min} \leq x_1(t) \leq \mathcal{Y}_s^{max},\; x_2(t) + x_3(t) \leq 2U_b\}$.

where A^d, $B^d = [B_u^d \;\; B_r^d \;\; E^d]$ and C are the pulsatile matrices defined in Section 3 and $B^o = [1\ 0\ 0\ 0\ 0]'$. This way, B^o determines how the integrating disturbance $d_1(k)$ $[mg/dL]$ affects the glycemia state $x_1(k)$ (or system output). Moreover, the process noise covariance $Q_{KF} = E[(G\,w(k-1))(G\,w(k-1))'] = G\,E[w(k-1)w(k-1)']\,G'$ and since, $\sigma^2 = E[w(k-1)w(k-1)']$, results in $Q_{KF} = G \cdot \sigma^2 \cdot G'$, being $G = [0 \;\; k_i \;\; k_i \;\; 0 \;\; 0 \;\; 0 \;\; k_d]'$ the disturbance input distribution matrix. Furthermore, the measurement noise $v(k)$ is assumed as zero-mean white noise $v(k) \sim N(0, R_{KF})$ with covariance $R_{KF} = \sigma^2_{CGM}$.

The augmented state x_{aug} is estimated by the following time-varying Kalman filter (KF) algorithm:

$$\hat{x}_{aug}(k|k) = A_{aug}\hat{x}_{aug}(k|k-1) + B_{aug}u_{aug} + K(k)(y(k) - C\hat{x}_{aug}(k|k-1)), \tag{11}$$

where $\hat{x}_{aug} = [\hat{x},\ \hat{d}_1,\ \hat{d}_2]'$ is the augmented estimated state, and

$$\begin{aligned} P(k|k-1) &= A_{aug}P(k-1|k-1)A'_{aug} + Q_{KF}, \\ K(k) &= P(k|k-1)C'(CP(k|k-1)C' + R_{KF})^{-1}, \\ P(k|k) &= (I - K(k)C)P(k|k-1), \end{aligned}$$

are the covariance of the *a-priori* estimation error $x(k) - \hat{x}(k|k-1)$, the KF gain and the covariance of the *a-posteriori* estimation error $x(k) - \hat{x}(k|k)$, respectively. The KF is initialized at $\hat{x}(0) = [G_b \;\; U_b \;\; U_b \;\; 0 \;\; 0]'$, $\hat{d}_1(0) = 0$, $\hat{d}_2(0) = 0$ and $P(0|0) = P(\infty|\infty)$, where the solution of a discrete algebraic Riccati equation calculates $P(\infty|\infty)$ according to system (11). Since the estimated states are positive physiological variables, a KF with inequality constraints is employed (see: *2.4. Estimate projection with inequality constraints, [52]*).

From Figure 2, it can be seen, that in spite of the fact that meals are announced with different misestimation errors, the estimated glycemia ($\hat{x}_1$) and insulin on board ($\hat{IOB}$) follow an offset-free behavior in fasting and postprandial periods. In this sense, note that $d_1(k)$ is moved onto a manifold that cancels meal uncertainty effects on glycemia state (i.e.: when meals are unannounced (UA), d_1 increases in such a way that compensates meal uncertainty impact on glycemia state). Note, that this observer is designed to cancel output disturbances, and consequently, Ra is estimated according to the nominal model.

4.2. Input Disturbance Observer (IDO)

Following the same characterization of disturbance dynamics, in this case, it is assumed that uncertainty in the carb counting, denoted by $d_1(k)$ $[g/min]$, is driven by a double integrated white noise process $w(k) \sim N(0, \sigma^2)$. This way, $B_r^d r(k) = B_r^d[\hat{r}(k) + d_1(k)] = B_r^d\hat{r}(k) + B_r^d d_1(k)$, being $r(k)$ the meal ingest rate $[g/min]$ and $\hat{r}(k)$ the carb counting per sampling time $[g/min]$. We use this disturbance model to ensure offset-free estimation for a large class of meal profiles. In this case, the augmented model is given by (11), but replacing B^o by $B_1^i = B_r^d$ in matrix A_{aug}.

Although this observer explicitly considers the meal dynamic, the augmented double integrator state, $d_1(k)$, implicitly assumes that the plant-model mismatch comes exclusively from this kind of disturbances. Therefore, others source of disturbance, like unmodeled glucose-insulin dynamics, sensor noise, etc., will be explained as a meal ingestion, which may cause an aggressive insulin delivery by the controller. Hence, we proposed to modify B_1^i by $B_2^i = \theta_5 \cdot RF \cdot B^o + \mu \cdot B_r^d$, being θ_5 the meal absorption time constant $[min]$, $RF = \theta_3[mg/(dL \cdot g)]$, $B^o = [0.01\ 0\ 0\ 0\ 0]'$ and $\mu \in [0, 1]$ a tuning parameter to adjust the aggressiveness (signal-to-noise ratio) of the state observer. Figure 3 shows that despite the fully input observer with B_1^i is more sensible to unannounced meals (fast rejection), the estimated rate of glucose appearance in plasma ($\hat{Ra}_{B_1^i}$) is affected by uncertainty and noise. On the other hand, the effect of the lumped disturbance d_1 on the meal subsystem and glucose dynamic (input observer B_2^i) provides a smoother estimation of Ra (see $\hat{Ra}_{B_2^i}$ in Figure 3). μ is set heuristically at 0.5 for all patients.

5. Pulsatile MPC formulation

In this section, a novel MPC formulation for system (4) is presented, by extending the so-called impulsive zone MPC (iZMPC) presented in [53, 35] to the pulsatile case (pZMPC). The glucose

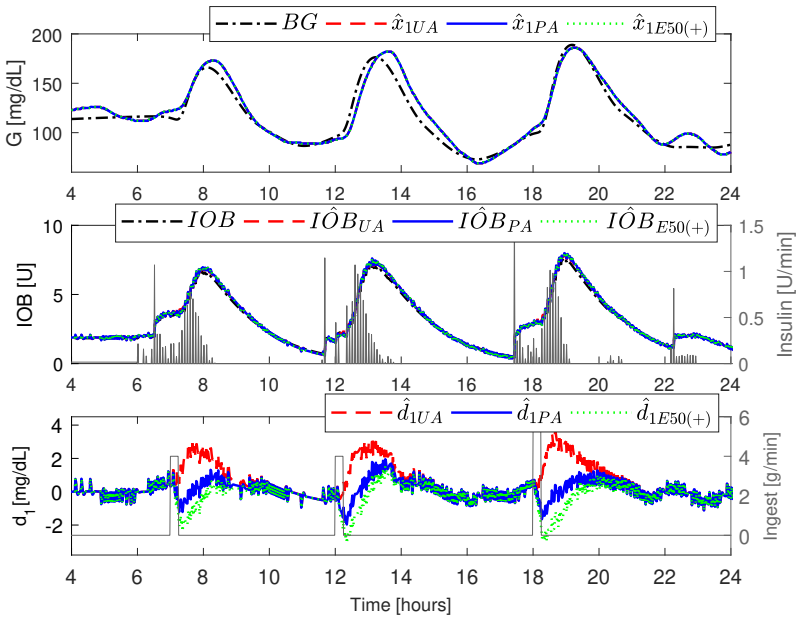

Figure 2: Performance of the output disturbance observer (ODO) under open-loop, considering unannounced (UA), perfectly announced (PA) and announcement with $+50\%$ estimation error ($E50(+)$) meal ingest. KF setting: $k_i = 1 \cdot 10^{-2}$, $k_d = 1$, $\sigma^2 = 1[mg^2/dL^2]$ and $\sigma^2_{CGM} = 6.51[mg^2/dL^2]$. Patient: Adult 004.

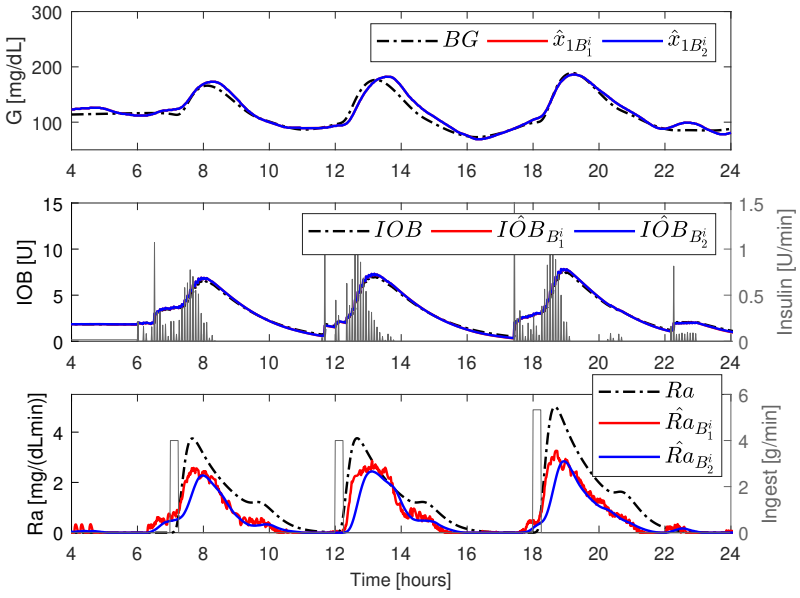

Figure 3: Performance of the input disturbance observer (IDO) considering $B_1^i = B_r^d$ (red) and $B_2^i = \theta_5 \cdot RF \cdot B^o + \mu \cdot B_r^d$ (blue) under open-loop, unannounced meal case. KF setting: $k_i = 1 \cdot 10^{-2}$, $k_d = 1$, $\sigma^2 = 1[mg^2/dL^2]$, $\sigma^2_{CGM} = 6.51[mg^2/dL^2]$ and $\mu = 0.5$. Patient: Adult 004.

(and state) predictions are based on the discrete-time pulsatile system (9), and the control objective is to drive (and maintain) the blood glucose to a safety zone given by $\mathcal{Y}^{Tar}$, while fulfilling the input and state constraints in the path. The controller is designed for both, the announced (or partially-announced) and the unannounced meal cases. For the former, the meal signal, $\hat{r}$, is the estimated meal ingest rate (or carb counting per sampling time) and the estimated state at the current time, $\hat{x} = \hat{x}(k|k)$, is calculated by the disturbance observer ODO. For the latter, since no

meals are announced ($\hat{r} \equiv 0$), the meal effect is estimated by the disturbance observer IDO, which copes with Ra estimation in cases of unannounced scenarios.

Let consider the sets $\mathcal{Y}_s^{Tar} = C\mathcal{X}_s^{Tar}$, where $\mathcal{X}_s^{Tar}$ is a generalized equilibrium set with respect to $\mathcal{X}^{Tar}$, and both $\mathcal{X}^{Tar} \subseteq \mathcal{X}(t)$, for all $t \geq 0$, and $C\mathcal{X}^{Tar} = \mathcal{Y}^{Tar}$ (as defined in subsection 3.1). The cost function of the optimization problem that the MPC solves on-line reads

$$V_N(\hat{x}, \hat{r}, \mathcal{Y}_s^{Tar}; \mathbf{u}, u_a, y_a) \doteq V_{dyn}(\hat{x}, \hat{r}; \mathbf{u}, u_a, y_a) + V_s(\mathcal{Y}_s^{Tar}; u_a, y_a),$$

where

$$V_{dyn}(\hat{x}, \hat{r}; \mathbf{u}, u_a, y_a) \doteq \sum_{j=0}^{N-1} (Cx(j) - y_a)^T Q (Cx(j) - y_a) + (u(j) - u_a)^T R (u(j) - u_a),$$

with $Q > 0$ and $R > 0$, is a term devoted to steer the system to the artificial equilibrium variables $(u_a, y_a) \in \mathcal{U}_s \times \mathcal{Y}_s$, and $V_s(\mathcal{Y}_s^{Tar}; u_a, y_a) \doteq p\left(dist_{\mathcal{Y}_s^{Tar}}(y_a)\right)$, with $p > 0$, and $dist_{\mathcal{A}}(a)$ representing the distance from the point a to the set $\mathcal{A}$, is a stationary cost devoted to steer y_a to the target equilibrium $\mathcal{Y}_s^{Tar}$. As usual in MPC with economic objectives [54, 55], the stationary term V_s can be designed to account for objectives that are specific for each application. In section 5.1, the form of such a cost term is discussed for the case of the AP.

In the latter cost, $\hat{x}$, $\hat{r}$ and $\mathcal{Y}_s^{Tar}$ are optimization parameters, while $\mathbf{u} = \{u(0), u(1), \cdots, u(N-1)\}$, u_a and y_a, are the optimization variables, being N the control horizon. The optimization problem to be solved at the current time k by the MPC is given by

$P_{MPC}(\hat{x}, \hat{r}, \mathcal{Y}_s^{Tar})$:

$$\begin{aligned}
\min_{\mathbf{u}, u_a, y_a} \quad & V_N(\hat{x}, \hat{r}, \mathcal{Y}_s^{Tar}; \mathbf{u}, u_a, y_a) \\
s.t. \quad & \\
& x(0) = \hat{x}, \;\; r(0) = \hat{r}, \\
& x(j+1) = A^d x(j) + B_u^d u(j) + B_r^d r(j) + E^d, && j \in \mathbb{I}_{0:N-1} \\
& u(j) \in \mathcal{U}, && j \in \mathbb{I}_{0:N-1} \\
& \tilde{C}x(j) \in \tilde{C}\mathcal{X}(k), && j \in \mathbb{I}_{1:N} \\
& r(j) = 0, && j \in \mathbb{I}_{1:N-1} \\
& \tilde{C}x(N) = x_a, \\
& y_a = x_{1,a}, \\
& x_a = \tilde{C}A^d x_a + \tilde{C}B^d u_a + \tilde{C}E^d.
\end{aligned}$$

Given that only the first three states of model (9) are controllable, constraints can be imposed only on the first three states x_1, x_2 and x_3, by means of matrix $\tilde{C} = [I_3 \; 0_{3\times 2}]$. Furthermore, given that no future meals are considered, r is only used for the first prediction step, if available. Note, that it is assumed that meals are ingested during a sampling period T, although this formulation supports the distribution of the announcement in an arbitrary interval (D_t), in such a way that $D_t = nT$ with $n \in \mathbb{I}_{1:N-1}$. The constraint $\tilde{C}x(N) = x_a$ is the terminal constraint that forces the state at the end of control horizon N to reach the artificial equilibrium state $x_a = [x_{1,a}, x_{2,a}, x_{3,a}]' \in \mathbb{R}^3$. Furthermore, the constraint $x_a = \tilde{C}A^d x_a + \tilde{C}B^d u_a + \tilde{C}E^d$ forces the artificial variable pair (u_a, x_a) to be a feasible equilibrium of the discrete-time system (9) (not necessarily $\mathcal{X}_s$ in the transient regime). The state set $\mathcal{X}(k)$ is a discretization of set $\mathcal{X}(t)$ introduced in (6).

Once the Problem $P_{MPC}(\hat{x}, \hat{r}, \mathcal{Y}_s^{Tar})$ is solved, the (optimal) solution is denoted as $(\mathbf{u}^0, u_a^0, x_a^0)$, while the optimal cost function is given by $V_N^0(\hat{x}, \hat{r}, \mathcal{Y}_s^{Tar}) \doteq V_N(\hat{x}, \hat{r}, \mathcal{Y}_s^{Tar}; \mathbf{u}^0, u_a^0, x_a^0)$. The control law, derived from the application of a **receding horizon control** policy (RHC), is given by $\kappa_{MPC}(\hat{x}, \hat{r}, \mathcal{Y}_s^{Tar}) = u^0(0; x)$, where $u^0(0; x)$ is the first element of the solution sequence $\mathbf{u}^0(x)$.

The main properties of the resulting closed-loop - in the case the state is perfectly measured and no permanent disturbances are considered - are:
(i) The optimization problem $P_{MPC}(x(k), r, \mathcal{Y}_s^{Tar})$, considering $x(k+1) = A^d x(k) + B_u^d \kappa_{MPC}(x(k), 0, \mathcal{Y}_s^{Tar}) + E^d$, is recursively feasible, i.e., if the problem is feasible at $x(\hat{k})$, then it is feasible for all subsequent states $x(k)$, with $k \geq \hat{k}$.
(ii) Set $\mathcal{X}_s^{Tar}$ is stable for the closed loop $x(k+1) = A^d x(k) + B_u^d \kappa_{MPC}(x(k), 0, \mathcal{Y}_s^{Tar}) + E^d$, with a domain of attraction given by the controllable set, in N steps, to the **entire equilibrium set** of

system (9), $\mathcal{X}_N$. This means that $y(k) \to \mathcal{Y}_s^{Tar}$ for $k \to \infty$.
(iii) Assuming $x(k)$ reaches $\mathcal{X}_s^{Tar}$ at time $\hat{k}$ ($y(k)$ reaches $\mathcal{Y}_s^{Tar}$), then $x(t)$ will remains in $\mathcal{X}^{Tar}$ for all continuous-time $t \geq \hat{k}T$ ($y(t)$ will remains in $\mathcal{Y}^{Tar}$). This property follows from Definition 1, which accounts for the continuous-time system behavior at the equilibrium set.

The proofs of the latter statements follow similar steps than the one in [35], Theorem 3, and are omitted for the sake of brevity.

5.1. The term V_s

The stationary cost V_s is designed to account for the fact that, mainly in the short term, hypoglycemia is more dangerous than hyperglycemia. That is, V_s is defined by $V_s(\mathcal{Y}_s^{Tar}; u_a, y_a) \doteq \hat{p}\delta_{hyper}^2 + \check{p}\delta_{hypo}^2$, while the following constraint is added to P_{MPC} problem: $\mathcal{Y}_s^{min} - \delta_{hypo} \leq y_a \leq \mathcal{Y}_s^{max} + \delta_{hyper}$. Variables δ_{hypo} and δ_{hyper} are additional optimization variables, constrained to be positive (i.e., $\delta_{hypo} \geq 0$, $\delta_{hyper} \geq 0$), $\hat{p}$ and $\check{p}$ are the weights corresponding to hyper and hypoglycemia, respectively, and $\mathcal{Y}_s^{min}$ and $\mathcal{Y}_s^{max}$ are the limits values of $\mathcal{Y}_s^{Tar}$ (as defined in Section 2.4). This way, by selecting $\hat{p} \ll \check{p}$ an asymmetric cost function, which penalizes harder the hypoglycemic episodes, is obtained. In contrast to other MPC formulations for AP, this asymmetry operates exclusively on the stationary predicted regime, since the artificial variables (u_a, y_a) are generalized equilibrium pairs of the (controllable part of) system (4).

6. Optimal Basal-Bolus Calculator

To further exploit the advantages of pulsatile infusion mode (specifically, postprandial optimal boluses when meals are announced), an optimal basal-bolus calculator based on an event-triggered pZMPC is presented. Basically, the idea is to emulate the conventional FIT, but in an optimal way, in such a way that the controller is switched-on every time a meal is announced, and remains inactive otherwise (no RHC is implemented).

In this case, the cost function of the optimization problem, reads:

$$V_N(\hat{x}, \hat{r}; \mathbf{u}, u_s, \boldsymbol{\delta_{hyper}}, \boldsymbol{\delta_{hypo}}) = \sum_{j=0}^{N-1} \Big(\delta_{hyper}(j)^T \hat{Q} \delta_{hyper}(j) + \delta_{hypo}(j)^T \check{Q} \delta_{hypo}(j) + (u(j) - u_s)^T R (u(j) - u_s) \Big) + \delta_{hyper}(N)^T \hat{Q} \delta_{hyper}(N) + \delta_{hypo}(N)^T \check{Q} \delta_{hypo}(N)$$

with $\hat{Q} > 0$, $\check{Q} > 0$ and $R > 0$, is an asymmetric cost designed to steer the system directly to $\mathcal{Y}_s^{Tar}$ (without artificial variables), and (u_s, x_s) are just auxiliary equilibrium variable in $\mathcal{U}_s \times \mathcal{X}_s^{Tar}$ being, as before, $\mathcal{X}_s^{Tar}$ a generalized equilibrium set of (4), with $C\mathcal{X}_s^{Tar} = \mathcal{Y}_s^{Tar}$. The optimization problem to be solved by the event-triggered pZMPC, whenever a meal event is announced, reads:

$P_{MPC}(\hat{x}, \hat{r}, \mathcal{Y}_s^{Tar})$:

$$\begin{aligned}
\min_{\mathbf{u}, u_s, \boldsymbol{\delta_{hyper}}, \boldsymbol{\delta_{hypo}}} \quad & V_N(\hat{x}, \hat{r}, \mathcal{Y}_s^{Tar}; \mathbf{u}, u_s, \boldsymbol{\delta_{hyper}}, \boldsymbol{\delta_{hypo}}) \\
s.t. \quad & \\
& x(0) = \hat{x}, \;\; r(0) = \hat{r}, \\
& x(j+1) = A^d x(j) + B_u^d u(j) + B_r^d r(j) + E^d, \qquad j \in \mathbb{I}_{0:N-1} \\
& u(j) \in \mathcal{U}(k), \qquad j \in \mathbb{I}_{0:N-1} \\
& \tilde{C} x(j) \in \tilde{C}\mathcal{X}(k), \qquad j \in \mathbb{I}_{1:N} \\
& r(j) = 0, \qquad j \in \mathbb{I}_{1:N-1} \\
& \tilde{C} x(N) = x_s, \;\; x_s = \tilde{C} A^d x_s + \tilde{C} B^d u_s + \tilde{C} E^d, \\
& y_s = x_{1,s} \in \mathcal{Y}_s^{Tar} \\
& \mathcal{Y}_s^{min} - \delta_{hypo}(j) \leq C x(j) \leq \mathcal{Y}_s^{max} + \delta_{hyper}(j), \quad j \in \mathbb{I}_{0:N-1} \\
& \delta_{hypo}(j) \geq 0, \; \delta_{hyper}(j) \geq 0.
\end{aligned}$$

The constraints of the problem are basically the same of the original pZMPC of Section 5. The main difference is that no artificial variable are used (u_s and x_s are just auxiliary equilibrium variables, necessary to implement the distance function from the predicted state to the target set $\mathcal{X}_s^{Tar}$) and input constraints are given by $\mathcal{U} = \{u \in \mathbb{R}_{\geq 0} \mid u(0) \leq U_{max}, 0 \leq u(1) \leq 2U_b, \; u(j) =$

$u(j-1),\ \text{for}\ j \leq 2\}$. Under this scheme, the receding horizon policy (RHC) is not used, and the N control actions $\mathbf{u} = \{u(0), u(1), \cdots, u(N-1)\}$ are applied to the system whenever the pZMPC is triggered by a meal event. In summary, the main distinctive characteristics are: (i) the use of an infusion mode constraint to ensure a bolus and basal pattern along the control horizon, (ii) the use of an asymmetric transient stage cost and (iii) each time the controller is activated (meal event), the whole optimal input sequence is implemented. Furthermore, given that in this formulation the domain of attraction, $\mathcal{X}_N$, is reduced (controllable set, in N steps, to target equilibrium set of system (9)), the control horizon N must be enlarged.

7. Simulation Results

The benefits of the proposed pulsatile Zone Model Predictive Control (pZMPC) will be demonstrated by means of the commercially available UVA/Padova Type 1 Diabetes Metabolic Simulator (T1DMS2013, Academic Version) with a virtual population of 10 adult patients. Three main cases are simulated, to show how the controller behaves in realistic stressing scenarios. Firstly, an *hybrid closed-loop scheme* is presented, where the meals are announced, perfectly and affected by random misestimation errors. Secondly, the meals become completely unannounced, in a *fully closed-loop scheme*. Thirdly, an *event-triggered scheme* is proposed, where the pZMPC is activated each time a meal is announced, to emulate the conventional FIT set be simulator.

7.1. Description of the scenarios, outcome metrics and statistical analysis

For all the cases, three nominal meals per day are considered: breakfast (60 g CHO, at 7:00), lunch (60 g CHO, at 12:00) and dinner (80 g CHO, at 18:00), affected by random variations in mealtimes ($\pm 10\ min$) and meal size ($\pm 20\%$) (according to an uniform distribution). The simulation lasts 14 days, and a sampling time of $T = 5[min]$, with a pulse size of $\Delta T = 1[min]$ are considered. At the beginning (first 6 hs) the virtual patient glycemia is controlled by means of the FIT provided by the UVA/Padova simulator. After that, the insulin treatment (including both, basal rate and boluses) is exclusively managed by the proposed pZMPC. The observers are selected depending on the case: an ODO, for the announced-meal and event-triggered scenarios, and an IDO, for the unannounced instance. The model noise is the one corresponding to Dexcom G5 Mobile CGM, proposed by Vettoretti et al. [56] (warm-up period omitted), with $a_0 = 1.04$, $b_0 = -1.42[mg/dL]$, $c_1 = 1.17$, $\sigma^2_{CGM} = 6.51[mg^2/dL^2]$ and $a_1 = 0$ (no-trend noise). The insulin pump is the default one, provided by the simulator.

In order to assess the performance of the pZMPC, standard metrics (according to the International Consensus on Use of Continuous Glucose Monitoring [57]) are considered. The indexes are given by: mean glucose $(\overline{G}_m)$; glucose standard deviation (SD); coefficient of variation (CV); time in range $70-180\ mg/dL$; time in tight range $70-140\ mg/dL$; time above 180 and 250 mg/dL, ($G_m > 180$, $G_m > 250$); time below 70 and 54 mg/dL, ($G_m < 70$, $G_m < 54$); number of hypoglycemia events L1 ($G_m < 70\ mg/dL$) and L2 ($G_m < 54\ mg/dL$); Total Daily Insulin (TDI); and Glucose Management Indicator (GMI)[58], which gives an estimation of laboratory glycosylated hemoglobin (A1c). Postprandial periods (PP) are defined as a 4 hours interval from meal ingest, while night periods (NP) are established from 0:00-6:00hs. All metrics are expressed as median $[25th, 75th]$, with the statistical significance assessed by Wilcoxon signed-rank test. The mean ($\pm$ SD) is reported for hypoglycemia range, with statistical significance according to paired t-test.

7.2. Hybrid closed-loop scheme: meal announced case.

In this first case, the following scenarios are proposed: perfectly announced meal ingest (PA), announcement with carb counting estimation error following the regression curve (Fig.3, [59]) with uniform variability of 30% ($A_{30\%}$) and, announcement with $\pm 50\%$ estimation error ($A_{50\%}$), which is extreme misestimation condition. The ODO presented in Section 4.1 is used as state observer and the meals are directly informed, by considering $\hat{r} = C\hat{HO}/T$, being $C\hat{HO}$ the estimated carbohydrates of meal intake $[g]$, and T the sampling time $[min]$. Moreover, for all in-silico adults, the controller is tuned by setting $\hat{p} = 1 \cdot 10^9$, $\check{p} = 1 \cdot 10^7$, $Q = 1$ and $R \in [1, 100]$, with the main objective of minimizing the number of hypoglycemic events ($No.\ L1_{hypo}$ and $No.\ L2_{hypo}$) as well as maximizing the time on tight target range ($70 \leq G_m \leq 140\ mg/dL$). The control horizon is set on 6 hours ($N = 72$) following the American Diabetes Association (ADA) [4] recommendations.

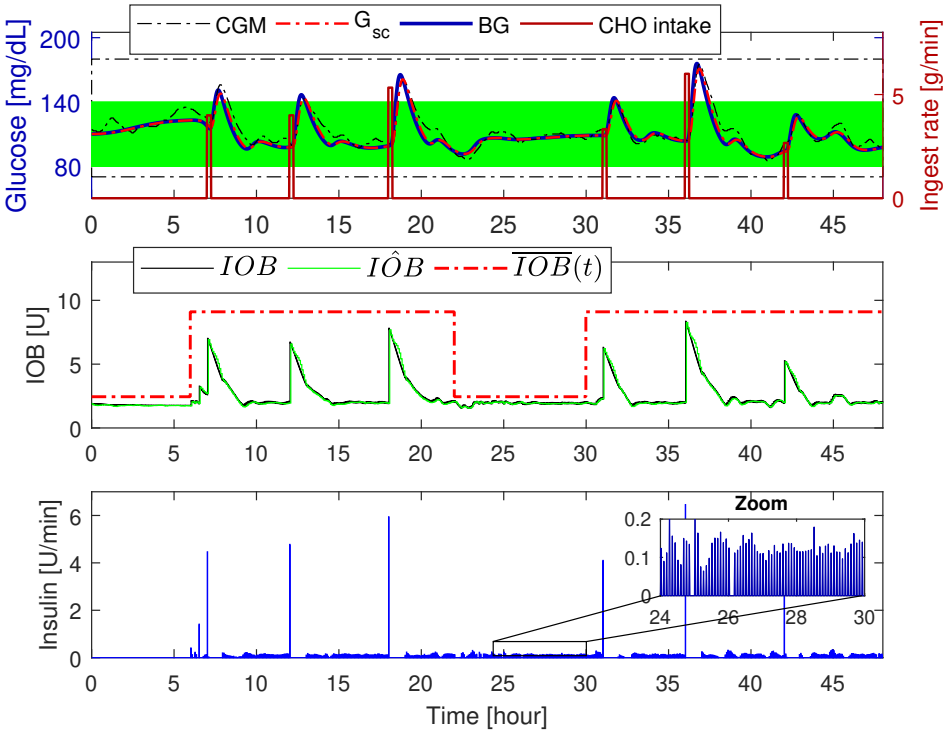

Figure 4: pZMPC under perfectly announced (PA) case. Above: CGM, subcutaneous glucose concentration (G_{sc}), blood glucose (BG) and meal ingest rate (r). Middle: insulin on board measurement IOB and estimation $I\hat{O}B$, with $\overline{IOB}(t) = 9.10[U]$ for $t \in [6,\ 22)$ hs and $\overline{IOB}(t) = 2.10[U]$ for $t \in [22,\ 6)$ hs. Below: insulin pulses $u[U/min]$. Patient: Adult 002.

Figure 4 shows the behavior of the controller when meals are perfectly announced. Insulin is administered in a pulsatile way, fulfilling the glycemia and insulin pharmacokinetics constraints. Moreover, since meals are assumed to be ingested during just one sampling period ($r(0) = \hat{CHO}/T;\ r(j) = 0,\ j > 0$) and the meal absorption subsystem assumes a complete carbohydrate meal profile, the controller compensates the disturbance by a feedback (optimal) super-bolus, which is an expected infusion delivery for this case. Moreover, during fasting periods (i.e.: night period 24:00-30:00 hs, Fig.4) the pZMPC administrates a pulsatile basal infusion ($u_s \simeq 0.1[U/min]$) which steers the glycemia to the output equilibrium set (according to the equilibrium characterization presented in Section 3.1).

On the other hand, Figure 5 shows the performance of the controller when meals are announced with a rounding error of $\pm 50\%$ ($A_{50\%}$). In this case, when meals are overestimated (i.e.: $\hat{CHO} = 90[g](+50\%)$) the constraint on $\overline{IOB}_{[6,22)}$ becomes active ($\overline{IOB}_{[6,22)} = IOB_s + (CHO_{ub}/CR + \tau \cdot U_b) \simeq 9.10[U]$ with $IOB_s = 2.10[U]$, $CHO_{ub} = 90[g]$, $CR = 22.484[g/U]$, $\tau = 120[min]$ and $U_b = 0.0255[U/min]$) limiting the insulin infusion. As a result, the hypoglycemic risk related to insulin overdosing due to meal overestimation is reduced.

The performance metrics corresponding to the 14-day scenario are reported in Table 3. As it is expected, the glucose variability increases as the carb misestimation becomes higher, being statistical significant for the $A_{50\%}$ case ($SD = 26.047, p < 0.05$). From Figure 6, which shows the performance of the three scenarios, for the 10 adults, it can be seen that the glycemia variability ([25th,75th] percentiles) of $A_{50\%}$ is higher than the one of the $A_{30\%}$ and PA cases, specially during postprandial periods. Nevertheless, its coefficient of variation ($CV = 21.283, p < 0.05$) is below the upper limit of ($CV < 36\%$)[57], which is in accordance with an stable glucose profile. The time in target range ($70 \leq G_m \leq 180$) is acceptable for the 3 cases, being non-statistically different for $A_{30\%}$, and with a reduction of 1.289% for $A_{50\%}$ (mainly related with the increment of 1.495% reported in the $G_m > 180$ interval). No hypoglycemia events are reported for PA and $A_{30\%}$; while, for $A_{50\%}$ 0.104(0.235) L1 events are registered, due to patient 007. This can be explained, since this patient has an insulin sensitivity index ($S_I \doteq -dG_b/dU_b =$

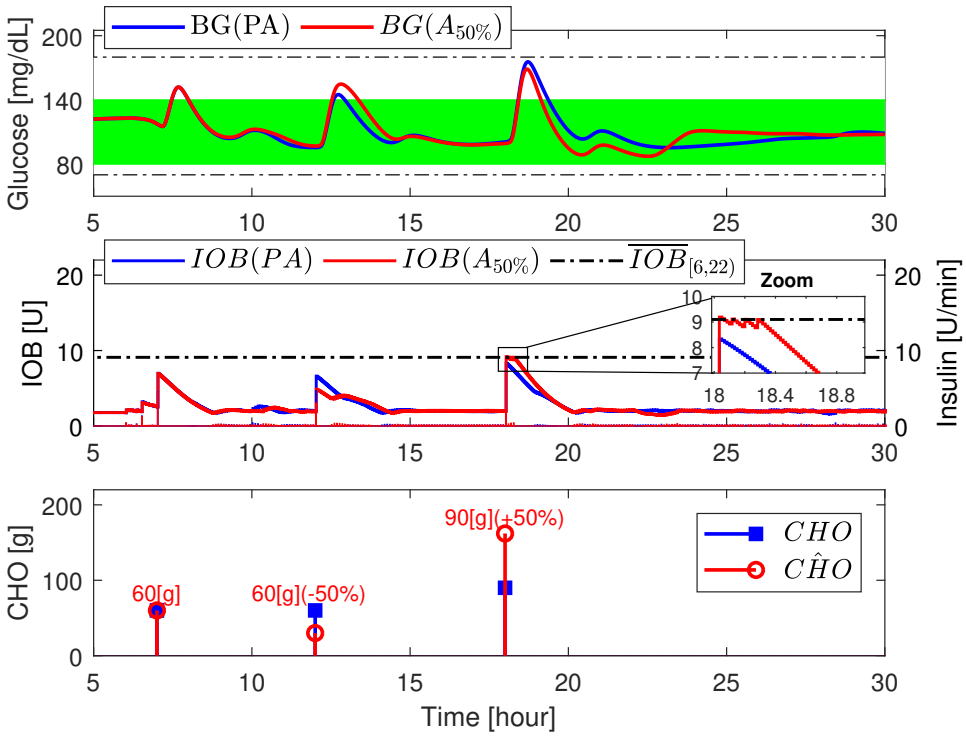

Figure 5: pZMPC when meals are informed with ±50% error. Above: Blood glucose concentration for PA (blue) and $A_{50\%}$ (red). Middle: IOB measurement for PA (blue) and $A_{50\%}$ (red), and diurnal IOB limit ($\overline{IOB}_{[6,22)}$). Below: carb counting for PA case (blue) and $A_{50\%}$ (red). The sign of percentage indicate the overestimated (+)/ underestimated (-) error. Patient: Adult 002.

θ_2/θ_1) of $4.413 \cdot 10^4[(mg/dL)/(U/min)]$ which is 2.5 times above the cohort mean value of $1.798 \cdot 10^4(1.266 \cdot 10^4)$ $[(mg/dL)/(U/min)]$.

For the 3 cases, the total daily insulin (TDI) is in order of $43[U/day]$ which is an expected value being $TDI = BW \cdot 0.53 = 70[kg] \cdot 0.53 \simeq 37[U/day]$. The mean glucose of misestimation cases does not show a significative differences regarding the *PA* case. The glucose management indicator (GMI) is in order of 6% for the 3 cases, and taking into account that non-significant L1 events happened, it can be concluded that the proposed hybrid closed-loop scheme ensures an appropriated A1c management despite of the carb counting errors.

7.3. Fully closed-loop scheme: meal unannounced case.

In this second case, we assess the performance of pZMPC when meals are not announced. The selected observer is the IDO, presented in Section 4.2, which allows for the estimation of meal absorption states ($\hat{x}_4, \hat{x}_5$), both related to the rate of glucose appearance in plasma ($\hat{Ra}$), when meals are unannounced. For all in-silico patients, the pZMPC is tuned by setting $\hat{p} = 1 \cdot 10^9$, $\check{p} = 1 \cdot 10^3$, $Q = 1 \cdot 10^3$ and $R \in [1, 100]$, tailored following the same objectives of the previous scheme. Penalty $\check{p}$ is reduced in order to increase the relative penalization of hypoglycemia, given that this scheme is more sensible to erratic glucose excursions (especially, related with *Ra* misestimation). Moreover, matrix Q is increased in order to diminish the glycemia excursion with respect to the euglycemia zone. This tuning parameter is critical, given that meals are sensed by means of the *Ra* estimation signal ($\hat{Ra}$), which has an inherently delay of $\simeq 50$ *min*, due to glucose absorption dynamics from the gut ($\simeq 40$ *min*) plus the glucose measurement delay from the subcutaneous space ($\simeq 10$ *min*). On the other hand, the IDO is tailored by setting $\mu = 0.5$, for all patients, to smooth down the *Ra* estimation.

Table 3: Performance metrics for hybrid closed-loop scheme under perfectly announced (PA), announcement with randomly 30% misestimation error ($A_{30\%}$) and announcement with $\pm 50\%$ error ($A_{50\%}$). An asterisk indicates statistical significance ($p < 0.05$) respect to PA case. (Overall).

	PA	$A_{30\%}$	$A_{50\%}$
Mean G_m $[mg/dL]$	114.013[112.197,117.590]	114.673[112.430,118.417]	114.025[110.467,117.317]
SD $[mg/dL]$	18.648[16.217,22.034]	21.014[16.828,23.827]	26.047[18.481,27.487]*
CV $[\%]$	16.464[14.573,19.639]	18.325[15.030,19.924]	21.283[16.736,23.430]*
$70 \leq G_m \leq 140$ $[\%time]$	88.577[85.804,90.681]	85.714[83.097,90.007]	85.950[82.304,90.086]
$70 \leq G_m \leq 180$ $[\%time]$	99.792[99.520,100.000]	99.626[98.622,99.911]	98.506[95.465,99.787]*
$G_m > 180$ $[\%time]$	0.208[0.000,0.481]	0.374[0.089,1.378]	1.495[0.213,4.536]*
$G_m > 250$ $[\%time]$	0.000[0.000,0.000]	0.000[0.000,0.000]	0.000[0.000,0.000]
$G_m < 70$ $[\%time]$	0.000[0.000,0.000] 0.000(0.000)	0.000[0.000,0.000] 0.000(0.000)	0.000[0.000 0.000] 0.128(0.334)
$G_m < 54$ $[\%time]$	0.000[0.000,0.000] 0.000(0.000)	0.000[0.000,0.000] 0.000(0.000)	0.000[0.000,0.000] 0.000(0.000)
$No.\ L1_{hypo}$	0.000[0.000,0.000] 0.000(0.000)	0.000[0.000,0.000] 0.000(0.000)	0.000[0.000,0.000] 0.104(0.235)
$No.\ L2_{hypo}$	0.000[0.000,0.000] 0.000(0.000)	0.000[0.000,0.000] 0.000(0.000)	0.000[0.000,0.000] 0.000(0.000)
TDI $[U]$	43.754[40.495,55.496]	43.576[40.226,55.248]	45.233[41.329,56.291]
GMI $[\%]$	6.037[5.994,6.123]	6.053[5.999,6.143]	6.038[5.952,6.116]

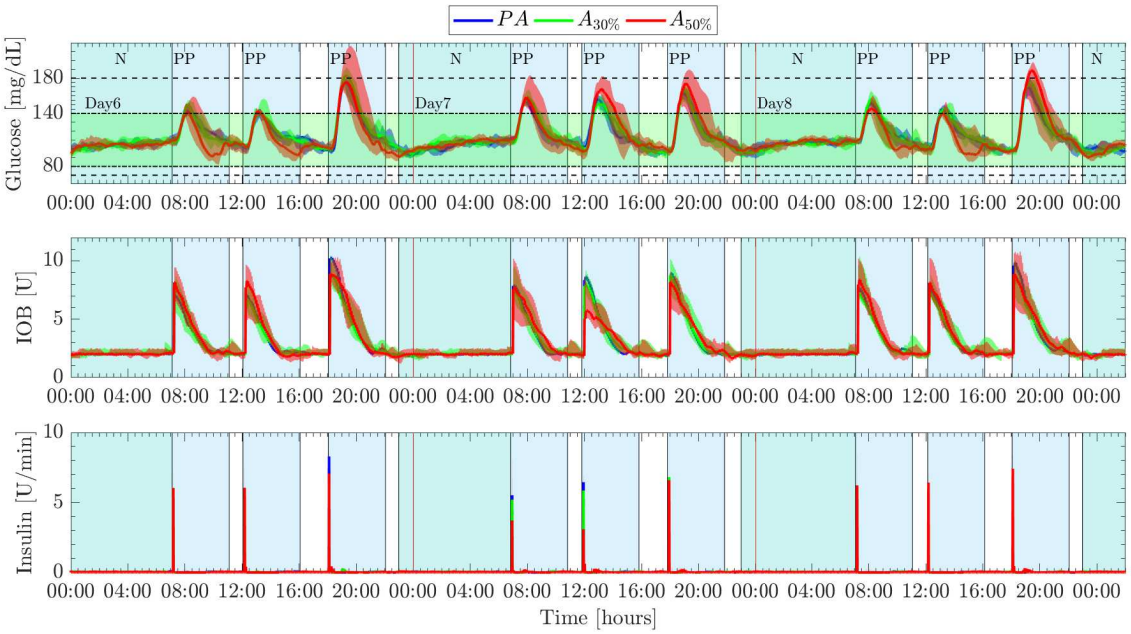

Figure 6: Hybrid closed-loop controller performance for PA, $A_{30\%}$ and $A_{50\%}$ cases. Glucose, IOB and insulin profiles are shown in terms of median (solid lines) surrounded by colored regions representing the $[25th, 75th]$ percentiles.

To properly assess the potential improvement in glycemia control achieved by the described scheme (pZMPC + IDO) when meals are not announced (UA_{FCL}), we also simulated the hybrid closed-loop scheme (pZMPC + ODO), but considering a missed announcement scenario (UA_{HCL}). That is, the control scheme of the previous subsection is simulated when some of the meal announcements are lost. Furthermore, the UA_{FCL} is compared with the $A_{30\%}$ case (which is the most realistic case presented in Section 7.2) to asses the significance of glycemia control degradation when meal announcement signal is eliminated from the loop.

Figure 7 shows that the performance of UA_{FCL} is considerably better than the one of UA_{HCL}: both, median and variability ([25th, 75th] percentiles) are smaller, which is an expected result given that for the former the meal intake is considered as an input disturbance, allowing the controller to provide a faster rejection when $\hat{Ra}$ is increasing. This effect can be seen in the insulin

Table 4: Performance metrics of fully closed-loop scheme (UA_{FCL}) respect to hybrid closed-loop scheme considering announced with 30% error($A_{30\%}$) and missed announced (UA_{HCL}) cases. An asterisk indicates statistical significance ($p < 0.05$) respect to UA_{FCL} case. (Overall).

	UA_{FCL}	$A_{30\%}$	UA_{HCL}
Mean G_m $[mg/dL]$	115.955[113.522,119.862]	114.673[112.430,118.417]	129.222[122.452,134.177]*
SD $[mg/dL]$	27.839[24.820, 31.446]	21.014[16.828,23.827]*	40.037[29.621,44.893]*
CV $[\%]$	23.863[22.532,26.237]	18.325[15.030,19.924]*	29.888[25.500, 34.188]*
$70 \leq G_m \leq 140$ $[\%time]$	80.653[79.513,86.116]	85.714[83.097,90.007]	70.722[68.851,77.322]*
$70 \leq G_m \leq 180$ $[\%time]$	96.243[92.570,97.928]	99.626[98.622,99.911]*	84.574[79.994,92.347]*
$G_m > 180$ $[\%time]$	3.757[2.072,7.430]	0.374[0.089,1.378]*	15.426[7.653,19.996]*
$G_m > 250$ $[\%time]$	0.000[0.000,0.000]	0.000[0.000,0.000]	0.188[0.000,1.110]*
$G_m < 70$ $[\%time]$	0.000[0.000,0.000] 0.024(0.056)	0.000[0.000,0.000] 0.000(0.000)	0.000[0.000,0.000] 0.0188(0.0596)
$G_m < 54$ $[\%time]$	0.000[0.000,0.000] 0.000(0.000)	0.000[0.000,0.000] 0.000(0.000)	0.000[0.000,0.000] 0.000(0.000)
$No.\ L1_{hypo}$	0.000[0.000,0.000] 0.007(0.022)	0.000[0.000,0.000] 0.000(0.000)	0.000[0.000,0.000] 0.0071(0.0226)
$No.\ L2_{hypo}$	0.000[0.000,0.000] 0.000(0.000)	0.000[0.000,0.000] 0.000(0.000)	0.000[0.000,0.000] 0.000(0.000)
TDI $[U]$	46.843[39.082,53.116]	43.576[40.226,55.248]	43.708[36.709,48.258]
GMI $[\%]$	6.084[6.025,6.177]	6.053[5.999,6.143]	6.401[6.239,6.519]*

administration pattern, where for the UA_{FCL} case the insulin delivery is higher during postprandial periods, allowing this way a better compensation of the glycemia excursion. Furthermore, from IOB estimation (Fig.7) it can be seen that, in spite of the fact the UA_{FCL} has a delay of $\simeq 50min$ with respect to the announced case ($A_{30\%}$), the IOB amplitude is in the same order of magnitude for both cases. This explains the fact that glycemia control is not seriously degraded when meals are unannounced.

The performance metrics on the 14-day scenario are presented in Table 4. The UA_{FCL} improves the postprandial control respect to UA_{HCL}, reducing the time above 180 mg/dL to 3.757%($p = 0.0046$), without a significant increment of hypoglycemia events. The results show that the increment of time below $G_m < 70$ mg/dL is non-statistically significant (UA_{FCL} : $0.024(0.056)$ vs UA_{HCL} : $0.0188(0.0596)$, $p = 0.85$), although the IDO is naturally more sensible to other disturbances (noise sensor, non modeled plant parts, etc.) than ODO. The glucose variability (SD) is decreased by a 30.466% (UA_{FCL} : 27.839 mg/dL vs UA_{HCL} : 40.037 mg/dL, $p < 0.05$), with an acceptable coefficient of variation ($CV < 36\%$) for the UA_{FCL} case. In addition, the mean glucose is reduced by a 11.5% (UA_{FCL} : 115.95 mg/dL vs UA_{HCL} : 129.22 mg/dL, $p = 0.0028$) which is in accordance with GMI improvement (UA_{FCL} : 6.084 % vs UA_{HCL} : 6.401 %, $p = 0.0028$). On the other hand, from comparison between UA_{FCL} and $A_{30\%}$ cases, we can argue that the glycemia control is not considerably degraded when meal announcement signal is removed from the loop. The time within target range ($70 \leq G_m \leq 180$) is only reduced by a 3.0% (UA_{FCL} : 96.243 vs $A_{30\%}$: 99.626, $p < 0.05$), being this fact mainly related to the increment of the time above 180 mg/dL for the UA_{FCL} scheme. No significant hypoglycemia increments are reported. Despite the glucose variability (SD) is higher for the UA_{FCL} case (UA_{FCL} : 27.839 mg/dL vs $A_{30\%}$: 21.014 mg/dL, $p < 0.01$), no significant differences are reported in the mean glycemia management. This is an expected result given that postprandial control is achieved by a sequence of pulses compensating $\hat{Ra}$ increments (in spite of the super-bolus mode of administration). These results suggest that the proposed scheme could replace the hybrid closed-loop under misestimation errors, avoiding the carbohydrate counting.

7.4. Circadian variability

The $A_{30\%}$ and U_{FCL} cases are assessed considering circadian variability of insulin sensitivity. The sensitivity is affected by sinusoidal variations with 24 hours period, random amplitude according to a uniform distribution of $\pm 30\%$ and random phase [60]. Under this scenario,

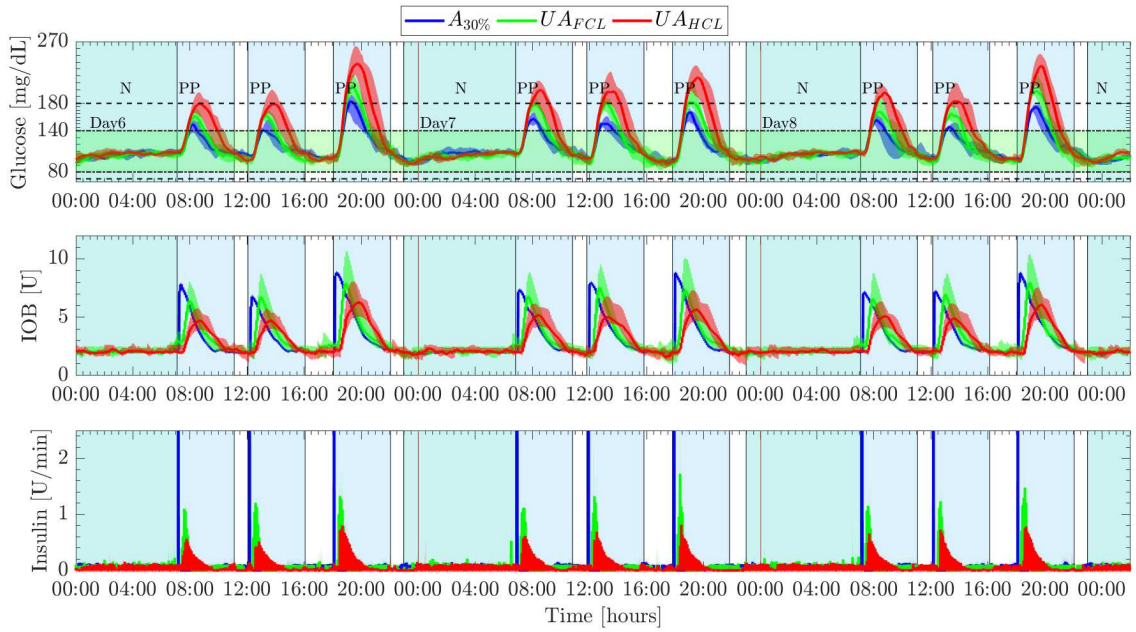

Figure 7: Comparison of the fully closed-loop scheme (UA_{FCL}) respect to hybrid closed-loop proposal when meals are announced with 30% error($A_{30\%}$) and missed announced (UA_{HCL}). Blood glucose, IOB and insulin profiles are shown in terms of median (solid lines) surrounded by colored regions representing the $[25th, 75th]$ percentiles.

non significative changes are observed respect to the nominal case. For $A_{30\%}$ case, the percentage of time in tight range is $85.186[83.831, 88.163](p = 0.791)$; in $70-180\ mg/dL$ range, $99.546[97.566, 99.679](p = 0.52)$ and above $180\ mg/dL$, $0.454[0.322, 2.434](p = 0.499)$. Neither L1 and L2 events are reported. On the other hand, for U_{FCL} case, the percentage of time in tight range is $79.223[76.034, 81.100](p = 0.212)$; in $70-180\ mg/dL$ range, $94.585[90.473, 96.976](p = 0.385)$; and above $180\ mg/dL$, $5.415\ [3.0237, 9.527]\ (p = 0.385)$. The percentage of time in hypoglycemia range (Gm<70) is $0.0352\ (0.0781)\ (p = 0.66)$ with $0.0143(0.03)\ (p = 0.343)$ L1 events. As for the nominal case, no L2 event is reported and the percentage of time in hypoglycemia range (Gm<54) is $0(0)$. This brief simulation suggest that the inherent robustness of the controller is able to account for this kind of variability. Future research should include the use of time-varying models (floquet) to better account for any circadian variability.

7.5. Event-triggered scheme: meal announced case.

In this third case, the performance of the event-triggerd pZMPC presented in Section 6 is evaluated. As for the hybrid closed-loop scheme, the output disturbance observer (ODO) is employed, restricting the simulations to perfectly announced case (PA). The control horizon was set in 14 hours ($N = 168$) for all patients, except for patient 003, for which it was increased to 24 hours ($N = 288$). Notice that this patient has a glucose effectiveness (θ_1) of $0.0010[min]$ which is 3.8 times below the cohort mean value of $0.0037[/min]$ (see Table 2).

Figure 8 shows that the proposed controller (denoted as FIT_{ET}) achieves a better postprandial performance than the conventional therapy, set by the UVA/Padova simulator (denoted as FIT_{CT}). In spite of the fact that both strategies have the same glucose target, the former is tuned to achieve a minimal postprandial hyperglycemia, which is in accordance with glycemia lower bound constraint activation (see [31]), while the latter is adjusted according to more conservative specifications (see: *Determination of CR and CF*, [23]). It is important to note, that the proposed strategy takes into account IOB constraints, avoiding insulin overdosing when meals are misestimated or remaining boluses still active. Furthermore, the pulsatile basal insulin delivery is updated whenever the pZMPC is triggered by a meal event (i.e., $U_b = u^0(2)$, when the pZMPC is inactive). Table 5 shows that the FIT_{ET} increases the time in tight target by a 15.4% (FIT_{ET} : 82.785% vs FIT_{CT} : 71.746%, $p < 0.05$) without statistical significant L1 events (no L2 events are reported). Therefore, since the mean glucose is reduced by a 9.15% (FIT_{ET} : 116.334 mg/dL vs

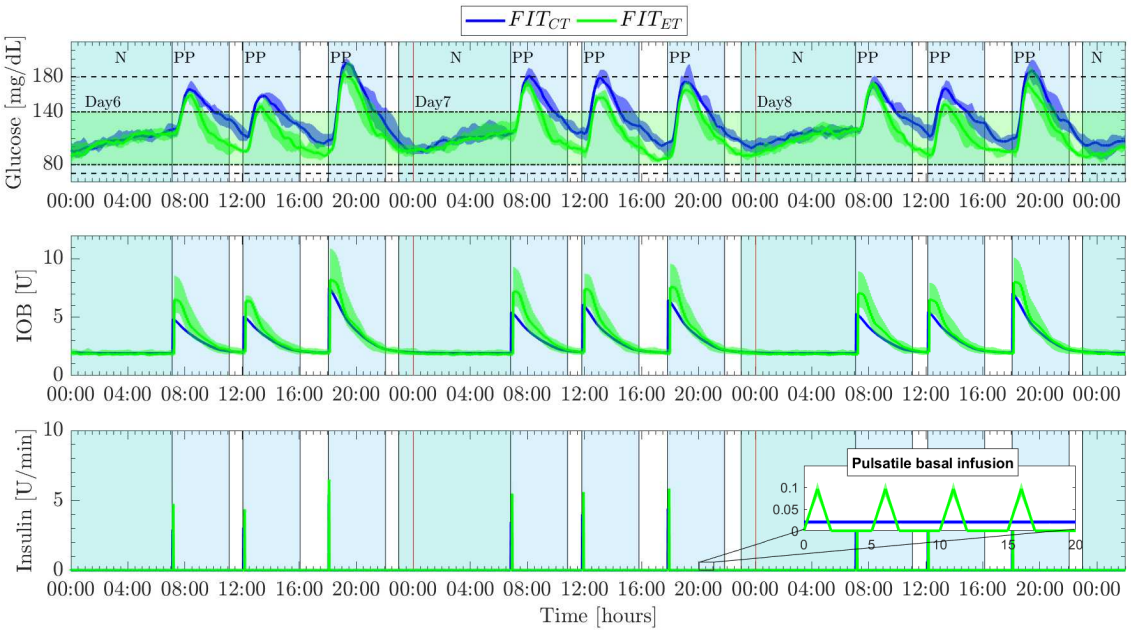

Figure 8: Comparison of the event-trigged scheme (FIT_{ET}) respect to conventional therapy (FIT_{CT}) under perfectly announced meal case. Blood glucose, IOB and insulin profiles are shown in terms of median (solid lines) surrounded by colored regions representing the $[25th, 75th]$ percentiles.

FIT_{CT} : 128.0461 mg/dL, $p < 0.05$) and the time in hypoglycemia range is not significant, the proposed strategy would impact on a enhancement of A1c management (GMI, FIT_{ET} : 6.093 % vs FIT_{CT} : 6.373 %, $p = 0.005$). In this context, the proposed controller could be used as an optimal basal-bolus calculator, designed for computing both, basal and bolus infusions, according to the solution of an optimization problem.

8. Conclusion

An AP based on a stable pZMPC with individualized model was proposed. The approach aims to steer blood glucose to target zone, by employing a pulsatile insulin administration for both, basal and bolus infusions. A daily state set considering normoglycemia range as well as insulin on board constraints was included in order to restrict the insulin infusion, especially during post prandial periods (i.e.: due to overestimated meal intake) and night intervals (i.e.: due to insulin stacking, circadian variability of insulin sensitivity, missing out a dinner, etc.). Furthermore, the presented controller was implemented taking into account announced as well as unannounced meal intake, employing dedicated disturbance observers. For the announced case (hybrid closed-loop scheme) the controller administrates insulin in a super-bolus mode since a fully carbohydrate meal ingest rate (during a sampling period) is assumed. Moreover, the performance was not significantly degraded when meals were announced with 30% error ($A_{30\%}$). On the other hand, for the unannounced case (fully closed-loop scheme, U_{FCL}), the Ra estimation (by means of an input disturbance observer) allowed an improvement of glycemia control respect to missed announced case (U_{HCL}). Moreover, this formulation achieved a behavior comparable with the hybrid scheme under regular carb counting misestimation errors ($A_{30\%}$). Furthermore, the $A_{30\%}$ and U_{FCL} cases were assessed considering circadian variability of insulin sensitivity, with not significant differences respect to nominal case. To take advantage of the pulsatile mode, the proposed controller was finally used as an optimal basal-bolus calculator. A better glycemia control respect to conventional FIT therapy was obtained thanks to the explicit use of predictions, state and inputs constraints, and asymmetric stage costs. Future research includes the explicit use of time-variant linear/nonlinear model for predictions, to better account for any kind a variability.

Table 5: Performance metrics of event-triggered scheme (FIT_{ET}) respect to conventional therapy (FIT_{CT}) set by simulator. An asterisk indicates statistical significance ($p < 0.05$) respect to FIT_{ET} case. (Overall).

	FIT_{ET}	FIT_{CT}
Mean G_m $[mg/dL]$	116.334[114.692,118.451]	128.046[125.987,136.855]*
SD $[mg/dL]$	23.356 [21.490,28.653]	25.288[21.574,28.935]
CV $[\%]$	19.406[18.651,24.983]	18.752[17.917,22.966]
$70 \leq G_m \leq 140$ $[\%time]$	82.785[86.547,86.547]	71.746[74.864,74.864]*
$70 \leq G_m \leq 180$ $[\%time]$	98.999[99.371,99.371]	96.572[95.930,95.930]
$G_m > 180$ $[\%time]$	1.001[0.630,0.630]	3.428[4.070,4.070]
$G_m > 250$ $[\%time]$	0.000[0.000,0.000]	0.000[0.000,0.000]
$G_m < 70$ $[\%time]$	0.000[0.000,0.000] 0.0169(0.0533)	0.000[0.000,0.000] 0.000(0.000)
$G_m < 54$ $[\%time]$	0.000[0.000,0.000] 0.000(0.000)	0.000[0.000,0.000] 0.000(0.000)
$No.\ L1_{hypo}$	0.000[0.000,0.000] 0.0071(0.0226)	0.000[0.000,0.000] 0.000(0.000)
$No.\ L2_{hypo}$	0.000[0.000,0.000] 0.000(0.000)	0.000[0.000,0.000] 0.000(0.000)
TDI $[U]$	46.551[39.497,52.454]	43.111[37.051,47.080]
GMI $[\%]$	6.093[6.053,6.143]	6.373[6.324,6.584]*

9. Acknowledgment

A. H. Gonzalez would like to thank the Argentinean Agency of Scientific and Technological Development (ANPCyT, under the FONCyT Grant PICT-2016-3613) and CONICET. Pablo S. Rivadeneira would like to thank to the Departamento Administrativo de Ciencia, Tecnología e Innovación (COLCIENCIAS) from the Government of Colombia for supporting this work with Grant 110180763081.

10. Appendices

10.1. Appendix A1

Next, the detailed steps to obtain discrete-time system (9) from the sampling of the continuous-time one (4), considering the pulsatile input (8) and constant meals along the period are given. The continuous-time solution of (4), on each periods T, can be written as:

$$\begin{aligned} x(t) = \varphi(t; x(kT), u(\cdot), r(\cdot)) &= e^{A(t-kT)}x(kT) + \int_{kT}^{t} e^{A(t-\zeta)}B_u u(\zeta)d\zeta \\ &+ \int_{kT}^{t} e^{A(t-\zeta)}d\zeta B_r r(kT) + \int_{kT}^{t} e^{A(t-\zeta)}d\zeta E, \end{aligned}$$

for $t \in [kT, (k+1)T]$, where the disturbance r is now out of the integral, because it is constant all along the time period $[kT, (k+1)T)$. To obtain a discrete-time system, the latter solution is sampled at times $t = kT$, $k \in \mathbb{N}$. Furthermore, taking into account that input $u(t)$ is null in $[kT + \Delta T,\ (k+1)T)$, it follows that:

$$\begin{aligned} x((k+1)T) &= e^{A((k+1)T-kT)}x(kT) + \int_{kT}^{kT+\Delta T} e^{A((k+1)T-\zeta)}d\zeta B_u u(kT) \\ &+ \int_{kT}^{(k+1)T} e^{A((k+1)T-\zeta)}d\zeta B_r r(kT) + \int_{kT}^{(k+1)T} e^{A((k+1)T-\zeta)}d\zeta E. \end{aligned}$$

Given that the model matrices are time-invariant, we can consider $kT = 0$ in the integrals, without loss of generality, and so

$$x((k+1)T) = e^{AT}x(kT) + \int_0^{\Delta T} e^{A(T-\zeta)}d\zeta B_u u(kT) + \int_0^{T} e^{A(T-\zeta)}d\zeta B_r r(kT) + \int_0^{T} e^{A(T-\zeta)}d\zeta E. \quad (12)$$

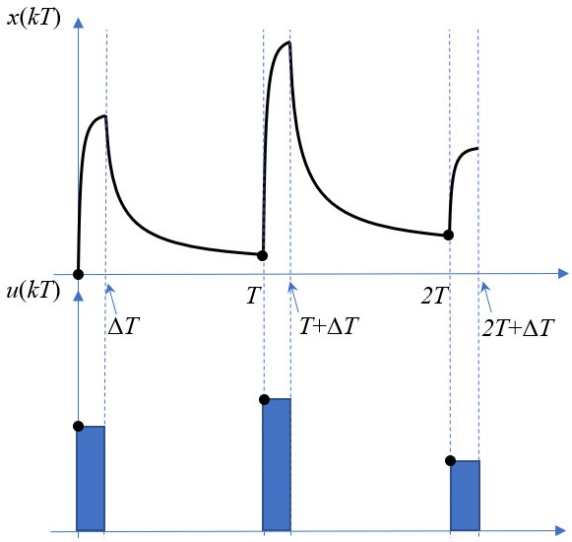

Figure 9: Pulsive scheme. Continuous-time evolution and sampled system.

But the second term of the latter equation can be written as

$$\int_0^{\Delta T} e^{A(T-\zeta)} d\zeta B_u u(kT) = e^{A(T-\Delta T)} \int_0^{\Delta T} e^{A(\Delta T-\zeta)} d\zeta B_u u(kT)$$

and then, equation (12) reads

$$\begin{aligned} x((k+1)T) &= e^{AT}x(kT) + e^{A(T-\Delta T)} \int_0^{\Delta T} e^{A(\Delta T-\zeta)} d\zeta B_u u(kT) + \int_0^{T} e^{A(T-\zeta)} d\zeta B_r r(kT) \\ &+ \int_0^{T} e^{A(T-\zeta)} d\zeta E = A^d x(kT) + B_u^d u(kT) + B_r^d r(kT) + E^d \end{aligned}$$

where $A^d = e^{AT}$, $B_u^d = e^{A(T-\Delta T)} \int_0^{\Delta T} e^{A(\Delta T-\zeta)} d\zeta B_u = e^{A(T-\Delta T)} A^{-1}(e^{A\Delta T} - I_5) B_u$, $B_r^d = \int_0^T e^{A(T-\zeta)} d\zeta B_r = A^{-1}(e^{AT} - I_5) B_r$ and $E^d = \int_0^T e^{A(T-\zeta)} d\zeta E = A^{-1}(e^{AT} - I_5) E$. Figure 9 shows an schematic plot of the pulsatile evolution of a system, where it can be seen that there are two different components: the first one corresponds to the response forced by the input u, while the other is a free response.

References

[1] I. D. Atlas, S. Edition, Online version of idf diabetes atlas, Available at: www.diabetesatlas.org (2015).

[2] A. Katsarou, S. Gudbjörnsdottir, A. Rawshani, D. Dabelea, E. Bonifacio, B. J. Anderson, L. M. Jacobsen, D. A. Schatz, Å. Lernmark, Type 1 diabetes mellitus, Nature reviews Disease primers 3 (2017) 17016.

[3] American Diabetes Association, Classification and diagnosis of diabetes: standards of medical care in diabetes—2019, Diabetes Care 42 (Supplement 1) (2019) S13–S28.

[4] American Diabetes Association, Glycemic targets: Standards of medical care in diabetes-2019, Diabetes Care 42 (Supplement 1) (2019) S61–S70.

[5] J. Walsh, R. Roberts, Pumping insulin: everything for success on an insulin pump and CGM, Torrey Pines Press, 2017.

[6] K. Howorka, Functional Insulin Treatment: Principles, Teaching Approach and Practice, Springer Science & Business Media, 2012.

[7] C. Cobelli, E. Renard, B. Kovatchev, Artificial pancreas: past, present, future, Diabetes 60 (11) (2011) 2672–2682.

[8] S. Trevitt, S. Simpson, A. Wood, Artificial pancreas device systems for the closed-loop control of type 1 diabetes: what systems are in development?, Journal of diabetes science and technology 10 (3) (2016) 714–723.

[9] G. M. Steil, Algorithms for a closed-loop artificial pancreas: the case for proportional-integral-derivative control, Journal of diabetes science and technology 7 (6) (2013) 1621–1631.

[10] R. Mauseth, I. B. Hirsch, J. Bollyky, R. Kircher, D. Matheson, S. Sanda, C. Greenbaum, Use of a "fuzzy logic" controller in a closed-loop artificial pancreas, Diabetes technology & therapeutics 15 (8) (2013) 628–633.

[11] M. Messori, G. P. Incremona, C. Cobelli, L. Magni, Individualized model predictive control for the artificial pancreas: In silico evaluation of closed-loop glucose control, IEEE Control Systems Magazine 38 (1) (2018) 86–104.

[12] A. Haidar, The artificial pancreas: How closed-loop control is revolutionizing diabetes, IEEE Control Systems Magazine 36 (5) (2016) 28–47.

[13] D. Shi, S. Deshpande, E. Dassau, F. J. Doyle III, Feedback control algorithms for automated glucose management in T1DM: the state of the art, in: The Artificial Pancreas, Elsevier, 2019, pp. 1–27.

[14] G. P. Incremona, M. Messori, C. Toffanin, C. Cobelli, L. Magni, Model predictive control with integral action for artificial pancreas, Control Engineering Practice 77 (2018) 86–94.

[15] R. Hovorka, et al., Nonlinear model predictive control of glucose concentration in subjects with type-1 diabetes, Physiological Measurement 25 (4) (2004) 905–920.

[16] R. Gondhalekar, E. Dassau, F. J. Doyle III, Velocity-weighting and velocity-penalty MPC of an artificial pancreas: Improved safety and performance, Automatica 91 (48) (2018) 105–117.

[17] D. Boiroux, A. K. Duun-Henriksen, S. Schmidt, K. Nørgaard, S. Madsbad, N. K. Poulsen, H. Madsen, J. B. Jørgensen, Overnight glucose control in people with type 1 diabetes, Biomedical Signal Processing and Control 39 (2018) 503–512.

[18] I. Hajizadeh, M. Rashid, S. Samadi, M. Sevil, N. Hobbs, R. Brandt, A. Cinar, Adaptive personalized multivariable artificial pancreas using plasma insulin estimates, Journal of Process Control 80 (2019) 26–40.

[19] D. Shi, E. Dassau, F. J. Doyle III, Multivariate learning framework for long-term adaptation in the artificial pancreas, Bioengineering & translational medicine 4 (1) (2019) 61–74.

[20] D. Boiroux, V. Bátora, M. Hagdrup, S. L. Wendt, N. K. Poulsen, H. Madsen, J. B. Jørgensen, Adaptive model predictive control for a dual-hormone artificial pancreas, Journal of Process Control 68 (2018) 105–117.

[21] G. C. Goodwin, A. M. Medioli, H. V. Phan, B. R. King, A. D. Matthews, Application of MPC incorporating stochastic programming to type 1 diabetes treatment, in: 2016 American Control Conference (ACC), IEEE, 2016, pp. 907–912.

[22] M. M. Seron, A. M. Medioli, G. C. Goodwin, A methodology for the comparison of traditional MPC and stochastic MPC in the context of the regulation of blood glucose levels in type 1 diabetics, in: 2016 Australian Control Conference (AuCC), IEEE, 2016, pp. 126–131.

[23] C. D. Man, F. Micheletto, D. Lv, M. Breton, B. Kovatchev, C. Cobelli, The UVA/Padova type 1 diabetes simulator: new features, Journal of diabetes science and technology 8 (1) (2014) 26–34.

[24] R. Hovorka, F. Shojaee-Moradie, P. V. Carroll, L. J. Chassin, I. J. Gowrie, N. C. Jackson, R. S. Tudor, A. M. Umpleby, R. H. Jones, Partitioning glucose distribution/transport, disposal, and endogenous production during IVGTT, American Journal of Physiology-Endocrinology and Metabolism 282 (5) (2002) E992–E1007.

[25] S. S. Kanderian, S. Weinzimer, G. Voskanyan, G. M. Steil, Identification of intraday metabolic profiles during closed-loop glucose control in individuals with type 1 diabetes (2009).

[26] J. B. Jørgensen, D. Boiroux, Z. Mahmoudi, An artificial pancreas based on simple control algorithms and physiological insight, IFAC-PapersOnLine 52 (1) (2019) 1018–1023.

[27] DiabetesHealth, Product reference guide january 2019, Available at: https://diabeteshealth.com/wp-content/uploads/2019/pdf/2019/InsulinPumps.pdf (2019).

[28] S. H. Song, S. S. McIntyre, H. Shah, J. D. Veldhuis, P. C. Hayes, P. C. Butler, Direct measurement of pulsatile insulin secretion from the portal vein in human subjects, The Journal of Clinical Endocrinology & Metabolism 85 (12) (2000) 4491–4499.

[29] L. S. Satin, P. C. Butler, J. Ha, A. S. Sherman, Pulsatile insulin secretion, impaired glucose tolerance and type 2 diabetes, Molecular aspects of medicine 42 (2015) 61–77.

[30] W. Regittnig, M. Urschitz, B. Lehki, M. Wolf, H. Kojzar, J. K. Mader, M. Ellmerer, T. R. Pieber, Insulin bolus administration in insulin pump therapy: Effect of bolus delivery speed on insulin absorption from subcutaneous tissue, Diabetes technology & therapeutics 21 (1) (2019) 44–50.

[31] G. C. Goodwin, A. M. Medioli, D. S. Carrasco, B. R. King, Y. Fu, A fundamental control limitation for linear positive systems with application to type 1 diabetes treatment, Automatica 55 (2015) 73–77.

[32] G. C. Goodwin, D. S. Carrasco, M. M. Seron, A. M. Medioli, A fundamental control performance limit for a class of positive nonlinear systems, Automatica 95 (2018) 14–22.

[33] H. M. Tolic, E. Mosekilde, J. Stuirs, Modeling the insulin-glucose feedback system: the significance of pulsatile insulin secretion, Journal of Theoretical Biology 207 (2000) 361–375.

[34] Y. Ruan, M. E. Wilinska, H. Thabit, R. Hovorka, Modeling day-to-day variability of glucose-insulin regulation over 12-week home use of closed-loop insulin delivery, IEEE Transactions on Biomedical Engineering 64 (6) (2017) 1412–1419.

[35] P. S. Rivadeneira, A. Ferramosca, A. H. González, Control strategies for non-zero set-point regulation of linear impulsive systems, IEEE Transactions on Automatic Control 69 (9) (2018) 2994–3001.

[36] P. S. Rivadeneira, J. L. Godoy, J. E. Serenoa, P. Abuin, A. Ferramosca, A. H. González, Impulsive MPC schemes for biomedical processes. application to type 1 diabetes, in: A. T. Azar (Ed.), Control applications for Biomedical Engineering Systems, ELSEVIER, 2019.

[37] C. M. Ramkisson, P. Herrero, J. Bondia, V. J., Unannounced meals in the artificial pancreas: Detection using continuous glucose monitoring, Sensors 18 (2018) 1–18. doi:10.3390/s18030884.

[38] A. El Fathi, M. R. Smaoui, V. Gingras, B. Boulet, A. Haidar, The artificial pancreas and meal control: an overview of postprandial glucose regulation in type 1 diabetes, IEEE Control Systems Magazine 38 (1) (2018) 67–85.

[39] S. Oviedo, J. Vehí, R. Calm, J. Armengol, A review of personalized blood glucose prediction strategies for T1DM patients, International journal for numerical methods in biomedical engineering 33 (6) (2017) e2833.

[40] E. M. Aiello, G. Lisanti, L. Magni, M. Musci, C. Toffanin, Therapy-driven deep glucose forecasting, Engineering Applications of Artificial Intelligence 87 (2020) 103255.

[41] C. D. Man, R. A. Rizza, C. Cobelli, Meal simulation model of the glucose-insulin system, IEEE Transactions on Biomedical Engineering 54 (10) (2007) 1740–1749.

[42] R. N. Bergman, Y. Z. Ider, C. R. Bowden, C. Cobelli, Quantitative estimation of insulin sensitivity., American Journal of Physiology-Endocrinology And Metabolism 236 (6) (1979) E667.

[43] I. Hajizadeh, M. Rashid, K. Turksoy, S. Samadi, J. Feng, M. Sevil, N. Frantz, C. Lazaro, Z. Maloney, E. Littlejohn, et al., Multivariable recursive subspace identification with application to artificial pancreas systems, IFAC-PapersOnLine 50 (1) (2017) 886–891.

[44] K. van Heusden, E. Dassau, H. C. Zisser, D. E. Seborg, F. J. Doyle III, Control-relevant models for glucose control using a priori patient characteristics, IEEE transactions on biomedical engineering 59 (7) (2011) 1839–1849.

[45] M. Messori, C. Toffanin, S. Del Favero, G. De Nicolao, C. Cobelli, L. Magni, Model individualization for artificial pancreas, Computer methods and programs in biomedicine (2016).

[46] C. Cobelli, G. Pacini, G. Toffolo, L. Sacca, Estimation of insulin sensitivity and glucose clearance from minimal model: new insights from labeled IVGTT, American Journal of Physiology-Endocrinology And Metabolism 250 (5) (1986) E591–E598.

[47] N. Magdelaine, L. Chaillous, I. Guilhem, J. Y. Poirier, M. Krempf, C. H. Moog, E. L. Carpentier, A long-term model of the glucose-insulin dynamics of type 1 diabetes, IEEE Transactions on Biomedical Engineering 62 (6) (2015) 1546 –1552.

[48] S. Dube, I. Errazuriz-Cruzat, A. Basu, R. Basu, The forgotten role of glucose effectiveness in the regulation of glucose tolerance, Current diabetes reports 15 (6) (2015) 31.

[49] J. Bondia, S. Romero-Vivo, B. Ricarte, J. L. Diez, Insulin estimation and prediction: a review of the estimation and prediction of subcutaneous insulin pharmacokinetics in closed-loop glucose control, IEEE Control Systems Magazine 38 (1) (2018) 47–66.

[50] P. Colmegna, F. Garelli, H. De Battista, R. Sánchez-Peña, Automatic regulatory control in type 1 diabetes without carbohydrate counting, Control Engineering Practice 74 (2018) 22–32.

[51] C. Cobelli, E. Carson, Introduction to modeling in physiology and medicine, Academic Press, 2019.

[52] D. Simon, Kalman filtering with state constraints: a survey of linear and nonlinear algorithms, IET Control Theory & Applications 4 (8) (2010) 1303–1318.

[53] P. Rivadeneira, A. Ferramosca, A. H. González, MPC with state window target control in linear impulsive systems, IFAC-PapersOnline 48 (23) (2015) 507–512.

[54] T. Alamo, A. Ferramosca, A. H. González, D. Limon, D. Odloak, A gradient-based strategy for the one-layer RTO+MPC controller, Journal of Process Control 24 (4) (2014) 435–447.

[55] A. Ferramosca, A. H. González, D. Limon, Offset-free multi-model economic model predictive control for changing economic criterion, Journal of Process Control 54 (2017) 1–13.

[56] M. Vettoretti, A. Facchinetti, G. Sparacino, C. Cobelli, Type-1 Diabetes Patient Decision Simulator for In Silico Testing Safety and Effectiveness of Insulin Treatments, IEEE Transactions on Biomedical Engineering 65 (6) (2017) 1281–1290.

[57] T. Danne, R. Nimri, T. Battelino, R. M. Bergenstal, K. L. Close, J. H. DeVries, S. Garg, L. Heinemann, I. Hirsch, S. A. Amiel, et al., International consensus on use of continuous glucose monitoring, Diabetes care 40 (12) (2017) 1631–1640.

[58] R. M. Bergenstal, R. W. Beck, K. L. Close, G. Grunberger, D. B. Sacks, A. Kowalski, A. S. Brown, L. Heinemann, G. Aleppo, D. B. Ryan, et al., Glucose management indicator (GMI): a new term for estimating A1C from continuous glucose monitoring, Diabetes care 41 (11) (2018) 2275–2280.

[59] T. Kawamura, C. Takamura, M. Hirose, T. Hashimoto, T. Higashide, Y. Kashihara, K. Hashimura, H. Shintaku, The factors affecting on estimation of carbohydrate content of meals in carbohydrate counting, Clinical Pediatric Endocrinology 24 (4) (2015) 153–165.

[60] E. J. Mansell, P. D. Docherty, J. G. Chase, Shedding light on grey noise in diabetes modelling, Biomedical Signal Processing and Control 31 (2017) 16–30.

Apéndice B

Pulsatile Zone MPC with asymmetric stationary cost for artificial pancreas based on a non-standard IOB constraint

Pulsatile Zone MPC with asymmetric stationary cost for artificial pancreas based on a non-standard IOB constraint

Pablo Abuin[a], Antonio Ferramosca[b], Chiara Toffanin[c], Lalo Magni[d], Alejandro H. Gonzalez[a]

[a]*Institute of Technological Development for the Chemical Industry (INTEC), CONICET-Universidad Nacional del Litoral (UNL), Güemes 3450, Santa Fe (3000), Argentina. (e-mail: alejgon@santafe-conicet.gov.ar)*
[b]*Department of Management, Information and Production Engineering, University of Bergamo Via Marconi 5, 24044 Dalmine (BG), Italy (e-mail: antonio.ferramosca@unibg.it)*
[c]*Department of Electrical, Computer and Biomedical Engineering, University of Pavia, 27100 Pavia, Italy*
[d]*Department of Civil and Architecture Engineering, University of Pavia, 27100 Pavia, Italy*

Abstract

This paper presents an improved version of the pulsatile Zone Model Predictive Control (pZMPC) for glycemic control in type 1 diabetic patients presented in [1]. Two main novelties were included: (i) a time-varying insulin on board constraint ($\overline{IOB}(t)$), which promotes a non-zero insulin delivery after a standard bolus infusion (increasing the system controllability during postprandial periods), and (ii) a soft-constrained version of the controller which ensures stability with an enlarged domain of attraction. Furthermore, a configuration method for the IOB constraint based on a carb counting regression model is proposed, and an algorithm is given to adjust the amplitude of the constraint based on glycemia rate of change information. In-silico results in the FDA-approved UVA/Padova simulator, under over/underestimation of meal amount, show a superiority of the glucose control over postprandial periods when the aforementioned ingredients are employed.

Keywords: Insulin on board, Carbohydrate counting error, Soft constraints, Model Predictive Control, Artificial pancreas

1. Introduction

Type 1 Diabetes Mellitus (T1DM) is a chronic disease characterized by a destruction of pancreatic β cells [2], which leads to a complete deficiency of endogenous insulin production, thus resulting in higher blood glucose (BG) levels (fasting BG: $>$ 126 mg/dL, postprandial BG (2hs): $\geq$ 200 mg/dL) [3]. It accounts for 5–15$\%$ of approximately 422 million worldwide patients with diabetes, and its incidence is increasing at a rate of 3.9$\%$ per year [2]. Due to the hyperglycemia condition, diabetic patients are prone to have long-term complications, such as nephropathy, neuropathy, coronary heart disease and peripheral artery disease, as well as short-term complications, such as, diabetic ketoacidosis (that is, acidosis due to the breakdown of lipids to ketones as an alternative source of glucose).

To restore euglycemia levels (fasting BG: $80-140$ mg/dL, peak postprandial BG (2hs): <180 mg/dL) [4], avoiding hypoglycemia episodes in the path (BG: <70 mg/dL, severe hypoglycemia leads to cerebral damage or even death), patients with T1DM require the delivery of insulin in an optimized manner. As result, the artificial pancreas (AP) was proposed as a medical device to control glycemia in a closed-loop mode, through a continuous glucose monitoring (CGM) sensor, an insulin pump (CSII), and a control algorithm, which based on the CGM readings, adjusts the insulin delivery. Several control algorithms have been proposed for current AP systems, including Proportional-Integral-Derivative (PID) [5], Fuzzy-Logic [6], and Model Predictive Control (MPC) [7, 8, 1], which have been tested under in-silico simulators (UVA/Padova [9], Cambridge [10], Medtronic Virtual Patient [11]) and also under in-vivo clinical trials [12, 13, 14]. Among all these control strategies, MPC has shown to be the most promissory one, because of its ability to compute optimal control actions (insulin for the single-hormonal, and insulin and glucagon for the bi-hormonal) based on the solution of a optimization problem that takes into account a mathematical prediction model of the glucose-insulin dynamic, and input and output or state constraints. While input constraints often represent *physical limitations* of the actuators (*i.e.* insulin pump accuracy , operation range), and thus, can not been exceeded, output or state constraints are usually *desirable limitations* that may not be fulfilled depending on the disturbances affecting the system. It is often the function of the MPC

controller to determine in real time if the output or state constraints are not achievable, and relax them in some satisfactory manner (*i.e.* by penalizing the severity degree related to the constraint unfulfillment).

Even though insulin administration via intraperitoenal route has improved pharmacokinetic/pharmacodynamic properties [15, 16], the majority of AP systems administers the insulin subcutaneously, which for the rapid-acting insulin induces a lag of ~ 80 min since the insulin is infused until its peak effect (*i.e.* 50 min for insulin absorption and 30 min for insulin action) [17, 18]. Therefore, the non-negligible dynamic between injections and their effects in the blood needs to be explicitly considered. A reported well known phenomenon occurring when this dynamic is disregarded or underestimated by the controller is insulin stacking - a phenomenon frequently intensified by closed-loop algorithms that infuse insulin continuously [5, 19]. To counteract this effect that increase the risk of hypoglycemic events, safety modules based on the estimation and limitation of the plasma insulin and/or the insulin on board (IOB) - insulin depot remaining at the subcutaneous tissue before entering circulation - have been proposed [20]. In the context of MPC controllers this safety limitation is accounted for, directly, through constraints in states associated with plasma insulin and/or IOB [21, 1] or, indirectly, through constraints on the insulin delivery rate $u(t)$ [U/min] [22, 23]. Regarding the former, it is important to mention, that several works [24, 20] have considered an external feedback loop, called safety auxiliary feedback element (SAFE), to keep IOB inside predefined limits in non-constrained formulations.

Furthermore, since the major disturbance corresponds to meal ingestion, which is normally counteracted by insulin carb-boluses, IOB constraints with exponential decay curves have been employed [8, 24, 25], which mimics the pharmacokinetic (PK) profile corresponding to bolus injections [26]. This way, the control performance does not deteriorate significantly, while hypoglycemic episodes are avoided. However, forcing this mode of infusion, may be not optimal for meals with slow absorption dynamics, where a better blood glucose control is achieved by a bolus plus a non-zero flow delivery [27], or when an *'extended bolus'* (square wave) posterior to the bolus injection is desired in, a so-called, *'dual-wave infusion policy'* [28, 29]. Moreover, since the IOB constraint is normally designed based on the estimated '*carb/correction bolus*' of the conventional therapy [20, 30, 31], it could be restrictive in case of underestimated meal ingest and/or overestimated functional insulin therapy (FIT) parameters, so significantly reducing the T1DM controllability at hyperglycemic conditions. Studies have reported that T1DM patients are prone to underestimate large meals [32, 33, 34], which impacts on BG control, denoting an increased risk of hyperglycemic episodes. Furthermore, due to the exponential decay rate, insulin delivery could be limited in case of an unannounced meal intake during the postprandial period of the configured bolus delivery. Therefore, it could be desirable to have an IOB constraint which, in addition to a bolus infusion, allows for a non-zero insulin delivery over a predefined time interval. As it will be detailed below, the study and modification of the IOB constraint is one of the main contributions of this work.

Concerning the MPC formulations for APs, the majority of them lacks of stabilizing ingredients (terminal cost function and terminal constraint). To the best of the current author's knowledge, some exceptions can be found in [7, 35, 36, 37, 38, 39]. To avoid increasing the computational cost related to terminal ingredients consideration (*i.e.* terminal set handling by additional constraints), prediction horizon sufficiently large such that the terminal state reaches an equilibria condition are usually employed [40]. This way, since meals represent the major perturbation, and taking into account that the postprandial period after a well-configured carb-bolus lasts ~ 4 h, prediction horizons of $6 - 10$ h are used. In addition, most of them are formulated by minimizing the deviation between the predicted glycemia and a fixed set-point (*i.e.* integral MPC [41], set-point enhanced MPC [42, 40]) or a set-interval (*i.e.* zone MPC [8, 30]). Therefore, since the constraints and the terminal conditions of the optimization related problem will depend on the selected target, if it is changed (*i.e.* blood glucose zone varying over the day [30], time-varying setpoint in accordance to blood glucose level [40]), the controller feasibility could be lost. Furthermore, imposing hard state or output constraints can be overly conservative or render the optimization problem infeasible in the closed-loop operation (for example, due to unmodelled glucose-insulin effects, intraday-variations of insulin sensitivity, sensor noise, among others). Even though a possible remedy is to soften the state constraints by penalizing (in the AP context, see [22, 40]), standard soft-constrained formulations do not provide stability guarantees. Therefore, as an additional contribution of this work, the pulsatile Zone Model Predictive Control presented in Abuin et. al. [1], which is an MPC for tracking zone regions under changing operation conditions and has recursive feasibility and stability guarantees by design (under nominal conditions)[43], was extended to the soft-constrained case, based on Zeilinger et. al. [44] proposal. This way, under the assumption that a not-necessary feasible equilibrium (in the hard sense) is reached at the end of the control horizon (*i.e.* meals fully absorbed during prediction horizon), the recursive feasibility and stability of the closed-loop are

guaranteed for all time. Furthermore, because of the proper use of constraints, the domain of attraction is increased.

Finally, since the glucose control problem of T1DM is highly asymmetric (the consequences of hypoglycemia are faster and more detrimental than those of hyperglycemia, in the single-hormone AP there is no antagonist control action to insulin, insulin can not be removed, etc.) we added: a) an asymmetric stage cost which, by penalizing harder hypoglycemic excursions over the prediction horizon, promotes the convergence of the predicted trajectory to the artificial set-point from above, and b) an asymmetric stationary cost, both to decrease the artificial setpoint convergence at hyperglycemic conditions (and thus, decreasing the controller overreaction) and to encourage the insulin suspension as the blood glucose is below the target zone. Moreover, as a special setting, we extended the aforementioned stationary cost by including a velocity-dependent function which modifies the artificial setpoint convergence to the zone in accordance with the glycemic rate of change.

According to the aforementioned discussion, the main novelties of this work are:

1. A novel time-varying constraint for the insulin on board (IOB) is proposed, which promotes a non-zero insulin flow after a bolus delivery, so increasing the system controllability during postprandial periods. Furthermore, a configuration method of the constraint based on a carb counting regression model is proposed, and an algorithm is given, to adjust the amplitude of the constraint, according to the glycemia rate of change.
2. A soft-constrained version of the pulsatile zone MPC (pZMPC) introduced in Abuin et al. [1] is proposed, which ensures stability with an enlarged domain of attraction.

After the introduction given in Section 1 the article is organized as follows. Section 2 presents the glucose–insulin model and the time-varying constraints of the blood glucose problem under insulin therapy. In Section 3 the non-standard IOB constraint is formulated and a configuration methodology according to a carb counting regression model is explained. An extended algorithm is included to deal with a relaxation of constraint amplitude in the case of excessive glycemia rise. In Section 4, the discretization schemes are formulated in order to get a pulsatile representation of the glucose-insulin model. Then, in Section 5, the pulsatile zone MPC is presented and the soft-constrained formulation is detailed. In Section 6, in-silico trials are performed considering different settings of the non-standard IOB constraint and carb counting estimation errors. Finally, in Section 7, a complete discussion concerning glycemic control under the novel IOB constraint is fulfilled, and some concluding remarks are given.

2. Control-oriented model

According to control purposes, and regarding its inherent descriptive capability and parameter interpretability, the following physiological long-term minimal model based on Ruan et. al. [45] proposal, is considered:

$$\begin{aligned} \dot{x}(t) &= Ax(t) + B_u u(t) + B_r r(t) + E, \;\; x(0) = x_0, \\ y(t) &= Cx(t), \end{aligned} \tag{2.1}$$

where $x(t) = [x_1(t) \;\; x_2(t) \;\; x_3(t) \;\; x_4(t) \;\; x_5(t)]'$, with x_1 being the blood glucose concentration [mg/dL], x_2 being the insulin delivery rate in plasma [U/min], x_3 being the insulin delivery rate in the subcutaneous compartment [U/min], x_4 being the rate of carbohydrate absorption from the gut [g/min] and x_5 being the glucose delivery rate from the stomach [g/min]. The output $y(t)$ is given by the state component x_1, *i.e.*, the glycemia to be controlled. Furthermore, $u(t)$ denotes the exogenous insulin infusion rate [U/min] and $r(t)$ the carbohydrate amount (CHO) eaten in the unit of time [g/min]. The state matrices are given by:

$$A = \begin{pmatrix} -\theta_1 & -\theta_2 & 0 & \theta_3 & 0 \\ 0 & -\frac{1}{\theta_4} & \frac{1}{\theta_4} & 0 & 0 \\ 0 & 0 & -\frac{1}{\theta_4} & 0 & 0 \\ 0 & 0 & 0 & -\frac{1}{\theta_5} & \frac{1}{\theta_5} \\ 0 & 0 & 0 & 0 & -\frac{1}{\theta_5} \end{pmatrix}, \; B_u = \begin{pmatrix} 0 \\ 0 \\ \frac{1}{\theta_4} \\ 0 \\ 0 \end{pmatrix}, \; B_r = \begin{pmatrix} 0 \\ 0 \\ 0 \\ 0 \\ \frac{1}{\theta_5} \end{pmatrix}, \; E = \begin{pmatrix} \theta_0 \\ 0 \\ 0 \\ 0 \\ 0 \end{pmatrix}, \; C = \begin{pmatrix} 1 \\ 0 \\ 0 \\ 0 \\ 0 \end{pmatrix}', \;$$

where θ_2 is the insulin sensitivity [mg/(dL·U)] (it measures the ability of insulin to enhance the disappearance of glucose from plasma, both by inhibiting glucose production and by stimulating glucose utilization in

insulin-dependent tissues) and θ_3 is the raise factor [mg/(dL·g)] (change in blood glucose concentration per unit of time when 1 g of CHO is absorbed), being the rate of glucose appearance in plasma $R_a = \theta_3 x_4(t)$ [mg/(dL·min)]. Moreover, θ_1 is the glucose effectiveness [/min] or glucose self-regulation effect to promote its own metabolism (*i.e.* stimulating glucose uptake by peripheral tissues and suppressing hepatic glucose release) and θ_0 the endogenous glucose production at basal levels EGP_b ($\theta_0 = \theta_1 G_b + \theta_2 U_b$, being G_b and U_b the glucose and insulin rate at basal levels) [mg/(dL · min)]. The insulin absorption kinetics is expressed by θ_4 (time-to-maximum effective insulin concentration) [min] while the time constant related to the meal absorption subsystem is represented by θ_5 (or time-of-maximum appearance rate of glucose in gut) [min].

The unconstrained set of equilibrium pairs (u_s, x_s) of system (2.1) (which are obtained by making $\dot{x}(t) = 0$ in (2.1)), is given by the pairs $(u_s, x_s) \in \mathbb{R}_{\geq 0} \times \mathbb{R}^5_{\geq 0}$ that fulfills $x_{s,1} = (\theta_0 - \theta_2 u_s)/\theta_1$, $x_{2,s} = x_{3,s} = u_s$ and $x_{4,s} = x_{5,s} = 0$. Among all the pairs (u_s, x_s) constituting an equilibrium condition, the one corresponding to basal conditions is denoted (U_b, x_b), where $x_b := [x_{1,b} \;\; x_{2,b} \;\; x_{3,b} \;\; x_{4,b} \;\; x_{5,b}]' = [G_b \;\; U_b \;\; U_b \;\; 0 \;\; 0]'$, U_b is the basal insulin dose and G_b is the basal glycemia, *i.e.*, a fasting normoglycemia value ($G_b \approx 110$ [ml/dL]). The basal regime refers simultaneously to equilibrium and fasting conditions (there is no equilibrium with meals). Furthermore, it is possible to define glycemia and insulin basal sets (G_b^{Tar} and U_b^{Tar}, with $G_b^{Tar} = (\theta_0 - \theta_2 U_b^{Tar})/\theta_1$), instead of basal points, to reinforce the idea that there is a complete zone of values G_b, (*i.e.* $80 \leq G_b \leq 140$ [mg/dL]) where the blood glucose concentration is considered normal.

Remark 1. *Due to the affine term, E, basal conditions are explicitly accounted for in model* (2.1) *(i.e. $G_b = (\theta_0 - \theta_2 U_b)/\theta_1$). This way, the input u can be expressed as*

$$u(t) := U_b + \tilde{u}(t), \tag{2.2}$$

in such a way that both, the basal U_b and bolus/postprandial $\tilde{u}(t)$ infusions are accounted for simultaneously, allowing null insulin infusion when $u(t) \equiv 0$. This consideration significantly increases the system controllability when, for instance, a complete reduction of the basal delivery is needed after an insulin 'super-bolus' (i.e. optimal insulin delivery for meals with full CHO content), or a postprandial hypoglycemia episode is unavoidable for any non-null basal delivery.

Remark 2. *Under the assumption that $\theta_1 \approx 0$ (see [46, 47]), FIT tools can be derived from the analysis of the dynamic model* (2.1)*. Owing to this, the correction factor (or insulin sensitivity factor) $CF = \theta_2$ [mg/(dL U)], the raise factor $RF = \theta_3$ [mg/(dL g)], and the carbohydrate-to-insulin ratio (or the number of carbohydrates covered by 1 unit of insulin) $CR = \theta_2/\theta_3$ [g/U]. It is important to mention, that since the glucose self-regulation effect is not accounted (i.e. note that it counteracts the insulin effect on BG reduction), the mentioned parameters are conservative in sense of the optimal achievable values [48, 49, 50].*

Remark 3. *The so-called insulin-on-board (IOB) - that is, the amount of insulin remaining in the body from the previous insulin boluses - can also be expressed in terms of the system* (2.1) *states. Indeed, according to [51], the IOB is given by $IOB(t) := \int_0^t (u(\tau) - x_2(\tau))\, d\tau$. Since $u(\tau) - x_2(\tau) = \theta_4(\dot{x}_2(\tau) + \dot{x}_3(\tau))$, then $IOB(t) = \theta_4(x_2(t) + x_3(t))$ (where it is assumed $x_2(0) = 0$ and $x_3(0) = 0$).*

Remark 4. *According to the superposition of basal and bolus (or postprandial) components of the input $u(t)$, and the model* (2.1) *linearity, it is possible to denote the state variable by the superposition of this two component $x_i(t) = x_{i,b} + \tilde{x}_i(t)$, $i = \{1, 2, 3\}$. The same follows for the IOB, $IOB(t) = IOB_b + \tilde{IOB}(t)$.*

2.1. Time-varying input and state constraints

System (2.1) is assumed to be constrained in both, states and input, such that $u \in \mathcal{U}$, $x \in \mathcal{X}$, where $\mathcal{U}$ is given by $\mathcal{U} = \{u \in \mathbb{R}_{\geq 0} \mid u \leq U_{max}\}$, with $U_{max} \approx 15$ [U/min] (*i.e.*: maximum infusion dose of insulin pumps) [52]. Furthermore, $\mathcal{X}$ is assumed to be time-varying along the day, to account for additional insulin requirements over postprandial periods. For the sake of simplicity, let consider a meal-related event [1] of amplitude $C\hat{H}O_0$ [g] at $t = t_0$. Then, for $t \geq t_0$,

$$\mathcal{X}(t) := \{x \in \mathbb{R}^5_{\geq 0} \mid G_{hypo} \leq x_1(t) \leq G_{hyper},\; \theta_4(x_2(t) + x_3(t)) \leq \overline{IOB}(t)\}, \tag{2.3}$$

[1] Meal announcement through the estimated carbohydrate content $C\hat{H}O$.

where $\overline{IOB}(t) = IOB_{b,max} + I\tilde{O}B_{max}(t; t_0, C\hat{H}O_0)$, being $IOB_{b,max}$ a constant associated with basal/equilibrium conditions [2] and $I\tilde{O}B_{max}(t; t_0, C\hat{H}O_0)$ a time-varying term accounting for insulin delivery over the postprandial period, which is explicitly defined in Section 3 and it can be configured according to an admissible carb bolus, $U_0 = C\hat{H}O_0/CR$. To avoid insulin overdoses due to an overestimated $C\hat{H}O$, U_0 can be computed using a fixed meal size upper bound (*i.e:* 55 g for all $C\hat{H}O$) [31], meal size classification levels (*i.e.:* small meals $C\hat{H}O < 35$ g, medium meals $C\hat{H}O \in [35, 65)$ g, large meals ≥ 65 g) [53, 31], or an assumed CHO counting error model (*i.e.* $C\hat{H}O = f(CHO)$) as it will be detailed next, in Section (3.2). The bounds for x_1 are given by $G_{hypo} = 60$ and $G_{hyper} = 300$ [mg/dL]. Note that $\mathcal{X}(t)$ is unbounded from above for x_4, x_5, which is consistent with the fact that these two state components (associated to the meal ingestion) are uncontrollable. The constrained equilibrium set is given by the pairs (u_s, x_s) that fulfill $0 \leq u_s \leq U_{b,max}$, with $U_{b,max} := (\theta_0 - \theta_1 G_{b,min})/\theta_2$, $G_{hypo} \leq x_{1,s} \leq G_{hyper}$ and $\theta_4(x_{2,s} + x_{3,s}) \leq IOB_{b,max}$. Note that equilibrium is, by definition, associated with a basal condition, since equilibrium implies a fasting state, *i.e.*, $x_{4,s} = x_{5,s} = 0$. Furthermore, it is clear that every feasible equilibrium state is in $\mathcal{X}(t)$, for all $t \geq t_0$.

Remark 5. *In contrast to [1], where a piecewise IOB constraint was employed, with fixed bounds over diurnal and nocturnal periods, in this work, we propose a time-varying IOB constraint according to an admissible insulin absorption pattern after a meal-related event. As a result, the constraint is only relaxed when a carb bolus is required, ensuring glycemia compensation over postprandial periods, and avoiding insulin over delivery during fasting periods (i.e. increased risk of hypoglycemia events overnight interval due to a blunted sympathoadrenal response to falling blood glucose concentration [54, 55]). Moreover, in comparison with the piecewise IOB constraint, where infeasibility problems could arise if a meal-related event takes place in the vicinity of constraint tightening; by using a time-varying profile - in accordance to the insulin absorption dynamic - the risk of infeasibility is decreased.*

3. Non-standard IOB constraint

Several types of time-varying IOB constraints have been proposed for AP control algorithms ([56, 8, 24, 31]), the majority of which were designed to accomplish IOB decay curves after the standard bolus injections. However, this model of infusion is right only for meals with rapid-absorption dynamics *i.e.* high degree of carbohydrate content, but may be significantly restrictive for those with slow absorption dynamics (*i.e.* high proportion of protein/fat, low glycemic index(GI)) where at least, theoretically, a better glycemic control is achieved by a bolus followed by non-zero insulin flow [27]. Moreover, since the IOB constraint is usually configured according to the estimated CHO counting ($C\hat{H}O$), the insulin delivery could be insufficient when the meal intake is underestimated, thus augmenting the time in hyperglycemia and increasing the blood glucose variability. As it will be shown later, employing this type of IOB decay curve, the insulin infusion could be too restrictive in the case of unannounced meals posterior to constraint triggering. In this section, a time-varying less restrictive IOB constraint is proposed, which permits a bolus infusion followed by a non-null insulin delivery over a configurable time interval. Furthermore, by means of a carbohydrate counting error model, the constraint is set to avoid hypoglycemia episodes due to CHO overestimation. An algorithm is proposed to augment the IOB constraint amplitude according to the rate of change (ROC) of blood glucose.

3.1. $I\tilde{O}B_{max}$ formulation

Given that the postprandial insulin on board is given by $I\tilde{O}B(t) = \theta_4(\tilde{x}_2(t) + \tilde{x}_3(t))$, its time evolution for a predefined insulin pattern can be obtained by solving the insulin subsystem. For instance, assuming a standard bolus therapy of amplitude $U_0 = C\hat{H}O_0/CR$ applied at some $t_0 \geq 0$, the $I\tilde{O}B(t)$ profile results $I\tilde{O}B(t) = U_0 e^{-(t-t_0)/\theta_4}(1 + \frac{1}{\theta_4}(t - t_0))$ (see Appendix (8.1)), which can be employed as an upper bound constraint for insulin administration. Even though this mode of constraint may be optimal for carb/correction boluses adequately computed, it could be too restrictive when a high insulin dose is required (*i.e.* if an underestimated CHO - or an overestimated CR ratio - is employed for the constraint setting). Moreover, the insulin infusion could be wrongly limited when additional boluses are required to

[2] Given that $IOB(t) = \theta_4(x_2(t) + x_3(t))$, it is possible to define a maximal basal infusion $U_{b,max} := (\theta_0 - \theta_1 G_{b,min})/\theta_2$, such that $IOB_{b,max} = \theta_4(x_{2,b,max} + x_{3,b,max}) = \theta_4 2U_{b,max}$, being $G_{b,min}$ a minimal safety basal value of G ($G_{b,min} \approx 70$ [mg/dL]).

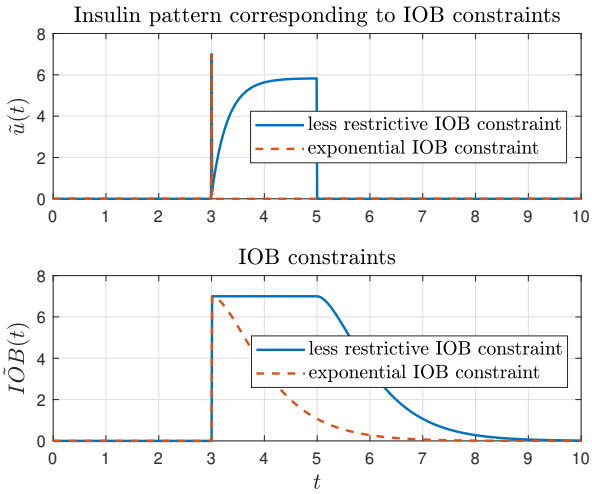

Figure 1: Upper panel. Insulin patterns related to (i) non-standard IOB constraint (single bolus followed by an exponential increasing flow, in black), and (ii) exponential IOB constraint (single bolus, in dashed red). Lower panel. Proposed non-standard IOB constraint (in black) and exponential IOB constraint (in dashed red). The time of meal announcement is $t_0 = 3$ h while $t_f = 5$ h. For both constraints: $U_0 = 7$ U.

compensate for unannounced meals, or when a non-null insulin administration after the bolus injection is needed (dual-wave policy). Therefore, designing an IOB postprandial constraint that accounts for insulin infusions over a predefined time interval after the meal announcement could be advantageous. This way, we define the non-standard IOB constraint as the one that permits a single bolus infusion followed by a non-zero insulin delivery period in which IOB remains constant. The following definition formalizes this new concept:

Definition 1. *Let consider a meal-related event of amplitude $C\hat{H}O_0$ at time $t_0 \geq 0$. So, the "non-standard insulin on board constraint" $I\tilde{O}B_{max}(t; t_0, C\hat{H}O_0)$, $t \geq t_0$, is given by*

$$I\tilde{O}B_{max}(t; t_0, C\hat{H}O_0) := \begin{cases} 0 & t = t_0, \\ U_0 & t \in (t_0, t_f], \\ U_0 e^{-(t-t_f)/\theta_4}(1 + \frac{1}{\theta_4}(t - t_f)) & t \in (t_f, \infty), \end{cases} \tag{3.1}$$

where $U_0 = C\hat{H}O_0/CR$ is the amplitude of the insulin bolus (that takes into account the estimated carb amount $C\hat{H}O$ and the carbohydrate-to-insulin ratio CR), and $t_f > t_0$ is a finite time that will be specified later, according to additional insulin requirements. In the sequel, we will denote $\Delta T_{IOB} = t_f - t_0$.

Note that the difference between the proposed upper bound constraint and that consisting in just using $I\tilde{O}B_{max}(t) = U_0 e^{-(t-t_0)/\theta_4}(1 + \frac{1}{\theta_4}(t - t_0))$, which is a limit case of the former when $\Delta T_{IOB} \to 0$, is that now, for a non-zero ΔT_{IOB}, the upper bound is considered constant. This way, according to insulin requirements, an additional flow (over basal delivery) is permitted during postprandial period to better compensate different types of meals. The hyperglycemia excursion degree respect to the euglycemic zone will be handled by selecting an appropriate value for ΔT_{IOB} while the hypoglycemia risk will be managed by U_0 setting (see Section 3.2). Figure 1, lower panel, shows a schematic plot of both type of constraints, the proposed less restrictive and the exponential one. A question that naturally arises at this point is that concerning the form of the input (insulin pattern) that corresponds to the proposed constraint. The next Theorem shows the feasible insulin infusion pattern that fulfills with equality the $I\tilde{O}B_{max}$ [3] constraint.

Theorem 3.1. *Consider the system* (2.1) *at basal initial conditions and a meal-related event of amplitude $C\hat{H}O_0$ at time $t_0 \geq 0$. The "non-standard IOB constraint" of Definition*(1)*, results from the insulin*

[3]For the sake of clarity, in the sequel, we will omit the parameters of the non-standard IOB constraint defined in 3.1, referring interchangeably to this, by $I\tilde{O}B_{max}$.

subsystem solution under the following insulin pattern:

$$\tilde{u}(t) := \begin{cases} U_0 & t = t_0, \\ \frac{IOB_0}{2\theta_4}(1 - e^{-\frac{2}{\theta_4}(t-t_0)}) & t \in (t_0, t_f], \\ 0 & t \in (t_f, \infty), \end{cases} \tag{3.2}$$

where $U_0 = C\hat{H}O_0/CR$ *and* IOB_0 *is the value of* $I\tilde{O}B(t)$ *right after the insulin bolus, i.e.,* $IOB_0 := I\tilde{O}B(t_0^+) = \theta_4(\tilde{x}_2(t_0^+) + \tilde{x}_3(t_0^+))$ [4].

Proof. Consider the insulin pattern described by (3.2), with $t_0 \geq 0$ and $t_f > t_0$, and consider, without loss of generality, that the system is at steady state at t_0 (*i.e.*, $x_2(t_0) = x_3(t_0) = U_b$, where U_b is the basal insulin delivery). Since we are analyzing the system behavior after meal announcement, only the postprandial state components will be considered. After the impulse, at t_0, states $\tilde{x}_3$ and $\tilde{x}_2$ are given by $\tilde{x}_2(t_0^+) = 0$ and $\tilde{x}_3(t_0^+) = \frac{U_0}{\theta_4}$ and, so, $IOB_0 := I\tilde{O}B(t_0^+) = U_0$.

On the other hand, over the interval $(t_0^+, t_f]$, $I\tilde{O}B(t)$ is constant, so $\dot{I\tilde{O}B}(t) = 0$ and, consequently, $I\tilde{O}B(t) = IOB_0$, for $t \in (t_0^+, t_f]$, due to continuity of $I\tilde{O}B(t)$.

From system (2.1), $\dot{\tilde{x}}_2(t) + \dot{\tilde{x}}_3(t) = \frac{-1}{\theta_4}(\tilde{u}(t) - \tilde{x}_2(t))$, and given that $\dot{I\tilde{O}B}(t) = \theta_4(\dot{\tilde{x}}_2(t) + \dot{\tilde{x}}_3(t)) = 0$, it results that $\tilde{x}_2(t) = \tilde{u}(t)$. Then, replacing $\tilde{x}_2(t)$ by $\tilde{u}(t)$ in $I\tilde{O}B(t)$, it follows that $\tilde{x}_3(t) = \frac{IOB_0}{\theta_4} - \tilde{u}(t)$. Taking $\dot{\tilde{x}}_3(t) = -\dot{\tilde{u}}(t)$ and accounting that $\dot{\tilde{x}}_3(t) = \frac{-1}{\theta_4}\tilde{x}_3(t) + \frac{1}{\theta_4}\tilde{u}(t)$, with $\tilde{x}_3(t) = \frac{IOB_0}{\theta_4} - \tilde{u}(t)$, it results that the insulin infusion $\tilde{u}(t)$ must satisfy the following differential equation

$$\dot{\tilde{u}}(t) = \frac{-2}{\theta_4}\tilde{u}(t) + \frac{IOB_0}{\theta_4^2}, \tag{3.3}$$

in order to get a constant IOB profile. Solving the aforementioned differential equation, we have the following insulin profile $\tilde{u}(t) = \frac{IOB_0}{2\theta_4}(1 - e^{-(2/\theta_4)(t-t_0)})$ over the predefined interval $(t_0, t_f]$. If the system is not at steady state, then $IOB_0 \neq U_0$, but the proof follows the same steps. □

Remark 6. *Despite the non-standard IOB constraint (Definition 1) was formulated assuming basal initial conditions, in order to clear up the explanation; its applicability could be limited when such a condition is not satisfied (i.e. constraint updating during the postprandial period of a meal-related event, see later in Section 3.3). This way, in Appendix 8.2, a complete definition under non-steady state initial conditions is presented, and it is shown, that also results from the solution of the insulin subsystem under the insulin pattern* (3.3)*.*

Theorem 3.1 helps us to understand what type of insulin pattern is indirectly forced/constrained by the non-standard IOB constraint, when this latter is active: an impulse (or thin pulse) followed by an increasing dose up to a given time t_f.

To have a first insight into the effect of the upper bound $I\tilde{O}B_{max}$ in the general meal compensation, some preliminary simulations are carried out next. Figure (2) shows the BG control when the $I\tilde{O}B_{max}$ constraint is configured in accordance with $CR = \theta_2/\theta_3$, under different ΔT_{IOB} periods. As it can be seen, if ΔT_{IOB} is increased, both for the perfectly announced (60 g at 7:00 h and 80g at 18:00 h) as well as the underestimated (60 (-50%) g at 12:00 h) meal-related events, the time span where BG is above the 140 [mg/dL] limit is reduced. Particularly, for the underestimated event, it can be observed that the increment of ΔT_{IOB} promotes the insulin infusion over a prolonged interval of time, and thus, a faster euglycemia restitution. In addition, if an unannounced meal occurs over the interval where $I\tilde{O}B_{max}$ is active (*i.e.* snack of 50 g at 20 h), the hyperglycemia episode is better counteracted by the IOB constraints with wider ΔT_{IOB} periods. Note that if $\Delta T_{IOB} = 150$ [min], insulin infusions of higher amplitude are admitted, and thus, a better BG compensation is achieved. On the other hand, if meals are overestimated, since the IOB constraint amplitude is augmented for the aforementioned configurations, the risk of hypoglycemic episodes will be increased. Anyway, as it will be shown in Section 3.2, by handing the $I\tilde{O}B_{max}$ upper bound, the risk can be managed to tolerable levels. From this discussion, it is possible to infer, that based on "a priori" carbohydrate counting error information, the upper bound U_0 and time interval ΔT_{IOB} of the $I\tilde{O}B_{max}$ can be computed in order to guarantee that commensurate insulin infusions will be applied.

[4] Note that if the system is at steady state at t_0, then $IOB_0 = U_0$

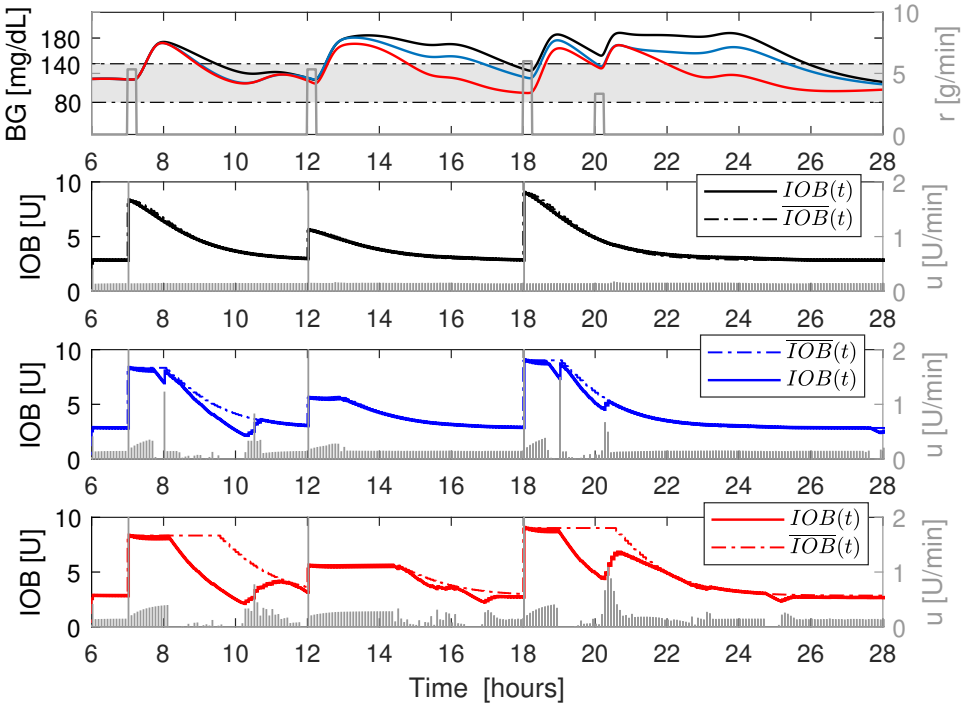

Figure 2: Blood glucose control employing the non-standard IOB constraint, with different sizes of ΔT_{IOB} interval. Case 1: $\Delta T_{IOB} = 0$ [min], standard bolus case (black). Case 2: $\Delta T_{IOB} = 60$ [min] (black). Case 3: $\Delta T_{IOB} = 150$ [min] (red). Meal-related events: 60 g at 7:00 h, 60 (-50%) g at 12:00 h, and 80 g at 18:00 h followed by an unannounced meal snack of 50 g at 20:00 h. IOB(t): estimated IOB by a dedicated observer (ODO, [1]). $\overline{IOB}(t)$: IOB constraint for insulin delivery over fasting and postprandial periods. The sign of percentage indicates the overestimated ($+$)/underestimated ($-$) error.

Remark 7. *It is important to mention that by restricting $IOB(t) \leq I\tilde{O}B_{max}(t; t_0, C\hat{H}O_0)$, the insulin on board state $IOB(t)$ is bounded by the $I\tilde{O}B_{max}(t; t_0, C\hat{H}O_0)$ profile. Furthermore, since $I\tilde{O}B_{max}(t; t_0, C\hat{H}O_0)$ has an associated insulin delivery pattern $\tilde{u}(t)$ (Theorem 3.1), then the maximal accumulated insulin dosage over $[t_0, \infty)$ will be $U_0 + \int_{t_0}^{\Delta T_{IOB}} \tilde{u}(t)dt$. Therefore, by including the restriction $IOB(t) \leq I\tilde{O}B_{max}(t; t_0, C\hat{H}O_0)$, a) $IOB(t)$ will not exceeded $I\tilde{O}B_{max}(t; t_0, C\hat{H}O_0)$ for a given t, and b) $\int_{t_0}^{\infty} u(t)dt \leq U_0 + \int_{t_0}^{\Delta T_{IOB}} \tilde{u}(t)dt$. Notice that, $IOB(t) = h * u(t)$, where $*$ denotes the convolution operator and h represents the impulse response of the insulin pharmacokinetic system. Then, $h * u(t) \leq h * \tilde{u}(t)$, and consequently, by integrating both sides, from t_0 to ∞, and by Fubini's theorem, results in $\int_{t_0}^{\infty} u(t)dt \leq U_0 + \int_{t_0}^{\Delta T_{IOB}} \tilde{u}(t)dt$. In other words, the maximal accumulated dose over a given interval will be restricted by the maximal dose allowed by the restriction. On the other hand, if the constraint is only considered on the maximal dose, $u(t) \leq U_{max}(C\hat{H}O_0)$, not on the pattern followed by the $IOB(t)$, the time-invariant upper bound limit $I\tilde{O}B_{max} = U_{max}(C\hat{H}O_0)$ is a feasible restriction. In this case, the accumulated dose over $[t_0, \infty)$ keeps unbounded. Notice $I\tilde{O}B_{max}(t; t_0, C\hat{H}O_0) \leq I\tilde{O}B_{max}(C\hat{H}O_0)$ for all $t \geq t_0$.*

3.2. Accounting for CHO counting error models

Provided that the proposed IOB constraints $I\tilde{O}B_{max}$ is a function of $C\hat{H}O$, through U_0 in (3.1), possible errors in the carb counting should be explicitly considered. Previous studies attempting to quantify the carbohydrate counting error in T1DM patients have reported that they tend to overestimate small meals and underestimate large meals. Thus, an increment of hyperglycemia episodes has been reported in clinical trials, both under open-loop [34, 33] and closed-loop [57]. If the IOB constraint is configured according to $C\hat{H}O$, insulin over-delivery could occur for the first case, so increasing the hypoglycemic risk, while for the second case, the insulin infusion might be insufficient to compensate for hyperglycemia episodes. To account for these potential carb counting errors, the IOB constraint should be designed to avoid insulin over-delivery when meal ingest is overestimated, ensuring an adequate infusion when meals are underestimated.

Since $I\tilde{O}B_{max}$ has an interval of non-zero insulin infusion after the bolus- those in which $\dot{I\tilde{O}B}(t) = 0$, the accumulated dose can be incremented without augmenting the bolus amplitude. Moreover, from the solution of (3.3) over the time interval $(t_0^+, t_f]$, it can be seen that this type of constraint forces the reduction of the insulin delivery posterior to bolus and, consequently, the risk of insulin over-delivery diminishes.

Let us now consider a carbohydrate counting regression model, $\hat{CHO} = f(CHO; \beta)$, where f is a known function of the carbohydrate amount, CHO, and the fitted parameters β (with abuse of notation, $f(CHO) := f(CHO; \beta)$). Furthermore, for a fixed CHO_0, assume a known meal prediction interval, given by $f(CHO_0) \pm \Delta\hat{CHO}_0$, where $\Delta\hat{CHO}_0$ is a term related to prediction error variability [58]. The key idea is to get a prediction interval for the actual carb amount CHO, also called '*calibration interval*', according to a given carbohydrate counting $\hat{CHO}_0$ (see Figure (3)). This way, we will consider an announced $\hat{CHO}_0$ and a fitted regression model, $\hat{CHO} = f(CHO)$, with upper/lower bounds of the prediction interval, given by $f_{ub}(CHO) = f(CHO) + \Delta\hat{CHO}$ and $f_{lb}(CHO) = f(CHO) - \Delta\hat{CHO}$, respectively. Employing approximated methods for inverse regression [59], the upper and lower bounds for the actual carb intake can be estimated by $CHO_{lb} = f_{lb}^{-1}(\hat{CHO}_0)$ and $CHO_{ub} = f_{ub}^{-1}(\hat{CHO}_0)$. Furthermore, the expected value of CHO, $\mathbb{E}(CHO) = \overline{CHO}$, is given by $\overline{CHO} = f^{-1}(\hat{CHO}_0)$. From Figure (3) (1.a), it can be seen the aforementioned bounds for an estimated $\hat{CHO}_0 = 80$ [g]. Moreover, in Figure (3) (1.b,1,c), two additional carbohydrates counting regression model based on real data [32, 33] are presented. Since for the mentioned studies the prediction intervals were not reported, it was assumed that $f_{lb}(CHO) := k_{lb} f(CHO)$ and $f_{ub}(CHO) := k_{ub} f(CHO)$ for some constants $k_{lb}, k_{ub} > 0$ (heteroscedasticity of variance) in order to deal with the observed variability of the CHO counting error (defined as $\tilde{CHO} := \hat{CHO} - CHO$) against the meal CHO count (see Figure 1 (C) in [34] and Figure 3 in [33]).

Now, based on the estimated lower/upper bounds for the actual carb amount, $CHO_{lb} = f_{lb}^{-1}(\hat{CHO}_0)$ and $CHO_{ub} = f_{ub}^{-1}(\hat{CHO}_0)$, respectively, the non-standard IOB constraint (Definition 1) is configured in such a way that: i) $U_0 = CHO_{lb}/CR$, and ii) $\Delta T_{IOB} = \Delta T_{IOBub}$, where ΔT_{IOBub} is a time interval such that the maximal accumulated insulin dose is CHO_{ub}/CR (see. Lemma 1). This way, $U_0 = CHO_{lb}/CR$ limits the bolus amplitude at the worst case, that is, when the actual carb amount $CHO = CHO_{lb}$, while $\Delta T_{IOB} = \Delta T_{IOBub}$ guarantees that the accumulated insulin dose over ΔT_{IOB} will be the required for all $CHO \leq CHO_{ub}$, according to the conventional therapy rule *i.e.* CHO/CR. As detailed next, the expected value of the CHO, $\overline{CHO} = f^{-1}(\hat{CHO}_0)$, will be informed to the pZMPC and the state observer as the best available meal estimation.

The following lemma states an analytical expression for the ΔT_{IOBub} period.

Lemma 1. *Let us consider an insulin pattern fulfilling equation* (3.3) *with* $U_0 = CHO_{lb}/CR$ *and* $\Delta T_{IOB} = \Delta T_{IOBub}$*, in such away that the accumulated insulin dose over the aforementioned interval is given by* CHO_{ub}/CR*. Then,* ΔT_{IOBub} *fulfills the following non-linear equation*

$$\Delta T_{IOBub} + \frac{\theta_4 e^{-2\Delta T_{IOBub}/\theta_4}}{2} = \frac{\theta_4}{2}\left(4\frac{CHO_{ub} - CHO_{lb}}{CHO_{lb}} + 1\right). \tag{3.4}$$

Proof. Given the insulin pattern (3.3), the accumulated dose over $\Delta T_{IOB} = t_f - t_0$ can be calculated as $\int_{t_0}^{t_f} \tilde{u}(t)\, dt = U_0 + \int_{t_0^+}^{t_f} \tilde{u}(t)\, dt$. Furthermore, by hypothesis, if $\Delta T_{IOB} = \Delta T_{IOBub}$, with $U_0 = CHO_{lb}/CR$, the accumulated dose over the time period is CHO_{ub}/CR. Then, $CHO_{ub}/CR = CHO_{lb}/CR + \int_{t_0^+}^{t_f} \tilde{u}(t)\, dt$, and consequently, $\int_{t_0^+}^{t_f} \tilde{u}(t)\, dt = (CHO_{ub} - CHO_{lb})/CR$. Since, $\tilde{u}(t) = \frac{IOB_0}{2\theta_4}(1 - e^{-\frac{2}{\theta_4}(t-t_0)})$ for $t \in (t_0, t_f]$, and defining $\tau := t - t_0$, results

$$\int_0^{\Delta T_{IOB}} \frac{IOB_0}{2\theta_4}(1 - e^{-\frac{2}{\theta_4}\tau})\, d\tau = \frac{CHO_{ub} - CHO_{lb}}{CR}, \tag{3.5}$$

where $IOB_0 = U_0$ since it is assumed that the system is at steady state before t_0. From the solution of (3.5), with $U_0 = CHO_{lb}/CR$, the non-lineal equality (3.4) follows. □

Assumption 1. *It is important to mention that the aforementioned configuration of the* $I\tilde{O}B_{max}$ *resides on the assumption of a significant carb counting error model of the cohort under study. In this sense, hypoglycemic episodes could arise if the carb counting error model assumes that the patient is underestimating meal size, while in fact, he/she is overestimating these one. Anyway, this effect can be counteracted, by setting carb counting error models with gradual degree of accuracy i.e., start with models which considers*

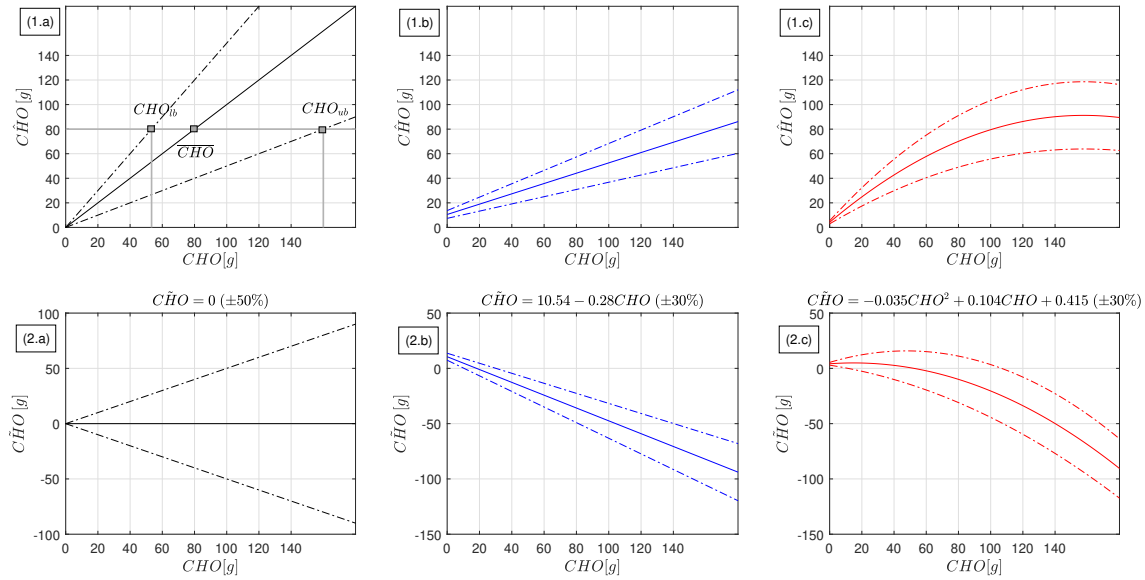

Figure 3: Upper plot: CHO estimation ($C\hat{H}O$) against meal CHO amount according to the regression model $C\hat{H}O = f(CHO)$ (filled line) $\pm$ variability interval in the CHO estimation (dash-dot lines). Model 1 (black): nominal model, $f(CHO) = CHO$. Model 2 (black): linear regression model, $f(CHO) = 10.54 + 0.72CHO$ [34]. Model 3 (red): polynomial regression model, $f(CHO) = -0.05CHO^2 + 1.104CHO + 0.415$ [33]. Note the significant variability in the CHO amount $[CHO_{lb}, CHO_{ub}]$, according to a given CHO estimation. Lower plot: CHO estimation error, $C\tilde{H}O = C\hat{H}O - CHO$, against meal CHO amount.

overestimation of meal amount, and depending on the hypo/hyperglycemia ratio, employ models for underestimation case. On the other hand, even though, an accurate model of the patient under study could be found, if its variability is miss-estimated, hypoglycemic/hyperglycemic episodes could arise depending on CHO_{ub}/CHO_{lb} ratio.

Remark 8. *Since U_0 also depends on the carbohydrate-to-insulin ratio (CR), if CR differs from the real patient value, insulin delivery could be excessive in case of an underestimated value. Although this issue was not considered in the present work, assuming a regression model for CR, the proposed constraint can be configured to avoid hypoglycemia episodes.*

3.3. Adaptive $I\tilde{O}B_{max}$

Although the mentioned configuration for the IOB constraint avoids an excessive insulin delivery in case of overestimated meal ingests, it could be restrictive when the meal ingests are underestimated. That is, even though an interval of constant IOB is allowable for the insulin delivery, it could not be enough to compensate a postprandial hyperglycemic event. Therefore, in this section, an algorithm for the constraint modulation is introduced, which allows an increment of the $I\tilde{O}B_{max}$ amplitude according to the rate of change (ROC) of blood glucose. This way, if i) the ROC of glycemia, $\dot{G}(t)$, is higher than a predefined threshold $\dot{G}_{th}$, and ii) the ROC of the ROC of glycemia, $\ddot{G}(t)$, is positive (*i.e.* meal effect on the glycemia acceleration is higher than the related to insulin absorption), the $I\tilde{O}B_{max}$ constraint is relaxed allowing a bolus delivery of higher amplitude (Algorithm 1). Hence, if the blood glucose is increasing in such a way that the aforementioned conditions are satisfied, and taking into account, that at least for meals with a high glycemic index, the optimal delivery consists of a bolus infusion (*i.e.* it is assumed that meal announcements before the meal ingestion time are not considered), then by relaxing constraint amplitude, commensurable insulin infusions can be applied. Mainly, if the actual carb amount CHO is higher than the lower bound CHO_{lb}, employed to constraint setting.

Figure (4) shows the blood glucose control under three configurations of the IOB constraint, indicated as: $\tilde{I}OB^{UB}_{max}$, $\tilde{I}OB^{LB}_{max}$, and $\tilde{I}OB^{LBa}_{max}$. In $\tilde{I}OB^{UB}_{max}$, the constraint upper bound is set in $U_0 = CHO_{ub}/CR$, in order to admit, at the meal announcement time, carb boluses for actual carb amounts $CHO \leq CHO_{ub}$. The time interval of constant IOB is fixed in $\Delta T_{IOB} = 0$. In $\tilde{I}OB^{LB}_{max}$, the

Algorithm 1 $I\tilde{O}B_{max}$ updating according to $\dot{G}$ and $\ddot{G}$ estimation

Require: $C\hat{H}O_0$, $\dot{G}_{th}$, CHO_{ub}, CHO_{lb}, CR, $IOB_{b,max}$, δ_{CHO} (discretization step for the carb amount calibration interval), and δ_{PP} (postprandial period).

1: Set $I\tilde{O}B_{max}$, with $U_0 = CHO_{lb}/CR$ and $\Delta T_{IOB} = \Delta T_{IOBub}$ (Lemma 1).
2: Fix the $IOB_{b,max}$ relaxed amplitude step size, $\Delta U_0 = (CHO_{ub} - CHO_{lb})/(CRn_{sp})$, where $n_{sp} = int((CHO_{ub} - CHO_{lb})/\delta_{CHO})$.
3: Initialize $t_k = t_0$.
4: **while** $|t_k - t_0| \leq \delta_{PP}$ and $n_{sp} > 0$ **do**
5: Estimate $\dot{G}(t_k)$ and $\ddot{G}(t_k)$.
6: **if** $\dot{G}(t_k) > \dot{G}_u$ and $\ddot{G}(t_k) > 0$ **then**
7: Compute $\tilde{x}_i(t_k) = x_i(t_k) - x_{ib,max}$, where $x_i(t_k)$ is an insulin-related state (i.e. estimated by a dedicated state observer, see ODO in [1]) and $x_{ib,max} = IOB_{b,max}/(2\theta_4)$ $(i = 2, 3)$.
8: Update the $I\tilde{O}B_{max}$ in accordance with Appendix 8.2 by setting: $\tilde{x}_{2,0} = \tilde{x}_2(t_k)$, $\tilde{x}_{3,0} = \tilde{x}_3(t_k)$, $\Delta T_{IOB} = 0$ and $U_0 = \Delta U_0$.
9: $n_{sp} = n_{sp} - 1$.
10: **end if**
11: $t_k = t_k + T_s$.
12: **end while**

constraint is configured according to enunciated method in Section 3.2, that is, $U_0 = CHO_{lb}/CR$ (to limit bolus amplitude at the worst case) and $\Delta T_{IOB} = \Delta T_{IOBub}$ (to ensure the maximal accumulated dose is the corresponding to CHO_{ub}). In $\tilde{I}OB^{LBa}_{max}$, the constraint is assembled as it is detailed in Algorithm 1. A threshold of $\dot{G}_{th} = 2$ [mg/(dL min)] was considered in accordance with the expected ROC of the blood glucose concentration when underestimated meal amounts are tackled. Furthermore, the discretization step for the carb amount calibration interval (δ_{CHO}) was set in 10 g, while the admissible interval for constraint updating (δ_{PP}) in 240 min (which is in accordance with a 4h postprandial period). For all configurations, the nominal carb counting error model (model 1, Figure 3) with $k_{lb} = 2$ (to deal with overestimated meal amounts by +100 %) and $k_{ub} = 0.5$ (to deal with underestimated meal amounts by -50 %) was employed to CHO_{ub}, $\overline{CHO}$, and CHO_{lb} estimation. In this sense, it is important to mention, that for all meal-related events (45 g at 7:00 h, 80 g at 12:00 h and 130 g at 18:00 h), a fixed carb counting of 80 g was considered, and thus, $CHO_{lb} = 40$ g, $\overline{CHO} = 80$ g, and $CHO_{ub} = 160$ g. This way, when the meal is overestimated (*i.e.* 45 g at 7:00h), due to configured CHO_{lb} limit (CHO_{lb} <45), the hypoglycemia episode reported for the $\tilde{I}OB^{UB}_{max}$ case is avoided for both, $\tilde{I}OB^{LB}_{max}$ and $\tilde{I}OB^{LBa}_{max}$ settings. On the other hand, if the meal ingest is underestimated (130 g at 18:00 h), due to constraint relaxation, insulin administrations of higher amplitude are allowed for the $\tilde{I}OB^{LBa}_{max}$ setting. Consequently, the hyperglycemic peak is reduced, achieving a similar performance than the $\tilde{I}OB^{UB}_{max}$ case. As a result, by the $\tilde{I}OB^{LBa}_{max}$ configuration for the IOB constraint, insulin overdoses due to overestimated meal amount are prevented, while hyperglycemic conditions are diminished when the reported meal amount is underestimated. As it will be shown in Section 6, this configuration of the $I\tilde{O}B_{max}$ constraint is promising, mainly, when carb counting errors are tackled.

Remark 9. *Notice that the Algorithm 1 for $I\tilde{O}B_{max}$ updating follows the recommendations for dealing with uncertainty in meal amount proposed by Townsend et. al. [60], that is, decide the magnitude of the bolus based on the minimum amount of consumed carbohydrate and/or reduce the insulin flow when the maximum blood glucose level occurs (since the insulin effect begins to dominate the blood glucose response). In addition, it can be related to the IOB constraint modification curve, in accordance with the blood glucose concentration, proposed in [42].*

Remark 10. *In Algorithm 1, the threshold for the ROC of the glycemia can be set by user (i.e. see Table 2.6 in [28]) or estimated according to the expected ROC following an allowable insulin pattern and considering an actual meal ingest higher than CHO_{lb}. Furthermore, $\dot{G}(t)$ and $\ddot{G}(t)$ are estimated using an Euler discretization ($T_s = 5$ min), and a KF algorithm, as it is detailed in [61].*

Remark 11. *Even though releasing the IOB constraint amplitude is more favourable when meals are underestimated, since an insulin delivery by a bolus mode will be achieved (which is optimal, even when*

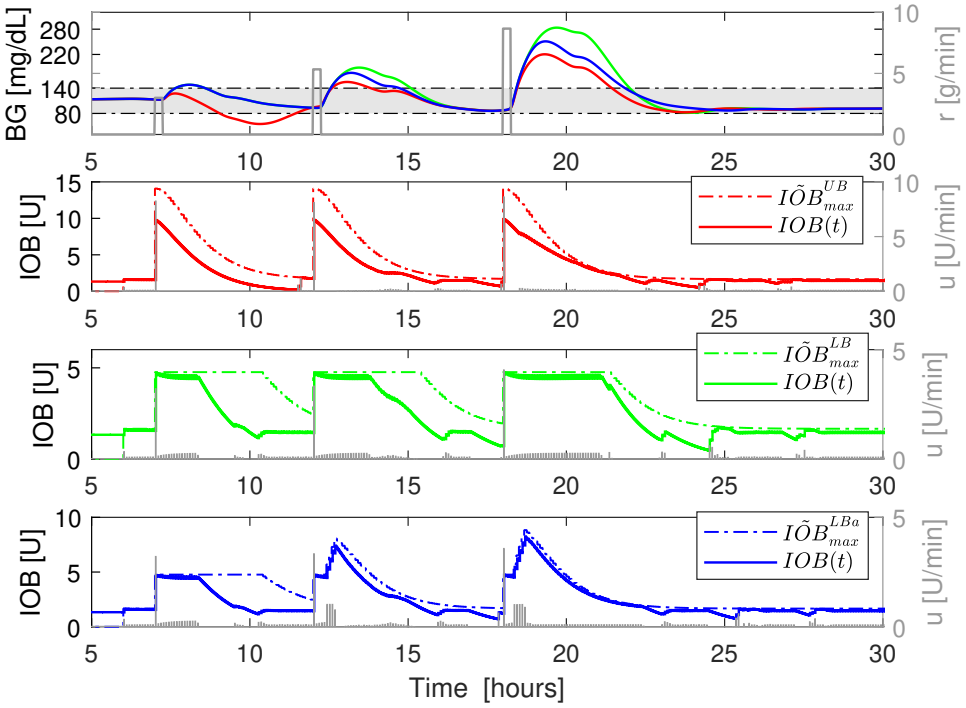

Figure 4: Blood glucose profiles employing the $\tilde{I}OB^{UB}_{max}$ (red), $\tilde{I}OB^{LB}_{max}$ (green), and $\tilde{I}OB^{LBa}_{max}$ (black) configurations for the $\tilde{I}OB_{max}$ constraint. A fixed carb counting of 80 g was announced to the controller and state observer during the meal-related events ($C\hat{H}O = 80$ g). Actual meal amounts: 45 g at 7:00 h, 80 g at 12:00 h and 130 g at 18:00 h.

insulin infusion is delayed [62]), it would be not necessarily safe. For instance, if meals are actually overestimated, and threshold conditions (detailed in Algorithm 1) are satisfied, hypoglycemic episodes could arise due to an excessive delivery during the glycemia up-hill phase. Hence, in this configuration of the non-standard constraint, threshold conditions establishment is crucial to avoid false positive activation.

Remark 12. *Notice that since $I\tilde{O}B_{max}(t_k) \leq I\tilde{O}B_{max}(t_k + T_s)$ during constraint updating, if this mode of constraint is employed in an MPC controller, recursive feasibility will be preserved for all t_k.*

4. Discrete-time model for pulsatile input signals

To be able to use the continuous-time model (2.1) as prediction models in an MPC controller, they should be previously sampled. As it is detailed in [62, 27] a better BG control could be achieved by means of short-duration insulin actions: meals with both rapid and slow absorption times with respect to insulin action time, at least theoretically, demands a shot bolus of insulin (in the second case, followed by a non-zero insulin profile). So, we select the pulsatile scheme proposed in [1] which, for a given sampling time T_s and a pulse duration $0 < \Delta < 1$, considers the following input form:

$$u(t) \quad = \quad \begin{cases} u(kT_s), & t \in [kT_s, kT_s + \Delta T_s), \\ 0, & t \in [kT_s + \Delta T_s, (k+1)T_s), \quad k \in \mathbb{I}_{[0,\infty)}. \end{cases}$$

This input leads to the following discrete-time sub-models:

$$x((k+1)T_s) \quad = \quad A^d x(kT_s) \; + \; B^d_u u(kT_s) \; + \; B^d_r r(kT_s) + E^d, \tag{4.1}$$

where $k \in \mathbb{I}_{[0,\infty)}$ represents kT_s, and the pulsatile discrete-time matrices are given by:

$$\begin{aligned} A^d \quad &:= \quad e^{AT_s}, \\ B^d_u \quad &:= \quad e^{A(T_s - \Delta T_s)} A^{-1} (e^{A\Delta T_s} - I_5) B_u, \end{aligned}$$

$$\begin{aligned} B_r^d &:= A^{-1}(e^{AT_s} - I_5)B_r, \\ E^d &:= A^{-1}(e^{AT_s} - I_5)E. \end{aligned}$$

Matrices A^d, B_r^d and E^d are the discrete-time counterpart of A, B_r and E, respectively, for the fixed time period T_s, when r and E are piece-wise constant with a period T_s. On the other side, B_u^d, which depends on ΔT_s, accounts for the effect of the input u, which is null from ΔT_s to T_s. Furthermore, the time-varying state constraints set, $\mathcal{X}(t)$, can be sampled by considering $\mathcal{X}(k) := \mathcal{X}(kT_s)$, $k \in \mathbb{I}_{[0,\infty)}$. Further details on the discrete-time version of a linear system under pulsatile inputs can be found in [1].

Remark 13. *The characterization of equilibria for pulsatile systems requires some care to account for some bounds on the free responses (those going from ΔT_s to T_s at each period). See Definition 1, in [1], for further details. For the sake of simplicity, we assume that equilibria are directly characterized by pairs (u_s, x_s) fulfilling the condition $x_s = A^d x_s + B_u^d u_s + E^d$ and, because of the pulsatile nature of the inputs, these equilibria do not coincide with the continuous-time equilibria. Feasible equilibria are those equilibrium pairs (u_s, x_s) that also fulfill $0 \leq u_s \leq U_{b,max}$, $G_{hypo} \leq x_{1,s} \leq G_{hyper}$ and $\theta_4(x_{2,s} + x_{3,s}) \leq IOB_{b,max}$.*

5. Pulsatile MPC formulation

In this section, a pulsatile zone MPC (pZMPC, which is an extension of the one originally introduced in [1]) that explicitly incorporates the IOB constraints discussed in the previous sections is presented.

The glucose (and state) predictions are based on the discrete-time pulsatile representation (4.1), introduced in the previous section. The control objective is to drive (and maintain) the blood glucose to a safety zone given by $G^{Tar} := \{G \in \mathbb{R}_{\geq 0} | \, \underline{G} \leq G \leq \overline{G}\}$, denoted as normoglycemia zone, where $\underline{G} = 90$ and $\overline{G} = 120$ [mg/dL]. Furthermore, the input and state constraints must be fulfilled at any time. Unless stated otherwise, the estimated state at current time k, given by $\hat{x}$, is computed based on an 'output disturbance observer' (ODO), which provides an offset-free estimation when the plant-model mismatch is an impulse, a step, or a ramp (see [1] for details). Although the pZMPC is designed for both, the announced (or partially announced) and the unannounced meal cases, in the present work, only the announced meal case will be considered. This way, the estimated carb-counting at a given time k, denoted as $C\hat{H}O(k)$ [g], is assumed to be consumed during an arbitrary interval, D_t, in such a way that the rate of oral ingested carbohydrates announced to the controller is specified by the sequence $\hat{\mathbf{r}}(k) = \{\hat{r}_i\}_{i=0}^{N-1}$, with $\hat{r}_i = C\hat{H}O(k)/Dt$ [g/min] for $i \in [0, n)$ and $\hat{r}_i = 0$ for $i \in [n, N-1]$, being $n = D_t/T_s < N-1$ the meal duration (in sampling times) and N the control horizon.

The cost function of the optimization problem to be solved by the MPC, reads:

$$V_N(\hat{x}, \hat{\mathbf{r}}, G^{Tar}; \mathbf{u}, u_a, y_a, \delta_{\mathbf{hyper}}, \delta_{\mathbf{hypo}}) \doteq V_{dyn}(\hat{x}, \hat{\mathbf{r}}; \mathbf{u}, u_a, y_a, \delta_{\mathbf{hyper}}, \delta_{\mathbf{hypo}}) + V_s(G^{Tar}; u_a, y_a). \quad (5.1)$$

where

$$V_{dyn}(\hat{x}, \hat{\mathbf{r}}; \mathbf{u}, u_a, y_a, \delta_{\mathbf{hyper}}, \delta_{\mathbf{hypo}}) := \sum_{j=0}^{N-1} \|\delta_{hyper}(j)\|_{\hat{Q}}^2 + \|\delta_{hypo}(j)\|_{\hat{Q}}^2 + \| \, (u(j) - u_a) \, \|_R^2, \quad (5.2)$$

with $\mathbf{u} = \{u(0), u(1), \cdots, u(N-1)\}$ being the sequence of future control actions, $\delta_{\mathbf{hyper}} = \{\delta_{hyper}(0), \delta_{hyper}(1), \cdots, \delta_{hyper}(N-1)\}$ and $\delta_{\mathbf{hypo}} = \{\delta_{hypo}(0), \delta_{hypo}(1), \cdots, \delta_{hypo}(N-1)\}$ being deviation variables from y_a associated to the hyper and hypoglycemic episodes, respectively, with $\delta_{hyper}(j) \geq 0$, $\delta_{hypo}(j) \geq 0$, $j \in \mathbb{I}_{0:N-1}$, $\check{Q} \gg \hat{Q} > 0$, and $R > 0$ being penalization matrices, and (u_a, y_a) being auxiliary input and output variables associated to an equilibrium pair (u_a, x_a) at the end of the control horizon N. V_{dyn} is a cost term devoted to steer the predictions to the auxiliary pair (u_a, y_a) in the predicted transient regime. Furthermore,

$$V_s(G^{Tar}; u_a, y_a) := p\left(dist_{G^{Tar}}(y_a)\right),$$

with $p > 0$, and $dist_{\mathcal{A}}(a)$ representing the distance from the point a to the set $\mathcal{A}$, is a stationary cost devoted to steer the auxiliary output y_a to the target G^{Tar}. Notice that, in comparison with [1], two additional optimization variables sequences, $\delta_{\mathbf{hyper}}$ and $\delta_{\mathbf{hypo}}$, were included to obtain an asymmetric stage cost, which allows commanding the way the predicted trajectory reaches the artificial set-point y_a. Thus, by setting

$\check{Q} \gg \hat{Q} > 0$, the predicted trajectory converges to y_a from above, decreasing hypoglycemic excursions respect to the artificial set-point over the prediction horizon.

Before introducing the MPC optimization problem, the different state and input sets will be expressed in their polytopic form, to simplify the notation. That is, sets $\mathcal{U}$ and $\mathcal{X}(k)$, $k \in \mathbb{I}_{[0,\infty)}$, are rewritten as $H_u u \leq b_u$ and $H_x x \leq b_x(k)$, respectively, where

$$H_u = \begin{pmatrix} 1 \\ -1 \end{pmatrix}, b_u = \begin{pmatrix} U_{max} \\ 0 \end{pmatrix} \tag{5.3}$$

$$H_x = \begin{pmatrix} 1 & 0 & 0 & 0 & 0 \\ -1 & 0 & 0 & 0 & 0 \\ 0 & \theta_4 & \theta_4 & 0 & 0 \end{pmatrix}, b_x(k) = \begin{pmatrix} G_{hyper} \\ G_{hypo} \\ IOB_{b,max} + I\tilde{O}B(k; k_0, C\hat{H}O_0) \end{pmatrix} \tag{5.4}$$

being k_0 an arbitrary time (in sample times) where a meal-related event of amplitude $C\hat{H}O_0$ occurs. Furthermore, for basal conditions, matrices b_u and b_x takes the form

$$b_u^b = \begin{pmatrix} U_{b,max} \\ 0 \end{pmatrix}, b_x^b = \begin{pmatrix} G_{hyper} \\ G_{hypo} \\ IOB_{b,max} \end{pmatrix}. \tag{5.5}$$

The equilibrium condition for a pair (u_s, x_s), corresponding to the discrete-time system (4.1), $x_s = \tilde{C}A^d x_s + \tilde{C}B_u^d u_s + \tilde{C}E^d$, where $\tilde{C} = [I_3 \ \ 0_{3\times 2}]$ is a matrix devoted to isolate the first three states (which are the controllable ones), can be expressed as $H_s[u_s \ x_s]' = b_s$, where $H_s = [-\tilde{C}B_u^d \ \ \tilde{C}(I_5 - A^d)]$ and $b_s = \tilde{C}E^d$.

Remark 14. *Given that the insulin subsystem is positive (see in [63]), then for any nonnegative initial state and for any nonnegative input its state and output are nonnegative. Consequently, since* $u(j) \geq 0$ *and* $\hat{x}(0) \geq 0$ *(nonnegative constraints are imposed in the estimated states, see [1]), the nonnegativity of the insulin subsystem solution* $(x_2(j), x_3(j))$ *is guaranteed for any* $j \in \mathbb{I}_{0:N-1}$.

Then, the optimal control problem to be solved by the MPC, at each event $(\hat{x}, \hat{\mathbf{r}}, G^{Tar}, k)$, is given by

$P_N(\hat{x}, \hat{\mathbf{r}}, G^{Tar}, k)$:

$$\begin{aligned}
\min_{\mathbf{u}, u_a, y_a, \delta_{\mathbf{hyper}}, \delta_{\mathbf{hypo}}} \quad & V_N(\hat{x}, \hat{\mathbf{r}}, G^{Tar}; \mathbf{u}, u_a, y_a, \delta_{\mathbf{hyper}}, \delta_{\mathbf{hypo}}) \\
s.t. \quad & \\
& x(0) = \hat{x}, \\
& x(j+1) = A^d x(j) + B_u^d u(j) + B_r^d \hat{r}(j) + E^d, && j \in \mathbb{I}_{0:N-1} \\
& H_u u(j) \leq b_u, && j \in \mathbb{I}_{0:N-1} \\
& H_x x(j) \leq b_x(k+j), && j \in \mathbb{I}_{0:N-1} \\
& \tilde{C}x(N) = x_a, \\
& H_s[u_a \ x_a]' = b_s, \\
& H_x x_a \leq b_x^b, \\
& H_u u_a \leq b_u^b, \\
& y_a = x_{1,a}, \\
& -\delta_{hypo}(j) \leq Cx(j) - y_a \leq \delta_{hyper}(j), && j \in \mathbb{I}_{0:N-1} \\
& \delta_{hypo}(j) \geq 0, \ \delta_{hyper}(j) \geq 0, && j \in \mathbb{I}_{0:N-1}
\end{aligned} \tag{5.6}$$

Note that the state constraint (fourth constraint) is updated each time a meal related-event is announced (or eventually, detected by a meal detector algorithm in case of unannounced scenario) to the controller, so the whole optimization problem depends on this event (*i.e.,* we have an event-based MPC). Let k_0 be the time where a meal-related event of amplitude $C\hat{H}O_0$ arises, then the third component of $b_x(k_0 + i)$ is given by $IOB_{b,max} + I\tilde{O}B(k_0 + i; k_0, C\hat{H}O_0)$ with $i \in \mathbb{I}_{[0,H]}$, being H a predefined horizon such that $I\tilde{O}B(k_0 + H; k_0, C\hat{H}O_0) \approx 0$ (*i.e.:* a basal condition is reached at the end of the horizon). Furthermore, the first constraint accounts for the initialization of the estimated state, while the second to third, account for the system dynamics and input constraint. The fifth constraint is a terminal condition that forces the state at the end of control horizon N to reach a feasible auxiliary equilibrium state $x_a = [x_{1,a}, x_{2,a}, x_{3,a}]' \in \mathbb{R}^3$,

with $\tilde{C} = [I_3 \;\; 0_{3\times 2}]$ (x_a is forced to be a feasible basal equilibrium by constraints sixth to eighth). The ninth constraint links the output auxiliary variable y_a to the state auxiliary variable x_a. Finally, the last three constraints establish the relationship between y_a and the asymmetric deviation variables $\delta_{\mathbf{hyper}}$ and $\delta_{\mathbf{hypo}}$.

Once the Problem $P_N(\hat{x}, \hat{\mathbf{r}}, G^{Tar}, k)$ is solved, the (optimal) solution is denoted as $(\mathbf{u}^0, u_a^0, x_a^0, \delta^0_{\mathbf{hyper}}, \delta^0_{\mathbf{hypo}})$, while the optimal cost function is given by $V_N^0(\hat{x}, \hat{\mathbf{r}}, G^{Tar})$ $:= V_N(G^{Tar}; \mathbf{u}^0, u_a^0, x_a^0, \delta^0_{\mathbf{hyper}}, \delta^0_{\mathbf{hypo}})$. The time-varying control law, derived from the application of a **receding horizon control** policy (RHC), is given by $\kappa_{MPC}(\hat{x}, \hat{\mathbf{r}}, G^{Tar}, k) := u^0(0)$, where $u^0(0)$ is the first element of the solution sequence $\mathbf{u}^0$.

Remark 15. *The fourth constraint, as it was said, is an an event-based constraint which makes the whole problem $P_N(\hat{x}, \hat{\mathbf{r}}, G^{Tar}, k)$ event based. Indeed, the set $\mathcal{X}(t)$, defined in* (3.1)*, depends on a meal-related event $C\hat{H}O_0$ at an arbitrary meal time t_0, in such a way that $\mathcal{X}(t)$ is enlarged over postprandial period $t \geq t_0$. Because of this constraint, the recursive feasibility and stability of the resulting pZMPC controller can be ensured only in periods of time after meal announcements.*

Remark 16. *In comparison with the standard target-tracking MPC formulation, where the set-point tracking problem is treated as a regulation problem under suitable coordinate transformation, in the presented formulation, by means of an artificial set point y_a which can move to any feasible steady-state, the domain of attraction $\mathcal{X}_N$, that is, the set of states which can admissibility be steered to the target zone is increased.*

Next, a softening of the constraints is proposed to ensure the recursive feasibility at any time.

5.1. Soft constrained MPC setup

In order to avoid infeasibility issues related to hard state constraints, they can be relaxed by adding slack variables and minimizing the amount of constraint violation in the pZMPC cost. Following the soft constrained formulation presented in [44], two different types of slack variables, denoted as $\epsilon = \{\epsilon(0), \epsilon(1), \cdots, \epsilon(N-1)\}$ and ϵ_s, were included to soft both, transient and stationary state constraints, respectively. The main objective of this formulation, which is an extension of one introduced in [1], is to relax both the state and terminal constraints (enlarging the domain of attraction), while maintaining the condition that ensures stability.

The proposed soft-constrained pZMPC problem reads

$P_N^s(\hat{x}, \hat{\mathbf{r}}, G^{Tar}, k)$:

$$
\begin{aligned}
\min_{\mathbf{u}, u_a, y_a, \delta_{\mathbf{hyper}}, \delta_{\mathbf{hypo}}, \epsilon, \epsilon_s} \quad & V_N^s(\hat{x}, \hat{\mathbf{r}}, G^{Tar}; \mathbf{u}, u_a, y_a, \delta_{\mathbf{hyper}}, \delta_{\mathbf{hypo}}, \epsilon, \epsilon_s) := V_N(\hat{x}, \hat{\mathbf{r}}, G^{Tar}; \mathbf{u}, u_a, y_a, \delta_{\mathbf{hyper}}, \delta_{\mathbf{hypo}}) \\
& + \textstyle\sum_{j=0}^{N-1} \|(\epsilon(j) + \epsilon_s)\|_S^2 + \|\epsilon_s\|_S^2 \\
s.t. \quad & \\
& x(0) = \hat{x}, \\
& x(j+1) = A^d x(j) + B_u^d u(j) + B_r^d \hat{r}(j) + E^d, && j \in \mathbb{I}_{0:N-1} \\
& H_u u(j) \leq b_u, && j \in \mathbb{I}_{0:N-1} \\
& H_x x(j) \leq b_x(k+j) + \epsilon(j) + \epsilon_s, && j \in \mathbb{I}_{0:N-1} \\
& \tilde{C} x(N) = x_a, \\
& y_a = x_{1,a}, \\
& H_s [u_a \; x_a]' = b_s, \\
& H_x x_a \leq b_x^b + \epsilon_s, \\
& H_u u_a \leq b_u^b, \\
& -\delta_{hypo}(j) \leq Cx(j) - y_a \leq \delta_{hyper}(j) && j \in \mathbb{I}_{0:N-1} \\
& \delta_{hypo}(j) \geq 0, \delta_{hyper}(j) \geq 0, && j \in \mathbb{I}_{0:N-1} \\
& \epsilon(j) \geq 0, \epsilon_s \geq 0, && j \in \mathbb{I}_{0:N-1}
\end{aligned}
\tag{5.7}
$$

where S is symmetric positive semi-definite matrix, defined by

$$
S = \begin{pmatrix} p_{G_{hyper}} & 0 & 0 \\ 0 & p_{G_{hypo}} & 0 \\ 0 & 0 & p_{IOB} \end{pmatrix}, \tag{5.8}
$$

and whose entries are the weights related to upper and lower bounds of glycemia constraint, $p_{G_{hyper}}$ and $p_{G_{hypo}}$, respectively, and the weight corresponding to IOB limit p_{IOB}.

In contrast to the hard state constraint formulation - nominal MPC problem $P_N(\hat{x}, \hat{\mathbf{r}}, G^{Tar}, k)$ (5.6)- in this case both the state constraints and the terminal set for tracking are relaxed. In this way, the state constraints (fourth constraint) are relaxed by the slack variables $\epsilon(j)$ and ϵ_s - allowing the hard state constraints to be violated over the transient period - while the terminal set for tracking (eighth constraint) relaxed by ϵ_s - allowing the artificial pair (x_a, u_a) to move any steady state (seventh constraint) satisfying only the input constraint (ninth constraint). As a result, the domain of attraction (for the same control horizon) is increased with respect to the nominal MPC formulation as well as the nominal MPC formulation with only state constraints relaxed. In spite of the fact, by softening the mentioned constraints, the recursive feasibility is preserved, even when, the hard state constraints are not fulfilled (i.e., when tight state constraints are employed for safety reasons and unexpected disturbances take place), the stability guarantee will be lost if a non-cautious design is considered. In this sense, by employing $\epsilon(j) + \epsilon_s$ as the slack variable for each state constraint (fourth constraint), and taking into account, both the equality terminal constraint (fifth constraint) and the terminal set constraint (eighth constraint), it is ensured that the terminal state, $x(N)$, will lie inside the state constraints relaxed by the amount ϵ_s, and will not require further constraint relaxation (i.e. $\epsilon_N = 0$, where ϵ_N is the slack variable of the terminal state defined by $H_x x(N) \leq b_x^b + \epsilon_s + \epsilon_N$). Consequently, considering the optimal solution of the $P_N^s(\hat{x}, \hat{\mathbf{r}}, G^{Tar}, k)$ problem at a time k, denoted as $(\mathbf{u}^0, u_a^0, x_a^0, \delta_{\mathbf{hyper}}^0, \delta_{\mathbf{hypo}}^0, \epsilon^0, \epsilon_s^0)$, then the shifted slack variable sequence $\epsilon = \{\epsilon_s^0(1;\hat{x}), ..., \epsilon_s^0(N-1;\hat{x}), 0, \epsilon_s^0\}$, where $\epsilon_s^0(j;\hat{x}) = \epsilon^0(j;\hat{x}) - \epsilon_s^0$, will be feasible for a successor state at time $k+1$ (i.e., $x^+ = A^d\hat{x} + B_u^d u^0(0;\hat{x})$, no model mismatch and fasting conditions considered). In this sense, following standard stability proofs (for details, see [44]), it can be proved that the system controlled by the proposed formulation preserves asymptotic stability to the zone. It is important to mention, that if only the state constraints are relaxed, the stability guarantee of the nominal formulation $P_N(\hat{x}, \hat{\mathbf{r}}, G^{Tar}, k)$ is preserved (i.e., it can be interpreted as the soft constrained formulation with $\epsilon_s \equiv 0$). However, this approach could degrade the controller performance, mainly, when short control horizons are used and meal-related events of higher amplitude are present.

Remark 17. *The penalty term $\sum_{j=0}^{N-1} \|(\epsilon_j + \epsilon_s)\|_s^2$, which is included in the cost V_N^s to minimize the constraint violation as long as possible, competes with the dynamic and stationary costs, V_{dyn} and V_s, respectively, which are devoted to steer the glycemia to the target zone, G^{Tar}. As a result, if the state constraints are configured without considering physiological ranges, the controller performance (i.e., its capability to bring high glucose levels back to target) could deteriorate. For example, if the IOB constraint described in Section 3 is set by employing an overestimated carbohydrate-to-insulin ratio CR, then the upper bound U_0 could be too small so producing hyperglycemia episodes.*

6. Simulations results

In this section, the pulsatile Zone Model Predictive Control (pZMPC) will be assessed under different settings of the $I\tilde{O}B_{max}$ constraint, by means of the commercially available UVA/Padova simulator (T1DMS2013, Academic Version) with a virtual population of 10 adult patients. The controller will be implemented by YALMIP toolbox for optimization and modeling in MATLAB [64].

6.1. Controller personalization & tuning

The controller customization resides mainly on individualized glucose-insulin models (2.1) identified as described in [1]. Despite the fact that a controller tuning according to patient specific information (*i.e.* carbohydrate-to-insulin ratio, correction factor, body weight, euglycemic zone, etc.) [41, 65] is a desirable feature of MPC controllers applied to AP systems, in the sequel, the same configuration will be used for all in-silico subjects (except for one patient, denoted as Adult 007, whose insulin sensitivity is significantly higher than the cohort value [5]). Notice the main objective will be to evaluate the pZMPC performance under different settings of the $I\tilde{O}B_{max}$, instead of judging its behavior under optimal controller tuning. Anyway, based on "a priori" clinical knowledge and BG records under closed-loop operation, iterative algorithms for MPC tuning could be added to improve its performance.

[5] Notice that this patient has an insulin sensitivity index, $S_I := -\left.\frac{\partial x_1}{\partial u}\right|_{ss} = \frac{\theta_2}{\theta_1}$, of $4.413 \cdot 10^4$ [(mg/dL)/(U/min)] which is 2.5 times above the cohort value of $1.445 \cdot 10^4 [1.081 \cdot 10^4, 2.286 \cdot 10^4]$ (median $[25th, 75th]$). For details, see Table 2 in [1].

Table 1: pZMPC weighting parameters

	$\hat{\mathbf{Q}}$	$\check{\mathbf{Q}}$	$\mathbf{R}$	$\hat{\mathbf{p}}$	$\check{\mathbf{p}}$	$\mathbf{pG_{hyper}}$	$\mathbf{pG_{hypo}}$	$\mathbf{pIOB}$
all cohort (except Adult 007)	1	$0.5 \cdot 10^2$	1	10^6	10^9	1	10^9	10^9
Adult 007	1	$0.5 \cdot 10^3$	1	10^4	10^9	1	10^9	10^9

As it was detailed in Section 5, to cost to be minimized includes (i) an asymmetric stage cost, which measures the glycemia excursion within the control horizon, penalizing BG deviation from above and below the artificial reference by $\hat{Q}$ and $\check{Q}$, respectively, (ii) an offset cost, which measures the distance between the artificial reference and the target zone, and (iii) a penalty cost related to constraint violation. Consequently, to reduce the hypoglycemic excursion during the control horizon, and thus, over closed-loop operation, the stage cost was configured by setting $\check{Q} \gg \hat{Q}$. Furthermore, an asymmetric offset cost was considered, both to decrease the controller overreaction when the artificial reference is above the target zone (*i.e.* hyperglycemia condition during postprandial period), and to promote the pump-attenuation when the artificial reference is below the target zone (*i.e.* hypoglycemic episode overnight period). In this vein, from [1], $V_s(G^{Tar}; u_a, y_a) \doteq \hat{p}\delta^2_{hyper,s} + \check{p}\delta^2_{hypo,s}$, where $\hat{p}$ and $\check{p}$ are the weights corresponding to hyper and hypoglycemia, respectively, and $\delta_{hypo,s}$ and $\delta_{hyper,s}$ nonnegative optimization variables such that $\underline{G} - \delta_{hypo,s} \leq y_a \leq \overline{G} + \delta_{hyper,s}$. This way, by selecting $\check{p} \gg \hat{p}$, with $\check{Q} \ll \hat{p}$, the convergence to the zone is harder penalized when y_a approaches below ($y_a \nearrow \underline{G}$). On the other hand, the soft constraint weights were fixed in accordance with the severity implication of constraint unfulfillment. Table 3 shows the parameter setting of the pZMPC cost function for the study cohort. The control horizon was set to 6 hours ($N = 72$) in order to ensure that the terminal state satisfies the equilibrium condition posterior to meal ingestion ($(x_4, x_5) = (0, 0)$). For the discrete-time system under pulsatile input, a sampling time of $T_s = 5$ [min] with a pulse size of $\Delta T_s = 1$ [min] was considered.

Depending on the IOB constraint configuration, the pZMPC was implemented in three ways: (i) $pZMPC_{UB}$: $U_0 = CHO_{ub}/CR$ and $\Delta T_{IOB} = 0$, (ii) $pZMPC_{LB}$: $U_0 = CHO_{lb}/CR$ and $\Delta T_{IOB} = \Delta T_{IOBub}$, and (iii) $pZMPC_{LBa}$: $U_0 = CHO_{lb}/CR$, $\Delta T_{IOB} = \Delta T_{IOBub}$, $\delta_{CHO} = 10$ [g], and $\dot{G}_{th} = 2$ [mg/(dL min)] for all cases. In cases (ii) and (iii) the time interval of constant IOB, ΔT_{IOBub}, was set according to Lemma 1 under a fixed carb estimation of $C\hat{H}O = 80$ g. Moreover, $\overline{CHO} = f^{-1}(C\hat{H}O)$, which is the expected value for the CHO ingestion following the regression model $C\hat{H}O = f(CHO)$, was announced to the pZMPC controller and to the output disturbance observer (ODO). It is important to note that for the aforementioned configurations, the total accumulated dose over the postprandial period is equal. This allows us to make fair comparisons.

6.2. Description of the scenarios and outcome metrics

The simulation lasts 14 days, and for all cases, three nominal meals per day were considered: breakfast (60 g CHO, at 7:00), lunch (60 g CHO, at 12:00) and dinner (80 g CHO, at 18:00), affected by random variations in mealtimes ($\pm$ 10 min) and meal size ($\pm$ 20 %). The meal scenarios are performed with: (i) error on meal carbohydrate amount overestimated by 50%, (ii) error on meal carbohydrate amount underestimated by 50%, and (iii) errors on meal carbohydrate amount following the regression curve (Figure (3), model 2) with uniform variability ($\pm 30\%$), reduction of fraction of intestinal absorption of CHO (15%), and intraday variability of insulin sensitivity. The CGM model noise is the one corresponding to Dexcom G5 Mobile CGM, proposed by Vettoretti et al. [66] with a sampling time of $T = 5$ [min].

To evaluate the performance of the proposed controller, the following indices [4] were considered: mean glucose ($\overline{G}$), glucose standard deviation (G_{SD}), coefficient of variation (CV), percentage of time spent in the euglycemic range $70 - 180$ mg/dL (Tt), percentage of time in the tight euglycemic range $70 - 140$ mg/dL (Ttt), percentage of time above 180 mg/dL (T_{180}) and percentage of time spent below 70 and 54 mg/dL (T_{70} and T_{54}, respectively). $No.\,L1_{hypo}$ and $No.\,L2_{hypo}$ denote the number of hypoglycemia events L1 ($G < 70$ mg/dL) and L2 ($G < 54$ mg/dL). For each of these metrics, the median and the interquartile range ($IQR : [25th, 75th]$) over the specific pool of patients were reported. Postprandial periods (PP) are defined as a 4 hours interval from meal ingest, while night periods (NP) are established from 0:00–6:00 h. The statistical significance of possible improvements obtained with $pZMPC_{LB}$ and $pZMPC_{LBa}$, with respect to $pZMPC_{UB}$, were evaluated through the Wilcoxon signed-rank test (significance level 5%). Moreover, the safety (reduction of hypoglycemia) and efficacy (attenuation of hyperglycemia) of the proposals were quantitatively evaluated using the control variability grid analysis (CVGA). This tool

provides a simultaneous visual and numerical assessment of the overall quality of glycemic control, where a single point (case study) represents the couple of 2.5 and 97.5 percentiles of BG values reached by a virtual patient during a single day.

6.3. Meal size overestimated by 50% *(scenario i)*

In this case, the meal carbohydrate amount was overestimated by 50%. Although this carbohydrate error variability is high compared with the values reported in the bibliography (*i.e.* average absolute estimation error of $11.3 \pm 14.7\%$ for meals > 40 g [67]), we use it to stress the controller and grade the robustness of the IOB constraint under severe conditions in carb estimation. Furthermore, since the error in the CHO counting was considered respect with to the perfectly announced case, the IOB constraint was configured by employing the nominal regression curve (model 1, Figure 3) with a variability of 50%. That is, for an estimated $C\hat{H}O$ [g], the upper and lower bound for the IOB setting were $CHO_{ub} = f_{ub}^{-1}(C\hat{H}O)$ and $CHO_{lb} = f_{lb}^{-1}(C\hat{H}O)$, with $f_{ub}(CHO) = 1.5f(CHO)$ and $f_{lb}(CHO) = 0.5f(CHO)$.

As shown in Figure 5 (a), both the configurations $pZMPC_{LB}$ and $pZMPC_{LBa}$, reduce the hypoglycemia events during postprandial periods, at the cost of a modest increase in the hyperglycemic range. Such a result is confirmed in the CVGA plot (Figure 5 (b)), where, in comparison with the $pZMPC_{UB}$ setting (which is characterized by a marked increase in the region of hyperglycemia over-correction), the minimum glycemia levels are moved to normoglycemia zone. Note that 0.71% and 0% of the cases studies were in zone C for $pZMPC_{LB}$ and $pZMPC_{LBa}$, respectively, vs 30% for $pZMPC_{UB}$, which shows the additional protection given by the IOB constraint, with $U_0 = CHO_{lb}/CR$, in case of an overestimated meal ingest. These results are corroborated in Table 2, where it can be seen a significant reduction of the time below 70 mg/dL for both, $pZMPC_{LB}$ and $pZMPC_{LBa}$ configurations.

Remark 18. *In spite of this fact, the IOB constraint was set in accordance with an assumed CHO counting calibration interval* $[CHO_{lb}, CHO_{ub}]$*, where (i)* $U_0 = CHO_{lb}/CR$ *and (ii)* $\Delta T_{IOB} \propto CHO_{ub}/CR$ *(Lemma 1), if the current* $CHO_{lb}^* < CHO_{lb}$*, the hypoglycemic risk due to controller over-reaction will be increased. Remember that for a meal-related event of amplitude* $C\hat{H}O_0$*, the expected value of CHO,* $\overline{CHO} = f^{-1}(C\hat{H}O_0)$*, is announced to pZMPC controller, and thus, as* $CHO_{lb}^* \ll CHO_{lb} < \overline{CHO}$*, the IOB protection against carb counting overestimation will be decreased. Although was not considered in this scenario, to deal with* CR *subestimation (i.e., due to an increased insulin sensitivity) a safety factor can be added to CR, that is,* $CR = \lambda CR_n$ *(where* $\lambda \geq 1$ *and* $CR_n = \theta_2/\theta_3$*).*

Table 2: Performance metrics of $pZMPC_{LB}$, $pZMPC_{LBa}$ and $pZMPC_{UB}$ considering a meal size overestimated by 50%. An asterisk indicates statistical significance ($p-$value < 0.05) respect to $pZMPC_{UB}$ case (postprandial period).

	$pZMPC_{LB}$	$pZMPC_{LBa}$	$pZMPC_{UB}$
$\overline{G}$ [mg/dL]	126.74[124.82,129.78]*	126.63[122.93,129.92]*	108.24[106.46,110.65]
G_{SD} [mg/dL]	22.49[19.54,26.13]	22.04[20.70,25.64]	23.18[22.24,26.28]
CV [%]	17.22[15.99,20.93]*	16.99[16.81,20.05]*	21.78[20.78,24.65]
Tt [%]	98.87[98.15,99.69]	99.07[98.23,100.00]	98.25[96.99,99.76]
Ttt [%]	71.04[68.46,78.45]*	71.57[67.49,78.48]*	86.25[83.29,88.41]
T_{180} [%]	1.13[0.31,1.85]*	0.83[0.00,1.77]	0.00[0.00,0.195]
T_{70} [%]	0.00[0.00,0.00]*	0.00[0.00,0.00]*	1.13[0.24,2.77]
T_{54} [%]	0.00[0.00,0.00]	0.00[0.00,0.00]	0.00[0.00,0.08]
$No.\ L1_{hypo}$	0.00[0.00,0.00]*	0.00[0.00,0.00]*	0.21[0.07,1.43]
$No.\ L2_{hypo}$	0.00[0.00,0.00]	0.00[0.00,0.00]	0.00[0.00,0.00]

6.4. Meal size underestimated by 50% *(scenario ii)*

In case of underestimation of meal carbohydrate amount by 50 $\%$, for all configurations, it is noticed an increment of hyperglycemic episodes (Figure 6). Furthermore, for the $pZMPC_{LB}$ setting, the percentage of case studies in zone C and D increments to 17.14% and 0.71%, respectively. This can be explained by the fact the IOB is forced to be below a constant safety limit, given by $U_0 = CHO_{lb}/CR$, and consequently, if the hyperglycemia excursion is high enough, a controller over-correction could be induced, so increasing the risk of postprandial hypoglycemia events. Nevertheless, for the $pZMPC_{LBa}$ setting, since the amplitude of

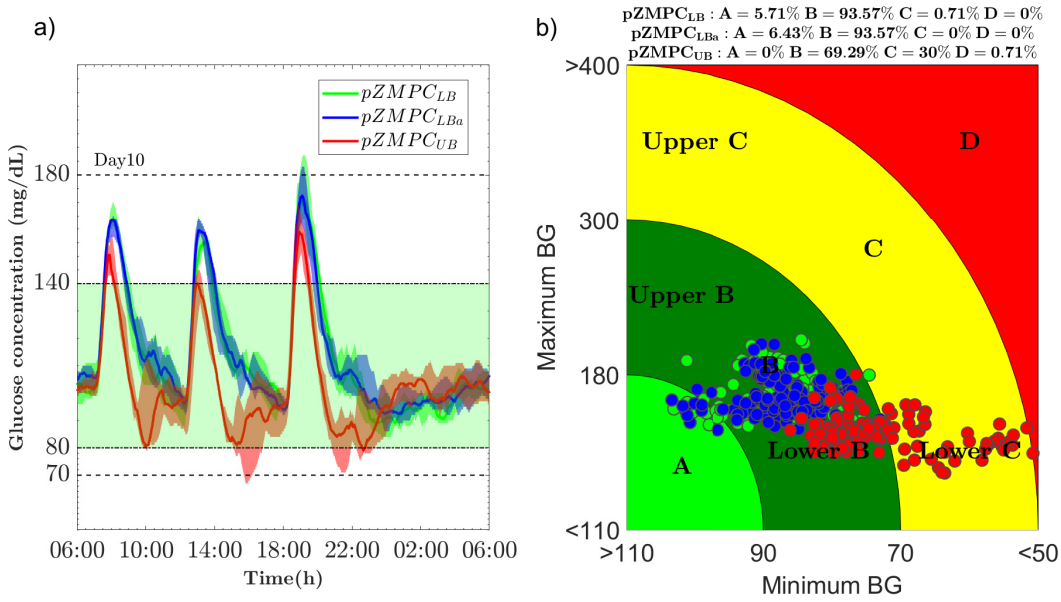

Figure 5: (a) Simulated CGM profiles achieved by $pZMPC_{LB}$, $pZMPC_{LBa}$, and $pZMPC_{UB}$ on 10 T1DM virtual subjects at a single day (Day 10). CGM profiles are shown in terms of median (solid lines) surrounded by colored regions representing the $[25th, 75th]$ percentiles. (b) CVGA plot for 10 T1DM virtual subjects during the 14 days scenario. Each point represents the combination of the 2.5 and 97.5 percentiles reached by a virtual patient during a single day. Case: overestimated CHO with $(+50\%)$ error.

the IOB constraint can be relaxed according to ROC glycemia conditions (Algorithm 1), insulin infusions of higher amplitude are allowed, avoiding the risk of controller over-reaction when an excessive BG excursion is noticed. It is important to mention that meals with high glycemic index are considered, hence, the optimal insulin delivery will be infusions with a bolus pattern. Furthermore, as it is confirmed in Table 3, the time spent above 180 mg/dL is $15.65\%(p = 0.089)$ for $pZMPC_{LBa}$ vs $23.22\%(p = 0.0091)$ for $pZMPC_{LB}$, which is consistent with the better regulation achieved by bolus infusions in case of meals whose effect precede the insulin response (*i.e.* $\theta_5 < \theta_4$ in (2.1)).

It is important to mention that the controller over-delivery under the $pZMPC_{LB}$ setting can be mitigated by using a velocity-dependent stationary cost. Thus, if $\dot{G}(t) < 0$ (down-hill phase), the main idea is to adapt the $\hat{p}$ weight, decreasing it whenever an increased falling of $G(t)$ is noticed. For this purpose, we adopted the velocity-weighting function presented by [8] to the $pZMPC_{LB}$ setting, denoting it by $pZMPC_{LB}(\dot{G})$. [6]. From Figure 7, it can be seen, that by this configuration the percentage of case studies in zone C and D are significantly decreased in comparison with $pZMPC_{LB}$ setting, which discloses the underlying advantages of using a velocity-dependent stationary cost when the non-standard constraint is employed. In other words, by this configuration, the degree of accumulated insulin dose over the postprandial period is managed by cost, while the maximum accumulated dosage and the IOB pattern are established by the IOB constraint.

[6]For the $pZMPC_{LB}(\dot{G})$ setting the following velocity-dependent stationary cost function is employed: $\hat{p}(\dot{G}) := \hat{p}$ if $\dot{G} \geq 0$, $\hat{p}(\dot{G}) := \alpha$ if $\dot{G} \leq -1$, and $\hat{p}(\dot{G}) := \frac{1}{2}[\cos(\dot{G}\pi)(1-\alpha) + (1+\alpha)]$\$ otherwise. For all cases, $\alpha = 1$.

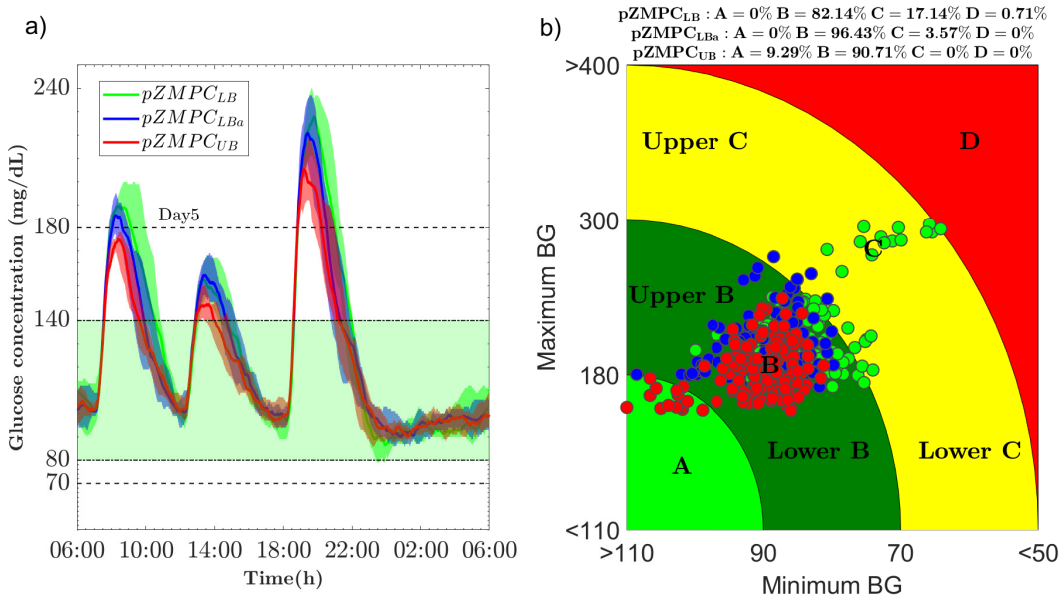

Figure 6: (a) Simulated CGM profiles achieved by $pZMPC_{LB}$, $pZMPC_{LBa}$, and $pZMPC_{UB}$ on 10 T1DM virtual subjects at a single day (Day 5). CGM profiles are shown in terms of median (solid lines) surrounded by colored regions representing the $[25th, 75th]$ percentiles. (b) CVGA plot for 10 T1DM virtual subjects during the 14 days scenario. Each point represents the combination of the 2.5 and 97.5 percentiles reached by a virtual patient during a single day. Case: underestimated CHO with (-50%) error.

Table 3: Performance metrics of $pZMPC_{LB}$, $pZMPC_{LBa}$ and $pZMPC_{UB}$ considering a meal size underestimated by 50%. An asterisk indicates statistical significance ($p-$value < 0.05) respect to $pZMPC_{UB}$ case (postprandial period).

	$pZMPC_{LB}$	$pZMPC_{LBa}$	$pZMPC_{UB}$
$\overline{G}$ [mg/dL]	154.15[148.93,160.51]*	147.72[141.96,154.66]	139.97[136.15,148.20]
G_{SD} [mg/dL]	32.51[29.38,36.90]*	29.28[27.21,35.32]	24.36[22.51,29.79]
CV [%]	21.72[18.83,23.72]*	20.14[18.74,23.65]	17.53[16.78,21.04]
Tt [%]	76.76[66.56,83.83]*	84.35[77.32,92.56]	93.91[85.56,97.93]
Ttt [%]	31.82[26.45,42.53]*	40.11[32.48,53.81]	52.86[36.54,62.58]
T_{180} [%]	23.22[16.17,33.44]*	15.65[7.44,22.68]	6.09[2.07,14.44]
T_{70} [%]	0.00[0.00,0.03]	0.00[0.00,0.00]	0.00[0.00,0.00]
T_{54} [%]	0.00[0.00,0.00]	0.00[0.00,0.00]	0.00[0.00,0.00]
$No.\ L1_{hypo}$	0.00[0.00,0.00]	0.00[0.00,0.00]	0.00[0.00,0.00]
$No.\ L2_{hypo}$	0.00[0.00,0.00]	0.00[0.00,0.00]	0.00[0.00,0.00]

6.5. Meal content estimated based on Roversi et. al. [34] regression model (scenario iii)

In this case, the pZMPC was assessed employing the CHO counting regression model presented in [34] (model 2, Figure 3) which was identified based on Brazeau et. al. [32] real data. In order to account for the maximum variability reported in [34], a uniform random variability of $\pm 30\%$ was added. Furthermore, an intraday variability of insulin sensitivity was simulated by sinusoidal variations, with random amplitude according to a uniform distribution of $\pm 30\%$, and random phase [68]. Moreover, the fraction of intestinal absorption was reduced by 15% to consider an overestimated raise factor (or carbohydrate factor) given by $RF = \theta_3$ [mg/(dLg)]. Notice that θ_3 was identified in [1] under nominal conditions of intestinal absorption.

From Figure 8 (a) it can be seen that both, in $pZMPC_{LB}$ and $pZMPC_{LBa}$, the hypoglycemic excursion during postprandial periods is decreased. Furthermore, from Figure 8 (b), it is noted that scatter plots for $pZMPC_{LB}$ and $pZMPC_{LBa}$ configurations are within A and B regions, denoting that the overall glucose control performance is not compromised. Moreover, Table 4 shows a significant ($p < 0.05$) reduction of the time below 70 mg/dL for $pZMPC_{LB}$ and $pZMPC_{LBa}$ settings. Although the percentage

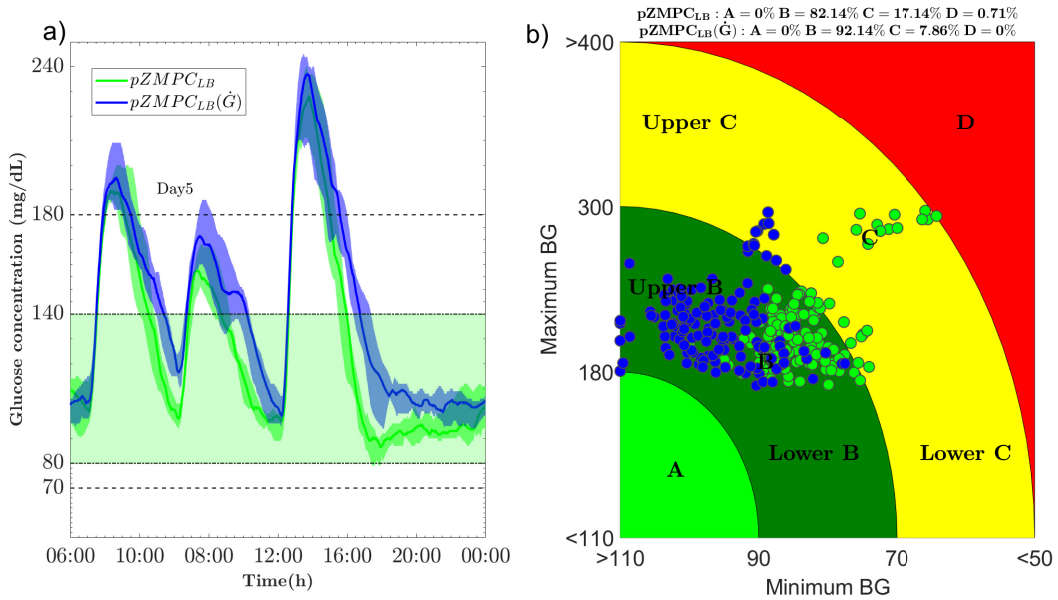

Figure 7: (a) Simulated CGM profiles achieved by $pZMPC_{LB}$ and $pZMPC_{LB}(\dot{G})$ on 10 T1DM virtual subjects at a single day (Day 12). CGM profiles are shown in terms of median (solid lines) surrounded by colored regions representing the $[25th, 75th]$ percentiles. (b) CVGA plot for 10 T1DM virtual subjects during the 14 days scenario. Each point represents the combination of the 2.5 and 97.5 percentiles reached by a virtual patient during a single day. Case: underestimated CHO with (-50%) error.

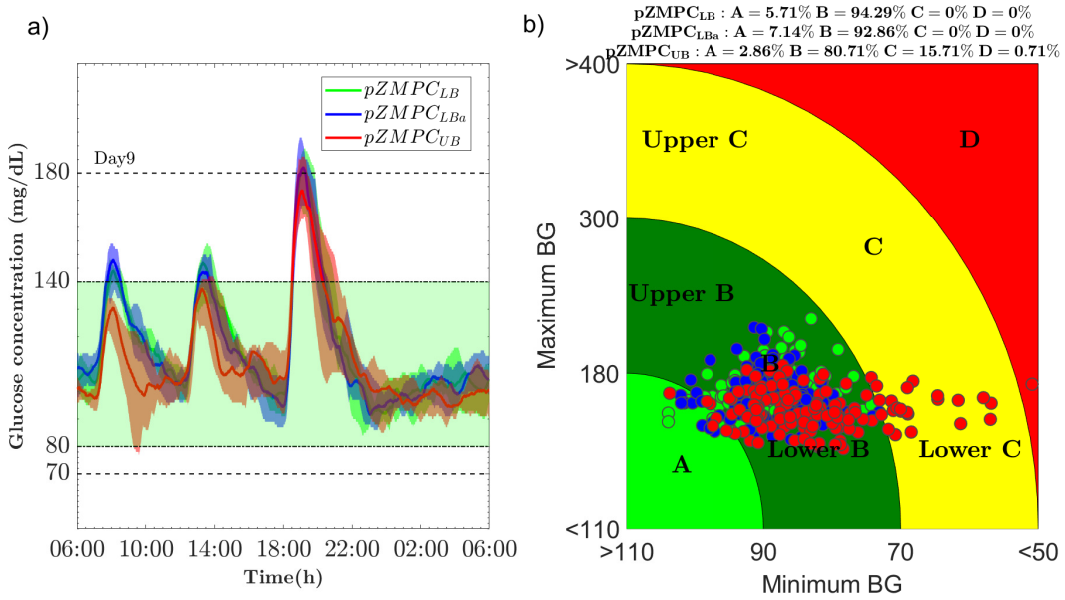

Figure 8: (a) Simulated CGM profiles achieved by $pZMPC_{LB}$, $pZMPC_{LBa}$, and $pZMPC_{UB}$ on 10 T1DM virtual subjects at a single day (Day 9). CGM profiles are shown in terms of median (solid lines) surrounded by colored regions representing the $[25th, 75th]$ percentiles. (b) CVGA plot for 10 T1DM virtual subjects during the 14 days scenario. Each point represents the combination of the 2.5 and 97.5 percentiles reached by a virtual patient during a single day. Case: carbohydrate counting error following the regression model presented in [34] with uniform variability of $(\pm 30\%)$.

time above 180 mg/dL is $1.19\%(p = 0.12)$ for $pZMPC_{LB}$ and $1.44\%(p = 0.13)$ for $pZMPC_{LBa}$, its increment is not significant respect to $pZMPC_{LB}$ case, suggesting that the aforementioned settings does not compromise meaningfully the BG control. It is important to remark, that a non-significant statistical difference is observed between metrics of $pZMPC_{LB}$ and $pZMPC_{LBa}$ settings, which reveals that the former might be satisfactory at meal events with ordinary error variability, and under the assumption, of a known carbohydrate counting model.

Table 4: Performance metrics of $pZMPC_{LB}$, $pZMPC_{LBa}$ and $pZMPC_{UB}$ considering the carbohydrate counting error model given in [34] with uniform variability of ($\pm 30\%$). An asterisk indicates statistical significance ($p < 0.05$) respect to $pZMPC_{UB}$ case (postprandial period).

	$pZMPC_{LB}$	$pZMPC_{LBa}$	$pZMPC_{UB}$
$\overline{G}$ [mg/dL]	130.70[127.75,131.32]*	127.93[127.02,130.38]*	120.85[118.24,125.97]
G_{SD} [mg/dL]	20.83[20.09,24.52]	22.43[20.85,26.62]	23.33[20.49,24.89]
CV [%]	16.00[15.62,18.69]	18.05[16.29,19.74]	18.94[16.45,21.16]
Tt [%]	98.81[97.81,99.90]	98.49[96.46,99.72]	98.98[96.87,99.62]
Ttt [%]	67.61[63.80,73.94]*	70.27[66.16,72.64]*	79.346[74.79,82.24]
T_{180} [%]	1.19[0.10,2.19]	1.44[0.28,3.54]	0.45[0.00,0.65]
T_{70} [%]	0.00[0.00,0.00]*	0.00[0.00,0.00]*	0.36[0.00,1.51]
T_{54} [%]	0.00[0.00,0.00]	0.00[0.00,0.00]	0.00[0.00,0.00]
$No.\ L1_{hypo}$	0.00[0.00,0.00]*	0.00[0.00,0.00]*	0.07[0.00,0.29]
$No.\ L2_{hypo}$	0.00[0.00,0.00]	0.00[0.00,0.00]	0.00[0.00,0.00]

7. Discussion

7.1. Non-standard IOB constraint

Automatic blood glycemic control is the core objective of AP systems. In spite of the fact that several control algorithms have been formulated, insulin stacking problems have been reported in the subcutaneous route of insulin administration. Owing to this, safety systems based on IOB estimation and limitation have been employed, both for constrained as well as unconstrained control algorithms. Since normally the major perturbation corresponds to meal ingestion, which is usually counteracted by carb-correction bolus, IOB constraints with an exponential decay curve have been adopted. However, employing this mode of constraint, insulin delivery could be limited to a single bolus over the postprandial period, thus reducing the glucose-insulin system controllability. In this work, a novel IOB constraint that allows a non-zero insulin delivery after bolus administration is proposed to overcome this kind of problem.

Even though fully automated APs - without meal announcement - are preferred in contrast to hybrid APs configurations, due to the considerable delay between the insulin action and the meal-glucose absorption, the achievement of the former in a fully automated manner is limited (at least, under subcutaneous route of insulin infusion). Consequently, meal announcements are usually required, demanding an effort for the T1DM patients to estimate the carbohydrate content. Studies have reported that T1DM patients are prone to estimate carbohydrate content with errors, being normally overestimated for small meals while underestimated for large meals (*i.e.* fear of hypoglycemia). Although several trials have assessed the impact of CHO counting error, both 'in-silico' [67, 69] and under outpatient conditions [57], none have considered explicitly "a-priori" information related to CHO counting error. This way, as a second contribution of this work, based on an assumed CHO counting regression model, a method to configure the proposed IOB constraint was designed. Moreover, an extended algorithm was formulated, to relax the IOB constraint in case of an excessive blood glucose increment.

Therefore, concerning the "non-standard constraint" under the mentioned configuration, the following results can be summarized:

i. In the case of an overestimated meal, hypoglycemia episodes are significantly decreased (in both, $pZMPC_{LB}$ and $pZMPC_{LBa}$ configurations), by arranging the non-standard IOB constraint upper bound in a conservative value, $U_0 = CHO_{lb}/CR$. Notice that this result is observed, even when the expected meal amount, $\overline{CHO}$, which is $\overline{CHO} > CHO_{lb}$, is announced to the controller and to the state observer. For larger variability in the carbohydrate counting error, a disturbance observer robust to CHO miss-estimation should be considered. Even tough, non-significant hypoglycemic episodes were reported for the $pZMPC_{LBa}$ configuration, it is important to remark, that it is highly dependent on the threshold conditions used for constraint triggering. Owing to this, in scenarios with high variability (i.e., delayed meal announcement, increased insulin sensitivity) residual information could be added to cope with false-positive activation.

ii. In the case of underestimated meal amount, although $\Delta T_{IOB} > 0$ increases the glucose-insulin system controllability, it is observed an augmented risk of hypoglycemic episodes (particularly, for patients with high insulin sensitivity). This can be explained by the fact, that according to the $I\tilde{O}B_{max}$ upper limit mentioned in item ii), a restrictive insulin administration is allowed over the postprandial period, and consequently, high hyperglycemic excursions could be promoted. Therefore, in spirit to guide the blood glucose concentration to the euglycemic zone, a controller over-correction could be induced, and thus, due to the amplitude restrictive setting of the constraint, a delayed insulin absorption and action will take place. Facing this situation, three options could be handled: i) decrease ΔIOB interval (notice, that according to Lemma 1, it is calculated considering only accumulated dose respect to conventional therapy, and thus a hypoglycemia-free behavior is not guaranteed), ii) adjust the constraint upper bound as suggested by the adaptive $I\tilde{O}B_{max}$ algorithm (Section 3.3), or iii) employ a velocity-dependent asymmetric stationary cost (as it was shown in Section 6.4). Although all these, pare down the extended insulin delivery, it is preferable to the second and the third one, since ii) allows for insulin administration of higher amplitude during the up-hill phase (and thus, also reduces hyperglycemic episodes) while iii) commands the accumulated dose over the down-hill period (and thus, mitigate the hypoglycemic risk due to a prolonged infusion).

iii. Taking into account a real carb counting scenario (Brazeau et. al. dataset [32]), and under the assumption of a known carbohydrate counting model, performances achieved by $pZMPC_{LB}$ and $pZMPC_{LBa}$ settings are not statically different. Consequently, under scenarios with not-extensive meal announcement errors, additional insulin requirements can be managed by the $pZMPC_{LB}$ setting. Since this configuration does not depend on triggering conditions, the risk of the controller overreaction due to false positive activation is reduced.

Although it was not simulated in the present work, since the formulated IOB constraint allows for the administration of a non-zero insulin profile after bolus, it may be employed considering meals with slow absorption dynamic (*i.e.:* high protein/high lipid diet) or when drugs to reduce gastric emptying are administered. In this sense, following Goodwin et. al. [27] and assuming $\theta_4 > \theta_5$ in 2.1, a suitable upper bound for U_0 and ΔT_{IOB} for the $I\tilde{O}B_{max}$ can be reached.

It is important to mention that the aforementioned configuration of the IOB constraint, might be applied to increase the robustness of partial feedforward-feedback strategies for APs [70]; that is, strategies where instead of inputting the exact amount of carbohydrates contained in the meal, provides an indication of the meal size. This way, a reduction on the load associated to carb-counting could be performed in a safety manner.

7.2. MPC formulation

Although several MPC algorithms have been proposed for APs, few of them account for stability issues: [7, 71] use an infinite prediction horizon but neither input nor state constraints are considered, while [36] considers constraints and bases the stability on the use of artificial variables under an impulsive scheme. In the same vein, the strategy proposed [1] bases its benefits on the use of artificial variables and impulsive/pulsatile schemes, and adds a time-varying constraint that improves the general closed-loop performance. The soft-constrained pZMPC proposed in this work also ensures stability but shows several extra benefits in contrast to [1]. The main advantages of the proposed controller are listed below:

i. *Recursive Feasibility.* Despite the pZMPC presented in [1] has an extended domain of attraction and it can track any admissible target set (zone) in an admissible fashion, it's assumed that the system evolution satisfies state constraints for all time. However, imposing hard state or output constraints can be overly conservative or render the optimization problem infeasible in closed-loop operation. For example, in medical device systems, where due to safety issues, tighter constraints are usually used. Consequently, in other to overpass this situation, and preserve the desirable properties of the pZMPC, a soft version was employed [44] which preserves stability guarantee, even when, the terminal constraint is relaxed. This way, a larger domain of attraction is obtained, being the optimization problem feasible, even for initial conditions outside the hard constraint. It is important to mention that because of the equality terminal constraint, it is required that the terminal state reaches an equilibrium condition. Hence, since large disturbances correspond to meal ingestion, the control horizon should be designed such that the meals are fully absorbed at the end of the horizon. However, by employing a T1DM invariant set [63] as a terminal condition, the control horizon could be reduced.

ii. *Stability.* The pZMPC formulation, both under hard- and soft constraints, and assuming that the state is perfectly measured and no permanent disturbances are considered, satisfies the basic stability assumptions. As a result, for any feasible initial state $x_0 \in \mathcal{X}_N$ (or $x_0 \in \mathcal{X}_N^s$ soft case, with $\mathcal{X}_N \subseteq \mathcal{X}_N^s$) and for a given target operation zone G^{Tar} , the glucose-insulin system controlled by the proposed MPC $\kappa_{MPC}(\hat{x}, \hat{\mathbf{r}}, G^{Tar}, k)$ is stable, fulfills the constraints throughout the time evolution and asymptotically converges to a steady output $y_s \in G^{Tar}$.

iii. *Performance.* Up to the authors' knowledge, the main benefits of the proposed controller concern its generally good performance. In comparison to other MPC formulations for APs, characterized by computing the carb-bolus according to conventional therapy rules, and thus, being the main role of the controller to counteract plant-model mismatches, the proposed controller computes the carb-bolus infusion directly from the optimization problem solution. As a result, insulin over-delivery could occur if hypoglycemic excursions are not accounted over the prediction horizon, even though, $G(j) > G_{hypo}$ fulfillment can be managed by p_{Gmin} penalization (see. Section 5.1, soft constrained MPC). Owing to this, an asymmetric stage cost was incorporated to manage the hypo- and hyperglycemia deviation with respect to an auxiliary variable y_a over the prediction horizon. Even though, in [1], an asymmetric offset cost has been proposed to deal with hypo and hyperglycemia episodes during closed-loop operation, since the former employs a sequence of deviation variables, a better handle of glycemia excursion is achieved. Future works: add a velocity-dependent stationary cost to mitigate controller over actuation during glycemia down-hill phase (i.e., crucial to avoid hypoglycemic events during insulin sensitivity transitions).

8. Appendix

8.1. IOB profile under FIT therapy

Consider the system (2.1) at non-basal conditions and a meal-event of amplitude $C\hat{H}O_0$ at t_0. Then, the $I\tilde{O}B(t)$ profile when a bolus of U_0 amplitude is applied at t_0, is given by

$$I\tilde{O}B(t) = \theta_4(\tilde{x}_3(t_0^+) + \tilde{x}_2(t_0^+) + \frac{\tilde{x}_3(t_0^+)}{\theta_4}(t - t_0))e^{-(t-t_0)\theta_4}, \tag{8.1}$$

where $\tilde{x}_2(t_0^+) = \tilde{x}_2(t_0)$ and $\tilde{x}_3(t_0^+) = \tilde{x}_3(t_0) + U_0/\theta_4$. Notice that the bolus amplitude related to meal-event (carb bolus), can be computed in accordance with bolus calculator standard rules [72]. Hence, $U_0 = C\hat{H}O_0/CR - I\tilde{O}B_0$, where CR is the carbohydrate-to-insulin [g/U] and $I\tilde{O}B_0 = \theta_4(\tilde{x}_2(t_0) + \tilde{x}_3(t_0))$ is the remaining insulin on board from previous boluses. If basal initial conditions are assumed, then $I\tilde{O}B(t) = U_0 e^{-(t-t_0)/\theta_4}(1 + \frac{1}{\theta_4}(t - t_0))$ with $U_0 = C\hat{H}O_0/CR$.

8.2. Non-standard IOB constraint at non-basal initial conditions

Let consider the system (2.1) at non-basal initial conditions and meal-related event of amplitude $C\hat{H}O_0$ at time $t_0 \geq 0$. Then, the "non-standard IOB constraint at non-basal initial conditions" $I\tilde{O}B_{max}(t; t_0, C\hat{H}O_0, \tilde{x}_{2,0}, \tilde{x}_{3,0})$, $t \geq t_0$, is specified by

$$I\tilde{O}B_{max}(t; t_0, C\hat{H}O_0, \tilde{x}_{2,0}, \tilde{x}_{3,0}) := \begin{cases} \theta_4(\tilde{x}_{2,0} + \tilde{x}_{3,0}) & t = t_0, \\ \theta_4(\tilde{x}_{2,0} + \tilde{x}_{3,0} + \frac{U_0}{\theta_4}) & t \in (t_0, t_f], \\ \theta_4(\tilde{x}_{2,0} + \tilde{x}_{3,0} + \frac{U_0}{\theta_4} + (\tilde{x}_{3,0} + \frac{U_0}{\theta_4})\frac{1}{\theta_4}(t - t_f))e^{-(t-t_f)/\theta_4} & t \in (t_f, \infty), \end{cases} \tag{8.2}$$

where $\tilde{x}_{2,0}$ and $\tilde{x}_{3,0}$ are the initial values of the insulin-related states to the IOB constraint (i.e. $I\tilde{O}B_{max,0} = \theta_4(\tilde{x}_{2,0} + \tilde{x}_{3,0})$), and $U_0 = C\hat{H}O_0/CR - I\tilde{O}B_{max,0}$ according to conventional FIT therapy (note that the reaming IOB due to previous carb bolus is taken into account). Following similar steps to Theorem 3.1, it can be demonstrated that the aforementioned constraint, results from the insulin subsystem solution under the insulin pattern given in Section 3.1 with $IOB_0 := I\tilde{O}B(t_0^+) = \theta_4(\tilde{x}_2(t_0^+) + \tilde{x}_3(t_0^+))$, and $\tilde{x}_2(t_0^+) = x_{2,0}$ and $\tilde{x}_3(t_0^+) = x_{3,0} + U_0/\theta_4$.

Remark 19. *In comparison with the Definition 1, we see that in this case, the initial conditions of the constraint must be considered every time we want to update it (i.e. when another meal-related event has happened, an excessive rate of change of glycemia is measured, among others). Consequently, they can be obtained from (i) the insulin-related states previously computed when the constraint was triggered, or (ii) by reconciling them according to an estimation of the actual insulin states (i.e. by using a state observer).*

References

[1] P. Abuin, P. Rivadeneira, A. Ferramosca, A. González, Artificial pancreas under stable pulsatile mpc: Improving the closed-loop performance, Journal of Process Control 92 (2020) 246–260.

[2] A. Katsarou, S. Gudbjörnsdottir, A. Rawshani, D. Dabelea, E. Bonifacio, B. J. Anderson, L. M. Jacobsen, D. A. Schatz, Å. Lernmark, Type 1 diabetes mellitus, Nature reviews Disease primers 3 (2017) 17016.

[3] American Diabetes Association, Classification and diagnosis of diabetes: standards of medical care in diabetes—2019, Diabetes Care 42 (Supplement 1) (2019) S13–S28.

[4] T. Danne, R. Nimri, T. Battelino, R. M. Bergenstal, K. L. Close, J. H. DeVries, S. Garg, L. Heinemann, I. Hirsch, S. A. Amiel, et al., International consensus on use of continuous glucose monitoring, Diabetes care 40 (12) (2017) 1631–1640.

[5] G. M. Steil, Algorithms for a closed-loop artificial pancreas: the case for proportional-integral-derivative control, Journal of diabetes science and technology 7 (6) (2013) 1621–1631.

[6] R. Mauseth, I. B. Hirsch, J. Bollyky, R. Kircher, D. Matheson, S. Sanda, C. Greenbaum, Use of a "fuzzy logic" controller in a closed-loop artificial pancreas, Diabetes technology & therapeutics 15 (8) (2013) 628–633.

[7] M. Messori, G. P. Incremona, C. Cobelli, L. Magni, Individualized model predictive control for the artificial pancreas: In silico evaluation of closed-loop glucose control, IEEE Control Systems Magazine 38 (1) (2018) 86–104.

[8] R. Gondhalekar, E. Dassau, F. J. Doyle III, Velocity-weighting and velocity-penalty MPC of an artificial pancreas: Improved safety and performance, Automatica 91 (48) (2018) 105–117.

[9] C. D. Man, F. Micheletto, D. Lv, M. Breton, B. Kovatchev, C. Cobelli, The UVA/Padova type 1 diabetes simulator: new features, Journal of diabetes science and technology 8 (1) (2014) 26–34.

[10] R. Hovorka, F. Shojaee-Moradie, P. V. Carroll, L. J. Chassin, I. J. Gowrie, N. C. Jackson, R. S. Tudor, A. M. Umpleby, R. H. Jones, Partitioning glucose distribution/transport, disposal, and endogenous production during IVGTT, American Journal of Physiology-Endocrinology and Metabolism 282 (5) (2002) E992–E1007.

[11] S. S. Kanderian, S. Weinzimer, G. Voskanyan, G. M. Steil, Identification of intraday metabolic profiles during closed-loop glucose control in individuals with type 1 diabetes (2009).

[12] J. R. Castle, J. El Youssef, L. M. Wilson, R. Reddy, N. Resalat, D. Branigan, K. Ramsey, J. Leitschuh, U. Rajhbeharrysingh, B. Senf, et al., Randomized outpatient trial of single-and dual-hormone closed-loop systems that adapt to exercise using wearable sensors, Diabetes care 41 (7) (2018) 1471–1477.

[13] M. Messori, J. Kropff, S. Del Favero, J. Place, R. Visentin, R. Calore, C. Toffanin, F. Di Palma, G. Lanzola, A. Farret, et al., Individually adaptive artificial pancreas in subjects with type 1 diabetes: a one-month proof-of-concept trial in free-living conditions, Diabetes Technology & Therapeutics 19 (10) (2017) 560–571.

[14] R. Sánchez-Peña, P. Colmegna, F. Garelli, H. De Battista, D. García-Violini, M. Moscoso-Vásquez, N. Rosales, E. Fushimi, E. Campos-Náñez, M. Breton, et al., Artificial pancreas: clinical study in latin america without premeal insulin boluses, Journal of diabetes science and technology 12 (5) (2018) 914–925.

[15] C. Toffanin, L. Magni, C. Cobelli, Artificial pancreas: In silico study shows no need of meal announcement and improved time in range of glucose with intraperitoneal vs. subcutaneous insulin delivery, IEEE Transactions on Medical Robotics and Bionics 3 (2) (2021) 306–314.

[16] J. Lo Presti, A. Galderisi, F. J. Doyle III, H. C. Zisser, E. Dassau, E. Renard, C. Toffanin, C. Cobelli, Intraperitoneal insulin delivery: Evidence of a physiological route for artificial pancreas from compartmental modeling, Journal of diabetes science and technology (2022) 19322968221076559.

[17] M. E. Wilinska, L. J. Chassin, H. C. Schaller, L. Schaupp, T. R. Pieber, R. Hovorka, Insulin kinetics in type-1 diabetes: continuous and bolus delivery of rapid acting insulin, IEEE Transactions on Biomedical Engineering 52 (1) (2004) 3–12.

[18] B. W. Bequette, Challenges and recent progress in the development of a closed-loop artificial pancreas, Annual reviews in control 36 (2) (2012) 255–266.

[19] P. Colmegna, E. Cengiz, J. Garcia-Tirado, K. Kraemer, M. D. Breton, Impact of accelerating insulin on an artificial pancreas system without meal announcement: an in silico examination, Journal of Diabetes Science and Technology 15 (4) (2021) 833–841.

[20] J. Bondia, S. Romero-Vivo, B. Ricarte, J. L. Diez, Insulin estimation and prediction: a review of the estimation and prediction of subcutaneous insulin pharmacokinetics in closed-loop glucose control, IEEE Control Systems Magazine 38 (1) (2018) 47–66.

[21] I. Hajizadeh, M. Rashid, A. Cinar, Plasma-insulin-cognizant adaptive model predictive control for artificial pancreas systems, Journal of process control 77 (2019) 97–113.

[22] M. Messori, M. Ellis, C. Cobelli, P. D. Christofides, L. Magni, Improved postprandial glucose control with a customized model predictive controller, in: 2015 American control conference (ACC), IEEE, 2015, pp. 5108–5115.

[23] C. Ellingsen, E. Dassau, H. Zisser, B. Grosman, M. W. Percival, L. Jovanovič, F. J. Doyle III, Safety constraints in an artificial pancreatic β cell: an implementation of model predictive control with insulin on board, Journal of diabetes science and technology 3 (3) (2009) 536–544.

[24] E. Fushimi, N. Rosales, H. De Battista, F. Garelli, Artificial pancreas clinical trials: Moving towards closed-loop control using insulin-on-board constraints, Biomedical Signal Processing and Control 45 (2018) 1–9.

[25] M. F. Villa-Tamayo, F. León-Vargas, M. García-Jaramillo, P. S. Rivadeneira, Glycemic control strategy based on an impulsive mpc with safety layer coupling for iob limitation, IEEE Control Systems Letters 5 (5) (2020) 1669–1674.

[26] H. Zisser, L. Robinson, W. Bevier, E. Dassau, C. Ellingsen, F. J. Doyle III, L. Jovanovic, Bolus calculator: a review of four "smart" insulin pumps, Diabetes technology & therapeutics 10 (6) (2008) 441–444.

[27] G. C. Goodwin, M. M. Seron, A performance bound for optimal insulin infusion in individuals with type 1 diabetes ingesting a meal with slow postprandial response, Automatica 103 (2019) 531–537.

[28] J. Walsh, R. Roberts, Pumping insulin: everything for success on an insulin pump and CGM, Torrey Pines Press, 2017.

[29] K. J. Bell, C. E. Smart, G. M. Steil, J. C. Brand-Miller, B. King, H. A. Wolpert, Impact of fat, protein, and glycemic index on postprandial glucose control in type 1 diabetes: implications for intensive diabetes management in the continuous glucose monitoring era, Diabetes care 38 (6) (2015) 1008–1015.

[30] R. Gondhalekar, E. Dassau, F. J. Doyle III, Periodic zone-mpc with asymmetric costs for outpatient-ready safety of an artificial pancreas to treat type 1 diabetes, Automatica 71 (2016) 237–246.

[31] P. Colmegna, F. Garelli, H. De Battista, R. Sánchez-Peña, Automatic regulatory control in type 1 diabetes without carbohydrate counting, Control Engineering Practice 74 (2018) 22–32.

[32] A. Brazeau, H. Mircescu, K. Desjardins, C. Leroux, I. Strychar, J. Ekoé, R. Rabasa-Lhoret, Carbohydrate counting accuracy and blood glucose variability in adults with type 1 diabetes, Diabetes research and clinical practice 99 (1) (2013) 19–23.

[33] T. Kawamura, C. Takamura, M. Hirose, T. Hashimoto, T. Higashide, Y. Kashihara, K. Hashimura, H. Shintaku, The factors affecting on estimation of carbohydrate content of meals in carbohydrate counting, Clinical Pediatric Endocrinology 24 (4) (2015) 153–165.

[34] C. Roversi, M. Vettoretti, S. Del Favero, A. Facchinetti, G. Sparacino, H.-R. Consortium, Modeling carbohydrate counting error in type 1 diabetes management, Diabetes technology & therapeutics 22 (10) (2020) 749–759.

[35] P. Soru, G. De Nicolao, C. Toffanin, C. Dalla Man, C. Cobelli, L. Magni, A. H. Consortium, et al., Mpc based artificial pancreas: strategies for individualization and meal compensation, Annual Reviews in Control 36 (1) (2012) 118–128.

[36] A. H. González, P. S. Rivadeneira, A. Ferramosca, N. Magdelaine, C. H. Moog, Stable impulsive zone model predictive control for type 1 diabetic patients based on a long-term model, Optimal Control Applications and Methods 41 (6) (2020) 2115–2136.

[37] A. H. González, P. S. Rivadeneira, A. Ferramosca, N. Magdelaine, C. H. Moog, Impulsive zone mpc for type i diabetic patients based on a long-term model, IFAC-PapersOnLine 50 (1) (2017) 14729–14734.

[38] P. S. Rivadeneira, A. Ferramosca, A. H. González, Impulsive zone model predictive control with application to type i diabetic patients, in: 2016 IEEE Conference on Control Applications (CCA), IEEE, 2016, pp. 544–549.

[39] M. Penet, Robust nonlinear model predictive control based on constrained saddle point optimization: Stability analysis and application to type 1 diabetes, Ph.D. thesis, Supélec (2013).

[40] D. Boiroux, A. K. Duun-Henriksen, S. Schmidt, K. Nørgaard, S. Madsbad, N. K. Poulsen, H. Madsen, J. B. Jørgensen, Overnight glucose control in people with type 1 diabetes, Biomedical Signal Processing and Control 39 (2018) 503–512.

[41] G. P. Incremona, M. Messori, C. Toffanin, C. Cobelli, L. Magni, Model predictive control with integral action for artificial pancreas, Control Engineering Practice 77 (2018) 86–94.

[42] J. B. Lee, E. Dassau, R. Gondhalekar, D. E. Seborg, J. E. Pinsker, F. J. Doyle III, Enhanced model predictive control (empc) strategy for automated glucose control, Industrial & engineering chemistry research 55 (46) (2016) 11857–11868.

[43] A. Ferramosca, D. Limon, A. H. González, D. Odloak, E. F. Camacho, Mpc for tracking zone regions, Journal of Process Control 20 (4) (2010) 506–516.

[44] M. N. Zeilinger, M. Morari, C. N. Jones, Soft constrained model predictive control with robust stability guarantees, IEEE Transactions on Automatic Control 59 (5) (2014) 1190–1202.

[45] Y. Ruan, M. E. Wilinska, H. Thabit, R. Hovorka, Modeling day-to-day variability of glucose–insulin regulation over 12-week home use of closed-loop insulin delivery, IEEE Transactions on Biomedical Engineering 64 (6) (2016) 1412–1419.

[46] N. Magdelaine, L. Chaillous, I. Guilhem, J.-Y. Poirier, M. Krempf, C. H. Moog, E. Le Carpentier, A long-term model of the glucose–insulin dynamics of type 1 diabetes, IEEE Transactions on Biomedical Engineering 62 (6) (2015) 1546–1552.

[47] A. Bock, G. François, D. Gillet, A therapy parameter-based model for predicting blood glucose concentrations in patients with type 1 diabetes, Computer methods and programs in biomedicine 118 (2) (2015) 107–123.

[48] G. C. Goodwin, D. S. Carrasco, A. M. Medioli, B. R. King, C. Stephen, Nonlinear insulin to carbohydrate rule for treatment of type 1 diabetes, IFAC-PapersOnLine 48 (11) (2015) 198–203.

[49] C. Toffanin, R. Visentin, M. Messori, F. Di Palma, L. Magni, C. Cobelli, Toward a run-to-run adaptive artificial pancreas: In silico results, IEEE Transactions on Biomedical Engineering 65 (3) (2017) 479–488.

[50] M. Schiavon, C. Dalla Man, C. Cobelli, Insulin sensitivity index-based optimization of insulin to carbohydrate ratio: in silico study shows efficacious protection against hypoglycemic events caused by suboptimal therapy, Diabetes technology & therapeutics 20 (2) (2018) 98–105.

[51] N. Magdelaine, P. S. Rivadeneira, L. Chaillous, A.-L. Fournier-Guilloux, M. Krempf, T. MohammadRidha, M. Ait-Ahmed, C. H. Moog, Hypoglycaemia-free artificial pancreas project, IET systems biology 14 (1) (2020) 16–23.

[52] Medtronic, MiniMed 640G System User Guide, rev. 1 (1 2015).

[53] F. H. El-Khatib, C. Balliro, M. A. Hillard, K. L. Magyar, L. Ekhlaspour, M. Sinha, D. Mondesir, A. Esmaeili, C. Hartigan, M. J. Thompson, et al., Home use of a bihormonal bionic pancreas versus insulin pump therapy in adults with type 1 diabetes: a multicentre randomised crossover trial, The Lancet 389 (10067) (2017) 369–380.

[54] R. Hovorka, D. Elleri, H. Thabit, J. M. Allen, L. Leelarathna, R. El-Khairi, K. Kumareswaran, K. Caldwell, P. Calhoun, C. Kollman, et al., Overnight closed-loop insulin delivery in young people with type 1 diabetes: a free-living, randomized clinical trial, Diabetes care 37 (5) (2014) 1204–1211.

[55] K. A. Matyka, E. C. Crowne, P. J. Havel, I. A. Macdonald, D. Matthews, D. B. Dunger, Counter-regulation during spontaneous nocturnal hypoglycemia in prepubertal children with type 1 diabetes., Diabetes Care 22 (7) (1999) 1144–1150.

[56] C. Toffanin, H. Zisser, F. J. Doyle III, E. Dassau, Dynamic insulin on board: incorporation of circadian insulin sensitivity variation, Journal of diabetes science and technology 7 (4) (2013) 928–940.

[57] V. Gingras, R. Rabasa-Lhoret, V. Messier, M. Ladouceur, L. Legault, A. Haidar, Efficacy of dual-hormone artificial pancreas to alleviate the carbohydrate-counting burden of type 1 diabetes: A randomized crossover trial, Diabetes & metabolism 42 (1) (2016) 47–54.

[58] D. C. Montgomery, E. A. Peck, G. G. Vining, Introduction to linear regression analysis, John Wiley & Sons, 2021.

[59] G. Jones, P. Lyons, Approximate graphical methods for inverse regression, Journal of Data Science 7 (1) (2009) 61–72.

[60] C. Townsend, M. M. Seron, G. C. Goodwin, B. R. King, Control limitations in models of t1dm and the robustness of optimal insulin delivery, Journal of diabetes science and technology 12 (5) (2018) 926–936.

[61] E. Dassau, B. W. Bequette, B. A. Buckingham, F. J. Doyle, Detection of a meal using continuous glucose monitoring: implications for an artificial β-cell, Diabetes care 31 (2) (2008) 295–300.

[62] G. C. Goodwin, D. S. Carrasco, M. M. Seron, A. M. Medioli, A fundamental control performance limit for a class of positive nonlinear systems, Automatica 95 (2018) 14–22.

[63] T. MohammadRidha, P. S. Rivadeneira, N. Magdelaine, M. Cardelli, C. H. Moog, Positively invariant sets of a t1dm model: Hypoglycemia prediction and avoidance, Journal of the Franklin Institute 356 (11) (2019) 5652–5674.

[64] J. Löfberg, Yalmip : A toolbox for modeling and optimization in matlab, in: In Proceedings of the CACSD Conference, Taipei, Taiwan, 2004.

[65] Z. Cao, R. Gondhalekar, E. Dassau, F. J. Doyle, Extremum seeking control for personalized zone adaptation in model predictive control for type 1 diabetes, IEEE Transactions on Biomedical Engineering 65 (8) (2017) 1859–1870.

[66] M. Vettoretti, A. Facchinetti, G. Sparacino, C. Cobelli, Type-1 diabetes patient decision simulator for in silico testing safety and effectiveness of insulin treatments, IEEE Transactions on Biomedical Engineering 65 (6) (2017) 1281–1290.

[67] F. Reiterer, G. Freckmann, L. del Re, Impact of carbohydrate counting errors on glycemic control in type 1 diabetes, IFAC-PapersOnLine 51 (27) (2018) 186–191.

[68] E. J. Mansell, P. D. Docherty, J. G. Chase, Shedding light on grey noise in diabetes modelling, Biomedical Signal Processing and Control 31 (2017) 16–30.

[69] C. Roversi, M. Vettoretti, S. Del Favero, A. Facchinetti, P. Choudhary, G. Sparacino, Impact of carbohydrate counting error on glycemic control in open-loop management of type 1 diabetes: Quantitative assessment through an in silico trial, Journal of Diabetes Science and Technology (2021) 19322968211012392.

[70] A. El Fathi, M. R. Smaoui, V. Gingras, B. Boulet, A. Haidar, The artificial pancreas and meal control: an overview of postprandial glucose regulation in type 1 diabetes, IEEE Control Systems Magazine 38 (1) (2018) 67–85.

[71] L. Magni, D. M. Raimondo, C. Dalla Man, G. De Nicolao, B. Kovatchev, C. Cobelli, Model predictive control of glucose concentration in type i diabetic patients: An in silico trial, Biomedical Signal Processing and Control 4 (4) (2009) 338–346.

[72] S. Schmidt, K. Nørgaard, Bolus calculators, Journal of diabetes science and technology 8 (5) (2014) 1035–1041.

Apéndice C

Artificial pancreas under periodic MPC for trajectory tracking: handling circadian variability of insulin sensitivity

Artificial pancreas under periodic MPC for trajectory tracking: handling circadian variability of insulin sensitivity

Pablo Abuin * **Antonio Ferramosca** ** **Chiara Toffanin** ***
Lalo Magni **** **Alejandro H. Gonzalez** *

* *Institute of Technological Development for the Chemical Industry (INTEC), CONICET-Universidad Nacional del Litoral (UNL), Santa Fe, Argentina. Email: pabloabu.g@gmail.com*
** *Department of Management, Information and Production Engineering, University of Bergamo, Bergamo Italy*
*** *Department of Electrical, Computer and Biomedical Engineering, University of Pavia, Pavia, Italy*
**** *Department of Civil and Architecture Engineering, University of Pavia, Pavia, Italy*

Abstract: Closed-loop glycemic control algorithms have demonstrated the ability to improve glucose regulation in patients with type 1 diabetes mellitus (T1D), both in silico and clinical trials. Many of the proposed control strategies have been developed, based on time-invariant linear models, without considering the parametric variations of T1DM subjects. In this work, a pulsatile Zone Model Predictive Control (pZMPC) is proposed, which explicitly considers patterns of intra-day insulin sensitivity (S_I), according to the latest updates of the FDA-approved UVA/Padova simulator. Results show a significant improvement in the performance, which *a-priori* justifies the increment in the controller complexity.

Keywords: Insulin sensitivity variations, trajectory tracking, MPC, Artificial Pancreas

1. INTRODUCTION

Blood glucose regulation in type 1 diabetes (T1D) patients is not an easy task: glucose metabolism is affected by several factors during the day, such as daily variations in subject physiological parameters, different composition of ingested meals, physical activity, irregular pattern of sleep, stress, illness, menstrual cycle, etc (Kudva et al., 2014; Mansell et al., 2017). Among them, circadian variability (24-h) of insulin sensitivity (S_I) is a well known phenomenon that occurs in T1D subjects, characterized by a periodic insulin sensitivity pattern, being lower, on average, at breakfast in comparison with lunch and dinner (Hinshaw et al., 2013). Although this pattern has been associated with the effect of counter-regulatory hormones (i.e. cortisol, melatonin, growth hormone) (Schrezenmeir et al., 1993) or the so-called dawn phenomena, a study conducted by (Hinshaw et al., 2013) did not find such a link, arguing that the modulation of diurnal patterns of S_I could be more related to sleep architecture. Moreover, in comparison with healthy S_I pattern, they noted a large inter-subject variability in T1D patients, which was later corroborated by (Visentin et al., 2015) who, using a minimal model for S_I estimation, detected 7 classes of S_I profiles.

Several mathematical models of the S_I profile have been proposed employing piecewise, sinusoidal and variable basis (Mansell et al., 2017). Indeed, this effect has been included in the UVA/Padova Maximal Model (Visentin et al., 2018) by modifying parameters, such as k_{p3} and V_{mx}, according to a given S_I class. In addition, some control algorithms have been formulated considering intra-patient variability, but few of them have explicitly taken into account the periodicity of the S_I patterns due to circadian variability, to make predictions. Recently, some new adaptive strategies were also proposed. By taking into account that the meal intake and physical activity follow a periodicity pattern, (Ortmann et al., 2017) has proposed a Gaussian-process controller with an offset free Model Predictive Controller (MPC) approach to make predictions under the mini-pig model. Moreover, (Toffanin et al., 2013) used the circadian S_I variability to formulate a dynamic Insulin-on-Board (IOB) constraint for the MPC controller previously presented in (Patek et al., 2012). Finally, (Gondhalekar et al., 2016) proposed to include a periodic reference in order to tackle S_I circadian variability, avoiding overnight hypoglycemia.

In this work, we explicitly consider S_I intra-day variability in the prediction model, which leads to the concept of basal trajectories - in contrast to basal fixed levels. Basal trajectories increase the general system controllability, to better avoid hypo and hyperglycemia episodes. On the one hand, when the S_I is high, a reasonable option is to keep the glycemia in a high basal level, to counteract eventual falls due to miss-estimation of the S_I. On the other hand, when the S_I is low, a reasonable option is to keep the glycemia in a low basal level, to prevent the insufficient effect of insulin boluses that compensate meals. Further benefits of MPC that are exploited in this work are: the consideration of 'zones objectives' around the basal glycemic trajectories, which define the normoglycemia range and avoid over control (Gondhalekar et al., 2016, 2018; Abuin et al., 2020); asymmetric cost functions (penalizing harder hypoglycemic than hyperglycemic episodes) (Gondhalekar et al., 2016; Abuin et al., 2020); and the use of pulsatile insulin infusions (González et al., 2020; Abuin et al., 2020), which better

reproduces the pump behavior both, in basal and postprandial scenarios.

Notation: $\mathbb{R}$ and $\mathbb{I}$ are the sets of real and integer numbers. $\mathbb{R}^n_{[a,b]}$ ($\mathbb{R}^n_{(a,b)}$) is the set of real vectors x, of dimension n, which component-wise fulfill $a \leq x \leq b$ ($a < x < b$). Similarly, $\mathbb{I}_{[a,b]}$ ($\mathbb{I}_{(a,b)}$) is the set of integers k such that $a \leq k \leq b$ ($a < k < b$). The n-norm for vectors $x \in \mathbb{R}^n$, with $n \in \mathbb{I}_{[1,\infty)}$, is denoted $\|x\|_n$. Given a set $\mathcal{X} \subseteq \mathbb{R}^n$, $\mathcal{P}(\mathcal{X})$ is the power set of $\mathcal{X}$ (i.e., the set of all subsets of $\mathcal{X}$). $x(\cdot) : \mathbb{R}_{[a,b]} \to \mathbb{R}^n_{[c,d]}$ denotes the continuous-time functions, that goes from $t \in [a, b]$ to real vectors in $\mathbb{R}^n_{[c,d]}$. Similarly, $\mathbf{x} : \mathbb{I}_{[a,b]} \to \mathbb{R}^n_{[c,d]}$ represents the discrete-time sequences, that goes from $k \in [a, b]$ to vectors in $\mathbb{R}^n_{[c,d]}$.

2. PHYSIOLOGICAL BLOOD GLUCOSE-INSULIN MODEL

The following affine continuous-time time-varying state space model, which is a physiological minimal model based on (Ruan et al., 2016), is considered to describe the **glucose-insulin subsystem** under intra-day variations of insulin sensitivity ($S_I(t)$):

$$\dot{x}(t) = A_x(t)x(t) + B_u u(t) + B_z z(t) + E, \;\; x(0) = x_0, \quad (1)$$

where $x(t) = [x_1(t) \;\; x_2(t) \;\; x_3(t)]'$ denotes the system state, with $x_1 = G$ being the blood glucose concentration [mg/dL], x_2 being the insulin delivery rate in plasma [U/min] and x_3 being the insulin delivery rate in the subcutaneous compartment [U/min], and $u(t)$ denotes the exogenous insulin infusion rate [U/min]. Variable z is a state representing the **meal absorption subsystem**, which is in turn described by the following subsystem:

$$\dot{z}(t) = A_z z(t) + B_r r(t), \;\; z(0) = z_0, \quad (2)$$

where $z(t) = [z_1(t) \;\; z_2(t)]'$, with z_1 being the rate of carbohydrate absorption from the gut [g/min] and z_2 being the glucose delivery rate from the stomach [g/min], and $r(t)$ is the rate of carbohydrate (CHO) intake [g/min].
The subsystems matrices are given by:

$$A_x(t) = \begin{bmatrix} -\theta_1 & -\theta_2(t) & 0 \\ 0 & -\frac{1}{\theta_4} & \frac{1}{\theta_4} \\ 0 & 0 & -\frac{1}{\theta_4} \end{bmatrix}, \; B_u = \begin{bmatrix} 0 \\ 0 \\ \frac{1}{\theta_4} \end{bmatrix}, \; E = \begin{bmatrix} \theta_0 \\ 0 \\ 0 \end{bmatrix},$$
$$B_z = \begin{bmatrix} \theta_3 & 0 \\ 0 & 0 \\ 0 & 0 \end{bmatrix}, \; A_z = \begin{bmatrix} -\frac{1}{\theta_5} & \frac{1}{\theta_5} \\ 0 & -\frac{1}{\theta_5} \end{bmatrix}, \; B_r = \begin{bmatrix} 0 \\ \frac{1}{\theta_5} \end{bmatrix}, \quad (3)$$

where $\theta_2(\cdot) : \mathbb{R}_{[0,\infty)} \to \mathbb{R}_{[\theta_{2min}, \theta_{2max}]}$ is the insulin sensitivity under intra-day variations [mg/(dL·U)] , θ_3 is the raise factor [mg/(dL·g)] and θ_1 is the glucose effectiveness [/min] or glucose self-regulation effect to promote its own metabolism. Furthermore, θ_0 is the extrapolated endogenous glucose production (EGP) at zero glucose and insulin levels [mg/(dL·min)], θ_4 is the insulin absorption kinetics time constant [min], and θ_5 is the meal absorption subsystem time constant [min].
The outputs of subsystem (1) are given by $G(t) = C_1 x(t)$, where $C_1 = [1\; 0\; 0]$ (glycemia to be controlled), and $IOB(t) = C_2 x(t)$ where $C_2 = [0 \;\; \theta_4 \;\; \theta_4]$ (insulin on board, to be constrained for safety reasons).

Assumption 1. *Parameter $\theta_2(\cdot) : \mathbb{R}_{[0,\infty)} \to \mathbb{R}_{[\theta_{2min}, \theta_{2max}]}$ is assumed be $\theta_2(t) := \bar{\theta}_2 + \tilde{\theta}_2(t)$, $t \geq 0$, where $\bar{\theta}_2 > 0$ is a constant nominal value, and $\tilde{\theta}_2(t)$ is a periodic one, accounting for the insulin sensitivity variations due to circadian rhythms: i.e., $\tilde{\theta}_2(t) = \tilde{\theta}_2(t+T)$, for all $t \geq 0$, being T the circadian cycle equal to 24 hours (or 1440 minutes). Furthermore, $\theta_2(t) > 0$ for all $t \geq 0$.*

Subsystems (1) and (2), with $\theta_2(t) \equiv \bar{\theta}_2$, are referred to as the **nominal system**. Note that due to the affine term (E), physiological basal conditions are explicitly accounted for in subsystem (1), since null values of u does not produce null values of G, even in fasting periods where $r(t) \equiv 0$ and $z(t) \equiv 0$.

2.1 Constraints under circadian insulin sensitivity variations

The input and states of subsystem (1) are assumed to be constrained to belong to sets $\mathcal{U}$ and $\mathcal{X}$, respectively. Set $\mathcal{U}$, on one hand, accounts for the positivity and the maximal infusion dose of the insulin pump, and it is given by:

$$\mathcal{U} := \mathbb{R}_{[0, u_{max}]}, \quad (4)$$

with $u_{max} = 15$ [U] (*i.e.*: maximum infusion dose of insulin pumps). Given that - for safety reasons - $IOB(t) = \theta_4(x_2(t) + x_3(t))$ should have different maximum values for different periods of the day, and system (1) is time-variant, the state constraints set $\mathcal{X}$ is defined as a time-variant set. The idea is to consider $\mathcal{X}(\cdot) : \mathbb{R}_{[0,\infty)} \to \mathcal{P}(\mathcal{X})$ periodic, with period T; that is $\mathcal{X}(t) = \mathcal{X}(t+T)$, for all $t \geq 0$. More precisely, the state constraint set $\mathcal{X}(t)$ is given by:

$$\mathcal{X}(t) := \{x \in \mathcal{X} \mid x_{min} \leq Cx \leq x_{max}(t)\}, \quad t \geq 0, \quad (5)$$

with $C = [C_1, C_2]'$, $x_{min} = [G_{hypo}, 0]'$, and $x_{max}(t) = [G_{hyper}, IOB_{max}(t)]'$. $G_{hypo} = 60$ [mg/dL], $G_{hyper} = 250$ [mg/dL], and $IOB_{max}(\cdot) := \theta_4(x_{b,2}(\cdot) + x_{b,3}(\cdot)) + CHO(\cdot)/CR$, with CR representing the carbohydrate-to-insulin ratio, that provides the nominal bolus given by the ratio $CHO(\cdot)/CR$. Moreover, $(x_{b,2}, x_{b,3})$ represent the value of states (x_2, x_3) at a basal trajectory, which will be defined later on.

2.2 Basal conditions analysis

Subsystems (1) and (2) without meal intakes ($r(t) \equiv 0$ and $z(t) \equiv 0$) are referred to as the 'system under basal conditions' and, in such fasting scenario, subsystem (1) describes the whole system dynamic.

Nominal case. For the nominal case (i.e. $\theta_2(t) \equiv \bar{\theta}_2$), the equilibrium set of subsystem (1) is given by a set of pairs (u_s, x_s) fulfilling the condition $x_s = [x_{s,1}, x_{s,2}, x_{s,3}]' = [\frac{\theta_0 - \bar{\theta}_2 u_s}{\theta_1}, u_s, u_s]'$. If, in addition, the input and state constraints are considered, the state equilibrium set is defined as the set of all state x_s that belongs to $\mathcal{X}$, for which there exists some u_s belonging to $\mathcal{U}$. We denote this latter set $\mathcal{X}_s$ and the corresponding input set, $\mathcal{U}_s$.
Among the pairs $(x_s, u_s) \in \mathcal{X}_s \times \mathcal{U}_s$ we define the nominal basal equilibrium (x_b, u_b) as the one corresponding to a specific value of $x_{s,1} := \bar{G}_b$, where $\bar{G}_b$ represents a fixed **basal level for the glucose** (usually $\bar{G}_b = 110$ [mg/dL]). This way, we have a basal equilibrium state $x_b = [\bar{G}_b, u_b, u_b]'$, and a basal equilibrium input $u_b = \frac{\theta_0 - \theta_1 \bar{G}_b}{\bar{\theta}_2}$. See Figure 1 for a schematic plot of $\mathcal{X}_s$ (blue line) and x_b (green point).

Time-varying case. If now $\theta_2(t) = \bar{\theta}_2 + \tilde{\theta}_2(t)$, with a periodic $\theta_2(t) = \theta_2(t+T)$, for $t \geq 0$, **the whole concept of equilibrium is lost**, i.e., there is no longer an input that maintains the state fixed in time. However, as long as $\theta_2(t)$ is not large enough to cause feasibility problems, it is still possible to define a trajectory such that $G(t) = x_1(t)$ remains

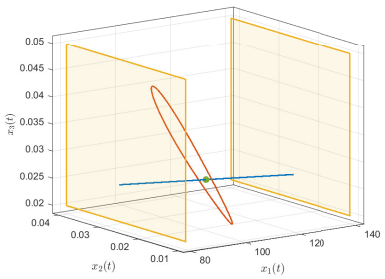

Fig. 1. Equilibrium set $\mathcal{X}_s$ (blue line), basal state x_b (green point) and basal trajectory corresponding to $\bar{G}_b = 110$ (red periodic trajectory), for subsystem (1). The yellow planes represents bounds for $G = x_1$

fixed at $\bar{G}_b$, while the other two states $x_2(t)$ and $x_3(t)$ are periodic as it is $\theta_2(t)$. This trajectory of period T, defined as $x_b(t) := [x_{b,1}(t), x_{b,2}(t), x_{b,3}(t)]' = [\bar{G}_b, x_{b,2}(t), x_{b,3}(t)]'$, $t \geq 0$, corresponds to a periodic input $u_b(t)$, and can be obtained explicitly as follows:

$$x_b(t) = \begin{bmatrix} x_{b,1}(t) \\ x_{b,2}(t) \\ x_{b,3}(t) \end{bmatrix} = \begin{bmatrix} \bar{G}_b \\ \frac{\theta_0 - \bar{G}_b\theta_1}{\theta_2(t)} \\ \frac{\theta_0 - \bar{G}_b\theta_1}{\theta_2(t)} - \frac{(\theta_0 - \bar{G}_b\theta_1)\theta_4\dot{\theta}_2(t)}{\theta_2^2(t)} \end{bmatrix}, \quad (6)$$

with $u_b(t) = x_{b,3}(t) + \theta_4 \dot{x}_{b,3}(t)$. Figure 1 shows a schematic plot of $x_b(t)$ (red trajectory).

The latter periodic trajectory $x_b(t)$ is, however, one of many possible (the one that maintains $x_1(t)$ at $\bar{G}_b$). In a more general framework, we may propose a problem to find out the basal state and input trajectories, such that state $x_1(t)$ approaches as long as possible (i.e., fulfilling the constraints) a general G_b^{ref}, periodic in $[0, T]$. The following definition summarizes this new concept:

Definition 1 (Basal state and input trajectories)**.** *Consider subsystem* (1) *constrained by $\mathcal{X}$ and $\mathcal{U}$, and a given glycemia periodic reference $G_b^{ref}(\cdot) : \mathbb{R}_{[0,\infty)} \to \mathbb{R}_{[G_{hypo}, G_{hyper}]}$, with period T (i.e., $G_b^{ref}(t) = G_b^{ref}(t+T)$, for $t \geq 0$). A basal state and input trajectories are given by the periodic state trajectory $x_b(\cdot) : \mathbb{R}_{[0,\infty)} \to \mathcal{X}$ and the corresponding input $u_b(\cdot) : \mathbb{R}_{[0,\infty)} \to \mathcal{U}$ that minimizes $\|C_1 x_b(t) - G_b^{ref}(t)\|$, for $t \geq 0$.*

Remark 1. *Note that the concept of basal state and input trajectories can be also defined for LTI models. However, the periodic (and significant) variability of S_I (which is not considered in LTI models) may reinforce low values of G, so producing hypoglycemic episodes.*

3. IDENTIFICATION OF CIRCADIAN S_I RHYTHMS

In order to obtain an estimation of the periodic insulin sensitivity pattern, $\theta_2(t)$, a constrained optimization problem was formulated by imposing a periodicity constraint on the time-varying parameter. Furthermore, physiological constraints were added for $\theta_2(t)$ estimation, such that $\theta_2(t) \in \Theta$, with $\Theta = \mathbb{R}_{[0.8\alpha\bar{\theta}_2, 1.2\bar{\theta}_2]}$ ($\alpha = 0.4$) and $\bar{\theta}_2$ being the insulin sensitivity nominal value. A variability of $\pm 20\%$ was assumed, as reported in (Visentin et al., 2015). The system period was fixed in a daily basis ($T = 1440$ min) so the circadian insulin sensitivity rhythm can be computed as the solution of the following constrained convex quadratic problem:

$$\begin{aligned} \theta_2^* = \arg \min_{\theta_2, \theta_{2T}, \mathbf{s}} \; & \textstyle\sum_{j=1}^{N_{CI}} \|G_m(j) - G(j)\|_2^2 + \lambda_1 \|s(j)\|_2^2 \\ & + \lambda_2 \|\Delta\theta_{2T}(j)\|_1 \\ s.t. \; & G(j) = C_1 [\tfrac{(q-1)I}{T_s} - A_x(j)]^{-1} (B_u u(j) \\ & + B_z z(j) + E), \quad j \in \mathbb{I}_{[0,N_{CI}]}, \\ & z(j) = [\tfrac{(q-1)I}{T_s} - A_z]^{-1} B_r r(j), \; j \in \mathbb{I}_{[0,N_{CI}]}, \\ & \theta_2(j) \leq \theta_{2T}(j) + s(j), \quad j \in \mathbb{I}_{[0,N_{CI}]}, \\ & \theta_2(j) \geq \theta_{2T}(j) - s(j), \quad j \in \mathbb{I}_{[0,N_{CI}]}, \\ & \theta_{2T}(j) = \theta_{2T}(j+T), \theta_2(j) \in \Theta, \; j \in \mathbb{I}_{[0,N_{CI}]} \\ & s(j) \geq 0, \quad j \in \mathbb{I}_{[0,N_{CI}]}, \end{aligned}$$

where θ_2^* is the optimal estimation of the daily circadian S_I pattern, $\lambda_1, \lambda_2 > 0$ are penalty scalars, $G_m(j)$ denotes the measured BG, $G(j)$ is the BG predicted by the model, q is a forward shift operator ($qx(j) := x(j+1)$), θ_{2T} is an auxiliary periodic variable, and s a dispersion/slack variable. $A_x(j)$ indicates that the state space matrix varies throughout the prediction horizon, due to the time variability of $\theta_2(j)$ (Euler discretization). N_{CI} is the length of the dataset ($N_{days} \cdot (288/day)$, if $T_s = 5$ min). Due to the inherent inter-day variability of the insulin sensitivity, $\theta_2(t) \approx \theta_2(t+T)$ (quasi-periodic behavior), so the periodic constraint was relaxed via the slack variable $s(j)$, whose variations are penalized by the l-2 norm regularization term (weighted by $\lambda_1 \geq 0$). In addition, since the S_I profile follows a piecewise constant evolution, a sparsity-promotion term of the first order time differences, given by $\Delta\theta_{2T}(j) = \theta_{2T}(j) - \theta_{2T}(j-1)$, was included in order to detect S_I transitions over periods of flat S_I progression.

4. DISCRETE-TIME LTV MODELING FOR PULSIVE INPUT SIGNALS

In order to use the continuous-time models (1) and (2) as prediction models in an MPC controller, they should be previously sampled. We select in this work the pulsatile scheme proposed in (Abuin et al., 2020) which, for a given sampling time T_s (such that T is a multiple of T_s) and a pulse duration $0 < \Delta < T_s$, consists in the following discrete-time sub-models:

$$\begin{aligned} x(k+1) &= F_x(k, x(k), u(k), z(k)), \\ z(k+1) &= F_z(z(k), r(k)), \\ G(k) &= C_1 x(k), \quad IOB(k) = C_2 x(k), \end{aligned} \quad (7)$$

where $k \in \mathbb{I}_{[0,\infty)}$ represents kT_s, $F_x(\cdot, x(\cdot), u(\cdot), z(\cdot)) := A_x^d(\cdot)x(\cdot) + B_u^d(\cdot)u(\cdot) + B_z^d(\cdot)z(\cdot) + E^d(\cdot)$ and $F_z(z(\cdot), r(\cdot)) := A_z^d z(\cdot) + B_r^d r(\cdot)$. The time varying pulsatile discrete-time matrices are: $A_x^d(k) := e^{A_x(kT_s)T_s}$, $B_u^d(k) := e^{A_x(kT_s)(T_s - \Delta T_s)} A_x^{-1}(kT_s)(e^{A_x(kT_s)\Delta T_s} - I_3)B_u$, $B_z^d(k) := A_x^{-1}(kT_s)(e^{A(kT_s)T_s} - I_3)B_z$, $E^d(k) := A_x^{-1}(kT_s)(e^{A_x(kT_s)T_s} - I_3)E$, $A_z^d := e^{A_z T_s}$, and $B_r^d := A_z^{-1}(e^{A_z T_s} - I_2)B_r$ (Abuin et al., 2020).

Note that in the previous discretization it was assumed that $\theta_1 \neq 0$ (in such a way that A_x is invertible) and time varying parameters are assumed constant during the sampling-time interval T_s, that is, $\theta_2(t) := \theta_2(kT_s)$, $t \in [kT_s, (k+1)T_s)$, $k \in \mathbb{I}_{[0,\infty)}$ (zero-order hold assumption). Furthermore, the time-varying state constraints set, $\mathcal{X}(t)$, can be sampled by considering $\mathcal{X}(k) := \mathcal{X}(kT_s)$, $k \in \mathbb{I}_{[0,\infty)}$.

5. PULSATILE MPC FORMULATIONS

In this section, a pulsatile MPC controller devoted to track the **basal state and input trajectories** is presented, which is based on concepts introduced in (Limon et al., 2015) and (Abuin et al., 2020). Although the MPC is designed for both, the announced

(or partially-announced) and the unannounced meal cases, in the present work only the (not in advanced) announced meal case will be considered. The general control problem can be defined as follows:

Definition 2 (Control problem: basal trajectory tracking)**.** *Consider system* (7) *constrained by* $\mathcal{X}(k)$, $k \in \mathbb{I}_{[0,\infty)}$ *and* $\mathcal{U}$, *and a desired basal reference for the blood glucose* $\mathbf{G}_b^{ref} : \mathbb{I}_{[0,\infty)} \to \mathbb{R}_{[G_{hypo},G_{hyper}]}$, *with period* T, *which is a sampled version of* $G_b^{ref}(\cdot)$, *in Definition 1, and* T *is now the period in sampling times. Then, given the estimated states* $\hat{x}$ *and* $\hat{z}$ *and the meal announcement* $\hat{r}$, *at the current time* k, *the control problem consists in steering the system to the basal state and input trajectory*[1]*, denoted as* $\mathbf{x}_b(\cdot) : \mathbb{I}_{[0,\infty)} \to \mathcal{X}$ *and* $\mathbf{u}_b(\cdot) : \mathbb{I}_{[0,\infty)} \to \mathcal{U}$, *which minimize* $\|C_1 x_b(k) - G_b^{ref}(k)\|$, *for all* $k \geq 0$.

To account for the latter control problem, the following MPC schemes are proposed.

5.1 Basal trajectory tracking, two stage approach

Given $G_b^{ref}(k)$, over the period $[0, T]$, we solve first the **basal trajectory computation problem**, $\mathcal{BTC}(\mathbf{G}_b^{ref})$, to obtain $\mathbf{u}_b$ and $\mathbf{x}_b$:

$$\begin{aligned} \min_{\bar{\mathbf{u}}_b, \bar{\mathbf{x}}_b} \; & V_{traj}(\mathbf{G}_b^{ref}; \bar{\mathbf{u}}_b, \bar{\mathbf{x}}_b) \\ s.t. \; & \bar{u}_b(j) \in \mathcal{U}, \;\; \bar{x}_b(j) \in \mathcal{X}(k+j), \qquad j \in \mathbb{I}_{[0,T]} \\ & \bar{x}_b(j+1) = F_x(k+j, \bar{x}_b(j), \bar{u}_b(j), 0), \\ & \bar{x}_b(0) = F_x(k+T-1, \bar{x}_b(T-1), \bar{u}_b(T-1), 0), \end{aligned} \tag{8}$$

with $\mathcal{U}$, $\mathcal{X}$ given by (4) - (5), respectively, and V_{traj} given by:

$$V_{traj}(\mathbf{G}_b^{ref}; \bar{\mathbf{u}}_b, \bar{\mathbf{x}}_b) := \sum_{j=0}^{T-1} S \|C_1 \bar{x}_b(j) - G_b^{ref}(j)\|_2^2, \tag{9}$$

with $S > 0$ being an appropriate positive penalty.

The solution of problem $\mathcal{BTC}(\mathbf{G}_b^{ref})$ is given by $\bar{\mathbf{x}}_b^0(\cdot) : \mathbb{I}_{[0,T]} \to \mathcal{X}$ and $\bar{\mathbf{u}}_b^0(\cdot) : \mathbb{I}_{[0,T]} \to \mathcal{U}$, which fulfills $\bar{x}_b^0(0) = \bar{x}_b^0(T)$ and $\bar{u}_b^0(0) = \bar{u}_b^0(T)$, respectively. Note that if $G_b^{ref}(k)$ is reachable over the period $[0, T]$, then $V_{traj}(\mathbf{G}_b^{ref}; \bar{\mathbf{u}}_b^0, \bar{\mathbf{x}}_b^0) = 0$, since in such case, the blood glucose reference can be followed by means of a feasible insulin trajectory, and following a feasible state trajectory, over $[0, T]$. Otherwise, $V_{traj}(\mathbf{G}_b^{ref}; \bar{\mathbf{u}}_b^0, \bar{\mathbf{x}}_b^0) > 0$, but given that the later optimization problem is convex, the solution $\bar{\mathbf{u}}_b^0$ and $\bar{\mathbf{x}}_b^0$ is unique.

Once $\bar{\mathbf{u}}_b^0$ and $\bar{\mathbf{x}}_b^0$ are obtained from $\mathcal{BTC}(\mathbf{G}_b^{ref})$, **the basal state and input trajectories**[2], $\mathbf{u}_b$ and $\mathbf{x}_b$, are obtained by concatenating $\bar{\mathbf{u}}_b^0$ and $\bar{\mathbf{x}}_b^0$ over all the positive discrete times, in such a way that $u_b(k) = u_b(k+T)$ and $x_b(k) = x_b(k+T)$, respectively, for all $k \geq 0$.

Consider now the estimated states[3] $\hat{x}$, $\hat{z}$ and the carb counting, $\hat{r}$, at the current time k. The meal announcement sequence $\mathbf{r} : \mathbb{I}_{[0,T]} \to \mathbb{R}_{[0,r_{max}]}$, is such that $r(k) = \hat{r}$ if $k = 0$, and $r(k) = 0$, otherwise. Then, the MPC **trajectory tracking problem**, $\mathcal{MPC}_{\mathcal{TT}}(\hat{x}, \hat{z}, \mathbf{r}, \mathbf{u}_b, \mathbf{x}_b, k)$, to be solved at each time k, is given by:

$$\begin{aligned} \min_{\mathbf{u}} \; & V_{track}(\hat{x}, \hat{z}, \mathbf{r}, \mathbf{u}_b, \mathbf{x}_b, k; \mathbf{u}) \\ s.t. & x(0) = \hat{x}, \;\; z(0) = \hat{z} \\ & x(j+1) = F_x(k+j, x(j), u(j), z(j)), \quad j \in \mathbb{I}_{[0,N]} \\ & z(j+1) = F_z(z(j), r(j)), \qquad\qquad\quad j \in \mathbb{I}_{[0,N]} \\ & u(j) \in \mathcal{U}, \;\; x(j) \in \mathcal{X}(k+j), \qquad j \in \mathbb{I}_{[0,N-1]} \\ & x(N) = x_b(N), \end{aligned} \tag{10}$$

where $N<T$ is the control horizon and V_{track} is given by:

$$\begin{aligned} V_{track}(\hat{x}, \hat{z}, \mathbf{r}, \mathbf{u}_b, \mathbf{x}_b, k; \mathbf{u}) := & \sum_{j=0}^{N-1} Q \|x(j) - x_b(k+j))\|_2^2 \\ & + R \|u(j) - u_b(k+j)\|_2^2, \end{aligned} \tag{11}$$

with $Q>0$ and $R>0$ being positive definite penalty matrices. In problem $\mathcal{MPC}_{\mathcal{TT}}(\hat{x}, \hat{z}, \mathbf{r}, \mathbf{u}_b, \mathbf{x}_b, k)$, $\hat{x}$, $\hat{z}$, $\mathbf{u}_b$, $\mathbf{x}_b$, $\mathbf{r}$ are parameters, while $\mathbf{u} : \mathbb{I}_{[0,N]} \to \mathcal{U}$ is the optimization variable. Once problem $\mathcal{MPC}_{\mathcal{TT}}$ is solved, the optimal solution is denoted $\mathbf{u}^0$, with an associated state sequence $\mathbf{x}^0$. Following the receding horizon control (RHC) policy, only the first optimal input/dose, $u^0(0)$, is applied to the patient, time goes from k to $k+1$, and the whole problem $\mathcal{MPC}_{\mathcal{TT}}$ is solved again. It can be shown that the control scheme derived from the application of $\mathcal{MPC}_{\mathcal{TT}}$ - provided that Problem $\mathcal{BTC}$ has a unique solution - steers the system feasibly to $\mathbf{u}_b, \mathbf{x}_b$ as $k \to \infty$.

5.2 Basal trajectory tracking, single stage approach

Now, based on the use of artificial trajectory, originally introduced in (Limon et al., 2015), the core idea is to merge both, $\mathcal{BTC}$ and $\mathcal{MPC}_{\mathcal{TT}}$ problems, in a single one, denoted by $\mathcal{MPC}_{\mathcal{BTT}}$. Given $\hat{x}$, $\hat{z}$, $\hat{r}$ and $\mathbf{G}_b^{ref}$, at the current time k, the cost function of the problem to be solved at k is given by:

$$\begin{aligned} V_N(\hat{x}, \hat{z}, \mathbf{r}, \mathbf{G}_b^{ref}, k; \mathbf{u}, \mathbf{u}_a, \mathbf{x}_a) := & V_{track}(\hat{x}, \hat{z}, \mathbf{r}; \mathbf{u}, \mathbf{u}_a, \mathbf{x}_a) \\ & + V_{traj}(\mathbf{G}_b^{ref}, k; \mathbf{u}_a, \mathbf{x}_a) \end{aligned} \tag{12}$$

where

$$\begin{aligned} V_{track}(\hat{x}, \hat{z}, \mathbf{r}; \mathbf{u}, \mathbf{u}_a, \mathbf{x}_a) := & \sum_{j=0}^{N-1} Q \|x(j) - x_a(j))\|_2^2 \\ & + R \|u(j) - u_a(j)\|_2^2, \end{aligned} \tag{13}$$

is a term designed to steer the system to the artificial trajectory variables $\mathbf{u}_a : \mathbb{I}_{[0,T]} \to \mathcal{U}$, $\mathbf{x}_a : \mathbb{I}_{[0,T]} \to \mathcal{X}$, in the transient regime, and

$$V_{traj}(\mathbf{G}_b^{ref}, k; \mathbf{u}_a, \mathbf{x}_a) := \sum_{j=0}^{T-1} S \|C_1 x_a(j) - G_b^{ref}(k+j)\|_2^2 \tag{14}$$

is a term devoted to steer the state artificial trajectory to the desired basal reference $\mathbf{G}_b^{ref}$.

The optimization problem $\mathcal{MPC}_{\mathcal{BTT}}(\hat{x}, \hat{z}, \mathbf{r}, \mathbf{G}_b^{ref}, k)$ to be solved by the MPC is then given by:

$$\begin{aligned} \min_{\mathbf{u}, \mathbf{u}_a, \mathbf{x}_a} \; & V_N(\hat{x}, \hat{z}, \mathbf{r}, \mathbf{G}_b^{ref}, k; \mathbf{u}, \mathbf{u}_a, \mathbf{x}_a) \\ s.t. & x(0) = \hat{x}, \;\; z(0) = \hat{z} \\ & x(j+1) = F_x(k+j, x(j), u(j), z(j)), \quad j \in \mathbb{I}_{[0,N]} \\ & z(j+1) = F_z(z(j), r(j)), \qquad\qquad\quad j \in \mathbb{I}_{[0,N]} \\ & u(j) \in \mathcal{U}, \;\; x(j) \in \mathcal{X}(k+j), \qquad j \in \mathbb{I}_{[0,N-1]} \\ & x(N) = x_a(N), \\ & x_a(j+1) = F_x(k+j, x_a(j), u_a(j), 0), \; j \in \mathbb{I}_{[0,T-1]} \\ & u_a(j) \in \mathcal{U}, \quad x_a(j) \in \mathcal{X}(k+j), \qquad j \in \mathbb{I}_{[0,T-1]} \\ & x_a(0) = F_x(k+T-1, x_a(T-1), u_a(T-1), 0). \end{aligned} \tag{15}$$

Notice that this approach is convenient (i) to allow changes in $\mathbf{G}_b^{ref}$ profile, that are instantaneously accounted for in the single optimization problem (i.e., terminal constraint does not

[1] That can be seen as a sampled version of $x_b(\cdot)$ and $u_b(\cdot)$, of Definition 1

[2] Note that $\bar{\mathbf{u}}_b^0$ and $\bar{\mathbf{x}}_b^0$ are defined over $[0, T]$ while the basal state and input trajectories, $\mathbf{x}_b$ and $\mathbf{u}_b$, are defined over $[0, \infty)$

[3] The states x and z are assumed to be estimated by an output disturbance observer (ODO) as the one presented in Abuin et al. (2020)

depend on a pre-computed basal trajectory), and (ii) to enlarge the domain of attraction of the controller (i.e., due to the fact of having a basal reachable trajectory as a decision variable instead of a particular one).

5.3 Basal tube tracking

The idea now is to extend the latter formulation to the case of zone control, that is, control schemes in which the control objective is to follow a region or zone of possible values of G (or a tube made of several zones varying over the time) instead of a particular reference. Taking advantage of the use of artificial variables, this extension can be made by replacing the trajectory cost (14), V_{traj}, by

$$V_{traj}(\mathbf{G}_b^{ref}, k; \mathbf{u}_a, \mathbf{x}_a, \mathbf{G}*) := \sum_{j=0}^{T-1} S\|C_1 x_a(j) - G^*(j)\|_2^2,$$

where $G^*(j)$ is an additional optimization variable, only restricted by $G^*(j) \in [G_b^{ref}(k+j) - G_{b,min}^z, G_b^{ref}(k+j) + G_{b,max}^z]$, being $G_{b,min}^z$ and $G_{b,max}^z$ the lower and upper bounds of the zone, respectively. Moreover, following the ideas presented in (Abuin et al., 2020, Section 6), it is possible to consider asymmetric tubes, by harder penalizing the excursion of $G(t)$ under the reference value $\mathbf{G}_b^{ref}$.

For the sake of brevity, we do not analyse here the feasibility and stability of the proposed control schemes. However, they can proved by following similar steps as in (Limon et al., 2015).

6. SIMULATIONS RESULTS

The performance of the proposed MPC formulations is evaluated through the commercially available UVA/Padova simulator (T1DMS2013, Academic Version) with a virtual average adult patient ($CR = 22.48$ [g/U]). Sensitivity insulin variations are added, acting on k_{SI}, according to randomly-noisy smoothed variation of the nominal profile reported in (Visentin et al., 2015, 2018). The identification of $\theta_2(t)$ is done offline following what is presented in Section 3. The controller parameters are $Q = 1$, $R = 1$, and $S = 10^2$ for all the cases.

6.1 Assessment of the $\mathcal{MPC}_{\mathcal{TT}}$ and $\mathcal{MPC}_{\mathcal{BTT}}$ formulations: nominal vs time-varying prediction model

In this first case, we evaluate the MPC formulations, with and without trajectory planning, $\mathcal{MPC}_{\mathcal{TT}}$ and $\mathcal{MPC}_{\mathcal{BTT}}$, respectively, when a nominal and a time-varying prediction model is employed. For both configurations, a prediction horizon $N = 30$ (2.5 hours) was proposed, to highlight the potential strengths of defining the planned reachable basal trajectory as a decision variable instead of a fix trajectory. The blood glucose reference was fixed in a constant value, $G_b^{ref} = 110$ [mg/dL].

Figure 2 shows the glycemia evolution under the $\mathcal{MPC}_{\mathcal{TT}}$ employing a nominal LTI (red) and a LTV (blue) prediction model. It can be seen, that the LTV setting manages the insulin delivery in accordance to the circadian variations of $S_I(t)$. As expected, the insulin delivery is reduced in an anticipatory way when a S_I transition from a low S_I^l to a high S_I^h level is predicted over the control horizon (i.e. IOB reduction from 10:00 to 12:00 hs). Similarly, it is increased when a S_I transition from a high to a low level is forecasted (i.e. IOB increment from 16:00 to 18:00 hs). In addition, the meal related-events are better counteracted by the LTV configuration, increasing, for the same carb content, the bolus amplitude over intervals of reduced S_I (i.e. IOB at 7:00 and 12:00 hs, being $CHO = 80$ g).

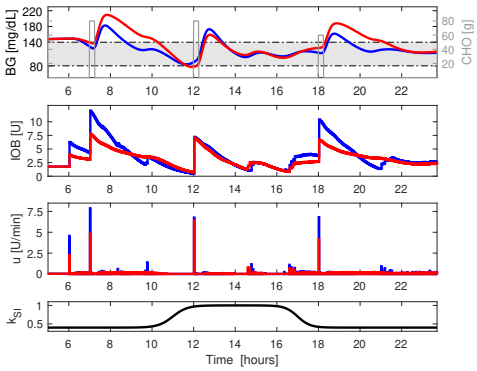

Fig. 2. Blood glucose control employing the $\mathcal{MPC}_{\mathcal{TT}}$ formulation, under nominal LTI (red) and LTV (blue) settings. Insulin sensitivity modulation pattern $k_{SI}(t)$.

Nevertheless, for the $\mathcal{MPC}_{\mathcal{TT}}$ formulation, since its domain of attraction is smaller, a higher number infeasibility episodes are reported (mainly during post prandial intervals, where the BG level is augmented, and thus, feasible control sequences might not be found). See Table 1 for a 7 days scenario.

Table 1. Infeasibility episodes (IE) over 7 days scenario

	$\mathcal{MPC}_{\mathcal{TT}}$		$\mathcal{MPC}_{\mathcal{BTT}}$	
	LTI	LTV	LTI	LTV
#IE	15	52	1	0

6.2 Assessment of the $\mathcal{MPC}_{\mathcal{BTT}}$ formulation: constant vs time-varying G_b^{ref}

In this second case, the idea is to assess the $\mathcal{MPC}_{\mathcal{BTT}}$ performance when a time-varying G_b^{ref} is considered, in such a way that $G_b^{ref}(t) = \lambda(t)G_{b,max}^{ref} + (1-\lambda(t))G_{b,min}^{ref}$, with $\lambda(t) = (\theta_2^{ref}(t) - \theta_{2min}^{ref})/(\theta_{2max}^{ref} - \theta_{2min}^{ref})$. Notice that $\theta_2^{ref}(t) = \max(\theta_2(t) - \overline{\theta_2}, 0)$ to filter eventual non-physiological insulin sensitivity reductions (*i.e.,* $\theta_2(t)$ falling down during postprandial intervals due to structural identifiability limits). To increase the safety from hypoglycemic episodes during intervals of high S_I, the bounds of the time-reference were set in $G_{b,max}^{ref} = 140$ mg/dL and $G_{b,min}^{ref} = 110$ mg/dL. The insulin sensitivity pattern was augmented in 25% (*i.e.,* $k_{SI}^{high}(t) = 1.25 k_{SI}(t)$).

As shown in Figure 3 (i), hypoglycemic episodes are reduced when the aforementioned reference is employed, since it forces the system to steer higher BG levels during periods of high S_I. This strategy allows us to deal with the case in which the identified $\theta_2(t)$ underestimates the actual $S_I(t)$ pattern (*i.e.,* inter-day variability of circadian S_I). Furthermore, if an asymmetric tracking cost is added, the transient evolution before the convergence to the reachable basal trajectory better counteracts the hypoglycemic excursions, thus improving the closed-loop performance. A prediction horizon of $N = 60$ (5 hs) was used in order to increase the influence of the transient regimen effect in the optimization problem $\mathcal{MPC}_{\mathcal{BTT}}$.

6.3 Assessment of the $\mathcal{MPC}_{\mathcal{BTT}}$ (tube): time-varying G_b^{ref}

Finally, in this third case, the $\mathcal{MPC}_{\mathcal{BTT}}$ is compared to $\mathcal{MPC}_{\mathcal{BTT}}$ (tube), where zones are used as control objectives instead of a fixed trajectory. In order to highlight the potential advantages of the latter proposal, a disturbance on the expected circadian variation of $S_I(t)$, given by a physical exercise

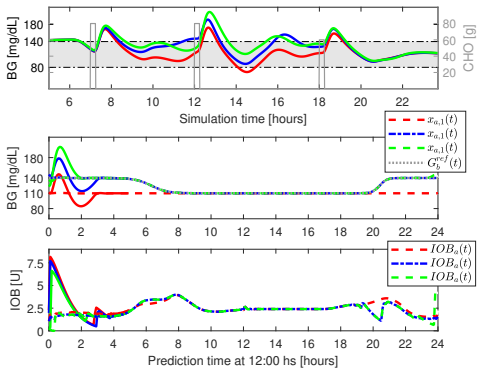

Fig. 3. Blood glucose control using the $\mathcal{MPC}_{\mathcal{BTT}}$ formulation, under: (i) $G_b^{ref} = 110$ mg/dL (red), (ii) $G_b^{ref}(t)$ (blue), and (iii) $G_b^{ref}(t)$ and asymmetric stage cost, $\check{Q}/\hat{Q} = 5 \cdot 10^2$, (green).

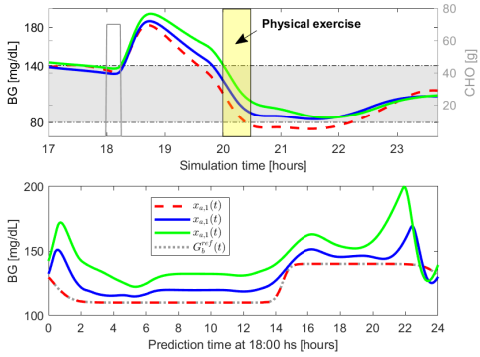

Fig. 4. Blood glucose profile when the control objective is to follow a zone of basal periodic trajectories. $\mathcal{MPC}_{\mathcal{BTT}}$: (red dash-dot line). $\mathcal{MPC}_{\mathcal{BTT}}$ (tube): $G^z_{b,max} = 30$ (blue filled line). $\mathcal{MPC}_{\mathcal{BTT}}$ (wider tube): $G^z_{b,max} = 60$ (green filled line). $G^z_{b,min} = 10$.

episode (moderate exercise 30 min, model C (Dalla Man et al., 2009)) at 20:00 hs was simulated. For both configurations, the time-varying reference proposed in Section 6.2 was considered.

Figure 4 (i) shows that when zones of wider amplitude are employed, the hypoglycemic risk after meal ingestion is reduced. Notice that the periodic basal trajectories (Figure 4 (ii)) are now free to move over a wider zone. The asymmetric cost allows the controller to better anticipate hypoglycemic episodes.

7. CONCLUSION

In this work, a novel trajectory tracking MPC controller that accounts for circadian variability is proposed for the artificial pancreas problem. Although the formulation is (slightly) more complex than classical MPCs, the performance of the simulation on the average virtual patient case-study (in both, the handling of hyper and hypoglycemic episodes) suggests that the strategy may be a first step in a new form of tackling the AP problem under MPC.

REFERENCES

Abuin, P., Rivadeneira, P., Ferramosca, A., and González, A. (2020). Artificial pancreas under stable pulsatile mpc: Improving the closed-loop performance. *Journal of Process Control*, 92, 246–260.

Dalla Man, C., Breton, M.D., and Cobelli, C. (2009). Physical activity into the meal glucose—insulin model of type 1 diabetes: In silico studies.

Gondhalekar, R., Dassau, E., and Doyle III, F.J. (2018). Velocity-weighting and velocity-penalty MPC of an artificial pancreas: Improved safety and performance. *Automatica*, 91(48), 105–117.

Gondhalekar, R., Dassau, E., and Doyle III, F.J. (2016). Periodic zone-mpc with asymmetric costs for outpatient-ready safety of an artificial pancreas to treat type 1 diabetes. *Automatica*, 71, 237–246.

González, A.H., Rivadeneira, P.S., Ferramosca, A., Magdelaine, N., and Moog, C.H. (2020). Stable impulsive zone model predictive control for type 1 diabetic patients based on a long-term model. *Optimal Control Applications and Methods*, 41(6), 2115–2136.

Hinshaw, L., Dalla Man, C., Nandy, D.K., et al. (2013). Diurnal pattern of insulin action in type 1 diabetes: implications for a closed-loop system. *Diabetes*, 62(7), 2223–2229.

Kudva, Y.C., Carter, R.E., Cobelli, C., Basu, R., and Basu, A. (2014). Closed-loop artificial pancreas systems: physiological input to enhance next-generation devices. *Diabetes care*, 37(5), 1184–1190.

Limon, D., Pereira, M., de la Pena, D.M., Alamo, T., Jones, C.N., and Zeilinger, M.N. (2015). Mpc for tracking periodic references. *IEEE Transactions on Automatic Control*, 61(4), 1123–1128.

Mansell, E.J., Docherty, P.D., and Chase, J.G. (2017). Shedding light on grey noise in diabetes modelling. *Biomedical Signal Processing and Control*, 31, 16–30.

Ortmann, L., Shi, D., Dassau, E., Doyle, F.J., Leonhardt, S., and Misgeld, B.J. (2017). Gaussian process-based model predictive control of blood glucose for patients with type 1 diabetes mellitus. In *2017 11th Asian Control Conference (ASCC)*, 1092–1097. IEEE.

Patek, S.D., Magni, L., Dassau, E., Karvetski, C., Toffanin, C., De Nicolao, G., Del Favero, S., Breton, M., Dalla Man, C., Renard, E., et al. (2012). Modular closed-loop control of diabetes. *IEEE Transactions on Biomedical Engineering*, 59(11), 2986–2999.

Ruan, Y., Wilinska, M.E., Thabit, H., and Hovorka, R. (2016). Modeling day-to-day variability of glucose–insulin regulation over 12-week home use of closed-loop insulin delivery. *IEEE Transactions on Biomedical Engineering*, 64(6), 1412–1419.

Schrezenmeir, J., Tatò, F., Tatò, S., Laue, C., and Beyer, J. (1993). Differences between basal and postprandial circadian variation of insulin sensitivity in healthy subjects and type 1 diabetics. In *Hormones in Lipoprotein Metabolism*, 45–64. Springer.

Toffanin, C., Zisser, H., Doyle III, F.J., and Dassau, E. (2013). Dynamic insulin on board: incorporation of circadian insulin sensitivity variation. *Journal of diabetes science and technology*, 7(4), 928–940.

Visentin, R., Campos-Náñez, E., Schiavon, M., Lv, D., Vettoretti, M., Breton, M., Kovatchev, B.P., Dalla Man, C., and Cobelli, C. (2018). The uva/padova type 1 diabetes simulator goes from single meal to single day. *Journal of diabetes science and technology*, 12(2), 273–281.

Visentin, R., Dalla Man, C., Kudva, Y.C., Basu, A., and Cobelli, C. (2015). Circadian variability of insulin sensitivity: physiological input for in silico artificial pancreas. *Diabetes technology & therapeutics*, 17(1), 1–7.

Apéndice D

Characterization of SARS-CoV-2 Dynamics in the Host

Characterization of SARS-CoV-2 Dynamics in the Host

Pablo Abuin[a], Alejandro Anderson[a], Antonio Ferramosca[b,c], Esteban A. Hernandez-Vargas[d,e], Alejandro H. Gonzalez[a]

[a]*Institute of Technological Development for the Chemical Industry (INTEC), CONICET-UNL, Santa Fe, Argentina*
[b]*Department of Management, Information and Production Engineering, University of Bergamo, Italy*
[c]*CONICET - CCT Santa Fe, Argentina.*
[d]*Instituto de Matemáticas, Universidad Nacional Autonoma de Mexico, Boulevard Juriquilla 3001, Querétaro, Qro., 76230, México*
[e]*Frankfurt Institute for Advanced Studies, 60438 Frankfurt am Main, Germany.*
Corresponding authors: alejgon@santafe-conicet.gov.ar, vargas@fias.uni-frankfurt.de

Abstract

While many epidemiological models were proposed to understand and handle COVID-19, too little has been invested to understand human viral replication and the potential use of novel antivirals to tackle the infection. In this work, using a control theoretical approach, validated mathematical models of SARS-CoV-2 in humans are characterized. A complete analysis of the main dynamic characteristic is developed based on the reproduction number. The equilibrium regions of the system are fully characterized, and the stability of such regions are formally established. Mathematical analysis highlights critical conditions to decrease monotonically SARS-CoV-2 in the host, as such conditions are relevant to tailor future antiviral treatments. Simulation results validates the aforementioned system characterization.

Keywords: SARS-CoV-2 infection, In-host model, Equilibrium sets characterization, Stability analysis.

1. Introduction

By December 2019, an outbreak of cases with pneumonia of unknown etiology was reported in Wuhan, Hubei province, China [1]. On January 7, a novel betacoronavirus was identified as the etiological agent by the Chinese Center of Disease Control and Prevention (CCDC), and subsequently named as Severe Acute Respiratory Syndrome Coronavirus 2 (SARS-CoV-2) [2]. On February 11, the World Health Organization (WHO) named the disease as Coronavirus disease 2019 (COVID-19) [3]. Although prevention and control measures were implemented rapidly, from the early stages in Wuhan and other key areas of Hubei [4], the first reported cases outside of China showed that the virus was starting to spread around the world [5].

On March 11, with more that 111.800 cases in 114 countries, and 4921 fatalities cases, COVID-19 was declared a pandemic by the WHO [5]. So far, with more than 7.000.000 total cases confirmed in 213 countries and territories [6, 7], and an estimated case-fatality rate (CFR) of 5.7% (H1N1 pandemic, CFR$<$1%)[8], the potential health risks are evident.

The virus spreads mainly from person-to-person through respiratory droplets produced when an infected person coughs, sneezes or talks [9]. The nonexistence of vaccines or specific therapeutic treatments, preventive measures such as social and physical distancing, hand washing, cleaning and disinfection of surfaces and the use of face masks, among others, have been implemented in order to decrease the transmission of the virus.

Epidemiological mathematical models [10, 11, 12, 13] have been proposed to predict the spread of the disease and evaluate the potential impact of infection prevention and control measures in outbreak management [14]. However, mathematical models at intra-host level that could be useful to understand the SARS-CoV-2 replication cycle and interaction with immune system as well as the pharmacological effect of potential drug therapies [15, 16] are needed. So far, there are approximately 109 trials (including those not yet recruiting, active, or completed) to asses pharmacological therapy for the treatment of COVID-19 in adult patients[17], including antiviral drugs (i.e. Hydroxychloroquine, Remdesivir, Favipiravir, Lopinavir/Ritonavir, Ribavirin), immunomodulatory agents (i.e. Tocilizumab) and immunoglobulin therapy, among others. Recently, Hernandez-Vargas et. al. [18] proposed different intra-host mathematical models (2 based on target cell-limited model, with and without latent phase, and another considering immune response) for 9 patients with COVID-19. Numerical results in [18] showed intra-host reproductive number values consistent to influenza infection (1.7-5.35).

Although models in [18] have been fitted to COVID-19 patients data, a control theoretical approach is needed to characterize the model dynamics. Even when the equilibrium states are known, a formal stability analysis is needed to understand the model behavior and, mainly, to design efficient control strategies. Note that the target cell model has been employed previously taking into account pharmacodynamic (PD) and pharmacokinetic (PK) models of antiviral therapies [19, 20], and this can be potentially done also for COVID-19.

In this context, the main contribution of this article is twofold. First, a full characterization of equilibrium and stability proprieties is performed for the COVID-19 target cell-limited model [18]. Then, formal properties concerning the state variables behavior before convergence - including an analysis of the virus peak times - are given. A key aspect in the target cell model for acute infections shows some particularities such as it has a minimal nontrivial stable equilibrium set, whose stability does not depend on the reproduction number. On the other side, assuming a basic reproduction number greater than 1, the virus would not be cleared before the target cells decreases below under a given critical value, which is independent of the initial conditions.

The article is organized as follows. Section 2 presents the general in-host target cell-limited model used to represent SARS-CoV-2 infection dynamic. Section 3 characterizes the equilibrium sets of the system, and establishes their formal asymptotic stability, by proving both, the attractivity of the equilibrium set in a given domain, and its $\epsilon - \delta$ (Lyapunov) local stability. Then, in Section 4, some dynamical properties of the system are stated, concerning the values of the states at the infection time $t = 0$. In Section 5 the general model for the SARS-CoV-2 infection is described and the general characteristics of the infection are analyzed. Finally, Section 6 gives the conclusion of the work, while several mathematical formalisms - necessary to support the results of Sections 3 and 4 - are presented in Appendix 6.

1.1. Notation

$\mathbb{R}$ and $\mathbb{I}$ denote the real and integer numbers, respectively. The real vector space of dimension n is denoted as $\mathbb{R}^n$. $\mathbb{R}^n_{\geq 0}$ represents the vectors of dimension n whose components are equal or greater than zero. The distance from a point $x \in \mathbb{R}^n$ to a set $\mathcal{X} \subset \mathbb{R}^n$ is defined by $\|x\|_{\mathcal{X}} := \inf_{z \in \mathcal{X}} \|x - z\|_2$, where $\|\cdot\|_2$ denotes the norm-2. The open ball of radius ϵ around a point $x \in \mathbb{R}^n$, with respect to set $\mathcal{X}$, is defined as $\mathbb{B}_\epsilon(x) := \{z \in \mathcal{X} : \|x - z\|_2 < \epsilon\}$. For the real function $f(z) = ze^z$, the so-called Lambert function is defined as the inverse of $f(\cdot)$, i.e., $W(z) := f^{-1}(z)$ in such a way that $W(f(z)) = z$.

2. SARS-CoV-2 in-host mathematical model

Although incomplete by definition, mathematical models of in-host virus dynamic improve the understanding of the interactions that govern infections and, more importantly, permit the human intervention to moderate their effects [21]. Basic in-host infection dynamic models usually include the susceptible cells, infected cells, and the pathogen particles [22]. Among the most used mathematical models, the target cell-limited model has been employed to represent and control HIV infection [23, 24, 25], influenza [26, 27, 28, 19], Ebola [29], dengue [30, 31] among others.

In this work, we consider the mathematical model proposed by Hernandez-Vargas [18] given by the following set of ordinary differential equations (ODEs) :

$$\dot{U}(t) = -\beta U(t)V(t), \qquad U(0) = U_0, \tag{2.1a}$$

$$\dot{I}(t) = \beta U(t)V(t) - \delta I(t), \qquad I(0) = I_0 = 0, \tag{2.1b}$$

$$\dot{V}(t) = pI(t) - cV(t), \qquad V(0) = V_0, \tag{2.1c}$$

where U $[cells]$, I $[cells]$ and V $[copies/mL]$ represent the susceptible cells, the infected cells, and the virus load, respectively. The parameter β $[(copies/mL)^{-1}day^{-1}]$ is the infection rate of susceptible cells by the virus. δ $[day^{-1}]$ is the death rate of I. p $[(copies/mL)day^{-1}cells^{-1}]$ is the replication rate of free virus from the infected cells I. c $[day^{-1}]$ is the degradation (or clearance) rate of virus V. The effects of immune responses are not explicitly described in this model, but they are implicitly included in the death rate of infected cells (δ) and the clearance rate of virus (c) [27].

The parameter values of the target cell model were fitted by [18] using viral kinetics reported by [32] in patients with COVID-19. The Differential Evolution (DE) algorithm was shown to be more robust to initial guesses of parameters than other mentioned methods [33]. Akaike information criterion (AIC) was used

to compare the goodness-of-fit for models that evaluate different hypotheses in [18]. The target cell model showed better fitting than exponential growth and logarithmic decay models as well as the target cell model with eclipse phase [18].

The model (2.1) is non-negative, which means that $U(t) \geq 0$, $I(t) \geq 0$ and $V(t) \geq 0$, for all $t \geq 0$. If we denote $x(t) := (U(t), I(t), V(t))$, then the states are constrained to belong to the invariant set:

$$\mathbb{X} := \{x \in \mathbb{R}^3_{\geq 0}\}. \tag{2.2}$$

Another meaningful set is the one consisting in all the states in $\mathbb{X}$ with strictly positive amount of virus and susceptible cells, i.e.,

$$\mathcal{X} := \{x \in \mathbb{X} : U > 0,\ V > 0\}. \tag{2.3}$$

Note that the set $\mathcal{X}$ is an open set.

The initial conditions of (2.1) are assumed such at a healthy steady state before the infection time $t = 0$, i.e., $V(t) = 0$, $I(t) = 0$, and $U(t) = U_0$, for $t < 0$. At time $t = 0$, a small quantity of virions enters to the host body and, so, a discontinuity occurs in $V(t)$. Indeed, $V(t)$ jumps from 0 to a small positive value V_0 at $t_0 = 0$ (formally, $V(t)$ has a discontinuity of the first kind at t_0, i.e., $\lim_{t\to 0^-} V(t) = 0$ while $\lim_{t\to 0^+} V(t) = V_0 > 0$). The same scenario arises, for instance, when an antiviral treatment affects either parameter p or β. The jump of p or β can be considered as a discontinuity of the first kind. In any case, for the time after the discontinuity, the virus may spread or be cleared in the body, depending on its infection effectiveness. The following (mathematical) definition is given

Definition 1 (Spreadability of the virus in the host)**.** *Consider system* (2.1)*, constrained by the positive set* $\mathbb{X}$*, at some time* t_0*, with* $U(t_0) > 0$*,* $I(t_0) \geq 0$ *and* $V(t_0) > 0$ *(i.e.,* $x(t_0) = (U(t_0), I(t_0), V(t_0)) \in \mathcal{X}$*). Then, it is said that the virus spreads in the host for* $t > t_0$ *if there exists at least one* $t^* > t_0$ *such that* $\dot{V}(t^*) > 0$*.*

The latter definition states that the virus spreads in the body host if $V(t)$ has at least one local maximum. On the other hand, the virus does not spread if $V(t)$ is strictly decreasing for all $t > t_0$. As it will be stated later on (Property 1), $\lim_{t\to\infty} V(t) = 0$ for system (2.1), independently of the fact that the virus reaches or not a maximum (this is a key difference between acute and chronic infection models [21, 22]).

The infection severity can be related with the virus spreadability established in Definition 1. Liu et.al. [34] have shown that patients with severe COVID-19 tend to have a high viral load and a long virus shedding period. The mean viral load of severe cases was around 60 times higher than that of mild cases, suggesting that higher viral loads might be associated with severe clinical outcomes. Furthermore, they found that the viral load of severe cases remained significantly higher for the first 12 days after the appearance of the symptoms than those of corresponding mild cases. Mild cases were also found to have an early viral clearance, with 90% of these patients repeatedly testing negative on reverse transcription polymerase chain reaction (RT-PCR) by day 10 post symptoms onset (pso). By contrast, all severe cases still tested positive at or beyond day 10 pso. In addition, Zheng et.al. [35] reported (from a study with 96 SARS-CoV-2 patients, 22 with mild and 74 with severe disease) a longer duration of SARS-CoV-2 in lower respiratory samples of severe patients. For patients with severe disease the virus permanence was significantly longer (21 days, 14-30 days) than in patients with mild disease (14 days, 10-21 days; p=0.04). Moreover, higher viral loads were detected in respiratory samples, although no differences were found in stool and serum samples. While these findings suggest that reducing the viral load through clinical means and strengthening management should help to prevent the spread of the virus, they are preliminary and it remains controversial whether virus persistence is necessary to drive the dysfunctional immune response characteristic of COVID-19 patients [36].

Remark 1. *Note that the virus spreadability may or may not cause a severe infection (a disease that eventually causes host death) which depends on how much time the virus is above a given value.*

To properly establish conditions under which the virus does not spread for $t > 0$ (i.e., after the infection time $t = 0$) the so-called intra-host basic reproduction number is defined next.

Definition 2. *The intra-host basic reproduction number $\mathcal{R}$ is defined as the number of infected cells (or virus particles) that are produced by one infected cell (or virus particle), at a given time. Its mathematical expression is given by:*

$$\mathcal{R}(t) := U(t)\frac{\beta p}{c\delta}. \tag{2.4}$$

Particularly, for $t = 0$, this number describes the number of infected cells produced by one infected cell, when a small amount of virus, V_0, is introduced into a healthy stationary population of uninfected target cells, U_0,

$$\mathcal{R}_0 := U_0\frac{\beta p}{c\delta}. \tag{2.5}$$

A discussion about the way this value is obtained is given in Appendix 6. The relation between the basic reproduction number at the infection time ($\mathcal{R}_0$) and the virus spreadiblity is stated in the next theorem.

Theorem 2.1. *Consider the system* (2.1)*, constrained by the positive set $\mathbb{X}$, at the beginning of the infection, i.e., $U(0) = U_0 > 0$, $I(0) = 0$ and $V(0) = V_0 > 0$ (i.e., $x(0) = (U(0), I(0), V(0)) \in \mathcal{X}$). Then, a sufficient condition (not necessary) for the virus not to spread in the host is given by $\mathcal{R}_0 < 1$.*

Proof: In Theorem 4.1, Section 4, it is shown that if the virus spreads, then $\mathcal{R}_0 > 1$. This means that (contrapositive of the statement) if $\mathcal{R}_0 \leq 1$ (particularly, $\mathcal{R}_0 < 1$), then the virus does not spread in the host body. □

Before proceeding with a full dynamic analysis of system (2.1), let us define first the so-called critical value of the susceptible cells, which is a threshold to properly understand the spread of the virus.

Definition 3. *The critical value for U, $\mathcal{U}_c$, is defined as*

$$\mathcal{U}_c := \frac{c\delta}{p\beta} = \frac{U_0}{\mathcal{R}_0}, \tag{2.6}$$

which, for fixed system parameters β, p, δ and c, is a constant.

Note that $U(t) < \mathcal{U}_c$ if and only if $\mathcal{R}(t) < 1$, for every $t \geq 0$.

2.1. Equilibrium set characterization

By equating $\dot{U}$, $\dot{I}$ and $\dot{V}$ to zero in (2.1), it can be shown that the system only has healthy equilibria of the form $x_s = (U_s, 0, 0)$, with U_s being an arbitrary positive value, i.e., $U_s \in [0, \infty)$. Thus, there is only one equilibrium set, which is the disease-free one, and it is defined by

$$\mathcal{X}_s := \{(U, I, V) \in \mathbb{R}^3 : U \in [0, \infty),\ I = 0,\ V = 0\}. \tag{2.7}$$

To examine the stability of the equilibrium points in $\mathcal{X}_s$, system (2.1) can be linearized at a general state $x_s \in \mathcal{X}_s$. From (2.1) we have $\dot{U} = f(U, I, V)$, $\dot{I} = g(U, I, V)$, $\dot{V} = h(U, I, V)$. Then, the Jacobian matrix is given by

$$J = \begin{pmatrix} \frac{\partial f}{\partial U} & \frac{\partial f}{\partial I} & \frac{\partial f}{\partial V} \\ \frac{\partial g}{\partial U} & \frac{\partial g}{\partial I} & \frac{\partial g}{\partial V} \\ \frac{\partial h}{\partial U} & \frac{\partial h}{\partial I} & \frac{\partial h}{\partial V} \end{pmatrix} = \begin{pmatrix} -\beta V & 0 & -\beta U \\ \beta V & -\delta & \beta U \\ 0 & p & -c \end{pmatrix},$$

which evaluated at any point $x_s \in \mathcal{X}_s$ reads

$$A_s = \begin{pmatrix} 0 & 0 & -\beta U_s \\ 0 & -\delta & \beta U_s \\ 0 & p & -c \end{pmatrix}.$$

with $U_s \in [0, \infty)$. Then, the eigenvalues $(\lambda_1, \lambda_2, \lambda_3)$ are given by the solution to $Det(A_s - \lambda I) = 0$, i.e.,

$$\lambda[-\lambda^2 - (c + \delta)\lambda + (\beta U_s p - c\delta)] = 0.$$

The first eigenvalue is trivially given by $\lambda_1 = 0$. The other two, are given by:

$$\lambda_{2,3} = -\frac{(c+\delta) \pm \sqrt{(c+\delta)^2 + 4c\delta(\frac{U_s}{\mathcal{U}_c} - 1)}}{2}.$$

To analyze the eigenvalues qualitatively, note that for $U_s = \mathcal{U}_c$

$$\lambda_{2,3} = -\frac{(c+\delta) \pm (c+\delta)}{2},$$

which means that $\lambda_2 = 0$ and $\lambda_3 = -(c+\delta) < 0$ (given that $c, \delta > 0$). Furthermore, $\lambda_2 < 0$ and $\lambda_3 < 0$ for $U_s < \mathcal{U}_c$; and $\lambda_2 > 0$ and $\lambda_3 < 0$ for $U_s > \mathcal{U}_c$. Since the maximum eigenvalue is the one dominating the stability behavior of the equilibrium under consideration, it is possible to infer how the system behaves near some segments of $\mathcal{X}_s$. The first intuition is that the equilibrium set

$$\mathcal{X}_s^1 := \{(U, I, V) \in \mathbb{R}^3 : U \in [0, \mathcal{U}_c),\ I = 0,\ V = 0\} \tag{2.8}$$

is stable, and that the equilibrium set

$$\mathcal{X}_s^2 := \{(U, I, V) \in \mathbb{R}^3 : U \in [\mathcal{U}_c, \infty),\ I = 0,\ V = 0\} \tag{2.9}$$

is unstable. These are just intuitions, given that one of the eigenvalues of the linearized system is null and so the linear approximation cannot be used to fully determine the stability of the nonlinear system (Theorem of Hartman-Grobman [37, 38]). To formally prove the asymptotic stability of $\mathcal{X}_s^1$ in a given domain, it is necessary to show its global attractivity (in such domain) and local ϵ-δ stability.

3. Asymptotic stability of the equilibrium sets

A key point to analyze the general asymptotic stability (AS) of system (2.1) is to consider stability of the complete equilibrium sets $\mathcal{X}_s^1$ and $\mathcal{X}_s^2$, and not of the single points inside them (as defined in Definitions 5, 6 and 7, in Appendix 6). As it is shown in the next subsections, there is no single AS equilibrium points in this system, although there is an AS equilibrium set (i.e., $\mathcal{X}_s^1$).

As stated in Definition 7, in Appendix 6, the AS of $\mathcal{X}_s^1$ requires both, attractivity and $\epsilon - \delta$ stability, which are stated in the next two subsections, respectively. Then, in Subsection 3.3 the AS theorem is formally stated.

3.1. Attractivity of set $\mathcal{X}_s^1$ in $\mathcal{X}$

Before proceeding with the formal theorems of the attractivity of $\mathcal{X}_s^1$, let us consider the following key property of system (2.1) concerning the attractivity of $\mathcal{X}_s$.

Property 1 (Attractivity of $\mathcal{X}_s$)**.** *Consider system* (2.1) *constrained by the positive set $\mathbb{X}$, at some arbitrary time t_0, with $U(t_0) > 0$, $I(t_0) \geq 0$ and $V(t_0) > 0$ (i.e., $x(t_0) = (U(t_0), I(t_0), V(t_0)) \in \mathcal{X}$). Then, $U_\infty := \lim_{t\to\infty} U(t)$ is a constant value smaller than $U(t_0)$, $I_\infty := \lim_{t\to\infty} I(t) = 0$ and $V_\infty := \lim_{t\to\infty} V(t) = 0$, which means that $x(t) = (U(t), I(t), V(t))$ tends to some state in $\mathcal{X}_s$.*

Proof: Since $\dot{U}(t) \leq 0$ for all $t \geq 0$ and all $(U(t_0), I(t_0), V(t_0)) \in \mathcal{X}$, by (2.1a) $U(t)$ is a decreasing function (no oscillation can occur). Since $U(t_0) > 0$ and $V(t_0) > 0$, then $U_\infty = \lim_{t\to\infty} U(t)$ is a constant value in $[0, U(t_0))$. Given that $U(t)$ converges to a finite fixed value, then $\dot{U}(t) = 0$ as $t \to \infty$ by (2.1a). This implies - by the same equation (2.1a) - that $U(t)V(t) = 0$ as $t \to \infty$ and, so, from equation (2.1b), that $\dot{I}(t) = -\delta I(t)$ as $t \to \infty$. Then $I_\infty = \lim_{t\to\infty} I(t) = 0$. Finally, by equation (2.1c)), $\dot{V}(t) = -\delta V(t)$ as $t \to \infty$. Then $V_\infty = \lim_{t\to\infty} V(t) = 0$, which completes the proof. □

Property 1 states that $\mathcal{X}_s$ is an attractive set for system (2.1), in $\mathcal{X}$, but not the smallest attractive set. Next, conditions are given to show that the smallest attractive set is given by $\mathcal{X}_s^1$.

Theorem 3.1 (Attractivity of $\mathcal{X}_s^1$)**.** *Consider system* (2.1) *constrained by the positive set $\mathbb{X}$. Then, the set $\mathcal{X}_s^1$ defined in* (2.8) *is the smallest attractive set in $\mathcal{X}$. Furthermore, $\mathcal{X}_s^2$, defined in* (2.9)*, is not attractive.*

Proof: The proof is divided into two parts. First it is proved that $\mathcal{X}_s^1$ is an attractive set, and then, that it is the smallest one.

Attractivity of $\mathcal{X}_s^1$: The attractivity of $\mathcal{X}_s$ in $\mathcal{X}$ was already proved in Property 1. So, to prove the attractivity of $\mathcal{X}_s^1$ in $\mathcal{X}$ (and to show that $\mathcal{X}_s^2$ is not attractive) it remains to demonstrate that $U_\infty \in [0, \mathcal{U}_c)$. From system (2.1), by replacing (2.1a) in (2.1b), it follows that

$$\dot{I}(t) = \beta U(t)V(t) - \delta I(t) = -\dot{U}(t) - \delta I(t), \tag{3.1}$$

which implies that

$$I(t) = (-\frac{1}{\delta})(\dot{I}(t) + \dot{U}(t)). \tag{3.2}$$

Rearranging (2.1c) yields

$$V(t) = \frac{1}{c}(pI(t) - \dot{V}(t)). \tag{3.3}$$

Then, replacing (3.2) in (3.3), we have

$$V(t) = [p(-\frac{1}{\delta})(\dot{I}(t) + \dot{U}(t)) - \dot{V}(t)]\frac{1}{c}. \tag{3.4}$$

Finally, by substituting (3.4) in (2.1a), and multiplying by $1/U(t)$ both sides of the equation (without loss of generality we assume that $U(t) \neq 0$), it follows that

$$\frac{1}{U(t)}\dot{U}(t) = \frac{\beta p}{c\delta}\dot{U}(t) + \frac{\beta p}{c\delta}\dot{I}(t) + \frac{\beta}{c}\dot{V}(t). \tag{3.5}$$

This latter equation can be integrated, for general initial conditions U_0, I_0 and V_0, as follows:

$$\ln(\frac{U(t)}{U_0}) = \frac{\beta p}{c\delta}(U(t) - U_0) + \frac{\beta p}{c\delta}(I(t) - I_0) + \frac{\beta}{c}(V(t) - V_0). \tag{3.6}$$

Now, by defining $U_\infty := \lim_{t\to\infty} U(t)$, $I_\infty := \lim_{t\to\infty} I(t)$, $V_\infty := \lim_{t\to\infty} V(t)$, and recalling from Property 1 that $I_\infty = V_\infty = 0$, the latter equation for $t \to \infty$, reads

$$\begin{aligned}
\ln(\frac{U_\infty}{U_0}) &= \frac{\beta p}{c\delta}(U_\infty - U_0) + \frac{\beta p}{c\delta}(I_\infty - I_0) + \frac{\beta}{c}(V_\infty - V_0) \\
&= \frac{\beta p}{c\delta}U_\infty - \mathcal{R}_0 - \frac{\beta p}{c\delta}I_0 - \frac{\beta}{c}V_0 \\
&= \frac{\beta p}{c\delta}U_\infty - \mathcal{R}_0 + \mathcal{K}_0,
\end{aligned} \tag{3.7}$$

where $\mathcal{R}_0 := \frac{\beta p}{c\delta}U_0$ (as it was defined in (2.5)) and

$$\mathcal{K}_0 := -\frac{\beta}{c}(\frac{p}{\delta}I_0 + V_0). \tag{3.8}$$

Note that $\mathcal{R}_0$ is a function of U_0 while $\mathcal{K}_0$ is a function of I_0 and V_0, and, furthermore, $\mathcal{R}_0 > 0$ and $\mathcal{K}_0 < 0$ for every $x_0 = (U_0, I_0, V_0) \in \mathcal{X}$. Then, after some manipulation, (3.7) reads

$$-\frac{\beta p}{c\delta}U_\infty e^{-\frac{\beta p}{c\delta}U_\infty} = -\frac{\beta p}{c\delta}U_0 e^{-\mathcal{R}_0}e^{\mathcal{K}_0} = -\mathcal{R}_0 e^{-\mathcal{R}_0}e^{\mathcal{K}_0}. \tag{3.9}$$

Now, by denoting

$$z = z(\mathcal{R}_0, \mathcal{K}_0) := -\mathcal{R}_0 e^{-\mathcal{R}_0}e^{\mathcal{K}_0} \tag{3.10}$$

and

$$y := -\frac{\beta p}{c\delta}U_\infty, \tag{3.11}$$

the latter equation can be written as

$$W(z) = y, \tag{3.12}$$

or

$$W(-\mathcal{R}_0 e^{-\mathcal{R}_0} e^{\mathcal{K}_0}) = -\frac{\beta p}{c\delta} U_\infty, \tag{3.13}$$

where $W(\cdot)$ is a Lambert function. Figure 1 shows the graph of such a function, where it can be seen that it has two branches, denoted as W_p and W_m. However, $W(\cdot) = W_p(\cdot)$ in this case, since $W_m \to -\infty$ for $z \to 0^-$, which has not biological sense (note that U_∞ is a finite value in $[0, U_0)$). Also $-1/e < z(\mathcal{R}_0, \mathcal{K}_0) \leq 0$ for $\mathcal{R}_0 > 0$ and $\mathcal{K}_0 < 0$ (Figure 2 shows a plot of function $z(\mathcal{R}_0, \mathcal{K}_0)$ for negative values of $\mathcal{K}_0$ and positive values of $\mathcal{R}_0$), and W_p maps $(-1/e, 0]$ into $(-1, 0]$, which implies that

$$1 > -W(z(\mathcal{R}_0, \mathcal{K}_0)) \geq 0, \tag{3.14}$$

for $\mathcal{R}_0 > 0$ and $\mathcal{K}_0 < 0$. Thus, by (3.13), it follows that

$$\begin{aligned} U_\infty &= -\frac{c\delta}{\beta p} W(-\mathcal{R}_0 e^{-\mathcal{R}_0} e^{\mathcal{K}_0}) \\ &= -\mathcal{U}_c W(-\mathcal{R}_0 e^{-\mathcal{R}_0} e^{\mathcal{K}_0}) \\ &\in [0, \mathcal{U}_c), \end{aligned} \tag{3.15}$$

which completes the proof.

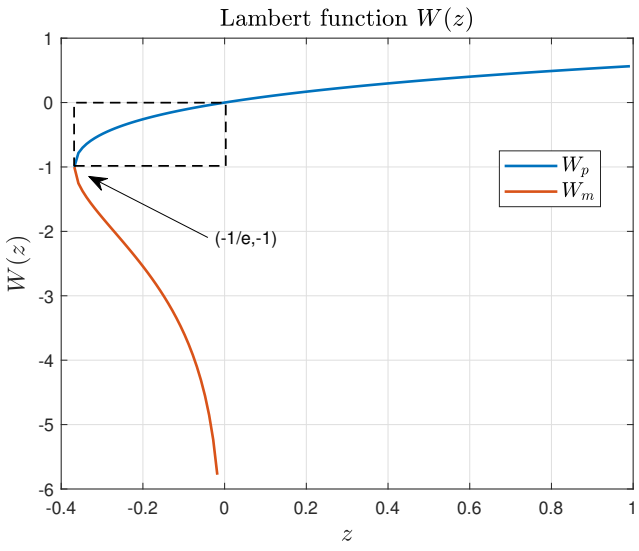

Figure 1: Lambert function. $W(z)$ has two branches, denoted as W_p (in blue) and W_m (in red). Both branches are defined for $z \in [-1/e, 0]$; however $\lim_{z\to 0^-} W_p = 0$ while $\lim_{z\to 0^-} W_m = -\infty$, which means that only the branch W_p will be used in our analysis, as it is shown in the proof of Theorem 3.1.

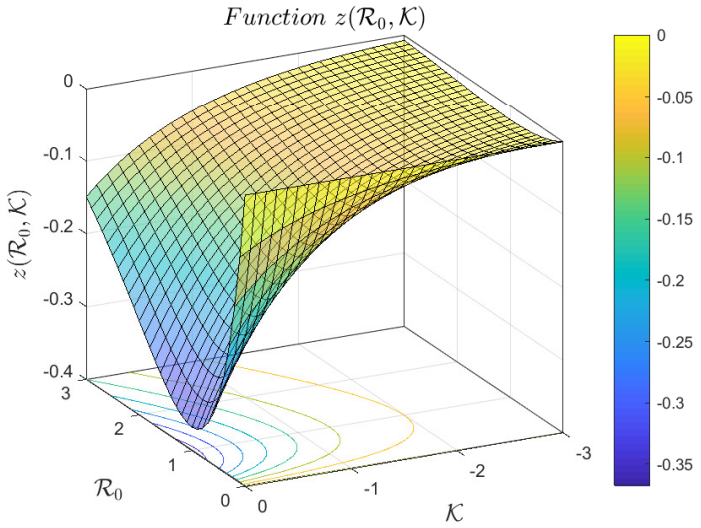

Figure 2: Function $z(\mathcal{R}_0, \mathcal{K}_0)$, for $\mathcal{R}_0 \geq 0$ and $\mathcal{K}_0 \leq 0$. Note that $z(\mathcal{R}_0, \mathcal{K}_0) > -1/e = -0.3679$ for all values of $\mathcal{R}_0 \geq 0$ and $\mathcal{K}_0 \leq 0$.

$\mathcal{X}_s^1$ is the smallest attractive set: It is clear from the previous analysis, that any initial state $x_0 = (U_0, I_0, V_0)$ in $\mathcal{X}$ converges to a state $x_\infty = (U_\infty, 0, 0)$ with $U_\infty \in [0, \mathcal{U}_c)$. This means that $\mathcal{X}_s^2$ is not attractive in $\mathcal{X}$. Let us consider now a state $x_s \in \mathcal{X}_s^1$ and an arbitrary small ball of radius $\epsilon > 0$, w.r.t. $\mathcal{X}$, around it, $\mathbb{B}_\epsilon(x_s) \in \mathcal{X}$. Take two arbitrary initial states $x_{0,1} = (U_{0,1}, I_{0,1}, V_{0,1})$ and $x_{0,2} = (U_{0,2}, I_{0,2}, V_{0,2})$ in $\mathbb{B}_\epsilon(x_s)$, such that $U_{0,1} \neq U_{0,2}$ and $V_{0,1} \neq V_{0,2}$. These two states converge, according to equation (3.15), to $x_{\infty,1} = (U_{\infty,1}, 0, 0)$ and $x_{\infty,2} = (U_{\infty,2}, 0, 0)$, respectively, with $U_{\infty,1}, U_{\infty,2} \in [0, \mathcal{U}_c)$. Given that function $z(R, K)$ is monotone (injective) in $\mathcal{R}_0$ (and so in U_0) and $W(z)$ is monotone (injective) in z, then $U_{\infty,1} \neq U_{\infty,2}$. This means that, although both initial states converge to some state in $\mathcal{X}_s^1$, they necessarily converge to different points. Therefore neither single states $x_s \in \mathcal{X}_s^1$ nor subsets of $\mathcal{X}_s^1$ are attractive in $\mathcal{X}$. So, $\mathcal{X}_s^1$ is the smallest attractive set and the proof is concluded. □

Remark 2. *Note that $\mathcal{X}_s^1$ and $\mathcal{X}_s^2$ are in the closure of the open set $\mathcal{X}$, which is not in $\mathcal{X}$. In other words, Theorem 3.1 shows that any initial state in $\mathcal{X}$ converges to a point onto the boundary of $\mathcal{X}$ that does not belong to $\mathcal{X}$. Furthermore note that, an initial state of the form $(U_0, 0, 0)$, $U_0 > \mathcal{U}_c$, (i.e., a state in $\mathcal{X}_s^2$) cannot be attracted by any set since it is an equilibrium state (every state in $\mathcal{X}_s^2$ will remains unmodified). This is the reason why it is not possible to consider the attractivity of $\mathcal{X}_s^2$ in $\mathcal{X}$.*

3.2. Local $\epsilon - \delta$ stability of $\mathcal{X}_s^1$

The next theorem shows the formal Lyapunov (or $\epsilon - \delta$) stability of the equilibrium set $\mathcal{X}_s^1$.

Theorem 3.2. *Consider system* (2.1) *constrained by the positive set* $\mathbb{X}$*. Then, the equilibrium set $\mathcal{X}_s^1$ defined in* (2.8) *is locally $\epsilon - \delta$ stable.*

Proof: Let us consider a particular equilbrium point $x_s := (U_s, 0, 0)$, with $U_s \in [0, \mathcal{U}_c)$ (i.e., $x_s \in \mathcal{X}_s^1$). Then a Lyapunov function candidate is given by (similar to one used in [39] for chronic infections)

$$J(x) := U - U_s - U_s \ln(\frac{U}{U_s}) + I + \frac{\delta}{p} V. \tag{3.16}$$

This function is continuous in $\mathbb{X}$, is positive for all nonegative $x \neq x_s$ and, furthermore, $J(x_s) = 0$. Function J evaluated at the solutions of system (2.1) reads:

$$\begin{aligned} \frac{\partial J(x(t))}{\partial t} &= \frac{\partial J}{\partial x}\dot{x}(t) = \begin{bmatrix} \frac{dJ}{dU} & \frac{dJ}{dI} & \frac{dJ}{dV} \end{bmatrix} \begin{bmatrix} -\beta U(t)V(t) \\ \beta U(t)V(t) - \delta I(t) \\ pI(t) - cV(t) \end{bmatrix} \\ &= \begin{bmatrix} (1 - \frac{U_s}{U(t)}) & 1 & \frac{\delta}{p} \end{bmatrix} \begin{bmatrix} -\beta U(t)V(t) \\ \beta U(t)V(t) - \delta I(t) \\ pI(t) - cV(t) \end{bmatrix} \end{aligned}$$

$$= (-\beta U(t)V(t) + U_s\beta V(t)) + (\beta U(t)V(t) - \delta I(t)) + (\delta I(t) - \frac{\delta c}{p}V(t))$$
$$= U_s\beta V(t) - \frac{\delta c}{p}V(t) = V(t)(U_s\beta - \frac{\delta c}{p}). \quad (3.17)$$

Now, given $U_s \in [0, \mathcal{U}_c)$, with $\mathcal{U}_c = \frac{\delta c}{\beta p}$, it follows that $\dot{J}(x(t)) \leq 0$ for every $x \in \mathbb{X}$ (note that it is not true that $\dot{J}(x(t)) < 0$ for $x \neq x_s$, as shown next, in Remark 3). Then, J is a Lyapunov function for system (2.1), which means that each $x_s \in \mathcal{X}_s^1$ is $\epsilon - \delta$ stable (see Theorem 6.1 in Appendix 1). Therefore, it is easy to see that the equilibrium set $\mathcal{X}_s^1$ is also $\epsilon - \delta$ stable, which completes the proof. □

Remark 3. *Note that, in the latter proof, it is not true that $\dot{J}(x(t)) < 0$ for every nonegative $x \neq x_s$. If for instance, the function $\dot{J}(x(t))$ is evaluated at $\hat{x}_s = (\hat{U}, 0, 0)$, with $\hat{U} \neq U_s$, we have that $\dot{J}(\hat{x}_s(t)) = 0$. In fact, $\dot{J}(x(t))$ is null along the whole U axis, given that this axis is an equilibrium set. This means that the (individual) states in $\mathcal{X}_s^1$ are $\epsilon - \delta$ stable, but not attractive.*

A schematic plot of such a behavior can be seen in Figure 3.

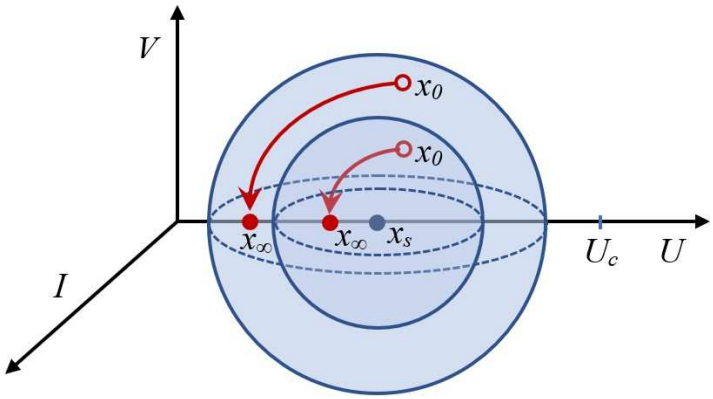

Figure 3: Every point in $\mathcal{X}_s^1$ is $\epsilon - \delta$ stable but not attractive. Initial states x_0 starting arbitrarily close to x_s remain (for all $t \geq 0$) arbitrarily close to x_s, but do not converge to x_s. As a consequence, set $\mathcal{X}_s^1$ is AS but the points inside it are not.

Remark 4. *A similar behavior can be seen in system $\dot{x} = Ax$, when $A = [0\ -1;\ 0\ -1\ ]$, or the 2-state Kermack-McKendrick epidemic model [40, 41]: $\dot{S} = \beta SI$, $\dot{I} = \beta SI - \delta I$, being S the susceptible and I the infected individuals. In this latter model, $\mathcal{R}_0 := (\delta/\beta)S_0$ and the critical value for S is $S_c = \delta/\beta$. The AS set is given by all the states of the form $x_s := (S_s, 0)$, with $S_s \in [0, S_c)$. Furthermore, for this system, the maximum of I occurs when $S = S_c$.*

3.3. Asymptotic stability of $\mathcal{X}_s^1$

In the next Theorem, based on the previous results concerning the attractivity and $\epsilon - \delta$ stability of $\mathcal{X}_s^1$, the asymptotic stability is formally stated.

Theorem 3.3. *Consider system* (2.1) *constrained by the positive set $\mathbb{X}$. Then, the set $\mathcal{X}_s^1$ defined in* (2.8) *is smallest asymptotically stable (AS) equilibrium set, with a domain of attraction given by $\mathcal{X}$.*

Proof: The proof follows from Theorems 3.1, which states that $\mathcal{X}_s^1$ is the smallest attractive in $\mathcal{X}$, and 3.2, which states the local $\epsilon - \delta$ stability of $\mathcal{X}_s^1$. □

A critical consequence of the latter Theorem is that no equilibrium point in $\mathcal{X}_s$ (neither in $\mathcal{X}_s^1$, nor in $\mathcal{X}_s^2$) can be used as setpoint in a control strategy design. The effect of antivirals (pharmocodynamic), for instance, is just to reduce the virus infectivity (by reducing the infection rate β) or the production of infectious virions (by reducing the replication rate p) [21]. So, the previous stability analysis is still valid for such controlled systems, since only a modification of some of the parameters defining $\mathcal{U}_c$ is done. In such a context, only a controller able to consider the whole set $\mathcal{X}_s^1$ as a target (a set-based control strategy, as zone MPC [42, 43]) will be fully successful in controlling system (2.1). Further details concerning antiviral treatments are given next, in Section 4.1.

4. Characterization for different initial conditions

In this section some further properties of system (2.1) concerning its dynamic are stated, based on the initial conditions at the infection time $t = 0$. The objective is to fully characterize the states behavior in a qualitative way, including the times at which the virus and the infected cells reach their peaks. First, Property 2 states some characteristics of U_∞ for different initial conditions. Then, Theorem 4.1 states a general relationship between the peak times of V and I and the time at which U reaches its critical value $\mathcal{U}_c$.

Property 2. *Consider system* (2.1)*, constrained by the positive set* $\mathbb{X}$*, at the beginning of the infection, i.e.,* $U(0) = U_0 > 0$*,* $I(0) = 0$ *and* $V(0) = V_0 > 0$ *(i.e.,* $x(0) = (U(0), I(0), V(0)) \in \mathcal{X}$*). Consider also that* V_0 *is small enough to describe the beginning of the infection. Then,*

i. $U_\infty \to 0$ *when* $U_0 \to \infty$ *or* $U_0 \to 0$*.*

ii. $U_\infty \to \mathcal{U}_c$ *when* $U_0 \to \mathcal{U}_c$*.*

iii. $0 < U_\infty(U_{0,1}, I_0, V_0) < U_\infty(U_{0,2}, I_0, V_0) < \mathcal{U}_c$*, for initial conditions* $U_{0,1} < U_{0,2} < \mathcal{U}_c$*.*

iv. $0 < U_\infty(U_{0,2}, I_0, V_0) < U_\infty(U_{0,1}, I_0, V_0) < \mathcal{U}_c$*, for initial conditions* $\mathcal{U}_c < U_{0,1} < U_{0,2}$*.*

Proof: If $I_0 = 0$ and $V_0 \approx 0$ then $\mathcal{K}_0 \approx 0$. Therefore $W(-\mathcal{R}_0 e^{\mathcal{K}_0 - \mathcal{R}_0}) \approx W(-\mathcal{R}_0 e^{-\mathcal{R}_0})$, and $U_\infty \approx -\mathcal{U}_c W(-\mathcal{R}_0 e^{-\mathcal{R}_0})$ by (3.13).

i. $W(-\mathcal{R}_0 e^{-\mathcal{R}_0}) \to 0$ when $-\mathcal{R}_0 e^{-\mathcal{R}_0} \to 0$, which means that either $\mathcal{R}_0 \to 0$ or $\mathcal{R}_0 \to \infty$. This implies that $U_0 \to 0$ or $U_0 \to \infty$, respectively.

ii. $W(-\mathcal{R}_0 e^{-\mathcal{R}_0}) \to -1$ when $-\mathcal{R}_0 e^{-\mathcal{R}_0} \to -1/e$, which is true if $\mathcal{R}_0 \to 1$ or, the same, when $U_0 \to \mathcal{U}_c$.

iii. $z(\mathcal{R}_0) = -\mathcal{R}_0 e^{-\mathcal{R}_0}$ is strictly decreasing for $\mathcal{R}_0 \in (0, 1)$ (note that $\mathcal{R}_{01} := \frac{c\delta U_{0,1}}{\beta p}$ and $\mathcal{R}_{02} := \frac{c\delta U_{0,2}}{\beta p}$ are in $(0, 1)$, since they are smaller than $\mathcal{U}_c$), while $-W_p(\cdot)$ is strictly decreasing in $(-1/e, 0)$. So, $0 < -W_p(-\mathcal{R}_{01} e^{-\mathcal{R}_{01}}) < -W_p(-\mathcal{R}_{02} e^{-\mathcal{R}_{02}}) < 1$, which implies that $0 < U_\infty(U_{0,1}, I_0, V_0) < U_\infty(U_{0,2}, I_0, V_0) < \mathcal{U}_c$.

iv. $z(\mathcal{R}_0) = -\mathcal{R}_0 e^{-\mathcal{R}_0}$ is strictly increasing for $\mathcal{R}_0 \in (1, \infty)$, while $-W_p(\cdot)$ is strictly decreasing in $(-1/e, 0)$. So, $0 < -W_p(-\mathcal{R}_{02} e^{-\mathcal{R}_{02}}) < -W_p(-\mathcal{R}_{01} e^{-\mathcal{R}_{01}}) < 1$, which implies that $0 < U_\infty(U_{0,2}, I_0, V_0) < U_\infty(U_{0,1}, I_0, V_0) < \mathcal{U}_c$. Figure 4 shows U_∞ as a function of U_0, taking V_0 as a parameter. □

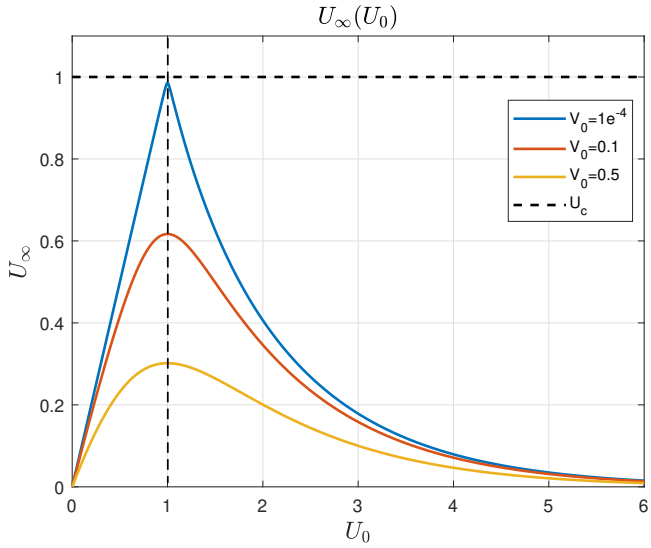

Figure 4: According to equation (3.13), $U_\infty(U_0)$ is plotted for different values of V_0. All parameters are equal to 1 for simplicity, which means that $\mathcal{U}_c = 1$.

Theorem 4.1 (Virus behavior from the infection time)**.** *Consider system* (2.1)*, constrained by the positive set* $\mathbb{X}$*, at the beginning of the infection, i.e.,* $U(0) = U_0 > 0$*,* $I(0) = 0$ *and* $V(0) = V_0 > 0$*. If the virus spreads (according to Definition 1), then* $\mathcal{R}_0 > 1 + \alpha(0)$*, for some* $\alpha(0) > 0$ *(or, the same,* $U_0 > \mathcal{U}_c$*) and there exist positive times* $\check{t}_V$*,* $\hat{t}_I$*,* t_c *and* $\hat{t}_V$*, such that* $\check{t}_V < \hat{t}_I < t_c < \hat{t}_V$*, where* $\check{t}_V$ *and* $\hat{t}_V$ *are the times at which* $V(t)$ *reaches a local minimum and a local maximum, respectively,* $\hat{t}_I$ *is the time at which* $I(t)$ *reaches a local maximum, and* t_c *is the time at which* $U(t)$ *reaches* $\mathcal{U}_c$*. Furthermore,* $\dot{V}(t) < 0$ *for all* $t > \hat{t}_V$*.*

Proof: First, note that $\dot{V}(0) = pI(0) - cV(0) < 0$ since the initial conditions are $I(0) = 0$ and $V(0) > 0$. Even more, by hypothesis the virus spreads, which means that $V(t)$ reaches a local maximum at some time $\hat{t}_V > 0$. Therefore, $V(t)$ must reach a local minimum at some $0 < \check{t}_V < \hat{t}_V$. Now, by Lemma 1 in the Appendix, it is $\mathcal{R}(\check{t}_V) > 1$ and $\mathcal{R}(\hat{t}_V) < 1$, respectively, and it is easy to see that $\mathcal{R}(t)$ is a decreasing function, so it follows that $\mathcal{R}_0 > \mathcal{R}(\check{t}_V) > 1$. Then there exists $\alpha(0) > 0$ such that $\mathcal{R}_0 > 1 + \alpha(0)$ and, besides, $0 < \check{t}_V < t_c < \hat{t}_V$. From the minimum and maximum conditions of V, at times $\check{t}_V$ and $\hat{t}_V$, we have $\dot{V}(\check{t}_V) = 0$, $\ddot{V}(\check{t}_V) > 0$ and $\dot{V}(\hat{t}_V) = 0$, $\ddot{V}(\hat{t}_V) < 0$, respectively. After some algebraic computation, it is easy to see that $\dot{I}(\check{t}_V) > 0$ and $\dot{I}(\hat{t}_V) < 0$, which means that $I(t)$ must reach a maximum at some time $\hat{t}_I$, fulfilling $\check{t}_V < \hat{t}_I < \hat{t}_V$. Moreover, it must be

$$\dot{I}(\hat{t}_I) = \beta U(\hat{t}_I)V(\hat{t}_I) - \delta I(\hat{t}_I) = 0. \tag{4.1}$$

Given that $\dot{V}(t) > 0$ for $\check{t}_V < t < \hat{t}_V$ (it goes from its minimum to its maximum), then by (2.1.a), $I(\hat{t}_I) > \frac{c}{p}V(\hat{t}_I)$. Replacing this latter condition in (4.1), it follows that

$$(\beta U(\hat{t}_I) - \frac{\delta c}{p})V(\hat{t}_I) > \beta U(\hat{t}_I)V(\hat{t}_I) - \delta I(\hat{t}_I) = 0, \tag{4.2}$$

which implies that $\mathcal{R}(\hat{t}_I) = \frac{\beta p U(\hat{t}_I)}{\delta c} > 1$ and, then, $\hat{t}_I < t_c$. Therefore, $t_0 < \check{t}_V < \hat{t}_I < t_c < \hat{t}_V$, which concludes the proof. □

Remark 5. *The value of* $\alpha(0)$ *is necessary to properly understand and characterize the system behavior according to the initial conditions and parameters. Opposite to what happens, for instance, in epidemiological models (SIR, etc.), where* $\mathcal{R}_0 > 1$ *is a necessary and sufficient condition for the disease to spread in a population, in our case* $\mathcal{R}_0 > 1$ *is not a sufficient condition for the virus to spread in the host body. The only thing Theorem 4.1 ensures (by its contrapositive) is that a sufficient condition for the virus to not spread in the host body at time* $t > 0$ *is given by* $\mathcal{R}_0 < 1$ *(or* $U(0) < \mathcal{U}_c$*). See Figure 6, lower plot, for an example. The value of* $\alpha(0)$ *can be computed numerically and it is usually small in comparison with* $\mathcal{R}_0$ *(for all the patients simulated in Section 5,* $\alpha(0) < 1 \times 10^{-4}$*).*

To clarify the results of this section, Figures 5 and 6 show a phase portrait and a state time evolution corresponding to system (2.1), when all parameters are equal to 1 (for simplicity), which means that $\mathcal{U}_c = 1$. The first plot (Figure 5) depicts how every state trajectory - even those starting close to $\mathcal{X}_s^2$ - converges to $\mathcal{X}_s^1$. As stated in Property 2, U_∞ approaches $\mathcal{U}_c$ from below, as $U(0)$ approaches $\mathcal{U}_c$ from above. Also it can be seen how the virus load starts do decrease only once $U(t)$ is smaller than $\mathcal{U}_c$, as stated in Theorem 4.1. On the other hand, the second plot (Figure 6) shows the time evolution of U, I and V, for two different initial conditions. In the upper plot, initial conditions are selected such that $1 + \alpha(0) < \mathcal{R}_0$, while in the lower plot, the initial conditions produce $1 < \mathcal{R}_0 < 1 + \alpha(0)$. As it can be seen, only in the first case the virus spread in the host body (i.e., $\dot{V}(t) > 0$, for some $t > 0$), as stated in Theorem 4.1.

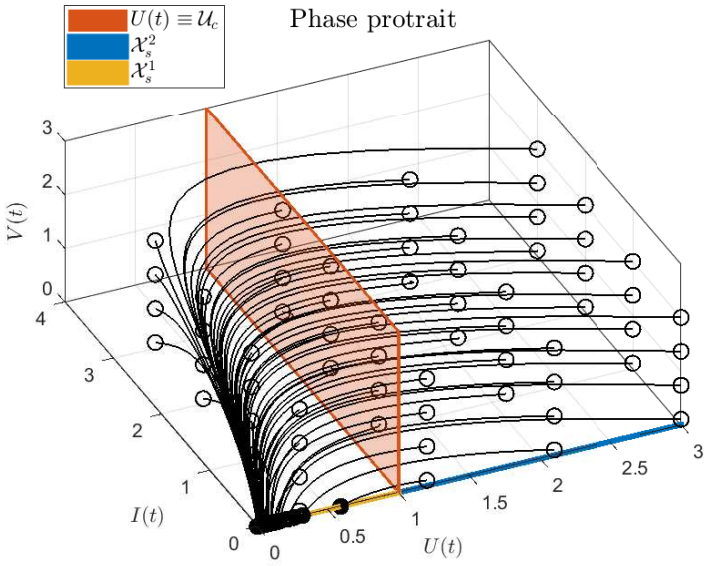

Figure 5: Phase portrait of system (2.1), with unitary parameters. Empty circles represent the initial states, while solid circles represent final states. Note that only the initial states with $U_0 > \mathcal{U}_c = 1$ corresponds to scenarios with $\mathcal{R}_0 > 1$.

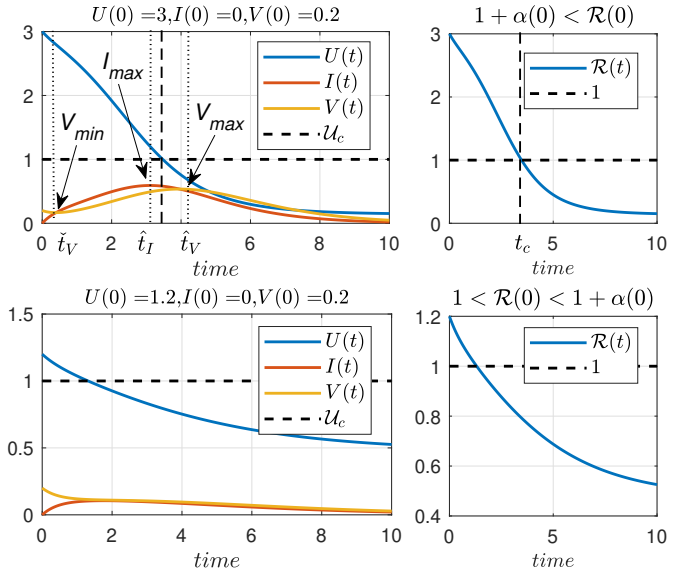

Figure 6: Time evolution of U, I and V, with unitary parameters β, δ, p, c, for initial conditions $U_0 = 3, I_0 = 0, V_0 = 0.2$ (upper plot) and $U_0 = 1.2, I_0 = 0, V_0 = 0.12$ (lower plot).

4.1. Remarks concerning antivirals treatments

Even though the analysis of potential antiviral treatments is out of the scope of this work, in this section some comments concerning the implications of Theorem 4.1 (and the system characterization) will be made. The antiviral effect can be modeled as a reduction of the virus infectivity in the presence of reverse transcriptase inhibitors (by reducing the infection rate β) and/or as a reduction in the production of infectious virions in the presence of protease inhibitors (by reducing the replication rate p). Let us assume that the antiviral pharmacodynamics (PD) corresponding to an antiviral is modeled as $p(1 - \eta(t_r))$ (the analysis for β is almost the same), being $\eta(t_r) \in (0, 1)$ the effectiveness of the antiviral and t_r the time of treatment initiation. The antiviral pharmacokynetics (PK) is not considered, for simplicity, which means that the antivirals instantaneously modify η at time t_r. Then, as the virus monotonically goes to zero only once $U(t)$

is below U_c, the antiviral will be effective (in the sense that the virus load starts decreasing as the treatment begins, and it does not increase again) only if the value of $\eta(t_r)$ is such that $U(t_r) < \mathcal{U}_c(t_r) := \frac{c\delta}{p(1-\eta(t_r))\beta}$ (i.e., such that $\mathcal{R}(t_r) < 1 + \alpha(t_r) \approx 1$). This condition defines a threshold for the antiviral effectiveness (say, a minimal critical value $\eta^c(t_r)$) that may explain, from a pure mathematical point of view, why some antiviral may not work for some patients.

From a control theory point of view, the assertions made in Theorem 4.1 means that a control strategy devoted to steers $V(t)$ to zero at any time by administering a time-variant dose of antivirals (for instance by using $\eta(t) < \eta^c(t)$, for $t > t_r$), may be counterproductive. Indeed, to slow down $V(t)$ by decreasing p or β, implies that $\mathcal{U}_c = \frac{c\delta}{p\beta}$ increases, but also soften the decreasing behavior of $U(t)$. As a result, the time t_c (and so, the virus peak time $\hat{t}_V$) may be delayed, which means that $V(t)$ is maintained in a high level for a longer time. According to preliminary simulations, the delay of the virus peak may be significantly long for antiviral with maximal effectiveness smaller than the critical value.

A formal (and detailed) mathematical analysis of the antiviral effect in COVID-19 is the main topic of a future work.

5. Characterization of the SARS-CoV-2 target cell model

In this section, the model parameters in (2.1) will be associated to the patients labeled as A, B, C, D, E, F, G, H and I - reported in [32]. The initial number of target cells U_0 is estimated as approximately 10^7 cells [18]. I_0 is assumed to be 0 while V_0 is determined by interpolation considering an incubation period of 7 days (note, that V_0 ranges from 0.02 to 5.01 $copies/mL$ which is below the detectable level of about 100 $copies/mL$). Moreover, the onset of the symptoms is assumed to occurs 4 to 7 days after the infection time (day 0, Figure 7 and 8). The parameters and the initial conditions (U_0, I_0 and V_0, with $t_0 = 0$ the infection time) of each patient are collected in Table 1.

Table 1: Target limited cell model parameter values for different patients with COVID-19 [18].

Patient	β	δ	p	c
A	9.98×10^{-8}	0.61	9.3	2.3
B	1.77×10^{-7}	14.11	20.2	0.8
C	8.89×10^{-7}	79.51	134.4	0.4
D	3.15×10^{-8}	45.51	620.2	2.0
E	5.61×10^{-8}	7.51	96.4	5.0
F	1.41×10^{-8}	37.61	995.0	0.6
G	1.77×10^{-8}	8.21	338.4	5.0
H	1.58×10^{-8}	21.11	927.8	1.8
I	4.46×10^{-9}	4.21	994.6	4.3

According to the system analysis of the previous sections, some relevant dynamical values are shown in Table 2. Constant $\alpha(0)$ (defined in Theorem 4.1) is smaller than 10×10^{-4} for all the patients, so it is not taken into account for the study.

Table 2: Characterization Parameters of patients with COVID-19.

Patient	$\mathcal{U}_c$	U_∞	$\mathcal{R}_0$	$\mathcal{K}_0$	$\hat{t}_I$	t_c	$\hat{t}_V$	V_{max}
A	1.51×10^6	1.36×10^4	6.61	-2.17×10^{-7}	10.16	10.24	10.58	1.73×10^7
B	3.15×10^6	4.88×10^5	3.18	-6.87×10^{-8}	11.54	12.26	12.32	4.35×10^6
C	2.66×10^5	4.81×10^{-10}	37.57	-6.89×10^{-7}	1.43	1.67	1.69	1.47×10^7
D	4.65×10^6	1.67×10^6	2.15	-4.89×10^{-9}	9.04	9.42	9.44	2.33×10^7
E	6.94×10^6	4.58×10^6	1.44	-3.48×10^{-9}	15.02	15.16	15.24	4.03×10^6
F	1.61×10^6	2.03×10^4	6.21	-7.28×10^{-9}	7.12	7.76	7.78	1.42×10^8
G	6.84×10^6	4.43×10^6	1.46	-1.1×10^{-9}	14.80	14.92	15.00	1.44×10^7
H	2.59×10^6	2.3×10^5	3.86	-2.72×10^{-9}	5.16	5.44	5.48	1.577×10^8
I	4.08×10^6	1.14×10^6	2.45	-3.21×10^{-10}	9.28	9.38	9.50	2.60×10^8

Figures 7 and 8 show the dynamics of V and U. As expected, the states converge to $\mathcal{X}_s^1$, although significantly different behaviors can be observed for the different patients. From Figure 8 it can be seen that the healthy cells final value U_∞ is reduced in cases of patients with large values of $\mathcal{R}_0$, in spite all simulations have the same initial U_0. This can be explained from the fact that $W(\mathcal{R}_0 e^{-\mathcal{R}_0} e^{\mathcal{K}_0})$ is monotonically decreasing for $\mathcal{R}_0 > 1$ (see Figures 1 and 2), and therefore, $0 < U_\infty(\mathcal{R}_{01}) < U_\infty(\mathcal{R}_{02})$ for $R_{01} > R_{02} > 1$ (see Property 2, above). Note that the susceptible cells of patient C converges to U_∞ equals to 4.810×10^{-10} $[cell]$, which can be explained by the fact that this patient has a reproduction number ($\mathcal{R}_0$) of 37.57, which is 5.2 times above the cohort mean value of 7.21. Figure 7 and Table 2 show that the viral load of patient C reaches the peak at 1.69 days post infection (dpi) (40.56 hours post infection, hpi).

Furthermore, from Figure 7, it can be seen that for all the cases the viral load spreads (i.e.: the virus presents a peak) although $\mathcal{R}_V(0) < 0$ for all patients (i.e., $I_0 = 0$). This can be justified since $U_0 \gg \mathcal{U}_c$ and, therefore, $\mathcal{R}_0$ will be greater than $1 + \alpha(0)$ for all patients (note that, $\alpha(0) < 10 \times 10^{-4}$). Moreover, from Table 2, we can corroborate that $\hat{t}_I > t_c > \hat{t}_V$ which is in accordance to what is stated in Theorem 4.1.

Concerning the immune response, this model makes the assumption that it is constant and independent on viral load as well as infected cells. Furthermore, neither innate or adaptive response are modeled, being the viral load dynamic mainly limited by target cells availability. Since recent studies have shown a dysfunctional immune response (i.e.: lymphogenia, desregulated secretion of pro-inflammatory cytokines, excessive infiltration of monocytes, macrophages and T cells, among others) [36, 44], this effect should be added in the proposed model, in order to have a more reliable representation (and, eventually, a more realistic control objective). In addition, a more reliable standard to measure the severity of disease could be related with the viral spreadability as well as the deregulated inflammatory response.

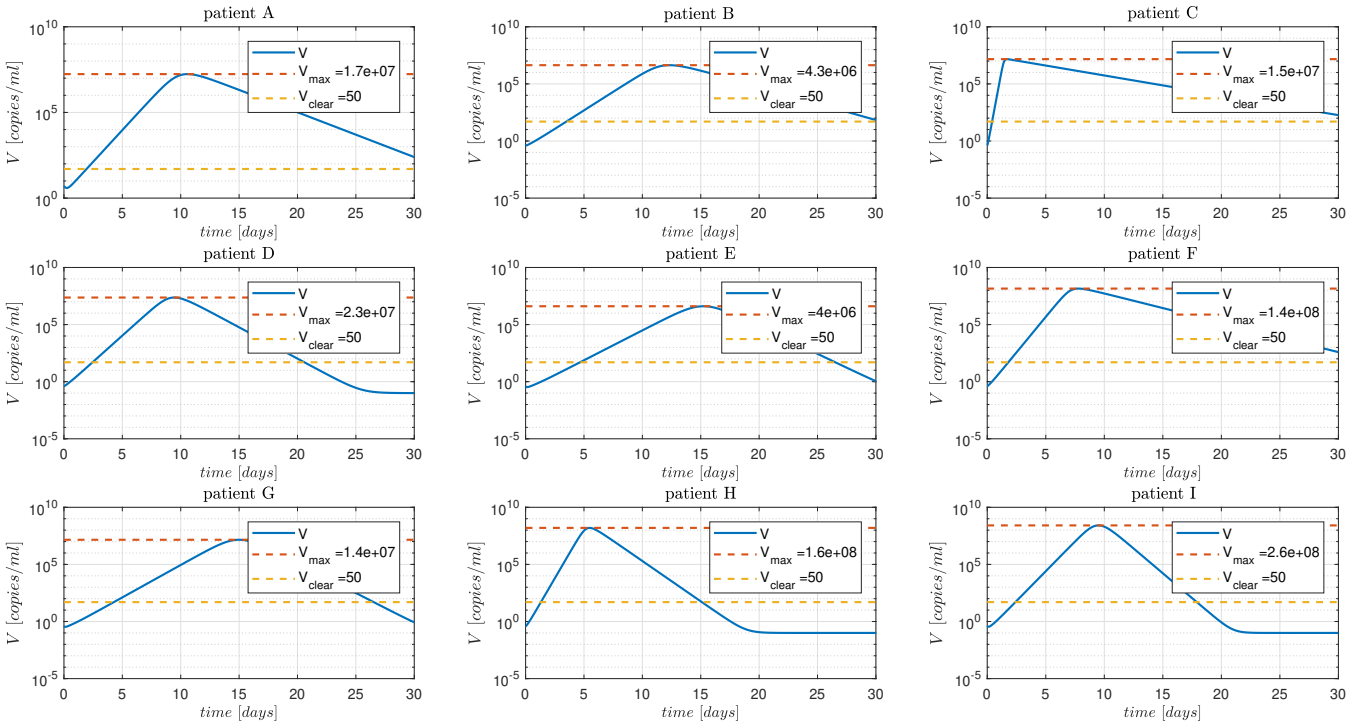

Figure 7: SARS-CoV-2 Dynamics. The continuous blue line is the simulation with parameter values presented in [18]. The patient labeling is as presented in [32]. V_{clear} denotes a value of 50 [copies/ml] under which the virus is not detectable and it is considered is cleared.

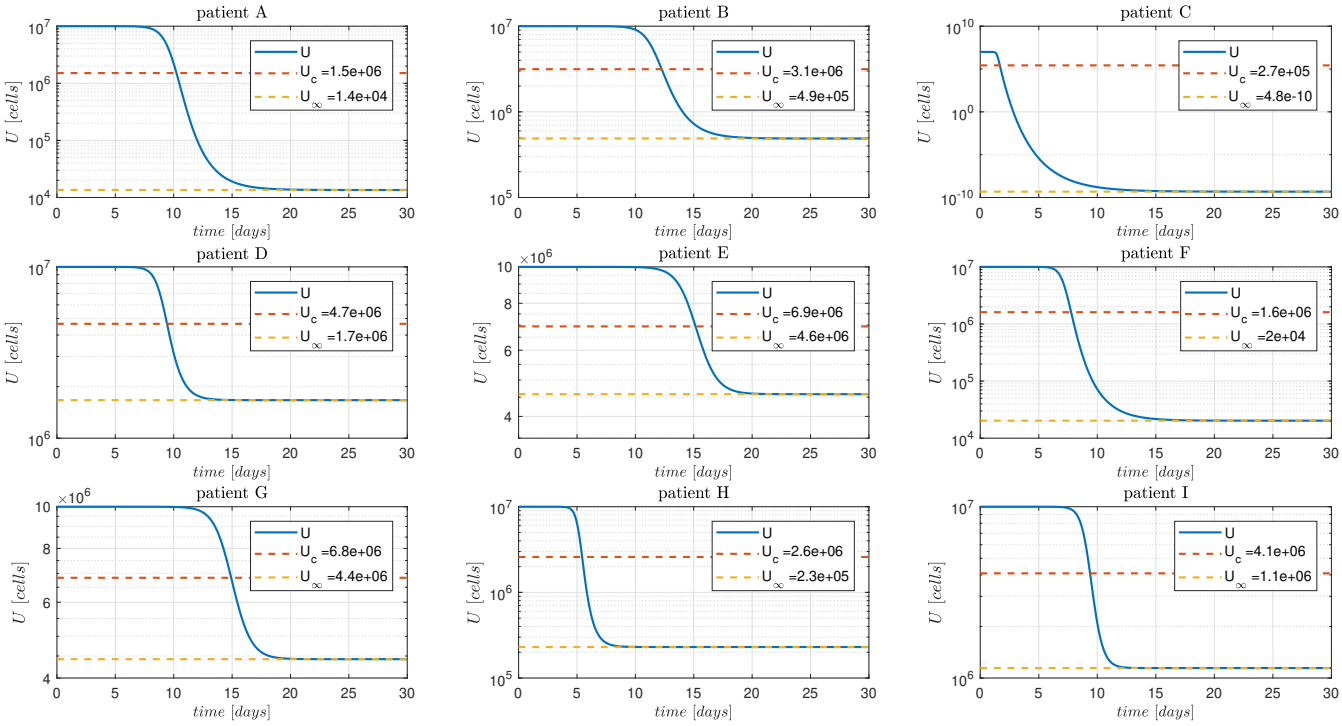

Figure 8: Susceptible cells dynamics. The continuous blue line is the simulation with parameter values presented in [18]. The patient labeling is as presented in [32]. Simulation for the patient C shows a very low value of U_∞ (practically zero), which suggests that the selected value of $U_0 = 1.0e^7$ may be large.

6. Conclusions

In this work a full dynamical characterization of a COVID-19 in-host target-cell model is performed. It is shown that there exists a minimal stable equilibrium set depending only on the system parameters. Furthermore, it is shown that there exists a parameter-depending threshold for the susceptible cells that fully characterizes the virus and infected cells qualitative behavior. Simulations demonstrate the potential utility of such system dynamic characterization to tailor the most valuable pipeline drugs against SARS-CoV-2.

Appendices

Appendix 1. Stability theory

In this section some basic definitions and results are given concerning the asymptotic stability of sets and Lyapunov theory, in the context of non-linear continuous-time systems. All the following definitions are referred to system

$$\dot{x}(t) = f(x(t)), \quad x(0) = x_0, \tag{6.1}$$

where x is the system state constrained to be in $\mathbb{X} \subseteq \mathbb{R}^n$, f is a Lipschitz continuous nonlinear function, and $\phi(t; x)$ is the solution for time t and initial condition x.

Definition 4 (Equilibrium set)**.** *Consider system 6.1 constrained by $\mathbb{X}$. The set $\mathcal{X}_s \subset \mathbb{X}$ is an equilibrium set if each point $x \in \mathcal{X}_s$ is such that $f(x) = 0$ (this implying that $\phi(t; x) = x$ for all $t \geq 0$).*

Definition 5 (Attractivity of an equilibrium set)**.** *Consider system 6.1 constrained by $\mathbb{X}$. A closed equilibrium set $\mathcal{X}_s \subset \mathbb{X}$ is attractive in $\mathcal{X} \subset \mathbb{X}$ if $\lim_{t\to\infty} \|\phi(t; x)\|_{\mathcal{X}_s} = 0$ for all $x \in \mathcal{X}$.*

Any set containing an attractive set is attractive, so the significant attractivity concept in a constrained system is given by the smallest one.

Definition 6 ($\epsilon - \delta$ local stability of an equilibrium set)**.** *Consider system 6.1 constrained by $\mathbb{X}$. A closed equilibrium set $\mathcal{X}_s \subset \mathbb{X}$ is $\epsilon - \delta$ locally stable if for all $\epsilon > 0$ it there exists $\delta > 0$ such that in a given boundary of $\mathcal{X}_s$, $\|x\|_{\mathcal{X}_s} < \delta$, it follows that $\|\phi(t;x)\|_{\mathcal{X}_s} < \epsilon$, for all $t \geq 0$.*

Definition 7 (Asymptotic stability (AS) of an equilibrium set)**.** *Consider system 6.1 constrained by $\mathbb{X}$. A closed equilibrium set $\mathcal{X}_s \in \mathbb{X}$ is asymptotically stable (AS) in $\mathcal{X} \subset \mathbb{X}$ if it is $\epsilon - \delta$ locally stable and attractive in $\mathcal{X}$.*

Theorem 6.1 (Lyapunov theorem [45])**.** *Consider system 6.1 constrained by $\mathbb{X}$ and an equilibrium state $x_s \in \mathcal{X}_s \subset \mathbb{X}$. Let consider a function $V(x) : \mathbb{R}^n \to \mathbb{R}$ such that $V(x) > 0$ for $x \neq x_s$, $V(x_s) = 0$ and $\dot{V}(x(t)) \leq 0$, denoted as Lyapunov function. Then, the existence of such a function implies that $x_s \in \mathcal{X}_s$ is $\epsilon - \delta$ locally stable. If in addition $\dot{V}(x(t)) < 0$ for all $x \neq x_s$ and $\dot{V}(x_s) = 0$, then $x_s \in \mathcal{X}_s$ is asymptotically stable.*

Appendix 2. Derivation of the basic reproduction number $\mathcal{R}_0$

The derivation of the basic reproduction number $\mathcal{R}_0$ will be given by means of the concept of next-generation matrix [46]. Consider system (2.1) and the healthy equilibrium $x_0 = (U_0, 0, 0)$, which is stable in the absence of virus. Of the complete state of system (2.1), $x = (U, I, V)$, only two states depend on infected cells, that is I and V. Let us rewrite the ODEs for this two states in the form

$$\begin{aligned} \dot{I}(t) &= \mathcal{F}_I(x) - \mathcal{G}_I(x) \\ \dot{V}(t) &= \mathcal{F}_V(x) - \mathcal{G}_V(x) \end{aligned}$$

where $\mathcal{F}_i(x)$, $i = \{I, V\}$, is the rate of appearance of new infections in compartment i, while $\mathcal{G}_i(x)$, $i = \{I, V\}$, is the rate of other transitions between compartment i and the other infected compartments, that is

$$\begin{array}{lll} \mathcal{F}_I(x) = \beta U(t) V(t) & \text{and} & \mathcal{G}_I(x) = \delta I(t) \\ \mathcal{F}_V(x) = 0 & \text{and} & \mathcal{G}_V(x) = -pI(t) + cV(t) \end{array}$$

If we now define

$$F = \left[\begin{array}{cc} \dfrac{\partial \mathcal{F}_I(x)}{\partial I} & \dfrac{\partial \mathcal{F}_I(x)}{\partial V} \\ \dfrac{\partial \mathcal{F}_V(x)}{\partial I} & \dfrac{\partial \mathcal{F}_V(x)}{\partial V} \end{array} \right]_{x=x_0} = \left[\begin{array}{cc} 0 & \beta U_0 \\ 0 & 0 \end{array} \right]$$

and

$$G = \left[\begin{array}{cc} \dfrac{\partial \mathcal{G}_I(x)}{\partial I} & \dfrac{\partial \mathcal{G}_I(x)}{\partial V} \\ \dfrac{\partial \mathcal{G}_V(x)}{\partial I} & \dfrac{\partial \mathcal{G}_V(x)}{\partial V} \end{array} \right]_{x=x_0} = \left[\begin{array}{cc} \delta & 0 \\ -p & c \end{array} \right]$$

then matrix FG^{-1}, represents the so-called *next-generation matrix*. Each (i, j) entry of such a matrix represents the expected number of secondary infections in compartment i produced by an infected cell introduced in compartment j. The spectral radius of this matrix, that is, the maximum absolute value of its eigenvalues, defines the basic reproduction number $\mathcal{R}_0$.

For the specific case of system (2.1), the *next-generation matrix* is given by

$$FG^{-1} = \left[\begin{array}{cc} \dfrac{\beta p U_0}{c\delta} & \dfrac{\beta U_0}{c} \\ 0 & 0 \end{array} \right]$$

Therefore, the basic reproduction number $\mathcal{R}_0$ is given by

$$\mathcal{R}_0 =: \frac{\beta p U_0}{c\delta}$$

Notice that $\mathcal{R}_0$ coincides with the entry $(1, 1)$ of matrix FG^{-1}, thus meaning that $\mathcal{R}_0$ represents the expected number of secondary infections produced in compartment I by an infected cell originally in I.

Appendix 3. Technical lemma

The next Lemma characterizes the virus minimum and maximum times, for system (2.1), in terms of the value of the reproduction number $\mathcal{R}(t)$.

Lemma 1. *Consider system* (2.1)*, constrained by the positive set* $\mathbb{X}$*, at the beginning of the infection* $t = 0$*, with* $U(0) > 0$*,* $I(0) \geq 0$ *and* $V(0) > 0$ *(i.e.,* $x(0) = (U(0), I(0), V(0)) \in \mathcal{X}$*). Then,*

i. if $V(t)$ *reaches a local minimum at time* $t_V^* > t_0$*, then* $\mathcal{R}(t_V^*) > 1$*,*

ii. if $V(t)$ *reaches a local maximum at time* $t_V^* > t_0$*, then* $\mathcal{R}(t_V^*) < 1$*, and*

iii. if $V(t)$ *reaches an inflection point at time* $t_V^* > t_0$ *(a point in which* $\dot{V} = 0$ *and* $\ddot{V} = 0$*), then* $t_V^* = t_c$*, where* t_c *is the (unique) time at which* $\mathcal{R}$ *reaches 1 (i.e.,* $\mathcal{R}(t_c) = 1$ *or, the same,* $U(t_c) = \mathcal{U}_c$*).*

Proof: Any of the three hypothesis ($V(t)$ reaches a local minimum, a local maximum or a inflection point) implies that

$$\dot{V}(t_V^*) = pI(t_V^*) - cV(t_V^*) = 0, \tag{6.2}$$

which means that

$$V(t_V^*) = p/cI(t_V^*). \tag{6.3}$$

Consider the critical case of an inflection point, i.e.,

$$\ddot{V}(t_V^*) = p\dot{I}(t_V^*) - c\dot{V}(t_V^*) = p\dot{I}(t_V^*) = 0. \tag{6.4}$$

Thus $\dot{I}(t_V^*) = 0$ which, by (2.1.b) at t_V^*, is equivalent to

$$\dot{I}(t_V^*) = \beta U(t_V^*)V(t_V^*) - \delta I(t_V^*) = 0. \tag{6.5}$$

Now, by (6.3), we have

$$(\frac{\beta p}{c}U(t_V^*) - \delta)I(t_V^*) = 0. \tag{6.6}$$

Given that $I(t_V^*) > 0$ (note that $I(t)$ is positive for all $t > 0$), then $\frac{\beta p}{c}U(t_V^*) - \delta = 0$, or

$$\mathcal{R}(t_V^*) = \frac{\beta p}{c\delta}U(t_V^*) = 1. \tag{6.7}$$

This way if an inflection point does occurs at t_V^*, then $t_V^* = t_c$, where t_c is the time at which $\mathcal{R} = 1$. This proves item (iii).

Furthermore, if V reaches a local minimum at t_V^*, then $\ddot{V}(t_V^*) > 0$ (instead of $\ddot{V}(t_V^*) = 0$, as it is in (6.4), which by (6.3) implies that

$$\mathcal{R}(t_V^*) = \frac{\beta p}{c\delta}U(t_V^*) > 1. \tag{6.8}$$

This proves item (i).

On the other hand, if V reaches a local maximum at t_V^*, then $\ddot{V}(t_V^*) < 0$ (instead of $\ddot{V}(t_V^*) = 0$, as it is in (6.4)), which by (6.3) implies that

$$\mathcal{R}(t_V^*) = \frac{\beta p}{c\delta}U(t_V^*) < 1. \tag{6.9}$$

This proves item (ii). □

References

[1] H. Lu, C. W. Stratton, Y.-W. Tang, Outbreak of pneumonia of unknown etiology in wuhan china: the mystery and the miracle, Journal of Medical Virology (2020).

[2] A. E. Gorbalenya, Severe acute respiratory syndrome-related coronavirus–the species and its viruses, a statement of the coronavirus study group, BioRxiv (2020).

[3] Who director-general's remarks at the media briefing on 2019-ncov on 11 february 2020, https://www.who.int/dg/speeches/detail/who-director-general-s-remarks-at-the-media-briefing-on-2019-ncov/on-11-february-2020, accessed: 2020-04-15.

[4] Report of the who-china joint mission on coronavirus disease 2019 (covid-19), https://www.who.int/docs/default-source/coronaviruse/who-china-joint-mission-on-covid-19-final-report.pdf, accessed: 2020-04-14.

[5] Who timeline - covid-19, https://www.who.int/news-room/detail/08-04-2020-who-timeline---covid-19, accessed: 2020-04-14.

[6] Coronavirus disease 2019 (covid-19) situation report – 86, https://www.who.int/docs/default-source/coronaviruse/situation-reports/20200415-sitrep-86-covid-19.pdf/sfvrsn=c615ea20_6, accessed: 2020-04-15.

[7] Covid-19 dashboard by the center for systems science and engineering (csse) at johns hopkins university, https://coronavirus.jhu.edu/map.html, accessed: 2020-04-15.

[8] Who director-general's opening remarks at the media briefing on covid-19 - 3 march 2020, https://www.who.int/dg/speeches/detail/who-director-general-s-opening-remarks-at-the-media-briefing-on/covid-19-3-march-2020, accessed: 2020-04-14.

[9] How covid-19 spreads, https://www.cdc.gov/coronavirus/2019-ncov/prevent-getting-sick/how-covid-spreads.html, accessed: 2020-04-15.

[10] G. Giordano, F. Blanchini, R. Bruno, P. Colaneri, A. Di Filippo, A. Di Matteo, M. Colaneri, et al., A sidarthe model of covid-19 epidemic in italy, arXiv preprint arXiv:2003.09861 (2020).

[11] M. A. Acuna-Zegarra, A. Comas-Garcia, E. Hernandez-Vargas, M. Santana-Cibrian, J. X. Velasco-Hernandez, The sars-cov-2 epidemic outbreak: a review of plausible scenarios of containment and mitigation for mexico, medRxiv (2020).

[12] J. M. Read, J. R. Bridgen, D. A. Cummings, A. Ho, C. P. Jewell, Novel coronavirus 2019-ncov: early estimation of epidemiological parameters and epidemic predictions, MedRxiv (2020).

[13] A. Y. Alanis, S. Member, E. A. Hernandez-vargas, F. Nancy, D. Ríos-rivera, Neural Control for Epidemic Model of Covid-19 with a Complex Network Approach, IEEE Latin America Transactions 100 (2020).

[14] R. M. Anderson, H. Heesterbeek, D. Klinkenberg, T. D. Hollingsworth, How will country-based mitigation measures influence the course of the covid-19 epidemic?, The Lancet 395 (10228) (2020) 931–934.

[15] C. Liu, Q. Zhou, Y. Li, L. V. Garner, S. P. Watkins, L. J. Carter, J. Smoot, A. C. Gregg, A. D. Daniels, S. Jervey, et al., Research and development on therapeutic agents and vaccines for covid-19 and related human coronavirus diseases (2020).

[16] O. Mitjà, B. Clotet, Use of antiviral drugs to reduce covid-19 transmission, The Lancet Global Health (2020).

[17] J. M. Sanders, M. L. Monogue, T. Z. Jodlowski, J. B. Cutrell, Pharmacologic treatments for coronavirus disease 2019 (covid-19): A review, JAMA (2020).

[18] E. A. Hernandez-Vargas, J. X. Velasco-Hernandez, In-host modelling of COVID-19 kinetics in humans, medRxiv (2020).

[19] G. Hernandez-Mejia, A. Y. Alanis, M. Hernandez-Gonzalez, R. Findeisen, E. A. Hernandez-Vargas, Passivity-based inverse optimal impulsive control for influenza treatment in the host, IEEE Transactions on Control Systems Technology (2019).

[20] A. Boianelli, N. Sharma-Chawla, D. Bruder, E. A. Hernandez-Vargas, Oseltamivir pk/pd modeling and simulation to evaluate treatment strategies against influenza-pneumococcus coinfection, Frontiers in cellular and infection microbiology 6 (2016) 60.

[21] E. A. Hernandez-Vargas, Modeling and Control of Infectious Diseases in the Host: With MATLAB and R, Academic Press, 2019.

[22] S. M. Ciupe, J. M. Heffernan, In-host modeling, Infectious Disease Modelling 2 (2) (2017) 188–202.

[23] A. S. Perelson, D. E. Kirschner, R. De Boer, Dynamics of hiv infection of cd4+ t cells, Mathematical biosciences 114 (1) (1993) 81–125.

[24] M. Legrand, E. Comets, G. Aymard, R. Tubiana, C. Katlama, B. Diquet, An in vivo pharmacokinetic/pharmacodynamic model for antiretroviral combination, HIV Clinical trials 4 (3) (2003) 170–183.

[25] A. S. Perelson, R. M. Ribeiro, Modeling the within-host dynamics of hiv infection, BMC biology 11 (1) (2013) 96.

[26] E. W. Larson, J. W. Dominik, A. H. Rowberg, G. A. Higbee, Influenza virus population dynamics in the respiratory tract of experimentally infected mice., Infection and immunity 13 (2) (1976) 438–447.

[27] P. Baccam, C. Beauchemin, C. A. Macken, F. G. Hayden, A. S. Perelson, Kinetics of influenza a virus infection in humans, Journal of virology 80 (15) (2006) 7590–7599.

[28] A. M. Smith, A. S. Perelson, Influenza a virus infection kinetics: quantitative data and models, Wiley Interdisciplinary Reviews: Systems Biology and Medicine 3 (4) (2011) 429–445.

[29] V. K. Nguyen, S. C. Binder, A. Boianelli, M. Meyer-Hermann, E. A. Hernandez-Vargas, Ebola virus infection modeling and identifiability problems, Frontiers in microbiology 6 (2015) 257.

[30] R. Nikin-Beers, S. M. Ciupe, The role of antibody in enhancing dengue virus infection, Mathematical biosciences 263 (2015) 83–92.

[31] R. Nikin-Beers, S. M. Ciupe, Modelling original antigenic sin in dengue viral infection, Mathematical medicine and biology: a journal of the IMA 35 (2) (2018) 257–272.

[32] R. Wölfel, V. M. Corman, W. Guggemos, M. Seilmaier, S. Zange, M. A. Müller, D. Niemeyer, T. C. Jones, P. Vollmar, C. Rothe, M. Hoelscher, T. Bleicker, S. Brünink, J. Schneider, R. Ehmann, K. Zwirglmaier, C. Drosten, C. Wendtner, Virological assessment of hospitalized patients with COVID-2019, Nature (2020) 1–10doi:10.1038/s41586-020-2196-x.
URL http://www.nature.com/articles/s41586-020-2196-x

[33] C. E. Torres-Cerna, A. Y. Alanis, I. Poblete-Castro, M. Bermejo-Jambrina, E. A. Hernandez-vargas, A Comparative study of Differential Evolution Algorithms for Parameter Fitting Procedures, IEEE World Congress on Computational Intelligence (WCCI) (2016) In pressdoi:10.1109/CEC.2016.7744385.

[34] Y. Liu, L.-M. Yan, L. Wan, T.-X. Xiang, A. Le, J.-M. Liu, M. Peiris, L. L. Poon, W. Zhang, Viral dynamics in mild and severe cases of covid-19, The Lancet Infectious Diseases (2020).

[35] S. Zheng, J. Fan, F. Yu, B. Feng, B. Lou, Q. Zou, G. Xie, S. Lin, R. Wang, X. Yang, et al., Viral load dynamics and disease severity in patients infected with sars-cov-2 in zhejiang province, china, january-march 2020: retrospective cohort study, bmj 369 (2020).

[36] M. Z. Tay, C. M. Poh, L. Rénia, P. A. MacAry, L. F. Ng, The trinity of covid-19: immunity, inflammation and intervention, Nature Reviews Immunology (2020) 1–12.

[37] P. Hartman, Ordinary Differential Equations, Birkhauser, 1982.

[38] L. Perko, Differential equations and dynamical systems, Vol. 7, Springer Science & Business Media, 2013.

[39] A. Nangue, Global stability analysis of the original cellular model of hepatitis c virus infection under therapy, American Journal of Mathematical and Computer Modelling 4 (3) (2019) 58–65.

[40] F. Brauer, C. Castillo-Chavez, C. Castillo-Chavez, Mathematical models in population biology and epidemiology, Vol. 2, Springer, 2012.

[41] F. Brauer, The kermack–mckendrick epidemic model revisited, Mathematical biosciences 198 (2) (2005) 119–131.

[42] A. Ferramosca, D. Limon, A. H. González, D. Odloak, E. F. Camacho, MPC for tracking zone regions, Journal of Process Control 20 (4) (2010) 506–516.

[43] A. H. González, P. S. Rivadeneira, A. Ferramosca, N. Magdelaine, C. H. Moog, Stable impulsive zone mpc for type 1 diabetic patients based on a long-term model, Optimal Control Application and MethodsTo appear (2020).

[44] B. Diao, C. Wang, Y. Tan, X. Chen, Y. Liu, L. Ning, L. Chen, M. Li, Y. Liu, G. Wang, et al., Reduction and functional exhaustion of t cells in patients with coronavirus disease 2019 (covid-19), Frontiers in Immunology 11 (2020) 827.

[45] H. K. Khalil, J. W. Grizzle, Nonlinear systems, Vol. 3, Prentice hall Upper Saddle River, NJ, 2002.

[46] P. van den Driessche, Reproduction numbers of infectious disease models, Infectious Disease Modelling 2 (3) (2017) 288–303.

Apéndice E

Dynamical Characterization of Antiviral Effects in COVID-19

Dynamical Characterization of Antiviral Effects in COVID-19

Pablo Abuin[a], Alejandro Anderson[a], Antonio Ferramosca[b], Esteban A. Hernandez-Vargas[c], Alejandro H. Gonzalez[a]

[a]*Institute of Technological Development for the Chemical Industry (INTEC), CONICET-UNL, Santa Fe, Argentina (e-mail: alejgon@santafe-conicet.gov.ar)*
[b]*Department of Management, Information and Production Engineering, University of Bergamo, Via Marconi 5, 24044, Dalmine (BG), Italy (e-mail: antonio.ferramosca@unibg.it)*
[c]*Frankfurt Institute for Advanced Studies, 60438 Frankfurt am Main, Germany (e-mail: vargas@fias.uni-frankfurt.de)*

Abstract

Mathematical models describing SARS-CoV-2 dynamics and the corresponding immune responses in patients with COVID-19 can be critical to evaluate possible clinical outcomes of antiviral treatments. In this work, based on the concept of virus spreadability in the host, antiviral effectiveness thresholds are determined to establish whether or not a treatment will be able to clear the infection. In addition, the virus dynamic in the host - including the time-to-peak and the final monotonically decreasing behavior - is characterized as a function of the time to treatment initiation. Simulation results, based on nine patient data, show the potential clinical benefits of a treatment classification according to patient critical parameters. This study is aimed at paving the way for the different antivirals being developed to tackle SARS-CoV-2.

Keywords: SARS-CoV-2, In-host model, Dynamic characterization, Antiviral effectiveness.

1. Introduction

With more than 140 million cases confirmed so far (April 2021) in 220 countries [1, 2], coronavirus disease COVID-19, caused by SARS-CoV-2 virus, continues spreading around the globe without neither effective treatment available to date. In fact, the estimated worldwide case-fatality rate (CFR) for COVID-19 is about $2\% - 3\%$, which is almost 15 times higher than the CFR of seasonal influenza (0.0962%) [3, 4].

Currently, several clinical studies about the potentiality of repurposed antiviral agents (*i.e.*, Remdesivir, Favipiravir, Lopinavir/Ritonavir, Ribavirin, etc.) to ameliorate the viral spreading in the host are underway [5]. The clinical observations suggest that prophylaxis with approved doses could prevent SARS-CoV-2 infection and reduce viral shedding [6, 7], but these reports suffer from a number of limitations. For instance, there is no certainty that the undefined benefits are not outweighed by the acute toxicity of the specific antiviral agents. To overcome this impasse, randomized clinical trials with adequate potency should be performed [8]. On the other hand, despite some reported dosing recommendation to treat COVID-19 [9, 10], the efficacy of these proposed therapies cannot be guaranteed due to a paucity of data regarding the optimal dose of the antivirals [11]. In a race to find medical therapies to improve outcomes in patients with COVID-19 further studies are needed to elucidate the benefits of adapting antiviral agents.

An important strategy to help to find the optimal dose of drugs is the pharmacological modelling based on in-vitro drug testing. This approach could suggest whenever the prophylaxis with an appropriate doses of antiviral agents could prevent SARS-CoV-2 infection or control the replication cycle of the virus [12]. In this regard, recent studies have concentrated on the potential of a quantitative comprehension of COVID-19 dynamics [13, 14, 15, 16]. Within-host mathematical models demonstrated useful insights about SARS-CoV-2 infection dynamics and its interactions with the immune system. More important, such results invoke the potential utility of assessing targets for drug development.

The target cell-limited model, widely used to represent several diseases such as Influenza [17, 18], Ebola [19], HIV [20, 21], Hepatitis viruses [22], among others, has been linked to adjust the viral kinetics in infected patients with COVID-19 reported by [23]. While a complete analysis of the main dynamic characteristic for the target cell model was developed to evaluate SARS-CoV-2 infection [24], there is no extensive analysis of the effects of the existent pharmacological therapy for this model, with some remarkable exceptions [14, 25, 16, 26].

The main contribution of this work - that can be seen as an extension of [24] - is to provide a formal mathematical analysis of the SARS-CoV-2 dynamics under the effect of antiviral treatments, which may help to understand how to schedule the different therapies in function of the host parameters. A quantitative classification stating whether or not an antiviral will be effective - in terms of its capability to died out the virus in a reasonable period of time - is made, showing that their effectiveness could vary significantly between subjects.

After the introduction given in Section 1 the article is organized as follows. Section 2 proposes a general three-states "in-host" model to represent COVID-19 infection dynamics under the effect of antivirals drugs and formalizes the concepts of virus spreadability and critical values for the uninfected cells. Then, in Section 3, the antiviral effectiveness is analyzed, as the ability to avoid the virus to spread in the host. Both, the inhibition effect on the replication rate of the virus and the inhibition effect on the infection rate of susceptible healthy cells are studied. In Section 5, the results of Section 3 are extensively demonstrated by simulating different treatments scenarios for nine patients from the literature. Finally, Section 6 gives the discussion of the work, while several mathematical formalism - necessary to support the main results of article - are given in Appendix 7.

2. Within-Host COVID-19 infection model under antiviral effect

Mathematical models of within-host virus dynamic helps to improve the understanding of the interactions that govern infections and permits the human intervention to moderate their effects [27]. Basic models usually include the cells the pathogen infects, the pathogen particles, and their life cycle [28] and, opposite to one can expect, they vary little in its structure from one infectious disease to another.

The goal of this section is to formally consider the effect of antivirals into an acute infection model ([17, 13, 24]) to obtain a controlled system, *i.e.* a system with certain control actions - given by the administered antiviral drugs- that allows one to (even partially) modified the whole system dynamic according to some control objectives. Antivirals have the potential to inhibit the virus replication, reducing the advance of the infection over the target cells population of the infected host (*i.e.*: epithelial cells in the respiratory tract for H1N1 [17], cells with ACE2-TMPRSS2 complex for SARS-CoV-2, mainly nasal and bronchial epithelial cells due to their high expression of ACE2 [29]). Several antivirals are being tested for COVID-19 treatment, with different results concerning both, their inhibition effect on the virus replication and their toxicity. Based on their potential therapeutic targets over the SARS-CoV-2 lifecycle, they can be classified in those which prevent virus entry into the host cell (*i.e.*: potential antiviral drugs -Umifenovir, Camostat/Nafamostat-) and those which inhibit virus replication into the infected cells, mainly blocking viral protease and/or viral RNA replicase (*i.e.*: potential antiviral drugs - Lopinavir, Remdesivir, Favipiravir, Penciclovir) [30, 11, 31, 32, 33]. Consequently, the antiviral effect can be modeled as a reduction of the virus infectivity in the presence of inhibitors (by reducing the infection rate) and/or as a reduction in the replication of infectious virions (by reducing the virus replication rate) [5, 16]. In any case, the effectiveness of a treatment is limited and depends on the patient parameters (which in turn depends on his/her clinical state). Next, the following closed-loop mathematical model - based on the open-loop ones presented in [13, 24] - is considered:

$$\dot{U}(t) = -\beta(1-\eta_\beta(t))U(t)V(t), \qquad U(0) = U_0, \tag{2.1a}$$

$$\dot{I}(t) = \beta(1-\eta_\beta(t))U(t)V(t) - \delta I(t), \qquad I(0) = I_0, \tag{2.1b}$$

$$\dot{V}(t) = p(1-\eta_p(t))I(t) - cV(t), \qquad V(0) = V_0, \tag{2.1c}$$

where U (cell), I (cell) and V (copies/mL) represent the uninfected cells, the infected cells, and the virus concentration; parameter β ((copies/mL)$^{-1}$day^{-1}) is the infection rate; δ (day^{-1}) is the death rates of I, p ((copies/mL) day^{-1}cells^{-1}) is the viral replication rate, and c (day^{-1}) is the viral clearance rate. The effects of immune responses are not explicitly described in this model, but they are implicitly included in the death rate of infected cells (δ) and the clearance rate of virus (c) [17]. The antiviral inhibition effects $\eta_\beta(t)$ and $\eta_p(t)$ - one affecting the infection rate β and the other affecting the replication rate p - are assumed to jump from 0 to the values $\eta_\beta \in [0,1)$ and $\eta_p \in [0,1)$ - representing the full inhibition treatment effects - at the treatment time $t_{tr} > 0$ (*i.e.*, the pharmacokinetic of the antivirals is assumed to have time constants significantly smaller than the ones of the open-loop system, and, so, it is neglected):

$$\eta_\beta(t) = \begin{cases} 0 & t < t_{tr} \\ \eta_\beta & t \geq t_{tr} \end{cases}, \quad \eta_p(t) = \begin{cases} 0 & t < t_{tr} \\ \eta_p & t \geq t_{tr} \end{cases}. \tag{2.2}$$

Remark 1. *The assumption that the antiviral treatment is maintained indefinitely for $t \geq t_{tr}$ relies on the further assumption that once the virus load V is under a given low threshold value (for instance $V < 100$ $(copies/mL)$) it cannot grow up again, independently of value of U. However, it is worth to remark that according to the stability analysis made in [24], if the antiviral treatment is interrupted before U reaches the threshold value $\mathcal{U}_c$ (defined next, in Definition 3), a virus rebound may occurs. To model better viral eradication, it can be either assumed that the amount of virus is zero after certain threshold, or to change the ODE model for the stochastic version which can abstract viral eradication.*

System (2.1) is positive, which means that $U(t) \geq 0$, $I(t) \geq 0$ and $V(t) \geq 0$, for all $t \geq 0$. We denote $x(t) := (U(t), I(t), V(t))$ the state vector, and

$$\mathbb{X} := \{x \in \mathbb{R}^3_{\geq 0}\}, \tag{2.3}$$

the state constraints set.

The initial conditions of (2.1), which represent a healthy steady state before the infection, are assumed to be $V(t) = 0$, $I(t) = 0$, and $U(t) = U_0 > 0$, for $t < 0$. Then, at time $t = 0$, a small quantity of virions enters the host body and, so, a discontinuity occurs in $V(t)$. Indeed, $V(t)$ jumps from 0 to a small positive value V_0 at $t = 0$ (formally, $V(t)$ has a discontinuity of the first kind at t_0, *i.e.*, $\lim_{t\to 0^-} V(t) = 0$ while $\lim_{t\to 0^+} V(t) = V_0 > 0$). This way, for the time after the infection, the virus may spread or being cleared depending on its infection effectiveness. To properly determine what such a spread means, the following (mathematical) definition is given ([24])

Definition 1 (Spreadability of the virus in the host)**.** *Consider system* (2.1)*, constrained by the positive set $\mathbb{X}$, with $V(t) = 0$, $I(t) = 0$, and $U(t) = U_0 > 0$, for $t < 0$. Consider also that at time $t = 0$, $V(t)$ jumps from 0 to a small positive value V_0. Then, it is said that the virus spreads (in some degree) in the host for $t \geq 0$ if $\dot{V}(t) > 0$ for some $t > 0$. If the virus does not spread in the host, it is said that it is cleared for $t \geq 0$.*

Definition 1 states that the virus spreads in the host, for $t \geq 0$, if $V(t)$ increases at some time $t > 0$, and so, given that $\lim_{t\to\infty} V(t) = 0$ (as it is shown in [24]), it reaches at least one local maximum at some positive time. On the other hand, the virus is cleared for $t \geq 0$ if $V(t)$ is strictly decreasing for all $t > 0$, which means that $V(t)$ has neither local minima nor local maxima at any $t > 0$ (as stated in [24], $V(t)$ has at most one minimum and one maximum, provided $\eta_\beta(t) \equiv 0$ and $\eta_p(t) \equiv 0$ for all $t \geq 0$). An infectious disease can be related to the virus peak and/or the period of permanence of the virus in the host [19], and both effects are related to an increase of the virus load at some time after the infection. This is the reason why the spreadability is defined based on the virus positive derivative. A second reason supporting Definition 1 is its use in the determination of antiviral effectiveness (in Section 3): antivirals producing values of η_β and η_p able to clear the virus can be considered effective.

2.1. Reproduction number and critical value for the uninfected cells

To formally establish conditions under which the virus does or does not spread for $t > 0$, some basic concepts need to be defined. Let consider, at this stage, that $\eta_\beta(t) \equiv 0$ and $\eta_p(t) \equiv 0$ for all $t \geq 0$ (*i.e.*, untreated case).

Definition 2. *The within-host basic reproduction number $\mathcal{R}$ is defined as the number of infected cells (or virus particles) that are produced by one infected cell (or virus particle), over a course of its life-span. Its mathematical expression is given by $\mathcal{R}(t) := U(t)\frac{\beta p}{c\delta}$. Particularly, for $t = 0$, this number describes the number of virus particles produced by a virus particle when a small amount of virus, V_0, is introduced into a healthy stationary population of uninfected target cells, U_0, $\mathcal{R}_0 := U_0\frac{\beta p}{c\delta}$.*

A second number, which is closely related to the first one, is the critical value for the uninfected/susceptible cells such that the virus starts to decrease.

Definition 3. *The critical number of susceptible cells U, $\mathcal{U}_c$, is defined as $\mathcal{U}_c := \frac{c\delta}{p\beta}$, which for fixed system parameters β, p, δ and c, is a constant.*

Note that $U(t) < \mathcal{U}_c$ if and only if $\mathcal{R}(t) < 1$, for every $t \geq 0$. The basic reproduction number $\mathcal{R}(t)$ and the critical number $\mathcal{U}_c$ completely describe dynamic (2.1). In [24], a full characterization of the equilibrium sets, their stability and the full behavior of each variable are made. There, it is stated that the (trivial and

asymptotically stable) equilibrium set $\mathcal{X}_s := \{(U, I, V) \in \mathbb{R}^3 : U \in [0, \infty),\ I = 0,\ V = 0\}$ can be divided into two sets, determined by $\mathcal{U}_c$, being the first the smallest asymptotically stable equilibrium set and, the second, unstable (Theorem 3.3, in [24]). Furthermore, provided that virus spread for $t \geq 0$, it is also stated (Theorem 4.1) that there exist positive times $\check{t}_V$, $\hat{t}_I$, t_c and $\hat{t}_V$, such that $\check{t}_V < \hat{t}_I < t_c < \hat{t}_V$, where $\check{t}_V$ and $\hat{t}_V$ are the times at which $V(t)$ reaches a local minimum and a local maximum, respectively, $\hat{t}_I$ is the time at which $I(t)$ reaches a local maximum, and t_c is the time at which $U(t)$ reaches $\mathcal{U}_c$. In addition, $\dot{V}(t) < 0$ for all $t > \hat{t}_V$, which completely characterizes the system behavior.

3. Antiviral treatment effectiveness

The time to initiate treatment t_{tr} is assumed to be between the minimum and maximum time of V, *i.e.*, $\check{t}_V < t_{tr} < \hat{t}_V$ (although some simulations will be performed for $t_{tr} > \hat{t}_V$, for the sake of completeness). The full antiviral effect η_p and η_β are limited by the inhibitory potential of the drug (expressed in terms of EC_{50}, or drug concentration for inhibiting 50% of antigen particles) and its cytotoxic effect (expressed in terms of IC_{50}, or drug concentration which causes death to 50% of susceptible cells) [32, 34].

As the antiviral treatment reduces the system parameter in some amount, it will quantitatively modify the virus behavior. Particularly, the virus peak time will be modified from $\hat{t}_V$ (untreated patient case) to $\hat{t}_{V,tr}$ (treated patient case). However, given that the treatment is initiated when the virus is increasing (*i.e.*, between $\check{t}_V$ and $\hat{t}_V$), then the new peak will occur at the same time or after the treatment time, *i.e.*, $\hat{t}_{V,tr} \geq t_{tr}$. This way, even when the virus peak will always be smaller with a treatment (smaller peaks are obtained for smaller values of p and β), the time at which this peak takes place can be smaller or greater than the one without any treatment. This effect, usually disregarded in many studies concerning the effectiveness of antivirals, could be critical to define whether or not a given antiviral is able to prevent a severe disease. Indeed, in some cases, antivirals significantly delay the virus peaks, largely increasing the time of permanence of the virus in the host. In order to qualitatively assess antiviral effectiveness according to the time of the virus peak, the following classification is made:

Definition 4 (Antiviral treatment effectiveness)**.** *Consider system* (2.1)*, constrained by the positive set* $\mathbb{X}$*, such that the virus spreads in the host from time* $t = 0$*, which implies that:* $U(0) > \mathcal{U}_c$*,* $I(0) = 0$ *and* $V(0) > 0$*. Consider also that, at time* t_{tr}*, with* $\check{t}_V < t_{tr} < \hat{t}_V$*, an antiviral treatment is initiated such that* $\eta_p(t)$ *and/or* $\eta_\beta(t)$ *jump from* 0 *to* $\eta_p \in [0,\ 1)$ *and/or* $\eta_\beta \in [0,\ 1)$*, respectively (as stated in* (2.2)*). Then, the treatment is said to be effective if the virus peaks at a time* $\hat{t}_{V,tr} < \hat{t}_V$*, being the latter the virus peak time for the untreated viral dynamics (i.e., when* $\eta_p = \eta_\beta = 0$*). Otherwise, if* $\hat{t}_{V,tr} \geq \hat{t}_V$*, it is said that the treatment is ineffective.*

Definition 4 is closely related to the capacity of the antiviral drug to clear the infection (or, the same, cutting off its spread) in such a way that it could: a) decline the viral grow at the treatment time, and, so, the virus clearance starts when the therapy is initiated, or b) hasten the virus peak, and, so, even though the virus clearance is not started at treatment time, it begins prior to the untreated case. Note also that Definition 4 accounts for three typical antiviral effect metrics: the area under the virus curve (AUC) and the duration of infection (DI) [35], in a direct way, and the difference of viral loads at the time-to-peak ΔV[14], in an indirect way.

3.1. Antiviral effectiveness characterization

In this subsection it is shown that the effectiveness of antivirals depends on weather η_p and/or η_β are greater or smaller than a specified threshold, which is a function of the parameters and the time of the treatment initiation. In order to characterize such thresholds, the within-host basic reproduction number $\mathcal{R}$ at treatment time t_{tr} is computed as follows:

$$\mathcal{R}(t_{tr}) = \frac{U(t_{tr})p(1-\eta_p)\beta(1-\eta_\beta)}{c\delta}, \tag{3.1}$$

where $\check{t}_V < t_{tr} < \hat{t}_V$. The critical values of η_p and η_β are the ones that make $\mathcal{R}(t_{tr}) = 1$, *i.e.*:

$$\eta_p^c(t_{tr}) \quad := \quad 1 - \frac{c\delta}{U(t_{tr})\beta p} \tag{3.2}$$

$$\eta_\beta^c(t_{tr}) \quad := \quad 1 - \frac{c\delta}{U(t_{tr})\beta p} = \eta_p^c(t_{tr}). \tag{3.3}$$

From equations 3.2 and 3.3 it can be inferred that $\eta_p^c(t_{tr})$ and $\eta_\beta^c(t_{tr})$ are increasing functions of $U(t_{tr})$. Figure 1 shows the time behavior of $\eta_p^c(t_{tr})$ for the nine COVID-19 patients identified in Section 4. Note that $\eta_p^c(t_{tr}) \approx 1 - c\delta/(U_0\beta p)$ for $t_{tr} \to t_0$ and $\eta_p^c(t_{tr}) \approx 1 - c\delta/(\mathcal{U}_c\beta p) = 0$ for $t_{tr} \to \hat{t}_V$ ($t_c \approx \hat{t}_V$). Similar results concerning the critical drug efficacy with respect to the availability of target cells at the treatment time were reached in [36], for acute models, although the authors focused the analysis on treatment starting at the beginning of the infection.

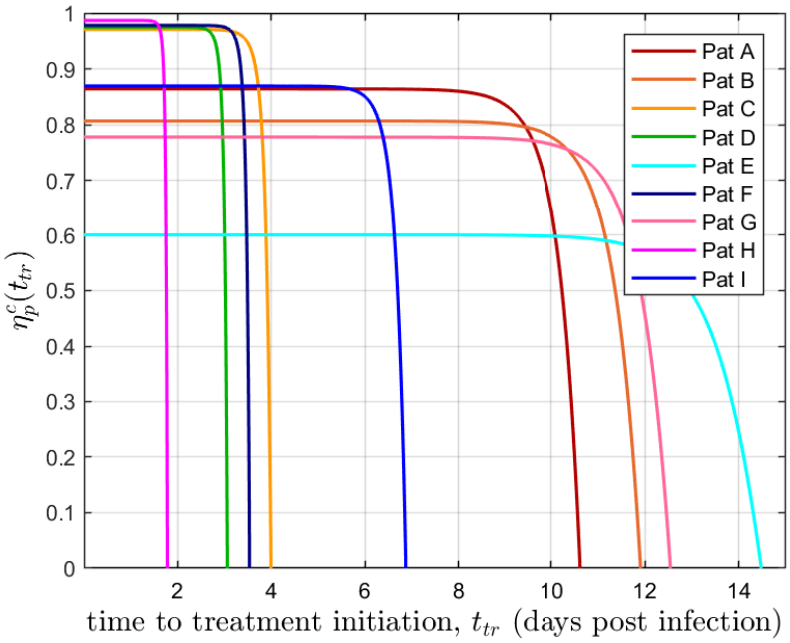

Figure 1: $\eta_p^c(t_{tr})$ vs t_{tr} corresponding to the nine patients simulated in Section 4

The following theorem determines the effectiveness of antivirals in terms of $\eta_p^c(t_{tr})$ and $\eta_\beta^c(t_{tr})$, by considering them separately. In the next subsection, the combined effect will be studied.

Theorem 3.1. *Consider system* (2.1)*, constrained by the positive set* $\mathbb{X}$*. Consider that the virus spreads in the host for* $t \geq 0$*, which implies that:* $U(0) > \mathcal{U}_c$*,* $I(0) = 0$ *and* $V(0) > 0$*. Consider also that, at time* t_{tr}*, with* $\check{t}_V < t_{tr} < \hat{t}_V$ *(when the virus is increasing), an antiviral treatment is initiated such that* $\eta_p(t)$ *or* $\eta_\beta(t)$ *jumps from* 0 *to* $\eta_p \in [0,\ 1)$ *or* $\eta_\beta \in [0,\ 1)$*, respectively (as stated in* (2.2)*). Then,*

i. if the inhibition effect is such that $\eta_p > \eta_p^c(t_{tr})$ *(or* $\eta_\beta > \eta_\beta^c(t_{tr})$*) then the maximum of* $V(t)$ *occurs at* t_{tr}*, which is smaller than* $\hat{t}_V$ *by hypothesis. In this case* ***the antiviral treatment is effective****.*

ii. for two antiviral treatment, 1 and 2, with inhibition effects η_p^1, η_p^2 *such that* $\eta_p^c(t_{tr}) < \eta_p^1 < \eta_p^2$ *(or two inhibition effects* $\eta_\beta^1, \eta_\beta^2$ *such that* $\eta_\beta^c(t_{tr}) < \eta_\beta^1 < \eta_\beta^2$*), there exist a time* $t^* > t_{tr}$ *(large enough) such that* $V_2(t) < V_1(t)$*, for all* $t \in (t_{tr}, t^*]$*, being* $V_1(t)$ *and* $V_2(t)$ *the virus corresponding to treatments* η_p^1 *and* η_p^2*, respectively. In this case* ***both treatments are effective, and treatment 2 is more efficient than treatment 1****.*

iii. if the inhibition effect is such that $\eta_p < \eta_p^c(t_{tr})$ *(or* $\eta_\beta < \eta_\beta^c(t_{tr})$*), then the virus reaches a maximum at a time* $\hat{t}_{V,tr} > t_{tr}$*. Furthermore, there exists a time* $t^e = t^e(\eta_p, t_{tr})$ *- denoted as early treatment time - such that* $\hat{t}_{V,tr} > \hat{t}_V$ *for* $t_{tr} \in (\check{t}_V, t^e]$*. In this case* ***the antiviral treatment is ineffective****.*

iv. for two antiviral treatment, 1 and 2, with inhibition effects η_p^1, η_p^2 *such that* $\eta_p^1 < \eta_p^2 < \eta_p^c(t_{tr})$ *with* $t_{tr} \in (\check{t}_V, t^e(\eta_p, t_{tr})]$ *(or for two inhibition effects* $\eta_\beta^1, \eta_\beta^2$ *such that* $\eta_\beta^1 < \eta_\beta^2 < \eta_\beta^c(t_{tr})$*), it is* $\hat{t}_{V,tr}^2 > \hat{t}_{V,tr}^1 > \hat{t}_V$*, being* $\hat{t}_{V,tr}^1$ *and* $\hat{t}_{V,tr}^2$ *the virus maximum time corresponding to treatments* η_p^1 *and* η_p^2*, respectively. In this case* ***both treatments are ineffective, but treatment 1 is more efficient than treatment 2****, which is a rather counter-intuitive fact.*

Sketch of Proof: For the sake of simplicity and clarity the proof is based on the approximation of system (2.1) described in Section 7.2. In such a case, system (2.1) is approximated by $\dot{U}(t) = -\beta U(t)V(t)$, $\dot{V}(t) \approx (\mathcal{R}(t)-1)\delta V(t)$ and $I(t) \approx \frac{c}{p}V(t)$. Only antiviral treatments affecting parameter p are tackled , since the results follows from conditions on $\mathcal{R}(t)$ and parameters β and p affect $\mathcal{R}$ in the same way.

i. Since $\check{t}_V < t_{tr} < \hat{t}_V$ (by hypothesis) and $\hat{t}_V \approx t_c$, then by Theorem 4.1 in [24], $\mathcal{R}(t) > 1$ for $t < t_{tr}$. Given that $\eta_p > \eta_p^c(t_{tr})$, then by (3.1) $\mathcal{R}(t)$ jumps to a value smaller than one at t_{tr}, *i.e.*, $\mathcal{R}(t_{tr}^-) > 1$ and $\mathcal{R}(t_{tr}) < 1$ (where $\mathcal{R}(t_{tr}^-) := \lim_{t\to t_{tr}^-} \mathcal{R}(t)$). Given that $U(t)$ is strictly decreasing, $\mathcal{R}(t) < 1$ for $t > t_{tr}$. From equation $\dot{V}(t) \approx (\mathcal{R}(t)-1)\delta V(t)$, it follows that $\dot{V}(t) < 0$ for all $t > t_{tr}$. So, given that is assumed that $V(t)$ is increasing when the treatment is initiated, its maximum occurs at t_{tr}.

ii. Let us consider that for all $t \geq t_{tr}$, $V_i(t)$ and $U_i(t)$ are the virus and the susceptible cells for treatment $i = 1, 2$, *i.e.*, the treatment under the inhibition effect η_p^i, and $\mathcal{R}_i(t) = \frac{U_i(t)(1-\eta_p^i)p\beta}{c\delta}$ with $U_1(t_{tr}) = U_2(t_{tr})$ and $V_1(t_{tr}) = V_2(t_{tr})$. By hypothesis $\eta_p^c(t_{tr}) < \eta_p^1 < \eta_p^2$, then $\mathcal{R}_2(t_{tr}) < \mathcal{R}_1(t_{tr})$ and $\mathcal{R}_i(t) < 1$ for all $t \geq t_{tr}$ and $i = 1, 2$. Since $U_i(t)$ is a continuous function for $i = 1, 2$, there is a positive time $t^* > t_{tr}$ such that $\mathcal{R}_2(t) < \mathcal{R}_1(t)$ for all $t \in [t_{tr}, t^*]$. From equation $\dot{V}_i(t) \approx (\mathcal{R}_i(t)-1)\delta V_i(t)$ it follows that $\dot{V}_2(t) < \dot{V}_1(t) < 0$ for all $t \in (t_{tr}, t^*]$ (note that $\dot{V}$ is not defined on t_{tr}). As it is shown in Section 5.1, for real data patients, t^* is large enough such that $V(t^*) \approx 0$.

iii. Since $\check{t}_V < t_{tr} < \hat{t}_V$ (by hypothesis) and $\hat{t}_V \approx t_c$, then by Theorem 4.1 in [24], $\mathcal{R}(t) > 1$ for $t < t_{tr}$. Given that $\eta_p < \eta_p^c(t_{tr})$, then by (3.1) $\mathcal{R}(t)$ jumps, at t_{tr}, from $\mathcal{R}(t_{tr}^-) = \frac{U(t_{tr})p\beta}{c\delta}$ to the smaller value $\mathcal{R}(t_{tr}) = \frac{U(t_{tr})p(1-\eta_p)\beta}{c\delta}$, which is still greater than one; *i.e.*, $\mathcal{R}(t_{tr}^-) > \mathcal{R}(t_{tr}) > 1$. From the fact that $\mathcal{R}(t_{tr}) > 1$, it follows that $\dot{V}(t_{tr}) > 0$, and given that $\mathcal{R}(t)$ is decreasing for $t > t_{tr}$, there exists a time $\hat{t}_{V,tr} > t_{tr}$ such that $\mathcal{R}(\hat{t}_{V,tr}) = 1$, in which case, it is

$$\dot{V}(\hat{t}_{V,tr}) \approx (\mathcal{R}(\hat{t}_{V,tr})-1)\delta V(\hat{t}_{V,tr}) = 0, \tag{3.4}$$

$$\ddot{V}(\hat{t}_{V,tr}) \approx -\frac{p\beta^2}{c}U(\hat{t}_{V,tr})V(\hat{t}_{V,tr}) + (\mathcal{R}(\hat{t}_{V,tr})-1)^2\delta^2 V(\hat{t}_{V,tr}) < 0. \tag{3.5}$$

This means that $V(t)$ reaches a maximum at time $\hat{t}_{V,tr} > t_{tr}$. Now, we need to prove that there exists a time $t^e(\eta_p, t_{tr})$ such that for $t_{tr} \in (\check{t}_V, t^e)$ it is $\hat{t}_{V,tr} > \hat{t}_V$. According to Lemma 1 in Section 7.1, there exists a time $t^e = t^e(\eta_p, t_{tr})$, smaller than $\hat{t}_V$, such that for a treatment time $t_{tr} \in (\check{t}_V, t^e]$, $\hat{t}_{V,tr}$ is a decreasing function of $\mathcal{R}(t_{tr})$, for $\mathcal{R}(t_{tr}) > 1$. This implies that smaller values of $\mathcal{R}(t_{tr})$ (greater values of η_p) correspond to larger times at which $\mathcal{R}(t)$, $t > t_{tr}$, reaches 1, *i.e.*, smaller values of $\mathcal{R}(t_{tr})$, correspond to larger values of $\hat{t}_{V,tr}$. So, from the fact that $\mathcal{R}(t_{tr}^-) > \mathcal{R}(t_{tr})$ (being $\mathcal{R}(t_{tr}^-)$ the value of $\mathcal{R}$ at t_{tr} if no treatment is applied), it follows that $\hat{t}_{V,tr} > \hat{t}_V > t_{tr}$, for $t_{tr} \in (\check{t}_V, t^e]$. As it is shown in Sections 5.1 and 5.2, for real data patients, (the maximal) t^e is close to $\hat{t}_V$.

iv. Since $\eta_p^1 < \eta_p^2 < \eta_p^c(t_{tr})$, by hypothesis, then $1 < \mathcal{R}_2(t_{tr}) < \mathcal{R}_1(t_{tr})$, being $\mathcal{R}_1(t_{tr}) = \frac{U(t_{tr})p(1-\eta_p^1)\beta}{c\delta}$ and $\mathcal{R}_2(t_{tr}) = \frac{U(t_{tr})p(1-\eta_p^2)\beta}{c\delta}$. Therefore, by following the same steps of the previous item, it follows that $\hat{t}_{V,tr}^2 > \hat{t}_{V,tr}^1 > \hat{t}_V$, being $\hat{t}_{V,tr}^1$ and $\hat{t}_{V,tr}^2$ the maximum times of the virus corresponding to η_p^1 and η_p^2, respectively. □

Remark 2. *Item (iii) of Theorem 3.1 establishes just the existence of $t^e > \check{t}_V$ such that for treatments starting at $t_{tr} \in (\check{t}_V, t^e]$, the new virus peak time is larger than the one corresponding to the untreated case, i.e., $\hat{t}_{V,tr} > \hat{t}_V$. However, it should be noted that for parameters coming from real patient data, (the maximal) t^e is indeed close to $\hat{t}_V$. This means that the time period where treatments can be ineffective is in most of the cases similar to $(\check{t}_V, \hat{t}_V)$, i.e., comparable with the time period where the virus is growing. Figures in Section 5 confirm this fact.*

A main consequence of item (*iii*) of Theorem 3.1 is that early treatments, if no effective, could be more detrimental than late ones. Another critical point to be remarked is that when an early treatment is not strong enough to avoid the virus spreadability right after t_{tr}, the highest the antiviral effectiveness η_p (or η_β) is, the longer time the virus remains in the host, since the maximum time $\hat{t}_{V,tr}$ is delayed, as established in item (iv). As a result, antivirals could be detrimental as treated patients would need to be isolated for larger periods of time than untreated ones.

Note that even when virus peak time can be delayed for some treatments, the virus peak will be always smaller than the one without any treatment. Furthermore, the fraction of dead cells at the end of the infection (D_∞) will be always greater if no antiviral is administrated. Indeed, $D_\infty := 1 - U_\infty/U(t_{tr})$ and, according to [24], $U_\infty = -\mathcal{U}_c^{tr} W(-\mathcal{R}(t_{tr})e^{-(\mathcal{R}(t_{tr})+\mathcal{K}(t_{tr}))})$, with $\mathcal{U}_c^{tr} = U(t_{tr})/R(t_{tr})$, $\mathcal{K}(t_{tr}) = \frac{\beta}{c}(\frac{p(1-\eta_p)}{\delta} I(t_{tr}) - V(t_{tr})) = \mathcal{R}(t_{tr})I(t_{tr}) - \frac{\beta}{c}V(t_{tr})$ and $W(\cdot)$ being the Lambert function. Therefore:

$$D_\infty = 1 + \frac{W(-\mathcal{R}(t_{tr})e^{-(\mathcal{R}(t_{tr})+\mathcal{K}(t_{tr}))})}{\mathcal{R}(t_{tr})}. \tag{3.6}$$

Consequently, if treatment is started early, such that $\mathcal{R}(t_{tr}) \gg \mathcal{K}(t_{tr})$, then the fraction of dead cells can be approximated as $D_\infty = 1 + \frac{W(-\mathcal{R}(t_{tr})e^{-\mathcal{R}(t_{tr})})}{\mathcal{R}(t_{tr})}$, which is equal to 0 if $R(t_{tr}) \leq 1$. Note that, by definition, $W(-\mathcal{R}(t_{tr})e^{-\mathcal{R}(t_{tr})}) = -\mathcal{R}(t_{tr})$ for $R(t_{tr}) \leq 1$, so $D_\infty = 1 + (-\mathcal{R}(t_{tr})/\mathcal{R}(t_{tr})) = 0$. On the other hand, if $\mathcal{R}(t_{tr}) > 1$ then $W(-\mathcal{R}(t_{tr})e^{-\mathcal{R}(t_{tr})}) \in (-1, 0]$ is monotonically increasing with $\mathcal{R}(t_{tr})$ (see Figure 1, in [24]). Hence, the fraction of dead cells at the end of infection is a monotonically increasing function of $\mathcal{R}(t_{tr})$, for $\mathcal{R}(t_{tr}) > 1$. Moreover, as the treatment time is delayed, $\mathcal{K}(t_{tr})$ grows, being D_∞ a monotonically increasing function of $\mathcal{R}(t_{tr})$, even for $\mathcal{R}(t_{tr}) \leq 1$.

3.2. Antiviral effectiveness considering the combined effect on η_β and η_p

Theorem 3.1 describes the behavior of the virus under the effect of an inhibitor reducing the infection rate β or the replication rate p. If both effects (η_β and η_p) are simultaneously included in the model, it can be computed a region - in the η_β, η_p space - for which condition $\mathcal{R}(t_{tr}) < 1$ is fulfilled. This way, instead of independent critical values $\eta_\beta^c(t_{tr})$ and $\eta_p^c(t_{tr})$ corresponding to each parameter, there is an entire set of critical combinations that makes a treatment effective. This set depends on treatment time t_{tr} and is placed on the boundary of the effective set

$$\mathcal{H}^c(t_{tr}) := \{(\eta_\beta, \eta_p) \in [0,1] \times [0,1] : \eta_p > 1 - \frac{c\delta}{U(t_{tr})\beta p(1-\eta_\beta)}\}. \tag{3.7}$$

Clearly, every pair $(\eta_\beta, \eta_p) \in \mathcal{H}^c(t_{tr})$ fulfills condition $\mathcal{R}(t_{tr}) < 1$ and, reciprocally, every pair $(\eta_\beta, \eta_p) \notin \mathcal{H}^c(t_{tr})$ fulfills condition $\mathcal{R}(t_{tr}) > 1$. Figure 2 shows a plot of set $\mathcal{H}^c(t_{tr})$ in the plane $(\eta_\beta \times \eta_p)$, corresponding to parameters $\beta = 0.5$, $\delta = 0.2$, $p = 2$ and $c = 5$, with $U(t_{tr}) = 3$.

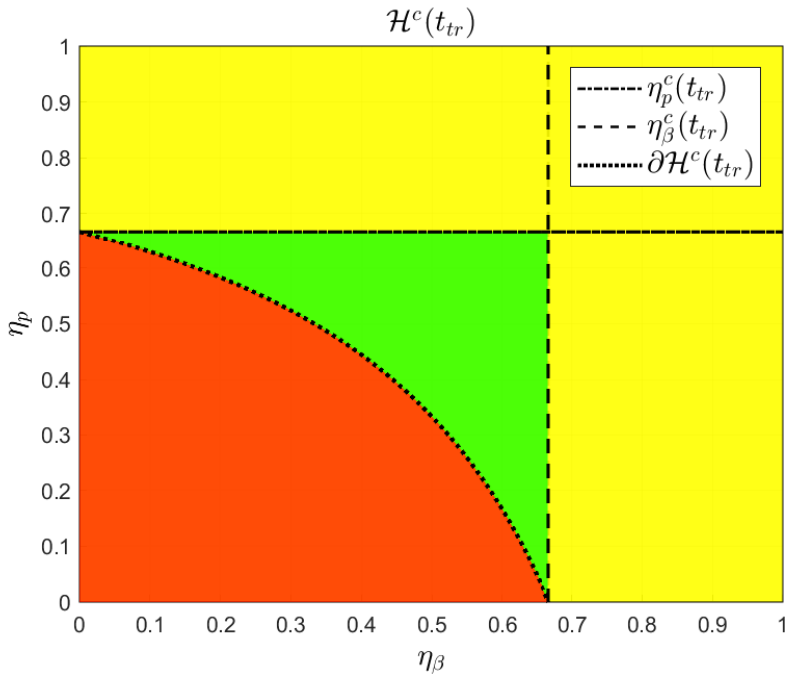

Figure 2: $\mathcal{H}^c(t_{tr})$ is given by the yellow and the green regions, considering the following system parameters: $\beta = 0.5$, $\delta = 0.2$, $p = 2$ and $c = 5$, with $U(t_{tr}) = 3$. The critical boundary of $\mathcal{H}^c(t_{tr})$, denoted by $\partial\mathcal{H}^c(t_{tr})$, represents the critical pairs of η_β and η_p such that $\mathcal{R}(t_{tr}) = 1$.

As it can be seen, for every inhibition effect pair $(\eta_\beta, \eta_p) \notin \mathcal{H}^c(t_{tr})$ (*i.e.* a point inside the red region in Figure 2) the antiviral treatment is ineffective. On the other hand, as it is shown in Theorem 3.1, for every pair (η_β, η_p) such that $\eta_\beta > \eta_\beta^c(t_{tr})$ or $\eta_p > \eta_p^c(t_{tr})$ (the yellow region in Figure 2) the antiviral treatment is effective. Finally, for pairs in the region inside $\mathcal{H}^c(t_{tr})$ with $\eta_\beta < \eta_\beta^c(t_{tr})$ and $\eta_p < \eta_p^c(t_{tr})$ (which does not fit conditions in Theorem 3.1 and it is represented by the green region in Figure 2) the antiviral treatment is still effective.

4. Within-Host Modeling of COVID-19

In this section, the parameters of model (2.1) are estimated using viral load data of nine patients, labeled as A, B, C, D, E, F, G, H and I, reported by Woelfel et. al. [23]. We follow a similar procedure as in Vargas et. al. [13]. Since the viral load is measured in Log10 scales, the model fitting was fulfilled by minimizing the root mean squared of logarithmic error (RMSLE), denoted as:

$$RMSLE = \sqrt{\frac{1}{n}\sum_{i=1}^{n}(log(y_i) - log(\bar{y}_i))^2}, \tag{4.1}$$

where n is the number of measurements, y_i the model predictive output, and $\bar{y}_i$ the experimental measurement. Since the minimization of 4.1 implies a nonlinear optimization problem, with highly dependence on initial conditions, the Differential Evolution (DE) algorithm [37, 27] was employed as a global optimization algorithm, which has shown to be robust to initial guesses of parameters [38].

Even though it is still debatable which compartments SARS-CoV-2 can infect, there is a common agreement that the viral shedding take places mainly in the respiratory epithelial cells (due to the high expression of ACE2) with direct viral toxicity of the infected cells [29]. Therefore, following previous works of mathematical modelling for influenza infection in humans, the value of U_0 was taken as about 4×10^8 (cells) for all patients [17]. Furthermore, I_0 was assumed to be 0 (cells) and V_0 was estimated (using a regression model, since the viral at the day of infection was not provided) [13] to be about 0.31 (copies/mL). Moreover, in order to avoid identifiability problems related with the fact that only viral titters are employed to model fitting , the viral clearance parameter (c) was set in 2.4 (day^{-1}), which is in accordance with previous estimates for influenza and HIV [39, 17]. The parameters and initial conditions at the time of infection, $t = 0$ days post infection (dpi), of each patient are collected in Tables 1 and 2. Since the viral load was measured after the onset of the symptoms, an incubation period of 7 days was assumed from the time of infection, according to [13].

Table 1: Target cell-limited model parameter values for COVID-19 patients [13].

Patient	β	δ	p	c
A	1.35×10^{-7}	0.61	0.2	2.4
B	1.26×10^{-7}	0.81	0.2	2.4
C	5.24×10^{-7}	0.51	0.2	2.4
D	7.92×10^{-10}	1.21	361.6	2.4
E	1.51×10^{-7}	2.01	0.2	2.4
F	5.74×10^{-10}	0.81	382	2.4
G	1.23×10^{-7}	0.91	0.2	2.4
H	2.62×10^{-9}	1.61	278.2	2.4
I	3.08×10^{-10}	2.01	299	2.4

The time evolution of U, I and V is shown in Figure 3, for each patient. As it can be seen, the plot confirms the results given in Theorem 4.1 (see [24]) concerning the minimum and maximum times of V, the maximum time of I and the time when U reaches $\mathcal{U}_c$ (*i.e.*, when $\mathcal{R}(t)$ reaches 1). Figure 3 also supports the approximation made in Section 7.2, by showing that the peaks of virus concentration and infected cells occur approximately at the same time at which U reaches $\mathcal{U}_c$. All these temporal metrics , together with the values of $\mathcal{U}_c$ (the critical target cell value), U_∞ (the final value of U at the end of infection), $\mathcal{R}_0$ and $V(\hat{t}_V)$ (virus concentration at time-to-peak) are shown in Table 2, for the nine simulated patients.

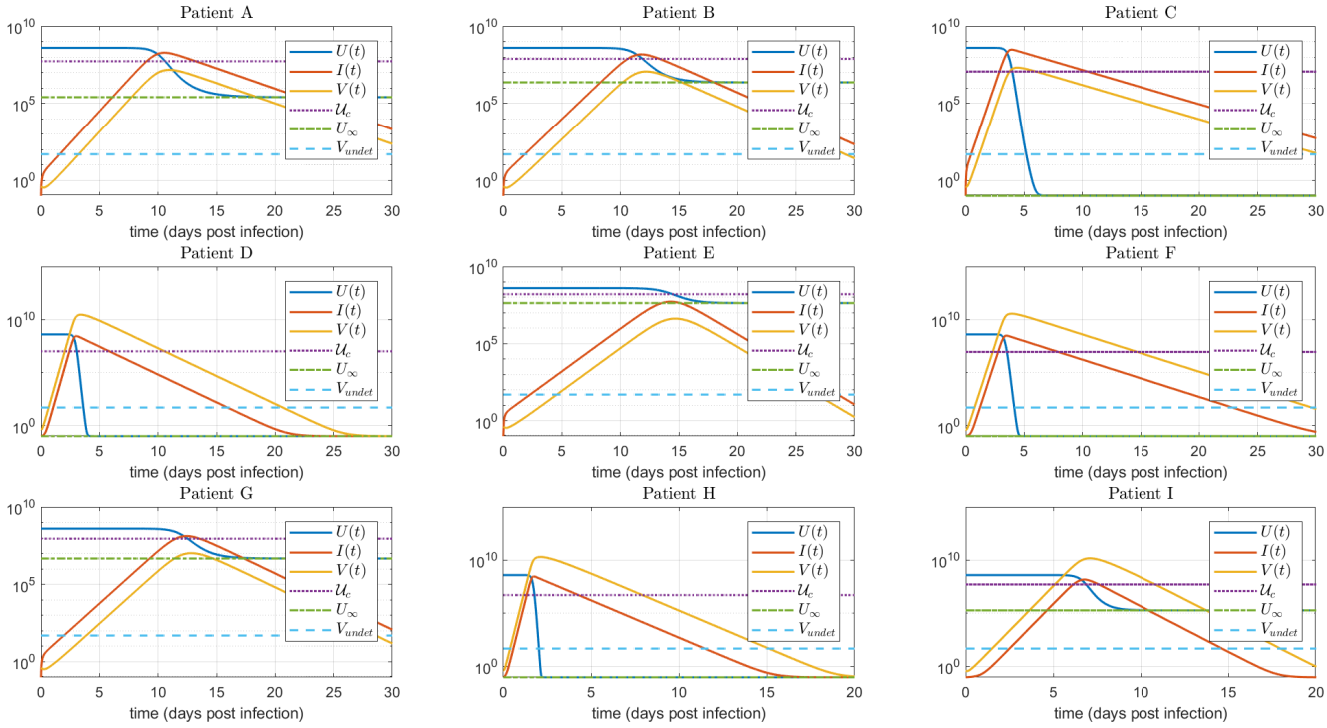

Figure 3: U,I,V time evolution for the untreated case. As stated in Theorem 4.1, in [24], $\check{t}_V < \hat{t}_I < t_c < \hat{t}_V$, where $\check{t}_V$ and $\hat{t}_V$ are the times at which $V(t)$ reaches a local minimum and a local maximum, respectively, $\hat{t}_I$ is the time at which $I(t)$ reaches a local maximum, and t_c is the time at which $U(t)$ reaches $\mathcal{U}_c$. Furthermore, as stated in Section 7.2, $\check{t}_V \approx 0$ and $\hat{t}_I \approx t_c \approx \hat{t}_V$. $V_{undet} = 100$ (copies/mL) stands for the undetectable level of the virus load.

Table 2: Parameter Characterization of COVID-19 patients. The times are given in days post infection (dpi).

Patient	$\mathcal{U}_c$	U_∞	$\mathcal{R}_0$	$\check{t}_V$	$\hat{t}_I$	t_c	$\hat{t}_V$	$V(\hat{t}_V)$
A	0.54×10^8	0.26×10^6	7.35	0.22	10.53	10.61	10.95	1.50×10^7
B	0.77×10^8	0.23×10^7	5.17	0.24	11.81	11.90	12.20	1.18×10^7
C	0.12×10^8	0.00	34.22	0.06	3.94	3.99	4.42	2.10×10^7
D	0.10×10^8	0.00	39.47	0.02	3.00	3.05	3.39	2.90×10^{10}
E	1.60×10^8	4.27×10^7	2.50	0.23	14.31	14.47	14.69	0.42×10^7
F	0.09×10^8	0.00	45.12	0.03	3.48	3.53	3.93	3.55×10^{10}
G	0.90×10^8	0.47×10^7	4.50	0.25	12.44	12.53	12.83	1.04×10^7
H	0.05×10^8	0.00	75.57	0.00	1.73	1.77	2.11	2.02×10^{10}
I	0.52×10^8	0.19×10^6	7.64	0.07	6.77	6.86	7.09	1.50×10^{10}

Remark 3. *In comparison with other coronavirus diseases, such as MERS and SARS, where the virus load peak takes place after the onset of symptoms ($7-10$ days post infection) [40], for SARS-CoV-2 infection it is not clear the temporal interval where the viral load reaches a peak. A recent study linking epidemiological and viral load data, suggests that the viral load peak occurs during the day of symptom onset [40]. However, observation of viral load in infected macaques [41, 42] denotes that the viral peak from nose and throat swabs happens during the 1-3 days post infection. Therefore, since the target cell model fitting was conducted using SARS-CoV-2 viral load measured after the onset of the symptoms [23], the estimated time-to-peak ($\hat{t}_V$) in Table 2 is subject to practical identifiability problems, which as was indicated in Theorem 3.1 and will be shown in Section 5, is a main parameter to evaluate antiviral effectiveness. Due to this reason, an uncertainty analysis computing the likelihood-based confidence intervals [43] for each parameter was done. In Figure 4 such analysis is shown for the 95% confidence interval of parameter p, where it*

can be seen the high degree of uncertainty in the estimated $\hat{t}_V$ for patients A, C, F and G (approximately 5 days).

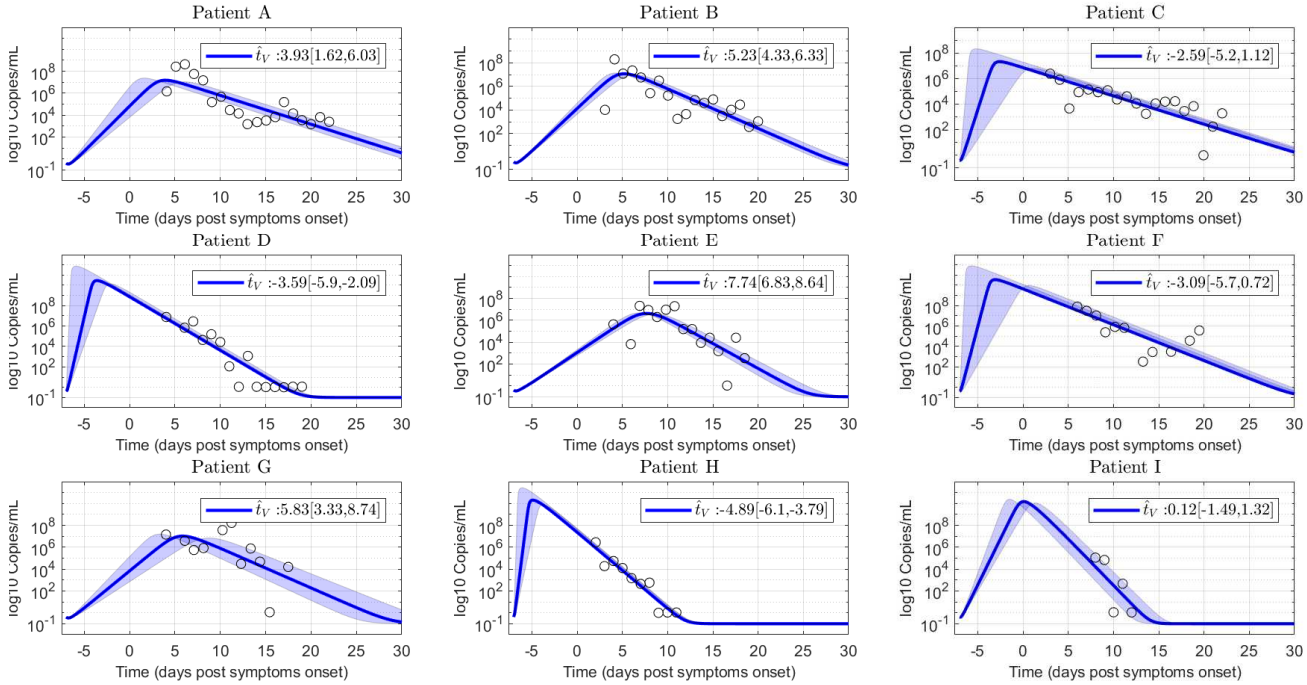

Figure 4: Uncertainty analysis on viral load evolution for p-parameter 95% confidence interval. Note the uncertainty in viral load peak. Empty dots are data of COVID-19 patients.

5. Simulation Results

To evaluate the results concerning the antiviral treatment effectiveness, several simulations involving the nine patients introduced in Section 4 were performed. First, the virus spreading interval - the time between the estimated day of infection (-7 days post symptoms onset (dpo)) and the time-to-peak of viral load ($\hat{t}_V$) - are considered in Section 5.1, to assess the results of Theorem 3.1. Due to the reported variability on the estimated time-to-peak (Figure 4), we decided to initialize the treatments taking into account the relative time with respect to the estimated $\hat{t}_V$, instead of using a fixed time for all the population. Furthermore, the (maximal) early treatment time (t^e) of each patient was computed numerically, being of the order of $0.77\ [0.74, 0.79]\hat{t}_V$.

Then, in Section 5.2, the case when the antiviral therapy is started before and after the untreated time-to-peak $\hat{t}_V$ is simulated, in order to analyze the effectiveness of a subpotent/potent antiviral drug as treatment time t_{tr} is delayed. Finally, in Section 5.3 the synergistic effects of antiviral therapies blocking the viral replication p and the host cell infection β are studied, taking into account the combined drug effect analysis presented in Section 3.2.

To numerically assess the viral kinetics evolution, the following infected-related metrics are employed: i) the difference of viral loads with and without treatment at time-to-peak, $\Delta V = V(\hat{t}_V) - V(\hat{t}_{V,tr})$, which is a measure of the viral reduction at time-to-peak respect to the untreated case [14]; ii) the duration of infection, DI, defined as the time spent by the viral titer curve over a detection limit (*i.e.*: 100 copies/ml), which is a measure of the viral shedding interval and can also be used, as an indicator of the time a patient is infectious, requiring isolation or quarantine to prevent onward infection [44]; and iii) the time-to-peak $\hat{t}_V$, which is an indicator of the viral replication rate and can be employed, as an estimation of the time window available for effective treatment [45]. For the sake of simplicity, unless otherwise stated, the approximation presented in Section 7.2, in the Appendix, is used for simulation analysis.

5.1. Treatment initiated at different times, during viral spreading interval ($t_{tr} \in (\check{t}_V, \hat{t}_V)$)

Scenario 1: Treatment is initiated at viral load detection level ($t_{tr} = t_{DL}$)

Figure 5 shows the simulated virus load evolution corresponding to each of the nine patients, when the antiviral therapy is started at the first positive PCR test time ($t_{tr} = t_{DL}$, being t_{DL} the time at which the virus reaches the value $V(t_{DL}) = 100$ copies/mL), which is about $0.3\hat{t}_V \approx 0.40t^e$. Consequently, all the patients fall in the case $\check{t}_V < t_{tr} < t^e < \hat{t}_V$ which means that we are under the hypothesis of Theorem 3.1 and, furthermore, the treatment time belongs to the early treatment time interval. To properly asses the antiviral replication inhibition effect, increasing values of η_p were used. First we started with small values of η_p, η_p^1 and η_p^2, fulfilling the condition $\eta_p < \eta_p^c(t_{tr})$ (item iii in Theorem 3.1, ineffective treatment). Then η_p was set to values approximately equal to $\eta_p^c(t_{tr})$, η_p^3 and η_p^4, to reinforce the counter-intuitive fact that larger inhibition effects fulfilling $\eta_p < \eta_p^c(t_{tr})$ produce larger virus peak times (item iv in Theorem 3.1). Finally, η_p was increased to two values larger than $\eta_p^c(t_{tr})$, η_p^5 and η_p^6, (items i and ii in Theorem 3.1), to show that higher inhibition effects produce faster eradication of the virus V. For the simulations, efficacies equally spaced from $\eta_p^c(t_{tr})$ were used, such that: $\eta_p^1 = 0.5\eta_p^c(t_{tr})$, $\eta_p^2 = 0.75\eta_p^c(t_{tr})$, $\eta_p^3 = 0.90\eta_p^c(t_{tr})$, $\eta_p^4 = \eta_p^c(t_{tr}) + 0.1(1 - \eta_p^c(t_{tr}))$, $\eta_p^5 = \eta_p^c(t_{tr}) + 0.25(1 - \eta_p^c(t_{tr}))$, and $\eta_p^6 = \eta_p^c(t_{tr}) + 0.5(1 - \eta_p^c(t_{tr}))$, for all patients.

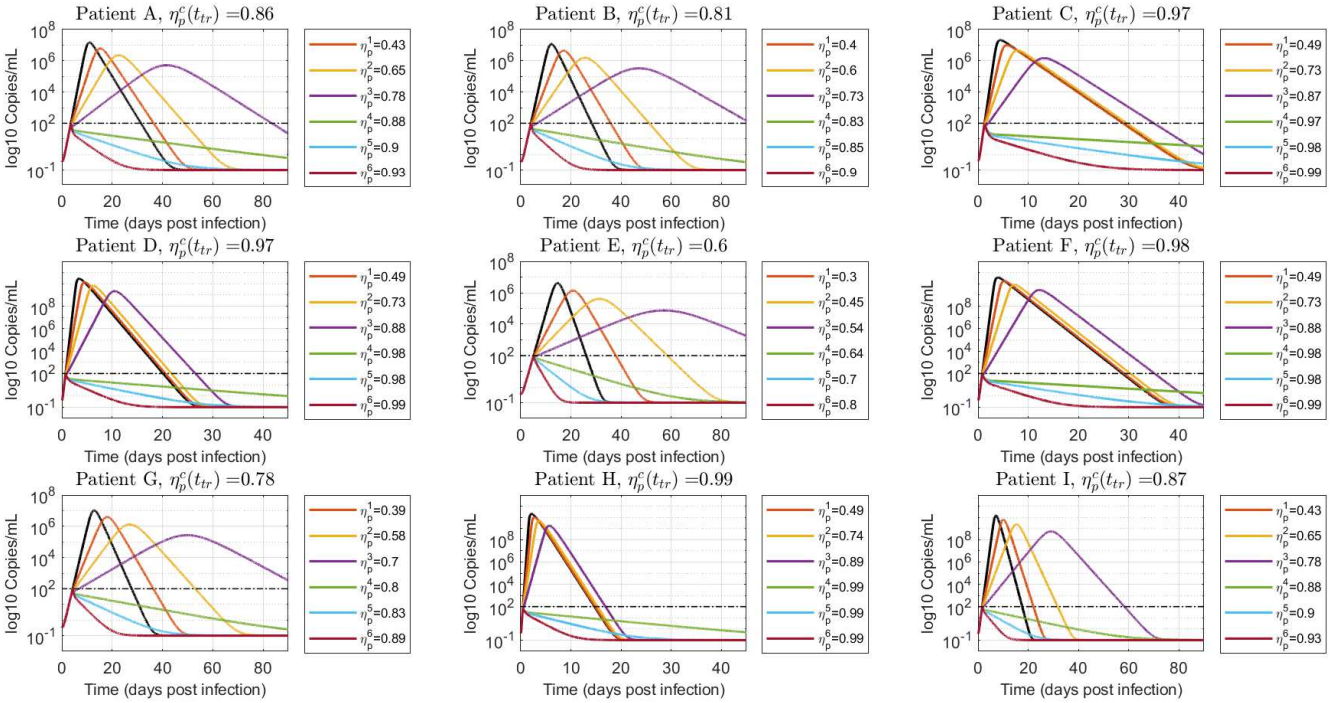

Figure 5: Free virus behavior when treatment is started at viral load detection level ($t_{tr} = t_{DL}$). Values of η_p smaller (η_p^1, η_p^2), approximately equal (η_p^3, η_p^4) and greater (η_p^5, η_p^6) than η_p^c are simulated to demonstrate the results in Theorem 3.1. The black line denotes the untreated case ($\eta_p = 0$).

As expected, effective treatments produce an instantaneous decline of the viral load, with a monotonically decreasing viral shedding interval as the antiviral efficacy is incremented. On the other hand, ineffective treatments cause a delay in time to peak, significantly increasing the duration of viral shedding as η_p is augmented from 0 to η_p^c. Even when the viral load peak is a monotonically decreasing function of η_p (by following similar steps than the ones in Lemma 1 it can be shown that $\partial V(\hat{t}_{V,tr})/\partial \mathcal{R} = (\delta/\beta)(1 - \frac{1}{\mathcal{R}})$, for $\mathcal{R} := \mathcal{R}(t_{tr}) \geq 1$, with $\mathcal{R}(t_{tr}) = (1 - \eta_p)p\beta/(c\delta)$), the patient will be PCR-positive for longer periods of time. This means that isolation and precautions measures with treated patients should be carefully considered, depending on the antiviral effectiveness.

Figure 6 shows a box-plot of the infected-related metrics for the antiviral effectiveness assessment. For an effective antiviral therapy ($\eta_p > \eta_p^c(t_{tr})$), the difference of viral loads at time-to-peak (ΔV) is above

the 2 logs threshold [14] and the duration of infection (DI) is below the 30 days limit (according [46], the viral shedding interval for untreated COVID-19 patients is in order of 30 days) which is in conformity with an effective viral clearance strategy. On the other hand, for an ineffective antiviral therapy ($\eta_p < \eta_p^c(t_{tr})$), even tough ΔV is monotonically increasing with η_p, the duration of infection is increased as a subpotent drug efficacy is employed. This means that the delay of the virus peak associated to ineffective treatments is significant in terms of the infected-related metrics.

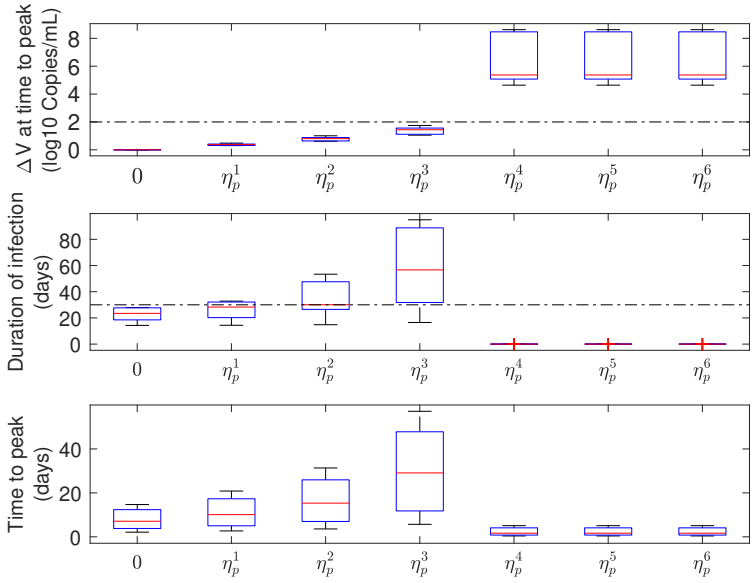

Figure 6: Infection-related metrics as function of η_p ($t_{tr} = t_{DL}$), for antiviral effectiveness assessment (all patients). Note that, $\eta_p^1 = 0.5\eta_p^c(t_{tr})$, $\eta_p^2 = 0.75\eta_p^c(t_{tr})$, $\eta_p^3 = 0.90\eta_p^c(t_{tr})$, $\eta_p^4 = \eta_p^c(t_{tr}) + 0.1(1 - \eta_p^c(t_{tr}))$, $\eta_p^5 = \eta_p^c(t_{tr}) + 0.25(1 - \eta_p^c(t_{tr}))$, and $\eta_p^6 = \eta_p^c(t_{tr}) + 0.5(1 - \eta_p^c(t_{tr}))$, being $\eta_p^c(t_{tr})$ the critical drug efficacy of each patient at time to treatment initiation, t_{tr}.

Scenario 2: treatment initiated in the course of viral spreading

Figures 7 and 8 show the virus load evolution when the antiviral therapy is started in the course of viral spreading, at $t_{tr} \approx 0.7t^e$ and $t_{tr} \approx t^e$, respectively. The viral load over the time has the same qualitative behavior than in the previous case. However, the duration of the infection is longer as the inhibition effect approaches $\eta_p^c(t_{tr})$ from below and from above (*i.e.*: η_p^3 and η_p^4 cases, violet and green lines in Figures 7 and 8). Indeed, for values of drug effectiveness in the vicinity of $\eta_p^c(t_{tr})$, the viral duration interval is augmented - even for effective therapies - since V has already reached a relatively high value at the treatment time. This behavior is confirmed in box-plots 9 and 10, where a sudden increase of the duration of infection happens when the antiviral efficacy is near the critical value. However, as the treatment time is delayed this behavior is mitigated (see box-plot 10) due to the natural increment of $V(t_{tr})$ (recall that $\dot{V}(t) \approx (\mathcal{R}(t_{tr}) - 1)\delta V(t)$, for $t > t_{tr}$, so larger values of $V(t_{tr})$ produce larger values of $|\dot{V}(t)|$). It is important to remark that, even when an increased duration of the viral shedding is reported for the effective treatment case in the boundary of critical drug effectiveness ($\eta_p \approx \eta_p^c$), the viral load peak occurs previous to $\hat{t}_V$, in accordance with items i and ii of Theorem 3.1.

5.2. Treatment initiated at different times, with the same effectiveness

In order to analyze the viral kinetics when the antiviral therapy is initiated at different times over the infection period (*i.e.*, before and after $\hat{t}_V$), we studied the temporal dependence of infection-related metrics corresponding to fixed subpotent/potent drug effectiveness. Based on the uncertainty analysis presented in Section 4, patient B was selected as a representative patient, whose critical drug efficacy $\eta_p^c(t_{tr}) \approx 0.81$ for $t_{tr} < t^e$ (see Figure 1, being $t^e \approx 0.77\hat{t}_V = 9.39$ dpi). The treatment initial times were: $t_{tr1} = 4$,

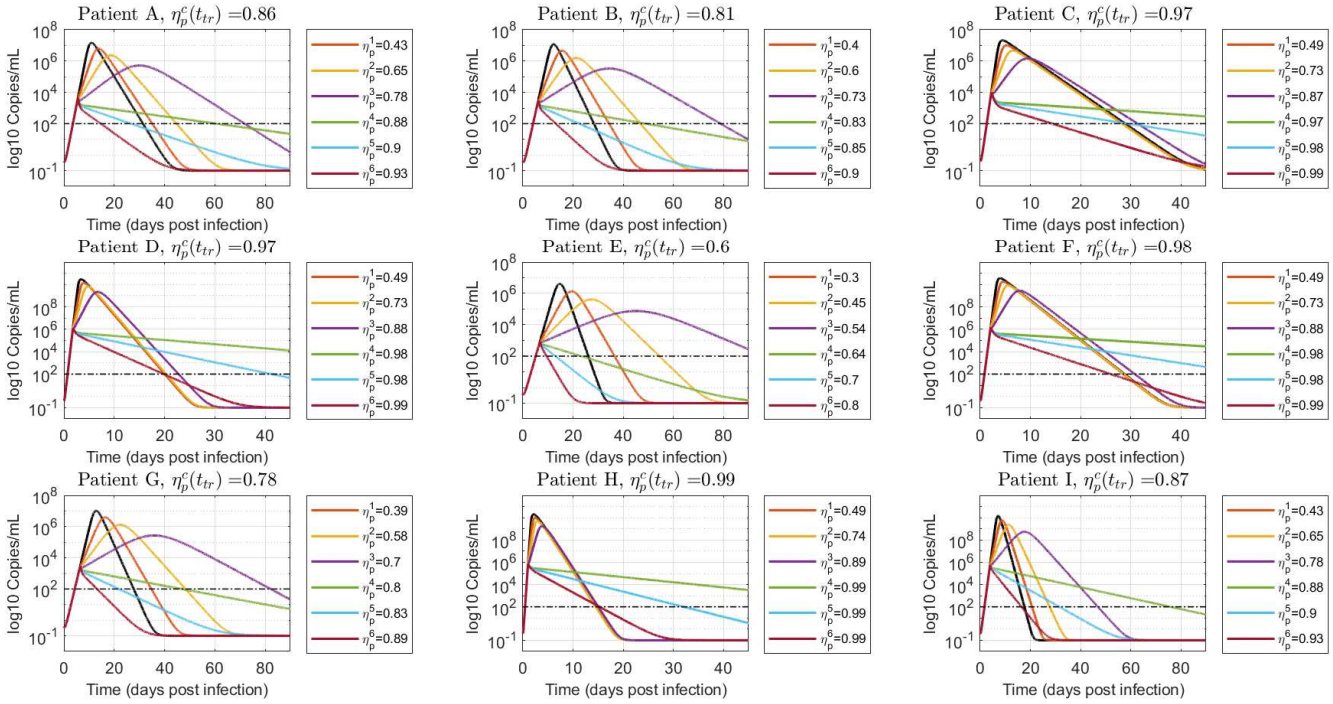

Figure 7: Viral load time evolution with treatment initial time given by $t_{tr} = 0.7t^e$. Values of η_p smaller, approximately equal and greater than η_p^c are simulated to demonstrate the results in Theorem 3.1.The black line denotes the untreated case ($\eta_p = 0$).

$t_{tr2} = 6$, $t_{tr3} = 9$, $t_{tr4} = 17$, $t_{tr5} = 20$ and $t_{tr6} = 25$ dpi. Figure11 (left) shows that if the treatment is initiated with an ineffective therapy ($\eta_p = 0.73$), the time-to-peak ($\hat{t}_{V,tr}$) and the duration of infection (DI) decrease as the treatment time is delayed. This can be explained by the fact that, for the same effectiveness, $\hat{t}_{V,tr}$ is reduced as $V(t_{tr})$ is augmented. Equations (7.4) and (7.5) in Lemma 1 show that for a fixed $\mathcal{R} \geq 1$, $k_1(\mathcal{R}) \geq 0$ and $k_2(\mathcal{R}) \leq 0$ are increasing functions of $V(t_{tr})$ (*i.e.*: $k_1(\mathcal{R}) = 0$ and $k_2(\mathcal{R}) = -1/(\delta(\mathcal{R}-1))$ for $V(t_{tr}) \to 0$ while $k_1(\mathcal{R}) = 1/((1-\mathcal{R})^2 + \mathcal{R})$ and $k_2(\mathcal{R}) = -1/(\delta\mathcal{R})$ for $V(t_{tr}) \to \delta/\beta$, being $\delta/\beta < V(\hat{t}_V)$). Therefore, since $\hat{t}_{V,tr} = k_2 \ln(k_1) + t_{tr}$ (according to equation (7.3)), it can be inferred that $\hat{t}_{V,tr}$ is monotonically decreasing with $V(t_{tr})$. Moreover, comparing the viral load at the time-to-peak, it can be deduced that $V(\hat{t}_{V,tr2}) > V(\hat{t}_{V,tr1})$ for an ineffective therapy started at two treatment times $t_{tr2} > t_{tr1}$ during the beginning of the infection (assuming that $U(t_{tr1}) \approx U(t_{tr2})$).

By following similar steps as in Lemma 1, the viral load at the time-to-peak can be written as: $V(\hat{t}_{V,tr}) = V(t_{tr}) + (p/c)U(t_{tr}) - (\delta/\beta)(\ln(\mathcal{R}_{tr}) + 1)$ and, therefore, $V(\hat{t}_{V,tr2}) - V(\hat{t}_{V,tr1}) = V(t_{tr2}) - V(t_{tr1}) > 0$. However, from Figure 11 (left) it can be seen that $V(\hat{t}_{V,tr})$ is of the order of $(3 \sim 4) \times 10^5$ (copies/ml) , independently of the treatment initiation time. This can be explained by the fact that the difference of viral load at $\hat{t}_{V,tr}$, for therapies started at different times, depends mainly on the deviation between the viral loads at treatment times, which normally are several order of magnitude below $V(\hat{t}_{V,tr})$. For example, $V(\hat{t}_{V,tr1}) = 3.29 \times 10^5$, $V(\hat{t}_{V,tr2}) = 3.30 \times 10^5$ and $V(\hat{t}_{V,tr3}) = 4.35 \times 10^5$ copies/ml while $V(t_{tr1}) = 1 \times 10^2$, $V(t_{tr2}) = 2.5 \times 10^3$ and $V(t_{tr3}) = 1.74 \times 10^5$ copies/ml. Consequently, the increment on the viral peak is not significant as the treatment is delayed, although the duration of infection is considerably reduced (*i.e.*: from 96 to 55 days). Note that the target cell-model assumes that the viral clearance in the convalescent phase is proportional to the virus load concentration at time-to-peak, which is in the same order of magnitude for the three cases. As a result, and taking into account that the viral peak is reached early as the treatment is delayed, a quickly viral deletion is observed for the postponed case. As a consequence, if a fixed subpotent drug is employed, delaying the treatment initiation time could reduce viral shedding interval, without significantly increasing the viral load at time-to-peak. It is important to remark that if η_p is reduced even more ($\eta_p \ll \eta^c$), the viral at time-to-peak follows the same behavior, although, the viral shedding interval is not-considerably decreased, since $\hat{t}_{V,tr} \approx \hat{t}_V$ as $\eta \to 0$

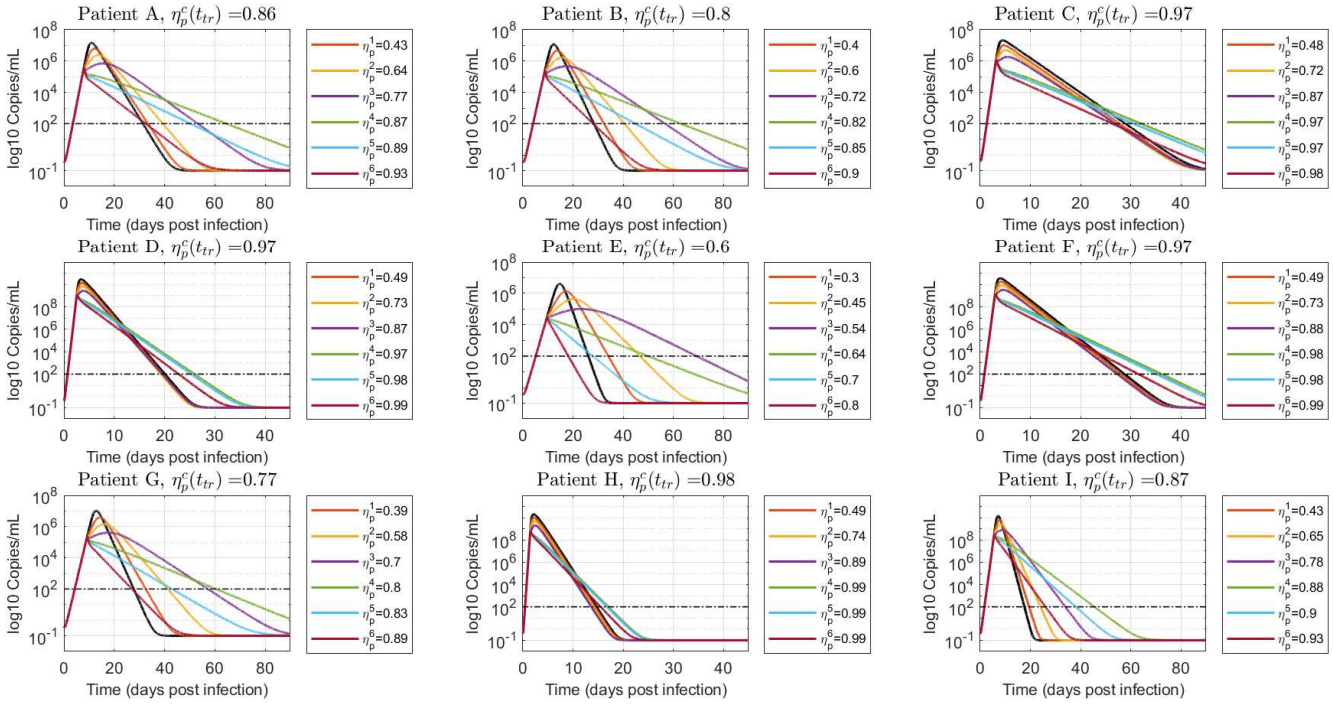

Figure 8: Viral load time evolution with treatment initial time given by $t_{tr} = t^e$. Values of η_p smaller, approximately equal and greater than η_p^c are simulated to demonstrate the results in Theorem 3.1. The black line denotes the untreated case ($\eta_p = 0$).

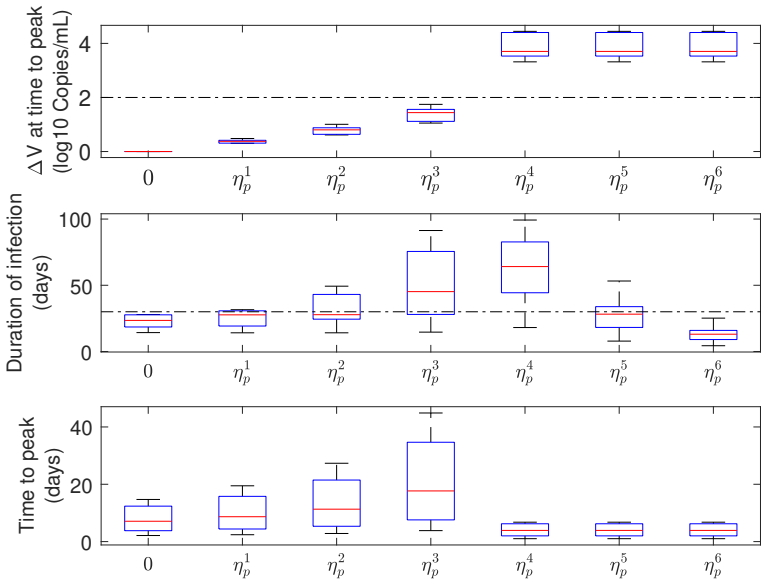

Figure 9: Infection-related metrics as function of η_p ($t_{tr} = 0.7t^e$), for antiviral effectiveness assessment (all patients).

($t_{tr} \in (\check{t}_V, \hat{t}_V)$). Hence, although a non-significant improvement on the duration of infection is achieved if the treatment is delayed, the viral outcomes continues to be acceptable.

On the other hand, if the ineffective therapy is initiated after the viral load peak, the duration of infection

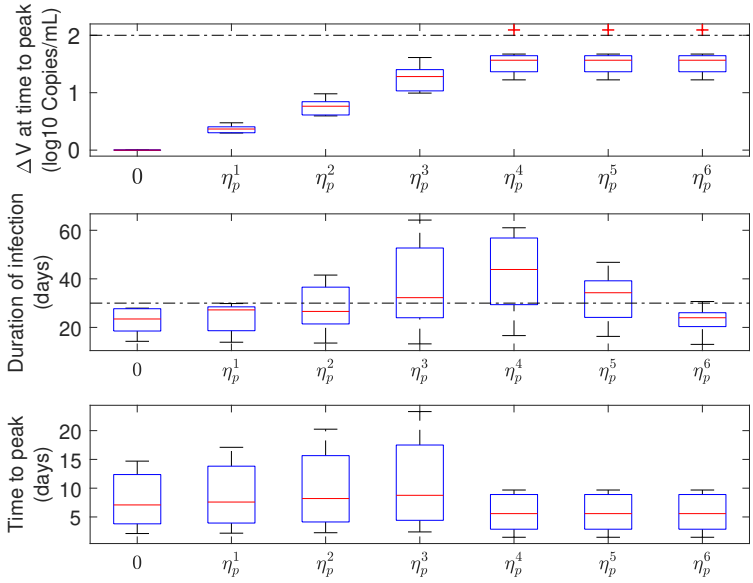

Figure 10: Infection-related metrics as function of η_p ($t_{tr} = t^e$), for antiviral effectiveness assessment (all patients).

is slightly reduced with respect to the previous case, since $R(t_{tr}) < 1$ at this time and, therefore, $\dot{V} = (\mathcal{R}(t_{tr}) - 1)\delta V(t)$ is a decreasing function of $V(t_{tr})$. In contrast to this, Figure 11 (right) shows that if an effective antiviral therapy is applied ($\eta_p = 0.9$) the duration of the infection is still decreased, since $\mathcal{R}_1(t_{tr4}) < \mathcal{R}_2(t_{tr4})$, being $\mathcal{R}_i$ the within-host basic reproduction number under a treatment with inhibition effect η_p^i (note that, $\eta_p^1 = 0.9$ and $\eta_p^2 = 0.73$ for patient B).

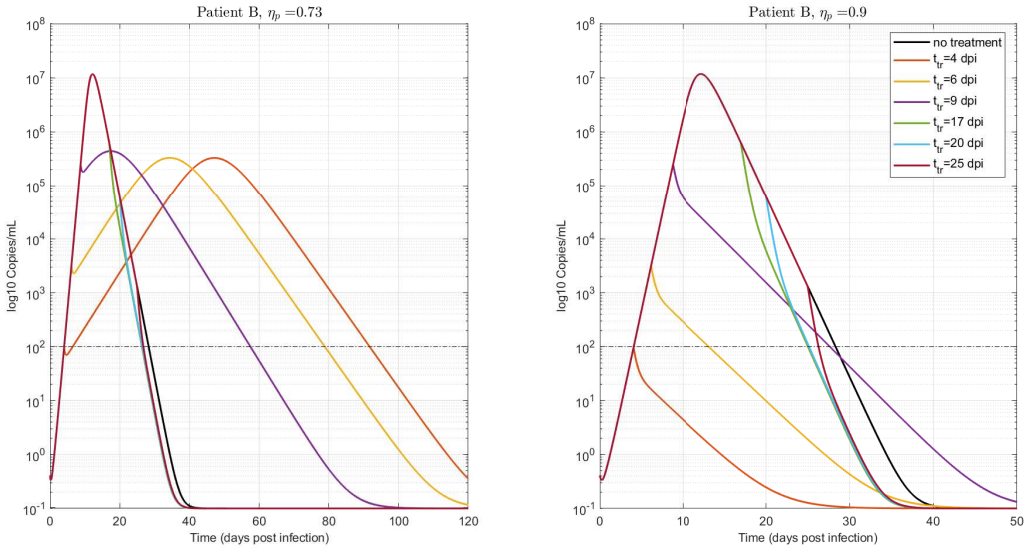

Figure 11: Virus time evolution for different treatment times, $t_{tr} = 4, 6, 8, 17, 20, 25$ (dpi). Two fixed values of η_p were used, smaller and bigger than $\eta_p^c(t_{tr})$: $\eta_p = 0.73$ (left) and $\eta_p = 0.9$ (right), respectively. $\eta_p^c(t_{tr}) \approx 0.81$ for $t_{tr} < t^e$. Patient B.

5.3. Treatment with antiviral inhibiting both viral infection (η_β) and viral replication rate (η_p)

Finally, the virus behavior was considered when a combined antiviral therapy inhibiting both, the viral infection rate (β) and the viral replication rate (p), was applied. Since the critical drug efficacy for acute models is defined during the viral spreading interval (Section 3.2), the treatment was initiated at $t_{tr} = 0.7t^e$, which is a value fulfilling $t_{tr} \in (\check{t}_V, \hat{t}_V)$.

For the sake of clarity, only Patient A was considered and the 3 previous infection-related metrics were assessed as functions of the antiviral inhibition effects η_p and η_β. Figure 12 shows that the antiviral is effective for every inhibition effect pair (η_β, η_p) fulfilling $(\eta_\beta, \eta_p) \in \mathcal{H}^c(t_{tr})$ (*i.e.*: yellow region of ΔV), in accordance with the results in Section 3.2. Moreover, as for the single inhibition cases, the duration of infection and the time-to-peak increase as the combined drug efficacy pair (η_β, η_p) tends to the boundary of $\mathcal{H}^c(t_{tr})$ ($\partial\mathcal{H}^c(t_{tr})$ in Figure 12). The difference of viral load at time-to-peak ΔV remains constant for every $(\eta_\beta, \eta_p) \in \mathcal{H}^c(t_{tr})$ since $V(\hat{t}_{V,tr}) = V(t_{tr})$ for effective treatments. In conclusion, the synergistic effect of drug effectiveness in combined therapies produces a reduction on the critical effectiveness with respect to single-therapies cases, with the same dynamical behavior over the boundary of $\mathcal{H}^c(t_{tr})$.

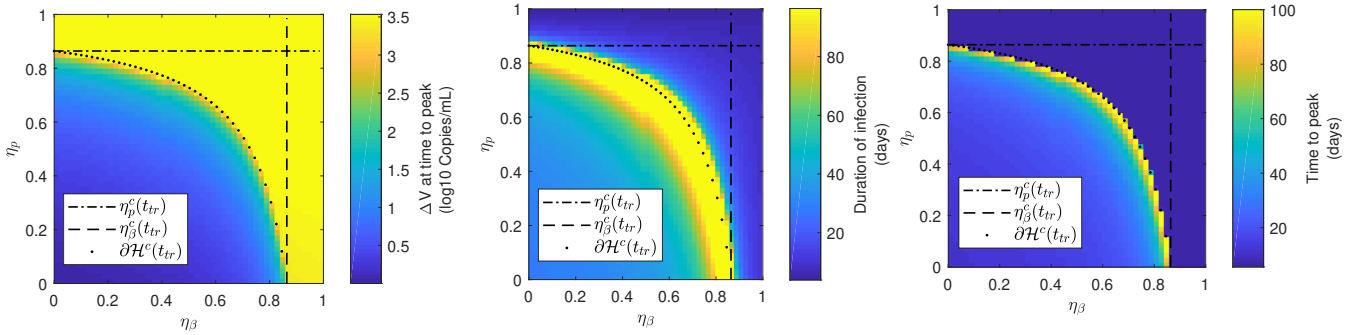

Figure 12: Infection-related metrics for antiviral effectiveness assessment as function of η_p and η_β ($t_{tr} = 0.7t^e$). Patient A.

6. Discussion

While several vaccines have been developed to prevent COVID-19 disease, it is imperative to evaluate potential therapies against SARS-CoV-2 infection. Among them, antiviral treatments are promissory strategies to increment the viral clearance "within-host", decreasing disease severity. In this sense, the drug effectiveness concept is crucial to evaluate the drug effect threshold above which the viral load starts declining [47]. Although this critical value has been described for chronic infections (e.g. HIV [47, 48], HCV [49]) it has not been studied yet for COVID-19. The critical drug efficacy can be understood in terms of the antiviral potency to decline viral spreading, in spite of guiding the system to an uninfected equilibrium, as it was introduced in Definition 4, Section 3.2. In addition, the critical inhibition effect of an antiviral depends on the treatment initiation time, and it has shown to be a monotonically decreasing function during the viral spreading interval (roughly speaking, during the time interval before the untreated virus peak).

Regarding the virus behavior for effective therapies ($\eta > \eta^c$), the viral load at time-to-peak is practically equal to $V(t_{tr})$ (*i.e.*, a treatment is considered effective if the virus starts to decrease at the very moment the treatment is initiated, by modifying either η_p, η_β, or both), so ΔV is larger for earlier treatments, being greater than the 2 log threshold for effective antiviral therapies started at $t_{tr} < t^e$ ($t^e \approx 0.77\hat{t}_V$). Nevertheless, for η approaching η^c (from above), the viral shedding interval is enlarged as the treatment is initiated during the infection growth. Therefore, if the therapeutic objective is to reduce both, the viral shedding interval and the viral peak, the efficacy level would need to overpass the critical value in a given quantity. From Figure 1 it can be seen that $\eta^c(t_{tr}) > 0.7$ for most of patients.

Simulations results suggest that for ineffective therapies, the virus would take longer to be cleared - rather than a monotonic decline, as in the previous case - reaching a peak and finally decreasing to zero. In spite of the fact that the viral load at time-to-peak decreases monotonically with η (ΔV increases as the inhibition effect jumps from 0 to $\eta > 0$), the time-to-peak increases as η approaches η^c (from below), which

results in a longer duration of infection, potentially requiring additional isolation measures for the treated patient.

Although an effective reduction of the viral load peak and the duration of infection could be achieved with early treatments (treatments started before the untreated peak), minor effects are attained with late ones. Particularly, Figure 11 corroborates a slight reduction on the viral shedding interval if a subpotent/potent drug therapy is employed after the time-to-peak. Consequently, taking into account that the viral load in COVID-19 patients presumably reaches the peak prior to the symptom onset, no further clinical improvements may be obtained if the therapy is started in this symptomatic phase (*i.e.*: notice that SARS-CoV-2 pathophysiology is characterized by a direct cytotoxic effect, endothelial cell damage, dysregulation of immune response, among others [29]).

The effectiveness of combined treatments affecting both, η_p and η_β, was also studied and an interdependent critical drug efficacy level was computed. Mathematically, the critical combination of values of η_p and η_β is placed on the boundary of the effective set $\mathcal{H}^c(t_{tr})$, which is a set in the (η_p, η_β) space. In comparison with single treatment cases (represented by the horizontal and vertical dash-dot lines in Figure 12), a reduced critical antiviral efficacy was reported for the combined case, denoting a reduction on the necessary drug effectiveness to reduce viral spreading. Moreover, the viral characteristic behavior in the vicinity of the critical drug efficacy (*i.e.*: increase of time-to-peak and duration of infection) was preserved for the combined case, as the pair (η_β, η_p) belongs to the critical boundary of $\mathcal{H}^c(t_{tr})$, which implies that the antiviral effectiveness characterization made in Theorem 3.1 for single treatments could be extended to combined therapies.

In sum, this work formalizes the existence of a critical drug efficacy for acute infection models, which could have implications in the extended viral shedding observed "in-silico" by [50] (for SARS-CoV-2 infections) and by [51] (for influenza) when the antiviral therapy is initiated early but with a subpotent drug efficacy. Moreover, it was shown the importance of initialization the antiviral therapy early (before viral load peak) in order to achieve a significant reduction of ΔV and DI [14, 52]. Although a time dependence was noticed for the critical drug efficacy $(\eta_p^c(t_{tr}), \eta_\beta^c(t_{tr}))$, since it is a decreasing function of t_{tr} (Figure 1), its behavior does not compromise the antiviral success if an effective therapy is started later.

The main clinical implications for acute infections, and, particularly, for the SARS-CoV-2 infection are: a) importance of viral load monitoring on probably infected COVID-19 patients (prophylactic use of antiviral therapy, previous to onset of symptoms, although adverse effects have been reported for potential antiviral drugs [30], which could limited their prophylactic usage in risk patients), b) isolation of treated patient, c) possible explanation of the increase of duration of infection showed in immune compromised COVID-19 patients.

7. Appendix

7.1. Virus peak time behavior under ineffective treatments

The next Lemma establishes conditions on the virus peak time as a function of $\mathcal{R}(t_{tr})$.

Lemma 1. *Consider* (2.1)*, constrained by the positive set* $\mathbb{X}$*, at the beginning of the infection* $t = 0$*, with* $U(0) > \mathcal{U}_c$*,* $I(0) \geq 0$ *and* $V(0) > 0$*. Consider that at some time* $t_{tr} > 0$*,* $\eta_p(t)$ *jumps from* 0 *to* $\eta_p > \eta_p^c$*, being* η_p^c *the critical value defined in* (3.2)*. Then, there exists* $t^e(\eta_p, t_{tr})$ *such that if* $t_{tr} \in (\check{t}_V, t^e]$*, the virus peak time* $\hat{t}_{V,tr}$ *(considering the treatment effect) is a decreasing function of* $\mathcal{R}(t_{tr})$*.*

Proof: Consider the approximation 7.10, in Section 7.2. Since $\eta_p(t)$ jumps from 0 to $\eta_p < \eta_p^c$, at t_{tr}, then $\mathcal{R}(t)$ jumps from $\mathcal{R}(t_{tr}^-)$ to $\mathcal{R}(t_{tr})$, with $\mathcal{R}(t_{tr}) \in (\mathcal{R}(t_{tr}^-), 1)$ and $\mathcal{R}(t_{tr}^-) > 1$. Then it is possible to approximate the explicit solutions for $U(t)$ and $V(t)$ (by approximating the $\ln(z)$ function in the time interval before the virus peak by $(z-1)(\frac{w_1}{z}+w_2)$, being w_1 and w_2 arbitrary constants, fulfilling $w_1+w_2 = 1$ [53]). So, $U(t)$, for $t > t_{tr}$, can be written as

$$U(t) = \frac{(B + \sqrt{B^2 - 4AC})k_{t_{tr}}^N e^{-(\beta/U(t_{tr}))\sqrt{B^2-4AC}(t-t_{tr})} - k_{t_{tr}}^D (B - \sqrt{B^2 - 4AC})}{2Ak_{t_{tr}}^D - 2Ak_{t_{tr}}^N e^{-(\beta/U(t_{tr}))\sqrt{B^2-4AC}(t-t_{tr})}}, \tag{7.1}$$

where

$$\begin{aligned}
k_{t_{tr}}^N &= 2AU(t_{tr}) + B - \sqrt{B^2 - 4AC}, \\
k_{t_{tr}}^D &= 2AU(t_{tr}) + B + \sqrt{B^2 - 4AC}, \\
A &= -\frac{p(1-\eta_p)}{c}U(t_{tr}) + \frac{\delta}{\beta}w_2, \\
B &= U(t_{tr})(\frac{\delta}{\beta}w_1 - \frac{\delta}{\beta}w_2 + V(t_{tr}) + \frac{p(1-\eta_p)}{c}U(tr)), \\
C &= -\frac{\delta}{\beta}U(t_{tr})^2 w_1.
\end{aligned}$$

A reasonable approximation, however, can be obtained by selecting $w_1 = 0$ and $w_2 = 1$ (also $w_1 = 0.2$ and $w_1 = 0.8$ gives a good result, but clearly the former selection significantly simplifies the expressions). In such a case, A, B, C, $k_{t_{tr}}^N$ and $k_{t_{tr}}^D$ read:

$$\begin{aligned}
A &\approx -U(t_{tr})\frac{p(1-\eta_p)}{c} + \frac{\delta}{\beta} = (1 - \mathcal{R}(t_{tr}))\frac{\delta}{\beta} < 0, \\
B &\approx U(t_{tr})(-\frac{\delta}{\beta} + V(t_{tr}) + U(t_{tr})\frac{p(1-\eta_p)}{c}) = -U(t_{tr})A + U(t_{tr})V(t_{tr}) > 0, \\
C &\approx 0, \\
k_{t_{tr}}^N &\approx 2AU(t_{tr}), \\
k_{t_{tr}}^D &\approx 2AU(t_{tr}) + 2B = 2U(t_{tr})V(t_{tr}),
\end{aligned}$$

being $\mathcal{R}(t_{tr}) = U(t_{tr})\frac{\beta p(1-\eta_p)}{c\delta}$. This way, $U(t)$ can be simplified as

$$\begin{aligned}
U(t) &= \frac{2B2AU(t_{tr})e^{-(\beta/U(t_{tr}))B(t-t_{tr})}}{2A2U(t_{tr})V(t_{tr}) - 2A2AU(t_{tr})e^{-(\beta/U(t_{tr}))B(t-t_{tr})}}, \\
&= \frac{(U(t_{tr})V(t_{tr}) - U(t_{tr})A)e^{-(\beta/U(t_{tr}))B(t-t_{tr})}}{V(t_{tr}) - Ae^{-(\beta/U(t_{tr}))B(t-t_{tr})}}
\end{aligned} \tag{7.2}$$

The time at which $U(t)$ reaches $\mathcal{U}_c^{tr}$ - *i.e.*, the time at which $\mathcal{R}(t)$ reaches 1 and $V(t)$ reaches its peak, denoted as $\hat{t}_{V,tr}$ (with $\hat{t}_{V,tr} \geq t_{tr}$) - can be explicitly computed as

$$\hat{t}_{V,tr} = k_2 \ln(k_1) + t_{tr}, \tag{7.3}$$

where

$$k_1 = \frac{V(t_{tr})\mathcal{U}_c^{tr}}{U(t_{tr})V(t_{tr}) - AU(t_{tr}) + A\mathcal{U}_c^{tr}}$$

$$k_2 \quad = \quad \frac{1}{\beta(A - V(t_{tr}))},$$

being $\mathcal{U}_c^{tr} = \frac{c\delta}{\beta p(1-\eta_p)}$ the critical value for U corresponding to the treatment parameter $p(1-\eta_p)$. Now, recalling that $\mathcal{R}(t_{tr}) = \frac{U(t_{tr})}{\mathcal{U}_c^{tr}}$, and denoting $U(t_{tr})$, $V(t_{tr})$ and $\mathcal{R}(t_{tr})$ as U, V and $\mathcal{R}$, respectively, for the sake of simplicity, k_1, k_2 can be rewritten as:

$$k_1(\mathcal{R}) = \frac{V}{\frac{\delta}{\beta}(1-\mathcal{R})^2 + \mathcal{R}V} > 0, \quad \forall \mathcal{R} > 1 \tag{7.4}$$

$$k_2(\mathcal{R}) = \frac{1}{\delta(1-\mathcal{R}) - \beta V} < 0, \quad \forall \mathcal{R} > 1 \tag{7.5}$$

This way, $\hat{t}_{V,tr} = \hat{t}_{V,tr}(\mathcal{R}) = k_2(\mathcal{R})\ln(k_1(\mathcal{R})) + t_{tr}$ represents the time of the virus peak in terms of $\mathcal{R}$. Note that $\hat{t}_{V,tr}(\mathcal{R})$ is defined only for $\mathcal{R} \geq 1$; indeed, $\hat{t}_{V,tr}(1) = t_{tr}$ since $k_1(1) = 1$, while $\hat{t}_{V,tr}(\mathcal{R}) > t_{tr}$ for $\mathcal{R} > 1$.

The idea now is to consider the derivative of $\hat{t}_{V,tr}$ with respect to $\mathcal{R}$, to show that it is negative for treatment times t_{tr} small enough. This derivative reads:

$$\frac{\partial \hat{t}_{V,tr}}{\partial \mathcal{R}} = \frac{\partial k_2}{\partial \mathcal{R}}\ln(k_1) + k_2\frac{1}{k_1}\frac{\partial k_1}{\partial \mathcal{R}}$$

where

$$\frac{\partial k_1}{\partial \mathcal{R}} = -\frac{V(\frac{2\delta}{\beta}(\mathcal{R}-1) + V)}{(\frac{\delta}{\beta}(1-\mathcal{R})^2 + \mathcal{R}V)^2} \tag{7.6}$$

$$\frac{\partial k_2}{\partial \mathcal{R}} = \frac{\delta}{(\delta(1-\mathcal{R}) - \beta V)^2}. \tag{7.7}$$

Since $\frac{\partial k_2}{\partial \mathcal{R}} > 0$ for $\mathcal{R} > 1$, condition $\frac{\partial \hat{t}_{V,tr}}{\partial \mathcal{R}} < 0$ can be written as

$$\ln(k_1) < -\frac{k_2}{k_1}\frac{\partial k_1}{\partial \mathcal{R}}(\frac{\partial k_2}{\partial \mathcal{R}})^{-1}. \tag{7.8}$$

Furthermore, given that $\ln(\cdot)$ is an increasing function on $(0, \infty]$, it follows that

$$k_1 < e^{-\frac{k_2}{k_1}\frac{\partial k_1}{\partial \mathcal{R}}(\frac{\partial k_2}{\partial \mathcal{R}})^{-1}}. \tag{7.9}$$

Then, by replacing (7.4), (7.5), (7.6) and (7.7) in inequality (7.9), we have:

$$\frac{\beta}{\delta}V < [(1-\mathcal{R})^2 + \mathcal{R}\frac{\beta}{\delta}V]e^{\frac{-2(1-\mathcal{R})^2 + 2\frac{\beta}{\delta}V(1-\mathcal{R}) - \frac{\beta}{\delta}^2V^2}{(1-\mathcal{R})^2 + \frac{\beta}{\delta}\mathcal{R}V}}$$

Now, for $\mathcal{R} > 1$ the exponent is negative, so function

$$f(\frac{\beta}{\delta}V) := [(1-\mathcal{R})^2 + \mathcal{R}\frac{\beta}{\delta}V]e^{\frac{-2(1-\mathcal{R})^2 + 2\frac{\beta}{\delta}V(1-\mathcal{R}) - \frac{\beta}{\delta}^2V^2}{(1-\mathcal{R})^2 + \frac{\beta}{\delta}\mathcal{R}V}}$$

starts at the positive value $(1-\mathcal{R})^2e^{-2}$, for $V = 0$, then increases to a maximum and finally decreases asymptotically to zero, for $V \to \infty$. So, there exists some interval of V, maybe small, such that $V < f(V)$. Figure 13 shows a plot of $f(V)$ for different values of $\mathcal{R} > 1$.

Finally, since we are considering the treatment time to belong to the increasing period of $V(t)$ (*i.e.*, $t_{tr} \in (\check{t}_V, \hat{t}_V)$, with $V(\check{t}_V) \approx 0$, then small values of $V(t)$ correspond to small values of t. So, a time interval $(\check{t}_V, t^e]$ exists such that $\hat{t}_{V,tr}$ is a decreasing function of $\mathcal{R}(t_{tr})$, and the proof is complete. Figure 14 shows the time evolution of $\mathcal{R}(t)$ when the antiviral treatment is initiated at $0.75\hat{t}_V$ and different antiviral

inhibition effects are considered, for the real data patients simulated in Sections 4 and 5. As it can be seen, larger values of η_p (or smaller values of $\mathcal{R}(t_{tr})$) corresponds always with larger values of $\hat{t}_{tr,V}$. □

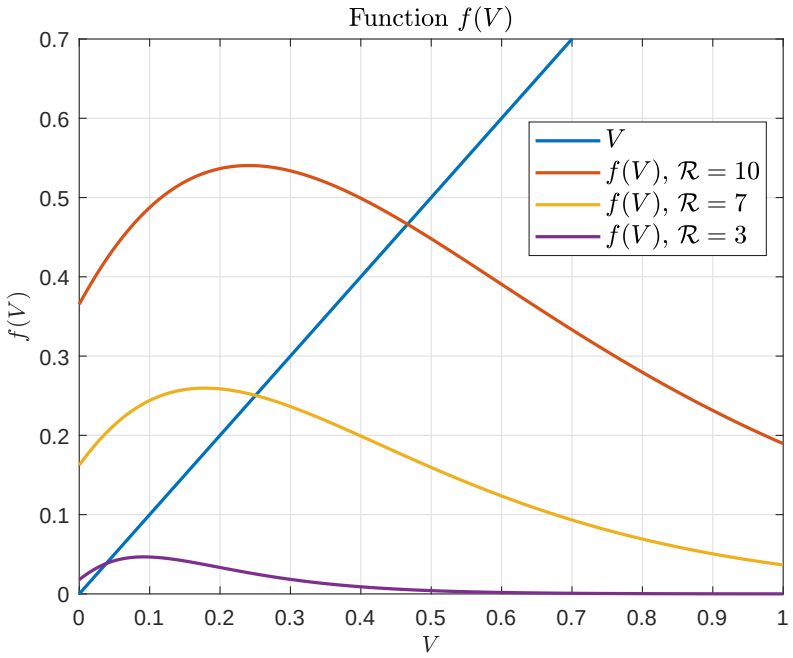

Figure 13: Qualitative plot of function $f(V)$ (arbitrary parameters) for different values of $\mathcal{R}$. As it can be seen - independently of the parameter values - if $\mathcal{R}(t_{tr}) > 1$ it there exists an interval of values of V, and a corresponding period of time such that $f(V) > V$.

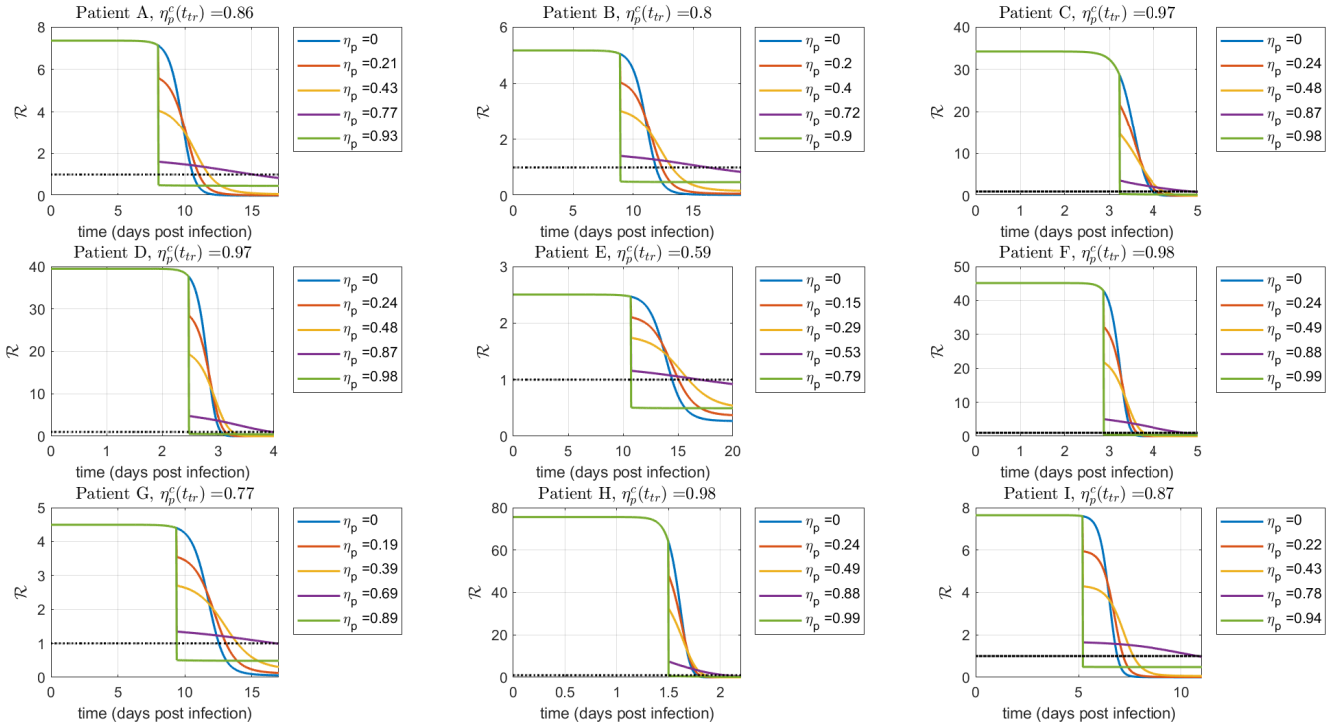

Figure 14: Evolution of $\mathcal{R}(t)$ when an antiviral treatment is initiated at a time of approximately $0.75\ \hat{t}_V$, and different antiviral inhibition effects η_p are considered, smaller and greater than the critical value η_p^c. The black dashed line represents $\mathcal{R} = 1$. As it can be seen, for values of $\eta_p < \eta_p^c$, $\mathcal{R}(t)$ crosses 1 at larger times for larger values of η_p as it is stated in Lemma 1. This implies that if $\eta_p < \eta_p^c$, larger values of η_p delays the virus peak time, as it is stated in Theorem 3.1.iii. Furthermore, the figure confirms that, for real patient date, t^e is close to $\hat{t}_V$.

7.2. System approximation

A characteristic of system (2.1) - that shows to be useful in the development of the main results of the work - is that for the untreated case ($\eta_\beta(t) \equiv 0$ and $\eta_p(t) \equiv 0$ for all $t \geq 0$), it can be simplified. Indeed, if we assume that virus is in quasi-steady state during viral spreading interval, which is a good assumption as long as $c \gg \delta$ (see [16], Equation (4), [54], [55], [49]), the three-states system (2.1) can be approximated by the following two-state equations:

$$\dot{U}(t) \approx -\beta U(t)V(t), \qquad U(0) = U_0, \tag{7.10a}$$

$$\dot{V}(t) \approx \frac{p\beta}{c} U(t)V(t) - \delta V(t), \qquad V(0) = V_0, \tag{7.10b}$$

where the infected cells state are given by $I(t) \approx \frac{c}{p}V(t)$. Note that equation (7.10.b) can be written as $\dot{V}(t) = (\mathcal{R}(t) - 1)\delta V(t)$. Then, according to Theorem 4.1 in [24], it is easy to see that $\hat{t}_V \to t_c$ from the right and $\hat{t}_I \to t_c$ from the left when $(c/\delta) \to \infty$, *i.e.*, the peaks of V and I tend to occur simultaneously, at time t_c. Figure 15 shows a phase portrait of system (2.1), without antiviral treatment, with a rather unrealistic parameter values ($\beta = 0.5$, $\delta = 0.2$, $p = 2$ and $c = 5$) but useful to exemplify how, after a relatively short time (and provided that $c > \delta$), the system reaches the manifold defined by the condition $I(t) = \frac{c}{p}V(t)$.

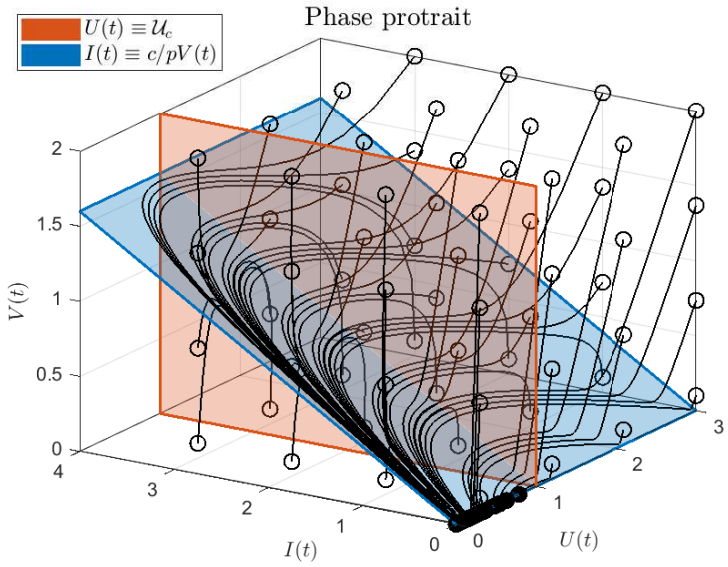

Figure 15: Phase portrait of system (2.1) with parameters $\beta = 0.5$, $\delta = 0.2$, $p = 2$ and $c = 5$, for different initial conditions not necessarily representing realistic cases. Empty circles represent the initial state, while solid circles represent final states. The red hyperplane corresponds to $U(t) \equiv \mathcal{U}_c$ (*i.e.*, the critical value of U, when $\mathcal{R}(t) = 1$) while the blue hyperplane corresponds to the fast manifold in which $I(t)$ and $V(t)$ are proportional (.i.e, $I(t) = c/pV(t)$). Note that only the initial states with $U_0 > \mathcal{U}_c = 1$ corresponds to scenarios with $\mathcal{R}_0 > 1$.

References

[1] Coronavirus disease 2019 (COVID-19) Situation Reports, https://www.who.int/emergencies/diseases/novel-coronavirus-2019/situation-reports, Accessed: 2020-12-28.

[2] COVID-19 Dashboard by the Center for Systems Science and Engineering (CSSE) at Johns Hopkins University, https://coronavirus.jhu.edu/map.html, Accessed: 2020-04-28.

[3] Y. Cao, A. Hiyoshi, S. Montgomery, Covid-19 case-fatality rate and demographic and socioeconomic influencers: worldwide spatial regression analysis based on country-level data, BMJ open 10 (11) (2020) e043560.

[4] M. S. Khan, I. Shahid, S. D. Anker, S. D. Solomon, O. Vardeny, E. D. Michos, G. C. Fonarow, J. Butler, Cardiovascular implications of COVID-19 versus influenza infection: a review, BMC medicine 18 (1) (2020) 1–13.

[5] O. Mitjà, B. Clotet, Use of antiviral drugs to reduce COVID-19 transmission, The Lancet Global Health (2020).

[6] J. Gao, Z. Tian, X. Yang, Breakthrough: Chloroquine phosphate has shown apparent efficacy in treatment of COVID-19 associated pneumonia in clinical studies, BioScience Trends 14 (02 2020). doi:10.5582/bst.2020.01047.

[7] X. Yao, F. Ye, M. Zhang, C. Cui, B. Huang, P. Niu, X. Liu, l. Zhao, E. Dong, C.-L. Song, S. Zhan, R. Lu, H. Li, D. Liu, In Vitro Antiviral Activity and Projection of Optimized Dosing Design of Hydroxychloroquine for the Treatment of Severe Acute Respiratory Syndrome Coronavirus 2 (SARS-CoV-2), Clinical infectious diseases : an official publication of the Infectious Diseases Society of America (03 2020). doi:10.1093/cid/ciaa237.

[8] A. Kalil, Treating COVID-19-Off-Label Drug Use, Compassionate Use, and Randomized Clinical Trials During Pandemics, JAMA 323 (03 2020). doi:10.1001/jama.2020.4742.

[9] P. Colson, J.-M. Rolain, J.-C. Lagier, P. Brouqui, D. Raoult, Chloroquine and hydroxychloroquine as available weapons to fight COVID-19, International Journal of Antimicrobial Agents 55 (2020) 105932. doi:10.1016/j.ijantimicag.2020.105932.

[10] N. H. Commission, et al., Translation: Diagnosis and Treatment Protocol for Novel Coronavirus Pneumonia (Trial Version 7), Infectious Microbes & Diseases (2020) 48–54.

[11] J. M. Sanders, M. L. Monogue, T. Z. Jodlowski, J. B. Cutrell, Pharmacologic Treatments for Coronavirus Disease 2019 (COVID-19): A Review, JAMA (2020).

[12] S. Tett, D. Cutler, R. Day, K. Brown, Bioavailability of hydroxychloroquine tablets in healthy volunteers, British journal of clinical pharmacology 27 (1989) 771–9. doi:10.1111/j.1365-2125.1989.tb03439.x.

[13] E. A. Hernandez-Vargas, J. X. Velasco-Hernandez, In-host Modelling of COVID-19 Kinetics in Humans, medRxiv (2020).

[14] A. Gonçalves, J. Bertrand, R. Ke, E. Comets, X. De Lamballerie, D. Malvy, A. Pizzorno, O. Terrier, M. Rosa Calatrava, F. Mentré, et al., Timing of antiviral treatment initiation is critical to reduce sars-cov-2 viral load, CPT: pharmacometrics & systems pharmacology 9 (9) (2020) 509–514.

[15] G. Giordano, F. Blanchini, R. Bruno, P. Colaneri, A. Di Filippo, A. Di Matteo, M. Colaneri, et al., A SIDARTHE model of COVID-19 Epidemic in Italy, arXiv preprint arXiv:2003.09861 (2020).

[16] K. S. Kim, K. Ejima, Y. Ito, S. Iwanami, H. Ohashi, Y. Koizumi, Y. Asai, S. Nakaoka, K. Watashi, R. N. Thompson, et al., Modelling SARS-CoV-2 Dynamics: Implications for Therapy, medRxiv (2020).

[17] P. Baccam, C. Beauchemin, C. A. Macken, F. G. Hayden, A. S. Perelson, Kinetics of influenza A virus infection in humans, Journal of virology 80 (15) (2006) 7590–7599.

[18] E. A. Hernandez-Vargas, E. Wilk, L. Canini, F. Toapanta, S. Binder, A. Uvarovskii, T. Ross, C. A. Guzman, A. Perelson, M. Meyer-Hermann, Effects of Aging on Influenza Virus Infection Dynamics, Journal of virology 88 (01 2014). doi:10.1128/JVI.03644-13.

[19] V. Nguyen, S. Binder, A. Boianelli, M. Meyer-Hermann, E. A. Hernandez-Vargas, Ebola Virus Infection Modelling and Identifiability Problems, Frontiers in microbiology 6 (05 2015). doi:10.3389/fmicb.2015.00257.

[20] L. Rong, A. Perelson, Modeling HIV persistence, the latent reservoir, and viral blips, Journal of theoretical biology 260 (2009) 308–31. doi:10.1016/j.jtbi.2009.06.011.

[21] A. S. Perelson, R. M. Ribeiro, Modeling the within-host dynamics of HIV infection, BMC biology 11 (1) (2013) 96.

[22] F. Graw, A. Perelson, Modeling viral spread, Annual Review of Virology 3 (11 2016). doi:10.1146/annurev-virology-110615-042249.

[23] R. Wölfel, V. M. Corman, W. Guggemos, M. Seilmaier, S. Zange, M. A. Müller, D. Niemeyer, T. C. Jones, P. Vollmar, C. Rothe, et al., Virological assessment of hospitalized patients with COVID-2019, Nature 581 (7809) (2020) 465–469.

[24] P. Abuin, A. Anderson, A. Ferramosca, E. A. Hernandez-Vargas, A. H. Gonzalez, Characterization of SARS-CoV-2 Dynamics in the Host, Annual Reviews in Control (2020).

[25] K. Wang, Z. Lu, X. Wang, H. Li, H. Li, D. Lin, Y. Cai, X. Feng, Y. Song, Z. Feng, et al., Current trends and future prediction of novel coronavirus disease (covid-19) epidemic in china: a dynamical modeling analysis, Mathematical biosciences and engineering 17 (4) (2020) 3052–3061.

[26] R. Ke, C. Zitzmann, R. M. Ribeiro, A. S. Perelson, Kinetics of sars-cov-2 infection in the human upper and lower respiratory tracts and their relationship with infectiousness, medRxiv (2020).

[27] E. A. Hernandez-Vargas, Modeling and Control of Infectious Diseases in the Host: With MATLAB and R, Academic Press, 2019.

[28] S. M. Ciupe, J. M. Heffernan, In-host modeling, Infectious Disease Modelling 2 (2) (2017) 188–202.

[29] A. Gupta, M. V. Madhavan, K. Sehgal, N. Nair, S. Mahajan, T. S. Sehrawat, B. Bikdeli, N. Ahluwalia, J. C. Ausiello, E. Y. Wan, et al., Extrapulmonary manifestations of COVID-19, Nature medicine 26 (7) (2020) 1017–1032.

[30] S. Jomah, S. M. B. Asdaq, M. J. Al-Yamani, Clinical efficacy of antivirals against novel coronavirus (COVID-19): A review, Journal of Infection and Public Health (2020).

[31] C. Liu, Q. Zhou, Y. Li, L. V. Garner, S. P. Watkins, L. J. Carter, J. Smoot, A. C. Gregg, A. D. Daniels, S. Jervey, et al., Research and development on therapeutic agents and vaccines for COVID-19 and related human coronavirus diseases (2020).

[32] M. Wang, R. Cao, L. Zhang, X. Yang, J. Liu, M. Xu, Z. Shi, Z. Hu, W. Zhong, G. Xiao, Remdesivir and chloroquine effectively inhibit the recently emerged novel coronavirus (2019-ncov) in vitro, Cell research 30 (3) (2020) 269–271.

[33] H. M. Dobrovolny, Quantifying the effect of remdesivir in rhesus macaques infected with SARS-CoV-2, Virology (2020).

[34] J.-M. Vergnaud, I.-D. Rosca, Assessing bioavailablility of drug delivery systems: mathematical modeling, CRC press, 2005.

[35] C. Hadjichrysanthou, E. Cauët, E. Lawrence, C. Vegvari, F. De Wolf, R. M. Anderson, Understanding the within-host dynamics of influenza A virus: from theory to clinical implications, Journal of The Royal Society Interface 13 (119) (2016) 20160289.

[36] H. M. Dobrovolny, R. Gieschke, B. E. Davies, N. L. Jumbe, C. A. Beauchemin, Neuraminidase inhibitors for treatment of human and avian strain influenza: A comparative modeling study, Journal of theoretical biology 269 (1) (2011) 234–244.

[37] R. Storn, K. Price, Differential evolution-a simple efficient adaptive scheme for global optimization, Tech. rep., Tech. Rep. TR-95-012, International Computer Science Institute, Berkeley ... (1995).

[38] C. E. Torres-Cerna, A. Y. Alanis, I. Poblete-Castro, M. Bermejo-Jambrina, E. A. Hernandez-Vargas, A comparative study of differential evolution algorithms for parameter fitting procedures, in: 2016 IEEE Congress on Evolutionary Computation (CEC), IEEE, 2016, pp. 4662–4666.

[39] E. A. Hernandez-Vargas, R. H. Middleton, Modeling the three stages in HIV infection, Journal of theoretical biology 320 (2013) 33–40.

[40] X. He, E. H. Lau, P. Wu, X. Deng, J. Wang, X. Hao, Y. C. Lau, J. Y. Wong, Y. Guan, X. Tan, et al., Temporal dynamics in viral shedding and transmissibility of COVID-19, Nature medicine 26 (5) (2020) 672–675.

[41] B. N. Williamson, F. Feldmann, B. Schwarz, K. Meade-White, D. P. Porter, J. Schulz, N. Van Doremalen, I. Leighton, C. K. Yinda, L. Pérez-Pérez, et al., Clinical benefit of remdesivir in rhesus macaques infected with SARS-CoV-2, BioRxiv (2020).

[42] V. J. Munster, F. Feldmann, B. N. Williamson, N. van Doremalen, L. Pérez-Pérez, J. Schulz, K. Meade-White, A. Okumura, J. Callison, B. Brumbaugh, et al., Respiratory disease in rhesus macaques inoculated with SARS-CoV-2, Nature (2020) 1–5.

[43] A. Raue, C. Kreutz, T. Maiwald, J. Bachmann, M. Schilling, U. Klingmüller, J. Timmer, Structural and practical identifiability analysis of partially observed dynamical models by exploiting the profile likelihood, Bioinformatics 25 (15) (2009) 1923–1929.

[44] H. M. Dobrovolny, M. B. Reddy, M. A. Kamal, C. R. Rayner, C. A. Beauchemin, Assessing mathematical models of influenza infections using features of the immune response, PloS one 8 (2) (2013) e57088.

[45] H. M. Dobrovolny, M. J. Baron, R. Gieschke, B. E. Davies, N. L. Jumbe, C. A. Beauchemin, Exploring cell tropism as a possible contributor to influenza infection severity, PloS one 5 (11) (2010) e13811.

[46] B. Zhou, J. She, Y. Wang, X. Ma, The duration of viral shedding of discharged patients with severe COVID-19, Clinical Infectious Diseases (2020).

[47] D. S. Callaway, A. S. Perelson, HIV-1 infection and low steady state viral loads, Bulletin of mathematical biology 64 (1) (2002) 29–64.

[48] Y. Huang, S. L. Rosenkranz, H. Wu, Modeling hiv dynamics and antiviral response with consideration of time-varying drug exposures, adherence and phenotypic sensitivity, Mathematical biosciences 184 (2) (2003) 165–186.

[49] H. Dahari, A. Lo, R. M. Ribeiro, A. S. Perelson, Modeling hepatitis C virus dynamics: liver regeneration and critical drug efficacy, Journal of theoretical biology 247 (2) (2007) 371–381.

[50] A. Goyal, E. F. Cardozo-Ojeda, J. T. Schiffer, Potency and timing of antiviral therapy as determinants of duration of SARS-CoV-2 shedding and intensity of inflammatory response, medRxiv (2020).

[51] P. Cao, J. M. McCaw, The mechanisms for within-host influenza virus control affect model-based assessment and prediction of antiviral treatment, Viruses 9 (8) (2017) 197.

[52] J. Wu, W. Li, X. Shi, Z. Chen, B. Jiang, J. Liu, D. Wang, C. Liu, Y. Meng, L. Cui, et al., Early antiviral treatment contributes to alleviate the severity and improve the prognosis of patients with novel coronavirus disease (COVID-19), Journal of internal medicine (2020).

[53] S. Kaushal, A. S. Rajput, S. Bhattacharya, M. Vidyasagar, A. Kumar, M. K. Prakash, S. Ansumali, Estimating Hidden Asymptomatics, Herd Immunity Threshold and Lockdown Effects using a COVID-19 Specific Model, arXiv preprint arXiv:2006.00045 (2020).

[54] H. Ikeda, S. Nakaoka, R. J. de Boer, S. Morita, N. Misawa, Y. Koyanagi, K. Aihara, K. Sato, S. Iwami, Quantifying the effect of Vpu on the promotion of HIV-1 replication in the humanized mouse model, Retrovirology 13 (1) (2016) 23.

[55] M. Nowak, R. M. May, Virus dynamics: mathematical principles of immunology and virology, Oxford University Press, UK, 2000.

Apéndice F

Optimal control strategies to tailor antivirals for acute infectious diseases in the host: A study case of COVID-19.

Optimal control strategies to tailor antivirals for acute infectious diseases in the host: A study case of COVID-19.

Mara Perez[a], Pablo Abuin[a], Marcelo Actis[b], Esteban A. Hernandez-Vargas[c], Alejandro H. Gonzalez[a]

[a]*Institute of Technological Development for the Chemical Industry (INTEC), CONICET-UNL, Santa Fe, Argentina.*
[b]*Facultad de Ingeniería Química (FIQ), Universidad Nacional del Litoral (UNL) and Consejo Nacional de Investigaciones científicas y técnicas (CONICET), Santa Fe, Argentina.*
[c]*Instituto de Matematicas, Unidad Juriquilla, UNAM, Mexico*

Abstract

Several mathematical models in SARS-CoV-2 have shown how target-cell model can help to understand the spread of the virus in the host and how potential candidates of antiviral treatments can help to control the virus. Concepts as equilibrium and stability show to be crucial to qualitative determine the best alternatives to schedule drugs, according to effectivity in inhibiting the virus infection and replication rates. Important biological events such as rebounds of the infections (when antivirals are incorrectly interrupted) can also be explained by means of a dynamic study of the target-cell model. In this work a full characterization of the dynamical behavior of the target-cell models under control actions is made and, based on this characterization, the optimal fixed-dose antiviral schedule that produces the smallest amount of dead cells (without viral load rebounds) is computed. Several simulation results - performed by considering real patient data - show the potential benefits of both, the model characterization and the control strategy.

Keywords: In-host acute infection model, Equilibrium sets characterization, Stability analysis, Model predictive control.

1. Introduction

Mathematical models of with-in infections can be used to characterize pathogen dynamics, optimize drug delivery, uncover biological parameters (including pathogen and infected cell half-lives), design clinical trials, among others. They have been employed to study chronic (*i.e.:* HIV[1, 2], hepatitis B[3, 4], hepatitis C[5, 6]) and acute (*i.e.:* influenza [7, 8, 9], dengue[10, 11], Ebola[12]) infections. Currently, they are based on ordinary differential equations (ODE), which allows to analyze these systems employing mathematical and computational tools. This way, in-host basic reproduction numbers ($\mathcal{R}$), stability analysis of equilibrium states, analytical/numerical solutions, can be computed [13, 14, 15, 16]. Most of them are based on the target-cell limited model to represent chronic/acute infections according to the infection resolution respect to the target cell production and natural death rates [17]. This way, the equilibrium states differ from isolated equilibrium points (*i.e.:* disease free and infected equilibria) for the former to a continuous of equilibrium points (*i.e.:* disease free equilibrium set) for the latter ones. Note that for acute infections, the only feasible equilibria is the disease

free, since the pathogen particles at the end of infection will be cleared independently of the in-host reproduction number [17, 7, 18]. The existence of healthy equilibrium set implies that stability analysis can be performed considering equilibrium sets as a generalization of equilibrium points, which gives an environment to employ set-theoretic methods [19, 20], widely used in the design of set-based controllers, although not fully employed for modeling characterization and control of acute infections. Some preliminary results, which will be discuss later in this chapter, can be found in [21].

The control of infection can be modelled considering immune response mechanisms, where the infection is self-controlled by a combination of a non-specific and specific reactions [22, 23, 24], or by drug therapies. The inclusion of pharmacokinetic (PK) and pharamacodynamic (PD) models of drug therapies allows the inclusion of therapeutic effects on the pathogen evolution [6, 17]. Therefore, the models parameters can be changed exogenously by dose frequency and quantity, naturally limited by the inhibitory potential of the drug (expressed in terms of EC50, or drug concentration for inhibiting 50% of antigen particles) and its cytotoxic effect (expressed in terms of IC50, or drug concentration which causes death to 50% of susceptible cells) [25]. Moreover, since drugs are normally administrated by pills or intravenous injections, instantaneous jumps are observed in the concentration of the drug in some tissues. This is mathematically conceptualized as a discontinuity of the first kind and gives rise to the so-called impulsive control systems [26]. This model representation has been used for optimal control and state-feedback control with constraints for infectious diseases, such as: influenza [9, 27] and HIV [28, 26]. Even though optimal dosage can be computed for chronic and acute models, the unstable healthy equilibrium of the former (under certain circumstances; for details, see [17, 14]) and the availability of target cells above a critical level for the latter (as it is discuss later), involve the duration of drug therapy, with the presence of viral rebounds when therapy is disrupted. This effect has been noticed for chronic [29] and acute [30] infections. Taking into account this scenario, in this work, we formalize the existence of an optimal single interval drug delivery such that viral rebounds are avoided. Even though, the presented analysis is valid for the target-cell limited model for acute infections, taking into account the current worldwide contextual situation (COVID-19 pandemic), we prove our results using an identified model of infected patients with SARS-CoV-2 virus [31, 21, 32].

After the introduction given in Section 1 the chapter is organized as follows. Section 2 presents the general "in the host" models used to represent infectious diseases. Section 4 studies the way the antivirals affect the dynamic of the model, emphasizing the fact that the stability analysis made in Section 3 remains unmodified and, so, any control strategy must be designed accounting for these details. In Section 5 control design able to exploit the stability model characterization is introduced, and its benefits are shown by simulating several cases, in Section 6. Finally, conclusions are given in Section 7.

1.1. Notation

First let us introduce some basic notation. We consider $\mathbb{R}^n$ as n-dimensional Euclidean space equipped with the euclidean distance between two points defined by $d(x, y) := \|x - y\| = [(x - y)'(x - y)]^{1/2}$. The euclidean distance from a point x to a set $\mathcal{Y}$ is given by $d(x, \mathcal{Y}) := \|x\|_{\mathcal{Y}} = \inf\{\|x - y\| \colon y \in \mathcal{Y}\}$.

With $\mathcal{X}$ we will denote the constraint set of $\mathbb{R}^3$, given by

$$\mathcal{X} := \mathbb{R}^3_{\geq 0} = \{(x_1, x_2, x_3) \in \mathbb{R}^3 : x_1 \geq 0, x_2 \geq 0 \text{ and } x_3 \geq 0\}.$$

We will consider $\mathcal{X}$ endowed with the *inherit topology* of $\mathbb{R}^3$, i.e. the open sets are intersections of open set of $\mathbb{R}^3$ with $\mathcal{X}$. Thus, an open ball in $\mathcal{X}$ with center in x and radius $\varepsilon > 0$ is given by $\mathcal{B}_\varepsilon(x) := \{y \in \mathcal{X} : \|x - y\| < \varepsilon\}$ and an ε-neighborhood of set $\mathcal{Y} \subset \mathcal{X}$ is given by $\mathcal{B}_\varepsilon(\mathcal{Y}) := \{x \in \mathcal{X} : \|x\|_\mathcal{Y} < \varepsilon\}$. Let $x \in \mathcal{Y}$, we say that x is an interior point of $\mathcal{Y}$ if the there exist $\varepsilon > 0$ such that $\mathcal{B}_\varepsilon(x) \subseteq \mathcal{Y}$. The interior of $\mathcal{Y}$ is the set of all interior points of $\mathcal{Y}$ and it is denoted by $\mathrm{int}(\mathcal{Y})$.

We will denote with $\to$ the limit of a function to a real number, including infinity. In the case of monotone convergence, decreasing or increasing, we will use the symbols $\searrow$ and $\nearrow$, respectively.

2. Review of the target-cell-limited model for in-host infection

Mathematical models of in-host virus dynamic have shown to be useful to understand of the interactions that govern infections and, more important, to allows external intervention to moderate their effects [23]. According to recent research in the area [17, 21], the following ordinary differential equations (ODEs) are used in this work to describe the interaction between uninfected target or susceptible cells U [cell/mm^3], infected cells I [cell/mm^3], and virus V [copies/mL]:

$$\dot{U}(t) = -\beta U(t)V(t), \qquad U(0) = U_0, \tag{2.1a}$$

$$\dot{I}(t) = \beta U(t)V(t) - \delta I(t), \qquad I(0) = I_0, \tag{2.1b}$$

$$\dot{V}(t) = pI(t) - cV(t), \qquad V(0) = V_0, \tag{2.1c}$$

where β [mL.day^{-1}/copies] is the infection rate of healthy U cells by external virus V, δ [day^{-1}] is the death rates of I, p [(copies.mm^3/cell.mL).day^{-1}] is the production rate of free virus from infected cells I, and c [day^{-1}] is degradation (or clearance) rate of virus V by the immune system.

System (2.1) is positive, which means that $U(t) \geq 0$, $I(t) \geq 0$ and $V(t) \geq 0$, for all $t \geq 0$. We denote $x(t) := (U(t), I(t), V(t))$ the state vector, and $\mathcal{X} = \mathbb{R}^3_{\geq 0}$ the state constraints set.

The initial conditions of (2.1), which represent a healthy steady state before the infection, are assumed to be $V(t) = 0$, $I(t) = 0$, and $U(t) = U_0 > 0$, for $t < 0$. Then, at time $t = 0$, a small quantity of virions enters the host body and, so, a discontinuity occurs in $V(t)$. Indeed, $V(t)$ jumps from 0 to a small positive value V_0 at $t = 0$ (formally, $V(t)$ has a discontinuity of the first kind at t_0, *i.e.*, $\lim_{t\to 0^-} V(t) = 0$ while $\lim_{t\to 0^+} V(t) = V_0 > 0$).

Although the solution of (2.1) for $t \geq t_0$, being t_0 an arbitrary time, is unknown, we know that it depends on the **basic reproduction number** $\mathcal{R} := \frac{\beta p}{c\delta}$ and the initial conditions $(U(t_0), I(t_0), V(t_0)) \in \mathcal{X}$. Since $U(t) \geq 0, V(t) \geq 0$, for all $t \geq t_0$, $U(t)$ is a non increasing function of t (by 2.1.a). From [21] and [16], if $c >> \delta$ (as it is always the case) system (2.1) can be approximated by $\dot{U}(t) \approx -\beta U(t)V(t)$, $\dot{V}(t) \approx (\frac{\beta p}{c}U(t) - \delta)V(t)$, $I(t) \approx \frac{c}{p}V(t)$. Then, since $U(t_0) > 0$, conditions for V to increase or decrease at t_0, are given by $U(t_0)\mathcal{R} > 1$ and $U(t_0)\mathcal{R} < 1$, respectively. This means that for $U(t_0)\mathcal{R} \leq 1$, $V(t)$ goes asymptotically to zero for $t \to \infty$. Otherwise, if $U(t_0)\mathcal{R} > 1$, $V(t)$ reaches a maximum $\hat{V}$ and then goes asymptotically to zero, for $t \to \infty$. In this latter case it is said that the virus **spreads in the host**, since there is at least one time instant for which $\dot{V} > 0$ [21]. The so called **critical value of** U, U^*, is

defined as

$$U^* := 1/\mathcal{R}, \tag{2.2}$$

where $\mathcal{R}$ is assumed to remain constant for all $t \geq t_0$. The critical value U^* can be seen as the counterpart of the "herd immunity" in the epidemiological SIR-type models: i.e., $U(t)$ reaches U^* approximately at the same time as $V(t)$ and $I(t)$ reach their peaks or, in other words, $V(t)$ and $I(t)$ cannot increase anymore once $U(t)$ is below U^*. This way, conditions $U(t_0)\mathcal{R} > 1$ and $U(t_0)\mathcal{R} \leq 1$ that determines if $V(t)$ increases or decreases for $t \geq t_0$ can be rewritten as $U(t_0) > U^*$ and $U(t_0) \leq U^*$, respectively. In what follows, we assume that $U(0) > U^*$ (or $U(0)\mathcal{R} > 1$), which corresponds to the case of the outbreak of the infection (i.e., the virus does spread in the host), at time $t = 0$.

Let us now define $U_\infty := \lim_{t\to\infty} U(t)$, $V_\infty := \lim_{t\to\infty} V(t)$ and $I_\infty := \lim_{t\to\infty} I(t)$, which are values that depend on $\mathcal{R}$ and the initial conditions $U(t_0), V(t_0)$, $I(t_0)$. According to [21], $V_\infty = I_\infty = 0$, while U_∞ is a value in $(0, U(t_0))$, which will be characterized in the next section.

3. Equilibria characterization and stability

To find the equilibrium set of model (2.1), with initial conditions $(U(t_0), V(t_0), I(t_0)) \in \mathcal{X}$ at an arbitrary time $t_0 \geq 0$, $\dot{U}(t)$, $\dot{I}(t)$ and $\dot{V}(t)$ need to be equaled to zero, in (2.1). According to [21, 16] there is only one equilibrium set in $\mathcal{X}$, which is a healthy one, and it is defined by

$$\mathcal{X}_s := \{(U, I, V) \in \mathcal{X} : \ I = 0, \ V = 0\}, \tag{3.1}$$

To examine the stability of the equilibrium points in $\mathcal{X}_s$, a first attempt consists in linearizing system (2.1) at some state $x_s := (U_s, I_s, V_s) \in \mathcal{X}_s$, and analyzing the eigenvalues of the Jacobian matrix. As it is shown in [21], this matrix has one eigenvalue at zero ($\lambda_1 = 0$), one always negative ($\lambda_2 < 0$) and a third one, λ_3, that is negative, zero or positive depending on if U_s is smaller, equal of greater than U^*, respectively.

Since the maximum eigenvalue λ_3 is the one determining the stability of the system, it is possible to separate set $\mathcal{X}_s$ into two subsets, according to its behaviour. Then, a first intuition is that the equilibrium subset

$$\mathcal{X}_s^{st} := \{(U, I, V) \in \mathcal{X} : U \in [0, U^*], \ I = 0, \ V = 0\} \tag{3.2}$$

is stable, and that the equilibrium subset

$$\mathcal{X}_s^{un} := \{(U, I, V) \in \mathcal{X} : U \in (U^*, +\infty), \ I = 0, \ V = 0\}, \tag{3.3}$$

is unstable. However, this is not a conclusive analysis, given that one of the eigenvalues of the linearized system is null and so the linear approximation cannot be used to fully determine the stability of a nonlinear system (Theorem of Hartman-Grobman [33, section 2.8, pag. 120]).

Formal asymptotic stability of set $\mathcal{X}_s^{st}$, together with its corresponding domain of attraction, is analyzed in the next subsection.

3.1. Asymptotic stability of the equilibrium sets

A key point to properly analyze the asymptotic stability (AS) of system (2.1) is to consider the stability of the equilibrium sets $\mathcal{X}_s^{st}$ and $\mathcal{X}_s^{un}$, instead of the single points inside them, as defined in Definitions 3.2, 3.3 and 3.5 in the next subsection. Indeed, even when every equilibrium point in $\mathcal{X}_s^{st}$ is $\epsilon - \delta$ stable, there is no single equilibrium point in such set that is locally attractive.

As stated in Definition 3.5, the AS of $\mathcal{X}_s^{st}$ requires both, attractivity and $\epsilon - \delta$ stability, which are stated in subsections 3.3 and 3.4, respectively. Finally, in subsection 3.5 the AS theorem is formally stated.

3.2. Stability theory

In this section some basic definitions and results are given concerning the asymptotic stability of sets and Lyapunov theory, in the context of non-linear continuous-time systems ([19], Appendix B). All the following definitions are referred to system

$$\dot{x}(t) = f(x(t)), \;\; x(0) = x_0, \tag{3.4}$$

where x is the system state constrained to be in $\mathcal{X} \subseteq \mathbb{R}^n$, f is a Lipschitz continuous nonlinear function, and $\phi(t; x)$ is the solution for time t and initial condition x.

Definition 3.1 (Equilibrium set)**.** *Consider system 3.4 constrained by $\mathcal{X}$. The set $\mathcal{X}_s \subset \mathcal{X}$ is an equilibrium set if each point $x \in \mathcal{X}_s$ is such that $f(x) = 0$ (this implying that $\phi(t; x) = x$ for all $t \geq 0$).*

Definition 3.2 (Attractivity of an equilibrium set)**.** *Consider system 3.4 constrained by $\mathcal{X}$ and a set $\mathcal{Y} \subseteq \mathcal{X}$. A closed equilibrium set $\mathcal{X}_s \subset \mathcal{X}$ is attractive in $\mathcal{Y}$ if $\lim_{t\to\infty} \|\phi(t; x)\|_{\mathcal{X}_s} = 0$ for all $x \in \mathcal{Y}$. If $\mathcal{Y}$ is a ε-neighborhood of $\mathcal{X}_s$ for some $\eta > 0$, we say that $\mathcal{X}_s$ is locally attractive.*

We define the *domain of attraction* (DOA) of an attractive set $\mathcal{X}_s$ for the system 3.4 to be the set of all initial states x such that $\|\phi(t; x)\|_{\mathcal{X}_s} \to 0$ as $t \to \infty$. We use the term *region of attraction* to denote any set of initial states contained in the domain of attraction.

A closed subset of an attractive set (for instance, a single equilibrium point) is not necessarily attractive. On the other hand, any set containing an attractive set is attractive, so the significant attractivity concept in a constrained system is given by the smallest one. Indeed, given two different attractive sets in $\mathcal{X}$ with the same DOA, one must be contained in the other. So the family of all attractive sets in $\mathcal{X}$ with the same DOA is a totally ordered set under the set inclusion (nested family). An arbitrary (finite, countable, or uncountable) intersection of nested nonempty closed subsets of a compact space is a nonempty compact set [34]. Then if one element of the family is bounded, and therefore compact, the intersection of all the family is a nonempty compact set. This set is the *smallest atractive set* we are referring to.

Definition 3.3 (Local $\epsilon - \delta$ stability of an equilibrium set)**.** *Consider system 3.4 constrained by $\mathcal{X}$. A closed equilibrium set $\mathcal{X}_s \subset \mathcal{X}$ is $\epsilon - \delta$ locally stable if for all $\epsilon > 0$ there exists $\delta > 0$ such that if $\|x\|_{\mathcal{X}_s} < \delta$ then $\|\phi(t; x)\|_{\mathcal{X}_s} < \epsilon$, for all $t \geq 0$.*

Unlike attractive sets, a set containing a locally $\epsilon - \delta$ stable equilibrium set is not necessarily locally $\epsilon - \delta$ stable. Even more, a closed subset of a locally $\epsilon - \delta$ stable equilibrium set (for instance, a single equilibrium point) is not necessarily locally $\epsilon - \delta$ stable. However, any (finite) union of equilibrium sets locally $\epsilon - \delta$ stable is also locally

$\epsilon - \delta$ stable. So the significant stability concept in a constrained system is given by the largest one.

Although a finite union of equilibrium set locally $\epsilon - \delta$ stable is also locally $\epsilon - \delta$ stable, in general we cannot extend this result to the case of arbitrary unions of points. Thus, even when every equilibrium point of an equilibrium set is locally $\epsilon - \delta$ stable, we cannot assure that the whole set would be locally $\epsilon - \delta$ stable. This is due to the fact that given a fixed ϵ the δ chosen for each point depend on the point and so the infimum of them could be zero. However, if in addition we also assume that the set is compact, then the stability of the set can be inherited from the stability of its points.

Lemma 3.4. *Let $\mathcal{X}_s$ be a compact equilibrium set. If every $x_s \in \mathcal{X}_s$ is $\epsilon - \delta$ locally stable, then $\mathcal{X}_s$ is $\epsilon - \delta$ locally stable.*

Proof. Given $\epsilon > 0$, there exists $\delta = \delta(x_s) > 0$ for each $x_s \in \mathcal{X}_s$ such that if $x \in B_{\delta(x_s)}(x_s)$ then $\phi(t; x) \in B_\epsilon(x_s)$ for $t \geq 0$. The family of δ-balls form a open cover of $\mathcal{X}_s$. Let us denote the union of this cover V, i.e. $V := \bigcup\{B_{\delta(x_s)}(x_s) : x_s \in \mathcal{X}_s\}$. Since $\mathcal{X}_s$ is compact and the complement of V is closed, then the distance between them is strictly positive, i.e. $\delta^* := d(\mathcal{X}_s, V^c) > 0$. Therefore, the δ^* neighborhood of the equilibrium set $\mathcal{X}_s$ is contained in V. Thus if $x \in B_{\delta^*}(\mathcal{X}_s) \subset V$ then $\phi(t; x) \in B_\epsilon(\mathcal{X}_s)$ for $t \geq 0$ .Therefore $\mathcal{X}_s$ is $\epsilon - \delta$ locally stable. □

Definition 3.5 (Asymptotic stability (AS) of an equilibrium set)**.** *Consider system 3.4 constrained by $\mathcal{X}$ and a set $\mathcal{Y} \subseteq \mathcal{X}$. A closed equilibrium set $\mathcal{X}_s \subset \mathcal{X}$ is asymptotically stable (AS) in $\mathcal{Y}$ if it is $\epsilon - \delta$ locally stable and attractive in $\mathcal{Y}$.*

Next, the theorem of Lyapunov, which refers to single equilibrium points and provides sufficient conditions for both, local $\epsilon - \delta$ stability and assymptotic stability, is introduced.

Theorem 3.6. (Lyapunov's stablity theorem [35, Theorem 4.1]) *Consider system 3.4 constrained by $\mathcal{X}$ and an equilibrium state $x_s \in \mathcal{X}_s$. Let $\mathcal{Y} \subset \mathcal{X}$ be a neighborhood of x_s and consider a function $V(x) : \mathcal{Y} \to \mathbb{R}$ such that $V(x) > 0$ for $x \neq x_s$, $V(x_s) = 0$ and $\dot{V}(x(t)) \leq 0$, denoted as Lyapunov function. Then, the existence of such a function in a neighborhood of x_s implies that $x_s \in \mathcal{X}_s$ is locally $\epsilon - \delta$ stable in $\mathcal{Y}$. If in addition $\dot{V}(x(t)) < 0$ for all $x \neq x_s$, then x_s is asymptotically stable in $\mathcal{Y}$.*

3.3. Attractivity of set $\mathcal{X}_s^{st}$

Before we deal with the attractivity of set $\mathcal{X}_s^{st}$, we need to delve into the behavior of U_∞. As is presented in [21], U_∞ can be expressed as a function of initial conditions as follows

$$U_\infty(U(t_0), I(t_0), V(t_0)) = -\frac{W(-\mathcal{R}U(t_0)e^{-\mathcal{R}(U(t_0)+I(t_0)+\frac{\delta}{p}V(t_0))})}{\mathcal{R}} \tag{3.5}$$

where $W(\cdot)$ is (the principal branch of) the Lambert function and $(U(t_0), I(t_0), V(t_0))$ are arbitrary initial conditions at a given time $t_0 \geq 0$. For each $\varepsilon \geq 0$ let us define a domain of $\mathcal{X}$ given by

$$\Omega(\varepsilon) = \{(U, I, V) \in \mathcal{X} : I \geq \varepsilon, V \geq \varepsilon\}. \tag{3.6}$$

The following Lemma describe the behavior of the maximum of U_∞ on each $\Omega(\varepsilon)$.

Lemma 3.7 (Maximum of the function U_∞)**.** *Consider the function U_∞ given by* (3.5) *and for each $\varepsilon \geq 0$ the domains $\Omega(\varepsilon)$ given by* (3.6)*. Then the maximum of $U_\infty(U, I, V)$ in $\Omega(\varepsilon)$ is reached in $(U^*, \varepsilon, \varepsilon)$. In particular, the maximum value of U_∞ over $\Omega(0)$ is reached in $(U^*, 0, 0)$ and is given by $U_\infty(U^*, 0, 0) = U^*$, where $U^* = 1/\mathcal{R}$.*

Proof. According to (3.5), U_∞ can be written as

$$U_\infty(U, I, V) = -\frac{W(-f(U, I, V))}{\mathcal{R}},$$

with $f(U, I, V) = \mathcal{R}Ue^{-\mathcal{R}(U+I+\delta/pV)}$. Since $-W(-\cdot)$ is an increasing (injective) function then $U_\infty(U, I, V)$ achieves its maximum over $\Omega(\varepsilon)$ at the same values as $f(U, I, V)$. Then, we focus our attention in finding the maximum (and the maximizing variables) of $f(U, I, V)$.

Through the change of variables $x = \mathcal{R}U$ and $y = \mathcal{R}(I + \delta/pV)$, f can be studied as a function of the form $g(x, y) = xe^{-(x+y)}$. Note that $(U, I, V) \in \Omega(\varepsilon)$ if and only if $x \geq 0$ and $y \geq \eta$ where $\eta := \mathcal{R}(1 + \frac{\delta}{p})\varepsilon \geq 0$. Therefore to find extremes of f in $\Omega(\varepsilon)$ it is enough to study the extreme points of g over $\Omega' = \{(x, y) \in \mathbb{R}^2_{\geq 0} : \ y \geq \eta\}$.

Since $\nabla g = [(1 - x)e^{-(x+y)}, -xe^{-(x+y)}]$ does not vanish and $g \to 0$ when $\|(x, y)\| \to \infty$, then the maximum is reached at the boundaries of Ω'. A simple analysis shows that g restricted to the boundary of Ω' achieves its maximum in $(1, \eta)$. This means that $f(U, I, V)$ achieves its maximum in $U = 1/\mathcal{R} = U^*$ and $I = V = \varepsilon$.

In particular, when $\varepsilon = 0$, $f(U, I, V)$ reaches its maximum in $(U^*, 0, 0)$. Furthermore,

$$U_\infty(U^*, 0, 0) = -\frac{W(-f(U^*, 0, 0))}{\mathcal{R}} = -\frac{W(-1/e)}{\mathcal{R}} = \frac{1}{\mathcal{R}} = U^*,$$

which concludes the proof. □

Let us now deal with attractivity of set $\mathcal{X}_s^{st}$. According to Definition 3.2, any set containing an attractive set is also attractive. So, we are in fact interested in finding the smallest closed attractive set in $\mathcal{X}\backslash\mathcal{X}_s^{un}$.

Theorem 3.8 (Attractivity of $\mathcal{X}_s^{st}$)**.** *Consider system* (2.1) *constrained by $\mathcal{X}$. Then, the set $\mathcal{X}_s^{st}$ defined in* (3.2) *is the smallest attractive set in $\mathcal{X}\backslash\mathcal{X}_s^{un}$. Furthermore, $\mathcal{X}_s^{un}$, defined in* (3.3)*, is not attractive.*

Proof. The proof is divided into two parts. First it is proved that $\mathcal{X}_s^{st}$ is an attractive set, and then, that it is the smallest one.

Attractivity of $\mathcal{X}_s^{st}$: To prove the attractivity of $\mathcal{X}_s^{st}$ in $\mathcal{X}$ (and to show that $\mathcal{X}_s^{un}$ is not attractive) we needs to prove that $U_\infty \in [0, U^*]$ for any initial conditions and values of $\mathcal{R}$. The minimum of U_∞ is given by $U_\infty = 0$, and it is reached when $U(t_0) = 0$ (for any value of $\mathcal{R}$, $I(t_0)$ and $V(t_0)$). The maximum of U_∞, on the other hand, is given by $U_\infty = U^*$, and it is reached only when $U(t_0) = U^*$ and $I(t_0) = V(t_0) = 0$ (for any value of $\mathcal{R}$), as it is shown in Lemma 3.7. Then, for any $(U(t_0), I(t_0), V(t_0)) \in \mathcal{X}$ and $\mathcal{R} > 0$, $U_\infty(\mathcal{R}, U(t_0), I(t_0), V(t_0)) \in [0, U^*]$, which means that $\mathcal{X}_s^{st}$ is attractive, and the proof of attractivity is complete.

Figure 1 shows how U_∞ behaves as function of $U(t_0)$ and $V(t_0)$, when $I(t_0) = 0$ and $I(t_0) = 5e^5$. The first one is the scenario corresponding to $t = 0$, when a certain amount of virus enters the healthy host.

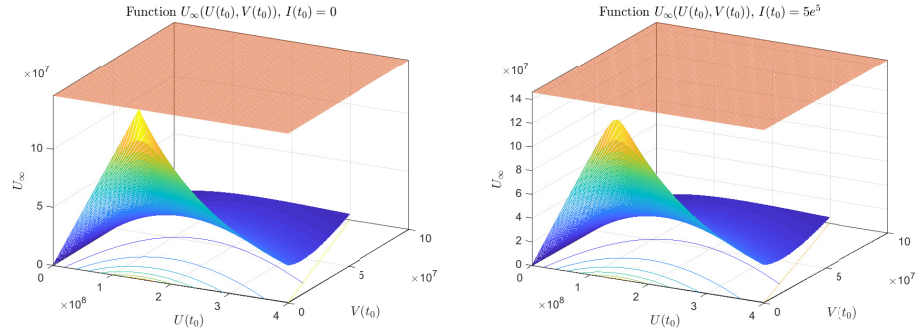

(a) U_∞ as function of $U(t_0)$ and $V(t_0)$, when $I(t_0) = 0$. The orange plane represents $U^* = 1/\mathcal{R} = 1.5e^8$. The maximum of U_∞ is reached when $U(t_0) = U^*$ and $V(t_0) = 0$, and is given by U^*. Patient A.

(b) U_∞ as function of $U(t_0)$ and $V(t_0)$, when $I(t_0) = 5e^5$. The orange plane represents $U^* = 1/\mathcal{R} = 1.5e^8$. The maximum of U_∞ is reached when $U(t_0) = U^*$ and $V(t_0) = 0$, and is smaller than U^*. Patient A.

Figure 1: Function $U_\infty(U(t_0), V(t_0))$, for different values of $I(t_0)$.

$\mathcal{X}_s^{st}$ is the smallest attractive set: It is clear from the previous analysis, that any initial state $x(t_0) = (U(t_0), I(t_0), V(t_0)) \in \mathcal{X}$ converges to a state $x_\infty = (U_\infty, 0, 0)$ with $U_\infty \in [0, U^*]$. This means that $\mathcal{X}_s^{un}$ is not attractive for any point in $\mathcal{X} \backslash \mathcal{X}_s$. However, to show that $\mathcal{X}_s^{st}$ is the smallest attractive set, we need to prove that every point $x_s \in \mathcal{X}_s^{st}$ is necessary for the attractiveness.

Let us consider a initial state of the form $(U^*, I(t_0), 0)$ with $I(t_0) \geq 0$. Since W is a bijective function from $(-1/e, 0)$ to $(-1, 0)$, then $U_\infty(\mathcal{R}, U^*, \cdot, 0)$ is bijective from $(0, +\infty)$ to $(0, U^*)$. Hence for every point $x_s \in \text{int}(\mathcal{X}_s^{st})$ there exists $I(t_0) \geq 0$ such that the initial state $(U^*, I(t_0), 0)$ converges to x_s. Since every interior point of $\mathcal{X}_s^{st}$ is necessary for the attractiveness, then the smallest closed attractive set is $\mathcal{X}_s^{st}$, and the proof is concluded. □

3.4. Local $\epsilon - \delta$ stability of $\mathcal{X}_s^{st}$

The next theorem shows the formal Lyapunov (or $\epsilon - \delta$) stability of the equilibrium set $\mathcal{X}_s^{st}$.

Theorem 3.9 (Local $\epsilon - \delta$ stability of $\mathcal{X}_s^{st}$)**.** *Consider system* (2.1) *constrained by* $\mathcal{X}$*. Then, the equilibrium set* $\mathcal{X}_s^{st}$ *defined in* (3.2) *is the largest locally* $\epsilon - \delta$ *stable.*

Proof. We proceed by analysing the stability of single equilibrium points $\bar{x} := (\bar{U}, 0, 0)$, with $\bar{U} \in (0, U_0]$ (i.e., $\bar{x} \in \mathcal{X}_s \backslash \{(0, 0, 0)\}$). For each $\bar{x}$ let us consider the following Lyapunov function candidate

$$J(x) := U - \bar{U} - \bar{U} \ln\left(\frac{U}{\bar{U}}\right) + I + \frac{\delta}{p} V. \tag{3.7}$$

This function is continuous in $\mathcal{X}$, is positive for all nonegative $x \neq \bar{x}$ and $J(\bar{x}) = 0$. Furthermore, for $x(t) \in \mathcal{X}$ and $t \geq 0$ we have

$$\dot{J}(x(t)) = \frac{\partial J}{\partial x}\dot{x}(t) = \begin{bmatrix} \frac{dJ}{dU} & \frac{dJ}{dI} & \frac{dJ}{dV} \end{bmatrix} \begin{bmatrix} -\beta U(t)V(t) \\ \beta U(t)V(t) - \delta I(t) \\ pI(t) - cV(t) \end{bmatrix}$$

$$= \begin{bmatrix} (1 - \frac{\bar{U}}{U(t)}) & 1 & \frac{\delta}{p} \end{bmatrix} \begin{bmatrix} -\beta U(t)V(t) \\ \beta U(t)V(t) - \delta I(t) \\ pI(t) - cV(t) \end{bmatrix}$$

$$= (-\beta U(t)V(t) + \bar{U}\beta V(t)) + (\beta U(t)V(t) - \delta I(t)) + \left(\delta I(t) - \frac{\delta c}{p}V(t)\right)$$
$$= \bar{U}\beta V(t) - \frac{\delta c}{p}V(t) = V(t)\left(\bar{U}\beta - \frac{\delta c}{p}\right),$$

where $\dot{x}(t)$ represents system (2.1). Function $\dot{J}(x(t))$ depends on $x(t)$ only through $V(t)$. So, independently of the value of the parameter $\bar{U}$, $\dot{J}(x(t)) = 0$ for $V(t) \equiv 0$. This means that for any single $x(0) \in \mathcal{X}_s$, $V(0) = I(0) = 0$ and so, $V(t) = 0$, for all $t \geq 0$. So $\dot{J}(x(t))$ is null for any $x(0) \in \mathcal{X}_s$ (i.e, it is not only null for $x(0) = \bar{x}$ but for any $x(0) \in \mathcal{X}_s$).

On the other hand, for $x(0) \notin \mathcal{X}_s$, function $\dot{J}(x(t))$ is negative, zero or positive, depending on if the parameter $\bar{U}$ is smaller, equal or greater than $U^* = \frac{\delta c}{\beta p}$, respectively, and this holds for all $x(0) \in \mathcal{X}$ and $t \geq 0$. So, for any $\bar{x} \in \mathcal{X}_s^{st}$, $\dot{J}(x(t)) \leq 0$ (particularly, for $\bar{x} = (\bar{U}, 0, 0) = (U^*, 0, 0)$, $\dot{J}(x(t)) = 0$, for all $x(0) \in \mathcal{X}$ and $t \geq 0$) which means that each $\bar{x} \in \mathcal{X}_s^{st}$ is locally $\epsilon - \delta$ stable (see Theorem 3.6).

Finally, when $\bar{U} = 0$, i.e. $\bar{x} = (0, 0, 0)$, we define the Lyapunov functional as $J(x) = U - I + \delta/pV$ and we proceed analogously as before to prove the local $\epsilon - \delta$ stability of the origin.

Therefore, since every state in $\mathcal{X}_s^{st}$ is locally $\epsilon - \delta$ stable and $\mathcal{X}_s^{st}$ is compact, by Lemma 3.4, the whole set $\mathcal{X}_s^{st}$ is locally $\epsilon - \delta$ stable.

Finally, since $\mathcal{X}_s^{st}$ is attractive in $\mathcal{X} \backslash \mathcal{X}_s^{un}$ then it is impossible for any $x \in \mathcal{X}_s^{un}$ to be $\epsilon - \delta$ stable, which implies that $\mathcal{X}_s^{st}$ is also the largest locally $\epsilon - \delta$ stable set in $\mathcal{X}_s$, which completes the proof. □

Remark 3.10. *In the latter proof, if we pick a particular $\bar{x} \in \mathcal{X}_s^{st}$, then $\dot{J}(x(t))$ is not only null for $x(0) = \bar{x}$ but for all $x(0) \in \mathcal{X}_s^{st}$, since in this case, $V(t) = 0$, for $t \geq 0$. This means that it is not true that $\dot{J}(x(t)) < 0$ for every $x \neq \bar{x}$, and this is the reason why we cannot use the last part of Theorem 3.6 to ensure the asymptotic stability of particular equilibrium points (or subsets of $\mathcal{X}_s^{st}$). In fact, they are $\epsilon - \delta$ stable, but not attractive.*

3.5. Asymptotic stability of $\mathcal{X}_s^{st}$

In the next Theorem, based on the previous results concerning the attractivity and $\epsilon - \delta$ stability of $\mathcal{X}_s^{st}$, the asymptotic stability is formally stated.

Theorem 3.11. *Consider system* (2.1) *constrained by the positive set $\mathcal{X}$. Then, the set $\mathcal{X}_s^{st}$ defined in* (3.2) *is the unique asymptotically stable (AS) equilibrium set, with a domain of attraction (DOA) given by $\mathcal{X} \backslash \mathcal{X}_s^{un}$. Furthermore, $\mathcal{X}_s^{un}$ is unstable.*

Proof. The proof follows from Theorems 3.8, which states that $\mathcal{X}_s^{st}$ is the smallest attractive in $\mathcal{X}$, and 3.9, which states that $\mathcal{X}_s^{st}$ is the largest locally $\epsilon - \delta$ stable set in $\mathcal{X}$. □

Figures 2 shows phase portrait plots of system (2.1), corresponding to different initial conditions.

3.6. U_∞ as function of initial conditions

In this section some characteristics of system (2.1) concerning the value of U_∞ as a function of the reproduction number $\mathcal{R}$ and the initial conditions are analyzed. Consider the next Property.

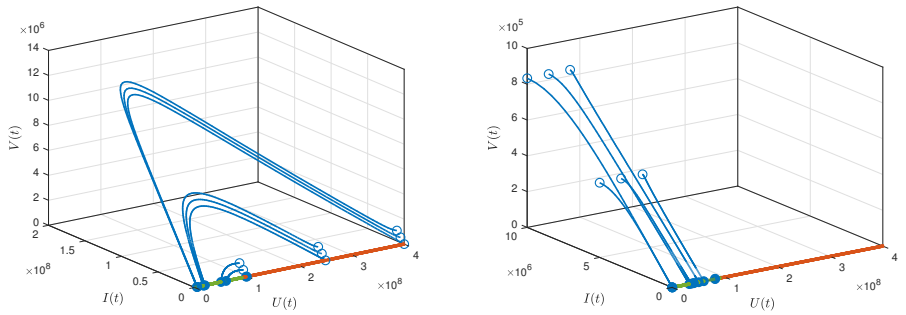

(a) (b)

Figure 2: Phase portrait for virtual patient A, described in Section 3.7. (a) Case $U(t_0) > U^*$. States arbitrarily close to $\mathcal{X}_s^{un}$ (in red), converges to $\mathcal{X}_s^{st}$ (in green), so the virus spreads in the host. (b) Case $U(t_0) < U^*$. States arbitrarily close to $\mathcal{X}_s^{st}$, converges to $\mathcal{X}_s^{st}$, so the virus does not spread in the host. Empty circles represent the initial state, while solid circles represent final states.

Property 3.12. *Consider system* (2.1) *with arbitrary initial conditions* $(U(t_0), I(t_0), V(t_0)) \in \mathcal{X}$*, for some* $t_0 \geq 0$*. Then:*

i. For any value of $U(t_0) > 0$, $I(t_0) > 0$, $V(t_0) > 0$, $U_\infty(\mathcal{R}, U(t_0), I(t_0), V(t_0)) \to 0$, *when* $\mathcal{R} \to \infty$*; while* $U_\infty(\mathcal{R}, U(t_0), I(t_0), V(t_0))$ *remains close to* $U(t_0)$ *when* $\mathcal{R} \to 0$*.*

ii. For $U(t_0) > U^*$ *and fixed* $I(t_0) > 0$, $V(t_0) > 0$ *and* $\mathcal{R} > 0$, $U_\infty(\mathcal{R}, U(t_0), I(t_0), V(t_0))$ *decreases when* $U(t_0)$ *increase, and* $U_\infty(\mathcal{R}, U(t_0), I(t_0), V(t_0)) < U^*$*. This means that the closer* $U(t_0)$ *is to* U^* *from above, the closer will be* U_∞ *to* U^* *from below.*

iii. For $U(t_0) < U^*$ *and fixed* $I(t_0) > 0$, $V(t_0) > 0$ *and* $\mathcal{R} > 0$, $U_\infty(\mathcal{R}, U(t_0), I(t_0), V(t_0))$ *increases with* $U(t_0)$*, and* $U_\infty(\mathcal{R}, U(t_0), I(t_0), V(t_0)) < U^*$*. This means that smaller values of* $U(t_0)$ *produce smaller values of* U_∞*, both below* U^**.*

iv. For any fixed $U(t_0)$ *and* $\mathcal{R} > 0$, $U_\infty(\mathcal{R}, U(t_0), I(t_0), V(t_0))$ *decrease with* $I(t_0)$ *and* $V(t_0)$*, and* $U_\infty(\mathcal{R}, U(t_0), I(t_0), V(t_0)) \leq U^*$*.*

v. For fixed $\mathcal{R} > 0$, $U(t_0) = U^*$ *and* $I(t_0) = V(t_0) = 0$, $U_\infty(\mathcal{R}, U(t_0), I(t_0), V(t_0))$ *reaches its maximum over* $\mathcal{X}$*, and the maximum value is given by* U^* *(see Lemma 3.7).*

The proof of the properties are omitted for brevity. However, Figures 1 and 3 show how U_∞ behaves for different values of initial conditions.

3.7. Simulation example

All along this work we use a virtual patient, denoted as patient A, to demonstrate the results of each section. The parameters of patient A were estimated by using viral load data of a RT-PCR COVID-19 positive patient —reported in [31] and used in [21, 32]— and are given by $\beta = 1.35 \times 10^{-7}$, $\delta = 0.61$, $p = 0.2$ and $c = 2.4$. The initial conditions are given by: $U_0 = 4 \times 10^8$, $I_0 = 0$ and $V_0 = 0.31$. Furthermore, the reproduction number is $\mathcal{R} = 1.84 \times 10^{-8}$, while the critical value for the susceptible

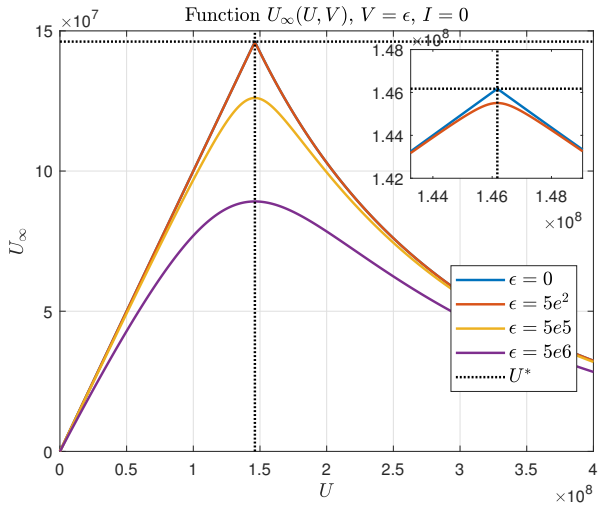

Figure 3: Function $U_\infty(U,V)$, for different values of ϵ, when $U \in [0, U_{\max}]$, $V = \epsilon$ and $I = 0$. As it can be seen, the supremum of U_∞ (given by U^*) is achieved when $U = U^*$ and $I \to 0$.

cells is $U^* = 5.44 \times 10^7$. The final value of U (if no antiviral treatment is applied) is given by $U_\infty = 2.57 \times 10^5$, which means that the area under the curve of V, given by $AUC_V := \int_0^\infty V(t)dt$, is 5.45×10^7 (see Remark 3.13). The peak of V is given by $\hat{V} = 1.98 \times 10^7$. Figure 4 shows the time response corresponding to patient A. As predicted, U_∞ is (significantly) smaller than U^*, which means that antivirals reducing (even for a finite period of time) either p or β will increase U_∞ and, so, will reduce the AUC_V and, probably, the peak of V.

Remark 3.13. *Note that from system* (2.1)*, by replacing* (2.1a) *in* (2.1b) *and then, after rearranging, in* (2.1c)*, $V(t)$ can be expressed as $V(t) = \frac{1}{c}[-\frac{p}{\delta}(\dot{I}(t) + \dot{U}(t)) - \dot{V}(t)]$. Therefore, the area under the curve of V, between times t_1 and t_2 is given by $AUC_V := \int_{t_1}^{t_2} V(t)dt = \frac{1}{c}[\frac{p}{\delta}(U(t_1) - U(t_2) + I(t_1) - I(t_2)) + V(t_1) - V(t_2)]$. Therefore, assuming $U(t_1) = U(t_0)$, $I(t_1) = I(t_0)$, $V(t_1) = V(t_0)$, with $U(t_0) \gg I(t_0)$, $U(t_0) \gg V(t_0)$, and $U(t_2) = U_\infty$, $I(t_2) = 0$ and $V(t_2) = 0$, which gives: $AUC_V \approx \frac{1}{c}[\frac{p}{\delta}(U(t_0) - U_\infty)]$. This way, if U_∞ is increased with respect to the value corresponding to the untreated case, the area under the curve of viral load decreases. Moreover, as it was shown in [16], the viral load at time to peak is monotonically decreasing with antiviral therapy reducing β or p.*

4. Inclusion of PK and PD of antiviral treatment

The idea now is to formally incorporate the pharmacodynamic (PD) and pharmacokinetics (PK) of antivirals into system 2.1, to obtain a controlled system, i.e. a system with certain control actions - given by the antivirals - that allows us to (even partially) modify the whole system dynamic according to some control objectives. In contrast to vaccines that kill the virus, antiviral just inhibits the virus infection and replication rates, so reducing the advance of the infections in the respiratory tract. The PD is introduced in system (2.1) as follows:

$$\dot{U}(t) = -\beta(1 - \eta(t))U(t)V(t), \tag{4.1a}$$

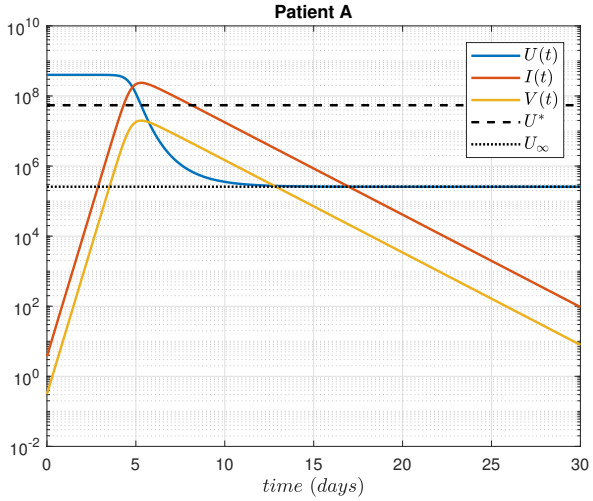

Figure 4: Time evolution of virtual patient A. As $c >> \delta$ (as it is always the case for real patient data), $I(t) \approx \frac{c}{p} V(t)$ for all $t \geq 0$.

$$\dot{I}(t) = \beta(1 - \eta(t))U(t)V(t) - \delta I(t) \tag{4.1b}$$

$$\dot{V}(t) = pI(t) - cV(t), \tag{4.1c}$$

where $\eta(t) \in [0, 1)$ represents the inhibition antiviral effects affecting the infection rate β (note that, according to [16], the effect of antivirals on the replication rate p, is analogous to the one on β, since both parameters affect in the same way the reproduction number $\mathcal{R}$).

On the other hand, the PK is modeled as a one compartment with an impulsive input action (to properly account for pills intakes or injections):

$$\dot{D}(t) = -\delta_D D(t), \;\; t \neq t_k, \tag{4.2a}$$

$$D(t_k) = D(t_k^-) + u_{k-1}, \;\; k \in \mathbb{I}, \tag{4.2b}$$

where D is the amount of drug available (with $D(0) = D_0 = 0$), δ_D is the drug elimination rate and the antiviral dose u_k enters the system impulsively at times $t_k := kT$, with $T > 0$ being a fix time interval and $k \in \mathbb{I}$. Time t_k^- denotes the time just before t_k, i.e., $D(t_k^-) = \lim_{\delta \to 0^+} D(t_k - \delta)$. Note that (4.2) is a continuous-time system impulsively controlled, which shows discontinuities of the first kind (jumps) at times t_k and free responses in $t \in [t_k, t_{k+1})$ (see [26] for details).

Finally, the way the drug D enters system (4.1) is by means of η as follows:

$$\eta(t) \;\; = \;\; \frac{D(t)}{D(t) + EC_{50}} \tag{4.3}$$

where EC_{50} represents the drug concentration in the blood where the drug is half-maximal. $\eta(t)$ is assumed to be in $[0, \eta_{\max})$, with $\eta_{\max} < 1$ (not full antiviral effect is considered, since this is an unrealistic scenario).

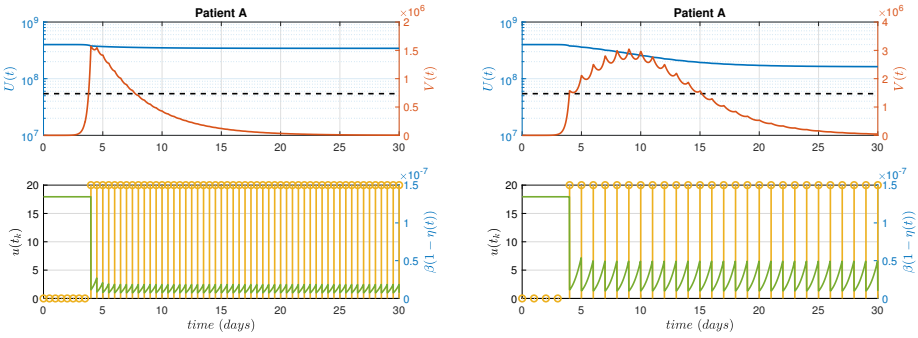

(a) (b)

Figure 5: (a) Time evolution of virtual patient A, with $u = 20$ mg of antivirals and $T = 1$ days. (b) Time evolution of virtual patient A, with $u = 20$ mg of antivirals and $T = 2$ days.

4.1. Impulsive scheme

Based on the PK and PD previous analysis, the complete Covid-19 infection model, taking into account an antiviral treatment (the controlled system) reads as follows:

$$\dot{U}(t) = -\beta(1-\eta(t))U(t)V(t), \quad t \neq t_k, \tag{4.4a}$$

$$\dot{I}(t) = \beta(1-\eta(t))U(t)V(t) - \delta I(t), \quad t \neq t_k, \tag{4.4b}$$

$$\dot{V}(t) = pI(t) - cV(t), \quad t \neq t_k, \tag{4.4c}$$

$$\dot{D}(t) = -\delta_D D(t), \quad t \neq t_k, \tag{4.4d}$$

$$D(t_k) = D(t_k^-) + u_{k-1}, \quad k \in \mathbb{I} \tag{4.4e}$$

with initial conditions given by $x_0 = (U_0, I_0, V_0, D_0)$. Given that $D(t) \geq 0$ for all $t \geq 0$, the constraint set $\mathcal{X}$ is enlarged to be $\tilde{\mathcal{X}} := \mathbb{R}^4_{\geq 0}$. Also, a constraint for the input, u, is defined as $\tilde{\mathbb{U}} := \{u \in \mathbb{R} : 0 \leq u \leq u_{\max}\}$, where $u_{\max}$ represent the maximal antiviral dosage ($u_{\max}$ is usually determined by the drug side effects and maximal effectivity, $0 \leq \eta_{\max} < 1$), while sets $\mathcal{X}$ is enlarged by considering $\tilde{\mathcal{X}} := \mathcal{X} \times \mathbb{R}_{\geq 0}$. A detailed study of the stability of impulsive systems can be seen in [36].

4.2. Simulation example

We resume here the simulation of the virtual patient A, to demonstrate the impulsive control actions describing the effects of antiviral administration. It is assumed that antivirals affect the infection rate β, while the initial condition for D is $D_0 = 0$, $\delta_D = 2$ (days^{-1}) and $EC_{50}^p = 75$ (mg). A scenario of 30 days was simulated, and a permanent dose of $u_k = 20$ (mg) of antivirals is administered each T days, starting at $t_i = 4$ days, with $T = 1$, $T = 2$ and $T = 0.5$. As shown in Figures 5a - 5b, the system response is quite different for different sampling times. For $T = 1$ days, the antiviral treatment is able to decreases V from the beginning. On the other hand, for $T = 2$, the treatment is unable to stop the spread of the virus (V continue increasing after the treatment is initiated), as it is shown in Figure 5b. Clearly, the effect of larger values of T is equivalent to smaller values of the dose u_k. In what follows, for the sake of clarity, T will be fixed in 1 day and only the (constant) value of the doses u_k - together with the initial and final time of the treatment - will be modified to analyze the different outcomes.

5. Control Strategies to Tailor Therapies

Control objectives in 'in host' infections can be defined in several ways. The peak of the virus load uses to be a critical index to minimize, since it is directly related to the severity of the infection and the ineffective capacity of the host. However, other indexes - usually put in a second place - are also important. This is the case of the time the infection lasts in the host over significant levels [16] - including virus rebounds after reaching a pseudo steady state, and the total viral load or infected cells at the end of the infection (i.e., the AUC of V and I). These latter indexes also informs (in a different manner) about the severity of the infection and the time during which the host is able to infect other individuals, and are directly determined by the amount of susceptible cells at the end of the infection. So the twofold control objective is defined as follows:

Definition 5.1 (Control objectives)**.** *The control objective for the closed-loop* (4.4) *consists in both, maximize the final value of susceptible/uninfected cells at the end of the infection, U_∞ and minimize the virus peak, $\hat{V}$. We denote these objectives a Objective 1 and 2, respectively.*

As it was said in the previous Section, antivirals affect the infection rate β, by the time-variant factor $(1-\eta(t))$. Accordingly, the reproduction number $\mathcal{R}$ will be also time varying, following the formula:

$$\mathcal{R}(t) := \frac{\beta(1-\eta(t))p}{c\delta}, \tag{5.1}$$

and the original reproduction number - i.e., the one corresponding to no treatment - will be denoted as $\mathcal{R}(0)$ for clarity ($\mathcal{R}(0)$ is the reproduction number at the outbreak of the infection, when $u_0 = 0$ and $\eta = 0$).

We will assume in the following a single interval antiviral treatment, consisting in a single fixed dose of antiviral, applied during a finite period of time. At the outbreak of the infection ($t = 0$), it is $(U(0), I(0), V(0)) := (U_0, 0, \epsilon)$, with $\epsilon > 0$ arbitrary small. Then, the single interval treatment is defined by the following input function:

$$u_k = u(t_k) = \begin{cases} 0 & \text{for } t_k \in [0, t_i), \\ u_i & \text{for } t_k \in [t_i, t_f], \\ 0 & \text{for } t_k \in (t_f, \infty). \end{cases} \tag{5.2}$$

where $t_i < \hat{t}(\mathcal{R}(0))$, being $\hat{t}(\mathcal{R}(0))$ the time of the peak of $V(\tau)$ when no treatment is implemented, $u_i \in [0, u_{\max}]$, and $t_f > t_i$, but finite. Note that after t_f, $u(t_k) = 0$, which means that $\eta(t) \to 0$ and $\mathcal{R} \to \mathcal{R}(0)$.

5.1. First control objective: maximizing the final value of the uninfected cells

The control problem we want to solve first reads as follows: for a given initial time, $t_i < \hat{t}$, find u_i (which has an associated $\mathcal{R}_i$, and η_i) and t_f (finite) to maximize $U_\infty = U_\infty(\mathcal{R}(0), U(t_f), I(t_f), V(t_f))$. This control problem accounts for the first control objective; next, somme comments will be made concerning the second one.

A critical point concerning antiviral treatments - that is usually disregarded - is that they are always transitory control actions, not permanent ones. It is not possible to maintain a given treatment for a long time, and its interruption must be explicitly considered in any antiviral schedule.

So, according to the stability results from the previous sections, the following Property holds:

Property 5.2 (Upper bound for U_∞)**.** *Consider system* (4.4) *with* $U(0) > U^*$ *(or* $U(0)\mathcal{R}(0) > 1$*). No matter which kind of antiviral treatment is implemented at time* t_i*, if it is interrupted at some finite time* $t_f > t_i$ *(as it is always the case), the system converges to an equilibrium state* $(U_\infty, 0, 0)$ *with* $U_\infty \leq U^*$*, being* U^* *the critical value for* U *corresponding to no antiviral treatment, i.e.,* $U^* = 1/\mathcal{R}(0)$*.*

Proof. We proceed by contradiction. Assume that $U_\infty > U^*$. Consider system (4.1) for $t \geq t_f$. Since the antiviral treatment is interrupted at time t_f, then $\eta(t) \searrow 0$, for $t \geq t_f$. By eq. (5.1) we have that $\mathcal{R}(t) \nearrow \mathcal{R}(0)$, for $t \geq t_f$. If we denote $U_c(t) = 1/\mathcal{R}(t)$ we have $U_c \searrow U^*$ for $t \geq t_f$. Since $U_\infty > U^*$ then $U_\infty > U_c(t)$ for $t > T$, with T large enough. Hence $(U(t), I(t), V(t))$ is converging to an equilibrium point in the unstable part, which is a contradiction. Therefore $U_\infty \leq U^*$, which concludes the proof. □

Remark 5.3. *From a clinical perspective, what Property 5.2 establishes is more than a simple upper bound for* U_∞*. It says that the best an antiviral treatment can do in terms of the* ***total amount of virus (or infected cells) at the end of the infection****,* $V_{\text{tot}} := \int_{t=0}^{\infty} V(t)dt \approx \int_{t=0}^{\infty} \frac{p}{c} I(t)dt$*, is to reach a minimal value intrinsically determined by the system parameters (*$\mathcal{R}(0)$*). Furthermore, the instantaneous* ***peak of*** $V(t)$*, for* $t > 0$*, which is the other critical index for the severity of the infection (whose minimization is the second control objective), is independent of the latter lower limit (as shown later on), and can be minimized while maintaining* V_{tot} *at its minimal value. This represents a new paradigm concerning what (and what not) antiviral treatments can do in acute infections.*

In the search of such a value, the next definition is stated.

Definition 5.4 (Goldilocks antiviral dose)**.** *The goldilocks antiviral dose (GAD),* $u^g = u^g(t_i)$*, is the one that, if applied at* $t_i < \hat{t}(\mathcal{R}(0))$*, produces* $U_\infty(\mathcal{R}^g, U(t_i), I(t_i), V(t_i)) = U^*$*, where* $\mathcal{R}^g$ *is determined by* u^g*, at steady state.*

Remark 5.5 (u^g computation)**.** *Given* t_i *and* $\mathcal{R}(0)$*,* $u^g = u^g(U(t_i), I(t_i), V(t_i)) = u^g(t_i)$ *can be obtained, numerically, by means of Algorithm 1.*

Algorithm 1: Computation of $u^g(t_i)$

```
u_k = 0, U* = 1/R(0);
Compute U_i, I_i and V_i by integrating system (2.1) from 0 to t_i, starting at
  (U_0, I_0, V_0);
Compute U(t_f) by integrating system (4.4) form t_i to t_f, starting at
  (U_i, I_i, V_i), with u_k;
while U(t_f) <= U* do
    u_k = u_k + 0.001;
    Compute U(t_f) by integrating system (4.4) form t_i to t_f, starting at
      (U_i, I_i, V_i), with u_k;
end
u^g = u_k;
```

Clearly, Goldilocks antiviral treatment cannot be applied indefinitely, since t_f is finite. However, it can be applied up to a time t_f large enough such that

$(U(t_f), I(t_f), V(t_f))$ is arbitrarily close to $(U^*, 0, 0)$ from above. This latter scenario is denoted as quasi steady state (QSS), and it allows us to introduce the following definition.

Definition 5.6 (Quasi optimal single interval antiviral treatment)**.** *Consider a given starting time, $t_i \in (0, \hat{t}(\mathcal{R}(0)))$. Then, the quasi optimal single interval antiviral treatment consists in applying u^g, up to a time t_f large enough for the the system to reach a QSS condition (i.e., $U(t_f) \approx U^*$ $I(t_f) \approx 0$, $V(t_f) \approx 0$).*

Remark 5.7. *Clearly, the latter definition refers to a quasi optimal single interval control action, because larger values of t_f will produce values of $U(t_f)$, $I(t_f)$ and $V(t_f)$ closer to U^*, 0 and 0, respectively, so $U_\infty(\mathcal{R}(0), U(t_f), I(t_f), V(t_f))$ will be closer to U^*.*

The next Theorem, which is one of the main contribution of the work, summarizes the latter results by means of a classification that consider every possible single interval treatment case.

Theorem 5.8 (Single interval antiviral treatment scenarios)**.** *Consider system* (2.1) *with initial conditions $(U(0), I(0), V(0)) = (U_0, 0, \epsilon)$, with $\epsilon > 0$ arbitrary small, and $\mathcal{R}(0)$ such that $U(0) > U^*$. Consider also single interval antiviral treatment (as the one defined in* (5.2)*), with a given starting time $t_i \in (0, \hat{t}(\mathcal{R}(0)))$, and a finite final time t_f. Define soft and strong treatments depending on if $u_i < u^g$ or $u_i > u^g$, respectively. Define also long and short term treatments depending on if the system reaches or does not reach a QSS at t_f. Then, the following scenarios can take place:*

i. Quasi optimal single interval antiviral treatment: if $u_i = u^g$, and t_f is such that $(U(t_f), I(t_f), V(t_f))$ reaches a QSS, then $U_\infty(\mathcal{R}(0), U(t_f), I(t_f), V(t_f)) \approx U^*$. Furthermore, the closer is $U(t_f)$ to U^* (or $I(t_f)$ and $V(t_f)$ to zero), the closer will be $U_\infty(\mathcal{R}(0), U(t_f), I(t_f), V(t_f))$ to U^*.

ii. Soft long-term antiviral treatment: if $(U(t_f), I(t_f), V(t_f))$ reaches a QSS, and $U(t_f) < U^*$, then $U_\infty(\mathcal{R}(0), U(t_f), I(t_f), V(t_f)) \approx U(t_f) < U^*$; i.e., $U(t)$ will remain approximately constant for $t \geq t_f$. Furthermore, the softer a soft long term antiviral treatment is, the smaller will be $U_\infty(\mathcal{R}(0), U(t_f), I(t_f), V(t_f))$.

*iii. Strong long-term antiviral treatment: if $(U(t_f), I(t_f), V(t_f))$ reaches a QSS, and $U(t_f) > U^*$, a **rebound** will necessarily take place at some time $\hat{\hat{t}} > t_f$ and, finally, the system will converge to an $U_\infty(\mathcal{R}(0), U(t_f), I(t_f), V(t_f)) < U^*$. Furthermore, the stronger a strong long term antiviral treatment is, the larger will be the rebound and the smaller will be $U_\infty(\mathcal{R}(0), U(t_f), I(t_f), V(t_f))$.*

iv. Short-term antiviral treatment: if $(U(t_f), I(t_f), V(t_f))$ does not reach a QSS (i.e, if $V(t_f) \not\approx 0$), then soft, strong and Goldilocks dose will necessarily produce values of $U_\infty(\mathcal{R}(0), U(t_f), I(t_f), V(t_f))$ significantly smaller than the one obtained by quasi optimal single interval treatment. In general, larger values of $V(t_f)$ will produce smaller values of $U_\infty(\mathcal{R}(0), U(t_f), I(t_f), V(t_f))$. This case includes the particular case where the treatment is interrupted at the very moment at which $U(t_f) = U^*$, but with $V(t_f) \not\approx 0$. This means that the critical value of U needs to be reached as a steady state, not as a transitory one.

Proof. The proof follows from the stability results shown in Sections 3, and (3.6):

i. Given that $u_i = u^g$ is implemented for $t \in [t_i, t_f]$, t_f is finite but large enough and $U_\infty(\mathcal{R}^g, U(t_i), I(t_i), V(t_i)) = U^*$, then $U(t_f)$ approaches U^* and $V(t_f)$ approaches zero, from above, as t_f increases. This means that at t_f, when the treatment is interrupted, $(U(t_f), I(t_f), V(t_f))$ is close to the unstable equilibrium set $\mathcal{X}_s^{un}$. Then, by Property 3.12.(ii), function $U_\infty(\mathcal{R}(0), U(t_f), I(t_f), V(t_f))$ is such that the closer $(U(t_f), I(t_f), V(t_f))$ is to the equilibrium point $(U^*, 0, 0)$, with $U(t_f) > U^*$, the closer will be $U_\infty(\mathcal{R}(0), U(t_f), I(t_f), V(t_f))$ to U^*, with $U_\infty < U^*$ (see the 'pine' shape of U_∞ around U^*, for $I \approx 0$, in Figure 3). Indeed, by the $\epsilon - \delta$ stability of the equilibrium state $(U^*, 0, 0)$, for each (arbitrary small) $\epsilon > 0$, it there exists $\delta > 0$, such that, if the system starts in a ball of radius δ centered at $(U^*, 0, 0)$, it will keeps indeterminately in the ball of radius ϵ centered at $(U^*, 0, 0)$. Furthermore, it is possible to define invariant sets around $(U^*, 0, 0)$ by considering the level sets of the Lyapunov function (3.7), with $\bar{U} = U^*$, or even the level sets of function $J(U, I, V) := U^* - U_\infty(\mathcal{R}, U, I, V)$, with a fixed $\mathcal{R} > 0$. This way, once the system enters any arbitrary small level set of the latter functions, it cannot leaves the set anymore. See, Figure 6.

ii. Given that $(U(t_f), I(t_f), V(t_f))$ approaches a steady state with $U(t_f) < U^*$, then $(U(t_f), I(t_f), V(t_f))$ is close to the stable equilibrium set $\mathcal{X}_s^{st}$, when the treatment is interrupted. Then, the system will converge to an equilibrium with $U_\infty(\mathcal{R}(0), U(t_f), I(t_f), V(t_f))$ close to $U(t_f)$. Softer antiviral treatment produces smaller values of $U(t_f)$ and, by Property 3.12.(iii), smaller values of $U(t_f)$ produce smaller values of $U_\infty(\mathcal{R}(0), U(t_f), I(t_f), V(t_f))$.

iii. Given that $(U(t_f), I(t_f), V(t_f))$ approaches a steady state with $U(t_f) > U^*$, then $(U(t_f), I(t_f), V(t_f))$ is close to the unstable equilibrium set, $\mathcal{X}_s^{un}$, when the treatment is interrupted. Then, the system will converges to an equilibrium in the stable equilibrium set, $\mathcal{X}_s^{st}$, with $U_\infty(\mathcal{R}(0), U(t_f), I(t_f), V(t_f)) < U^*$. Stronger antiviral treatment produces greater values of $U(t_f)$ and, by Property 3.12.(ii), values of $U(t_f)$ farther from U^*, from above, produce values of $U_\infty(\mathcal{R}(0), U(t_f), I(t_f), V(t_f))$ farther from U^*, from below. When $U(t_f)$ is significantly greater than U^*, no matter how large is t_f and how small is $V(t_f)$. Note that as long as t_f is finite, $(U(t_f), I(t_f), V(t_f))$ cannot reach $\mathcal{X}_s^{un}$, and so $V(t_f)$, even when arbitrary small, is greater than zero. So, once the treatment is interrupted, the system evolves to an equilibrium in $\mathcal{X}_s^{un}$. the system will evolve to an equilibrium in $\mathcal{X}_s^{st}$, with $U_\infty(\mathcal{R}(0), U(t_f), I(t_f), V(t_f))$ significantly smaller than U^*. Furthermore, to go from $U(t_f)$ to $U_\infty(\mathcal{R}(0), U(t_f), I(t_f), V(t_f))$, for $t > t_f$, the system significantly increase $V(t)$, and this effect is known as a rebound.

iv. Given that $(U(t_f), I(t_f), V(t_f))$ is a transitory state, then it does not approach any equilibrium. This means that $V(t_f)$ is significantly greater than 0, and according to Lemma 3.7, the maximum of $U_\infty(\mathcal{R}(0), U(t_f), I(t_f), V(t_f))$ over $\Omega(\varepsilon) = \left\{(U, I, V) \in \mathbb{R}^3_{\geq 0} : I \geq \varepsilon, V \geq \varepsilon\right\}$ is given by $-W(-\mathcal{R}U^* e^{-\mathcal{R}(U^* + \varepsilon + \frac{\delta}{p}\varepsilon)})/\mathcal{R}$, which is a decreasing function of ε, and reaches U^* only when $\varepsilon = 0$ (see Figure 3). Then, independently of the value of $U(t_f)$, $U_\infty(\mathcal{R}(0), U(t_f), I(t_f), V(t_f))$ will be (maybe significantly) smaller than the one obtained with quasi optimal single interval treatment, in which $\varepsilon \approx 0$.

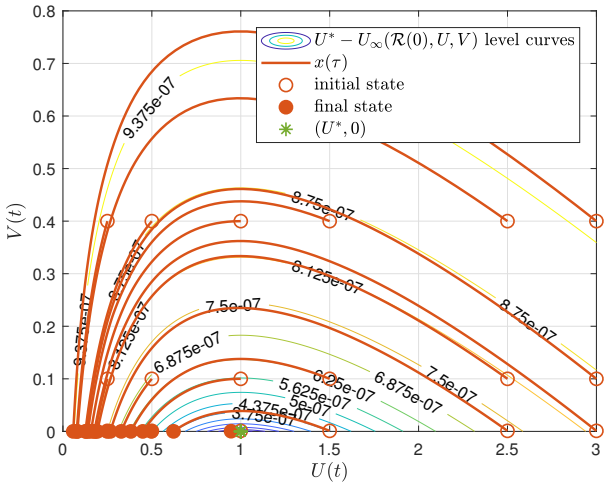

Figure 6: Phase Portrait for system (2.1) ($\beta = 1/2$, $\delta = 1/5$, $p = 2$, $c = 5$) in the U, V plane ($I = (c/p)V$), for different starting points (red lines), and level curves of function $J(U, I, V) := U^* - U_\infty(\mathcal{R}, U, I, V)$, $I = (c/p)V$. Function J is positive for all $(U, V) \neq (U^*, 0)$, is null at $(U^*, 0)$ and $\dot{J}(U, V) = 0$ along the solution of system (2.1) (since $U_\infty(\mathcal{R}, U, I, V)$ is). So its level sets are arbitrary small invariant sets around $(U^*, 0)$. Note that starting states close to $(U^*, 0)$ produce time evolution close to U^*, as determines the $\epsilon - \delta$ stability.

□

5.2. Second control objective: minimizing the virus peak

The quasi optimal single interval treatment clearly accounts for a steady state condition, given that any realistic treatment needs to be interrupted at a finite time. Furthermore, given that only one antiviral dose, u_i, is considered for the treatment, once the quasi optimal single interval treatment is determined ($u_i = u^g$), also is the peak (maximum over t) of the virus, $\hat{V}$: i.e., there is a unique $\hat{V}$ for each single interval control action, u_i.

However, if a more general control action is considered, in such a way that u_k assume several values in the interval from t_i to t_f, $\hat{V}$ can be arbitrarily reduced. Indeed, given that U_∞ depends only on the fact that $U \approx U^*$ and $V \approx 0$ at t_f, then stronger antiviral doses can be used at the beginning of the treatment to lower the peak of V. If for instance two consecutive single interval control actions are implemented —the first one with a high dose, applied from t_i to t_1, and the second one with the quasi optimal antiviral, $u^g(t_1)$, applied from t_1 to a large enough t_f— a lower peak of V will necessarily be obtained in contrast to one corresponding to the quasi optimal single interval control.

Although this chapter is not devoted to analyze control strategies different from the single interval one, it is worth to remark this latter point since it states that: (1) both control objectives are independent, in the the sense that if a given upper bound for V is stated from the the beginning (to avoid complication and/or to reduce the infectivity of the host) it is in general possible to design control strategies that both, make $V(t)$ not to overpasses the upper bound, and make $U_\infty \approx U^*$, and (2) the entire concept of a maximum or peak for V, for a given treatment, has sense only when $U_\infty \leq U^*$; since

otherwise, a rebounds of the virus will occurs once the treatment is interrupted, and a new peak for V may be reached.

Figures 11a and 11b, in the Simulation section, show an example of a two-steps interval treatment that produces a peak of V smaller than the one corresponding to the quasi optimal single interval one.

6. Simulation results

In this section each of the cases of Theorem 5.8, together with the case of two-steps interval control action of Subsection 5.2 are simulated for data coming from patient A, introduced in section 3.7 and 4.2. As it was already said, $\delta_D = 2$ (days^{-1}), $EC_{50}^p = 75$ (mg) and the sampling time is selected to be $T = 1$ day. Initial conditions are given by $(U_0, I_0, V_0) = (4 \times 10^8, 0, 0.31)$. Also, recall that $U^* = 5.44 \times 10^7$ and the untreated peak of V is given by $\hat{V} = 1.98 \times 10^7$.

6.1. Strong long-term treatment. Virus rebound

Figure 7a shows the time evolution of U (logarithmic scale), V, and u_k for patient A, when strong long-term antiviral treatment is implemented. The treatment starts at $t_i = 4$ days and finished at $t_f = 30$ days, while several strong doses are administered: $u_i = [21, 25, 35]$ mg.

As it can be seen, at t_f the value of U is greater than U^* while $V \approx 0$, so the viral load V rebounds after some time, producing a second (and larger) peak. More important, U_∞ ends up at a value significantly smaller than U^*. The values of U_∞ and $\hat{V}$ corresponding to the three doses are given by $U_\infty = [7.98 \times 10^6, 3.79 \times 10^6, 1.07 \times 10^5]$, and $\hat{V} = [4.84 \times 10^6, 7.86 \times 10^6, 1.34 \times 10^7]$, respectively.

To have a better idea of how the system behaves around state $(U^*, 0)$, Figure 7b shows the phase portrait in the space U, V, together with the level curves of the Lyapunov function $J(U, I, V) := U^* - U_\infty(\mathcal{R}(0), U, I, V)$. At time t_f, when the treatment is interrupted, $V(t_f) \approx 0$ and $U(t_f) > U^*$, so the system is close to an unstable equilibrium point. So, for $t > t_f$ the state is attracted to an equilibrium in the AS equilibrium set $\mathcal{X}_s^{st}$, following outer level curves of J. Outer level curves of J means both, a small U_∞ and a large $\hat{V}$.

6.2. Soft long-term treatment

Figure 8a shows the time evolution of U (logarithmic scale), V, and u_k, when soft long term antiviral treatment is implemented. The treatment starts at $t_i = 4$ days and finished at $t_f = 30$ days, while several soft doses are administered: $u_i = [4, 6, 8]$ mg.

As it can be seen, at t_f the value of U is smaller than U^*, while $V \approx 0$, so the viral load V decreases after the treatment is interrupted. The values of U_∞ and $\hat{V}$ corresponding to the three doses are given by $U_\infty = [8.98 \times 10^6, 1.90 \times 10^7, 3.25 \times 10^7]$, and $\hat{V} = [1.36 \times 10^7, 1.16 \times 10^7, 9.70e \times 10^6]$.

Figure 8b shows the phase portrait in the space U, V, together with the level curves of the Lyapunov function $J(U, I, V)$. At time t_f, when the treatment is interrupted, $V(t_f) \approx 0$ and $U(t_f) < U^*$, so the system is close to a stable equilibrium point. So, for $t > t_f$ the state remains almost unmodified.

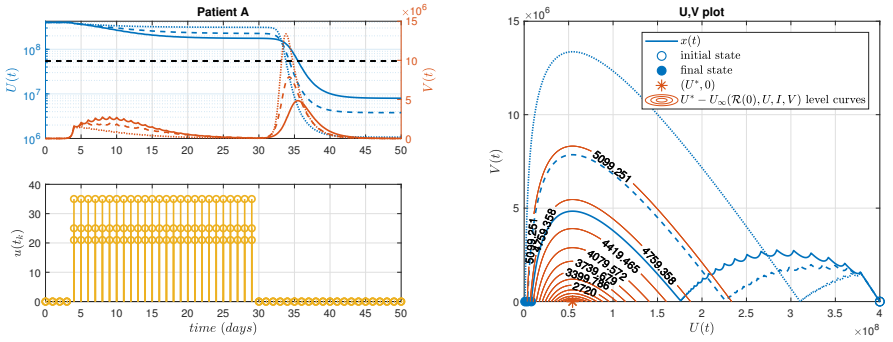

(a) (b)

Figure 7: (a) Time evolution of virtual patient A, with different doses of antiviral: $u_i = 21$ mg, solid line, $u_i = 25$ mg, dashed line, $u_i = 35$ mg, dotted line. (b) Phase portrait in the U, V space, and level curves of the Lyapunov function $J(U, I, V) := U^* - U_\infty(\mathcal{R}(0), U, I, V)$, around $(U^*, 0)$.

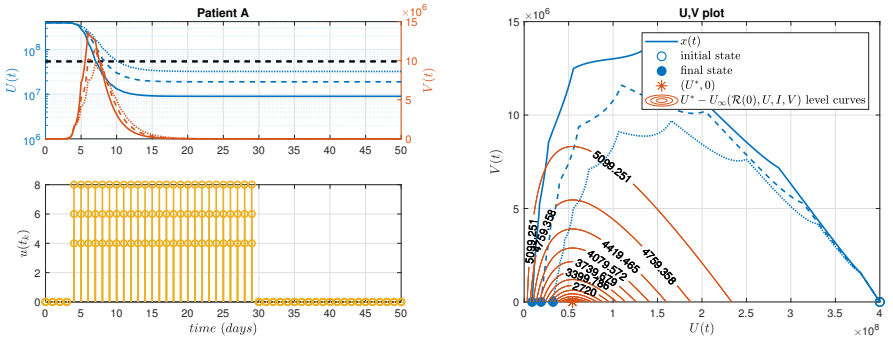

(a) (b)

Figure 8: (a) Time evolution of virtual patient A, with different doses of antiviral: $u_i = 4$ mg, solid line, $u_i = 6$ mg, dashed line, $u_i = 8$ mg, dotted line. (b) Phase portrait in the U, V space, and level curves of the Lyapunov function $J(U, I, V) := U^* - U_\infty(\mathcal{R}(0), U, I, V)$, around $(U^*, 0)$.

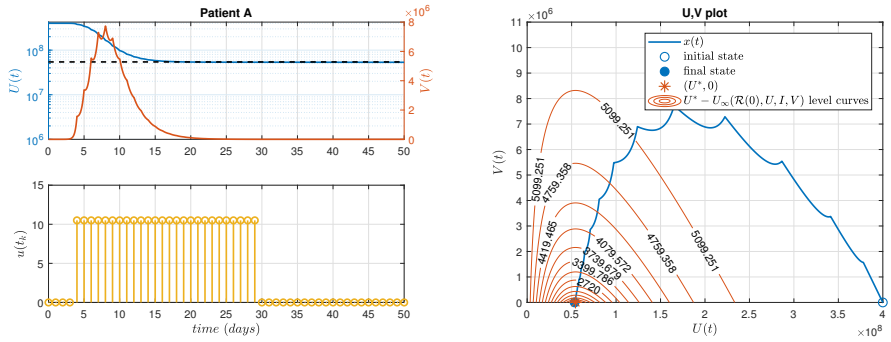

(a) (b)

Figure 9: (a) Time evolution of virtual patient A, with $u_i = u^g = 10.5$ mg of antivirals. (b) Phase portrait in the U, V space, and level curves of the Lyapunov function $J(U, I, V) := U^* - U_\infty(\mathcal{R}(0), U, I, V)$, around $(U^*, 0)$.

6.3. Quasi optimal single interval treatment

Figure 9a shows the time evolution of U (logarithmic scale), V, and u_k, when the quasi optimal single interval antiviral treatment is administered. The treatment starts at $t_i = 4$ days and finished at $t_f = 30$ days, while the Goldilocks dose is given by $u_i = u^g(t_i) = 10.5$ mg. The values of U_∞ and $\hat{V}$ are given by $U_\infty = 5.34 \times 10^7$ and $\hat{V} = 7.73 \times 10^6$, respectively

Figure 9b shows the phase portrait in the space U, V, together with the level curves of the Lyapunov function $J(U, I, V)$. As it can be seen, the system follows the only one trajectory that goes directly from (U_0, V_0) to $(U^*, 0)$: any other path goes necessarily to an equilibrium with $U_\infty < U^*$.

6.4. Short-term treatment

Figure 10a shows the time evolution of U (logarithmic scale), V, and u_k, when a short term treatment is implemented. The treatment starts at $t_i = 4$ days and finished at $t_f = 15$ days, while several doses - smaller and greater than $u^g(t_i)$ are administered: $u_i = [10, 15, 20, 25]$ mg. The values of U_∞ and $\hat{V}$ corresponding to the four doses are given by $U_\infty = [2.98 \times 10^6 7, 1.39 \times 10^7, 5.06 \times 10^7, 2.26 \times 10^7]$, and $\hat{V} = [8.05 \times 10^6, 4.98 \times 10^6, 6.67 \times 10^6, 1.01 \times 10^1]$.

Figure 10b shows the phase portrait in the space U, V. Given that trajectories go along the level curves of the Lyapunov function $J(U, I, V)$, any short term treatment - i.e., producing $V(t_f) \not\approx 0$ - will make the system to surround the state $(U^*, 0)$ by an outer level curve, thus finishing at some U_∞ significantly smaller than U^*. As before, outer level curves of J means both, a small U_∞ and a large $\hat{V}$.

6.5. Two-steps treatment, lowering the peak of V

Finally, a scenario is simulated to show that always it is possible to lower the the peak of V - while maintaining $U_\infty \approx U^*$ - if a control sequence more complex that the single interval one is implemented. Figure 11a shows the time evolution of U (solid blue line, logarithmic scale) and V (solid red line) corresponding to a two-steps interval control: the first step consisting in $u_i = 25$ mg, from $t_i = 4$ to $t_m = 30$ days, and the second one consisting in $u_i = u^g(t_m) = 5.6$ mg, from $t_m = 30$ to $t_f = 60$ (solid line). Also, the quasi optimal single interval control of Subsection 6.3 is shown, to compare

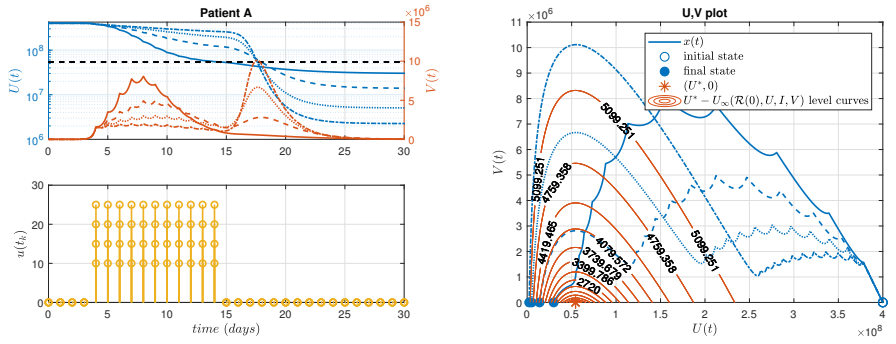

(a) (b)

Figure 10: (a) Time evolution of virtual patient A, with different doses of antiviral: $u_i = 10$ mg, solid line, $u_i = 15$ mg, dashed line, $u_i = 20$ mg, dotted line, and $u_i = 25$ mg, dashed-dotted line. (b) Phase portrait in the U, V space, and level curves of the Lyapunov function $J(U, I, V) := U^* - U_\infty(\mathcal{R}(0), U, I, V)$, around $(U^*, 0)$.

the performance (dashed line). As it can be seen, the peak of V is significantly reduced: from $\hat{V} = 7.73 \times 10^6$ to $\hat{V} = 2.57 \times 10^6$, while U_∞ is almost the same in both cases. Figure 11b shows the phase portraits of the two control strategies (solid line, two-steps control; dashed line, single interval control), where it can be seen also the reduction of the virus peak. This simple two-step strategy shows that with a more sophisticated control strategy (i.e., by means of a proper optimal control formulation) the virus peak can be arbitrarily reduced, maintaining the condition $U_\infty \approx U^*$. This is indeed, matter of future research.

7. Conclusions and future works

In this work, the stability and general long term behavior of UIV-type models have been fully analysed. A quasi optimal control action - consisting in the finite-time single interval antiviral treatment producing the minimal possible final amount of death cells - was found. The analysis shows also that more complex control strategies can account for both control objectives simultaneously: minimize the virus peak, while keeping the final amount of death cells at its maximum. A detailed analysis of subotimal scenarios permits to enumerate the following main results:

i. To apply soft antiviral treatment during a long time (even no treatment at all), expecting the non-infected cells would evolve alone to the critical value U^*, is not an option. Open loop U_∞ is in general significantly smaller than U^* (particularly for the reported values of $\mathcal{R}$ for the COVID-19).

ii. To apply strong antiviral treatment for a long time, expecting the virus will die out alone is not an option. Strong antiviral produces an values of U at the end of the treatment larger than U^*, but this final values are artificially stable steady states, since once the treatment is interrupted or reduced, a virus rebound will necessarily occurs at some future time, and U_∞ will be significantly smaller than U^*.

iii. To apply any antiviral treatment (soft or strong) for short period of time, such that the system is not able to reach a quasi steady state (i.e., when V at the end of

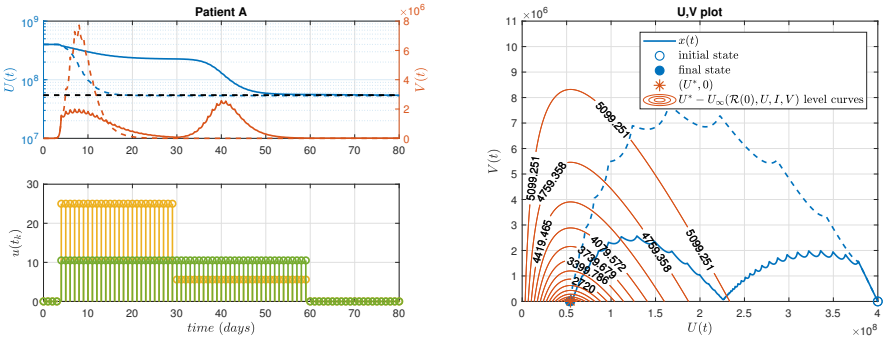

(a) (b)

Figure 11: (a) Time evolution of virtual patient A, with different doses of antiviral: $u_i = 25$ mg, from $t_i = 4$ to $t_m = 30$ days, and $u_i = u^g(t_m) = 5.6$ mg, from $t_m = 30$ to $t_f = 60$ (solid line). In dashed line is plotted the progression of target cells and viral particles considering the quasi optimal single interval treatment, given by $u_i = u^g(t_i) = 10$ mg from $t_i = 4$ to $t_f = 60$. (b) Phase portrait in the U, V space.

the treatment is not close to zero) is not an option. If the treatment is interrupted at a transient state, the initial conditions for the next time period are such that U_∞ will be significantly smaller than U^*.

iv. According to the latter results, the best option is to apply an antiviral treatment such that the system reaches a quasi steady state with $U \approx U^*$ and $V \approx 0$ at the end of the treatment. This is what we call "the quasi optimal single interval antiviral treatment", since it makes the system to approach the maximal final value of uninfected cells ($U_\infty \approx U^*$), without infection rebounds.

v. An important point to be remarked is that the quasi optimal single interval antiviral treatment does not determine the peak of the virus. Quasi optimal conditions for U_∞ are stationary, while condition for minimizing $\hat{V}$ are transitory, so both objective can be accounted for simultaneously.

Future works include the study of more complex control strategies (mainly model based control strategies as MPC and similar) and the explicit consideration of time-varying immune system.

References

[1] A. S. Perelson, D. E. Kirschner, R. De Boer, Dynamics of HIV infection of CD4+ T cells, Mathematical biosciences 114 (1) (1993) 81–125.

[2] A. S. Perelson, R. M. Ribeiro, Modeling the within-host dynamics of HIV infection, BMC biology 11 (1) (2013) 96.

[3] S. M. Ciupe, R. M. Ribeiro, P. W. Nelson, A. S. Perelson, Modeling the mechanisms of acute hepatitis b virus infection, Journal of theoretical biology 247 (1) (2007) 23–35.

[4] E. Herrmann, A. U. Neumann, J. M. Schmidt, S. Zeuzem, Hepatitis c virus kinetics, Antiviral therapy 5 (2) (2000) 85–90.

[5] A. U. Neumann, N. P. Lam, H. Dahari, D. R. Gretch, T. E. Wiley, T. J. Layden, A. S. Perelson, Hepatitis c viral dynamics in vivo and the antiviral efficacy of interferon-α therapy, Science 282 (5386) (1998) 103–107.

[6] L. Canini, A. S. Perelson, Viral kinetic modeling: state of the art, Journal of pharmacokinetics and pharmacodynamics 41 (5) (2014) 431–443.

[7] P. Baccam, C. Beauchemin, C. A. Macken, F. G. Hayden, A. S. Perelson, Kinetics of influenza A virus infection in humans, Journal of virology 80 (15) (2006) 7590–7599.

[8] A. M. Smith, A. S. Perelson, Influenza A virus infection kinetics: quantitative data and models, Wiley Interdisciplinary Reviews: Systems Biology and Medicine 3 (4) (2011) 429–445.

[9] G. Hernandez-Mejia, A. Y. Alanis, M. Hernandez-Gonzalez, R. Findeisen, E. A. Hernandez-Vargas, Passivity-based inverse optimal impulsive control for Influenza treatment in the host, IEEE Transactions on Control Systems Technology (2019).

[10] R. Nikin-Beers, S. M. Ciupe, The role of antibody in enhancing dengue virus infection, Mathematical biosciences 263 (2015) 83–92.

[11] R. Nikin-Beers, S. M. Ciupe, Modelling original antigenic sin in dengue viral infection, Mathematical medicine and biology: a journal of the IMA 35 (2) (2018) 257–272.

[12] V. Nguyen, S. Binder, A. Boianelli, M. Meyer-Hermann, E. A. Hernandez-Vargas, Ebola Virus Infection Modelling and Identifiability Problems, Frontiers in microbiology 6 (05 2015). doi:10.3389/fmicb.2015.00257.

[13] P. van den Driessche, Reproduction numbers of infectious disease models, Infectious Disease Modelling 2 (3) (2017) 288–303.

[14] A. Murase, T. Sasaki, T. Kajiwara, Stability analysis of pathogen-immune interaction dynamics, Journal of Mathematical Biology 51 (3) (2005) 247–267.

[15] H. L. Smith, P. De Leenheer, Virus dynamics: a global analysis, SIAM Journal on Applied Mathematics 63 (4) (2003) 1313–1327.

[16] P. Abuin, A. Anderson, A. Ferramosca, E. A. Hernandez-Vargas, A. H. Gonzalez, Dynamical characterization of antiviral effects in covid-19, arXiv preprint arXiv:2012.15585 (2020).

[17] S. M. Ciupe, J. M. Heffernan, In-host modeling, Infectious Disease Modelling 2 (2) (2017) 188–202.

[18] P. Cao, J. M. McCaw, The mechanisms for within-host influenza virus control affect model-based assessment and prediction of antiviral treatment, Viruses 9 (8) (2017) 197.

[19] J. B. Rawlings, D. Q. Mayne, M. Diehl, Model predictive control: theory, computation, and design, Vol. 2, Nob Hill Publishing Madison, WI, 2017.

[20] F. Blanchini, S. Miani, Set-theoretic methods in control, Springer, 2008.

[21] P. Abuin, A. Anderson, A. Ferramosca, E. A. Hernandez-Vargas, A. H. Gonzalez, Characterization of SARS-CoV-2 Dynamics in the Host, Annual Reviews in Control (2020).

[22] R. Eftimie, J. J. Gillard, D. A. Cantrell, Mathematical models for immunology: current state of the art and future research directions, Bulletin of mathematical biology 78 (10) (2016) 2091–2134.

[23] E. A. Hernandez-Vargas, Modeling and Control of Infectious Diseases in the Host: With MATLAB and R, Academic Press, 2019.

[24] H. M. Dobrovolny, M. B. Reddy, M. A. Kamal, C. R. Rayner, C. A. Beauchemin, Assessing mathematical models of influenza infections using features of the immune response, PloS one 8 (2) (2013) e57088.

[25] J.-M. Vergnaud, I.-D. Rosca, Assessing bioavailablility of drug delivery systems: mathematical modeling, CRC press, 2005.

[26] P. S. Rivadeneira, A. Ferramosca, A. H. González, Control strategies for nonzero set-point regulation of linear impulsive systems, IEEE Transactions on Automatic Control 63 (9) (2018) 2994–3001.

[27] G. Hernandez-Mejia, A. Alanis, E. A. Hernandez-Vargas, Inverse Optimal Impulsive Control Based Treatment of Influenza Infection, IFAC-PapersOnLine 50 (2017) 12185–12190. doi:10.1016/j.ifacol.2017.08.2272.

[28] P. S. Rivadeneira, C. H. Moog, Impulsive control of single-input nonlinear systems with application to hiv dynamics, Applied Mathematics and Computation 218 (17) (2012) 8462–8474.

[29] H. Dahari, A. Lo, R. M. Ribeiro, A. S. Perelson, Modeling hepatitis C virus dynamics: liver regeneration and critical drug efficacy, Journal of theoretical biology 247 (2) (2007) 371–381.

[30] H. M. Dobrovolny, R. Gieschke, B. E. Davies, N. L. Jumbe, C. A. Beauchemin, Neuraminidase inhibitors for treatment of human and avian strain influenza: A comparative modeling study, Journal of theoretical biology 269 (1) (2011) 234–244.

[31] R. Wölfel, V. M. Corman, W. Guggemos, M. Seilmaier, S. Zange, M. A. Müller, D. Niemeyer, T. C. Jones, P. Vollmar, C. Rothe, et al., Virological assessment of hospitalized patients with COVID-2019, Nature 581 (7809) (2020) 465–469.

[32] E. A. Hernandez-Vargas, J. X. Velasco-Hernandez, In-host Modelling of COVID-19 Kinetics in Humans, medRxiv (2020).

[33] L. Perko, Differential equations and dynamical systems, Vol. 7, Springer Science & Business Media, 2013.

[34] J. Kelley, General Topology, Dover Books on Mathematics, Dover Publications, 2017.

[35] H. K. Khalil, J. W. Grizzle, Nonlinear systems, Vol. 3, Prentice hall Upper Saddle River, NJ, 2002.

[36] A. D'Jorge, A. L. Anderson, A. Ferramosca, A. H. González, M. Actis, On stability of nonzero set-point for non linear impulsive control systems (2020). arXiv:2011.12085.

Bibliografía

[min, 2015] (2015). *MiniMed 640G System User Guide*. Medtronic. Rev. 1.

[Abuin et al., 2020a] Abuin, P., Anderson, A., Ferramosca, A., Hernandez-Vargas, E. A., and González, A. H. (2020a). Characterization of SARS-CoV-2 dynamics in the host. *Annual reviews in control*, 50:457–468.

[Abuin et al., 2021] Abuin, P., Anderson, A., Ferramosca, A., Hernandez-Vargas, E. A., and González, A. H. (2021). Dynamical characterization of antiviral effects in COVID-19. *Annual reviews in control*, 52:587–601.

[Abuin et al., 2022a] Abuin, P., Ferramosca, A., and González, A. H. (2022a). MPC-based artificial pancreas accounting for circadian variability of insulin sensitivity. In *2022 10th International Conference on Systems and Control (ICSC)*, pages 582–587. IEEE.

[Abuin et al., 2019] Abuin, P., Ferramosca, A., Rivadeneira, P. S., Godoy, J. L., and González, A. (2019). Control by pulses under MPC schemes, with applications to artificial pancreas. In *2019 XVIII Workshop on Information Processing and Control (RPIC)*, pages 265–270. IEEE.

[Abuin et al., 2023] Abuin, P., Ferramosca, A., Toffanin, C., Magni, L., and González, A. (2023). Pulsatile Zone MPC with asymmetric stationary cost for artificial pancreas based on a non-standard IOB constraint. *Journal of Process Control*, pages 1–29. En revisión.

[Abuin et al., 2022b] Abuin, P., Ferramosca, A., Toffanin, C., Magni, L., and Gonzalez, A. H. (2022b). Artificial pancreas under periodic MPC for trajectory tracking: handling circadian variability of insulin sensitivity. *IFAC-PapersOnLine*, 55(16):196–201.

[Abuin et al., 2020b] Abuin, P., Rivadeneira, P., Ferramosca, A., and González, A. (2020b). Artificial pancreas under stable pulsatile MPC: Improving the closed-loop performance. *Journal of Process Control*, 92:246–260.

[Abuin et al., 2022c] Abuin, P., Sánchez, I., Ferramosca, A., Toffanin, C., Magni, L., and González, A. (2022c). A basal trajectory-based framework for handling circadian variations of insulin sensitivity. pages 1–30, En redacción.

[Abuin et al., 2020c] Abuin, P., Sereno, J. E., Ferramosca, A., and González, A. H. (2020c). Closed-loop MPC-based artificial pancreas: Handling circadian variability of insulin sensitivity. In *2020 Argentine Conference on Automatic Control (AADECA)*, pages 1–6. IEEE.

[Aiello et al., 2020] Aiello, E. M., Lisanti, G., Magni, L., Musci, M., and Toffanin, C. (2020). Therapy-driven deep glucose forecasting. *Engineering Applications of Artificial Intelligence*, 87:103255.

[Allen et al., 2008] Allen, L. J., Brauer, F., Van den Driessche, P., and Wu, J. (2008). *Mathematical epidemiology*, volume 1945. Springer.

[American Diabetes Association, 2019] American Diabetes Association (2019). Classification and diagnosis of diabetes: standards of medical care in diabetes—2019. *Diabetes Care*, 42(Supplement 1):S13–S28.

[Anderson and Moore, 2012] Anderson, B. D. and Moore, J. B. (2012). *Optimal filtering*. Courier Corporation.

[Baccam et al., 2006] Baccam, P., Beauchemin, C., Macken, C. A., Hayden, F. G., and Perelson, A. S. (2006). Kinetics of influenza A virus infection in humans. *Journal of virology*, 80(15):7590–7599.

[Bergman et al., 1979] Bergman, R. N., Ider, Y. Z., Bowden, C. R., and Cobelli, C. (1979). Quantitative estimation of insulin sensitivity. *American Journal of Physiology-Endocrinology And Metabolism*, 236(6):E667.

[Bertachi et al., 2020] Bertachi, A., Biagi, L., Beneyto, A., Vehi, J., et al. (2020). Dynamic rule-based algorithm to tune insulin-on-board constraints for a hybrid artificial pancreas system. *Journal of Healthcare Engineering*, 2020.

[Best and Perelson, 2018] Best, K. and Perelson, A. S. (2018). Mathematical modeling of within-host zika virus dynamics. *Immunological reviews*, 285(1):81–96.

[Bisgaard Bengtsen and Møller, 2021] Bisgaard Bengtsen, M. and Møller, N. (2021). Mini-review: Glucagon responses in type 1 diabetes–a matter of complexity. *Physiological Reports*, 9(16):e15009.

[Blanchini and Miani, 2008] Blanchini, F. and Miani, S. (2008). *Set-theoretic methods in control*. Springer.

[Blanke et al., 2006] Blanke, M., Kinnaert, M., Lunze, J., Staroswiecki, M., and Schröder, J. (2006). *Diagnosis and fault-tolerant control*, volume 2. Springer.

[Bocharov et al., 2018] Bocharov, G., Volpert, V., Ludewig, B., Meyerhans, A., et al. (2018). *Mathematical immunology of virus infections*, volume 245. Springer.

[Bock et al., 2015] Bock, A., François, G., and Gillet, D. (2015). A therapy parameter-based model for predicting blood glucose concentrations in patients with type 1 diabetes. *Computer methods and programs in biomedicine*, 118(2):107–123.

[Boianelli et al., 2015] Boianelli, A., Nguyen, V. K., Ebensen, T., Schulze, K., Wilk, E., Sharma, N., Stegemann-Koniszewski, S., Bruder, D., Toapanta, F. R., Guzmán, C. A., et al. (2015). Modeling influenza virus infection: a roadmap for influenza research. *Viruses*, 7(10):5274–5304.

[Boiroux et al., 2018a] Boiroux, D., Bátora, V., Hagdrup, M., Wendt, S. L., Poulsen, N. K., Madsen, H., and Jørgensen, J. B. (2018a). Adaptive model predictive control for a dual-hormone artificial pancreas. *Journal of Process Control*, 68:105–117.

[Boiroux et al., 2018b] Boiroux, D., Duun-Henriksen, A. K., Schmidt, S., Nørgaard, K., Madsbad, S., Poulsen, N. K., Madsen, H., and Jørgensen, J. B. (2018b). Overnight glucose control in people with type 1 diabetes. *Biomedical Signal Processing and Control*, 39:503–512.

[Bondia et al., 2018] Bondia, J., Romero-Vivo, S., Ricarte, B., and Diez, J. L. (2018). Insulin estimation and prediction: a review of the estimation and prediction of subcutaneous insulin pharmacokinetics in closed-loop glucose control. *IEEE Control Systems Magazine*, 38(1):47–66.

[Bujarbaruah et al., 2020] Bujarbaruah, M., Zhang, X., Tanaskovic, M., and Borrelli, F. (2020). Adaptive stochastic mpc under time-varying uncertainty. *IEEE Transactions on Automatic Control*, 66(6):2840–2845.

[Cameron et al., 2012] Cameron, F., Niemeyer, G., and Bequette, B. W. (2012). Extended multiple model prediction with application to blood glucose regulation. *Journal of Process Control*, 22(8):1422–1432.

[Cameron et al., 2017] Cameron, F. M., Ly, T. T., Buckingham, B. A., Maahs, D. M., Forlenza, G. P., Levy, C. J., Lam, D., Clinton, P., Messer, L. H., Westfall, E., et al. (2017). Closed-loop control without meal announcement in type 1 diabetes. *Diabetes technology & therapeutics*, 19(9):527–532.

[Canini and Perelson, 2014] Canini, L. and Perelson, A. S. (2014). Viral kinetic modeling: state of the art. *Journal of pharmacokinetics and pharmacodynamics*, 41(5):431–443.

[Cao and McCaw, 2017] Cao, P. and McCaw, J. M. (2017). The mechanisms for within-host influenza virus control affect model-based assessment and prediction of antiviral treatment. *Viruses*, 9(8):197.

[Carlson et al., 2018] Carlson, F. B., Robertsson, A., and Johansson, R. (2018). Identification of ltv dynamical models with smooth or discontinuous time evolution by means of convex optimization. In *2018 IEEE 14th International Conference on Control and Automation (ICCA)*, pages 654–661. IEEE.

[Castle et al., 2018] Castle, J. R., El Youssef, J., Wilson, L. M., Reddy, R., Resalat, N., Branigan, D., Ramsey, K., Leitschuh, J., Rajhbeharrysingh, U., Senf, B., et al. (2018). Randomized outpatient trial of single-and dual-hormone closed-loop systems that adapt to exercise using wearable sensors. *Diabetes care*, 41(7):1471–1477.

[Chen et al., 2012] Chen, T., Ohlsson, H., and Ljung, L. (2012). On the estimation of transfer functions, regularizations and gaussian processes—revisited. *Automatica*, 48(8):1525–1535.

[Ciupe and Heffernan, 2017] Ciupe, S. M. and Heffernan, J. M. (2017). In-host modeling. *Infectious Disease Modelling*, 2(2):188–202.

[Cobelli and Carson, 2019] Cobelli, C. and Carson, E. (2019). *Introduction to modeling in physiology and medicine*. Academic Press.

[Colmegna et al., 2018] Colmegna, P., Garelli, F., De Battista, H., and Sánchez-Peña, R. (2018). Automatic regulatory control in type 1 diabetes without carbohydrate counting. *Control Engineering Practice*, 74:22–32.

[Committee and Committee:, 2022] Committee, A. D. A. P. P. and Committee:, A. D. A. P. P. (2022). 6. glycemic targets: standards of medical care in diabetes—2022. *Diabetes Care*, 45(Supplement_1):S83–S96.

[Dahari et al., 2007] Dahari, H., Lo, A., Ribeiro, R. M., and Perelson, A. S. (2007). Modeling hepatitis C virus dynamics: liver regeneration and critical drug efficacy. *Journal of theoretical biology*, 247(2):371–381.

[Dalla Man et al., 2009] Dalla Man, C., Breton, M. D., and Cobelli, C. (2009). Physical activity into the meal glucose—insulin model of type 1 diabetes: In silico studies.

[Dalla Man et al., 2007] Dalla Man, C., Rizza, R. A., and Cobelli, C. (2007). Meal simulation model of the glucose-insulin system. *IEEE Transactions on biomedical engineering*, 54(10):1740–1749.

[Del Favero et al., 2019] Del Favero, S., Toffanin, C., Magni, L., and Cobelli, C. (2019). Deployment of modular mpc for type 1 diabetes control: the italian experience 2008–2016. In *The Artificial Pancreas*, pages 153–182. Elsevier.

[Deshpande et al., 2023] Deshpande, S., Doyle, F. J., and Dassau, E. (2023). Glucose rate-of-change and insulin-on-board jointly weighted zone model predictive control. *IEEE Transactions on Control Systems Technology*.

[D'Jorge et al., 2020] D'Jorge, A., Anderson, A. L., Ferramosca, A., González, A. H., and Actis, M. (2020). On stability of nonzero set-point for non linear impulsive control systems.

[Dobrovolny et al., 2011] Dobrovolny, H. M., Gieschke, R., Davies, B. E., Jumbe, N. L., and Beauchemin, C. A. (2011). Neuraminidase inhibitors for treatment of human and avian strain influenza: A comparative modeling study. *Journal of theoretical biology*, 269(1):234–244.

[Dobrovolny et al., 2013] Dobrovolny, H. M., Reddy, M. B., Kamal, M. A., Rayner, C. R., and Beauchemin, C. A. (2013). Assessing mathematical models of influenza infections using features of the immune response. *PloS one*, 8(2):e57088.

[D'Jorge et al., 2022] D'Jorge, A., Anderson, A., Ferramosca, A., González, A. H., and Actis, M. (2022). On stability of nonzero set-point for nonlinear impulsive control systems. *Systems & Control Letters*, 165:105244.

[Eftimie et al., 2016] Eftimie, R., Gillard, J. J., and Cantrell, D. A. (2016). Mathematical models for immunology: current state of the art and future research directions. *Bulletin of mathematical biology*, 78(10):2091–2134.

[El-Khatib et al., 2017] El-Khatib, F. H., Balliro, C., Hillard, M. A., Magyar, K. L., Ekhlaspour, L., Sinha, M., Mondesir, D., Esmaeili, A., Hartigan, C., Thompson, M. J., et al. (2017). Home use of a bihormonal bionic pancreas versus insulin pump therapy in adults with type 1 diabetes: a multicentre randomised crossover trial. *The Lancet*, 389(10067):369–380.

[Ellingsen et al., 2009] Ellingsen, C., Dassau, E., Zisser, H., Grosman, B., Percival, M. W., Jovanovič, L., and Doyle III, F. J. (2009). Safety constraints in an artificial pancreatic β cell: an implementation of model predictive control with insulin on board. *Journal of diabetes science and technology*, 3(3):536–544.

[Ferramosca et al., 2010] Ferramosca, A., Limon, D., González, A. H., Odloak, D., and Camacho, E. F. (2010). Mpc for tracking zone regions. *Journal of Process Control*, 20(4):506–516.

[Fushimi et al., 2018] Fushimi, E., Rosales, N., De Battista, H., and Garelli, F. (2018). Artificial pancreas clinical trials: Moving towards closed-loop control using insulin-on-board constraints. *Biomedical Signal Processing and Control*, 45:1–9.

[Garcia-Tirado et al., 2018] Garcia-Tirado, J., Zuluaga-Bedoya, C., and Breton, M. D. (2018). Identifiability analysis of three control-oriented models for use in artificial pancreas systems. *Journal of diabetes science and technology*, 12(5):937–952.

[Godoy et al., 2018a] Godoy, J., Abuin, P., Rivadeneira, P., and González, A. (2018a). Modeling, identification and state estimation for artificial pancreas. Part I: Description of the model and identification procedure. In *Proceedings of the Congreso Argentino de Control Automático AADECA*, pages 1–6.

[Godoy et al., 2018b] Godoy, J., Abuin, P., Rivadeneira, P., and González, A. (2018b). Modeling, identification and state estimation for artificial pancreas. Part II: Study of the estimation problem. In *Proceedings of the Congreso Argentino de Control Automático AADECA*, pages 1–6.

[Gonçalves et al., 2021] Gonçalves, A., Maisonnasse, P., Donati, F., Albert, M., Behillil, S., Contreras, V., Naninck, T., Marlin, R., Solas, C., Pizzorno, A., et al. (2021). Sars-cov-2 viral dynamics in non-human primates. *PLoS computational biology*, 17(3):e1008785.

[Gondhalekar et al., 2016] Gondhalekar, R., Dassau, E., and Doyle III, F. J. (2016). Periodic zone-mpc with asymmetric costs for outpatient-ready safety of an artificial pancreas to treat type 1 diabetes. *Automatica*, 71:237–246.

[Gondhalekar et al., 2018] Gondhalekar, R., Dassau, E., and Doyle III, F. J. (2018). Velocity-weighting and velocity-penalty MPC of an artificial pancreas: Improved safety and performance. *Automatica*, 91(48):105–117.

[González et al., 2020] González, A. H., Rivadeneira, P. S., Ferramosca, A., Magdelaine, N., and Moog, C. H. (2020). Stable impulsive zone model predictive control for type 1 diabetic patients based on a long-term model. *Optimal Control Applications and Methods*, 41(6):2115–2136.

[Goodwin et al., 2006] Goodwin, G., Seron, M. M., and De Doná, J. A. (2006). *Constrained control and estimation: an optimisation approach*. Springer Science & Business Media.

[Goodwin et al., 2015a] Goodwin, G. C., Carrasco, D. S., Medioli, A. M., King, B. R., and Stephen, C. (2015a). Nonlinear insulin to carbohydrate rule for treatment of type 1 diabetes. *IFAC-PapersOnLine*, 48(11):198–203.

[Goodwin et al., 2018] Goodwin, G. C., Carrasco, D. S., Seron, M. M., and Medioli, A. M. (2018). A fundamental control performance limit for a class of positive nonlinear systems. *Automatica*, 95:14–22.

[Goodwin et al., 2015b] Goodwin, G. C., Medioli, A. M., Carrasco, D. S., King, B. R., and Fu, Y. (2015b). A fundamental control limitation for linear positive systems with application to type 1 diabetes treatment. *Automatica*, 55:73–77.

[Goodwin et al., 2016] Goodwin, G. C., Medioli, A. M., Phan, H. V., King, B. R., and Matthews, A. D. (2016). Application of mpc incorporating stochastic programming to type 1 diabetes treatment. In *2016 American Control Conference (ACC)*, pages 907–912. IEEE.

[Goodwin and Seron, 2019] Goodwin, G. C. and Seron, M. M. (2019). A performance bound for optimal insulin infusion in individuals with type 1 diabetes ingesting a meal with slow postprandial response. *Automatica*, 103:531–537.

[Gourishankar et al., 1977] Gourishankar, V., Kudva, P., and Ramar, K. (1977). Reduced-order observers for multivariable systems with inaccessible disturbance inputs. *International Journal of Control*, 25(2):311–319.

[Haddad and Chellaboina, 2008] Haddad, W. M. and Chellaboina, V. (2008). *Nonlinear dynamical systems and control: a Lyapunov-based approach*. Princeton university press.

[Hajizadeh et al., 2019a] Hajizadeh, I., Rashid, M., and Cinar, A. (2019a). Plasma-insulin-cognizant adaptive model predictive control for artificial pancreas systems. *Journal of process control*, 77:97–113.

[Hajizadeh et al., 2019b] Hajizadeh, I., Rashid, M., Samadi, S., Sevil, M., Hobbs, N., Brandt, R., and Cinar, A. (2019b). Adaptive personalized multivariable artificial pancreas using plasma insulin estimates. *Journal of Process Control*, 80:26–40.

[Hajizadeh et al., 2017] Hajizadeh, I., Rashid, M., Turksoy, K., Samadi, S., Feng, J., Sevil, M., Frantz, N., Lazaro, C., Maloney, Z., Littlejohn, E., et al. (2017). Multivariable recursive subspace identification with application to artificial pancreas systems. *IFAC-PapersOnLine*, 50(1):886–891.

[Harvey et al., 2014] Harvey, R. A., Dassau, E., Zisser, H., Seborg, D. E., and Doyle III, F. J. (2014). Design of the glucose rate increase detector: a meal detection module for the health monitoring system. *Journal of diabetes science and technology*, 8(2):307–320.

[Hernandez-Mejia et al., 2019] Hernandez-Mejia, G., Alanis, A. Y., Hernandez-Gonzalez, M., Findeisen, R., and Hernandez-Vargas, E. A. (2019). Passivity-based inverse optimal impulsive control for Influenza treatment in the host. *IEEE Transactions on Control Systems Technology*.

[Hernandez-Vargas and Velasco-Hernandez, 2020] Hernandez-Vargas, E. A. and Velasco-Hernandez, J. X. (2020). In-host Modelling of COVID-19 Kinetics in Humans. *medRxiv*.

[Hinshaw et al., 2013] Hinshaw, L., Dalla Man, C., Nandy, D. K., et al. (2013). Diurnal pattern of insulin action in type 1 diabetes: implications for a closed-loop system. *Diabetes*, 62(7):2223–2229.

[Hovorka et al., 2002] Hovorka, R., Shojaee-Moradie, F., Carroll, P. V., Chassin, L. J., Gowrie, I. J., Jackson, N. C., Tudor, R. S., Umpleby, A. M., and Jones, R. H. (2002). Partitioning glucose distribution/transport, disposal, and endogenous production during ivgtt. *American Journal of Physiology-Endocrinology and Metabolism*, 282(5):E992–E1007.

[Huang et al., 2012] Huang, M., Li, J., Song, X., and Guo, H. (2012). Modeling impulsive injections of insulin: towards artificial pancreas. *SIAM Journal on Applied Mathematics*, 72(5):1524–1548.

[Hughes et al., 2011] Hughes, C., Patek, S. D., Breton, M., and Kovatchev, B. P. (2011). Anticipating the next meal using meal behavioral profiles: A hybrid model-based stochastic predictive control algorithm for t1dm. *Computer methods and programs in biomedicine*, 102(2):138–148.

[Incremona et al., 2018] Incremona, G. P., Messori, M., Toffanin, C., Cobelli, C., and Magni, L. (2018). Model predictive control with integral action for artificial pancreas. *Control Engineering Practice*, 77:86–94.

[Jørgensen et al., 2019] Jørgensen, J. B., Boiroux, D., and Mahmoudi, Z. (2019). An artificial pancreas based on simple control algorithms and physiological insight. *IFAC-PapersOnLine*, 52(1):1018–1023.

[Juhl et al., 2012] Juhl, C. B., Gjedsted, J., Nielsen, M. F., and Schmitz, O. (2012). Increased action of pulsatile compared to non-pulsatile insulin delivery during a meal-like glucose exposure simulated by computerized infusion in healthy humans. *Metabolism*, 61(8):1177–1181.

[Kanderian et al., 2009] Kanderian, S. S., Weinzimer, S., Voskanyan, G., and Steil, G. M. (2009). Identification of intraday metabolic profiles during closed-loop glucose control in individuals with type 1 diabetes.

[Katsarou et al., 2017] Katsarou, A., Gudbjörnsdottir, S., Rawshani, A., Dabelea, D., Bonifacio, E., Anderson, B. J., Jacobsen, L. M., Schatz, D. A., and Lernmark, Å. (2017). Type 1 diabetes mellitus. *Nature reviews Disease primers*, 3:17016.

[Ke et al., 2021] Ke, R., Zitzmann, C., Ho, D. D., Ribeiro, R. M., and Perelson, A. S. (2021). In vivo kinetics of sars-cov-2 infection and its relationship with a person's infectiousness. *Proceedings of the National Academy of Sciences*, 118(49):e2111477118.

[Kim et al., 2021] Kim, K. S., Ejima, K., Iwanami, S., Fujita, Y., Ohashi, H., Koizumi, Y., Asai, Y., Nakaoka, S., Watashi, K., Aihara, K., et al. (2021). A quantitative model used to compare within-host sars-cov-2, mers-cov, and sars-cov dynamics provides insights into the pathogenesis and treatment of sars-cov-2. *PLoS biology*, 19(3):e3001128.

[Köhler et al., 2020] Köhler, J., Müller, M. A., and Allgöwer, F. (2020). A nonlinear tracking model predictive control scheme for dynamic target signals. *Automatica*, 118:109030.

[Kokotović et al., 1999] Kokotović, P., Khalil, H. K., and O'reilly, J. (1999). *Singular perturbation methods in control: analysis and design*. SIAM.

[Kölle et al., 2019] Kölle, K., Fougner, A. L., Lundteigen, M. A., Carlsen, S. M., Ellingsen, R., and Stavdahl, Ø. (2019). Risk analysis for the design of a safe artificial pancreas control system. *Health and Technology*, 9:311–328.

[Kudva et al., 2014] Kudva, Y. C., Carter, R. E., Cobelli, C., Basu, R., and Basu, A. (2014). Closed-loop artificial pancreas systems: physiological input to enhance next-generation devices. *Diabetes care*, 37(5):1184–1190.

[Lee et al., 2016] Lee, J. B., Dassau, E., Gondhalekar, R., Seborg, D. E., Pinsker, J. E., and Doyle III, F. J. (2016). Enhanced model predictive control (empc) strategy for automated glucose control. *Industrial & engineering chemistry research*, 55(46):11857–11868.

[Limon et al., 2009] Limon, D., Alamo, T., Raimondo, D. M., De La Peña, D. M., Bravo, J. M., Ferramosca, A., and Camacho, E. F. (2009). Input-to-state stability: a unifying framework for robust model predictive control. *Nonlinear Model Predictive Control: Towards New Challenging Applications*, pages 1–26.

[Limón et al., 2008] Limón, D., Alvarado, I., Alamo, T., and Camacho, E. F. (2008). Mpc for tracking piecewise constant references for constrained linear systems. *Automatica*, 44(9):2382–2387.

[Limon et al., 2015] Limon, D., Pereira, M., de la Pena, D. M., Alamo, T., Jones, C. N., and Zeilinger, M. N. (2015). Mpc for tracking periodic references. *IEEE Transactions on Automatic Control*, 61(4):1123–1128.

[Liu et al., 2019] Liu, S., Mao, Y., and Liu, J. (2019). Model-predictive control with generalized zone tracking. *IEEE Transactions on Automatic Control*, 64(11):4698–4704.

[Magdelaine et al., 2015] Magdelaine, N., Chaillous, L., Guilhem, I., Poirier, J.-Y., Krempf, M., Moog, C. H., and Le Carpentier, E. (2015). A long-term model of the glucose–insulin dynamics of type 1 diabetes. *IEEE Transactions on Biomedical Engineering*, 62(6):1546–1552.

[Magdelaine et al., 2020] Magdelaine, N., Rivadeneira, P. S., Chaillous, L., Fournier-Guilloux, A.-L., Krempf, M., MohammadRidha, T., Ait-Ahmed, M., and Moog, C. H. (2020). Hypoglycaemia-free artificial pancreas project. *IET Systems Biology*, 14(1):16–23.

[Man et al., 2014] Man, C. D., Micheletto, F., Lv, D., Breton, M., Kovatchev, B., and Cobelli, C. (2014). The uva/padova type 1 diabetes simulator: new features. *Journal of diabetes science and technology*, 8(1):26–34.

[Man et al., 2007] Man, C. D., Rizza, R. A., and Cobelli, C. (2007). Meal simulation model of the glucose-insulin system. *IEEE Transactions on Biomedical Engineering*, 54(10):1740–1749.

[Mansell et al., 2017] Mansell, E. J., Docherty, P. D., and Chase, J. G. (2017). Shedding light on grey noise in diabetes modelling. *Biomedical Signal Processing and Control*, 31:16–30.

[Manzoni et al., 2023] Manzoni, E., Rampazzo, M., Facchinetti, A., Sparacino, G., and Del Favero, S. (2023). Monitoring statistical properties of kalman filter residuals in an artificial pancreas to detect overnight pump malfunctions causing insulin suspension. *Control Engineering Practice*, 141:105673.

[Mauseth et al., 2013] Mauseth, R., Hirsch, I. B., Bollyky, J., Kircher, R., Matheson, D., Sanda, S., and Greenbaum, C. (2013). Use of a "fuzzy logic" controller in a closed-loop artificial pancreas. *Diabetes technology & therapeutics*, 15(8):628–633.

[Meneghetti et al., 2018] Meneghetti, L., Terzi, M., Del Favero, S., Susto, G. A., and Cobelli, C. (2018). Data-driven anomaly recognition for unsupervised model-free fault detection in artificial pancreas. *IEEE Transactions on Control Systems Technology*, 28(1):33–47.

[Messori et al., 2015] Messori, M., Ellis, M., Cobelli, C., Christofides, P. D., and Magni, L. (2015). Improved postprandial glucose control with a customized model predictive controller. In *2015 American control conference (ACC)*, pages 5108–5115. IEEE.

[Messori et al., 2018] Messori, M., Incremona, G. P., Cobelli, C., and Magni, L. (2018). Individualized model predictive control for the artificial pancreas: In silico evaluation of closed-loop glucose control. *IEEE Control Systems Magazine*, 38(1):86–104.

[Murphy and Weaver, 2016] Murphy, K. and Weaver, C. (2016). *Janeway's immunobiology*. Garland science.

[Murray, 2002] Murray, J. D. (2002). *Mathematical biology: I. An introduction*. Springer.

[Nangue, 2019] Nangue, A. (2019). Global Stability Analysis of the Original Cellular Model of Hepatitis C Virus Infection Under Therapy. *American Journal of Mathematical and Computer Modelling*, 4(3):58–65.

[Nguyen et al., 2015] Nguyen, V., Binder, S., Boianelli, A., Meyer-Hermann, M., and Hernandez-Vargas, E. A. (2015). Ebola Virus Infection Modelling and Identifiability Problems. *Frontiers in microbiology*, 6.

[Nikin-Beers and Ciupe, 2018] Nikin-Beers, R. and Ciupe, S. M. (2018). Modelling original antigenic sin in dengue viral infection. *Mathematical medicine and biology: a journal of the IMA*, 35(2):257–272.

[Nowak and May, 2000] Nowak, M. and May, R. M. (2000). *Virus dynamics: mathematical principles of immunology and virology*. Oxford University Press, UK.

[Ohlsson and Ljung, 2013] Ohlsson, H. and Ljung, L. (2013). Identification of switched linear regression models using sum-of-norms regularization. *Automatica*, 49(4):1045–1050.

[Ohlsson et al., 2010] Ohlsson, H., Ljung, L., and Boyd, S. (2010). Segmentation of arx-models using sum-of-norms regularization. *Automatica*, 46(6):1107–1111.

[Ortmann et al., 2017] Ortmann, L., Shi, D., Dassau, E., Doyle, F. J., Leonhardt, S., and Misgeld, B. J. (2017). Gaussian process-based model predictive control of blood glucose for patients with type 1 diabetes mellitus. In *2017 11th Asian Control Conference (ASCC)*, pages 1092–1097. IEEE.

[Oviedo et al., 2017] Oviedo, S., Vehí, J., Calm, R., and Armengol, J. (2017). A review of personalized blood glucose prediction strategies for t1dm patients. *International journal for numerical methods in biomedical engineering*, 33(6):e2833.

[Penet, 2013] Penet, M. (2013). *Robust Nonlinear Model Predictive Control based on Constrained Saddle Point Optimization: Stability Analysis and Application to Type 1 Diabetes*. PhD thesis, Supélec.

[Pérez et al., 2022] Pérez, M., Abuin, P., Actis, M., Ferramosca, A., Hernandez-Vargas, E. A., and González, A. H. (2022). Optimal control strategies to tailor antivirals for acute infectious diseases in the host: a study case of covid-19. In *Feedback Control for Personalized Medicine*, pages 11–39. Elsevier.

[Pillonetto et al., 2006] Pillonetto, G., Caumo, A., Sparacino, G., and Cobelli, C. (2006). A new dynamic index of insulin sensitivity. *IEEE transactions on biomedical engineering*, 53(3):369–379.

[Pillonetto et al., 2022] Pillonetto, G., Chen, T., Chiuso, A., De Nicolao, G., and Ljung, L. (2022). *Regularized system identification: Learning dynamic models from data*. Springer Nature.

[Rakovic and Levine, 2018] Rakovic, S. V. and Levine, W. S. (2018). Handbook of model predictive control.

[Raue et al., 2009] Raue, A., Kreutz, C., Maiwald, T., Bachmann, J., Schilling, M., Klingmüller, U., and Timmer, J. (2009). Structural and practical identifiability analysis of partially observed dynamical models by exploiting the profile likelihood. *Bioinformatics*, 25(15):1923–1929.

[Rawlings et al., 2017] Rawlings, J. B., Mayne, D. Q., and Diehl, M. (2017). *Model predictive control: theory, computation, and design*, volume 2. Nob Hill Publishing Madison, WI.

[Reiterer and Freckmann, 2019] Reiterer, F. and Freckmann, G. (2019). Advanced carbohydrate counting: an engineering perspective. *Annual Reviews in Control*, 48:401–422.

[Riddell et al., 2017] Riddell, M. C., Gallen, I. W., Smart, C. E., Taplin, C. E., Adolfsson, P., Lumb, A. N., Kowalski, A., Rabasa-Lhoret, R., McCrimmon, R. J., Hume, C., et al. (2017). Exercise management in type 1 diabetes: a consensus statement. *The lancet Diabetes & endocrinology*, 5(5):377–390.

[Riddell et al., 2020] Riddell, M. C., Scott, S. N., Fournier, P. A., Colberg, S. R., Gallen, I. W., Moser, O., Stettler, C., Yardley, J. E., Zaharieva, D. P., Adolfsson, P., et al. (2020). The competitive athlete with type 1 diabetes. *Diabetologia*, 63:1475–1490.

[Rilstone et al., 2021] Rilstone, S., Reddy, M., and Oliver, N. (2021). A pilot study of flat and circadian insulin infusion rates in continuous subcutaneous insulin infusion (csii) in adults with type 1 diabetes (first1d). *Journal of Diabetes Science and Technology*, 15(3):666–671.

[Rivadeneira et al., 2018] Rivadeneira, P. S., Ferramosca, A., and González, A. H. (2018). Control strategies for nonzero set-point regulation of linear impulsive systems. *IEEE Transactions on Automatic Control*, 63(9):2994–3001.

[Rivadeneira et al., 2019] Rivadeneira, P. S., Godoy, J. L., Serenoa, J. E., Abuin, P., Ferramosca, A., and González, A. H. (2019). Impulsive MPC schemes for biomedical processes. application to type 1 diabetes. In Azar, A. T., editor, *Control applications for Biomedical Engineering Systems*. ELSEVIER.

[Ruan et al., 2016] Ruan, Y., Wilinska, M. E., Thabit, H., and Hovorka, R. (2016). Modeling day-to-day variability of glucose–insulin regulation over 12-week home use of closed-loop insulin delivery. *IEEE Transactions on Biomedical Engineering*, 64(6):1412–1419.

[Ruan et al., 2017] Ruan, Y., Wilinska, M. E., Thabit, H., and Hovorka, R. (2017). Modeling day-to-day variability of glucose-insulin regulation over 12-week home use of closed-loop insulin delivery. *IEEE Transactions on Biomedical Engineering*, 64(6):1412–1419.

[Saad et al., 2012] Saad, A., Dalla Man, C., Nandy, D. K., Levine, J. A., Bharucha, A. E., Rizza, R. A., Basu, R., Carter, R. E., Cobelli, C., Kudva, Y. C., et al. (2012). Diurnal pattern to insulin secretion and insulin action in healthy individuals. *Diabetes*, 61(11):2691–2700.

[Sala-Mira et al., 2019] Sala-Mira, I., Díez, J.-L., Ricarte, B., and Bondia, J. (2019). Sliding-mode disturbance observers for an artificial pancreas without meal announcement. *Journal of Process Control*, 78:68–77.

[Samadi et al., 2018] Samadi, S., Rashid, M., Turksoy, K., Feng, J., Hajizadeh, I., Hobbs, N., Lazaro, C., Sevil, M., Littlejohn, E., and Cinar, A. (2018). Automatic detection and estimation of unannounced meals for multivariable artificial pancreas system. *Diabetes technology and therapeutics*, 20(3):235–246.

[Sanchez et al., 2023] Sanchez, I., Louembet, C., Actis, M., and Gonzalez, A. H. (2023). Characterization and computation of control invariant sets for linear impulsive control systems. *Nonlinear Analysis: Hybrid Systems*, 47:101271.

[Sánchez-Peña et al., 2018] Sánchez-Peña, R., Colmegna, P., Garelli, F., De Battista, H., García-Violini, D., Moscoso-Vásquez, M., Rosales, N., Fushimi, E., Campos-Náñez, E., Breton, M., et al. (2018). Artificial pancreas: clinical study in latin america without premeal insulin boluses. *Journal of diabetes science and technology*, 12(5):914–925.

[Satin et al., 2015] Satin, L. S., Butler, P. C., Ha, J., and Sherman, A. S. (2015). Pulsatile insulin secretion, impaired glucose tolerance and type 2 diabetes. *Molecular aspects of medicine*, 42:61–77.

[Schiavon et al., 2018] Schiavon, M., Dalla Man, C., and Cobelli, C. (2018). Insulin sensitivity index-based optimization of insulin to carbohydrate ratio: in silico study shows efficacious protection against hypoglycemic events caused by suboptimal therapy. *Diabetes technology & therapeutics*, 20(2):98–105.

[Schiavon et al., 2014] Schiavon, M., Dalla Man, C., Kudva, Y. C., Basu, A., and Cobelli, C. (2014). Quantitative estimation of insulin sensitivity in type 1 diabetic subjects wearing a sensor-augmented insulin pump. *Diabetes care*, 37(5):1216–1223.

[Schiavon et al., 2019] Schiavon, M., Visentin, R., Giegerich, C., Klabunde, T., Cobelli, C., and Dalla Man, C. (2019). Modeling subcutaneous absorption of long-acting insulin glargine in type 1 diabetes. *IEEE Transactions on Biomedical Engineering*, 67(2):624–631.

[Seron et al., 2016] Seron, M. M., Medioli, A. M., and Goodwin, G. C. (2016). A methodology for the comparison of traditional mpc and stochastic mpc in the context of the regulation of blood glucose levels in type 1 diabetics. In *2016 Australian Control Conference (AuCC)*, pages 126–131. IEEE.

[Shi et al., 2019] Shi, D., Dassau, E., and Doyle III, F. J. (2019). Multivariate learning framework for long-term adaptation in the artificial pancreas. *Bioengineering & translational medicine*, 4(1):61–74.

[Sikaris, 2014] Sikaris, K. A. (2014). Physiology and its importance for reference intervals. *The Clinical Biochemist Reviews*, 35(1):3.

[Simon, 2010] Simon, D. (2010). Kalman filtering with state constraints: a survey of linear and nonlinear algorithms. *IET Control Theory & Applications*, 4(8):1303–1318.

[Sontag, 2013] Sontag, E. D. (2013). *Mathematical control theory: deterministic finite dimensional systems*, volume 6. Springer Science & Business Media.

[Sopasakis et al., 2015] Sopasakis, P., Patrinos, P., Sarimveis, H., and Bemporad, A. (2015). Model predictive control for linear impulsive systems. *IEEE Transactions on Automatic Control*, 60(8):2277–2282.

[Soru et al., 2012] Soru, P., De Nicolao, G., Toffanin, C., Dalla Man, C., Cobelli, C., Magni, L., Consortium, A. H., et al. (2012). Mpc based artificial pancreas: strategies for individualization and meal compensation. *Annual Reviews in Control*, 36(1):118–128.

[Steil, 2013] Steil, G. M. (2013). Algorithms for a closed-loop artificial pancreas: the case for proportional-integral-derivative control. *Journal of diabetes science and technology*, 7(6):1621–1631.

[Stenvers et al., 2019] Stenvers, D. J., Scheer, F. A., Schrauwen, P., la Fleur, S. E., and Kalsbeek, A. (2019). Circadian clocks and insulin resistance. *Nature Reviews Endocrinology*, 15(2):75–89.

[Toffanin et al., 2017a] Toffanin, C., Messori, M., Cobelli, C., and Magni, L. (2017a). Automatic adaptation of basal therapy for type 1 diabetic patients: a run-to-run approach. *Biomedical Signal Processing and Control*, 31:539–549.

[Toffanin et al., 2017b] Toffanin, C., Visentin, R., Messori, M., Di Palma, F., Magni, L., and Cobelli, C. (2017b). Toward a run-to-run adaptive artificial pancreas: In silico results. *IEEE Transactions on Biomedical Engineering*, 65(3):479–488.

[Toffanin et al., 2013] Toffanin, C., Zisser, H., Doyle III, F. J., and Dassau, E. (2013). Dynamic insulin on board: incorporation of circadian insulin sensitivity variation. *Journal of diabetes science and technology*, 7(4):928–940.

[Tokarz et al., 2018] Tokarz, V. L., MacDonald, P. E., and Klip, A. (2018). The cell biology of systemic insulin function. *J Cell Biol*, 217(7):2273–2289.

[Van Cauter et al., 1997] Van Cauter, E., Polonsky, K. S., and Scheen, A. J. (1997). Roles of circadian rhythmicity and sleep in human glucose regulation. *Endocrine reviews*, 18(5):716–738.

[van den Driessche, 2017] van den Driessche, P. (2017). Reproduction numbers of infectious disease models. *Infectious Disease Modelling*, 2(3):288–303.

[van Heusden et al., 2011] van Heusden, K., Dassau, E., Zisser, H. C., Seborg, D. E., and Doyle III, F. J. (2011). Control-relevant models for glucose control using a priori patient characteristics. *IEEE transactions on biomedical engineering*, 59(7):1839–1849.

[Vegvari et al., 2016] Vegvari, C., Hadjichrysanthou, C., Cauet, E., Lawrence, E., Cori, A., De Wolf, F., and Anderson, R. M. (2016). How can viral dynamics models inform endpoint measures in clinical trials of therapies for acute viral infections? *PLoS One*, 11(7):e0158237.

[Visentin et al., 2018] Visentin, R., Campos-Náñez, E., Schiavon, M., Lv, D., Vettoretti, M., Breton, M., Kovatchev, B. P., Dalla Man, C., and Cobelli, C. (2018). The uva/padova type 1 diabetes simulator goes from single meal to single day. *Journal of diabetes science and technology*, 12(2):273–281.

[Visentin et al., 2015] Visentin, R., Dalla Man, C., Kudva, Y. C., Basu, A., and Cobelli, C. (2015). Circadian variability of insulin sensitivity: physiological input for in silico artificial pancreas. *Diabetes technology & therapeutics*, 17(1):1–7.

[Walsh and Roberts, 2017] Walsh, J. and Roberts, R. (2017). *Pumping insulin: everything for success on an insulin pump and CGM*. Torrey Pines Press.

[Wilinska et al., 2016] Wilinska, M. E., Budiman, E. S., Hayter, G. A., Taub, M. B., and Hovorka, R. (2016). Integrated closed-loop medication delivery with error model and safety check. US Patent 9,402,953.

[Wodarz, 2007] Wodarz, D. (2007). *Killer cell dynamics: mathematical and computational approaches to immunology*. Springer.

[Wölfel et al., 2020] Wölfel, R., Corman, V. M., Guggemos, W., Seilmaier, M., Zange, S., Müller, M. A., Niemeyer, D., Jones, T. C., Vollmar, P., Rothe, C., et al. (2020). Virological assessment of hospitalized patients with COVID-2019. *Nature*, 581(7809):465–469.

[Ziegler et al., 2021] Ziegler, R., Oliver, N., Waldenmaier, D., Mende, J., Haug, C., and Freckmann, G. (2021). Evaluation of the accuracy of current tubeless pumps for continuous subcutaneous insulin infusion. *Diabetes technology & therapeutics*, 23(5):350–357.

[Zou et al., 2020] Zou, H., Banerjee, P., Leung, S. S. Y., and Yan, X. (2020). Application of pharmacokinetic-pharmacodynamic modeling in drug delivery: development and challenges. *Frontiers in pharmacology*, 11:997.